Consistent Discretization of Maxwell's Equations on Polyhedral Grids

Vom Fachbereich 18
Elektrotechnik und Informationstechnik
der Technischen Universität Darmstadt

zur Erlangung
der Würde eines Doktor Ingenieurs (Dr.-Ing.)
genehmigte

DISSERTATION

von
Dipl.-Ing. Timo Euler
geboren in Schlüchtern

Referent:	Prof. Dr.-Ing. Thomas Weiland
Korreferent:	Prof. Dr. rer. nat. Jens Lang
Korreferent:	Prof. Dr. techn. Romanus Dyczij-Edlinger

Tag der Einreichung:	10.07.2007
Tag der mündlichen Prüfung:	22.10.2007

D17
Darmstädter Dissertation

Darmstadt, 2007

CONTENTS

ACKNOWLEDGEMENTS

Many people and institutions have provided support during the last years and thus helped me bring my research to a fruitful conclusion. Thanks. I explicitly thank

- Prof. Dr.-Ing. Thomas Weiland for advising my thesis and providing an excellent research environment,
- Prof. Dr. rer. nat. Jens Lang and Prof. Dr. techn. Romanus Dyczij-Edlinger for reviewing this thesis,
- the Technische Universität Darmstadt and the Computational Engineering Research Center at the Technische Universität Darmstadt for providing scholarships,
- my current and former colleagues at the Institut für Theorie Elektromagnetischer Felder of the Technische Universität Darmstadt, especially Dipl.-Ing. Andreas Paech and Dipl.-Ing. Denis Sievers, for the interesting discussions and a nice time,
- Prof. Dr.-Ing. Rolf Schuhmann for guiding the first steps into my research,
- the research community for stimulating discussions about and input for my work,
- my electrical engineering and mathematics teachers for igniting my interests in a wide field of scientific topics,
- my family and parents.

And I especially thank Esther Kraus for accompanying me during all these years.

ABSTRACT

This thesis introduces polyhedral cell shapes into the formalism of the Finite Integration Technique (FIT) and shows their practicability in electromagnetic simulations. Emphasis is put on a rigorous mathematical presentation.

The semi-discrete (discrete in space but continuous in time) and fully discrete Maxwell's Grid Equations of the FIT are developed from the continuous Maxwell's equations accentuating the connections to differential geometry and topology. The derivation of Maxwell's Grid Equations is valid for a set of arbitrary dual consistent grids allowing also for curved polyhedral cell shapes. This possibility has been known for quite some time, but material relations were only known for special cell shapes like hexahedra, tetrahedra, prisms, pyramids, or dual orthogonal grids. In this thesis, material relations for arbitrary polyhedral grid cells with straight edges and planar faces are derived. Examples from a wide range of electromagnetic applications show the practicability of these polyhedral grid cells in numerical simulations.

KURZFASSUNG

In dieser Arbeit werden Polyederelemente in die Methode der finiten Integration (FIT) eingeführt. Die praktische Anwendbarkeit in elektromagnetischen Simulationen wird gezeigt. Ein weiterer Schwerpunkt ist die rigorose mathematische Einbindung.

Die Gitter-Maxwell-Gleichungen der FIT werden in semi-diskreter (diskret im Raum und kontinuierlich in der Zeit) und in voll diskreter Form aus den kontinuierlichen Maxwellschen Gleichungen hergeleitet. Verbindungen zu den Disziplinen der Differentialgeometrie und Topologie werden ersichtlich. Die semi-diskreten und voll diskreten Gitter-Maxwell-Gleichungen gelten in der hergeleiteten Form für beliebige, duale, konsistente Gitter, einschließlich gekrümmten Polyedergittern. Obwohl diese Möglichkeit seit einiger Zeit bekannt ist, konnten die benötigten Materialbeziehungen bisher nur für spezielle Elementformen wie Hexaeder, Tetraeder, Prismen, Pyramiden oder dual orthogonale Gitter hergeleitet werden. In dieser Arbeit werden Materialbeziehungen für beliebige Polyeder mit planaren Flächen und geraden Kanten eingeführt. Beispiele aus verschiedenen elektromagnetischen Bereichen zeigen die praktische Anwendbarkeit in numerischen Simulationen.

1. INTRODUCTION

The macroscopic Maxwell's equations [64] describe many day-to-day electromagnetic phenomena. Complemented with suitable initial and boundary conditions assuring a unique solution, we call this system of equations *Maxwell's initial boundary value problem* (IBVP). This thesis discusses and extends a numerical method to approximately solve Maxwell's and similar IBVPs: The Finite Integration Technique (FIT) [92] [94] [95].

In general, numerical methods for solving partial differential equations can be classified into grid-based or non-grid-based schemes and into surface or volume discretizations. The FIT is a grid-based volume discretization scheme. The FIT is closely related to other numerical schemes like the cell-method [87], the Whitney-Finite Element Method (Whitney-FEM) [7], and certain Finite Difference (FD) and Finite Volume (FV) schemes. The shape of the grid cells used in the standard FIT is restricted to grids allowing for an orthogonal dual grid, usually conforming to an orthogonal coordinate system. The cube shown in Fig. 1.1a is an example conforming to a Cartesian grid. In [79], the FIT was extended to non-orthogonal hexahedral cells as the one shown in Fig. 1.1b. Using the close connection of the Whitney-FEM to the FIT, one can realize arbitrary tetrahedra [69], prisms [29], and pyramids [40] as shown in Fig. 1.1c to 1.1e, respectively. This still restricts the grid greatly, though. E.g. subgridding or interface coupling call for more flexible grid elements as shown in Fig. 1.1f and 1.1g.

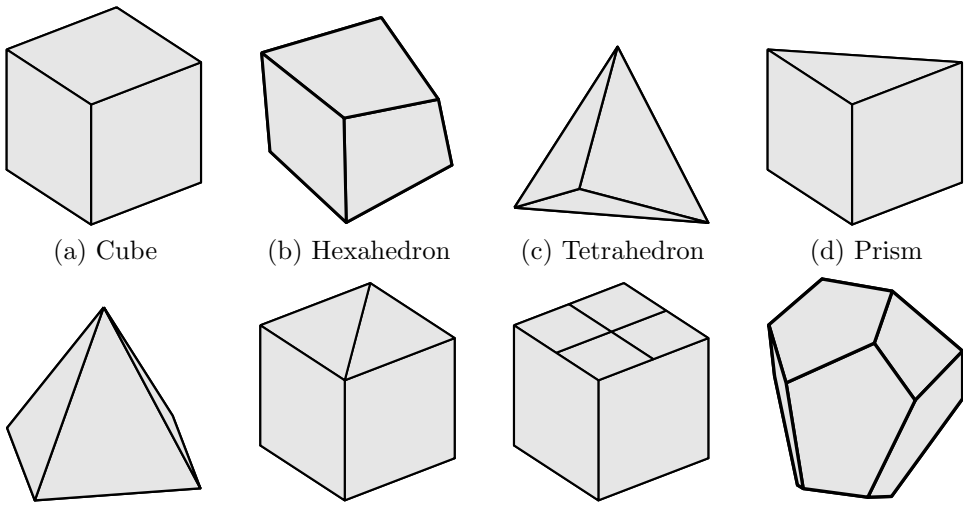

(a) Cube (b) Hexahedron (c) Tetrahedron (d) Prism

(e) Pyramid (f) Cube with additional edge (g) Cube with subgridding on top face (h) Polyhedral cell

Fig. 1.1: Example cell shapes.

The main aim of this thesis is to extend the FIT to facilitate arbitrary polyhedral cells with planar faces and straight edges. This allows e.g. for the treatment of all cells shown in Fig. 1.1 except for the hexahedron with curved faces in Fig. 1.1b. Very general polyhedral grids like the one shown in Fig. 1.2 are thus possible.

Fig. 1.2: Example polyhedral grid.

The idea of using polygonal or polyhedral grids is not new: The first nodal finite element basis functions for polygonal grids known to the author can be found in [90]. Further polygonal and polyhedral ideas and developments can e.g. be found in [14], [37], [45], [54], [57], and [82]. All these presentations only treat a small part of the computational framework of Maxwell's equations, though. In this thesis, the complete computational framework of the FIT is extended to polyhedral grids.

Since the start of numerical solution techniques for Maxwell's equations, it has been realized that the preservation of several properties of the continuous setting in the discrete schemes is very useful. The preservation of certain so-called *topological properties*[1] ensures e.g. the existence of discrete potentials. They also lead to charge conservation, which, besides being considered important by itself in some applications, renders a handy tool for detecting and localizing errors in the coding. Together with the preservation of so-called *metric properties*[2], conservation of energy and existence and uniqueness of solutions are assured in the discrete setting. We call a numerical solution technique preserving these topological and metric properties in the discrete setting a *consistent* discretization[3]. The FIT is such a consistent scheme.

Grid-based numerical schemes restricted to certain cell shapes often lack the flexibility

[1] The term *topological properties* basically refers to *geometric* properties of infinitesimal neighborhoods. The notion of *distance* is not required.

[2] The term *metric properties* here refers to properties requiring topological notions and further on the notion of a *metric*, that is basically of *distances*.

[3] At this place, the term *consistent* is not to be confused with the mathematical term of consistency of numerical schemes.

to realize grid transitions like subgridding or arbitrary interface coupling. To regain some flexibility, interpolations are employed for grid transitions. This often leads to the loss of the topological and metric properties and renders instable and non-convergent schemes. Even if some properties can be proven to hold, others might be unclear or hard to proof. E.g. for the subgridding scheme described in [73] a discrete charge conservation and stability has been shown. But the existence of discrete potentials has not been investigated, yet.

The idea of this thesis is to clarify the concepts of the FIT leading to the preservation of the topological and metric properties and then to fill in the missing parts for polyhedral cells. Therefore, known properties and concepts of the FIT are collected in a mathematical rigorous manner in parallel to the continuous setting. At certain points, missing parts are added. The connections to the mathematical fields of differential geometry and topology are emphasized.

It becomes clear that the topological properties in the FIT follow from the concept of using consistent grids. These consistent grids already allow for polyhedral cells with curved faces and edges. This has been known for quite some time [95], but here the concepts of the FIT are collected persistently for the general class of consistent grids separating the topological and metric parts. The metric properties then follow, if one can realize positive definite material relations.

Suitable material relations have not been known for arbitrary polyhedral cells before. The main achievement of this thesis is the realization of positive definite material relations for arbitrary polyhedra with straight edges and flat faces. They ensure the preservation of the metric properties in the discrete setting. The construction of the material relations is based on the work in [19] and requires the solution of continuous or discrete hierarchical boundary value problems (BVPs). Although convergence for the resulting scheme is not proven, the basic requirements are believed to be established and supported by numerical results.

The outline of the thesis is as follows: Chapter 2 establishes the continuous Maxwell's IBVP along with its topological and metric properties. In chapter 3, the FIT is described in exact analogy to the continuous setting capturing the discussed properties in a discrete sense. The semi-discrete (discrete in space but continuous in time) Maxwell's Grid Equations are discussed in chapter 3.2 while the fully discrete Maxwell's Grid Equations are discussed in chapter 3.3. The open question of material laws is answered in chapter 4 for arbitrary polyhedral cells with straight edges and flat faces. The electromagnetic problems in chapter 5 show different application scenarios for polytope, or more specifically polygonal and polyhedral, grid cells. The expected convergence rates are verified in the numerical experiments.

The main achievements of this thesis are:

- Symmetric positive definite material relations are developed for polyhedral cells with straight edges and flat faces in the framework of the FIT.
- Known concepts of the FIT are collected, separated into topological and metric concepts, in a mathematical rigorous manner for arbitrary consistent grids. The close connection to concepts from differential geometry and topology is emphasized.

Partial differential equations are often stated in the language of vector calculus. The topological and metric properties which we want to discuss separately are hidden in this language and mixed together, though. A clear separation is evident in the notation of differential geometry. So in order to discuss and separate the topological and metric properties, this text uses the language of differential geometry. Also, many formulas which in the language of vector calculus seem unconnected can actually be stated in one general form when using differential forms. The text will switch to a standard vector calculus formalism again for stating and discussing Maxwell's equations, as this is more commonly used in the engineering community and the generality is not needed any more at this point. Equivalently, a general notation is used for stating the general properties in the discrete setting in chapter 3, while for the concrete example of Maxwell's Grid Equations, (almost) standard FIT formalism is used.

2. CONTINUOUS MAXWELL'S EQUATIONS

The macroscopic Maxwell's equations first stated in [64] well describe many electromagnetic phenomena. They are comprised of a set of partial differential equations. The mathematical setting needed to state Maxwell's equations is presented e.g. in [18] or [59]. We shortly reproduce the most important mathematical tools in the language of differential geometry in chapter 2.1. As mentioned in the introduction, this simplifies the separation into topological and metric tools: Topological tools depend solely on the topology of the problem domain while metric tools also require a metric to be available. An introduction to this formalism used in electromagnetism can e.g. be found in [8] or [28].

In chapter 2.2, Maxwell's topological and metric laws are stated separately. The topological laws only make use of the topological tools while the metric laws also require the metric tools. Properties deduced only from the topological laws are called topological properties. Properties which also require the metric laws are called metric properties.

This separation into topological and metric tools, laws, and properties will be an important guideline for the discretization of Maxwell's equations in chapter 3. We will be able to fulfill Maxwell's topological laws exactly on a finite set of grid elements, while Maxwell's metric laws will only be approximated.

2.1 Continuous Mathematical Tools Needed to State Maxwell's Equations

2.1.1 Space-Time Domain

The quantities in Maxwell's equations are defined on a 4-dimensional space-time domain. We will only discuss their form in an inertial frame and separate the space-time into the 3-dimensional spatial domain Ω and the 1-dimensional temporal domain T. The problem domain is regarded as the Cartesian product of these spaces $\Omega \times \mathrm{T}$ as illustrated in Fig. 2.1. The spatial variable will be denoted by $\vec{r} \in \Omega$ and the temporal variable by $t \in \mathrm{T}$. This setting is suitable for most engineering applications and allows for the separate treatment of space and time in the discretization process.

Additionally, we restrict Ω to be a bounded contractible subset of $\mathbb{R}^3$ with smooth boundary $\partial\Omega$ and T to be bounded on one side, i.e. $\mathrm{T} = [t_0, \infty)$. The reasons for these restrictions are as follows:

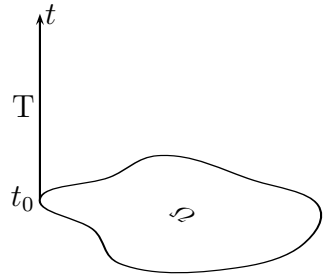

Fig. 2.1: Continuous problem domain $\Omega \times \mathrm{T}$.

- We take the spatial domain Ω to be bounded, as this is the case in many applications and requires us to give a rigorous treatment of the spatial boundary conditions in the discretization process in chapter 3.
- The spatial domain Ω is restricted to be contractible, as this allows us to leave cohomology considerations at the side; loosely speaking, we are thereby not treating the case of holes and loops in our domain. These cases do arise in the modeling of practical problems, though: E.g. a perfect electrically conducting box approximating a good conductor leads to a hole in the domain. Then, cohomology considerations are important for the correct use of potentials. For the interested reader, cohomology is treated extensively for the continuous and discrete Maxwell's equations in the quasistatic case in [42]. The treatment in this thesis can be extended to non-contractible domains by the concepts described in [42] if needed.
- By taking the spatial domain Ω as a subset of $\mathbb{R}^3$, Ω is orientable and the Riemannian metric is available. This is the standard setting for Maxwell's equations.
- The spatial boundary $\partial\Omega$ is assumed to be smooth as this simplifies the mathematical presentation. This is not the case for most engineering applications, though: E.g. a rectangular waveguide or the grid elements employed in the discretization exhibit edges and corners. There, we will have to lift this restriction. For discussion of domains with less regular boundaries, see e.g. [18] and [59].

2.1.2 Differential Forms, Vector Proxies, and Integration

The aim of this chapter is to introduce the notation of differential geometry used in this text. For the reader unfamiliar with differential geometry, the chapter tries to give a feeling for the concepts apparent in this notation that are important for the discretization of Maxwell's equations: The separation of topological and metric properties. E.g. for defining certain concepts such as integration, one does not need to use a metric. For a mathematically more rigorous introduction to differential geometry, one can e.g. consult the references [1], [18, pp. 296], or [53]. In [5], [28], [60], or [74], one finds introductions to Maxwell's equations stated in the language of differential geometry.

In the following, we will leave aside the time dependence t and only discuss quantities defined on the 3-dimensional spatial domain Ω. This can be considered as treating the quantities at a fixed point t_0 in time.

We first introduce the notation for paths, surfaces, and volumes in Ω in a unified manner. We will need them for defining the integral of physical quantities over these elements. The points, paths, surfaces, and volumes are called 0-, 1-, 2-, and 3-dimensional submanifolds, respectively:

Notation 2.1. We denote by $\boldsymbol{S}_s^k(\Omega)$ the *set of smooth oriented k-dimensional submanifolds* of the domain Ω.

Note that, in order to unify notation, we also have given an orientation to points. Later on, we will also need the oriented boundary of an oriented k-dimensional submanifold S^k:

Notation 2.2. The *oriented boundary* of an oriented k-dimensional submanifold S^k is denoted by ∂S^k. The orientation of the boundary is induced by the orientation of the submanifold S^k according to [53, pp. 113]. The boundary of a point S^0 is empty.

Let us first take a look at the standard vector analysis formulation of some electromagnetic quantities and how we integrate them over submanifolds:

From physical experience, one knows that the scalar electric potential $\varphi_e(\vec{r})$ is a quantity that is defined at (0-dimensional) points in space and can be, up to the arbitrary constant in its definition, measured pointwise. For a unified notation, we introduce the integration over a point S^0 as evaluation at that point:

$$\int_{S^0} \varphi_e(\vec{r}) \equiv \varphi_e(\vec{r})|_{\vec{r}=S^0} \tag{2.1a}$$

The electric field strength $\vec{E}(\vec{r})$ as a vector field is mathematically also defined pointwise, but physically can only be measured as the integral over oriented 1-dimensional paths in space. The resulting quantity is called electric voltage along that path S^1:

$$\int_{S^1} \vec{E}(\vec{r}) \cdot \vec{t}_{S^1} \, \mathrm{d}s \tag{2.1b}$$

where $\vec{t}_{S^1}$ denotes the unit tangential vector along the path S^1 and $\mathrm{d}s$ denotes the infinitesimal path length element. Any definition seeming to render a pointwise quantity here is actually interpreted as an infinitesimal limit of such an integration.

The magnetic flux density $\vec{B}(\vec{r})$ physically makes sense as the integral over oriented 2-dimensional surfaces which is called magnetic flux through these surfaces:

$$\int_{S^2} \vec{B}(\vec{r}) \cdot \vec{n}_{S^2} \, \mathrm{d}A \tag{2.1c}$$

where $\vec{n}_{S^2}$ denotes the unit vector normal to the surface S^2 and $\mathrm{d}A$ denotes the infinitesimal surface area element.

The electric charge density $\varrho_e(\vec{r})$ physically makes sense as integral over 3-dimensional volumes which is then called the electric charge in these volumes:

$$\int_{S^3} \varrho_e(\vec{r}) \, \mathrm{d}V \tag{2.1d}$$

where $\mathrm{d}V$ denotes the infinitesimal volume element.

Now the problem with this notation is twofold: Firstly, in the scalar and vector field quantities as well as in the infinitesimal integration elements, a metric seems to be necessary to define the integration. The process of integration can be defined without resorting to a metric, though. Secondly, in scalar and vector field notation, it is not clear over which kind of elements one can integrate the physical quantities. This leads e.g. to differing transformation rules of quantities that seem to be the same in the language of vector analysis.

The notation of differential geometry solves these problems. In the language of differential geometry, a quantity that makes sense only as integration over a k-dimensional manifold S^k is called a *differential form of degree* k, or in short *k-form*.

Notation 2.3. The space of *smooth*[1] *k-forms* on the domain Ω is denoted by $\mathcal{F}_s^k(\Omega)$.

Here, we will be satisfied by defining a k-form by its integral over k-dimensional manifolds:

Notation 2.4. The *integral of a k-form* $\omega^k \in \mathcal{F}_s^k(\Omega)$ over a k-dimensional manifold $S^k \in \boldsymbol{S}_s^k(\Omega)$ will be denoted by:

$$\int_{S^k} . : \quad \omega^k \in \mathcal{F}_s^k(\Omega) \longmapsto \int_{S^k} \omega^k \in \mathbb{R} \tag{2.2}$$

We formally also define the integral over the sum of two k-dimensional manifolds by:

$$\int_{S_a^k + S_b^k} \omega^k \equiv \int_{S_a^k} \omega^k + \int_{S_b^k} \omega^k, \qquad S_a^k,\, S_b^k \in \boldsymbol{S}_s^k(\Omega) \tag{2.3}$$

and the integral over a multiplication of a k-dimensional manifold with a scalar by:

$$\int_{\alpha S^k} \omega^k \equiv \alpha \int_{S^k} \omega^k, \qquad S^k \in \boldsymbol{S}_s^k(\Omega), \quad \alpha \in \mathbb{R} \tag{2.4}$$

So now instead of using the scalar and vector fields for the electromagnetic quantities as in equations (2.1a) to (2.1d), we can introduce the electric potential 0-form φ_e^0, the electric field strength 1-form e^1, the magnetic flux density 2-form b^2, and the electric charge density 3-form ϱ_e^3. Assuming the quantities known in standard vector analysis formulation, we could define the forms in integral terms by:

$$\int_{S^0} \varphi_e^0 \equiv \int_{S^0} \varphi_e(\vec{r}) \qquad \forall\, S^0 \in \boldsymbol{S}_s^0(\Omega) \tag{2.5a}$$

$$\int_{S^1} e^1 \equiv \int_{S^1} \vec{E}(\vec{r}) \cdot \vec{t}_{S^1}\, \mathrm{d}s \qquad \forall\, S^1 \in \boldsymbol{S}_s^1(\Omega) \tag{2.5b}$$

$$\int_{S^2} b^2 \equiv \int_{S^2} \vec{B}(\vec{r}) \cdot \vec{n}_{S^2}\, \mathrm{d}A \qquad \forall\, S^2 \in \boldsymbol{S}_s^2(\Omega) \tag{2.5c}$$

$$\int_{S^3} \varrho_e^3 \equiv \int_{S^3} \varrho_e(\vec{r})\, \mathrm{d}V \qquad \forall\, S^3 \in \boldsymbol{S}_s^3(\Omega) \tag{2.5d}$$

[1] In this chapter, we treat the space of smooth k-forms $\mathcal{F}_s^k$ to simplify the presentation: For definitions of the exterior derivative, Gauss' law, the partial integration formula, and the hodge operator we then can easily refer to the literature, e.g. [53]. This restriction is again not the case in most engineering applications, i.e. for the field solutions in regions with jumping material coefficients. The concepts can be generalized to k-forms with less regularity as will be done in chapter 4.

The scalar and vector fields φ_e, $\vec{E}$, $\vec{B}$, and ϱ_e are called the *vector proxies* of the differential forms φ_e^0, e^1, b^2, and ϱ_e^3:

Definition 2.1. The scalar and vector fields $\vec{\omega}^k$ with $\vec{\omega}^k(\vec{r}) \in \mathbb{R}^{\binom{3}{k}}$ associated with a k-form $\omega^k \in \mathcal{F}_s^k(\Omega)$ by

$$\int_{S^0} \vec{\omega}^0(\vec{r}) = \int_{S^0} \omega^0 \qquad \forall\, S^0 \in \boldsymbol{S}_s^0(\Omega), \qquad \text{for } k = 0 \tag{2.6a}$$

$$\int_{S^1} \vec{\omega}^1(\vec{r}) \cdot \vec{t}_{S^1}\, \mathrm{d}s = \int_{S^1} \omega^1 \qquad \forall\, S^1 \in \boldsymbol{S}_s^1(\Omega), \qquad \text{for } k = 1 \tag{2.6b}$$

$$\int_{S^2} \vec{\omega}^2(\vec{r}) \cdot \vec{n}_{S^2}\, \mathrm{d}A = \int_{S^2} \omega^2 \qquad \forall\, S^2 \in \boldsymbol{S}_s^2(\Omega), \qquad \text{for } k = 2 \tag{2.6c}$$

$$\int_{S^3} \vec{\omega}^3(\vec{r})\, \mathrm{d}V = \int_{S^3} \omega^3 \qquad \forall\, S^3 \in \boldsymbol{S}_s^3(\Omega), \qquad \text{for } k = 3 \tag{2.6d}$$

are called their *vector proxies*. The space of vector proxies of smooth k-forms will be denoted by $\vec{\mathcal{F}}_s(\mathcal{F}_s^k(\Omega))$, or in short $\vec{\mathcal{F}}_s^k(\Omega)$. We will use the symbol $\multimap$ to associate a k-form ω^k and its vector proxy $\vec{\omega}^k$:

$$\omega^k \quad \multimap \quad \vec{\omega}^k \tag{2.7}$$

Thus we can write for the k-forms and their vector proxies in equations (2.5) on the facing page:

$$\varphi_e^0 \quad \multimap \quad \varphi_e \tag{2.8a}$$

$$e^1 \quad \multimap \quad \vec{E}(\vec{r}) \tag{2.8b}$$

$$b^2 \quad \multimap \quad \vec{B}(\vec{r}) \tag{2.8c}$$

$$\varrho_e^3 \quad \multimap \quad \varrho_e \tag{2.8d}$$

Remark 2.1. In a n-dimensional space Γ^n, the vector proxies $\vec{\omega}^k \in \vec{\mathcal{F}}_s^k(\Gamma^n)$ are tensor fields:

$$\vec{\omega}^k : \mathbb{R}^n \longmapsto \mathbb{R}^{\binom{n}{k}} \tag{2.9}$$

For $n = 3$, we have scalar functions as vector proxies for ω^0 and ω^3 and 3-component vector fields as vector proxies for ω^1 and ω^2:

$$\vec{\omega}^0,\, \vec{\omega}^3 : \mathbb{R}^3 \longmapsto \mathbb{R}$$
$$\vec{\omega}^1,\, \vec{\omega}^2 : \mathbb{R}^3 \longmapsto \mathbb{R}^3$$

The mathematical tools for k-forms will be introduced in the following chapters by first stating equivalents in the standard vector analysis notation using vector proxies.

2.1.3 Topological Tools and Properties

The Trace Operator

Assume the electric field strength 1-form e^1 be given in the 3-dimensional domain Ω, i.e. $e^1 \in \mathcal{F}_s^1(\Omega)$. If we are only interested in the integrals of the electric field strength over

paths in some 2-dimensional surface $\Gamma^2 \subset \Omega$, we would like to restrict e^1 to the space of 1-forms on Γ^2 denoted by $\mathcal{F}_s^k(\Gamma^2)$. For the electric field strength vector proxy $\vec{E}$, this restriction to a vector field on a surface is achieved by restricting the tangential vector component to the surface:

$$\left(\vec{n}_{\Gamma^2} \times \left(\vec{E} \times \vec{n}_{\Gamma^2}\right)\right)\Big|_{\Gamma^2} \tag{2.10}$$

where $\vec{n}_{\Gamma^2}$ denotes again the oriented unit vector normal on Γ^2.

For arbitrary k-forms, such a restriction is achieved by the trace operator[2]:

Definition 2.2. The trace of a k-form ω^k defined on the manifold Ω onto an l-dimensional submanifold $\Gamma^l \subset \Omega$ denoted by

$$\mathrm{t}^k_{\Gamma^l}: \quad \omega^k \in \mathcal{F}_s^k(\Omega) \quad \longmapsto \quad \mathrm{t}^k_{\Gamma^l}\,\omega^k \in \mathcal{F}_s^k(\Gamma^l)$$

is defined for $l \geq k$ by fixing the integral over all k-dimensional submanifolds S^k of Γ^l:

$$\int_{S^k} \mathrm{t}^k_{\Gamma^l}\,\omega^k \equiv \int_{S^k} \omega^k \qquad \forall\, S^k \in \boldsymbol{S}_s^k(\Gamma^l) \tag{2.11}$$

For $l < k$, the trace is defined to be zero.

The equivalent of the trace operator on Γ^2 for the vector proxies of forms of all degrees reads:

$$\mathrm{t}^0_{\Gamma^2}\,\varphi_e^0 \quad \multimap \quad \varphi_e|_{\Gamma^2} \tag{2.12a}$$

$$\mathrm{t}^1_{\Gamma^2}\,e^1 \quad \multimap \quad \left(\vec{n}_{\Gamma^2} \times \left(\vec{E} \times \vec{n}_{\Gamma^2}\right)\right)\Big|_{\Gamma^2} \tag{2.12b}$$

$$\mathrm{t}^2_{\Gamma^2}\,b^2 \quad \multimap \quad \left(\vec{n}_{\Gamma^2} \cdot \vec{B}\right)\Big|_{\Gamma^2} \tag{2.12c}$$

$$\mathrm{t}^3_{\Gamma^2}\,\varrho_e^3 \quad \multimap \quad 0|_{\Gamma^2} \tag{2.12d}$$

The Exterior Product

The exterior product of k-forms is a generalization of the scalar product or cross product of their vector proxies. Thus we can use the exterior product to calculate energies or the Poynting vector.

Notation 2.5. The exterior product of a k-form ω^k with an l-form η^l is denoted by:

$$\wedge: \qquad \left(\omega^k, \eta^l\right) \in \mathcal{F}_s^k(\Omega) \times \mathcal{F}_s^l(\Omega) \quad \longmapsto \quad \omega^k \wedge \eta^l \in \mathcal{F}_s^{k+l}(\Omega)$$

For a definition, we refer to [42, pp. 220] and [53, p. 135] and here will only state examples for the exterior product in vector proxy language using the standard scalar multiplication, the scalar product and the vector product:

$$\varphi_e^0 \wedge \varrho_e^3 \quad \multimap \quad \varphi_e \varrho_e \tag{2.13a}$$

$$e^1 \wedge d^2 \quad \multimap \quad \vec{E} \cdot \vec{D} \tag{2.13b}$$

$$e^1 \wedge h^1 \quad \multimap \quad \vec{E} \times \vec{H} \tag{2.13c}$$

[2] The trace defined here is commonly called the tangential component of the trace or pullback in contrast to its normal component. See [18, p. 306] and [42, pp. 250] for further details.

We note that the exterior product is commutative or anti-commutative depending on the degree of the forms:

$$\omega^k \wedge \eta^l = (-1)^{kl}\, \eta^l \wedge \omega^k, \qquad \omega^k \in \mathcal{F}_s^k(\Omega),\, \eta^l \in \mathcal{F}_s^l(\Omega) \tag{2.14}$$

The Exterior Derivative and Gauss' Law

The exterior derivative acting on a k-form is the generalization of the gradient, curl, and divergence operators acting on the vector proxies. The Gauss' law will turn out a generalization of what is usually called Gauss' law in vector proxy language:

$$\int_{\Gamma^3} \operatorname{div} \vec{D}\, \mathrm{d}V = \int_{\partial\Gamma^3} \vec{D} \cdot \vec{n}_{\partial\Gamma^3}\, \mathrm{d}A \tag{2.15}$$

Here, the general version of Gauss' law is actually used to define the exterior derivative and thus holds by definition:

Definition 2.3. The *exterior derivative* of a k-form ω^k denoted by

$$\mathrm{d}^k : \quad \omega^k \in \mathcal{F}_s^k(\Omega) \longmapsto \mathrm{d}^k\, \omega^k \in \mathcal{F}_s^{k+1}(\Omega)$$

is defined for $k \in [0..2]$ as the unique $(k+1)$-form $\mathrm{d}^k\, \omega^k$ fulfilling the following Gauss' law:

$$\int_{S^{k+1}} \mathrm{d}^k\, \omega^k \equiv \int_{\partial S^{k+1}} \omega^k, \qquad \forall\, S^{k+1} \in \boldsymbol{S}_s^{k+1}(\Omega) \tag{2.16}$$

Remark 2.2. The $(k+1)$-form $\mathrm{d}^k\, \omega^k$ is completely defined by fixing its integral answer on all possible $(k+1)$-dimensional submanifolds of Ω as mentioned above; compare e.g. [48, p. 243] or [53, p. 125].

As mentioned above, the actions of the exterior derivative in vector proxy language are the gradient, curl, divergence, and the zero operator:

$$\mathrm{d}^0\, \varphi_e^0 \quad \multimap \quad \operatorname{grad} \varphi_e \tag{2.17a}$$
$$\mathrm{d}^1\, e^1 \quad \multimap \quad \operatorname{curl} \vec{E} \tag{2.17b}$$
$$\mathrm{d}^2\, b^2 \quad \multimap \quad \operatorname{div} \vec{B} \tag{2.17c}$$
$$\mathrm{d}^3\, \varrho_e^3 \quad \multimap \quad 0\, \varrho_e \tag{2.17d}$$

The last equation is stated formally into a space containing only the zero element and will be useful in the Poincaré Lemma stated later on.

Some more examples for the Gauss' law in vector proxy notation are:

$$\int_{\Gamma^1} \operatorname{grad} \varphi_e \cdot \vec{t}_{\Gamma^1}\, \mathrm{d}s = \int_{\partial\Gamma^1} \varphi_e \tag{2.18a}$$
$$\int_{\Gamma^2} \operatorname{curl} \vec{E} \cdot \vec{n}_{\Gamma^2}\, \mathrm{d}A = \int_{\partial\Gamma^2} \vec{E} \cdot \vec{t}_{\partial\Gamma^2}\, \mathrm{d}s \tag{2.18b}$$

The Sequence Property

In vector analysis, we have the following properties of the gradient, curl, and divergence operators:

$$\operatorname{curl}\operatorname{grad} = 0 \tag{2.19a}$$

$$\operatorname{div}\operatorname{curl} = 0 \tag{2.19b}$$

These properties are the equivalent of the sequence property for the exterior derivative:

Theorem 2.1. *The exterior derivative fulfills the sequence property:*

$$\mathrm{d}^{k+1}\,\mathrm{d}^k = 0 \tag{2.20}$$

Proof. The proof is easily done by using the definition of the exterior derivative (2.16) and the fact that the boundary of a boundary is empty, i.e. $\partial\partial = 0$. Then the following holds for any k-form $\omega^k \in \mathcal{F}_s^k(\Omega)$ and any manifold $S^{k+2} \in \boldsymbol{S}_s^{k+2}(\Omega)$:

$$\int_{S^{k+2}} \mathrm{d}^{k+1}\,\mathrm{d}^k\,\omega^k = \int_{\partial S^{k+2}} \mathrm{d}^k\,\omega^k = \int_{\partial\partial S^{k+2}} \omega^k = 0 \tag{2.21}$$

□

The sequence property is often graphically represent by the following diagram:

$$\mathcal{F}_s^0(\Omega) \xrightarrow{\mathrm{d}^0\,(=\mathrm{grad})} \mathcal{F}_s^1(\Omega) \xrightarrow{\mathrm{d}^1\,(=\mathrm{curl})} \mathcal{F}_s^2(\Omega) \xrightarrow{\mathrm{d}^2\,(=\mathrm{div})} \mathcal{F}_s^3(\Omega) \tag{2.22}$$

where it is assumed that the incoming operators map into the kernel of the outgoing operators.

The Poincaré Lemma

In vector analysis, the following existence statements of potentials are known:

$$\forall\,\vec{E}: \quad \operatorname{curl}\vec{E} = 0 \quad \Rightarrow \quad \exists\,\varphi_e: \quad \vec{E} = \operatorname{grad}\varphi_e \tag{2.23a}$$

$$\forall\,\vec{B}: \quad \operatorname{div}\vec{B} = 0 \quad \Rightarrow \quad \exists\,\vec{A}_m: \quad \vec{B} = \operatorname{curl}\vec{A}_m \tag{2.23b}$$

$$\forall\,\varrho_e: \quad 0\,\varrho_e = 0 \quad \Rightarrow \quad \exists\,\vec{D}: \quad \varrho_e = \operatorname{div}\vec{D} \tag{2.23c}$$

For differential forms, all these statements are summed up in the Poincaré Lemma. It is the converse of the sequence property: Given $\mathrm{d}^k\,\omega^k = 0$, does there always exist a ω^{k-1} such that $\omega^k = \mathrm{d}^{k-1}\,\omega^{k-1}$? The Poincaré Lemma states that this is true for contractible domains [9, pp. 132][3]:

Lemma 2.2 (Poincaré Lemma)**.** *Given a contractible domain Ω and a smooth k-form $\omega^k \in \mathcal{F}_s^k(\Omega)$, the following holds for $k \in [1..3]$:*

$$\mathrm{d}^k\,\omega^k = 0 \quad \Rightarrow \quad \exists\,\omega^{k-1} \in \mathcal{F}_s^{k-1}(\Omega): \quad \mathrm{d}^{k-1}\,\omega^{k-1} = \omega^k \tag{2.24}$$

[3] The generalization of the Poincaré Lemma to non-contractible domains is the deRham Theorem, see e.g. [48, p. 246].

A Partial Integration Formula

From the definition of the exterior derivative d^k and the exterior product $\wedge$, the following partial integration formula can be derived:

Theorem 2.3 (Partial integration formula)**.** *Given smooth k- and l-forms $\omega^k \in \mathcal{F}_s^k(\Omega)$ and $\eta^l \in \mathcal{F}_s^l(\Omega)$, and a $(k+l+1)$-dimensional manifold S^{k+l+1} in $\boldsymbol{S}_s^{k+l+1}(\Omega)$, the following holds:*

$$\int_{S^{k+l+1}} \mathrm{d}^k\,\omega^k \wedge \eta^l + (-1)^k \int_{S^{k+l+1}} \omega^k \wedge \mathrm{d}^l\,\eta^l = \int_{\partial S^{k+l+1}} \omega^k \wedge \eta^l \tag{2.25}$$

For a proof, the reader is referred to [48, pp. 246]. The main interesting examples of the partial integration formula (2.25) in vector proxy notation are:

$$\int_{S^3} \left(\operatorname{curl}\vec{E}\right) \cdot \vec{H} - \vec{E} \cdot \left(\operatorname{curl}\vec{H}\right)\,\mathrm{d}V = \int_{\partial S^3} \left(\vec{E} \times \vec{H}\right) \cdot \vec{n}_{\partial S^3}\,\mathrm{d}A \tag{2.26a}$$

$$\int_{S^3} (\operatorname{grad}\varphi_e) \cdot \vec{D} + \varphi_e \cdot \left(\operatorname{div}\vec{D}\right)\,\mathrm{d}V = \int_{\partial S^3} \left(\varphi_e \cdot \vec{D}\right) \cdot \vec{n}_{\partial S^3}\,\mathrm{d}A \tag{2.26b}$$

2.1.4 Metric Tools

In the preceding chapter, we outlined the topological tools needed to state IBVPs like the one arising from Maxwell's equations in the language of differential geometry. Several topological properties which follow without using a metric, i.e. the notion of distance, were stated. To state the material relations in Maxwell's equations and to define energy norms, we are still missing the metric tools, though.

The Hodge Operator

In vector proxy language, the most simple material relations are stated by a scalar multiplication[4]:

$$\vec{D} = \varepsilon\vec{E} \tag{2.27a}$$

$$\vec{H} = \nu\vec{B} \tag{2.27b}$$

Although at first sight, the scalar multiplication does only weight the vector proxies with the material constants ε and ν, the resulting quantities are actually interpreted as vector proxies of forms of a different degree. E.g. the electric flux density $\vec{D} = \varepsilon\vec{E}$ is now the vector proxy of a 2-form which is integrated over surfaces and not lines any more. So the topological tools of integration, exterior derivative, and exterior product act completely different on the new quantity.

The general concept of material relations in differential geometry is the *hodge operator*:

[4] More complex material relations can also be stated using a hodge operator. In this thesis, we only treat scalar material relations explicitly, though, as stated in chapter 2.2.2.

Notation 2.6. The *hodge operator* for an n-dimensional manifold Ω with a Riemannian, i.e. positive definite, metric α will be denoted by

$$\star_\alpha^n : \quad \omega^k \in \mathcal{F}_s^k(\Omega) \longmapsto \star_\alpha^n \omega^k \in \mathcal{F}_s^{n-k}(\Omega) \tag{2.28}$$

For a complete definition of the hodge operator, refer e.g. to [53, pp. 220] or [18, p. 302]. We will write $\star_\alpha$ as an abbreviation for $\star_\alpha^3$ and use $\star^n$ and $\star$ to denote the hodge operator based on the Euclidean metric.

So the equivalent statements of equations (2.27) in the language of differential geometry read:

$$d^2 = \star_\varepsilon e^1 \quad \multimap \quad \vec{D} = \varepsilon \vec{E} \tag{2.29a}$$

$$h^1 = \star_\nu b^2 \quad \multimap \quad \vec{H} = \nu \vec{B} \tag{2.29b}$$

Here we clearly see the change of the degree of the form and thereby know over which kind of manifolds we can integrate the quantities. There is no need to keep track of transformation rules as in the case of the vector proxies, where the electric field strength transforms covariantly while the electric flux density transforms contravariantly.

The Inner Product and the Norm

For the vector proxies, inner products $\langle\!\langle .|. \rangle\!\rangle_\alpha$ are defined using the material relation and integration:

$$\langle\!\langle \vec{E} | \vec{E} \rangle\!\rangle_\varepsilon \equiv \int_\Omega \varepsilon \vec{E} \cdot \vec{E} \, \mathrm{d}V \tag{2.30}$$

$$\langle\!\langle \vec{B} | \vec{B} \rangle\!\rangle_\nu \equiv \int_\Omega \nu \vec{B} \cdot \vec{B} \, \mathrm{d}V \tag{2.31}$$

The electric and magnetic energies W_e and W_m, respectively, are defined as one-half of the resulting energy norms $\|.\|_\varepsilon$ and $\|.\|_\nu$:

$$W_e \equiv \frac{1}{2} \|\vec{E}\|_\varepsilon^2 \equiv \frac{1}{2} \langle\!\langle \vec{E} | \vec{E} \rangle\!\rangle_\varepsilon \tag{2.32}$$

$$W_m \equiv \frac{1}{2} \|\vec{B}\|_\nu^2 \equiv \frac{1}{2} \langle\!\langle \vec{B} | \vec{B} \rangle\!\rangle_\nu \tag{2.33}$$

We can deduce that a general definition of the inner product for differential forms can also be written in terms of the hodge operator and the integration:

Definition 2.4. The *inner product* of two k-forms ω^k and η^k based on the Riemannian metric α is denoted by

$$\langle\!\langle .|. \rangle\!\rangle_\alpha : \quad \left(\omega^k, \eta^k\right) \in \mathcal{F}_s^k(\Omega) \times \mathcal{F}_s^k(\Omega) \longmapsto \langle\!\langle \omega^k | \eta^k \rangle\!\rangle_\alpha \in \mathbb{R} \tag{2.34}$$

and defined as:

$$\langle\!\langle \omega^k | \eta^k \rangle\!\rangle_\alpha \equiv \int_\Omega \omega^k \wedge \star_\alpha \eta^k \tag{2.35}$$

By requiring a Riemannian metric, the inner product defined above is positive definite. Therefore, the inner product canonically renders the norm $\|.\|_\alpha$ on the space of k-forms $\mathcal{F}_s^k(\Omega)$:

$$\|\omega^k\|_\alpha^2 \equiv \left\langle\!\left\langle \omega^k \middle| \omega^k \right\rangle\!\right\rangle_\alpha \tag{2.36}$$

We use the symbol $\|.\|$ for the norm based on the Euclidean metric and hodge operator.

2.2 Maxwell's Equations

In chapter 2.1, we have established the tools needed to state the IBVPs of Maxwell's equations in the language of differential geometry. The aim of introducing the language of differential geometry was twofold: Firstly, to separate the topological and the metric tools. Secondly, we are able to generalize many concepts, properties, and equations which seemed to be unrelated in the formalism of standard vector analysis. Both aims guide the discretization process in chapter 3.

For ease of readability, we use standard vector analysis notation in this chapter, though. From the presentation in chapter 2.1, we adopt the separation of Maxwell's equations into the topological laws in chapter 2.2.1, which only require topological operations like the gradient and integration, and into the material laws in chapter 2.2.2, which make use of a metric. Equivalently, we state so-called topological properties in chapter 2.2.3 which solely arise from Maxwell's topological laws and state so-called metric properties in chapter 2.2.4 which also make use of Maxwell's material laws.

In chapter 2.2.5, we complement Maxwell's equations with suitable boundary conditions to arrive at Maxwell's IBVP. We state existence and prove uniqueness of the solution to Maxwell's IBVP. In chapter 2.2.6, we capture the structural properties of Maxwell's equations in a graphical representation.

The spatial discretization of Maxwell's equations in chapter 3.2 will follow the same structure as used here for the continuous setting: The contents of chapters 3.2.1 to 3.2.6 are the discrete analogue of chapters 2.2.1 to 2.2.6.

2.2.1 Maxwell's Topological Laws

Maxwell's first and second law make use of topological concepts of the underlying domain Ω only. Thus we call them Maxwell's first and second topological law. In differential form[5] they read:

$$\boxed{\operatorname{curl} \vec{E}(\vec{r},t) = -\partial_t \vec{B}(\vec{r},t)} \qquad \forall\, \vec{r} \in \Omega,\ t \in \mathrm{T} \tag{2.37a}$$

$$\boxed{\operatorname{curl} \vec{H}(\vec{r},t) = \partial_t \vec{D}(\vec{r},t) + \vec{J}(\vec{r},t)} \qquad \forall\, \vec{r} \in \Omega,\ t \in \mathrm{T} \tag{2.37b}$$

[5] *Differential form* here means in the form using differential operators as opposed to the integral form in equations (2.38) on the following page. The use of the term *differential form* is not to be confused with the differential forms $\mathcal{F}_s^k(\Omega)$ introduced in chapter 2.1.

where $\vec{E}$ denotes the electric field strength, $\vec{B}$ the magnetic flux density, $\vec{H}$ the magnetic field strength, $\vec{D}$ the electric flux density, and $\vec{J}$ the electric current density. The temporal derivative is denoted by ∂_t.

We can also state Maxwell's first and second topological law in integral form:

$$\int_{\partial S^2} \vec{E}(\vec{r},t) \cdot \vec{t}_{\partial S^2} \,\mathrm{d}s = -\int_{S^2} \partial_t \vec{B}(\vec{r},t) \cdot \vec{n}_{S^2} \,\mathrm{d}A, \qquad \forall\, S^2 \in \boldsymbol{S}_s^2(\Omega),\ t \in \mathrm{T} \tag{2.38a}$$

$$\int_{\partial S^2} \vec{H}(\vec{r},t) \cdot \vec{t}_{\partial S^2} \,\mathrm{d}s = \int_{S^2} \Big(\partial_t \vec{D}(\vec{r},t) + \vec{J}(\vec{r},t)\Big) \cdot \vec{n}_{S^2} \,\mathrm{d}A, \qquad \forall\, S^2 \in \boldsymbol{S}_s^2(\Omega),\ t \in \mathrm{T} \tag{2.38b}$$

Note that the Maxwell's first topological law only connects the electric field strength $\vec{E}$ with the magnetic flux density $\vec{B}$ while Maxwell's second topological law only connects the magnetic field strength $\vec{H}$ with the electric flux density $\vec{D}$ and the electric source current $\vec{J}$. We identify them as topologically separate sets of quantities $(\vec{E}, \vec{B})$ and $(\vec{H}, \vec{D}, \vec{J})$. The connection between these quantities is established by the material laws in the next chapter.

2.2.2 Maxwell's Material Laws

The metric structure of the domain Ω comes into play in the material laws, also called material relations, metric laws, or constitutive laws. We will assume local, linear, isotropic, dispersion-free, and lossless material relations and non-moving media[6]. Maxwell's material laws connect the quantities of Maxwell's first and second topological equation:

$$\boxed{\vec{D}(\vec{r},t) = \varepsilon(\vec{r})\vec{E}(\vec{r},t)} \qquad \forall\, \vec{r} \in \Omega,\ t \in \mathrm{T} \tag{2.39a}$$

$$\boxed{\vec{H}(\vec{r},t) = \nu(\vec{r})\vec{B}(\vec{r},t)} \qquad \forall\, \vec{r} \in \Omega,\ t \in \mathrm{T} \tag{2.39b}$$

Equation (2.39a) is called Maxwell's electric material law and equation (2.39b) Maxwell's magnetic material law. We assume non-conducting materials to simplify the notation and thus do not include Ohm's conductive law[7]. The permittivity ε and the reluctivity ν are assumed to be local, linear, and constant in time. They are also assumed to be positive, i.e.:

$$\varepsilon(\vec{r}) > 0 \qquad \forall\, \vec{r} \in \Omega \tag{2.40a}$$

$$\nu(\vec{r}) > 0 \qquad \forall\, \vec{r} \in \Omega \tag{2.40b}$$

[6] Non-local, non-linear, non-isotropic [52, pp. 13], dispersive, or lossy [52, pp. 262] material relations as well as moving materials [52, pp. 256] can also be introduced, but they complicate the mathematical presentation.

[7] Ohm's law can easily be added, though. The term $\vec{J}$ in Maxwell's second topological equation (2.37b) then has to be defined as the sum of the source current density and the conduction current density.

2.2.3 Maxwell's Topological Properties

In this chapter, we present properties of Maxwell's equations, which only depend on Maxwell's topological laws and the topology of the domain Ω.

To shorten notation, we will often omit the explicit dependence of the scalar and vector field quantities on the spatial variable $\vec{r}$ and the temporal variable t.

Conservation of Charge

We first derive two conserved quantities purely from the topological Maxwell's equations and then recognize the terms as the standard expressions of electric and magnetic charge density.

Taking the divergence of equations (2.37), we get:

$$\operatorname{div}\operatorname{curl}\vec{E} = 0 = -\partial_t \operatorname{div}\vec{B} \tag{2.41a}$$

$$\operatorname{div}\operatorname{curl}\vec{H} = 0 = \partial_t \operatorname{div}\vec{D} + \operatorname{div}\vec{J} \tag{2.41b}$$

Defining the magnetic charge density ϱ_m and the electric charge density ϱ_e as[8]

$$\varrho_m \equiv \operatorname{div}\vec{B} \tag{2.42a}$$

$$\varrho_e \equiv \operatorname{div}\vec{D} \tag{2.42b}$$

we recognize equations (2.41a) and (2.41b) as the conservation of the electric and magnetic charge:

$$\boxed{\partial_t \varrho_m(\vec{r},t) = 0} \qquad \forall\, \vec{r} \in \Omega,\ t \in \mathrm{T} \tag{2.43a}$$

$$\boxed{\partial_t \varrho_e(\vec{r},t) + \operatorname{div}\vec{J}(\vec{r},t) = 0} \qquad \forall\, \vec{r} \in \Omega,\ t \in \mathrm{T} \tag{2.43b}$$

To stress the point: The conservation of charge only depends on the topological Maxwell's equations; the metric equations are not necessary for its derivation. Therefore, it is a purely topological property.

If the magnetic charge ϱ_m is assumed to be zero at a point t_1 in time, as physically motivated, we immediately deduce from equation (2.43a) that the magnetic charge is zero for all times $t \in \mathrm{T}$.

A Potential Formulation

Maxwell's equations are often formulated not in the field quantities used above, but in some potentials. Usually, this is done to simplify or unify the solution process for Maxwell's equations.

[8] We here take a mathematical point of view and define the magnetic and electric charge densities as conserved quantities resulting from Maxwell's first and second equation. From a physical perspective, one observes (no) magnetic and electric charges which have further properties and defines Maxwell's equations incorporating some of these observations.

Let us assume, as physically motivated, that the magnetic charge ϱ_m is zero at all times $t \in \mathrm{T}$. Then from equations (2.41a) and (2.42a) we know that the divergence of the magnetic flux density is zero at all times:

$$\operatorname{div} \vec{B} = 0 \tag{2.44}$$

The Poincaré Lemma in its form in equation (2.23b) on page 12 assures the existence of a vector field $\vec{A}_m$ such that:

$$\vec{B} = \operatorname{curl} \vec{A}_m \tag{2.45}$$

Plugging this into Maxwell's first topological law (2.37a) on page 15, we arrive at:

$$\begin{aligned} & \operatorname{curl} \vec{E} = -\partial_t \vec{B} = -\partial_t \operatorname{curl} \vec{A}_m \\ \Leftrightarrow \qquad & \operatorname{curl} \left(\vec{E} + \partial_t \vec{A}_m \right) = 0 \end{aligned} \tag{2.46}$$

Now the Poincaré Lemma in its form in equation (2.23a) on page 12 assures the existence of a scalar field φ_e such that:

$$\begin{aligned} & \vec{E} + \partial_t \vec{A}_m = -\operatorname{grad} \varphi_e \\ \Leftrightarrow \qquad & \vec{E} = -\partial_t \vec{A}_m - \operatorname{grad} \varphi_e \end{aligned} \tag{2.47}$$

Equivalently, one can write the other quantities and Maxwell's equations in terms of these potentials. The potentials are not unique, though. Uniqueness can be achieved by gauging the potentials. Well-known in this case are the Coulomb and the Lorentz gauge [42, p. 55] leading to different systems of equations to be solved.

Poynting's Theorem

We will derive another purely topological property: Poynting's Theorem. Let the otherwise arbitrary fields $(\vec{E}, \vec{B})$ and $(\vec{H}, \vec{D}, \vec{J})$ fulfill Maxwell's topological equations (2.37) on page 15. Multiplying equation (2.37b) by $\vec{E}$, integrating over the 3-dimensional volume S^3 and using equation (2.37a) after applying the integration by parts formula (2.26a) on page 13, we get:

$$\begin{aligned} \int_{S^3} \left(\partial_t \vec{D} \cdot \vec{E} + \vec{J} \cdot \vec{E} \right) \mathrm{d}V &= \int_{S^3} \left(\operatorname{curl} \vec{H} \right) \cdot \vec{E} \, \mathrm{d}V \\ &= \int_{S^3} \vec{H} \cdot \left(\operatorname{curl} \vec{E} \right) \mathrm{d}V - \int_{\partial S^3} \left(\vec{E} \times \vec{H} \right) \cdot \vec{n}_{\partial S^3} \, \mathrm{d}A \\ &= - \int_{S^3} \vec{H} \cdot \partial_t \vec{B} \, \mathrm{d}V - \int_{\partial S^3} \left(\vec{E} \times \vec{H} \right) \cdot \vec{n}_{\partial S^3} \, \mathrm{d}A \end{aligned}$$

Rearranging terms, we arrive at Poynting's Theorem:

$$\begin{aligned} \int_{S^3} \partial_t \vec{D} \cdot \vec{E} \, \mathrm{d}V + \int_{S^3} \vec{H} \cdot \partial_t \vec{B} \, \mathrm{d}V \\ + \int_{S^3} \vec{J} \cdot \vec{E} \, \mathrm{d}V + \int_{\partial S^3} \left(\vec{E} \times \vec{H} \right) \cdot \vec{n}_{\partial S^3} \, \mathrm{d}A = 0 \end{aligned} \tag{2.48}$$

Poynting's Theorem (2.48) is also a purely topological law. It is thus valid even for fields $(\vec{E}, \vec{B})$ and $(\vec{H}, \vec{D}, \vec{J})$ which are not related by Maxwell's material laws (2.39) on page 16. As such, the energy and loss terms do not have the standard physical meaning, which only evolves when taking fields related by the material laws. This will be done in the next chapter.

2.2.4 Maxwell's Metric Properties

In this chapter, we will present properties of Maxwell's equations, which depend on the topological and on the metric properties of the domain Ω. We use Maxwell's topological and material laws to derive these properties.

Conservation of Energy

Assume the set of fields $\vec{E}$, $\vec{B}$, $\vec{H}$, $\vec{D}$, and $\vec{J}$ fulfills Maxwell's topological laws (2.37) on page 15 as well as Maxwell's material laws (2.39) on page 16. Then we can rewrite Poynting's Theorem (2.48) as:

$$\partial_t \left\{ \underbrace{\frac{1}{2}\int_{S^3} \vec{D}\cdot\vec{E}\,\mathrm{d}V}_{\equiv W_e} + \underbrace{\frac{1}{2}\int_{S^3} \vec{B}\cdot\vec{H}\,\mathrm{d}V}_{\equiv W_m} \right\} + \underbrace{\int_{S^3} \vec{J}\cdot\vec{E}\,\mathrm{d}V}_{\equiv P_e} + \underbrace{\int_{\partial S^3} \left(\vec{E}\times\vec{H}\right)\cdot\vec{n}_{\partial S^3}\,\mathrm{d}A}_{\equiv P_P} = 0 \tag{2.49}$$

The terms W_e, W_m, P_e, and P_P are commonly called the electric energy, magnetic energy, electric losses, and the radiation losses of the volume S^3, respectively.

The energy and loss terms have the physical meaning of energies and losses of an electromagnetic field. Poynting's Theorem in its form (2.49) tells us that the energy in the system is conserved: The rate of change of the total electromagnetic energy $W \equiv W_e + W_m$ is equal to the negative of the losses by heat P_e and by radiation P_P.

According to our requirements (2.40) on page 16, the material constants $\varepsilon(\vec{r})$ and $\nu(\vec{r})$ are positive. So the electric and magnetic energies W_e and W_m defined above are positive definite and do define norms on the electric and magnetic fields:

$$W_e \equiv \frac{1}{2}\int_\Omega \varepsilon\vec{E}\cdot\vec{E}\,\mathrm{d}V = \|\vec{E}\|_\varepsilon^2 = \|\vec{D}\|_{\varepsilon^{-1}}^2 \tag{2.50a}$$

$$W_m \equiv \frac{1}{2}\int_\Omega \nu\vec{B}\cdot\vec{B}\,\mathrm{d}V = \|\vec{B}\|_\nu^2 = \|\vec{H}\|_{\nu^{-1}}^2 \tag{2.50b}$$

2.2.5 Maxwell's Initial Boundary Value Problem

In order to pose a mathematical problem with a unique solution, Maxwell's equations need to be complemented by suitable initial and boundary conditions. In general, a set of partial differential equations plus initial and boundary conditions is called an IBVP.

In this chapter, we state suitable boundary conditions for Maxwell's equations leading to Maxwell's IBVP. We consider existence and uniqueness of the solution to this IBVP and boundedness of the solution operator. In the discrete setting in chapter 3, we will go through the same steps. As the proofs for the discrete setting are less involved, we will be able to give them explicitly, whereas here in the continuous setting, we mostly refer to the literature.

An Initial Boundary Value Problem for Maxwell's Equations

We will allow for two different spatial *boundary conditions*: The *electric boundary condition* prescribes the tangential electric field strength, while the *magnetic boundary condition* prescribes the tangential magnetic field strength. To include both boundary conditions in the same problem, we will split the boundary $\partial\Omega$ of the domain Ω into two closed parts Γ_1 and Γ_2 as shown in Fig. 2.2. These parts are assumed to cover the complete boundary $\partial\Omega$, i.e.

$$\Gamma_1 \cup \Gamma_2 = \partial\Omega \tag{2.51}$$

and their interiors to be disjoint, i.e.

$$\mathring{\Gamma}_1 \cap \mathring{\Gamma}_2 = \varnothing \tag{2.52}$$

Imposing electric boundary conditions on Γ_1 means that we prescribe the tangential vector component of the electric field strength $\vec{E}$ on Γ_1 to some given value $\vec{E}_{\Gamma_1}(\vec{r}, t)$:

$$\vec{n}_{\Gamma_1}(\vec{r}) \times \left(\vec{E}(\vec{r}, t) \times \vec{n}_{\Gamma_1}(\vec{r})\right) = \vec{E}_{\Gamma_1}(\vec{r}, t) \qquad \forall\, \vec{r} \in \Gamma_1,\ t \in \mathrm{T} \tag{2.53a}$$

where $\vec{n}_{\Gamma_1}$ denotes the outward pointing unit normal vector on the surface Γ_1. In the homogeneous case, i.e. for $\vec{E}_{\Gamma_1} = 0$, we call this a *perfect electrically conducting (PEC) boundary condition.*

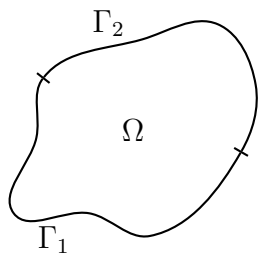

Fig. 2.2: Splitting of the boundary $\partial\Omega$ into two disjunct parts Γ_1 and Γ_2.

On Γ_2, we prescribe magnetic boundary conditions: The tangential vector component of the magnetic field strength $\vec{H}$ on Γ^2 is set to some given value $\vec{H}_{\Gamma_2}(\vec{r}, t)$:

$$\vec{n}_{\Gamma_2}(\vec{r}) \times \left(\vec{H}(\vec{r}, t) \times \vec{n}_{\Gamma_2}(\vec{r})\right) = \vec{H}_{\Gamma_2}(\vec{r}, t) \qquad \forall\, \vec{r} \in \Gamma_2,\ t \in \mathrm{T} \tag{2.53b}$$

In the homogeneous case, i.e. for $\vec{H}_{\Gamma_2} = 0$, we call this a *perfect magnetically conducting (PMC) boundary condition.*

As *initial condition* at $t = t_0$, we impose the electric field strength and the magnetic flux density to be known:

$$\vec{E}(\vec{r}, t_0) = \vec{E}_0(\vec{r}) \qquad \forall\, \vec{r} \in \Omega \tag{2.54a}$$

$$\vec{B}(\vec{r}, t_0) = \vec{B}_0(\vec{r}) \qquad \forall\, \vec{r} \in \Omega \tag{2.54b}$$

Remark 2.3. The boundary fields $\vec{E}_{\Gamma_1}$ and $\vec{H}_{\Gamma_2}$ actually are not arbitrary 3-dimensional vector fields on Γ_1 and Γ_2 but have to exhibit a zero normal component, i.e.:

$$\vec{E}_{\Gamma_1} \cdot \vec{n}_{\Gamma_1} = 0 \tag{2.55a}$$

$$\vec{H}_{\Gamma_2} \cdot \vec{n}_{\Gamma_2} = 0 \tag{2.55b}$$

In the notation of differential geometry introduced in chapter 2.1, the electric boundary condition reads: Given the 1-form $e^1_{\Gamma_1} \in \mathcal{F}^1_s(\Gamma_1)$, the electric boundary condition on Γ^1 imposes the following condition on the 1-form $e^1 \in \mathcal{F}^1_s(\Omega)$:

$$\mathrm{t}^1_{\Gamma_1}\, e^1 = e^1_{\Gamma_1} \tag{2.56a}$$

Thus we see that the traces of the forms live only on the boundary manifolds or rather their tangent spaces, i.e. $e^1_{\Gamma_1} \in \mathcal{F}^1_s(\Gamma_1)$. For the magnetic boundary condition imposed on the 1-form $h^1 \in \mathcal{F}^1_s(\Omega)$ to a given $h^1_{\Gamma_2} \in \mathcal{F}^1_s(\Gamma_2)$, one writes equivalently:

$$\mathrm{t}^1_{\Gamma_2}\, h^1 = h^1_{\Gamma_2} \tag{2.56b}$$

We can now finally state the IBVP to be solved: Assume the spatial domain Ω with boundary parts Γ_1 and Γ_2 and the temporal domain $\mathrm{T} = [\mathrm{t}_0, \infty)$ with boundary $t_0 = \partial\mathrm{T}$ to be given as defined above. Let the boundary data $\vec{E}_{\Gamma_1}(\vec{r}, t)$ be given for $\vec{r} \in \Gamma_1$, $t \in \mathrm{T}$ and the $\vec{H}_{\Gamma_2}(\vec{r}, t)$ for $\vec{r} \in \Gamma_2$, $t \in \mathrm{T}$, the initial data $\vec{E}_0(\vec{r})$ and $\vec{B}_0(\vec{r})$ for $\vec{r} \in \Omega$ as well as the source current $\vec{J}(\vec{r}, t)$ for $\vec{r} \in \Omega$, $t \in \mathrm{T}$. Then the system of Maxwell's topological laws (2.37) on page 15 and Maxwell's material laws (2.39) on page 16 together with the electric and magnetic boundary conditions (2.53) and the initial values (2.54) renders an IBVP in the unknowns $\vec{E}(\vec{r}, t)$, $\vec{B}(\vec{r}, t)$, $\vec{H}(\vec{r}, t)$, and $\vec{D}(\vec{r}, t)$:

$$\operatorname{curl} \vec{E}(\vec{r}, t) = -\partial_t \vec{B}(\vec{r}, t) \qquad \forall\, \vec{r} \in \Omega,\ t \in \mathrm{T} \tag{2.57a}$$

$$\operatorname{curl} \vec{H}(\vec{r}, t) = \partial_t \vec{D}(\vec{r}, t) + \vec{J}(\vec{r}, t) \qquad \forall\, \vec{r} \in \Omega,\ t \in \mathrm{T} \tag{2.57b}$$

$$\vec{D}(\vec{r}, t) = \varepsilon(\vec{r}) \vec{E}(\vec{r}, t) \qquad \forall\, \vec{r} \in \Omega,\ t \in \mathrm{T} \tag{2.57c}$$

$$\vec{H}(\vec{r}, t) = \nu(\vec{r}) \vec{B}(\vec{r}, t) \qquad \forall\, \vec{r} \in \Omega,\ t \in \mathrm{T} \tag{2.57d}$$

$$\vec{n}_{\Gamma_1}(\vec{r}) \times \Big(\vec{E}(\vec{r}, t) \times \vec{n}_{\Gamma_1}(\vec{r}) \Big) = \vec{E}_{\Gamma_1}(\vec{r}, t) \qquad \forall\, \vec{r} \in \Gamma_1,\ t \in \mathrm{T} \tag{2.57e}$$

$$\vec{n}_{\Gamma_2}(\vec{r}) \times \Big(\vec{H}(\vec{r}, t) \times \vec{n}_{\Gamma_2}(\vec{r}) \Big) = \vec{H}_{\Gamma_2}(\vec{r}, t) \qquad \forall\, \vec{r} \in \Gamma_2,\ t \in \mathrm{T} \tag{2.57f}$$

$$\vec{E}(\vec{r}, t_0) = \vec{E}_0(\vec{r}) \qquad \forall\, \vec{r} \in \Omega \tag{2.57g}$$

$$\vec{B}(\vec{r}, t_0) = \vec{B}_0(\vec{r}) \qquad \forall\, \vec{r} \in \Omega \tag{2.57h}$$

Equations (2.57) define *Maxwell's IBVP*.

Existence and Uniqueness of the Solution to Maxwell's Initial Boundary Value Problem

Theorem 2.4. *Maxwell's IBVP (2.57) with given smooth initial data*

$$\vec{E}_0(\vec{r}) \qquad \forall\, \vec{r} \in \Omega \tag{2.58a}$$

$$\vec{B}_0(\vec{r}) \qquad \forall\, \vec{r} \in \Omega \tag{2.58b}$$

smooth boundary data

$$\vec{E}_{\Gamma_1}(\vec{r}, t) \qquad \forall\, \vec{r} \in \Gamma_1,\ t \in \mathrm{T} \tag{2.59a}$$

$$\vec{H}_{\Gamma_2}(\vec{r}, t) \qquad \forall\, \vec{r} \in \Gamma_2,\ t \in \mathrm{T} \tag{2.59b}$$

fulfilling the compatibility conditions

$$\vec{n}_{\Gamma_1}(\vec{r}) \times \left(\vec{E}_0(\vec{r}) \times \vec{n}_{\Gamma_1}(\vec{r})\right) = \vec{E}_{\Gamma_1}(\vec{r}, t_0) \qquad \forall\, \vec{r} \in \Gamma_1 \tag{2.60a}$$

$$\vec{n}_{\Gamma_2}(\vec{r}) \times \left(\nu(\vec{r})\vec{B}_0(\vec{r}) \times \vec{n}_{\Gamma_2}(\vec{r})\right) = \vec{H}_{\Gamma_2}(\vec{r}, t_0) \qquad \forall\, \vec{r} \in \Gamma_2 \tag{2.60b}$$

and smooth source data

$$\vec{J}(\vec{r}, t) \qquad \forall\, \vec{r} \in \Omega,\ t \in \mathrm{T} \tag{2.61}$$

has a unique solution.

Proof. For a proof of existence and details on the assumed spaces of the boundary data and solution, the reader is referred to [18, pp. 255] [33, pp. 400] [59, pp. 146]. The proofs given there already extend to less smooth domains and material coefficients and render solutions in Sobolev-type spaces.

We will only proof uniqueness along the lines of [81, pp. 65], as this can be nicely translated into the discrete setting later on and shows an application of the topological and metric properties. The proof is by contradiction:

Assume there to be two different solutions $(\vec{E}_a, \vec{B}_a) \neq (\vec{E}_b, \vec{B}_b)$ to Maxwell's IBVP (2.57). The difference of the solution

$$(\vec{E}_\delta, \vec{B}_\delta) \equiv (\vec{E}_a, \vec{B}_a) - (\vec{E}_b, \vec{B}_b) \neq 0 \tag{2.62}$$

then also solves equations (2.57a) to (2.57d) with zero source current

$$\vec{J}_\delta = 0 \tag{2.63}$$

and the following zero boundary and initial conditions:

$$\vec{n}_{\Gamma_1}(\vec{r}) \times \vec{E}_\delta(\vec{r}, t) = 0 \qquad \forall\, \vec{r} \in \Gamma_1,\ t \in \mathrm{T} \tag{2.64a}$$

$$\vec{n}_{\Gamma_2}(\vec{r}) \times \vec{H}_\delta(\vec{r}, t) = 0 \qquad \forall\, \vec{r} \in \Gamma_2,\ t \in \mathrm{T} \tag{2.64b}$$

$$\vec{E}_\delta(\vec{r}, t_0) = 0 \qquad \forall\, \vec{r} \in \Omega \tag{2.64c}$$

$$\vec{B}_\delta(\vec{r}, t_0) = 0 \qquad \forall\, \vec{r} \in \Omega \tag{2.64d}$$

The conservation of energy (2.49) on page 19 also holds for the difference fields and renders:

$$\partial_t \left\{ \underbrace{\frac{1}{2}\int_\Omega \vec{D}_\delta \cdot \vec{E}_\delta \,\mathrm{d}V}_{W_{\delta,e}} + \underbrace{\frac{1}{2}\int_\Omega \vec{B}_\delta \cdot \vec{H}_\delta \,\mathrm{d}V}_{W_{\delta,m}} \right\}$$
$$= -\underbrace{\int_\Omega \vec{J}_\delta \cdot \vec{E}_\delta \,\mathrm{d}V}_{P_{\delta,e}} - \underbrace{\int_{\partial\Omega} \left(\vec{E}_\delta \times \vec{H}_\delta\right) \cdot \vec{n}_{\partial S^3} \,\mathrm{d}A}_{P_{\delta,P}} \tag{2.65}$$

Due to the zero source current from equation (2.63), the electric losses $P_{\delta,e}$ are zero. Due to the homogeneous boundary conditions in equations (2.64a) and (2.64b), the radiation losses $P_{\delta,P}$ are zero. Thus we know that the time derivative of the electric and magnetic field norms is zero:

$$\partial_t \left(\frac{1}{2}\|\vec{E}_\delta\|_\varepsilon^2 + \frac{1}{2}\|\vec{B}_\delta\|_\nu^2 \right) = 0 \tag{2.66}$$

$$\Leftrightarrow \qquad \partial_t \|\vec{E}_\delta\|_\varepsilon^2 = 0 \qquad \text{and} \qquad \partial_t \|\vec{B}_\delta\|_\nu^2 = 0 \tag{2.67}$$

So the electric and magnetic energy norms are constant in time. From equations (2.64c) and (2.64d), we know that the fields and therefore the energy norms are zero at the time t_0. Thus they are zero at all times:

$$\vec{E}_\delta = 0 \qquad \text{and} \qquad \vec{B}_\delta = 0 \qquad\qquad \forall\, \vec{r} \in \Omega,\ t \in \mathrm{T} \tag{2.68}$$

This contradicts equation (2.62) and therefore the solution must be unique. □

Boundedness of the Solution Operator to Maxwell's Initial Boundary Value Problem

We will derive the boundedness of the solution operator to Maxwell's IBVP (2.57). In the discrete setting we will show stability of the numerical scheme, which is basically uniform boundedness of a sequence of discrete solution operators.

To arrive at a suitable solution operator, let us rewrite Maxwell's IBVP (2.57) in the electric field strength $\vec{E}$ and the magnetic flux density $\vec{B}$ as unknowns. Define the combined unknown vector $\mathbf{x}$ as

$$\mathbf{x} = \begin{pmatrix} \vec{E}(\vec{r},t) \\ \vec{B}(\vec{r},t) \end{pmatrix} \tag{2.69}$$

the matrices $\mathbf{A}$ and $\mathbf{B}$ as

$$\mathbf{A} = \begin{pmatrix} \varepsilon(\vec{r}) & 0 \\ 0 & \nu(\vec{r}) \end{pmatrix}, \qquad \mathbf{B} = \begin{pmatrix} 0 & -\operatorname{curl}\nu(\vec{r}) \\ \nu(\vec{r})\operatorname{curl} & 0 \end{pmatrix} \tag{2.70}$$

the linear operator L by

$$\mathrm{L}\left(\mathbf{x}(\vec{r},t)\right) = \begin{pmatrix} \partial_t \mathbf{A}\mathbf{x}(\vec{r},t) + \mathbf{B}\mathbf{x}(\vec{r},t) \\ \vec{n}_{\Gamma_1}(\vec{r}) \times \left(\vec{E}(\vec{r},t) \times \vec{n}_{\Gamma_1}(\vec{r})\right) \\ \vec{n}_{\Gamma_2}(\vec{r}) \times \left(\vec{H}(\vec{r},t) \times \vec{n}_{\Gamma_2}(\vec{r})\right) \\ \mathbf{x}(\vec{r},t_0) \end{pmatrix} \tag{2.71}$$

and b by

$$b = \begin{pmatrix} \begin{pmatrix} -\vec{J}(\vec{r},t) \\ 0 \end{pmatrix} \\ \vec{E}_{\Gamma_1}(\vec{r},t) \\ \vec{H}_{\Gamma_2}(\vec{r},t) \\ \begin{pmatrix} \vec{E}_0(\vec{r}) \\ \vec{B}_0(\vec{r}) \end{pmatrix} \end{pmatrix} \tag{2.72}$$

Then we can rewrite Maxwell's IBVP (2.57) simply as

$$\mathrm{L}\mathbf{x} = b \tag{2.73}$$

where b is given and $\mathbf{x}$ is unknown. So actually, we are more interested in the inverse L^{-1} of the linear operator L, which we will call the *solution operator*. According to Theorem 2.4, we know a unique solution $\mathbf{x}$ to exist for the problem (2.73) and thus the inverse to be well defined. For a given b, the solution operator returns the solution $\mathbf{x}$ of the IBVP:

$$\mathbf{x} = \mathrm{L}^{-1}b \tag{2.74}$$

We are interested in the boundedness of the solution operator L^{-1} as defined in Definition E.1 on page 211. In order to simplify the analysis, we will restrict its domain, though: We assume homogeneous boundary conditions, i.e. $\vec{E}_{\Gamma_1}(\vec{r},t) = 0$ and $\vec{H}_{\Gamma_2}(\vec{r},t) = 0$, and zero source current, i.e. $\vec{J} = 0$. As norm on the range F of the solution operator, we will use the maximum energy of the electromagnetic field:

$$\|\mathbf{x}\|_F^2 \equiv \max_{t\in\mathrm{T}} \left(\|\vec{E}(\vec{r},t)\|_\varepsilon^2 + \|\vec{B}(\vec{r},t)\|_\nu^2 \right) \tag{2.75}$$

As norm on the domain U of the solution operator L^{-1}, we will use the electromagnetic energy of the initial fields:

$$\|b\|_U^2 \equiv \|\vec{E}_0(\vec{r})\|_\varepsilon^2 + \|\vec{B}_0(\vec{r})\|_\nu^2 \tag{2.76}$$

Theorem 2.5. *The solution operator* L^{-1} *to Maxwell's IBVP in reduced form in equation (2.73) is bounded under the assumption of homogeneous boundary conditions,* $\vec{E}_{\Gamma_1} = 0$ *and* $\vec{H}_{\Gamma_2} = 0$*, and zero source current,* $\vec{J} = 0$*, in the norms defined by equations (2.75) and (2.76).*

Proof. Using the conservation of energy (2.49) on page 19 we get immediately for any b in the domain of the solution operator, i.e. homogeneous boundary conditions and zero source currents, that the energy in the domain is constant:

$$\begin{aligned} & \partial_t \left(\frac{1}{2}\|\vec{E}(\vec{r},t)\|_\varepsilon^2 + \frac{1}{2}\|\vec{B}(\vec{r},t)\|_\nu^2 \right) = 0 \\ \Leftrightarrow \quad & \left(\|\vec{E}(\vec{r},t)\|_\varepsilon^2 + \|\vec{B}(\vec{r},t)\|_\nu^2 \right) = \|\vec{E}(\vec{r},t_0)\|_\varepsilon^2 + \|\vec{B}(\vec{r},t_0)\|_\nu^2 = \|b\|_U^2 \end{aligned}$$

Thus we know the maximum energy in time to be:

$$\|\mathbf{x}\|_F^2 = \|\mathrm{L}^{-1}b\|_F^2 = \max_{t\in\mathrm{T}} \left(\|\vec{E}(\vec{r},t)\|_\varepsilon^2 + \|\vec{B}(\vec{r},t)\|_\nu^2 \right) = \|b\|_U^2 \tag{2.77}$$

and get boundedness of the solution operator L^{-1} with the constant C in Definition E.1 on page 211 equal to unity. □

2.2.6 Maxwell's House

The diagram in Fig. 2.3 summarizes Maxwell's equations graphically and emphasizes the separation into topological and metric laws. This kind of diagram is called Tonti diagram after [86], Deschamps diagram after [28], or, in the special case of Maxwell's equations, Maxwell's house [9, pp. 134]. For completeness, we have included the (unphysical) magnetic source current density $\vec{K}$ and the magnetic charge density ϱ_m. The topological equations can be read off on the left and the right hand columns of Maxwell's house. The metric laws can be read off the connections of the left and right hand column. Thus we recognize two separate sets of quantities related internally only by topological laws. The connection between those two sets is established by the metric laws. Tab. 2.1 lists the quantities separated into those two sets.

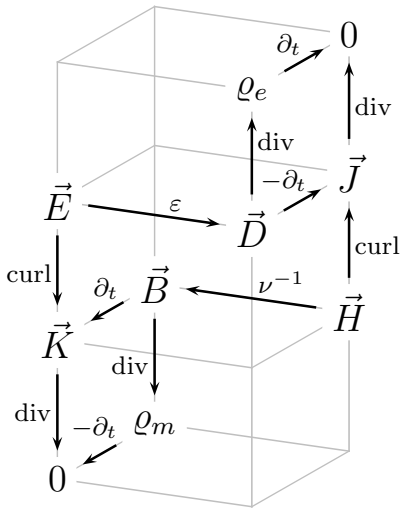

Fig. 2.3: Maxwell's house graphically represents Maxwell's equations: The equations can be read off by adding all incoming quantities at each node and setting it equal to the quantity at the node. An *incoming quantity* is defined for an incoming arrow as the attached operator applied to the quantity at the start of the arrow.

Set 1			Set 2		
$\vec{E}$	-	electric field strength	$\vec{H}$	-	magnetic field strength
$\vec{B}$	-	magnetic flux density	$\vec{D}$	-	electric flux density
$\vec{K}$	-	magnetic source current density	$\vec{J}$	-	electric source current density
ϱ_m	-	magnetic charge density	ϱ_e	-	electric charge density

Tab. 2.1: Quantities commonly used with Maxwell's equations. The quantities in set 1 are connected by the topological laws on the left hand side of Fig. 2.3. Shown in gray are the magnetic current and charge densities which are usually set to zero for physical reasons. The quantities in set 2 are connected by the topological laws on the right hand side of Fig. 2.3. The connection between both sets is established by the metric laws in the center of Fig. 2.3.

3. THE FINITE INTEGRATION TECHNIQUE ON CONSISTENT GRIDS

The Finite Integration Technique (FIT) described in [92], [94], and [95] provides a *consistent* way of discretizing Maxwell's equations. By *consistent*, we mean that basic topological properties of the continuous equations as stated in chapters 2.1.3 and 2.2.3 are preserved in the discrete setting. Although originally stated specifically for Maxwell's equations, the FIT encompasses a consistent discretization of a wide range of BVPs. Independently, the cell method [87] was developed starting from [86], which is based on very similar ideas and leads to equivalent formulations. Both methods are often categorized as Finite Difference (FD) or even Finite Volume (FV) methods, but although the same set of equations is derived in certain settings as for the FD and FV methods, the basic idea of consistently capturing important properties of the continuous Maxwell's equations is lost by this statement.

Another development took place in the Finite Element (FE) community: There, the preservation of the same topological properties was found to hold for the special class of Whitney-Finite Element Methods (Whitney-FEM) and was realized as an important quality of the discretization, see e.g. [9] [83]. A generalization to higher order FE can be found in [48] while an encompassing view is given in [2]. The lowest order Whitney-FEM is easily recast in the formalism of the FIT, as shown in appendix C.

Other terms have been established for the discrete setting of the FIT. Originating from different backgrounds or taking different points of view, it has e.g. been called Generalized Finite Differences [10] or Discrete Exterior Calculus [27] for general BVPs and Discrete Electromagnetism [21] or Lattice Electromagnetic Theory [84] for the special case of Maxwell's equations.

The FIT was originally stated for a pair of consistent dual orthogonal grids, which will be defined below. For these grids, discrete material relations are easily derived. In practical implementations, structured cubical grids are most often employed. In this chapter, we will state the FIT for a pair of general consistent dual grids allowing for arbitrary polyhedral grid cells. The construction of the discrete material relations for such general grids is left open, though. In chapter 4, a possible construction algorithm for the discrete material relations for planar-faced polyhedra will be described.

This chapter is outlined as follows: First, the spatial domain Ω is discretized by a primal grid Ω_h and its dual grid $\underset{\sim}{\Omega}_h$[1] along with the physical quantities and topological and metric

[1] Deviating from the standard FIT notation, we will place a tilde below symbols to denote a symbol related to the dual grid. This allows us to easily mark the electromagnetic quantities defined on the dual grid $\underset{\sim}{\Omega}_h$, i.e. write $\underset{\sim}{\widehat{\mathbf{h}}}$ for the magnetic voltage defined on the dual grid.

tools in chapter 3.1. The topological and metric tools and properties are introduced in parallel to the continuous setting in chapter 2.1.

Then Maxwell's equations are discretized in two steps: In chapter 3.2, the equations are discretized in the spatial variable but left continuous in the temporal variable. This semi-discrete formulation is often used with an analytical solution of the time dependence e.g. by a Fourier Transform. For a single frequency of this Fourier Transform, the resulting equations are referred to as time-harmonic equations. The resulting system of equations is called *Maxwell's spatially discrete grid equations*. The structure of the presentation is again in parallel to the continuous case: Maxwell's topological and metric grid equations and topological and metric properties are introduced in chapters 3.2.1 to 3.2.4 in parallel to the continuous chapters 2.2.1 to 2.2.4. In chapter 3.2.5, existence and uniqueness of the solution to Maxwell's grid IBVP with suitable boundary and initial conditions are proven along with discrete stability of the scheme. In chapter 3.2.6, the spatially discrete Maxwell's house is presented.

In a second step in chapter 3.3, Maxwell's Grid Equations are also discretized in the temporal variable. The spatially and temporally discrete equations are called *Maxwell's spatially and temporally discrete grid equations*. In chapters 3.3.1 to 3.3.4 Maxwell's topological and metric grid equations and topological tools and properties are introduced, again in parallel to the continuous presentation. Emphasis is put on the cell-based Newmark-Θ scheme described in [76] for which a preserved energy quantity is derived. In chapter 3.3.5, existence and uniqueness of the solution for the Newmark-Θ scheme with suitable boundary and initial conditions as well as discrete stability are proven.

The presentation of the continuous setting in chapter 2 put very rigid restrictions on the manifolds and differential forms: The domain Ω was assumed to have a smooth boundary and the spaces of smooth k-dimensional submanifolds $\boldsymbol{S}_s^k(\Omega)$ and smooth k-forms $\mathcal{F}_s^k(\Omega)$ were used. These assumptions allowed for a concise but somewhat consistent presentation of the continuous setting, but they are not fulfilled for standard engineering problems or the general polyhedral grid cells treated in this thesis. Standard engineering models and the polyhedral grids do exhibit corners and edges as well as jumping material coefficients. Thus the manifolds and k-forms are not smooth. Nevertheless, e.g. for the integration to make sense and Gauss' law to hold, they need to fulfill certain regularity properties. The author has not found a general enough mathematical setting to account for practical applications in the literature. E.g. the assumption of Lipschitz-continuous boundaries often used is too rigid as shown by the simple non-Lipschitz examples in [49, p. 27]. Also the cone property put forward in [59] seems too rigid. The setting put forward in [44] seems very promising for such a general setting, though.

We will wind out of this problem by simply assuming the manifolds to be *nice enough* for the things presented in chapter 2 to work. We denote the spaces of *nice enough* submanifolds by $\boldsymbol{S}^k(\Omega)$. The non-pathological manifolds with piecewise smooth boundary treated in the following do work. The k-forms are nevertheless still assumed to be smooth, as this is convenient and sufficient to present the discretization process in the FIT consistently without much new notation. We will present more general spaces of k-forms when they are needed in chapter 4.

3.1 Discrete Mathematical Tools Needed to State Maxwell's Grid Equations

3.1.1 Consistent Grids and their Duals

Instead of using standard grid types, e.g. hexahedral, tetrahedral, or prism-grids, we treat a more general class of *consistent grids*. Loosely speaking, a consistent grid is a tessellation of a domain into cells, faces, edges, and vertices that fit together correctly: Any cells, faces, edges touching each other have the same faces, edges, and vertices, respectively, in the touching part of their boundaries. A 2-dimensional example for a non-consistent and a consistent grid is shown in Fig. 3.1. For an example of a 3-dimensional consistent grid, see Fig. 3.2. We also require the elements to be piecewise smooth and to have no holes or loops. This leaves the elements quite arbitrary, e.g. they can have curved boundaries and edges and corners.

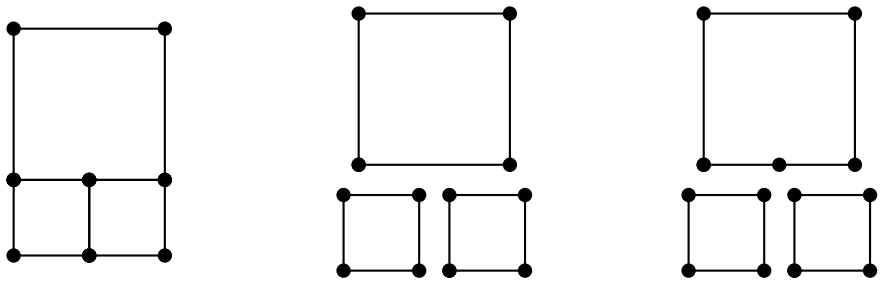

(a) Example 2-dimensional grid.

(b) Elements rendering (a) a non-consistent grid.

(c) Elements rendering (a) a consistent grid.

Fig. 3.1: Examples for 2-dimensional non-consistent and consistent grids: (a) This grid might be non-consistent or consistent, depending on the specific element shapes in the grid. (b) Example for a non-consistent grid: The grid elements cannot be put together consistently as the large rectangle is missing a vertex in the middle of its bottom edge that the small rectangles can be attached to. Often, these elements are put together using interpolation at the inconsistent edges. (c) Example for a consistent grid: The grid elements can be put together consistently as the large rectangle has a vertex and two small edges on its bottom side that the small rectangles can be attached to.

For reasons of clearness, we mainly treat the 3-dimensional case. A generalization to the n-dimensional case is easily achieved, though. The following definition of consistent grids follows closely the one given in [48]:

Definition 3.1 (Consistent grid)**.** A *consistent grid* Ω_h of a bounded contractible domain $\Omega \subset \mathbb{R}^3$ is a disjunct partition of the closure $\overline{\Omega}$ of the domain Ω into finite sets of 3-dimensional cells $\boldsymbol{S}^3(\Omega_h)$, 2-dimensional faces $\boldsymbol{S}^2(\Omega_h)$, 1-dimensional edges $\boldsymbol{S}^1(\Omega_h)$, and 0-dimensional vertices $\boldsymbol{S}^0(\Omega_h)$ with the following properties:

I. All cells, faces, edges, and vertices are piecewise smooth contractible open subsets of the domain Ω.

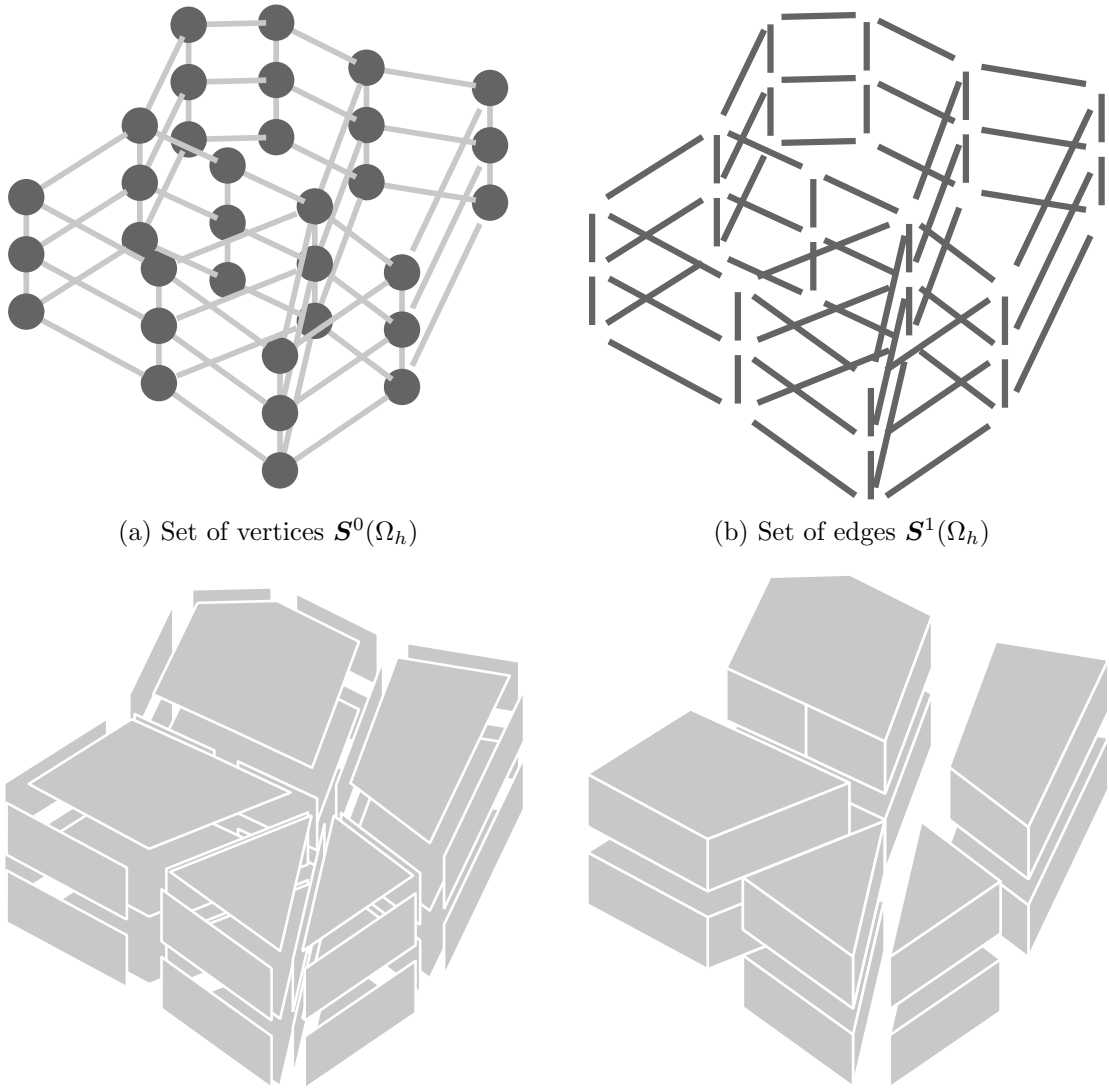

(a) Set of vertices $\boldsymbol{S}^0(\Omega_h)$

(b) Set of edges $\boldsymbol{S}^1(\Omega_h)$

(c) Set of faces $\boldsymbol{S}^2(\Omega_h)$

(d) Set of cells $\boldsymbol{S}^3(\Omega_h)$

Fig. 3.2: Example of a consistent grid Ω_h and the sets of its elements. In (a), also the edges are shown for better visualization. For clearness of the graphical representation, the depicted grid is uniform in one direction, which is in no way a requirement for a consistent grid.

II. The boundary of each cell is the union of the closure of faces; the boundary of each face is the union of the closure of edges; and the boundary of each edge consists of vertices.

III. Each vertex, edge, and face is contained in the boundary of an edge, face, or cell, respectively.

IV. For each face and edge of the grid, an arbitrary inner orientation[2] is chosen. Cells are positively oriented in accordance with the ambient (orientable) space Ω and the vertices are defined to be oriented positively.

The cells, faces, edges, and vertices are called *grid elements*. The number of grid elements in the set of k-dimensional elements $\boldsymbol{S}^k(\Omega_h)$ is denoted by n^k. The grid elements of the set $\boldsymbol{S}^k(\Omega_h)$ are assumed to be numbered from 1 to n^k and we denote the i-th element in $\boldsymbol{S}^k(\Omega_h)$ by $S_i^k(\Omega_h)$ or in short S_i^k.

It will later on be convenient to denote the corresponding submanifold of the grid element S_i^k by the same symbol. The context will allow us to distinguish between the interpretation of S_i^k as a grid element in $\boldsymbol{S}^k(\Omega_h)$ or as a submanifold in $\boldsymbol{S}^k(\Omega)$.

In the continuous setting, the domain Ω provided enough structure to state Maxwell's equations. In the discrete setting, it is convenient to introduce a second grid of the domain Ω, though. We choose this second grid $\underset{\sim}{\Omega}_h$ to be a *dual grid* of the consistent grid Ω_h:

Definition 3.2 (Dual grid)**.** A *dual grid* $\underset{\sim}{\Omega}_h$ of the consistent grid Ω_h is a partition of the interior $\mathring{\Omega}$ of Ω into finite sets of vertices $\underset{\sim}{\boldsymbol{S}}^0(\underset{\sim}{\Omega}_h)$, edges $\underset{\sim}{\boldsymbol{S}}^1(\underset{\sim}{\Omega}_h)$, faces $\underset{\sim}{\boldsymbol{S}}^2(\underset{\sim}{\Omega}_h)$, and cells $\underset{\sim}{\boldsymbol{S}}^3(\underset{\sim}{\Omega}_h)$, with the following properties:

I. All cells, faces, edges, and vertices of the dual grid $\underset{\sim}{\Omega}_h$ are piecewise smooth contractible open subsets of the domain Ω.

II. Each vertex $S_i^0 \in \boldsymbol{S}^0(\Omega_h)$ is associated with exactly one cell $\underset{\sim}{S}_i^3$, each edge $S_i^1 \in \boldsymbol{S}^1(\Omega_h)$ crosses exactly one face $\underset{\sim}{S}_i^2$, each face $S_i^2 \in \boldsymbol{S}^2(\Omega_h)$ is crossed by exactly one edge $\underset{\sim}{S}_i^1$, and each cell $S_i^3 \in \boldsymbol{S}^3(\Omega_h)$ contains exactly one vertex $\underset{\sim}{S}_i^0$.

III. The outer orientation[3] of the elements $\underset{\sim}{S}_i^k$ of the dual grid is induced by the inner orientation of its associated grid element S_i^{3-k}, as depicted in Fig. 3.3.

The elements of the set $\underset{\sim}{\boldsymbol{S}}^k(\underset{\sim}{\Omega}_h)$ are assumed to be numbered from 1 to $\underset{\sim}{n}^k$ with $\underset{\sim}{n}^k$ denoting the number of elements in $\underset{\sim}{\boldsymbol{S}}^k(\underset{\sim}{\Omega}_h)$. The element $\underset{\sim}{S}_i^k$ is called the *dual element of* S_i^{3-k} or *associated with the element* S_i^{3-k}.

[2] The term *inner orientation* refers to what is usually considered simply as orientation. We will use this term to distinguish it from the *outer orientation* of elements used below. See [17, pp. 184] and [11, pp. 10] for a definition and discussion.

[3] See [17, pp. 184] and [11, pp. 10] for a definition and discussion of inner and outer orientation.

Considering a consistent grid Ω_h and a choice of a dual grid $\underset{\sim}{\Omega}_h$, we will hereafter refer to the consistent grid Ω_h as *primal grid*.

By choosing the outer orientation as induced by the associated primal grid elements, the formula for the discrete grid exterior product given below becomes very simple, i.e. the discrete grid exterior product matrix introduced in [47, pp. 253] is the unity matrix. For further discussion of the choice of inner/outer orientation for the different quantities employed, see e.g. [88].

As for the primal grid elements, it will later on be convenient to denote the corresponding submanifold of the dual grid element $\underset{\sim}{S}_i^k$ by the same symbol. The context will allow us to differentiate between whether we interpret $\underset{\sim}{S}_i^k$ as a dual grid element in $\underset{\sim}{\boldsymbol{S}}^k(\Omega_h)$ or as a submanifold in $\boldsymbol{S}^k(\Omega)$.

Note that in contrast to the primal grid, the dual grid does not contain the boundary $\partial\Omega$ of the domain Ω. When stating discrete versions of partial differential equations, this poses problems and a special treatment of the boundary is needed. We are therefore tempted to include a discretization of the boundary $\partial\Omega$ in the dual grid $\underset{\sim}{\Omega}_h$. But this would destroy the simple duality to the primal grid Ω_h, introduce new notation that is not standard in the FIT, and might not seem very intuitive at this point. Therefore, we will stick to the dual grid $\underset{\sim}{\Omega}_h$ as a discretization of the interior of the domain $\mathring{\Omega}$ only and accept the need for a special treatment of the boundary $\partial\Omega$ later on. In chapter 3.2.1, we will have the specific example of Maxwell's topological laws at hand and intuitively derive a correct treatment without the need for much new notation. In appendix A, an *enhanced dual grid* is introduced with new notation and formulas for including a discretization of the boundary $\partial\Omega$ at this early technical stage.

The definition of dual grids leaves much leeway for the actual choice of a dual grid $\underset{\sim}{\Omega}_h$ for some given consistent grid Ω_h. The shape of the dual elements is not uniquely defined by the given requirements. See Fig. 3.4 for an example of a special choice of a dual grid for the top part of the primal grid in Fig. 3.2.

3.1.2 Chains, Cochains, Grid Integration, and the Grid Discretization Operator

In this chapter, we will develop the discrete counterparts on the primal and dual grid for the continuous integration paths, k-forms, and the integration of k-forms. The grid integration paths will be weighted collections of the grid elements and be called *chains*. The discrete equivalent of k-forms will be called *cochains* and return real numbers under the discrete integral operation for a chain to be defined. The connection between the continuous and discrete setting will be established by the *grid discretization operators*, which discretize continuous k-forms into discrete cochains on the primal and the dual grid.

The continuous submanifolds were flexible enough to use them as integration paths in the continuous setting. In the discrete setting, we will use weighted collections of grid elements for defining grid integration paths, called *k-chains*. When we want to describe the grid integration path along the edges of the part of a grid Ω_h depicted in Fig. 3.5

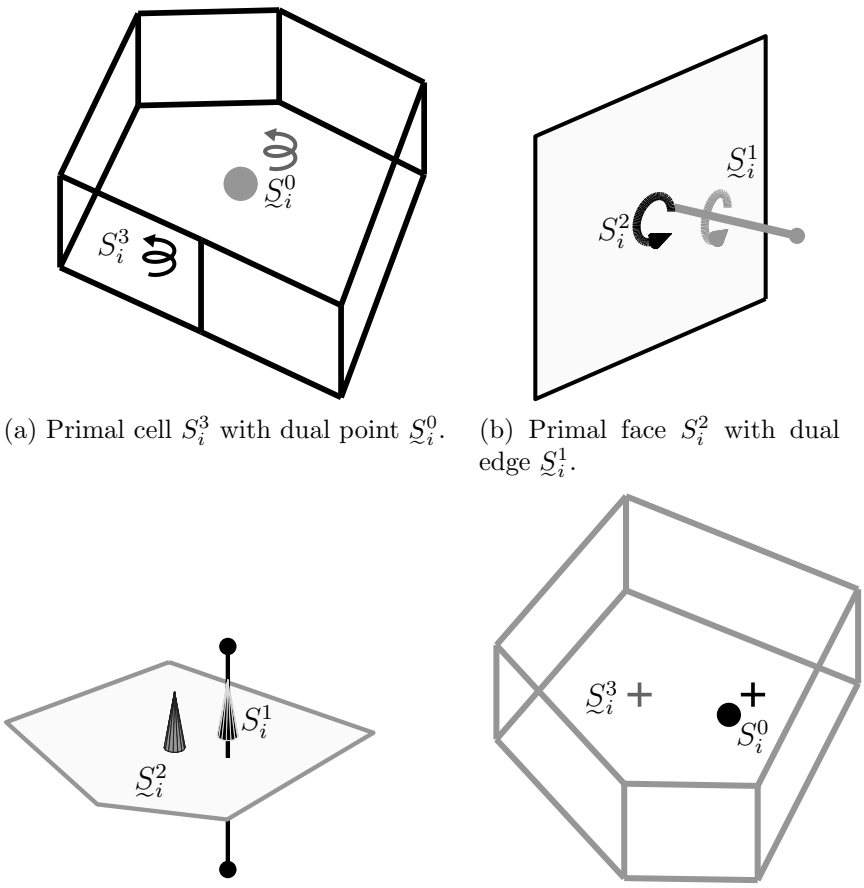

(a) Primal cell S_i^3 with dual point $\underset{\sim}{S}_i^0$.

(b) Primal face S_i^2 with dual edge $\underset{\sim}{S}_i^1$.

(c) Primal edge S_i^1 with dual face $\underset{\sim}{S}_i^2$.

(d) Primal point S_i^0 with dual cell $\underset{\sim}{S}_i^3$.

Fig. 3.3: Dual grid elements $\underset{\sim}{S}_i^k$ (shown in gray) with outer orientation induced by the inner orientation of the associated primal grid elements S_i^{3-k} (shown in black).

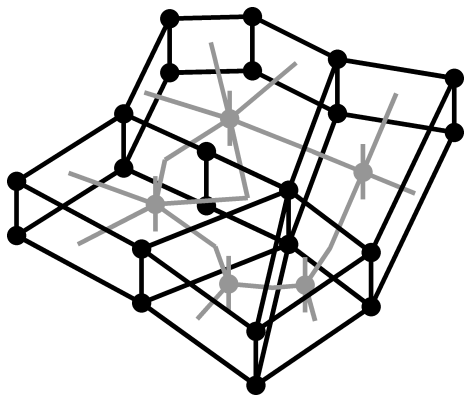

Fig. 3.4: Vertices and edges of a dual grid $\underset{\sim}{\Omega}_h$ (shown in gray) for the top part of the primal grid Ω_h (shown in black) displayed in Fig. 3.2. Note that the boundary of the domain is not included in the dual grid as defined here.

from the vertex S_1^0 to the vertex S_2^0, we will write this as the 1-chain $\boldsymbol{c}^1$ in the space of 1-chains $\boldsymbol{C}^1(\Omega_h)$:

$$\boldsymbol{c}^1 = S_1^1 + S_2^1 - S_3^1 \tag{3.1}$$

Collecting all the coefficients in front of the edges S_i^1 in the order of the edge numbering, we can represent the 1-chain also as a vector $\boldsymbol{c}^1 \in \mathbb{R}^{n^1}$:

$$\boldsymbol{c}^1 = \begin{pmatrix} +1 \\ +1 \\ -1 \\ 0 \\ \vdots \\ 0 \end{pmatrix} \tag{3.2}$$

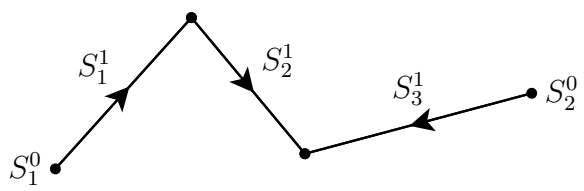

Fig. 3.5: Integration path example. Only some vertices and edges of a primal grid Ω_h are shown.

Let us put this into a formal definition for the primal grid:

Definition 3.3 (Primal chain)**.** The *space of primal chains* denoted by $\boldsymbol{C}^k(\Omega_h)$ is the vector space created by taking the k-dimensional elements of the primal grid Ω_h as a basis over the field[4] $\mathbb{R}$:

$$\boldsymbol{C}^k(\Omega_h) \equiv \operatorname{span}\left\{S_i^k : S_i^k \in \boldsymbol{S}^k(\Omega_h)\right\} \tag{3.3}$$

An element $\boldsymbol{c}^k$ of the space of primal chains $\boldsymbol{C}^k(\Omega_h)$ is called a *primal chain.* We will also denote by $\boldsymbol{c}^k$ its coefficient vector in the basis of the k-dimensional elements S_i^k and thus identify $\boldsymbol{C}^k(\Omega_h)$ with $\mathbb{R}^{n^k}$:

$$\boldsymbol{c}^k = \sum_{i=1}^{n^k} c_i^k S_i^k \tag{3.4}$$

where c_i^k denotes the i-th component of the vector $\boldsymbol{c}^k$.

The *space of dual chains* $\underset{\sim}{\boldsymbol{C}}^k(\underset{\sim}{\Omega}_h)$ is defined equivalently on the elements of the dual grid $\underset{\sim}{\Omega}_h$.

There is a discrete equivalent to the continuous boundary operator acting on the discrete chains: The primal and dual grid boundary operators $\boldsymbol{\partial}^k$ and $\underset{\sim}{\boldsymbol{\partial}}^k$, respectively. They

[4] We allow not only for coefficients in $\{+1, -1, 0\}$ but in all $\mathbb{R}$.

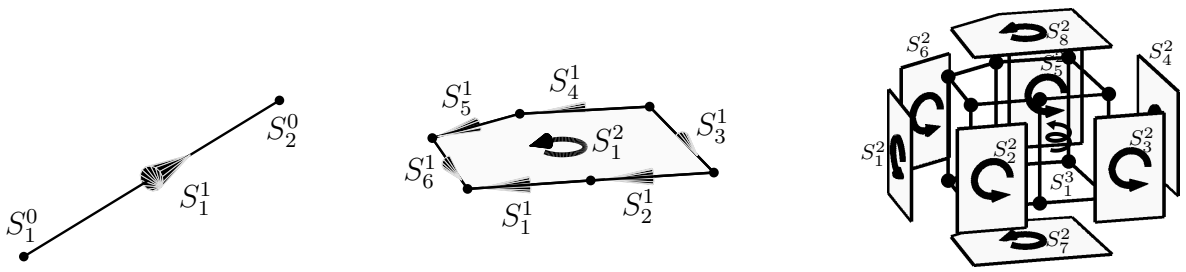

Fig. 3.6: Example grid elements and the elements in their boundaries.

act on a chain by picking out the grid elements in its boundary in the outward pointing direction. E.g. for the chain $\boldsymbol{c}^1$ defined by equation (3.1) and Fig. 3.5, the primal grid boundary operator returns the end points with adjusted signs:

$$\boldsymbol{\partial}^1 \boldsymbol{c}^1 = -S_1^0 + S_2^0 \tag{3.5}$$

For the example grid parts shown in Fig. 3.6, the primal grid boundary operator returns:

$$\boldsymbol{\partial}^1 S_1^1 = -S_1^0 + S_2^0 \tag{3.6a}$$
$$\boldsymbol{\partial}^2 S_1^2 = -S_1^1 - S_2^1 - S_3^1 + S_4^1 + S_5^1 + S_6^1 \tag{3.6b}$$
$$\boldsymbol{\partial}^3 S_1^3 = +S_1^2 + S_2^2 + S_3^2 - S_4^2 - S_5^2 - S_6^2 - S_7^2 + S_8^2 \tag{3.6c}$$

Definition 3.4 (Primal grid boundary operator)**.** The primal grid boundary operator, or primal boundary operator, denoted by $\boldsymbol{\partial}^k$

$$\boldsymbol{\partial}^k : \qquad \boldsymbol{c}^k \in \boldsymbol{C}^k(\Omega_h) \longmapsto \boldsymbol{\partial}^k \boldsymbol{c}^k \in \boldsymbol{C}^{k-1}(\Omega_h) \tag{3.7}$$

is defined in matrix terms operating on the coefficient vector $\boldsymbol{c}^k$ as

$$\left(\boldsymbol{\partial}^k\right)_{ij} = \begin{cases} +1 & \text{if } S_i^{k-1} \text{ lies in the boundary of } S_j^k \text{ with matching orientation,} \\ -1 & \text{if } S_i^{k-1} \text{ lies in the boundary of } S_j^k \text{ with opposite orientation,} \\ 0 & \text{otherwise} \end{cases} \tag{3.8}$$

As the primal grid boundary operator is a linear operator, we note:

$$\boldsymbol{\partial}^k \boldsymbol{c}^k = \sum_{i=1}^{n^k} c_i^k \boldsymbol{\partial}^k S_i^k \tag{3.9}$$

Further on, we can easily show that the boundary of a boundary in the discrete setting is also empty:

$$\boldsymbol{\partial}^{k-1} \boldsymbol{\partial}^k = 0 \qquad \forall\, k \in [1..3] \tag{3.10}$$

The *dual boundary operator* $\underset{\sim}{\boldsymbol{\partial}}^k$ is defined equivalently on the dual grid $\underset{\sim}{\Omega}_h$. Due to the duality of the grids, we notice the following relation:

$$\underset{\sim}{\boldsymbol{\partial}}^{k+1} = (-1)^{3-k} \left(\boldsymbol{\partial}^{3-k}\right)^{\mathrm{T}} \tag{3.11}$$

The discrete equivalents of the k-forms, which are integrated over k-submanifolds, are the discrete *k-cochains*, which we will integrate over k-chains. The simplest way of looking at a k-cochain $\boldsymbol{\omega}^k$ is as an assignment of real numbers $\omega_i^k \in \mathbb{R}$ to each k-element S_i^k of the grid, conveniently represented by the k-cochain coefficient vector also denoted by $\boldsymbol{\omega}^k$.

To get an idea what cochains are about, let us look at an example of how we can discretize the continuous electric field strength $\vec{E}(\vec{r},t)$, a 1-form, onto the edges of the primal grid Ω_h: For each edge S_i^1 of the primal grid, we can calculate the electric voltage $\widehat{\mathrm{e}}_i$ along that edge:

$$\widehat{\mathrm{e}}_i(t) \equiv \int_{S_i^1} \vec{E}(\vec{r},t)\cdot\vec{t}_{S_i^1}\,\mathrm{d}s \equiv L_i^1\vec{E}(\vec{r},t), \qquad \forall\, i\in[1..n^1], \qquad \forall\, t\in\mathrm{T} \tag{3.12a}$$

where we have introduced L_i^1 as the edge-wise grid discretization operator. Note that the symbol S_i^1 under the continuous integral sign now denotes the submanifold in Ω corresponding to the primal grid element S_i^1. Now we can collect the resulting coefficients in a vector called the *electric grid voltages* $\widehat{\mathbf{e}}$:

$$\widehat{\mathbf{e}}(t) \equiv \left[\int_{S_i^1} \vec{E}(\vec{r},t)\cdot\vec{t}_{S_i^1}\,\mathrm{d}s\right]_{i\in[1..n^1]} \equiv \mathrm{L}^1\vec{E}(\vec{r},t), \qquad \forall\, t\in\mathrm{T} \tag{3.12b}$$

where we have defined the edge grid discretization operator L^1. The electric grid voltages $\widehat{\mathbf{e}}$ will be called a 1-cochain. The operators L^k will be called *grid discretization operators*.

In view of equation (3.4), it seems very natural to define the discrete *grid integral* of the 1-cochain $\widehat{\mathbf{e}}$ over the 1-chain $\boldsymbol{c}^1$ as follows:

$$\int_{\boldsymbol{c}^1} \widehat{\mathbf{e}} = \int_{\sum_{i=1}^{n^1} c_i^1 S_i^1} \widehat{\mathbf{e}} \equiv \sum_{i=1}^{n^1} c_i^1 \int_{S_i^1} \widehat{\mathbf{e}} \equiv \sum_{i=1}^{n^1} c_i^1 \widehat{\mathrm{e}}_i = \left(\boldsymbol{c}^1\right)^{\mathrm{T}} \widehat{\mathbf{e}} \tag{3.13}$$

This definition of the discrete integral takes the sum of all 1-cochain coefficients $\widehat{\mathrm{e}}_i$ weighted by the corresponding 1-chain coefficients c_i^1. This is actually equal to the continuous integration of the original electric field strength $\vec{E}$ from equations (3.12) over the (weighted) submanifold corresponding to the 1-chain $\boldsymbol{c}^1$:

$$\begin{aligned}\int_{\boldsymbol{c}^1} \widehat{\mathbf{e}} &\equiv \sum_{i=1}^{n^1} c_i^1 \widehat{\mathrm{e}}_i = \sum_{i=1}^{n^1} c_i^1 \int_{S_i^1} \vec{E}(\vec{r},t)\cdot\vec{t}_{S_i^1}\,\mathrm{d}s \\ &= \int_{\sum_{i=1}^{n^1} c_i^1 S_i^1} \vec{E}(\vec{r},t)\cdot\vec{t}_{S_i^1}\,\mathrm{d}s\end{aligned} \tag{3.14}$$

Whether the integration symbol denotes a continuous integration or a discrete grid integration is apparent by looking at the integrand: A k-form requires a continuous integration while a k-cochain requires a grid integration.

We have introduced the cochains above as coefficient vectors. A more technical point of view is the interpretation of a cochain as an element in $\boldsymbol{C}^k(\Omega_h)'$, the dual of the space of chains. The chain space equipped with the scalar product of the coefficient vectors as inner product forms a Hilbert space. By Riesz' representation theorem, we are able to represent elements of the cochain space by elements of the chain space and thus arrive at the coefficient vectors used above. The grid integration is simply the dual pairing of a chain with a cochain. We will now put these concepts into a more formal definition:

Definition 3.5 (Primal cochain space)**.** The *space of primal k-cochains* $\mathcal{F}_h^k(\Omega_h)$ is defined as the dual of the space of primal k-chains $\boldsymbol{C}^k(\Omega_h)$:

$$\mathcal{F}_h^k(\Omega_h) \equiv \boldsymbol{C}^k(\Omega_h)' \tag{3.15}$$

So a *primal k-cochain* $\boldsymbol{\omega}^k \in \mathcal{F}_h^k(\Omega_h)$ is a linear function from the space of k-chains into $\mathbb{R}$:

$$\boldsymbol{\omega}^k : \quad \boldsymbol{c}^k \in \boldsymbol{C}^k(\Omega_h) \longmapsto \boldsymbol{\omega}^k\left(\boldsymbol{c}^k\right) \in \mathbb{R} \tag{3.16}$$

We will conveniently represent the k-cochain $\boldsymbol{\omega}^k$ by the coefficient vector of its representation in the k-chain space by Riesz' representation theorem. This coefficient vector will also be denoted by $\boldsymbol{\omega}^k \in \mathbb{R}^{n^k}$. The dual pairing of a k-cochain $\boldsymbol{\omega}^k$ with a k-chain $\boldsymbol{c}^k$ described by (3.16) is called *grid integration* of the k-cochain $\boldsymbol{\omega}^k$ over the k-chain $\boldsymbol{c}^k$ and we introduce the notation:

$$\int_{\boldsymbol{c}^k} \boldsymbol{\omega}^k \equiv \boldsymbol{\omega}^k\left(\boldsymbol{c}^k\right) = \left(\boldsymbol{c}^k\right)^{\mathrm{T}} \boldsymbol{\omega}^k = \sum_{i=1}^{n^k} c_i^k \omega_i^k \tag{3.17}$$

The *space of dual k-cochains* $\underset{\sim}{\mathcal{F}}_h^k(\underset{\sim}{\Omega}_h)$ and grid integration of a dual k-cochain $\underset{\sim}{\boldsymbol{\omega}}^k$ over a dual k-chain $\underset{\sim}{\boldsymbol{c}}^k$ are defined equivalently on the dual grid $\underset{\sim}{\Omega}_h$.

We will now generalize the connection of continuous k-forms with k-cochains by the *grid discretization operators* eluded to in equations (3.12):

Definition 3.6 (Primal grid discretization operator)**.** Let a k-form $\omega^k \in \mathcal{F}_s^k(\Omega)$ be given. Then the *primal grid discretization operator* L^k with

$$\mathrm{L}^k : \qquad \omega^k \in \mathcal{F}_s^k(\Omega) \longmapsto \mathrm{L}^k\omega^k \in \mathcal{F}_h^k(\Omega_h) \tag{3.18}$$

is defined by

$$\mathrm{L}^k\omega^k \equiv \left[L_i^k\omega^k\right]_{i\in[1..n^k]} \tag{3.19a}$$

$$L_i^k\omega^k \equiv \int_{S_i^k} \omega^k \tag{3.19b}$$

Equivalently, dual grid discretization operators $\underset{\sim}{\mathrm{L}}^k$ are defined rendering dual k-cochains $\underset{\sim}{\boldsymbol{\omega}}^k$ on the dual grid $\underset{\sim}{\Omega}_h$.

These grid discretization operators explain the terms *integral nodal, edge, face, and volume grid quantities* used in the FIT for the 0-, 1-, 2-, and 3-cochains, respectively. The grid discretization operators L^k are also called deRham maps. An illustration of the grid discretization operator L^0 for a 1-dimensional grid is given in Fig. 3.7.

Remark 3.1. As eluded to in equation (3.14), given a continuous k-form ω^k, the discrete integral of its grid discretization $\boldsymbol{\omega}^k$

$$\boldsymbol{\omega}^k \equiv \mathrm{L}^k\omega^k \qquad \in \mathcal{F}_h^k(\Omega_h) \tag{3.20}$$

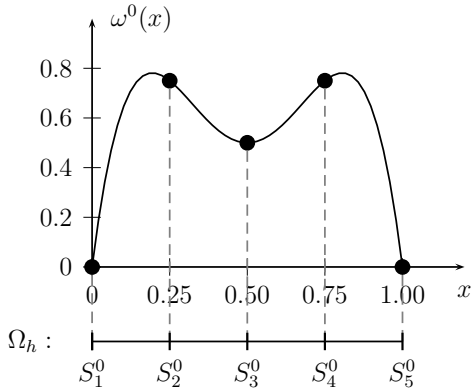

$$\mathrm{L}^0$$

$$\boldsymbol{\omega}^0 = \mathrm{L}^0\omega^0 = \begin{Bmatrix} 0 \\ 0.75 \\ 0.5 \\ 0.75 \\ 0 \end{Bmatrix}$$

Fig. 3.7: Illustration of the grid discretization operator L^0 for the one-dimensional grid Ω_h: The grid discretization operator L^0 discretizes the 0-form ω^0 onto the 0-cochain $\boldsymbol{\omega}^0$ by integrating the 0-form ω^0 over the points of the grid Ω_h or equivalently by evaluating it at the points S_i^0 of the grid.

over a k-chain $\boldsymbol{c}^k$ and the continuous integral of the k-form over the weighted submanifold corresponding to the k-chain $\boldsymbol{c}^k$ coincide by definition:

$$\int_{\boldsymbol{c}^k} \mathrm{L}^k \omega^k = \sum_{i=1}^{n^k} c_i^k \left(\mathrm{L}_i^k \omega^k\right) = \sum_{i=1}^{n^k} c_i^k \int_{S_i^k} \omega^k = \int_{\sum_{i=1}^{n^k} c_i^k S_i^k} \omega^k = \int_{\boldsymbol{c}^k} \omega^k \tag{3.21}$$

where we have used the definition of the discrete integral in equation (3.17), the definition of the coefficients of the grid discretization operator in equation (3.19b), as well as the definitions for the continuous integral in equations (2.3) and (2.4) on page 8 and interpret the term $\boldsymbol{c}^k$ in the last term on the right hand side as a weighted sum of submanifolds.

As examples of the grid discretization operators in vector proxy notation and in view of discretizing Maxwell's equations later on, let us discretize the field quantities encountered in Maxwell's equations onto the primal and dual grid. We will deviate slightly from the standard FIT notation by marking discrete quantities defined on the dual grid, i.e. dual cochains, by a tilde below the symbol:

$$\boldsymbol{\varphi}_e(t) = \mathrm{L}^0 \varphi_e(\vec{r}, t) = \left[\varphi_e(S_i^0, t)\right]_{i \in [1..n^0]}, \qquad \forall\, t \in \mathrm{T} \tag{3.22a}$$

$$\widehat{\mathbf{e}}(t) = \mathrm{L}^1 \vec{E}(\vec{r}, t) = \left[\int_{S_i^1} \vec{E}(\vec{r}, t) \cdot \vec{t}_{S_i^1}\, \mathrm{d}s\right]_{i \in [1..n^1]}, \qquad \forall\, t \in \mathrm{T} \tag{3.22b}$$

$$\widehat{\widehat{\mathbf{b}}}(t) = \mathrm{L}^2 \vec{B}(\vec{r}, t) = \left[\int_{S_i^2} \vec{B}(\vec{r}, t) \cdot \vec{n}_{S_i^2}\, \mathrm{d}A\right]_{i \in [1..n^2]}, \qquad \forall\, t \in \mathrm{T} \tag{3.22c}$$

$$\widehat{\widehat{\mathbf{k}}}(t) = \mathrm{L}^2 \vec{K}(\vec{r}, t) = \left[\int_{S_i^2} \vec{K}(\vec{r}, t) \cdot \vec{n}_{S_i^2}\, \mathrm{d}A\right]_{i \in [1..n^2]}, \qquad \forall\, t \in \mathrm{T} \tag{3.22d}$$

$$\widehat{\widehat{\widehat{\boldsymbol{\varrho}}}}_m(t) = \mathrm{L}^3 \varrho_m(\vec{r}, t) = \left[\int_{S_i^3} \varrho_m(\vec{r}, t)\, \mathrm{d}V\right]_{i \in [1..n^3]}, \qquad \forall\, t \in \mathrm{T} \tag{3.22e}$$

$$\underset{\sim}{\boldsymbol{\varphi}}_m(t) = \underset{\sim}{\mathrm{L}}^0 \varphi_m(\vec{r}, t) = \left[\varphi_m(\underset{\sim}{S}_i^0, t)\right]_{i \in [1..\underset{\sim}{n}^0]}, \qquad \forall\, t \in \mathrm{T} \tag{3.22f}$$

$$\underset{\sim}{\widehat{\mathbf{h}}}(t) = \underset{\sim}{\mathrm{L}}^1 \vec{H}(\vec{r}, t) = \left[\int_{\underset{\sim}{S}_i^1} \vec{H}(\vec{r}, t) \cdot \vec{t}_{\underset{\sim}{S}_i^1}\, \mathrm{d}s\right]_{i \in [1..\underset{\sim}{n}^1]}, \qquad \forall\, t \in \mathrm{T} \tag{3.22g}$$

$$\underset{\sim}{\widehat{\widehat{\mathbf{d}}}}(t) = \underset{\sim}{\mathrm{L}}^2 \vec{D}(\vec{r}, t) = \left[\int_{\underset{\sim}{S}_i^2} \vec{D}(\vec{r}, t) \cdot \vec{n}_{\underset{\sim}{S}_i^2}\, \mathrm{d}A\right]_{i \in [1..\underset{\sim}{n}^2]}, \qquad \forall\, t \in \mathrm{T} \tag{3.22h}$$

$$\underset{\sim}{\widehat{\widehat{\mathbf{j}}}}(t) = \underset{\sim}{\mathrm{L}}^2 \vec{J}(\vec{r}, t) = \left[\int_{\underset{\sim}{S}_i^2} \vec{J}(\vec{r}, t) \cdot \vec{n}_{\underset{\sim}{S}_i^2}\, \mathrm{d}A\right]_{i \in [1..\underset{\sim}{n}^2]}, \qquad \forall\, t \in \mathrm{T} \tag{3.22i}$$

$$\underset{\sim}{\widehat{\widehat{\widehat{\boldsymbol{\varrho}}}}}_e(t) = \underset{\sim}{\mathrm{L}}^3 \varrho_e(\vec{r}, t) = \left[\int_{\underset{\sim}{S}_i^3} \varrho_e(\vec{r}, t)\, \mathrm{d}V\right]_{i \in [1..\underset{\sim}{n}^3]}, \qquad \forall\, t \in \mathrm{T} \tag{3.22j}$$

We call $\boldsymbol{\varphi}_e(t)$ the electric scalar grid potentials, $\widehat{\mathbf{e}}(t)$ the electric grid voltages, $\widehat{\widehat{\mathbf{b}}}(t)$ the magnetic grid fluxes, $\widehat{\widehat{\mathbf{k}}}(t)$ the magnetic grid source currents, $\widehat{\widehat{\widehat{\boldsymbol{\varrho}}}}_m(t)$ the magnetic grid charges, $\underset{\sim}{\boldsymbol{\varphi}}_m(t)$ the magnetic scalar grid potentials, $\underset{\sim}{\widehat{\mathbf{h}}}(t)$ the magnetic grid voltages, $\underset{\sim}{\widehat{\widehat{\mathbf{d}}}}(t)$

the electric grid fluxes, $\underset{\sim}{\hat{\hat{\mathbf{j}}}}(t)$ the electric grid source currents, and $\underset{\sim}{\hat{\hat{\boldsymbol{\varrho}}}}_e(t)$ the electric grid charges. All these quantities are time dependent.

We have discretized the quantities of set 1 in Tab. 2.1 on the primal grid and those of set 2 on the dual grid. This choice will be discussed in chapter 3.2.

3.1.3 Discrete Topological Tools and Properties

In this chapter, we develop the discrete equivalents to the topological tools and properties introduced for the continuous setting in chapter 2.1.3: The discrete trace operator, the discrete exterior product, the discrete exterior derivative and the discrete Gauss' law, the discrete sequence property, the discrete Poincaré Lemma, and a discrete partial integration formula are introduced in parallel to the continuous statements.

Discrete Trace Operators

The trace operator in the continuous case restricts a k-form defined on a domain Ω to some l-dimensional subdomain $\Gamma^l \subset \Omega$. In the discrete setting, this corresponds to simply singling out the coefficients attached to elements in some l-dimensional region Γ_l of the grid Ω_h. So let us more formally define such a region as a *l-dimensional grid part* $\overline{\Gamma}^l_h$:

Definition 3.7 (Grid part)**.** By a *l-dimensional grid part* $\overline{\Gamma}^l_h$ of the primal grid Ω_h, we describe a collection of l-dimensional grid elements

$$\left\{S^l_i\right\}_{i\in \mathrm{I}^l_{\overline{\Gamma}^l_h}} \tag{3.23}$$

with index set $\mathrm{I}^l_{\overline{\Gamma}^l_h} \subset [1..n^l]$ together with all lower dimensional grid elements that lie in the closure of the boundary of any of those elements. The primal grid part $\overline{\Gamma}^l_h$ can again be interpreted as a consistent grid according to Definition 3.1 of the domain $\overline{\Gamma}^l$ defined as:

$$\overline{\Gamma}^l \equiv \overline{\bigcup_{i\in \mathrm{I}^l_{\overline{\Gamma}^l_h}} S^l} \tag{3.24}$$

For $k \leq l$, we will denote by $n^k_{\overline{\Gamma}^l_h}$ the number of the k-dimensional grid elements in $\overline{\Gamma}^l_h$ and by $\mathrm{I}^k_{\overline{\Gamma}^l_h} \subset [1..n^k]$ an index list of those elements.

Now we can define the discrete trace operator $\mathbf{T}^k_{\overline{\Gamma}^l_h}$ restricting a k-cochain defined on the primal grid Ω_h to the elements in the grid part $\overline{\Gamma}^l_h$: The discrete trace operator $\mathbf{T}^k_{\overline{\Gamma}^l_h}$ singles out the coefficients attached to k-dimensional grid elements in the grid part $\overline{\Gamma}^l_h$. E.g. the discrete trace operator onto the grid elements in the boundary of Ω_h, denoted by $\mathbf{T}^k_{\partial\Omega_h}$, renders a reduced coefficient vector with only the coefficients attached to the boundary elements. We will use discrete trace operators to impose the boundary conditions for a discrete IBVP.

Definition 3.8 (Primal grid trace operator)**.** Given a l-dimensional grid part $\overline{\Gamma}_h^l$ of the primal grid Ω_h, the *primal grid trace operator* $\mathbf{T}^k_{\overline{\Gamma}_h^l}$

$$\mathbf{T}^k_{\overline{\Gamma}_h^l}: \quad \boldsymbol{\omega}^k \in \mathcal{F}_h^k(\Omega_h) \longmapsto \mathbf{T}^k_{\overline{\Gamma}_h^l}\, \boldsymbol{\omega}^k \in \mathcal{F}_h^k(\overline{\Gamma}_h^l) \tag{3.25a}$$

is defined in matrix terms acting on the coefficient vectors $\boldsymbol{\omega}^k$ as:

$$\left(\mathbf{T}^k_{\overline{\Gamma}_h^l}\right)_{ij} = \begin{cases} +1 & \text{if } \mathrm{I}^k_{\overline{\Gamma}_h^l}(i) = j, \\ 0 & \text{otherwise} \end{cases} \tag{3.25b}$$

where $\mathrm{I}^k_{\overline{\Gamma}_h^l}(i)$ denotes the i-th index in the index list $\mathrm{I}^k_{\overline{\Gamma}_h^l}$.

The primal grid trace operator $\mathbf{T}^k_{\overline{\Gamma}_h^l}$ is usually only used for $k \leq l$. For $k > l$, it renders by definition a 0-dimensional coefficient vector.

We cannot impose boundary conditions on dual k-cochains, as the dual grid defined above does not include the boundary of Ω. Therefore we do not bother to define a dual grid trace operator. With the concrete example of Maxwell's Grid Equations at hand, we will describe in chapter 3.2 how to impose boundary conditions on quantities discretized on the dual grid.

Discrete Exterior Product

The discrete grid exterior product allows us to approximate energies in the domain Ω from the discrete quantities. E.g. the global electric energy W_e in the calculation domain defined as

$$W_e = \int_\Omega \vec{E} \cdot \vec{D}\, \mathrm{d}V \tag{3.26}$$

is approximated by the grid exterior product of the primal electric grid voltages $\widehat{\mathbf{e}}$ and the dual electric grid fluxes $\underset{\sim}{\widehat{\widehat{\mathbf{d}}}}$, which is simply the scalar product of their coefficient vectors:

$$(\widehat{\mathbf{e}})^{\mathrm{T}}\, \underset{\sim}{\widehat{\widehat{\mathbf{d}}}} \tag{3.27}$$

This expression is at best only an approximation of the continuous electric energy, as the grid exterior product of the grid projection of a continuous field is in general not equal to the integral of its continuous exterior product:

$$\left(\mathrm{L}^1\vec{E}\right)^{\mathrm{T}} \left(\underset{\sim}{\mathrm{L}}^2\vec{D}\right) \neq \int_\Omega \vec{E} \cdot \vec{D}\, \mathrm{d}V \tag{3.28}$$

For a nice enough family of grids, we expect convergence of the discrete quantity to the continuous one, though:

$$\left(\mathrm{L}^1\vec{E}\right)^{\mathrm{T}} \left(\underset{\sim}{\mathrm{L}}^2\vec{D}\right) \longrightarrow \int_\Omega \vec{E} \cdot \vec{D}\, \mathrm{d}V \tag{3.29}$$

The discrete grid exterior product defined below is, mathematically speaking, not an exterior product but a bilinear pairing of primal k-cochains $\boldsymbol{\omega}^k$ with dual $(3-k)$-cochains $\underset{\sim}{\boldsymbol{\eta}}^{3-k}$:

Definition 3.9 (Grid exterior product)**.** The *grid exterior product* $\wedge$

$$\wedge : \quad \left(\boldsymbol{\omega}^k, \underset{\sim}{\boldsymbol{\eta}}^{3-k}\right) \in \mathcal{F}_h^k(\Omega_h) \times \underset{\sim}{\mathcal{F}}_h^k(\underset{\sim}{\Omega}_h) \longmapsto \boldsymbol{\omega}^k \wedge \underset{\sim}{\boldsymbol{\eta}}^{3-k} \in \mathbb{R} \tag{3.30}$$

is defined as the scalar product of the coefficient vectors $\boldsymbol{\omega}^k$ and $\underset{\sim}{\boldsymbol{\eta}}^{3-k}$:

$$\boldsymbol{\omega}^k \wedge \underset{\sim}{\boldsymbol{\eta}}^{3-k} \equiv \left(\boldsymbol{\omega}^k\right)^{\mathrm{T}} \underset{\sim}{\boldsymbol{\eta}}^{3-k} \tag{3.31}$$

See [47] for further discussion of the grid exterior product and the fact that in our case it simply reduces to the scalar product of the two cochain coefficient vectors.

Remark 3.2. The grid exterior product defined above is a purely topological operator, as it only makes use of the topology of the grids and does not require any metric structure for its definition. The grid exterior product is also bilinear like the continuous exterior product. Nevertheless, it is at best an approximation to the continuous exterior product, as already stated for the concrete example in equation (3.28): For a k-form ω^k and a $(3-k)$-form η^{3-k}, the grid exterior product of its grid discretized cochains $\boldsymbol{\omega}^k$ and $\underset{\sim}{\boldsymbol{\eta}}^{3-k}$ is not equivalent to the integral of the continuous exterior product over the domain $\underset{\sim}{\Omega}$:

$$\boldsymbol{\omega}^k \wedge \underset{\sim}{\boldsymbol{\eta}}^{3-k} = L^k \omega^k \wedge \underset{\sim}{L}^{3-k} \eta^{3-k} \neq \int_\Omega \omega^k \wedge \eta^{3-k} \tag{3.32}$$

This is not surprising: Several different forms might render the same grid discretized cochains. The integral of their continuous exterior products might differ, but their grid exterior product then always stays the same.

Remark 3.3. As in the standard FIT, the discrete grid exterior product is defined here only as a pairing of primal k-cochains with dual $(3-k)$-cochains and delivers a real number interpreted as the global energy in the domain Ω. Local discrete energies, i.e. energy coefficients attached to some grid elements, are not readily available, as the local pairing of a primal cochain with a dual cochain is not defined. It would require some grid in a product space of the primal and the dual grid. Several interpretations for local quantities on such intermediate grids do exist, though:

In [78], the case of Cartesian coordinate grids is discussed: Each term $\widehat{\mathrm{e}}_i \widehat{\underset{\sim}{\mathrm{d}}}_i$ in the sum of the scalar product in equation (3.27) is interpreted as a local quantity attached to the volume defined by the Cartesian product of the associated primal edge S_i^1 with its dual face $\underset{\sim}{S}_i^2$. Thus the domain Ω is covered by three tilings of these volumes, one for each coordinate direction.

In [27, pp. 38], the case of simplicial (i.e. triangular or tetrahedral) grids is considered. There, local quantities are derived that are attached to the volumes defined by the convex hull of a primal grid element with its dual grid element. These volumes tile the domain Ω completely.

These approaches to a local interpretation do not seem very promising for the general consistent grids we are discussing here, though. In appendix A, we will take a different point of view and use the local material relations to define local energies in primal grid cells. We thus basically use the primal grid as product grid for the local discrete exterior products. This is consistent with the standard picture of local energies in primal grid cells used in the FEM. We will even derive a more general local exterior product. Not all questions will be answered, though, and a rigorous inclusion of a local grid exterior product in the picture of the FIT still needs to be achieved.

Discrete Exterior Derivatives and Discrete Gauss' Law

We will now define the equivalent of the continuous exterior derivatives (gradient, curl, and divergence) given in chapter 2.1.3 for the discrete case: the primal and dual grid exterior derivatives $\mathbf{D}^k$ and $\underset{\sim}{\mathbf{D}}^k$. In standard FIT notation, these are the primal and dual grid gradient, curl, and divergence operators:

$$\mathbf{G} = \mathbf{D}^0, \qquad \mathbf{C} = \mathbf{D}^1, \qquad \mathbf{S} = \mathbf{D}^2$$
$$\underset{\sim}{\mathbf{G}} = \underset{\sim}{\mathbf{D}}^0, \qquad \underset{\sim}{\mathbf{C}} = \underset{\sim}{\mathbf{D}}^1, \qquad \underset{\sim}{\mathbf{S}} = \underset{\sim}{\mathbf{D}}^2$$

Definition 3.10 (Primal grid exterior derivative)**.** The *primal grid exterior derivative* $\mathbf{D}^k$ of degree $k \in [0..2]$

$$\mathbf{D}^k : \quad \boldsymbol{\omega}^k \in \mathcal{F}_h^k(\Omega_h) \longmapsto \mathbf{D}^k\,\boldsymbol{\omega}^k \in \mathcal{F}_h^{k+1}(\Omega_h) \tag{3.33a}$$

is defined in its matrix representation as the transpose of the boundary operator $\boldsymbol{\partial}^{k+1}$ defined in Definition 3.4 on page 35:

$$\mathbf{D}^k \equiv \left(\boldsymbol{\partial}^{k+1}\right)^{\mathrm{T}} \tag{3.33b}$$

On the dual grid, the *dual grid exterior derivatives* $\underset{\sim}{\mathbf{D}}^k$ are defined accordingly.

In contrast to the continuous case, we have defined the discrete grid exterior derivative directly and therefore have to state and prove the discrete version of Gauss' law independently:

Theorem 3.1 (Primal grid Gauss' law)**.** *For any primal* $(k-1)$*-cochain* $\boldsymbol{\omega}^{k-1} \in \mathcal{F}_h^{k-1}(\Omega_h)$ *and any primal chain* $\boldsymbol{c}^k \in \boldsymbol{C}^k(\Omega_h)$*, the following holds:*

$$\int_{\boldsymbol{c}^k} \mathbf{D}^{k-1}\,\boldsymbol{\omega}^{k-1} = \int_{\boldsymbol{\partial}^k \boldsymbol{c}^k} \boldsymbol{\omega}^{k-1} \tag{3.34}$$

Proof. The proof of equation (3.34) is straight-forward: Using the definition of the discrete integral in equation (3.17) on page 37 and the definition of the grid exterior derivative $\mathbf{D}^k$ in equation (3.33b) we derive:

$$\begin{aligned}\int_{\boldsymbol{c}^k} \mathbf{D}^{k-1}\,\boldsymbol{\omega}^{k-1} &= \left(\boldsymbol{c}^k\right)^{\mathrm{T}} \left(\mathbf{D}^{k-1}\,\boldsymbol{\omega}^{k-1}\right) = \left(\left(\mathbf{D}^{k-1}\right)^{\mathrm{T}} \boldsymbol{c}^k\right)^{\mathrm{T}} \left(\boldsymbol{\omega}^{k-1}\right) \\ &= \left(\boldsymbol{\partial}^k \boldsymbol{c}^k\right)^{\mathrm{T}} \left(\boldsymbol{\omega}^{k-1}\right) = \int_{\boldsymbol{\partial}^k \boldsymbol{c}^k} \boldsymbol{\omega}^{k-1}\end{aligned} \tag{3.35}$$

□

The equivalence of the discrete magnetic charge in a grid cell and the outward magnetic flux through its boundary is an example of the primal grid Gauss' law in standard FIT notation:

$$\int_{S_i^3} \hat{\hat{\boldsymbol{\varrho}}}_m = \int_{S_i^3} \mathbf{S}\,\hat{\hat{\mathbf{b}}} = \left(\mathbf{S}\,\hat{\hat{\mathbf{b}}}\right)_i = \int_{\partial S_i^3} \hat{\hat{\mathbf{b}}} \tag{3.36}$$

We can prove the equivalent statement for the dual grid and call it the *dual discrete Gauss' law*. As the boundary of the domain Ω is not discretized by the dual grid, one has to keep in mind that its physical meaning is defective at the boundary, though.

It is interesting to note that the exterior derivatives commute with the primal grid discretization operators, i.e. one can exchange the order of exterior derivation (gradient, curl, and divergence) and grid discretization. The following commuting diagram represents this:

$$\begin{tikzcd}
\mathcal{F}_s^0(\Omega) \arrow[r, "\mathrm{d}^0\,(=\mathrm{grad})"] \arrow[d, "\mathrm{L}^0"'] & \mathcal{F}_s^1(\Omega) \arrow[r, "\mathrm{d}^1\,(=\mathrm{curl})"] \arrow[d, "\mathrm{L}^1"'] & \mathcal{F}_s^2(\Omega) \arrow[r, "\mathrm{d}^2\,(=\mathrm{div})"] \arrow[d, "\mathrm{L}^2"'] & \mathcal{F}_s^3(\Omega) \arrow[d, "\mathrm{L}^3"'] \\
\mathcal{F}_h^0(\Omega_h) \arrow[r, "\mathbf{D}^0\,(=\mathbf{G})"] & \mathcal{F}_h^1(\Omega_h) \arrow[r, "\mathbf{D}^1\,(=\mathbf{C})"] & \mathcal{F}_h^2(\Omega_h) \arrow[r, "\mathbf{D}^2\,(=\mathbf{S})"] & \mathcal{F}_h^3(\Omega_h)
\end{tikzcd} \tag{3.37}$$

In this diagram, we clearly see that the grid exterior derivatives are the discrete equivalents of the continuous exterior derivatives and their name is thus justified. The following theorem states validity of the commuting diagram:

Theorem 3.2. *The commuting diagram (3.37) holds, i.e. the grid exterior derivatives* $\mathbf{D}^k$ *and the continuous exterior derivatives* d^k *commute with the grid discretization operators* L^k*:*

$$\mathbf{D}^k\,\mathrm{L}^k = \mathrm{L}^{k+1}\,\mathrm{d}^k \tag{3.38}$$

Proof. Using the definition of the grid discretization operator in equations (3.19) on page 37 and Gauss' law (2.16) on page 11, we get for any k-form $\omega^k \in \mathcal{F}_s^k(\Omega)$:

$$\mathrm{L}^{k+1}\,\mathrm{d}^k\,\omega^k = \left[\int_{S_i^{k+1}} \mathrm{d}^k\,\omega^k\right]_{i\in[1..n^{k+1}]} = \left[\int_{\partial S_i^{k+1}} \omega^k\right]_{i\in[1..n^{k+1}]}$$

Now we can split the continuous integration over the boundary of S_i^{k+1} into its parts over the (corresponding manifolds of the) grid elements S_j^k using the discrete boundary operator $\boldsymbol{\partial}^{k+1}$

$$= \left[\sum_{j=1}^{n^k} \partial_{ji}^{k+1} \int_{S_j^k} \omega^k\right]_{i\in[1..n^{k+1}]} \tag{3.39}$$

use the definition of the discrete grid exterior derivative $\mathbf{D}^k$ in equation (3.33b)

$$= \left[\sum_{j=1}^{n^k} D_{ij}^k \int_{S_j^k} \omega^k\right]_{i\in[1..n^{k+1}]} \tag{3.40}$$

and finally again the definition of the grid discretization operator L^k to arrive at:

$$= \left[\sum_{j=1}^{n^k} D_{ij}^k L_j^k \omega^k\right]_{i\in[1..n^{k+1}]} = \mathbf{D}^k\,\mathrm{L}^k\omega^k \tag{3.41}$$

This proofs equation (3.38). □

At first sight, it might be surprising that such a commuting property does not hold for the dual grid. But as the boundary of Ω was not included in the dual grid, there is no chance of this commuting property to hold if the continuous k-forms are non-zero on $\partial\Omega$[5]. What is missing is the correct boundary treatment for the dual grid quantities. Appendix A gives a remedy by defining an enhanced dual grid including the boundary terms. As this is very technical, though, we will tread another path: In chapter 3.2, where we have the concrete example of Maxwell's equations at hand, the correct boundary treatment and the discrete partial integration formula will be developed intuitively.

Discrete Sequence Property

The following statements are fundamental in the FIT [95, pp. 298]:

$$\mathbf{C}\,\mathbf{G} = \mathbf{0}, \qquad \mathbf{S}\,\mathbf{C} = \mathbf{0} \tag{3.42}$$

$$\underset{\sim}{\mathbf{C}}\,\underset{\sim}{\mathbf{G}} = \mathbf{0}, \qquad \underset{\sim}{\mathbf{S}}\,\underset{\sim}{\mathbf{C}} = \mathbf{0} \tag{3.43}$$

This is the discrete equivalent of the continuous sequence property in chapter 2.1.3 on page 12. We will call it the discrete sequence property:

Theorem 3.3 (Primal discrete sequence property)**.** *For a consistent grid Ω_h with grid exterior derivatives $\mathbf{D}^k$ the following holds:*

$$\mathbf{D}^k\,\mathbf{D}^{k-1} = \mathbf{0} \qquad \forall\, k \in [1..2] \tag{3.44}$$

Proof. A nice indirect proof is available by resorting to the commuting property (3.38) on the preceding page, noting that any k-cochain is in the range of L^k, and using the continuous sequence property (2.20) on page 12.

Here, we will give a more direct proof: The sequence property can be viewed as a direct consequence of the boundary of a boundary being empty (equation (3.10)) and the grid exterior derivatives being the transpose of the boundary operator (equation (3.33b)):

$$\mathbf{D}^k\,\mathbf{D}^{k-1} = \left(\left(\boldsymbol{\partial}^k\right)^{\mathrm{T}}\left(\boldsymbol{\partial}^{k+1}\right)^{\mathrm{T}}\right)^{\mathrm{T}} = \mathbf{0} \tag{3.45}$$

□

An equivalent *dual discrete sequence property* holds for a dual grid $\underset{\sim}{\Omega}_h$ with grid exterior derivatives $\underset{\sim}{\mathbf{D}}^k$.

Discrete Poincaré Lemma

The converse of the sequence property is the question of the existence of potentials: Given $\mathbf{D}^k\,\boldsymbol{\omega}^k = 0$, does there always exist a $\boldsymbol{\omega}^{k-1}$ such that $\boldsymbol{\omega}^k = \mathbf{D}^{k-1}\,\boldsymbol{\omega}^{k-1}$? I.e. in standard

[5] Put positively, the commuting property does hold for the dual grid operators for all k-forms with zero trace on the boundary $\partial\Omega$ of the domain.

FIT notation, do the following existence of potentials statements hold:

$$\forall\, \widehat{\mathbf{e}} \in \mathbb{R}^{n^1} : \quad \mathbf{C}\,\widehat{\mathbf{e}} = \mathbf{0} \qquad \Rightarrow \qquad \exists\, \boldsymbol{\varphi} \in \mathbb{R}^{n^0} : \widehat{\mathbf{e}} = \mathbf{G}\,\boldsymbol{\varphi} \tag{3.46}$$

$$\forall\, \widehat{\widehat{\mathbf{b}}} \in \mathbb{R}^{n^2} : \quad \mathbf{S}\,\widehat{\widehat{\mathbf{b}}} = \mathbf{0} \qquad \Rightarrow \qquad \exists\, \widehat{\mathbf{a}} \in \mathbb{R}^{n^1} : \widehat{\widehat{\mathbf{b}}} = \mathbf{C}\,\widehat{\mathbf{a}} \tag{3.47}$$

$$\forall\, \widehat{\widehat{\boldsymbol{\varrho}}} \in \mathbb{R}^{n^3} : \quad \mathbf{0}\widehat{\widehat{\boldsymbol{\varrho}}} = \mathbf{0} \qquad \Rightarrow \qquad \exists\, \widehat{\widehat{\mathbf{b}}} \in \mathbb{R}^{n^2} : \widehat{\widehat{\boldsymbol{\varrho}}} = \mathbf{S}\,\widehat{\widehat{\mathbf{b}}} \tag{3.48}$$

For consistent grids of contractible domains, the discrete Poincaré Lemma in [48, p. 257][6] states:

Lemma 3.4 (Primal discrete Poincaré Lemma)**.** *Given a consistent grid Ω_h of a contractible domain Ω, the following holds for all k-cochains $\boldsymbol{\omega}^k \in \mathcal{F}_h^k(\Omega_h)$ and $k \in [1..3]$:*

$$\mathbf{D}^k\,\boldsymbol{\omega}^k = \mathbf{0} \qquad \Rightarrow \qquad \exists\, \boldsymbol{\omega}^{k-1} \in \mathcal{F}_h^{k-1}(\Omega_h) : \quad \mathbf{D}^{k-1}\,\boldsymbol{\omega}^{k-1} = \boldsymbol{\omega}^k \tag{3.49}$$

For the dual grid, an equivalent discrete Poincaré Lemma holds for $k \in [0..2]$.

A Discrete Partial Integration Formula

In the continuous setting, Poynting's Theorem given in chapter 2.2.3 is basically the application of the partial integration formula given in chapter 2.1.3. We will here state the discrete equivalent of this partial integration formula to be able to derive the discrete version of Poynting's Theorem later on.

As the boundary of the dual grid has not been treated yet, we will here give only the partial integration formula for dual quantities defined on the open dual grid $\underset{\sim}{\Omega}_h$. This can be interpreted as dual quantities that have zero trace on $\partial\Omega$. Therefore, the boundary term evident in the continuous partial integration formula (2.25) on page 13 is missing here:

Theorem 3.5 (Discrete partial integration formula)**.** *For any primal k-chochain $\boldsymbol{\omega}^k \in \mathcal{F}_h^k(\Omega_h)$ and any dual $(3-k-1)$-cochain $\underset{\sim}{\boldsymbol{\eta}}^{3-k-1} \in \underset{\sim}{\mathcal{F}}_h^{3-k-1}(\underset{\sim}{\Omega}_h)$, the following holds:*

$$\left(\mathbf{D}^k\,\boldsymbol{\omega}^k\right)^{\mathrm{T}} \underset{\sim}{\boldsymbol{\eta}}^{3-k-1} + (-1)^k \left(\boldsymbol{\omega}^k\right)^{\mathrm{T}} \left(\underset{\sim}{\mathbf{D}}^{3-k-1}\,\underset{\sim}{\boldsymbol{\eta}}^{3-k-1}\right) = 0 \tag{3.50}$$

Proof. Because of the duality of the primal and dual boundary operators $\boldsymbol{\partial}^{k+1}$ and $\underset{\sim}{\boldsymbol{\partial}}^{3-k}$ in equation (3.11) on page 35, the definition of the primal and dual grid exterior derivatives in equation (3.33b) on page 43 also renders duality of the primal and dual grid exterior derivatives:

$$\underset{\sim}{\mathbf{D}}^k = (-1)^{3-k} \left(\mathbf{D}^{3-k-1}\right)^{\mathrm{T}} \tag{3.51a}$$

$$\Leftrightarrow \qquad \mathbf{D}^k = (-1)^{k+1} \left(\underset{\sim}{\mathbf{D}}^{3-k-1}\right)^{\mathrm{T}} \tag{3.51b}$$

Plugging this into equation (3.50) directly shows its validity. □

Remark 3.4. In standard FIT notation, the duality relations (3.51) read (compare [95, p. 300]):

$$\underset{\sim}{\mathbf{G}} = -\,\mathbf{S}^{\mathrm{T}}, \qquad \underset{\sim}{\mathbf{C}} = \mathbf{C}^{\mathrm{T}}, \qquad \underset{\sim}{\mathbf{S}} = -\,\mathbf{G}^{\mathrm{T}} \tag{3.52}$$

[6] In [48, p. 257], actually the discrete deRham Theorem as generalization of the discrete Poincaré Lemma to grids of non-contractible domains is given.

3.1.4 Discrete Metric Tools

The topological tools outlined above have been stated solely using the topology, i.e. the incidence relations, of the consistent grids and their duals. We were able to capture main features like the Poincaré Lemma in the discrete setting. Now we will turn towards discrete equivalents of the metric tools outlined in chapter 2.1.4 on page 13. In discrete BVPs, the *discrete hodge operators* transform primal cochains into dual cochains and vice versa. They are used to approximate the continuous material relations. The *discrete inner products* and *discrete norms* derived from the discrete hodge operators approximate the continuous energy products and norms.

Discrete Hodge Operator

The *discrete hodge operators* establish discrete material relations just as in the continuous case in chapter 2.1.4 on page 13. We will use them later on in the discrete Maxwell's grid material laws, e.g. state Maxwell's first material law as:

$$\widehat{\underset{\sim}{\mathbf{d}}} = \mathbf{M}_\varepsilon \, \widehat{\mathbf{e}} \tag{3.53}$$

where $\mathbf{M}_\varepsilon$ denotes the permittivity discrete hodge operator and is also called the permittivity material matrix.

We actually can derive two sets of discrete hodge operators: The primal hodge operators $\mathbf{M}_\alpha^k$ act on primal k-cochains and return dual $(3-k)$-cochains:

$$\mathbf{M}_\alpha^k : \quad \boldsymbol{\omega}^k \in \mathcal{F}_h^k(\Omega_h) \longmapsto \mathbf{M}_\alpha^k \, \boldsymbol{\omega}^k \in \underset{\sim}{\mathcal{F}}_h^{3-k}(\underset{\sim}{\Omega}_h) \tag{3.54}$$

while the dual hodge operators $\underset{\sim}{\mathbf{M}}_\alpha^k$ act on dual k-cochains and return primal $(3-k)$-cochains:

$$\underset{\sim}{\mathbf{M}}_\alpha^k : \quad \underset{\sim}{\boldsymbol{\omega}}^k \in \underset{\sim}{\mathcal{F}}_h^k(\underset{\sim}{\Omega}_h) \longmapsto \underset{\sim}{\mathbf{M}}_\alpha^k \, \underset{\sim}{\boldsymbol{\omega}}^k \in \mathcal{F}_h^{3-k}(\Omega_h) \tag{3.55}$$

The subscript α is to denote the special choice of discrete metric and we will denote the discrete hodges approximating the Euclidean metric simply by $\mathbf{M}^k$ and $\underset{\sim}{\mathbf{M}}^k$.

There are ample choices for defining the discrete hodge operators. This is actually the point, where the standard FIT, the cell method and certain cases of FD, FE, and FV methods incorporated into the FIT framework might differ.

We will postpone the specific definition of the discrete hodge operators: The discrete hodges used in the standard FIT material relations for dual orthogonal grids are defined for $k = 1, 2$ in chapter 3.2.2, while a new type of discrete hodge operators for polyhedral grid elements will be defined in chapter 4 as the central achievement of this thesis.

Here, we will only list general requirements that the hodge operators to be defined do fulfill: In parallel to the assumption on the continuous hodges which they should approximate, we require the discrete hodge operators to be *linear* and *positive definite*. As they are linear, we can represent them by (square) matrices. The requirement of positive definiteness thus reads:

$$\left(\boldsymbol{\omega}^k\right)^{\mathrm{T}} \mathbf{M}_\alpha^k \, \boldsymbol{\omega}^k > 0 \qquad \forall \, \boldsymbol{\omega}^k \in \mathcal{F}_h^k(\Omega_h), \; \boldsymbol{\omega}^k \neq 0 \tag{3.56a}$$

$$\left(\underset{\sim}{\boldsymbol{\omega}}^k\right)^{\mathrm{T}} \underset{\sim}{\mathbf{M}}_\alpha^k \, \underset{\sim}{\boldsymbol{\omega}}^k > 0 \qquad \forall \, \underset{\sim}{\boldsymbol{\omega}}^k \in \underset{\sim}{\mathcal{F}}_h^k(\Omega_h), \; \underset{\sim}{\boldsymbol{\omega}}^k \neq 0 \tag{3.56b}$$

The positive definiteness allows us to define energy norms by the discrete hodge operators as done below and ensures that the discrete hodge operators are invertible.

We also require the discrete hodge operators to be symmetric, as this allows an easy proof of uniqueness of the solution and stability of the scheme by Poynting's Theorem. The requirement of symmetry is actually not necessary for uniqueness and stability, though. Several schemes using non-symmetric matrices do exist. For practical computations, symmetry is often advantageous for inverting the resulting system matrix.

Definition 3.11 (Primal discrete hodge operator)**.** The *primal discrete hodge operators* or simply *discrete hodge operators* are linear symmetric positive definite operators with domain and range as defined by equation (3.54). They can be represented by symmetric positive definite matrices. We also call the discrete hodge operators *discrete material matrices* or *discrete material relations.*

Due to the invertibility of the discrete hodge operators, we are able to choose the dual hodge operators as the inverse of the primal hodge operators (and vice versa):

$$\underset{\sim}{\mathbf{M}}^{k}_{\alpha^{-1}} \equiv \left(\mathbf{M}^{3-k}_{\alpha}\right)^{-1} \tag{3.57}$$

Thus we will not define a dual discrete hodge operator explicitly.

In order to derive local energy quantities and properties like a local Poynting's Theorem, we need a *local splitting* of the discrete hodge operators. For the discrete hodge operators defined later on, we will state a splitting into *local hodge operator parts* $\mathbf{M}^{k,m}_{\alpha}$ associated with the primal grid cells S^3_m such that we can calculate local energies in each primal grid cell[7]:

$$\mathbf{M}^{k}_{\alpha} = \sum_{m=1}^{n^3} \mathbf{M}^{k,m}_{\alpha} \tag{3.58}$$

The local hodge operator parts $\mathbf{M}^{k,m}_{\alpha}$ should at least be symmetric positive semi-definite. But in order to derive local energies, we further on require the local hodge operator parts $\mathbf{M}^{k,m}_{\alpha}$ to only act on quantities lying in the closure of their associated grid cells S^3_m and for those quantities to be symmetric positive definite. More specifically, using the discrete trace on the grid cells S^3_m denoted in short by $\mathbf{T}^{k}_{S^3_m}$, we define the *local reduced hodge operator parts* $\widehat{\mathbf{M}}^{k,m}_{\alpha}$ as

$$\widehat{\mathbf{M}}^{k,m}_{\alpha} : \boldsymbol{\omega}^k \in \mathcal{F}^k_h(S^3_m) \longmapsto \widehat{\mathbf{M}}^{k,m}_{\alpha}\boldsymbol{\omega}^k \in \underset{\sim}{\mathcal{F}}^{3-k}_h(S^3_m) \tag{3.59a}$$

$$\widehat{\mathbf{M}}^{k,m}_{\alpha} \equiv \mathbf{T}^{k}_{S^3_m}\, \mathbf{M}^{k,m}_{\alpha} \left(\mathbf{T}^{k}_{S^3_m}\right)^{\mathrm{T}} \tag{3.59b}$$

and require $\widehat{\mathbf{M}}^{k,m}_{\alpha}$ to be symmetric positive definite and the local hodge operator parts $\mathbf{M}^{k,m}_{\alpha}$ to be recaptured by:

$$\mathbf{M}^{k,m}_{\alpha} = \left(\mathbf{T}^{k}_{S^3_m}\right)^{\mathrm{T}} \widehat{\mathbf{M}}^{k,m}_{\alpha}\, \mathbf{T}^{k}_{S^3_m} \tag{3.60}$$

[7] The splitting of the hodge operators has been chosen into parts associated with the primal grid cells as the primal grid is viewed as the fundamental grid. We assume the primal grid to contain the subdivisions into parts that are of interest. Also, the hodge operators for polyhedral grids defined in chapter 4 do not even require to explicitly state a dual grid.

Definition 3.12 (Local splitting of the primal discrete hodge operator)**.** A splitting of the primal hodge operator $\mathbf{M}_\alpha^k$ into symmetric positive semi-definite matrices $\mathbf{M}_\alpha^{k,m}$ and symmetric positive definite matrices $\widehat{\mathbf{M}}_\alpha^{k,m}$ for $m \in [1..n^3]$ fulfilling equations (3.58), (3.59b), and (3.60) is called a *local splitting of the primal discrete hodge operator* $\mathbf{M}_\alpha^k$. The matrices $\mathbf{M}_\alpha^{k,m}$ are called *local hodge operator parts* or *local material matrices* and the matrices $\widehat{\mathbf{M}}_\alpha^{k,m}$ are called *local reduced hodge operator parts* or *local reduced material matrices.*

Discrete Inner Product and Norm

The discrete hodge operators defined above are used in the FIT to calculate global grid energy norms, e.g. the electric grid energy W_e^d is calculated as:

$$W_e^d = \frac{1}{2}\|\widehat{\mathbf{e}}\|_\varepsilon^2 = \frac{1}{2}\left(\widehat{\mathbf{e}}\right)^{\mathrm{T}} \mathbf{M}_\varepsilon\, \widehat{\mathbf{e}} \tag{3.61}$$

As in the continuous case, the discrete hodge operator together with the discrete grid exterior product render a global inner product that leads to the grid energy norms:

Definition 3.13 (Primal grid inner product)**.** The *primal grid inner product* $\langle\!\langle .|. \rangle\!\rangle_\alpha$

$$\langle\!\langle .|. \rangle\!\rangle_\alpha : \quad \left(\boldsymbol{\omega}^k, \boldsymbol{\eta}^k\right) \in \mathcal{F}_h^k(\Omega_h) \times \mathcal{F}_h^k(\Omega_h) \longmapsto \langle\!\langle \boldsymbol{\omega}^k | \boldsymbol{\eta}^k \rangle\!\rangle_\alpha \in \mathbb{R} \tag{3.62}$$

is defined in terms of the grid exterior product $\wedge$ defined in equation (3.31) on page 42 and the primal grid hodge operators $\mathbf{M}_\alpha^k$ as:

$$\langle\!\langle \boldsymbol{\omega}^k | \boldsymbol{\eta}^k \rangle\!\rangle_\alpha \equiv \boldsymbol{\omega}^k \wedge \left(\mathbf{M}_\alpha^k\, \boldsymbol{\eta}^k\right) = \left(\boldsymbol{\omega}^k\right)^{\mathrm{T}} \mathbf{M}_\alpha^k\, \boldsymbol{\eta}^k \tag{3.63}$$

As the discrete hodge operators $\mathbf{M}_\alpha^k$ are assumed to be symmetric positive definite, the primal grid inner product is symmetric and positive definite and thus truly an inner product. We define the following canonical *primal grid energy norm* $\|.\|_\alpha$:

$$\|\boldsymbol{\omega}^k\|_\alpha^2 \equiv \langle\!\langle \boldsymbol{\omega}^k | \boldsymbol{\omega}^k \rangle\!\rangle_\alpha = \left(\boldsymbol{\omega}^k\right)^{\mathrm{T}} \mathbf{M}_\alpha^k\, \boldsymbol{\omega}^k \tag{3.64}$$

The *dual inner grid product* $\langle\!\langle .|. \rangle\!\rangle_\alpha$ and the *dual grid energy norms* $\|.\|_\alpha$ are defined equivalently for the dual k-cochains using, in accordance with equation (3.57), the inverse material matrices $\left(\mathbf{M}_\alpha^{3-k}\right)^{-1}$.

3.2 Maxwell's Spatially Discrete Grid Equations

In chapter 3.1, we have established the tools needed to state the discrete version of Maxwell's equations in this chapter: Maxwell's Grid Equations. In this chapter, we establish Maxwell's Grid Equations with discretization only in the spatial variable and keep the time variable continuous. The resulting Maxwell's grid topological laws and metric laws are stated in chapters 3.2.1 and 3.2.2, respectively. From these, topological and metric properties are derived in chapters 3.2.3 and 3.2.4, respectively. In chapter 3.2.5, we complement Maxwell's Grid Equations by suitable discrete initial and boundary conditions to arrive at a discrete IBVP with unique solution. The discretization of given continuous initial and boundary values and given sources is also described. Maxwell's Grid Equations are recapitulated graphically in chapter 3.2.6 in the discrete version of Maxwell's house. All discrete derivations and presentations are in parallel to the continuous presentations in chapters 2.2.1 to 2.2.6.

Most results in this chapter can be found already in [95], but here we rigorously develop the concepts for arbitrary polyhedral grids, separate topological and metric concepts, and include a rigorous boundary treatment for the dual grid.

In the preceding chapter, we used general notations e.g. for the discrete exterior derivative. This highlighted general concepts of the discrete setting and emphasized the parallels to the continuous setting in chapter 2.1. For the specific problem of Maxwell's Grid Equations in this chapter, we resort to using (almost) standard FIT notation again. The generality is not needed any more and the text should be easier to read by researchers stemming from the FIT background.

3.2.1 Maxwell's Discrete Topological Laws

We here discretize Maxwell's topological laws from chapter 2.2.1 resulting in Maxwell's discrete topological laws. Looking at the continuous Maxwell's equations represented graphically in Maxwell's house in Fig. 2.3 on page 25, we see that there are two separate sets of electromagnetic quantities linked by the topological laws. We discretize one set of quantities on a consistent primal grid Ω_h and the other one on its dual grid $\underset{\sim}{\Omega}_h$. The electric field strength and all connected quantities are chosen to be discretized on the primal grid, as proposed in equations (3.22a) to (3.22j) on page 39. We could have easily chosen the magnetic field strength and all connected quantities to be discretized on the primal grid, though, leading to two different possibilities of discretization.

Let a primal spatial grid Ω_h and its dual grid $\underset{\sim}{\Omega}_h$ be given and assume them to be independent of time. The time variable $t \in \mathrm{T}$ is not yet discretized and we define semi-discrete quantities on the Cartesian product spaces $\Omega_h \times \mathrm{T}$ and $\underset{\sim}{\Omega}_h \times \mathrm{T}$ illustrated in Fig. 3.8.

We discretize Maxwell's first topological law by two different approaches arriving at the same discrete equation: First, we take a formal route making use of the rigorous definition of the primal grid discretization operators L^k and simply apply them to the differential version of Maxwell's first topological law (2.37a) on page 15. The second way is more intuitive and follows the standard route of the FIT by enforcing the integral version (2.38a)

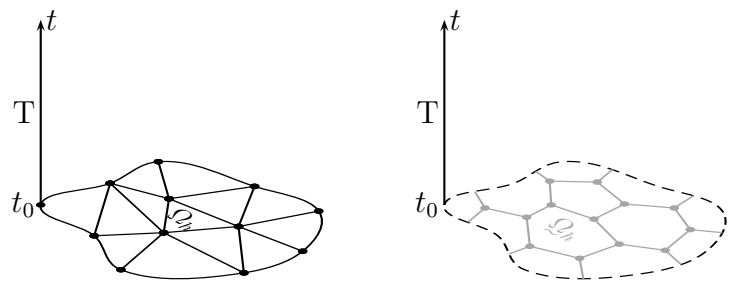

Fig. 3.8: Schematic sketch of the semi-discrete problem domains $\Omega_h \times \mathrm{T}$ and $\underset{\sim}{\Omega}_h \times \mathrm{T}$: The spatial domain Ω is discretized by the spatial primal grid Ω_h or the spatial dual grid $\underset{\sim}{\Omega}_h$ while the temporal domain T is kept continuous.

on page 16 on the finite set of faces of the primal grid. The two ways lead to the same discrete equations but emphasize different aspects of the discretization procedure.

First, we apply the 2-dimensional grid discretization operator L^2 defined by Definition 3.6 on page 37 to Maxwell's first topological law (2.37a) on page 15 in differential form and use the commuting property (3.38) on page 44 of the exterior derivatives with the grid discretization operators:

$$\begin{aligned} & \mathrm{L}^2 \operatorname{curl} \vec{E}(\vec{r},t) = \mathrm{L}^2 \left(-\partial_t \, \vec{B}(\vec{r},t) \right) && \forall\, t \in \mathrm{T} \\ \Leftrightarrow \quad & \mathbf{C}\, \mathrm{L}^1 \vec{E}(\vec{r},t) = -\partial_t \, \mathrm{L}^2 \vec{B}(\vec{r},t) && \forall\, t \in \mathrm{T} \end{aligned}$$

The grid discretization operators L^2 and the temporal derivative ∂_t commute due to the assumption of non-moving media and grids. Using the definition of the electric grid voltages $\widehat{\mathbf{e}}$ and the magnetic grid fluxes $\widehat{\widehat{\mathbf{b}}}$ in equations (3.22b) and (3.22c) on page 39, we arrive at *Maxwell's first topological grid law*:

$$\boxed{\mathbf{C}\, \widehat{\mathbf{e}}(t) = -\partial_t \, \widehat{\widehat{\mathbf{b}}}(t)} \qquad \forall\, t \in \mathrm{T} \tag{3.65}$$

We can also arrive at this equation by writing down the first Maxwell's topological equation (2.38a) on page 16 in integral form for each face S_i^2 of the primal grid:

$$\int_{S_i^2} \left(\operatorname{curl} \vec{E}(\vec{r},t) \right) \cdot \vec{n}_{S_i^2} \, \mathrm{d}A = \int_{S_i^2} -\partial_t \, \vec{B}(\vec{r},t) \cdot \vec{n}_{S_i^2} \, \mathrm{d}A \qquad \forall\, i \in [1..n^2],\, t \in \mathrm{T}$$

Using the continuous Gauss' law (2.18b) on page 11

$$\Leftrightarrow \quad \int_{\partial S_i^2} \vec{E}(\vec{r},t) \cdot \vec{t}_{\partial S_i^2} \, \mathrm{d}s = -\partial_t \int_{S_i^2} \vec{B}(\vec{r},t) \cdot \vec{n}_{S_i^2} \, \mathrm{d}A \qquad \forall\, i \in [1..n^2],\, t \in \mathrm{T}$$

the splitting of the left hand side integral into the contributions from the edges S_j^1 of the grid by employing the grid curl operator $\mathbf{C} = \mathbf{D}^1$ defined in equation (3.33b) on page 43

$$\Leftrightarrow \quad \sum_{j=1}^{n^1} C_{ij} \int_{S_j^1} \vec{E}(\vec{r},t) \cdot \vec{t}_{S_j^1} \, \mathrm{d}s = -\partial_t \int_{S_i^2} \vec{B}(\vec{r},t) \cdot \vec{n}_{S_i^2} \, \mathrm{d}A \quad \forall\, i \in [1..n^2],\, t \in \mathrm{T} \tag{3.66}$$

and finally the definition of the electric grid voltages $\widehat{\mathbf{e}}$ and the magnetic grid fluxes $\widehat{\widehat{\mathbf{b}}}$, we can collect all the equations and arrive at the same discrete equation:

$$\Leftrightarrow \qquad \mathbf{C}\,\widehat{\mathbf{e}}(t) = -\partial_t\,\widehat{\widehat{\mathbf{b}}}(t) \qquad\qquad \forall\, t \in \mathrm{T}$$

We basically have now done all the work by hand that was put before in the definition of the grid discretization operators L^k. But by this step-by-step approach, we are reminded that the integral version of Maxwell's first topological grid law is fulfilled exactly for each of the faces of the primal grid. It is easy to show that Maxwell's first topological grid law is then also exactly fulfilled on any combination of faces of the primal grid: When adding the corresponding equations, the inner edge contributions will cancel and leave only the terms corresponding to boundary edges of the union of the faces.

The discretization of Maxwell's second topological law is a bit more cumbersome, as we have not been rigorous enough in the definition of the dual grid, its cochains, and its exterior derivative operators: We did not include a discretization of the boundary of the domain $\partial\Omega$ and thus do not have a commuting property for the exterior derivatives with the dual grid discretization operators. In appendix A, an enhanced dual grid with such commuting properties is established, but this is fairly technical. So instead, we use the second possibility described above for discretizing the second Maxwell's topological law: We directly discretize its integral form. From the integral point of view, it will be very intuitive how to introduce the boundary terms into the standard FIT framework. By using a discrete equivalence principle, we do not even need any non-standard FIT notation to include the boundary terms.

Before we can start on this, we need to talk about the boundary of the domain $\partial\Omega$ in more detail, though. In the continuous case, we have introduced a splitting of the boundary $\partial\Omega$ into two disjunct boundary parts Γ_1 and Γ_2 on page 20. Electric boundary conditions are assumed on the boundary part Γ_1 and magnetic boundary conditions on the complementary boundary part Γ_2. Although this seem to be very simple boundary conditions, we are forced to introduce a rigorous boundary treatment paving the way for more complicated boundary conditions. We assume the primal grid Ω_h to be conforming to the boundary splitting, i.e. all boundary edges and faces are assumed to lie completely in one of the boundary parts as indicated in Fig. 3.9b[8]. Then we define the *primal boundary elements* as the elements lying in a boundary part Γ_j:

Definition 3.14. The primal grid elements lying in the boundary part Γ_j, i.e. for which we have

$$S_i^k \cap \overline{\Gamma}_j \neq \emptyset \tag{3.67}$$

are called *primal boundary grid elements* in the boundary part Γ_j. The set of all primal boundary grid elements in the boundary part Γ_j will be denoted by $\overline{\Gamma}_{j,h}$ and can be interpreted as a grid part of the grid Ω_h as defined on page 40. The number of k-dimensional primal boundary grid elements in the boundary grid part $\overline{\Gamma}_{j,h}$ will be denoted by $n^k_{\overline{\Gamma}_{j,h}}$ and the set of their indices by $\mathrm{I}^k_{\overline{\Gamma}_{j,h}}$.

[8] When only flat-faced polyhedral grid cells are available, as is the case later on, this restricts our domain Ω to be a flat-faced polyhedron. Otherwise, a polyhedral approximation of the boundary contour has to be introduced.

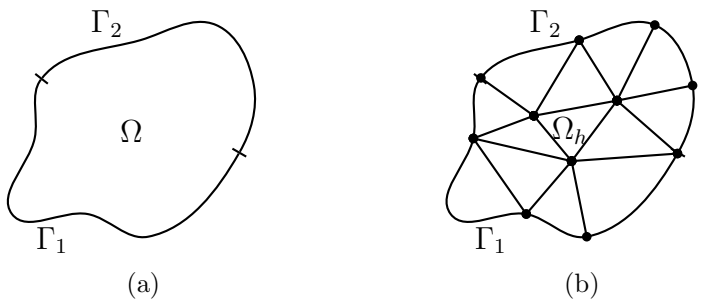

Fig. 3.9: Splitting of the boundary $\partial\Omega$. (a) The boundary of the domain Ω is split into two disjunct parts Γ_1 and Γ_2. We will later on assume electric boundary conditions on Γ_1 and magnetic boundary conditions on Γ_2. (b) The primal grid is assumed to conform to the boundary parts, i.e. all primal elements are either contained completely or not at all in a boundary part Γ_j.

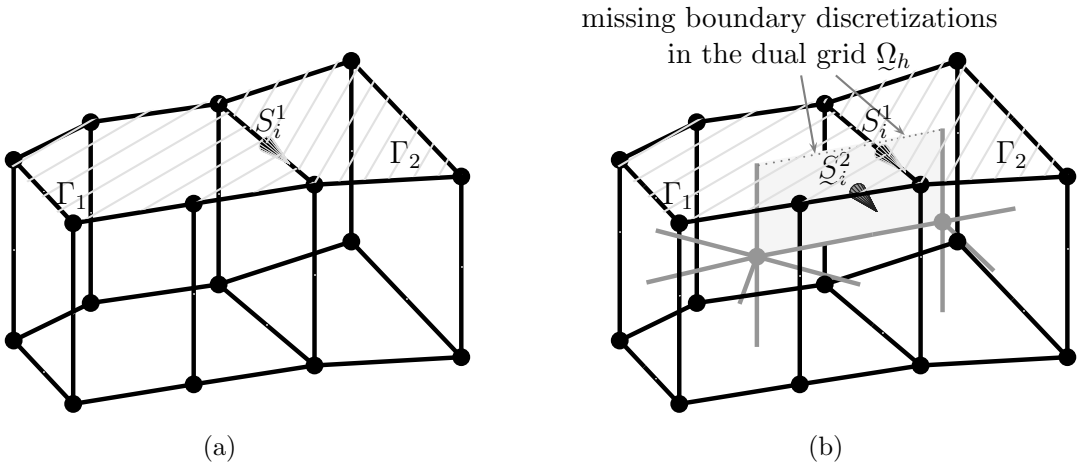

Fig. 3.10: Illustration of primal and dual grid elements at the boundary parts Γ_1 and Γ_2. (a) Part of the primal grid with the top faces in the boundary parts Γ_1 and Γ_2 as indicated. The primal edge S_i^1 belongs to both boundary parts Γ_1 and Γ_2 according to Definition 3.14. (b) Part of the dual grid is additionally shown. The dual face $\underset{\sim}{S}_i^2$ of the primal edge S_i^1 has incomplete boundary with respect to the boundary parts Γ_1 and Γ_2 according to Definition 3.15.

Note that the edges and vertices on the boundary of Γ_1 are also in the boundary of Γ_2 and thus lie in both boundary parts according to the above definition. Fig. 3.10a shows a boundary edge belonging to both boundary parts.

For the dual elements $\underset{\sim}{S}_i^{3-k}$ of primal boundary elements S_i^k, a part of the boundary discretization is missing. More specifically, the parts of the boundary of these dual elements lying in the boundary parts Γ_j

$$\partial \underset{\sim}{S}_i^{3-k} \cap \Gamma_j \tag{3.68}$$

are not discretized by the dual grid, as exemplified in Fig. 3.10b. In the discretization of Maxwell's second topological law, these elements have to be treated specifically. We call these elements *dual grid elements with incomplete boundary*:

Definition 3.15. For $k \in [0..2]$, we call the dual elements $\underset{\sim}{S}_i^{3-k}$ of the primal boundary elements S_i^k lying in the boundary part Γ_j *dual grid elements with incomplete boundary*

with respect to the boundary part Γ_j. The number of these elements will be denoted by $\underset{\sim}{n}^{2-k}_{\Gamma_{j,h}} = n^k_{\overline{\Gamma}_{j,h}}$ and the set of their indices by $\underset{\sim}{\mathrm{I}}^{2-k}_{\Gamma_{j,h}} = \mathrm{I}^k_{\overline{\Gamma}_{j,h}}$. Dual grid elements which are not incomplete with respect to any boundary part Γ_j are called *dual grid elements with complete boundary.*

An example of a dual face with incomplete boundary with respect to both boundary parts Γ_1 and Γ_2 is shown in Fig. 3.10b.

Now we can start to discretize Maxwell's second topological law (2.38b) on page 16 in integral form by enforcing it on the dual faces $\underset{\sim}{S}^k_i$ and using the continuous Gauss' law (2.16) on page 11:

$$\int_{\underset{\sim}{S}^2_i} \Big(\operatorname{curl} \vec{H}(\vec{r},t)\Big) \cdot \vec{n}_{\underset{\sim}{S}^2_i}\,\mathrm{d}A = \int_{\underset{\sim}{S}^2_i} \Big(\partial_t\, \vec{D}(\vec{r},t) + \vec{J}(\vec{r},t)\Big) \cdot \vec{n}_{\underset{\sim}{S}^2_i}\,\mathrm{d}A$$

$$\Leftrightarrow \qquad \int_{\partial \underset{\sim}{S}^2_i} \vec{H}(\vec{r},t) \cdot \vec{t}_{\partial \underset{\sim}{S}^2_i}\,\mathrm{d}s = \int_{\underset{\sim}{S}^2_i} \Big(\partial_t\, \vec{D}(\vec{r},t) + \vec{J}(\vec{r},t)\Big) \cdot \vec{n}_{\underset{\sim}{S}^2_i}\,\mathrm{d}A$$

We do have a problem discretizing the left hand term: As the dual grid only discretizes the interior $\mathring{\Omega}$ of the domain, the magnetic grid voltages $\underset{\sim}{\widehat{\mathbf{h}}}$ defined in equation (3.22g) on page 39 contain only the parts of the integration path that lie in the interior $\mathring{\Omega}$ of the domain. Thus for dual grid elements with incomplete boundary, we cannot directly rewrite the equation in terms of the magnetic grid voltages $\underset{\sim}{\widehat{\mathbf{h}}}$. So let us split the integral on the left hand side into the interior and the boundary contributions. We denote the interior part of the integration path by $\partial \underset{\sim}{S}^2_i \cap \mathring{\Omega}$ and assume its orientation induced by $\partial \underset{\sim}{S}^2_i$ as indicated in Fig. 3.11b. The boundary parts of the integration path are denoted by $\partial \underset{\sim}{S}^2_i \cap \Gamma_j$ again with the orientation induced by $\partial \underset{\sim}{S}^2_i$ as shown in Fig. 3.11b. Then the splitting of the left hand side integral reads:

$$\begin{aligned} \Leftrightarrow \quad & \int_{\partial \underset{\sim}{S}^2_i \cap \mathring{\Omega}} \vec{H}(\vec{r},t) \cdot \vec{t}_{\partial \underset{\sim}{S}^2_i}\,\mathrm{d}s + \sum_{j=1}^{2} \int_{\partial \underset{\sim}{S}^2_i \cap \Gamma_j} \vec{H}(\vec{r},t) \cdot \vec{t}_{\partial \underset{\sim}{S}^2_i \cap \Gamma_j}\,\mathrm{d}s \\ & = \int_{\underset{\sim}{S}^2_i} \Big(\partial_t\, \vec{D}(\vec{r},t) + \vec{J}(\vec{r},t)\Big) \cdot \vec{n}_{\underset{\sim}{S}^2_i}\,\mathrm{d}A \end{aligned} \tag{3.69}$$

With the definition of the dual grid curl operator $\underset{\sim}{\mathbf{C}} = \underset{\sim}{\mathbf{D}}^1$ and $\underset{\sim}{\widehat{\mathrm{h}}}_i$, $\underset{\sim}{\widehat{\widehat{\mathrm{d}}}}_i$, and $\underset{\sim}{\widehat{\widehat{\mathrm{j}}}}_i$ denoting the i-th component of the coefficient vectors $\underset{\sim}{\widehat{\mathbf{h}}}$, $\underset{\sim}{\widehat{\widehat{\mathbf{d}}}}$, and $\underset{\sim}{\widehat{\widehat{\mathbf{j}}}}$, defined in equations (3.22) on page 39, we can write in shorthand:

$$\Leftrightarrow \quad \sum_{j=1}^{\underset{\sim}{n}^1} \underset{\sim}{C}_{ij} \underset{\sim}{\widehat{\mathrm{h}}}_j(t) + \sum_{j=1}^{2} \int_{\partial \underset{\sim}{S}^2_i \cap \Gamma_j} \vec{H}(\vec{r},t) \cdot \vec{t}_{\partial \underset{\sim}{S}^2_i \cap \Gamma_j}\,\mathrm{d}s = \partial_t\, \underset{\sim}{\widehat{\widehat{\mathrm{d}}}}_i(t) + \underset{\sim}{\widehat{\widehat{\mathrm{j}}}}_i(t)$$

For all faces with complete boundary discretization, the boundary terms are zero as we have:

$$\partial \underset{\sim}{S}^2_i \cap \Gamma_j = \emptyset \tag{3.70}$$

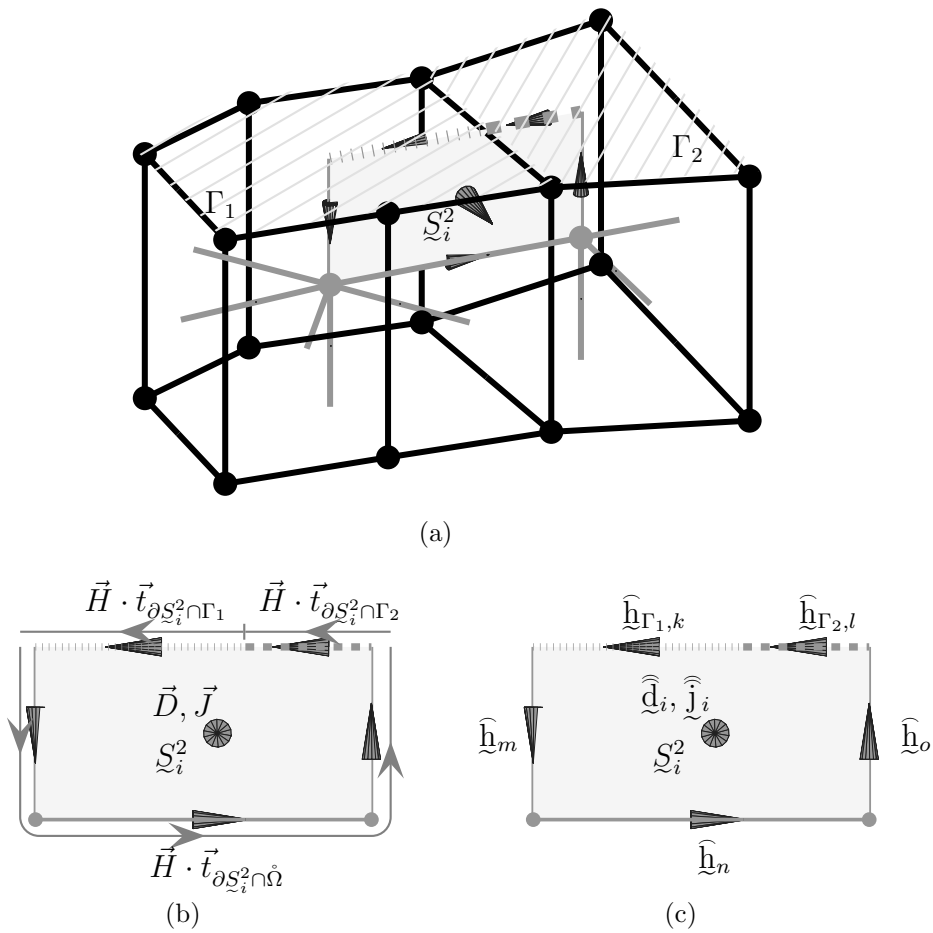

Fig. 3.11: Interpretations of the boundary terms as the missing magnetic field strength: (a) 3-dimensional view on the boundary parts. (b) 2-dimensional view on the dual face $\underset{\sim}{S}_i^2$ with incomplete boundary. The integral of the magnetic field strength $\vec{H}$ is split into the interior contribution and the contributions from the boundary parts Γ_1 and Γ_2 in equation (3.69). (c) The magnetic boundary grid voltages $\widehat{\underset{\sim}{\mathrm{h}}}_{\Gamma_1,k}$ and $\widehat{\underset{\sim}{\mathrm{h}}}_{\Gamma_2,l}$ are introduced in equations (3.71) to include the boundary contributions in equation (3.73). The indices k and l are such that $\underset{\sim}{\mathrm{I}}^1_{\underset{\sim}{\Gamma}_{1,h}}(k)=\underset{\sim}{\mathrm{I}}^1_{\underset{\sim}{\Gamma}_{2,h}}(l)=i$. (For better overview, the outer orientations of the dual grid elements are replaced consistently by an inner orientation in the figures.)

For the faces with incomplete boundary, it seems natural to introduce *dual boundary magnetic grid voltages* $\widehat{\underset{\sim}{\mathbf{h}}}_{\Gamma_j}$ discretizing the magnetic voltages along the missing boundary parts Γ_j:

$$\widehat{\underset{\sim}{\mathbf{h}}}_{\Gamma_j}(t)\equiv\left[\widehat{\underset{\sim}{\mathrm{h}}}_{\Gamma_j,l}(t)\right]_{l\in[1..\underset{\sim}{n}^1_{\underset{\sim}{\Gamma}_{j,h}}]}, \qquad \forall\, j\in[1,2] \tag{3.71a}$$

$$\widehat{\underset{\sim}{\mathrm{h}}}_{\Gamma_j,l}(t)\equiv\int_{\partial\underset{\sim}{S}_i^2\cap\Gamma_j}\vec{H}(\vec{r},t)\cdot\vec{t}_{\partial\underset{\sim}{S}_i^2\cap\Gamma_j}\,\mathrm{d}s,\quad i=\underset{\sim}{\mathrm{I}}^1_{\underset{\sim}{\Gamma}_{j,h}}(l),\quad \forall\, l\in[1..\underset{\sim}{n}^1_{\underset{\sim}{\Gamma}_{j,h}}],j\in[1,2] \tag{3.71b}$$

where $\underset{\sim}{\mathrm{I}}^1_{\underset{\sim}{\Gamma}_{j,h}}(l)$ denotes the l-th index in the index set $\underset{\sim}{\mathrm{I}}^1_{\underset{\sim}{\Gamma}_{j,h}}=\mathrm{I}^1_{\overline{\Gamma}_{j,h}}$. To get the above defined dual boundary magnetic grid voltages $\widehat{\underset{\sim}{\mathrm{h}}}_{\Gamma_j,l}$ into the correct places of our equation, we can use the primal trace operator $\mathbf{T}^1_{\overline{\Gamma}_{j,h}}$ onto the grid parts $\overline{\Gamma}_{j,h}$. Maxwell's second topological

law enforced on a dual grid face $\underset{\sim}{S}_i^2$ thus reads:

$$\sum_{j=1}^{\underset{\sim}{n}^1} \underset{\sim}{C}_{ij} \widehat{\underset{\sim}{\mathrm{h}}}_j(t) + \sum_{j=1}^{2} \sum_{l=1}^{n^1_{\overline{\Gamma}_{j,h}}} \left(\mathbf{T}^1_{\overline{\Gamma}_{j,h}}\right)_{li} \widehat{\underset{\sim}{\mathrm{h}}}_{\Gamma_j,l}(t) = \partial_t \widehat{\widehat{\underset{\sim}{\mathrm{d}}}}_i(t) + \widehat{\widehat{\underset{\sim}{\mathrm{j}}}}_i(t) \tag{3.72}$$

In Fig. 3.11c, we see an example of this local equation for a dual grid face incomplete with respect to both boundary parts Γ_1 and Γ_2. Collecting these local equations for all dual faces $\underset{\sim}{S}_i^2$ in matrix form renders *Maxwell's second topological grid law*:

$$\boxed{\underset{\sim}{\mathbf{C}}\, \widehat{\underset{\sim}{\mathbf{h}}}(t) + \sum_{j=1}^{2} \left(\mathbf{T}^1_{\overline{\Gamma}_{j,h}}\right)^{\mathrm{T}} \widehat{\underset{\sim}{\mathbf{h}}}_{\Gamma_j}(t) = \partial_t \widehat{\widehat{\underset{\sim}{\mathbf{d}}}}(t) + \widehat{\widehat{\underset{\sim}{\mathbf{j}}}}(t)} \qquad \forall\, t \in \mathrm{T} \tag{3.73}$$

This does look almost like the standard FIT version of Maxwell's second topological law, except for the term of the boundary magnetic grid voltages $\widehat{\underset{\sim}{\mathbf{h}}}_{\Gamma_j}$. This term is usually omitted, as it either is assumed to be zero for homogeneous magnetic boundary conditions or the corresponding equations are deleted from the system for electric boundary conditions. But for general boundary conditions or when the boundary quantities are needed e.g. for coupling to other domains, these terms are important and must not be neglected.

There is another interpretation of the boundary magnetic grid voltages $\widehat{\underset{\sim}{\mathbf{h}}}_{\Gamma_j}$. In the continuous case, we can introduce equivalent boundary current sheets $\vec{J}_{\Gamma_j}$ which force the tangential magnetic field to jump to zero just outside the domain Ω as indicated in Fig. 3.12b:

$$\vec{J}_{\Gamma_j} \equiv -\vec{n}_{\Gamma_j} \times \vec{H} \tag{3.74}$$

where $\vec{n}_{\Gamma_j}$ denotes the outward pointing normal unit vector on the boundary part Γ_j. In the discrete setting, this is even more intuitive than in the continuous case: Defining the *equivalent boundary grid current parts* $\widehat{\widehat{\underset{\sim}{\mathbf{j}}}}_{\Gamma_j}$ as

$$\widehat{\widehat{\underset{\sim}{\mathbf{j}}}}_{\Gamma_j}(t) \equiv -\left(\mathbf{T}^1_{\overline{\Gamma}_{j,h}}\right)^{\mathrm{T}} \widehat{\underset{\sim}{\mathbf{h}}}_{\Gamma_j}(t) \tag{3.75}$$

we can rewrite Maxwell's second topological grid law (3.73) as:

$$\boxed{\underset{\sim}{\mathbf{C}}\, \widehat{\underset{\sim}{\mathbf{h}}}(t) = \partial_t \widehat{\widehat{\underset{\sim}{\mathbf{d}}}}(t) + \widehat{\widehat{\underset{\sim}{\mathbf{j}}}}(t) + \sum_{j=1}^{2} \widehat{\widehat{\underset{\sim}{\mathbf{j}}}}_{\Gamma_j}(t)} \qquad \forall\, t \in \mathrm{T} \tag{3.76}$$

A local example for this interpretation is given in Fig. 3.12c. Note that the equivalent boundary grid current parts $\widehat{\widehat{\underset{\sim}{\mathbf{j}}}}_{\Gamma_j}$ only contain non-zero entries for indices corresponding to a dual face with incomplete boundary. Thus if $\mathbf{T}^1_{\Omega_h \setminus \overline{\Gamma}_{j,h}}$ denotes the primal trace operator onto all primal edges except for those on the boundary part $\overline{\Gamma}_{j,h}$, we have:

$$\mathbf{T}^1_{\Omega_h \setminus \overline{\Gamma}_{j,h}} \widehat{\widehat{\underset{\sim}{\mathbf{j}}}}_{\Gamma_j}(t) = 0 \qquad \forall\, t \in \mathrm{T} \tag{3.77}$$

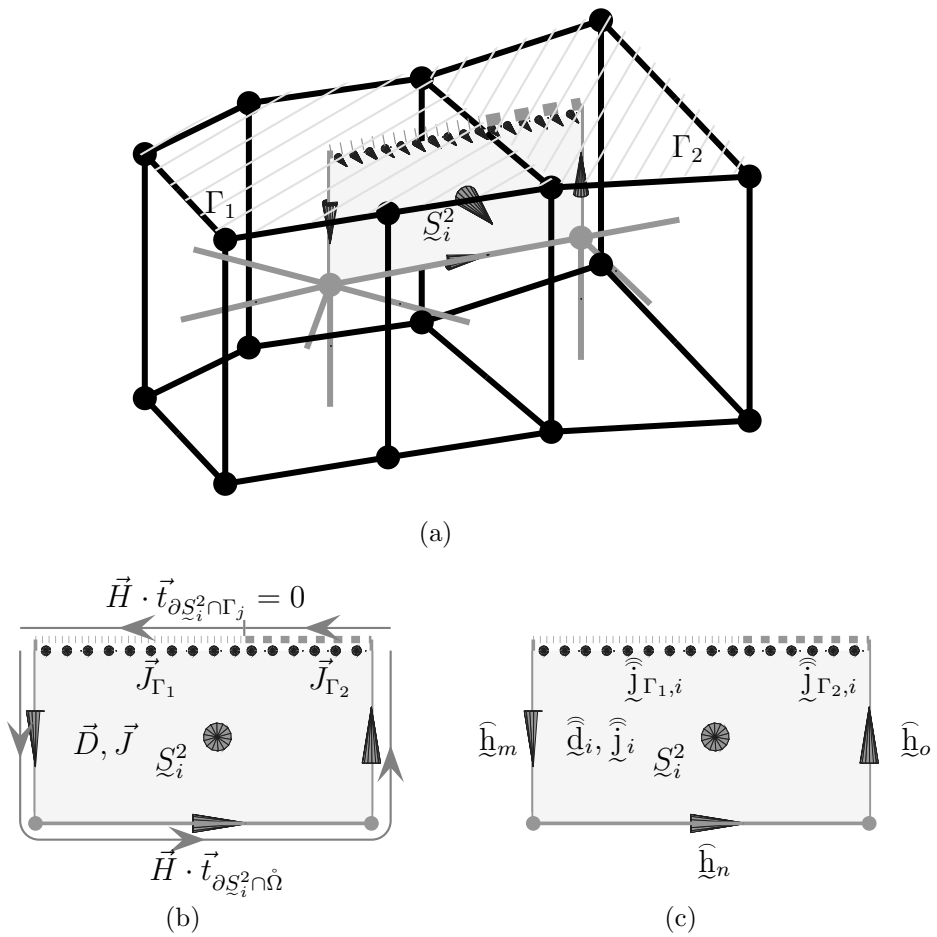

Fig. 3.12: Interpretations of the boundary terms as equivalent boundary currents: (a) 3-dimensional view on the boundary parts (c) 2-dimensional view on the dual face $\underset{\sim}{S}_i^2$ with open boundary. The equivalent boundary current sheets $\vec{J}_{\Gamma_j}$ force the tangential magnetic field strengths $\vec{H} \cdot \vec{t}_{\partial \underset{\sim}{S}_i^2 \cap \Gamma_j}$ just outside the calculation domain to zero. (c) The equivalent boundary grid currents $\hat{\hat{\underset{\sim}{\mathrm{j}}}}_{\Gamma_1,i}$ and $\hat{\hat{\underset{\sim}{\mathrm{j}}}}_{\Gamma_2,i}$ are introduced in equation (3.75) to include the boundary contributions in equation (3.76).

To even further shorten the notation, we define the complete *equivalent boundary grid current* $\hat{\hat{\underset{\sim}{\mathbf{j}}}}_{\partial\Omega}(t)$ as:

$$\hat{\hat{\underset{\sim}{\mathbf{j}}}}_{\partial\Omega}(t) \equiv \sum_{j=1}^{2} \hat{\hat{\underset{\sim}{\mathbf{j}}}}_{\Gamma_j}(t) \tag{3.78}$$

and write Maxwell's second topological grid law henceforth as

$$\boxed{\underset{\sim}{\mathbf{C}}\, \hat{\underset{\sim}{\mathbf{h}}}(t) = \partial_t\, \hat{\hat{\underset{\sim}{\mathbf{d}}}}(t) + \hat{\hat{\underset{\sim}{\mathbf{j}}}}(t) + \hat{\hat{\underset{\sim}{\mathbf{j}}}}_{\partial\Omega}(t)} \qquad \forall\, t \in \mathrm{T} \tag{3.79}$$

This form allows us to work with the standard FIT notation and minimal overhead.

3.2.2 Maxwell's Discrete Material Laws

For simplicity, we only consider local, linear, isotropic, dispersion-free, and lossless material coefficients and non-moving media as in the continuous case[9]. Further on, we assume the material coefficients to be constant in each primal grid cell. The permittivity and reluctivity in the primal cell S_i^3 are denoted by ε_i and ν_i, respectively. We derive Maxwell's discrete material laws also called Maxwell's metric grid equations in the form:

$$\boxed{\underset{\sim}{\widehat{\mathbf{d}}}(t) = \mathbf{M}_\varepsilon\, \widehat{\mathbf{e}}(t)} \qquad \forall\, t \in \mathrm{T} \tag{3.80a}$$

$$\boxed{\underset{\sim}{\widehat{\mathbf{h}}}(t) = \mathbf{M}_\nu\, \widehat{\mathbf{b}}(t)} \qquad \forall\, t \in \mathrm{T} \tag{3.80b}$$

Maxwell's discrete material laws only approximate the continuous material laws (2.39a) and (2.39b) on page 16. The material matrices $\mathbf{M}_\varepsilon$ and $\mathbf{M}_\nu$ will be realizations of primal discrete hodge operators $\mathbf{M}_\alpha^1$ and $\mathbf{M}_\alpha^2$, respectively, defined in Definition 3.11 on page 48. Therefore, they will be symmetric positive definite and thus invertible. We will use the terms *material matrices*, *discrete material relations*, and *discrete hodge operators* interchangeably. The discrete material laws connect the quantities of the primal and the dual grid and, to stress this point, are in contrast to the topological laws in general only approximations to their continuous counterparts.

Many commonly employed simulation schemes for differential equations can be interpreted in terms of the general FIT outlined here. They only differ in the specific choice of discrete material relations they use. The standard FIT on orthogonal (structured and unstructured) grids [92], the FIT on non-orthogonal grids [79], the cell-method [62] as well as certain versions of the Finite Volume and the Finite Element Method [63] and completely new geometrical methods [20] fit the general FIT framework as outlined here. The Mimetic Finite Difference Methods [6] [50] provide a similar framework to the FIT, also incorporating all these methods. Instead of emphasizing the discrete material relations, the Mimetic Finite Difference Methods emphasize a discrete realization of the inner product as basic tool, though.

In this thesis, we only discuss two different types of discrete material operators: The standard FIT operators for dual orthogonal grids are stated here due to their simplicity. The standard Whitney-FEM operators will be stated and extended to general polyhedral grids in chapter 4.

Standard FIT Material Operators

The standard FIT [92] only treats a fairly special class of grids: It requires a consistent grid and a choice of a dual grid where the dual edges/faces cut the primal faces/edges orthogonally. We will call such grids *dual orthogonal grids*. The discrete material laws for

[9] It is possible to extend the discrete material laws to more general media. Better approximations for material coefficients varying in a single cell are also available: In the standard FIT, it is possible to account for special tetrahedral fillings [85, pp. 16], edge- or face-average the material relations [35, pp. 77] or use conformal boundary techniques [101]. In the FEM, any square integrable material coefficients can be treated.

such grids can take a very simple form: They can be stated with diagonal material matrices[10]. We reproduce the standard FIT material matrices here as a specific example for discrete material relations and to state their local splitting as proposed in Definition 3.12 on page 49 which will be employed in the space and time discrete Newmark-Θ scheme on page 79.

The standard FIT hodge operators use the standard Riemannian measure of the primal and dual grid elements, i.e. their volume, surface, or length. We denote the standard Riemannian measure of the primal grid element S_i^k by $\left|S_i^k\right|$ and for the dual grid element $\underset{\sim}{S}_i^k$ by $\left|\underset{\sim}{S}_i^k\right|$.

For deriving the standard FIT (sFIT) permittivity matrix $\mathbf{M}_{\mathrm{sFIT},\varepsilon}$, let us consider the primal edge S_i^1 cutting its dual face $\underset{\sim}{S}_i^2$ orthogonally, as seen in Fig. 3.13a. Introducing an approximate electric flux density $D_{i,\mathrm{n}}$ normal on the dual face $\underset{\sim}{S}_i^2$ and an approximate electric field strength $E_{i,\mathrm{t}}$ tangential to the primal edge S_i^1 at the point of intersection, we approximate the first material law (2.39a) on page 16 by:

$$\frac{\underset{\sim}{\widehat{\widehat{\mathrm{d}}}}_i}{\left|\underset{\sim}{S}_i^2\right|} \equiv D_{i,\mathrm{n}} \approx \overline{\varepsilon}_i E_{i,\mathrm{t}} \equiv \overline{\varepsilon}_i \frac{\widehat{\mathrm{e}}_i}{\left|S_i^1\right|} \qquad \forall\, i \in [1..n^1] \tag{3.81}$$

where $\overline{\varepsilon}_i$ is the face-averaged permittivity:

$$\overline{\varepsilon}_i \equiv \sum_{m=1}^{n^3} \varepsilon_m \frac{\left|\underset{\sim}{S}_i^2 \cap S_m^3\right|}{\left|\underset{\sim}{S}_i^2\right|}, \qquad \forall\, i \in [1..n^1] \tag{3.82}$$

The term $\underset{\sim}{S}_i^2 \cap S_m^3$ signifies the intersection of the dual face $\underset{\sim}{S}_i^2$ with the primal cell S_m^3 and the term $|\underset{\sim}{S}_i^2 \cap S_m^3|$ its area. For a discussion of the approximation properties of this material relation, see [85, pp. 14].

Defining the diagonal permittivity matrix $\mathbf{M}_{\mathrm{sFIT},\varepsilon}$ as

$$\left(\mathbf{M}_{\mathrm{sFIT},\varepsilon}\right)_{ij} \equiv \delta_{ij}\overline{\varepsilon}_i \frac{\left|\underset{\sim}{S}_i^2\right|}{\left|S_i^1\right|} = \sum_{m=1}^{n^3} \delta_{ij}\varepsilon_m \frac{\left|\underset{\sim}{S}_i^2 \cap S_m^3\right|}{\left|\underset{\sim}{S}_i^2\right|}, \qquad \forall\, i,j \in [1..n^1] \tag{3.83}$$

where δ_{ij} denotes the Kronecker Delta, we can collect the discrete approximations of Maxwell's first material relation in equation (3.81) as:

$$\underset{\sim}{\widehat{\widehat{\mathbf{d}}}} = \mathbf{M}_{\mathrm{sFIT},\varepsilon}\, \widehat{\mathbf{e}} \tag{3.84}$$

The definition of the permittivity matrix in equation (3.83) naturally leads to the following splitting into cell-wise permittivity matrices $\mathbf{M}_{\mathrm{sFIT},\varepsilon}^{1,m}$ for each primal cell S_m^3 fulfilling the splitting formula (3.58) on page 48:

$$\left(\mathbf{M}_{\mathrm{sFIT},\varepsilon}^{1,m}\right)_{ij} \equiv \delta_{ij}\varepsilon_m \frac{\left|\underset{\sim}{S}_i^2 \cap S_m^3\right|}{\left|\underset{\sim}{S}_i^2\right|}, \qquad \forall\, i,j \in [1..n^1], \quad \forall\, m \in [1..n^3] \tag{3.85}$$

[10] A short reasoning for this possibility from the point of view of convergence analysis is given in [47, p. 256].

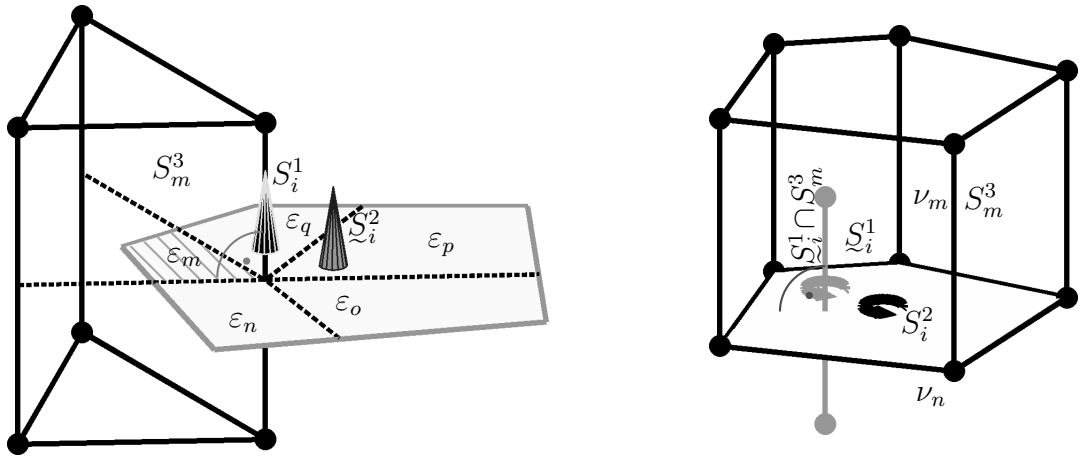

(a) Illustration for the first material law (3.83). The dual face part $\underset{\sim}{S}_i^2 \cap S_m^3$ is shown hatched.

(b) Illustration for the second material law (3.89). The dual edge part $\underset{\sim}{S}_i^1 \cap S_m^3$ is only the top part of the dual edge $\underset{\sim}{S}_i^1$ that lies inside the primal cell S_m^3.

Fig. 3.13: Illustrations for the standard FIT material laws requiring dual orthogonal grids. Each primal grid cell S_m^3 (shown in black) is assumed to be filled with a material with constant permittivity ε_m and constant reluctivity ν_m. The faces and edges of the dual grid (shown in gray) thus contain parts with different material constants. This leads to the material averaging in equations (3.82) and (3.88).

The local permittivity matrices $\mathbf{M}_{\mathrm{sFIT},\varepsilon}^{1,m}$ have only entries for the primal edges in the boundary of the grid element S_m^3 and their dual faces. Thus we can write them according to equation (3.60) on page 48 with the reduced local permittivity matrices $\widehat{\mathbf{M}}_{\mathrm{sFIT},\varepsilon}^{1,m}$:

$$\widehat{\mathbf{M}}_{\mathrm{sFIT},\varepsilon}^{1,m} = \mathbf{T}_{S_m^3}^1 \, \mathbf{M}_{\mathrm{sFIT},\varepsilon}^{1,m} \left(\mathbf{T}_{S_m^3}^1\right)^{\mathrm{T}} \tag{3.86}$$

For deriving the standard FIT reluctivity matrix $\mathbf{M}_{\mathrm{sFIT},\nu}$, let us consider the primal face S_i^2 being cut orthogonally by its dual edge $\underset{\sim}{S}_i^1$, as seen in Fig. 3.13b. Introducing an approximate magnetic field strength component $H_{i,\mathrm{t}}$ tangential to the dual edge $\underset{\sim}{S}_i^1$ and approximate magnetic flux density component $B_{i,\mathrm{n}}$ normal to the primal face S_i^2 at the point of intersection, we approximate the second material law (2.39b) on page 16 by:

$$\frac{\widehat{\underset{\sim}{\mathrm{h}}}_i}{\left|\underset{\sim}{S}_i^1\right|} \equiv H_{i,\mathrm{t}} \approx \overline{\nu}_i B_{i,\mathrm{n}} \equiv \overline{\nu}_i \frac{\widehat{\widehat{\mathrm{b}}}_i}{\left|S_i^2\right|}, \qquad \forall\, i \in [1..n^2] \tag{3.87}$$

where $\overline{\nu}_i$ is the edge-averaged reluctivity:

$$\overline{\nu}_i = \sum_{m=1}^{n^3} \nu_m \frac{\left|\underset{\sim}{S}_i^1 \cap S_m^3\right|}{\left|\underset{\sim}{S}_i^1\right|}, \qquad \forall\, i \in [1..n^2] \tag{3.88}$$

For a discussion of the approximation properties of this material relation, see again [85, pp. 14].

Defining the diagonal reluctivity matrix $\mathbf{M}_{\mathrm{sFIT},\nu}$ as

$$\left(\mathbf{M}_{\mathrm{sFIT},\nu}\right)_{ij} \equiv \delta_{ij}\overline{\nu}_i \frac{\left|\underset{\sim}{S}_i^1\right|}{\left|S_i^2\right|} = \sum_{m=1}^{n^3} \delta_{ij}\nu_m \frac{\left|\underset{\sim}{S}_i^1 \cap S_m^3\right|}{\left|\underset{\sim}{S}_i^1\right|}, \qquad \forall\, i,j \in [1..n^2] \tag{3.89}$$

we can collect the discrete approximations of Maxwell's second material law in equation (3.87) as:

$$\widehat{\underset{\sim}{\mathbf{h}}} = \mathbf{M}_{\mathrm{sFIT},\nu}\, \widehat{\overline{\mathbf{b}}} \tag{3.90}$$

We again see that the following local reluctivity matrices $\mathbf{M}^{2,m}_{\mathrm{sFIT},\nu}$ fulfill the splitting formula (3.58):

$$\left(\mathbf{M}^{2,m}_{\mathrm{sFIT},\nu}\right)_{ij} \equiv \delta_{ij}\nu_m \frac{\left|\underset{\sim}{S}_i^1 \cap S_m^3\right|}{\left|\underset{\sim}{S}_i^1\right|}, \qquad \forall\, i,j \in [1..n^2], \quad \forall\, m \in [1..n^3] \tag{3.91}$$

and these can again be written according to equation (3.60) with the reduced local reluctivity matrices $\widehat{\mathbf{M}}^{2,m}_{\mathrm{sFIT},\nu}$:

$$\widehat{\mathbf{M}}^{2,m}_{\mathrm{sFIT},\nu} = \mathbf{T}^2_{S_m^3}\, \mathbf{M}^{2,m}_{\mathrm{sFIT},\nu} \left(\mathbf{T}^2_{S_m^3}\right)^{\mathrm{T}} \tag{3.92}$$

Theorem 3.6. *The material matrices $\mathbf{M}_{\mathrm{sFIT},\varepsilon}$ and $\mathbf{M}_{\mathrm{sFIT},\nu}$ defined in equations (3.83) and (3.89) as well as the reduced local material matrices $\widehat{\mathbf{M}}^{1,m}_{\mathrm{sFIT},\varepsilon}$ and $\widehat{\mathbf{M}}^{2,m}_{\mathrm{sFIT},\nu}$ defined in equations (3.86) and (3.92) are symmetric positive definite.*

Proof. The matrices $\mathbf{M}_{\varepsilon,\mathrm{FIT}}$ and $\mathbf{M}_{\nu,\mathrm{FIT}}$ are diagonal and their entries strictly positive. Thus all their eigenvalues are positive and they are symmetric positive definite. For the reduced local material matrices, the same reasoning holds. □

3.2.3 Maxwell's Topological Properties

In this chapter, we derive properties depending solely on Maxwell's discrete topological laws (3.65) on page 51 and (3.79) on page 57. These properties are called Maxwell's topological properties and do not require Maxwell's discrete material laws or any metric tools. The presentation is in parallel to the continuous case in chapter 2.2.3.

Conservation of Charge

As in the continuous case on page 17, we can derive from each of Maxwell's topological grid equations a conserved discrete quantity. We will call these quantities the electric and magnetic grid charge.

Applying the primal grid divergence operator $\mathbf{S}$ to Maxwell's first topological law (3.65) on page 51, using the fact that the operators $\mathbf{S}$ and ∂_t commute and the sequence property (3.42) on page 45, we get:

$$\begin{aligned} & \mathbf{S}\,\mathbf{C}\,\widehat{\mathbf{e}}(t) = \mathbf{S}\left(-\partial_t\,\widehat{\mathbf{b}}(t)\right) \\ \Leftrightarrow \qquad & 0 = -\partial_t\,\mathbf{S}\,\widehat{\mathbf{b}}(t) \end{aligned} \tag{3.93}$$

Defining the magnetic grid charge $\widehat{\widehat{\boldsymbol{\varrho}}}_m(t)$ as

$$\widehat{\widehat{\boldsymbol{\varrho}}}_m(t) \equiv \mathbf{S}\,\widehat{\mathbf{b}}(t) \tag{3.94}$$

this states the conservation of the magnetic grid charge:

$$\boxed{\partial_t\,\mathbf{S}\,\widehat{\mathbf{b}}(t) = \partial_t\,\widehat{\widehat{\boldsymbol{\varrho}}}_m(t) = 0} \tag{3.95}$$

Remark 3.5. The discrete definition of the magnetic grid charge in equation (3.94) was completely independent of the definition of the continuous magnetic charge density ϱ_m in equation (2.42a) on page 17. Nevertheless, both definitions are consistent under the grid projections defined in equation (3.22c) and (3.22e) on page 39 due to the commuting property of the exterior derivative with the primal grid discretization operators given in Theorem 3.2 on page 44: Starting with the definition of the magnetic grid charge $\widehat{\widehat{\boldsymbol{\varrho}}}_m$ as grid projection of the continuous magnetic charge density ϱ_m

$$\widehat{\widehat{\boldsymbol{\varrho}}}_m(t) = \mathrm{L}^3\varrho_m(\vec{r},t) \tag{3.96}$$

using the definition of the continuous magnetic charge density ϱ_m in equation (2.42a) on page 17

$$= \mathrm{L}^3\,\mathrm{div}\,\vec{B}(\vec{r},t) \tag{3.97}$$

and the commuting property of the continuous and discrete divergence operators with the grid discretization operators L^k given in equation (3.38) on page 44, we arrive at the same definition as above:

$$= \mathbf{S}\,\mathrm{L}^2\vec{B}(\vec{r},t) = \mathbf{S}\,\widehat{\mathbf{b}}(t) \tag{3.98}$$

As a consequence, we know that the conservation of magnetic charge is exactly reproduced for each cell of the primal grid (and for any combination of primal cells) in the discrete setting by equation (3.95) and could have also been derived by a direct grid discretization of its continuous equivalent (2.43a) on page 17.

To derive the conservation law for the electric grid charge on the dual grid, we apply the dual grid divergence operator $\underset{\sim}{\mathbf{S}}$ to Maxwell's second topological grid law (3.79) on page 57. Using the sequence property for the dual grid in equation (3.43) on page 45 and commutativity of the time derivative with the dual grid divergence, we conclude:

$$\begin{aligned} & \underset{\sim}{\mathbf{S}}\,\underset{\sim}{\mathbf{C}}\,\widehat{\underset{\sim}{\mathbf{h}}}(t) = \underset{\sim}{\mathbf{S}}\left(\partial_t\,\widehat{\underset{\sim}{\mathbf{d}}}(t) + \widehat{\underset{\sim}{\mathbf{j}}}(t) + \widehat{\underset{\sim}{\mathbf{j}}}_{\partial\Omega}(t)\right) \\ \Leftrightarrow \qquad & 0 = \partial_t\,\underset{\sim}{\mathbf{S}}\,\widehat{\underset{\sim}{\mathbf{d}}}(t) + \underset{\sim}{\mathbf{S}}\,\widehat{\underset{\sim}{\mathbf{j}}}(t) + \underset{\sim}{\mathbf{S}}\,\widehat{\underset{\sim}{\mathbf{j}}}_{\partial\Omega}(t) \end{aligned} \tag{3.99}$$

Defining the electric grid charge $\underset{\sim}{\widehat{\widehat{\boldsymbol{\varrho}}}}{}_e^*(t)$ as

$$\underset{\sim}{\widehat{\widehat{\boldsymbol{\varrho}}}}{}_e^*(t) \equiv \underset{\sim}{\mathbf{S}}\, \underset{\sim}{\widehat{\widehat{\mathbf{d}}}}(t) \tag{3.100}$$

we arrive at the following conservation law for the electric grid charge:

$$\boxed{\partial_t\, \underset{\sim}{\widehat{\widehat{\boldsymbol{\varrho}}}}{}_e^*(t) = -\underset{\sim}{\mathbf{S}}\, \underset{\sim}{\widehat{\widehat{\mathbf{j}}}}(t) - \underset{\sim}{\mathbf{S}}\, \underset{\sim}{\widehat{\widehat{\mathbf{j}}}}{}_{\partial\Omega}(t)} \tag{3.101}$$

Remark 3.6. As suggested by the superscript $*$ for the defined electric grid charge $\underset{\sim}{\widehat{\widehat{\boldsymbol{\varrho}}}}{}_e^*$, the charge definition is not consistent with the electric grid charge $\underset{\sim}{\widehat{\widehat{\boldsymbol{\varrho}}}}{}_e$ defined in equation (3.22j). The reason is again the defect of the dual grid at the boundary $\partial\Omega$ of the domain: The electric grid charge $\underset{\sim}{\widehat{\widehat{\boldsymbol{\varrho}}}}{}_e^*$ does only count the electric fluxes through the (interior) dual faces, as is apparent in its definition in equation (3.100). Thus the electric fluxes through the boundary parts Γ_1 and Γ_2 are missing. We can interpret the electric grid charge $\underset{\sim}{\widehat{\widehat{\boldsymbol{\varrho}}}}{}_e^*$ to already contain an equivalent electric boundary charge that forces the normal electric flux density to jump to zero outside the domain.

Equivalently, the current divergence term $\underset{\sim}{\mathbf{S}}\, \underset{\sim}{\widehat{\widehat{\mathbf{j}}}}$ in the conservation law for the electric grid charge (3.101) is missing the electric currents flowing through the boundary parts Γ_1 and Γ_2. Both boundary terms, the missing electric fluxes and the electric currents, are contained in the term $\underset{\sim}{\mathbf{S}}\, \underset{\sim}{\widehat{\widehat{\mathbf{j}}}}{}_{\partial\Omega}$, though. This term represents the surface divergence of the equivalent boundary currents $\underset{\sim}{\widehat{\widehat{\mathbf{j}}}}{}_{\partial\Omega}$. Thus the conservation law for the electric grid charge (3.101) is correct, but one has to be careful with its interpretation. Defining boundary electric grid fluxes and boundary electric grid currents in parallel to the boundary magnetic grid voltages $\underset{\sim}{\widehat{\mathbf{h}}}_{\Gamma_j}$ in equation (3.71), one can arrive at a formulation where the terms do have direct equivalence to the continuous version in equation (2.43b) on page 17.

Potential Formulations

In parallel to the introduction of a continuous magnetic vector potential on page 17, we will show that under the assumption of absence of magnetic charges, we can introduce a magnetic vector potential $\widehat{\mathbf{a}}_m$ and rewrite the electric grid voltages $\widehat{\mathbf{e}}$ in terms of this magnetic vector potential and an electric scalar potential $\boldsymbol{\varphi}_e$.

Assuming no magnetic charges to exist at the time t_0, we get from the conservation law (3.95) that the magnetic charge is zero at all times:

$$\widehat{\widehat{\boldsymbol{\varrho}}}_m(t) = \mathbf{S}\, \widehat{\widehat{\mathbf{b}}}(t) = \widehat{\widehat{\boldsymbol{\varrho}}}_m(t_0) = 0 \qquad \forall\, t \in \mathrm{T} \tag{3.102}$$

Thus by the discrete Poincaré Lemma (3.47) on page 46 we know a magnetic vector potential $\widehat{\mathbf{a}}_m$ to exist, such that

$$\widehat{\widehat{\mathbf{b}}}(t) = \mathbf{C}\, \widehat{\mathbf{a}}_m(t) \qquad \forall\, t \in \mathrm{T} \tag{3.103}$$

Plugging this into Maxwell's first topological grid law (3.65) on page 51, we arrive at:

$$\begin{aligned} \mathbf{C}\, \widehat{\mathbf{e}}(t) &= -\partial_t \widehat{\widehat{\mathbf{b}}}(t) = -\partial_t\, \mathbf{C}\, \widehat{\mathbf{a}}_m(t) && \forall\, t \in \mathrm{T} \\ \Leftrightarrow \qquad \mathbf{C}\, (\widehat{\mathbf{e}}(t) + \partial_t \widehat{\mathbf{a}}_m(t)) &= 0 && \forall\, t \in \mathrm{T} \end{aligned} \tag{3.104}$$

Now the discrete Poincaré Lemma in its form (3.46) on page 46 assures existence of an electric scalar potential $\boldsymbol{\varphi}_e$ such that:

$$\begin{aligned} & \widehat{\mathbf{e}}(t) + \partial_t \widehat{\mathbf{a}}_m(t) = -\,\mathbf{G}\,\boldsymbol{\varphi}_e(t) && \forall\, t \in \mathrm{T} \\ \Leftrightarrow \quad & \widehat{\mathbf{e}}(t) = -\partial_t \widehat{\mathbf{a}}_m(t) - \mathbf{G}\,\boldsymbol{\varphi}_e(t) && \forall\, t \in \mathrm{T} \end{aligned} \tag{3.105}$$

The magnetic vector and electric scalar potentials are not unique and, as in the continuous case, special gauges can be used at this point to derive from Maxwell's Grid Equations a discrete system of equations with the desired properties.

Discrete Poynting's Theorem

We will derive a *global* discrete Poynting's Theorem and the *global* conservation of a discrete energy for discrete fields in the domain Ω. It will solely depend on Maxwell's topological grid laws and the topological tools introduced earlier without need for Maxwell's material grid laws. By calling it a *global* discrete Poynting's Theorem, we want to emphasize that it corresponds to the continuous Poynting's Theorem in equation (2.48) on page 18 with the integrals taken over the complete domain Ω and its boundary $\partial\Omega$, accordingly. A local interpretation can be found by discretizing only the local part of the calculation domain of interest, in the extreme case only one original grid cell, and using the resulting grid derivatives and material laws. A notation allowing directly for such local statements for primal grid cells is introduced in appendix A.

For the special case of a Cartesian coordinate grid using the standard FIT material relations, a local Poynting's Theorem was stated in [85, pp. 25]. Its global version is equivalent to the discrete Poynting's Theorem stated here.

Let us start with the term

$$\widehat{\underset{\sim}{\mathbf{h}}}^{\mathrm{T}} \left(\partial_t \widehat{\overline{\mathbf{b}}} \right) \tag{3.106}$$

where the magnetic grid voltages $\widehat{\underset{\sim}{\mathbf{h}}}$ and the magnetic grid fluxes $\widehat{\overline{\mathbf{b}}}$ are taken arbitrary, i.e. they need not fulfill Maxwell's magnetic material grid law (3.80b) on page 58. In the next section, assuming Maxwell's material laws to hold, we will interpret this term as the discrete magnetic energy in the domain Ω. Here, we will only assume Maxwell's topological grid laws to hold. Using Maxwell's first topological grid law (3.65) on page 51 and the duality of the discrete curl operators in equation (3.52) on page 46, we get:

$$= -\widehat{\underset{\sim}{\mathbf{h}}}^{\mathrm{T}} \left(\mathbf{C}\, \widehat{\mathbf{e}} \right) = -\left(\underset{\sim}{\mathbf{C}}\, \widehat{\underset{\sim}{\mathbf{h}}} \right)^{\mathrm{T}} \widehat{\mathbf{e}} \tag{3.107}$$

Now we can employ Maxwell's second topological grid law (3.79) on page 57 to arrive at:

$$= -\left(\partial_t \widehat{\overline{\underset{\sim}{\mathbf{d}}}} + \widehat{\overline{\underset{\sim}{\mathbf{j}}}} + \widehat{\overline{\underset{\sim}{\mathbf{j}}}}_{\partial\Omega} \right)^{\mathrm{T}} \widehat{\mathbf{e}} \tag{3.108}$$

Rearranging terms of this equality, we arrive at the global discrete Poynting's Theorem:

$$\boxed{\left(\partial_t \widehat{\overline{\underset{\sim}{\mathbf{d}}}} \right)^{\mathrm{T}} \widehat{\mathbf{e}} + \widehat{\underset{\sim}{\mathbf{h}}}^{\mathrm{T}} \left(\partial_t \widehat{\overline{\mathbf{b}}} \right) + \widehat{\overline{\underset{\sim}{\mathbf{j}}}}^{\mathrm{T}} \widehat{\mathbf{e}} + \widehat{\overline{\underset{\sim}{\mathbf{j}}}}_{\partial\Omega}^{\mathrm{T}} \widehat{\mathbf{e}} = 0} \tag{3.109}$$

This property is true for any two sets of fields $(\widehat{\mathbf{e}}, \widehat{\widehat{\mathbf{b}}})$ and $(\underset{\sim}{\widehat{\mathbf{h}}}, \underset{\sim}{\widehat{\widehat{\mathbf{d}}}}, \underset{\sim}{\widehat{\widehat{\mathbf{j}}}}_{\partial\Omega})$ fulfilling the first and second Maxwell's Grid Equations. The interpretation of the terms as grid energies and losses can only be established after also assuming Maxwell's material grid laws to hold. This will be done in the next section.

3.2.4 Maxwell's Metric Properties

In this chapter, we derive a property that requires both Maxwell's topological and material laws to hold: The conservation of grid energy.

Conservation of Grid Energy

We will define the grid energies and recognize Poynting's Theorem to render a conservation law for the electromagnetic grid energy.

Let us first introduce the electric and magnetic grid energies W_e^d and W_m^d:

$$W_e^d \equiv \frac{1}{2}\|\widehat{\mathbf{e}}\|_\varepsilon^2 = \frac{1}{2}\widehat{\mathbf{e}}^{\mathrm{T}}\,\mathbf{M}_\varepsilon\,\widehat{\mathbf{e}} \tag{3.110a}$$

$$W_m^d \equiv \frac{1}{2}\|\widehat{\widehat{\mathbf{b}}}\|_\nu^2 = \frac{1}{2}\widehat{\widehat{\mathbf{b}}}^{\mathrm{T}}\,\mathbf{M}_\nu\,\widehat{\widehat{\mathbf{b}}} \tag{3.110b}$$

The material matrices $\mathbf{M}_\varepsilon$ and $\mathbf{M}_\nu$ are realizations of discrete primal hodge operators. By Definition 3.11 on page 48, these are positive definite and the norm notation is thus justified. We conclude that the defined energies are always non-negative quantities. The total electromagnetic grid energy W^d is defined as the sum of the electric and magnetic grid energies:

$$W^d = W_e^d + W_m^d \tag{3.111}$$

For symmetric material matrices, the time derivative of the electric grid energy can be written as:

$$\partial_t W_e^d = \partial_t\left(\frac{1}{2}\widehat{\mathbf{e}}^{\mathrm{T}}\,\mathbf{M}_\varepsilon\,\widehat{\mathbf{e}}\right) = \left(\partial_t\,\mathbf{M}_\varepsilon\,\widehat{\mathbf{e}}\right)^{\mathrm{T}}\widehat{\mathbf{e}} \tag{3.112}$$

which, using Maxwell's first grid material law (3.80a) on page 58, is equal to

$$= \left(\partial_t \underset{\sim}{\widehat{\widehat{\mathbf{d}}}}\right)^{\mathrm{T}}\widehat{\mathbf{e}} \tag{3.113}$$

Using Maxwell's second grid material law (3.80b) on page 58, we can equivalently write the time derivative of the magnetic grid energy W_m^d as:

$$\partial_t W_m^d = \underset{\sim}{\widehat{\mathbf{h}}}^{\mathrm{T}}\left(\partial_t \widehat{\widehat{\mathbf{b}}}\right) \tag{3.114}$$

Now we see that the discrete Poynting's Theorem (3.109) delivers a conservation law for the electromagnetic grid energy:

$$\partial_t\left(W^d\right) + \underset{\sim}{\widehat{\widehat{\mathbf{j}}}}^{\mathrm{T}}\widehat{\mathbf{e}} + \underset{\sim}{\widehat{\widehat{\mathbf{j}}}}_{\partial\Omega}^{\mathrm{T}}\widehat{\mathbf{e}} = 0 \tag{3.115}$$

Defining the *electric grid losses* P_e^d as

$$P_e^d \equiv \underset{\sim}{\widehat{\mathbf{j}}}^{\mathrm{T}} \widehat{\mathbf{e}} \tag{3.116}$$

and the *equivalent boundary electric grid losses* P_P^d as

$$P_P^d \equiv \underset{\sim}{\widehat{\mathbf{j}}}_{\partial\Omega}^{\mathrm{T}} \widehat{\mathbf{e}} \tag{3.117}$$

we arrive at the final form of the electromagnetic grid energy conservation law:

$$\boxed{\partial_t \left(W^d\right) + P_e^d + P_P^d = 0} \tag{3.118}$$

The notation of the equivalent boundary electric grid losses P_P^d is deliberately chosen to remind of the continuous radiation losses P_P in equation (2.49) on page 19. Using the definition of the equivalent boundary currents in equation (3.75) on page 56, we notice that the equivalent boundary electric grid losses P_P^d realize the cross product of the electric and magnetic field strengths in the discrete setting:

$$P_P^d = -\sum_{j=1}^{2} \left(\left(\mathbf{T}_{\overline{\Gamma}_{j,h}}^{1} \right)^{\mathrm{T}} \underset{\sim}{\widehat{\mathbf{h}}}_{\Gamma_j} \right)^{\mathrm{T}} \widehat{\mathbf{e}} = -\sum_{j=1}^{2} \underset{\sim}{\widehat{\mathbf{h}}}_{\Gamma_j}^{\mathrm{T}} \mathbf{T}_{\overline{\Gamma}_{j,h}}^{1} \widehat{\mathbf{e}} \tag{3.119}$$

The equivalent boundary electric grid losses P_P^d do thus represent the radiation losses through the boundary parts Γ_1 and Γ_2.

3.2.5 Spatially Discrete Maxwell's Initial Boundary Value Problem

As in the continuous case, Maxwell's Grid Equations need to be supplemented by suitable initial and boundary conditions to arrive at a discrete IBVP with a unique solution. In this chapter, we will state such a discrete IBVP, show existence and uniqueness of a solution, and prove its stability for a family of grids.

A Discrete Initial Boundary Value Problem for Maxwell's Grid Equations

We assume the continuous Maxwell's IBVP in equations (2.57a) to (2.57h) on page 21 to be given along with the initial data $\vec{E}_0(\vec{r})$ and $\vec{B}_0(\vec{r})$, the boundary data $\vec{E}_{\Gamma_1}(\vec{r},t)$ and $\vec{H}_{\Gamma_2}(\vec{r},t)$, and the source current $\vec{J}(\vec{r},t)$. How do we arrive at an equivalent discrete IBVP? Maxwell's equations have already been translated into the continuous setting in this chapter. Now, we state how to discretize the initial and boundary data and the source current as well as how to impose the initial and boundary conditions in the discrete setting.

The temporal boundary data is discretized by the primal grid discretization operators L^k defined by equations (3.19) on page 37, which integrate the continuous data over the edges and faces of the primal grid:

$$\widehat{\mathbf{e}}_0 = \mathrm{L}^1 \vec{E}_0(\vec{r}) \tag{3.120}$$

$$\widehat{\mathbf{b}}_0 = \mathrm{L}^2 \vec{B}_0(\vec{r}) \tag{3.121}$$

We impose this discrete temporal boundary data on the discrete problem as:

$$\boxed{\widehat{\mathbf{e}}(t_0) = \widehat{\mathbf{e}}_0} \tag{3.122}$$

$$\boxed{\widehat{\widehat{\mathbf{b}}}(t_0) = \widehat{\widehat{\mathbf{b}}}_0} \tag{3.123}$$

For discretizing the electric boundary data, we introduce the primal boundary grid discretization operator $\mathrm{L}^1_{\overline{\Gamma}_{1,h}}$, which integrates the continuous data along the primal edges lying in the boundary part Γ_1:

$$\left(\mathrm{L}^1_{\overline{\Gamma}_{1,h}} \vec{E}_{\Gamma_1}(\vec{r},t)\right)_i = \int_{S^1_k} \vec{E}_{\Gamma_1}(\vec{r},t) \cdot \vec{t}_{S^1_k}\, \mathrm{d}s, \qquad k = \mathrm{I}^1_{\overline{\Gamma}_{1,h}}(i), \quad \forall\, i \in [1..n^1_{\overline{\Gamma}_{1,h}}] \tag{3.124}$$

Using the primal grid trace operator $\mathbf{T}^1_{\overline{\Gamma}_{1,h}}$ defined in Definition 3.8 on page 41, we can rewrite the boundary grid discretization operator $\mathrm{L}^1_{\overline{\Gamma}_{1,h}}$ in terms of the global grid discretization operator L^1 defined by Definition 3.6 on page 37 by

$$\mathrm{L}^1_{\overline{\Gamma}_{1,h}} \vec{E}_{\Gamma_1}(\vec{r},t) = \mathbf{T}^1_{\overline{\Gamma}_{1,h}}\, \mathrm{L}^1 \vec{E}_{\Gamma_1}(\vec{r},t) \tag{3.125}$$

where we have assumed that $\vec{E}_{\Gamma_1}$ is extended onto the complete domain Ω. The electric boundary data is then discretized by

$$\widehat{\mathbf{e}}_{\Gamma_1}(t) = \mathrm{L}^1_{\overline{\Gamma}_{1,h}} \vec{E}_{\Gamma_1}(\vec{r},t) \tag{3.126}$$

and imposed on Maxwell's Grid Equations as follows:

$$\boxed{\mathbf{T}^1_{\overline{\Gamma}_{1,h}}\, \widehat{\mathbf{e}}(t) = \widehat{\mathbf{e}}_{\Gamma_1}(t)} \qquad \forall\, t \in \mathrm{T} \tag{3.127}$$

Similarly, we discretize the magnetic boundary conditions by the dual boundary grid discretization operator $\underset{\sim}{\mathrm{L}}^1_{\underset{\sim}{\Gamma}_{2,h}}$ which integrates the magnetic field strength over the missing boundary parts of the dual faces $\underset{\sim}{S}^2_i$ with incomplete boundary in respect to Γ_2. Let us recall that the indices of these dual faces with incomplete boundary are collected in the index set $\underset{\sim}{\mathrm{I}}^1_{\underset{\sim}{\Gamma}_{2,h}}$. Thus we can write:

$$\left(\underset{\sim}{\mathrm{L}}^1_{\underset{\sim}{\Gamma}_{2,h}} \vec{H}_{\Gamma_2}(\vec{r},t)\right)_i = \int_{\partial \underset{\sim}{S}^2_k \cap \Gamma_2} \vec{H}_{\Gamma_2}(\vec{r},t) \cdot \vec{t}_{\partial \underset{\sim}{S}^2_k \cap \Gamma_2}\, \mathrm{d}s, \qquad k = \underset{\sim}{\mathrm{I}}^1_{\underset{\sim}{\Gamma}_{2,h}}(i), \quad \forall\, i \in [1..\underset{\sim}{n}^1_{\underset{\sim}{\Gamma}_{2,h}}] \tag{3.128}$$

In short, we write the discretization of the magnetic boundary data $\vec{H}_{\Gamma_2}(\vec{r},t)$ on the boundary part Γ_2 as:

$$\underset{\sim}{\widehat{\mathbf{h}}}_{\Gamma_2}(t) \equiv \underset{\sim}{\mathrm{L}}^1_{\underset{\sim}{\Gamma}_{2,h}} \vec{H}_{\Gamma_2}(\vec{r},t) \tag{3.129}$$

The discrete magnetic boundary condition is then imposed by equation (3.75) on page 56, which fixes the equivalent boundary current $\underset{\sim}{\widehat{\widehat{\mathbf{j}}}}_{\Gamma_2}$ as

$$\boxed{\underset{\sim}{\widehat{\widehat{\mathbf{j}}}}_{\Gamma_2}(t) = -\left(\mathbf{T}^1_{\overline{\Gamma}_{2,h}}\right)^{\mathrm{T}} \underset{\sim}{\widehat{\mathbf{h}}}_{\Gamma_2}(t)} \qquad \forall\, t \in \mathrm{T} \tag{3.130}$$

The source current $\vec{J}$ can be discretized by the dual grid discretization operator $\underset{\sim}{\mathrm{L}}^2$:

$$\underset{\sim}{\hat{\dot{\mathbf{j}}}} = \underset{\sim}{\mathrm{L}}^2 \vec{J} \tag{3.131}$$

Now Maxwell's semi-discrete grid IBVP reads:

$$\mathbf{C}\,\hat{\mathbf{e}}(t) = -\partial_t\,\hat{\hat{\mathbf{b}}}(t) \tag{3.132a}$$

$$\underset{\sim}{\mathbf{C}}\,\underset{\sim}{\hat{\mathbf{h}}}(t) = \partial_t\,\underset{\sim}{\hat{\hat{\mathbf{d}}}}(t) + \underset{\sim}{\hat{\hat{\mathbf{j}}}}(t) + \underset{\sim}{\hat{\hat{\mathbf{j}}}}_{\Gamma_1}(t) + \underset{\sim}{\hat{\hat{\mathbf{j}}}}_{\Gamma_2}(t) \tag{3.132b}$$

$$\underset{\sim}{\hat{\hat{\mathbf{d}}}}(t) = \mathbf{M}_\varepsilon\,\hat{\mathbf{e}}(t) \tag{3.132c}$$

$$\underset{\sim}{\hat{\mathbf{h}}}(t) = \mathbf{M}_\nu\,\hat{\hat{\mathbf{b}}}(t) \tag{3.132d}$$

$$\mathbf{T}^1_{\overline{\Gamma}_{1,h}}\,\hat{\mathbf{e}}(t) = \hat{\mathbf{e}}_{\Gamma_1}(t) \tag{3.132e}$$

$$\underset{\sim}{\hat{\hat{\mathbf{j}}}}_{\Gamma_2}(t) = -\left(\mathbf{T}^1_{\overline{\Gamma}_{2,h}}\right)^{\mathrm{T}}\,\underset{\sim}{\hat{\mathbf{h}}}_{\Gamma_2}(t) \tag{3.132f}$$

$$\hat{\mathbf{e}}(t_0) = \hat{\mathbf{e}}_0 \tag{3.132g}$$

$$\hat{\hat{\mathbf{b}}}(t_0) = \hat{\hat{\mathbf{b}}}_0 \tag{3.132h}$$

The initial data $\hat{\mathbf{e}}_0$ and $\hat{\hat{\mathbf{b}}}_0$, the boundary data $\hat{\mathbf{e}}_{\Gamma_1}(t)$ and $\underset{\sim}{\hat{\mathbf{h}}}_{\Gamma_2}(t)$, and the source currents $\underset{\sim}{\hat{\hat{\mathbf{j}}}}(t)$ are assumed to be given. Unknown are the electric grid voltages $\hat{\mathbf{e}}(t)$ except for their values on the boundary part Γ_1, the magnetic grid fluxes $\hat{\hat{\mathbf{b}}}(t)$, the electric grid fluxes $\underset{\sim}{\hat{\hat{\mathbf{d}}}}(t)$, the magnetic grid voltages $\underset{\sim}{\hat{\mathbf{h}}}(t)$, and the equivalent boundary grid currents $\underset{\sim}{\hat{\hat{\mathbf{j}}}}_{\Gamma_1}(t)$ on the boundary part Γ_1.

Existence and Uniqueness of the Solution to Maxwell's Semi-Discrete Initial Boundary Value Problem

Theorem 3.7. *Maxwell's semi-discrete IBVP (3.132) with given initial data*

$$\hat{\mathbf{e}}_0 \in \mathbb{R}^{n^1} \tag{3.133a}$$

$$\hat{\hat{\mathbf{b}}}_0 \in \mathbb{R}^{n^2} \tag{3.133b}$$

boundary data

$$\hat{\mathbf{e}}_{\Gamma_1}(t) \in \mathbb{R}^{n^1_{\overline{\Gamma}_{1,h}}} \qquad \forall\, t \in \mathrm{T} \tag{3.134a}$$

$$\underset{\sim}{\hat{\mathbf{h}}}_{\Gamma_2}(t) \in \mathbb{R}^{n^1_{\underset{\sim}{\Gamma}_{2,h}}} \qquad \forall\, t \in \mathrm{T} \tag{3.134b}$$

fulfilling the compatibility condition

$$\mathbf{T}^1_{\overline{\Gamma}_{1,h}}\,\hat{\mathbf{e}}_0 = \hat{\mathbf{e}}_{\Gamma_1}(t_0) \tag{3.135}$$

and source current

$$\underset{\sim}{\hat{\hat{\mathbf{j}}}}(t) \in \mathbb{R}^{\underset{\sim}{n}^2} \qquad \forall\, t \in \mathrm{T} \tag{3.136}$$

has a unique solution.

Proof. For ease of the presentation, we will assume only magnetic boundary conditions on all the boundary $\partial\Omega$ of the domain, i.e. we assume Γ_1 to be empty. The general treatment for electric and magnetic boundary conditions is found in appendix B on page 181.

In order to use the standard theory for systems of ordinary first order differential equations, we will rewrite Maxwell's semi-discrete IBVP (3.132) in the following standard form:

$$\partial_t \mathbf{A}\mathbf{x}(t) + \mathbf{B}\mathbf{x}(t) = \mathbf{b}(t) \tag{3.137a}$$

$$\mathbf{x}(t_0) = \mathbf{x}_0 \tag{3.137b}$$

Defining the unknown vector $\mathbf{x}$ as:

$$\mathbf{x}(t) = \begin{pmatrix} \widehat{\mathbf{e}}(t) \\ \widehat{\widehat{\mathbf{b}}}(t) \end{pmatrix} \tag{3.138}$$

the initial values $\mathbf{x}_0$ as

$$\mathbf{x}_0 = \begin{pmatrix} \widehat{\mathbf{e}}_0 \\ \widehat{\widehat{\mathbf{b}}}_0 \end{pmatrix} \tag{3.139}$$

the matrices $\mathbf{A}$ and $\mathbf{B}$ as

$$\mathbf{A} = \begin{pmatrix} \mathbf{M}_\varepsilon & 0 \\ 0 & \mathbf{M}_\nu \end{pmatrix}, \qquad \mathbf{B} = \begin{pmatrix} 0 & -\underset{\sim}{\mathbf{C}}\,\mathbf{M}_\nu \\ \mathbf{M}_\nu\,\mathbf{C} & 0 \end{pmatrix} \tag{3.140}$$

and the source vector $\mathbf{b}$ as

$$\mathbf{b}(t) = \begin{pmatrix} -\underset{\sim}{\widehat{\widehat{\mathbf{j}}}}(t) - \underset{\sim}{\widehat{\widehat{\mathbf{j}}}}_{\Gamma_2}(t) \\ 0 \end{pmatrix} \tag{3.141}$$

one can easily see that the standard form (3.137) results from the original system (3.132) when the electric boundary part Γ_1 is assumed to be empty, as stated above. We have eliminated the unknown quantities on the dual grid, i.e. the electric grid fluxes $\underset{\sim}{\widehat{\widehat{\mathbf{d}}}}$ and the magnetic grid voltages $\underset{\sim}{\widehat{\mathbf{h}}}$ which can be recovered uniquely by equations (3.132c) and (3.132d).

Existence and uniqueness of a solution to the problem (3.137) with a square invertible matrix $\mathbf{A}$ are covered by the standard theory for systems of ordinary first order differential equations [15, pp. 493]. The matrix $\mathbf{A}$ is easily seen to be invertible, as $\mathbf{M}_\varepsilon$ and $\mathbf{M}_\nu$ are symmetric positive definite. An explicit formula for the solution $\mathbf{x}$ in terms of matrix exponentials reads:

$$\mathbf{x}(t) = e^{-\mathbf{A}^{-1}\mathbf{B}(t-t_0)} \left(\mathbf{x}_0 + \int_{t_0}^{t} e^{\mathbf{A}^{-1}\mathbf{B}(t'-t_0)} \mathbf{A}^{-1}\mathbf{b}(t')\,\mathrm{d}t' \right) \tag{3.142}$$

That this $\mathbf{x}$ is truly a solution of problem (3.137) is easily checked by plugging it in. We now want to show uniqueness of the solution which can be done in parallel to the continuous case, as we have derived discrete analogues of all properties used in the continuous proof.

The proof will be by contradiction: Assume the existence of two different solutions $\mathbf{x}_a \neq \mathbf{x}_b$ to Maxwell's grid IBVP (3.132), or more appropriately to its reduced version (3.137). Then the difference of these solutions $\mathbf{x}_\delta = \mathbf{x}_a - \mathbf{x}_b \neq 0$ solves the following Maxwell's grid IBVP:

$$\mathbf{C}\,\widehat{\mathbf{e}}_\delta(t) = -\partial_t\,\widehat{\widehat{\mathbf{b}}}_\delta(t) \tag{3.143a}$$

$$\underset{\sim}{\mathbf{C}}\,\underset{\sim}{\widehat{\mathbf{h}}}_\delta(t) = \partial_t\,\underset{\sim}{\widehat{\widehat{\mathbf{d}}}}_\delta(t) + \underset{\sim}{\widehat{\widehat{\mathbf{j}}}}_{\Gamma_2,\delta}(t) \tag{3.143b}$$

$$\underset{\sim}{\widehat{\widehat{\mathbf{d}}}}_\delta(t) = \mathbf{M}_\varepsilon\,\widehat{\mathbf{e}}_\delta(t) \tag{3.143c}$$

$$\underset{\sim}{\widehat{\mathbf{h}}}_\delta(t) = \mathbf{M}_\nu\,\widehat{\widehat{\mathbf{b}}}_\delta(t) \tag{3.143d}$$

$$\underset{\sim}{\widehat{\widehat{\mathbf{j}}}}_{\Gamma_2,\delta}(t) = 0 \tag{3.143e}$$

$$\widehat{\mathbf{e}}_\delta(t_0) = 0 \tag{3.143f}$$

$$\widehat{\widehat{\mathbf{b}}}_\delta(t_0) = 0 \tag{3.143g}$$

The conservation law for the discrete electromagnetic energy (3.118) on page 66 also holds for the difference fields (with zero source current $\underset{\sim}{\widehat{\widehat{\mathbf{j}}}}$). Thus we derive that the time derivative of the total electromagnetic energy of the difference fields is zero:

$$\partial_t\left(W_\delta^d\right) + \underset{\sim}{\widehat{\widehat{\mathbf{j}}}}^{\mathrm{T}}_{\Gamma_2,\delta}\widehat{\mathbf{e}}_\delta = \partial_t\left(\frac{1}{2}\|\widehat{\mathbf{e}}_\delta\|_\varepsilon^2 + \frac{1}{2}\|\widehat{\widehat{\mathbf{b}}}_\delta\|_\nu^2\right) = 0$$

From equations (3.143f) and (3.143g) we know that the electric grid voltages and the magnetic grid fluxes and thus the electric and magnetic energies are zero at the time $t = t_0$. Thus the energies and fields are zero for all times $t > t_0$:

$$\begin{aligned} & \|\widehat{\mathbf{e}}_\delta(t)\|_\varepsilon + \|\widehat{\widehat{\mathbf{b}}}_\delta(t)\|_\nu = \|\widehat{\mathbf{e}}_\delta(t_0)\|_\varepsilon + \|\widehat{\widehat{\mathbf{b}}}_\delta(t_0)\|_\nu = 0 && \forall\, t \in \mathrm{T} \\ \Rightarrow \quad & \widehat{\mathbf{e}}_\delta(t) = 0 \quad \wedge \quad \widehat{\widehat{\mathbf{b}}}_\delta(t) = 0 && \forall\, t \in \mathrm{T} \end{aligned} \tag{3.144}$$

This contradicts the assumption of the solutions being different and therefore concludes the proof. □

Stability of the Semi-Discrete Maxwell's Initial Boundary Value Problem

As we have seen on page 23, Maxwell's continuous IBVP can be rewritten in the form

$$\mathrm{L}\mathbf{x} = b \tag{3.145}$$

where $\mathbf{x}$ denotes the continuous unknowns, b the given continuous initial, boundary, and source data, and L a linear operator

$$\mathrm{L}: \qquad U \longrightarrow F \tag{3.146}$$

As we will shortly see, we can also rewrite the semi-discrete Maxwell's IBVP (3.132) in the similar form

$$\mathrm{L}_h\mathbf{x}_h = b_h, \tag{3.147}$$

where the discrete unknown $\mathbf{x}_h$, data b_h, and operator L_h approximate the continuous unknown $\mathbf{x}$, data b, and operator L, respectively. The discrete operator L_h has domain U_h and range F_h:

$$\mathrm{L}_h : \qquad U_h \longrightarrow F_h \tag{3.148}$$

Assuming a fixed type of material relations to use, the discrete operator L_h and data b_h and thus also the discrete solution $\mathbf{x}_h$ depend solely on the specific grids Ω_h and $\underset{\sim}{\Omega}_h$ chosen for the discretization. Now one tries to find a sequence of grids $\{\Omega_h, \underset{\sim}{\Omega}_h\}_h$ such that the resulting sequence of discrete problems

$$\{\mathrm{L}_h \mathbf{x}_h = b_h\}_h \tag{3.149}$$

renders a sequence of solutions $\{\mathbf{x}_h\}_h$ that *converges* to the continuous solution $\mathbf{x}$ in some norm. Theorem E.1 on page 212 ensures *convergence* in a certain norm, if the sequence of discrete problems is *consistent* and *stable* in the same norms. Thus the terms *convergence*, *consistency*, and *stability* are always notions for a sequence of discrete problems with a sequence of solutions. Stability means uniform boundedness of the sequence of solution operators $\{\mathrm{L}_h^{-1}\}_h$, as seen from Definition E.3 on page 212. Consistency of the numerical solution scheme refers to the approximation property of the sequence of linear operators $\{\mathrm{L}_h\}_h$ as seen in Definition E.4 on page 212.

For many numerical schemes, consistency is more easily proven than stability. In the framework of the FIT, stability even for arbitrary sequences of consistent grids is fairly easy to prove, though. The consistency proof on the other hand hinges on the specific properties of the material matrices. Thus in this thesis, we will prove stability of the FIT but not consistency and thus not convergence. For the newly developed polyhedral material relations in chapter 4, a basic reasoning for consistency will be given, though.

So let us get back to the stability of the semi-discrete Maxwell's IBVP, or as we now can state more precisely: Of a sequence of semi-discrete problems resulting from the FIT scheme. We will not put any restriction on the sequence of these semi-discrete problems, other than each problem being a semi-discrete Maxwell's grid IBVP as described above. Thus even sequences with random discretization or coarser and coarser discretization will be proven to be stable. Such random discretizations will not have suitable consistency properties and do not render convergent schemes, though. As stated above, consistency for the specific sequence of discrete problems has to be examined independently to arrive at a convergence statement. Usually finer and finer grids, controlled by some grid parameter h, are defined to prove consistency for a sequence of discrete problems.

For each choice of grids $\{\Omega_h, \underset{\sim}{\Omega}_h\}$, we will denote the resulting FIT quantities by a subscript h. To shorten the presentation, we will simplify Maxwell's IBVP: Firstly, we assume only magnetic boundary conditions to be present, i.e. the electric boundary part Γ_1 is empty. This simplifies notation, but electric boundary conditions can easily be included in the stability proof. Secondly, we assume the source currents $\underset{\sim}{\widehat{\dot{\mathbf{j}}}}_h$ to be zero. This will simplify the proof, but non-zero source currents can also be included with little additional work. Thirdly, we assume homogeneous magnetic boundary conditions, i.e. the magnetic boundary voltages $\underset{\sim}{\widehat{\mathbf{h}}}_{\Gamma_2,h}$ are assumed zero. Non-homogeneous boundary conditions should also lead to stable schemes, but an easy proof was not achieved by the author.

So let us define the discrete problems (3.147) for this simplified semi-discrete Maxwell's IBVP: The unknown vector $\mathbf{x}_h$ will only consist of the electric grid voltages $\widehat{\mathbf{e}}_h$ and the magnetic grid fluxes $\widehat{\widehat{\mathbf{b}}}_h$, as defined in equation (3.138) with the additional subscript h to denote the special choice of grids. The operator L_h is defined in terms of the matrices $\mathbf{A}$ and $\mathbf{B}$ from equations (3.140), adding the subscript h, as:

$$\mathrm{L}_h\left(\mathbf{x}_h(t)\right) = \begin{pmatrix} \partial_t \mathbf{A}_h \mathbf{x}_h(t) + \mathbf{B}_h \mathbf{x}_h(t) \\ \mathbf{x}_h(t_0) \end{pmatrix} \tag{3.150}$$

The right hand side b_h is defined as

$$b_h = \begin{pmatrix} 0 \\ \mathbf{x}_{0,h} \end{pmatrix} \tag{3.151}$$

with the initial values $\mathbf{x}_{0,h}$ defined as in equation (3.139) again with the added subscript h. Equivalence of the resulting system (3.147) to the semi-discrete Maxwell's grid IBVP (3.132) under the assumptions of homogeneous magnetic boundary conditions on all of the boundary and no source currents to be present is easily shown. Note that the range F_h of the operator L_h has been restricted to have zero component in its first entry.

Now we have to specify the norms in which we want to discuss stability. As we do not have a recipe, yet, how to reconstruct a continuous solution from the semi-discrete solutions rendered by the FIT, we definitely have to consider semi-discrete norms, i.e. norms in the coefficient vectors of the discrete solution. For the norm in the domain U_h of the operator L_h, we will choose the discrete energy norms on the discrete spatial variable and the maximum norm in the continuous temporal variable:

$$\|\mathbf{x}_h\|_{U_h}^2 \equiv \max_{t\in \mathrm{T}} \left(\|\widehat{\mathbf{e}}_h(t)\|_\varepsilon^2 + \|\widehat{\widehat{\mathbf{b}}}_h(t)\|_\nu^2 \right) \tag{3.152}$$

As norm on the range F_h of the operator L_h, we will choose the discrete energy norms of the initial fields[11]:

$$\|b_h\|_{F_h}^2 \equiv \|\widehat{\mathbf{e}}_{0,h}\|_\varepsilon^2 + \|\widehat{\widehat{\mathbf{b}}}_{0,h}\|_\nu^2 \tag{3.153}$$

Theorem 3.8 (Stability)**.** *Let a sequence of semi-discrete Maxwell's grid IBVP be given in the reduced form of equation (3.147). Assume further on homogeneous magnetic boundary conditions on all of the boundary and no source currents to be present. Then the sequence of operators* L_h *is stable according to Definition E.3 in the discrete norms defined above.*

Proof. By Theorem 3.7 on page 68 we know that any of the operators L_h is invertible. So we are left to prove uniform boundedness of the inverse solution operators L_h^{-1}. We use the same tools as for the uniqueness proof in Theorem 3.7 on page 68, namely the conservation of grid energy according to equation (3.118) on page 66:

$$\partial_t \left(\frac{1}{2}\|\widehat{\mathbf{e}}_h(t)\|_\varepsilon^2 + \frac{1}{2}\|\widehat{\widehat{\mathbf{b}}}_h(t)\|_\nu^2 \right) = 0 \tag{3.154}$$

[11] As we have restricted the range F_h of the operator L_h to have zero component in its first entry, this does define a norm on F_h.

After temporal integration, we see that the discrete energy is constant in time:

$$\Leftrightarrow \qquad \|\widehat{\mathbf{e}}_h(t)\|_\varepsilon^2 + \|\widehat{\widehat{\mathbf{b}}}_h(t)\|_\nu^2 = \|\widehat{\mathbf{e}}_h(t_0)\|_\varepsilon^2 + \|\widehat{\widehat{\mathbf{b}}}_h(t_0)\|_\nu^2 \tag{3.155}$$

Now the square of the norm of the solution $\mathbf{x}_h$ can be calculated as:

$$\begin{aligned} \|\mathbf{x}_h\|_{U_h}^2 &= \max_{t\in \mathrm{T}} \left(\|\widehat{\mathbf{e}}_h(t)\|_\varepsilon^2 + \|\widehat{\widehat{\mathbf{b}}}_h(t)\|_\nu^2 \right) \\ &= \|\widehat{\mathbf{e}}_h(t_0)\|_\varepsilon^2 + \|\widehat{\widehat{\mathbf{b}}}_h(t_0)\|_\nu^2 = \|b_h\|_{F_h}^2 \end{aligned} \tag{3.156}$$

Replacing the solution $\mathbf{x}_h$ by the inverted given data $\mathrm{L}_h^{-1} b_h$ we get

$$\Rightarrow \qquad \|\mathrm{L}_h^{-1} b_h\|_{U_h} = \|b_h\|_{F_h} \tag{3.157}$$

This renders uniform boundedness of the inverse solution operator L_h^{-1} for all h with constant $C = 1$ and concludes the proof. □

Remark 3.7. Note that Theorem 3.8 does not put any requirements on the chosen grid sequence or the specific choice of discrete material relations other than that they fulfill the properties required by Definition 3.11 on page 48. Thus stability holds even for a sequence of coarser and coarser grids. In order to arrive at a convergent sequence, one has to choose a sequence which is consistent in the same norms in the same spaces U_h and F_h. The consistency requirement might force the range F_h of the operator L_h to contain fields with non-zero source currents, though. Thus, if one wants to prove convergence this way, it is actually necessary to extend the space F_h and the definition of its norm in the stability proof above to include fields with non-zero source currents.

Remark 3.8. We have shown stability in discrete norms. In order to arrive at convergence in continuous norms, reconstruction operators for the grid solutions $\mathbf{x}_h$ have to be defined and stability in continuous norms in the domain U and range F of the operator L has to be shown; see remark E.1 on page 213.

Remark 3.9. We have shown stability for the unbounded temporal domain $\mathrm{T} = [\mathrm{t}_0, \infty)$. This is sometimes called *strict stability*, e.g. in [97]. For stability analysis, often only bounded temporal domains $\mathrm{T} = [\mathrm{t}_0, \mathrm{t}_1]$ are considered. In this case, stable sequences of schemes might still show exponential growth of the solution in time, as long as a uniform bound does exist in the bounded temporal domain. Using the temporal maximum norm, this means that the spatial norms of the maximum of the solutions $\mathbf{x}_h$ must not exceed a certain value for the considered times $t \in \mathrm{T}$. Together with consistency, this still ensures convergence to the true solution in the bounded temporal domain T.

Remark 3.10. The stability proven above for the spatially discrete but temporally continuous Maxwell's IBVP is called *spatial stability* in the FIT community.

Remark 3.11. Considering an IBVP, some people refer to *stability with respect to (non-zero) initial conditions*, *stability with respect to (non-homogeneous) boundary conditions*, and *stability with respect to source terms*. As we have only included non-zero initial conditions, we have proven stability with respect to (non-zero) initial conditions. The other two terms imply non-homogeneous boundary conditions or source terms to be present, respectively.

Remark 3.12. An explicit stability proof is actually not necessary to prove convergence of the scheme. In [46, p. 17], the conservation of energy property is used directly to arrive at discrete error estimates in terms of discrete consistency errors of the material relations.

Remark 3.13. As we have seen, symmetry of the material matrices is not needed for the concept of stability. We have only proposed it in chapter 2.1.4 in order to simplify the presentation of the proof for stability of the space- and time-discrete Newmark-Θ scheme presented in chapter 3.3.2 on page 79.

3.2.6 Spatially Discrete Maxwell's House

Maxwell's house for the continuous Maxwell's equations in Fig. 2.3 on page 25 has an analogue in the semi-discrete case: The spatially discrete Maxwell's house depicted in Fig. 3.14. It captures Maxwell's topological and metric grid equations (3.65) on page 51, (3.79) on page 57, and (3.80a) and (3.80b) on page 58. The total grid currents $\underset{\sim}{\hat{\hat{\dot{\mathbf{j}}}}}^*$ are introduced as the sum of the source grid currents $\underset{\sim}{\hat{\hat{\dot{\mathbf{j}}}}}$ and the equivalent boundary grid currents $\underset{\sim}{\hat{\hat{\dot{\mathbf{j}}}}}_{\partial\Omega}$

$$\underset{\sim}{\hat{\hat{\dot{\mathbf{j}}}}}^* \equiv \underset{\sim}{\hat{\hat{\dot{\mathbf{j}}}}} + \underset{\sim}{\hat{\hat{\dot{\mathbf{j}}}}}_{\partial\Omega} \tag{3.158}$$

to shorten the notation. As was discussed in remark 3.5 on page 62, the dual grid charge $\underset{\sim}{\hat{\hat{\hat{\boldsymbol{\varrho}}}}}_e^*$ does also include equivalent boundary charges.

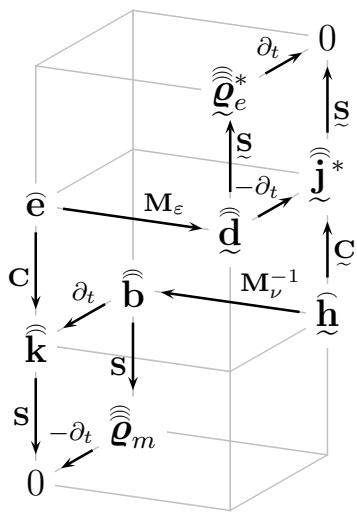

Fig. 3.14: The spatially discrete Maxwell's house represents the spatially discrete Maxwell's Grid Equations: The equations can be read off by adding all incoming quantities at each node and setting it equal to the quantity at the node. An *incoming quantity* is defined for an incoming arrow as the attached operator applied to the quantity at the start of the arrow. The superscript $*$ denotes dual quantities which include equivalent boundary terms to account for the missing boundary discretization in the dual grid.

3.3 Maxwell's Spatially and Temporally Discrete Grid Equations

In this chapter, we derive Maxwell's Grid Equations discretized in the temporal variable as well as in the spatial one. In chapter 3.3.1, we will take the first and second Maxwell's topological grid equations from chapter 3.2.1, which are discrete in space but continuous in time, and additionally discretize them in the temporal variable t. In chapter 3.3.2, Maxwell's material relations for the fully discrete quantities are first stated in general form. Then, a specific choice of metric relations rendering the cell-based Newmark-Θ time-stepping scheme introduced in [76] as a variant of the standard Newmark scheme [70] is proposed. In chapter 3.3.3, topological properties solely relying on Maxwell's discrete topological laws are derived. The metric properties in chapter 3.3.4 are derived for the specific case of the Newmark-Θ time-stepping scheme. Existence and uniqueness of a solution as well as stability for the fully discrete Maxwell's Grid Equations employing the Newmark-Θ time-stepping scheme are given in chapter 3.3.5.

All chapters proceed in analogue to the continuous case in chapter 2.2 and the semi-discrete case in chapter 3.2. No equivalent presentation for Maxwell's house is given for the fully discrete setting, though, as its representation in parallel to the preceding chapters is very complex and loses the simple overview.

3.3.1 Maxwell's Discrete Topological Laws

We will discretize Maxwell's semi-discrete topological grid laws stated in equations (3.65) on page 51 and (3.79) on page 57 in the temporal variable t on a primal temporal grid $\mathrm{T}_{\Delta t}$ and its dual $\underset{\sim}{\mathrm{T}}_{\Delta t}$, respectively. The semi-discrete domains $\Omega_h \times \mathrm{T}$ and $\underset{\sim}{\Omega}_h \times \mathrm{T}$ are thus discretized to the fully discrete domains $\Omega_h \times \mathrm{T}_{\Delta t}$ and $\underset{\sim}{\Omega}_h \times \underset{\sim}{\mathrm{T}}_{\Delta t}$ as represented by Fig. 3.15. In this chapter, we will take the temporal domain T to be unbounded, i.e.:

$$\mathrm{T} = (-\infty, \infty) \tag{3.159}$$

This relieves us from special treatment of the temporal boundary for the dual temporal grid $\underset{\sim}{\mathrm{T}}_{\Delta t}$. It could be included analogous to the discussion of spatially bounded domains Ω in chapter 3.2.1, though.

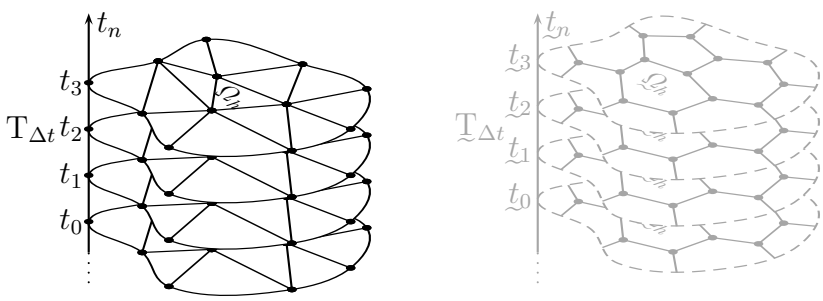

Fig. 3.15: Schematic sketch of the fully discrete problem domains $\Omega_h \times \mathrm{T}_{\Delta t}$ and $\underset{\sim}{\Omega}_h \times \underset{\sim}{\mathrm{T}}_{\Delta t}$: The spatial domain Ω is discretized by the spatial primal grid Ω_h or dual grid $\underset{\sim}{\Omega}_h$, while the temporal domain T is discretized by the temporal primal grid $\mathrm{T}_{\Delta t}$ or the temporal dual grid $\underset{\sim}{\mathrm{T}}_{\Delta t}$.

In order to keep any metric concept, i.e. here the temporal metric, out of the topological laws, we will introduce integral variables in time as done in [88]. This deviates from the notation of the traditional approach in the FIT, where a finite difference approximation for the time-discretization is directly put into the topological laws [95]. As pointed out in [88], the approach taken here has the advantage that the topological equations are again exactly fulfilled for grid projected analytical solutions and all approximations are put into the material relations.

The primal temporal grid $\mathrm{T}_{\Delta t}$ is introduced as a 1-dimensional consistent grid of the unbounded temporal domain T. This 1-dimensional consistent grid is defined in equivalence to Definition 3.1 on page 29 of a 3-dimensional consistent grid. For the nodes $S_n^0 \in \boldsymbol{S}^0(\mathrm{T}_{\Delta t})$ of the primal temporal grid, we will choose the more common notation t_n. For the edges $S_n^1 \in \boldsymbol{S}^1(\mathrm{T}_{\Delta t})$ of the primal temporal grid, we will choose the more common notation Δt_n which will also be used to denote the actual length of the edge:

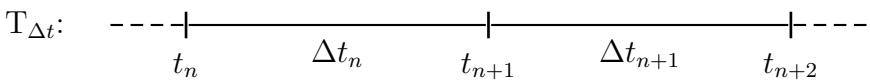

We can now integrate Maxwell's first topological grid law (3.65) on page 51 over the temporal grid edge Δt_n, i.e. from time t_n to t_{n+1}:

$$\begin{aligned} & \int_{\Delta t_n} \mathbf{C}\,\widehat{\mathbf{e}}(t)\,\mathrm{d}t = -\int_{\Delta t_n} \partial_t \widehat{\widehat{\mathbf{b}}}(t)\,\mathrm{d}t \\ \Leftrightarrow \quad & \int_{t_n}^{t_{n+1}} \mathbf{C}\,\widehat{\mathbf{e}}(t)\,\mathrm{d}t = -\int_{t_n}^{t_{n+1}} \partial_t \widehat{\widehat{\mathbf{b}}}(t)\,\mathrm{d}t \end{aligned} \tag{3.160}$$

Using the interchangeability of the time integral with the discrete curl operator due to constant grids in time, we arrive at:

$$\Leftrightarrow \quad \mathbf{C}\int_{t_n}^{t_{n+1}} \widehat{\mathbf{e}}(t)\,\mathrm{d}t = \widehat{\widehat{\mathbf{b}}}(t_n) - \widehat{\widehat{\mathbf{b}}}(t_{n+1}) \tag{3.161}$$

We now introduce the electric grid voltage pulses[12] $\overline{\widehat{\mathbf{e}}}^n$ as grid projection of the electric grid voltages $\widehat{\mathbf{e}}(t)$ onto the primal temporal edges Δt_n by the grid projection operator $L^1_{\mathrm{T}_{\Delta t},n}$:

$$\overline{\widehat{\mathbf{e}}}^n \equiv L^1_{\mathrm{T}_{\Delta t},n}\widehat{\mathbf{e}}(t) \equiv \int_{\Delta t_n} \widehat{\mathbf{e}}(t)\,\mathrm{d}t \tag{3.162}$$

and the magnetic grid fluxes $\widehat{\widehat{\mathbf{b}}}^n$ as the grid projection of the time-continuous magnetic grid fluxes $\widehat{\widehat{\mathbf{b}}}(t)$ onto the primal temporal nodes t_n by the grid projection operator $L^0_{\mathrm{T}_{\Delta t},n}$:

$$\widehat{\widehat{\mathbf{b}}}^n \equiv L^0_{\mathrm{T}_{\Delta t},n}\widehat{\widehat{\mathbf{b}}}(t) \equiv \widehat{\widehat{\mathbf{b}}}(t_n) \tag{3.163}$$

Then we can rewrite equation (3.161) as:

$$\boxed{\mathbf{C}\,\overline{\widehat{\mathbf{e}}}^n = \widehat{\widehat{\mathbf{b}}}^n - \widehat{\widehat{\mathbf{b}}}^{n+1}} \qquad \forall\, n \in \mathbb{Z} \tag{3.164}$$

[12] We will use the term *pulses* to denote time-integrated quantities.

We call this equation the local form of Maxwell's first topological grid law discrete in space and time. We call it the local form, as it states the relation for a single temporal edge Δt_n. It is comparable to the spatially local form of equation (3.66) on page 51 in the semi-discrete case, which is stated for single spatial faces S_i^2.

Maxwell's second topological grid law will be discretized on a dual temporal grid $\underset{\sim}{\mathrm{T}}_{\Delta t}$ of the primal grid $\mathrm{T}_{\Delta t}$. To keep notation fairly standard, the nodes $\underset{\sim}{S}_n^0 \in \underset{\sim}{\boldsymbol{S}}^0(\underset{\sim}{\mathrm{T}}_{\Delta t})$ and edges $\underset{\sim}{S}_n^1 \in \underset{\sim}{\boldsymbol{S}}^1(\underset{\sim}{\mathrm{T}}_{\Delta t})$ of the dual temporal grid $\underset{\sim}{\mathrm{T}}_{\Delta t}$ will be denoted by $\underset{\sim}{t}_n$ and $\underset{\sim}{\Delta t}_n$, respectively. The dual edge lengths will also be denoted by $\underset{\sim}{\Delta t}_n$. The dual grid $\underset{\sim}{\mathrm{T}}_{\Delta t}$ is assumed dual to the primal grid $\mathrm{T}_{\Delta t}$ in a 1-dimensional equivalent sense of Definition 3.2 on page 31:

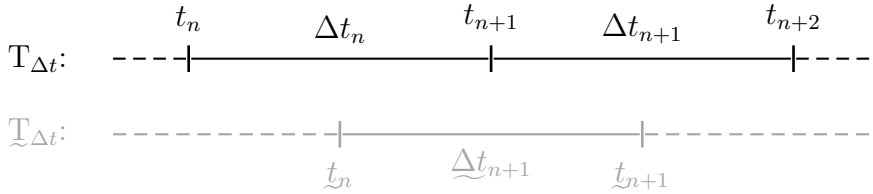

We discretize Maxwell's second topological grid equation (3.79) on page 57 by integrating it over a dual temporal edge $\underset{\sim}{\Delta t}_{n+1}$:

$$\begin{aligned} & \int_{\underset{\sim}{\Delta t}_{n+1}} \underset{\sim}{\mathbf{C}}\, \underset{\sim}{\widehat{\mathbf{h}}}(t)\,\mathrm{d}t = \int_{\underset{\sim}{\Delta t}_{n+1}} \left(\partial_t \underset{\sim}{\widehat{\widehat{\mathbf{d}}}}(t) + \underset{\sim}{\widehat{\widehat{\mathbf{j}}}}(t) + \underset{\sim}{\widehat{\widehat{\mathbf{j}}}}_{\partial\Omega}(t)\right)\,\mathrm{d}t \\ \Leftrightarrow \quad & \int_{\underset{\sim}{t}_n}^{\underset{\sim}{t}_{n+1}} \underset{\sim}{\mathbf{C}}\, \underset{\sim}{\widehat{\mathbf{h}}}(t)\,\mathrm{d}t = \int_{\underset{\sim}{t}_n}^{\underset{\sim}{t}_{n+1}} \left(\partial_t \underset{\sim}{\widehat{\widehat{\mathbf{d}}}}(t) + \underset{\sim}{\widehat{\widehat{\mathbf{j}}}}(t) + \underset{\sim}{\widehat{\widehat{\mathbf{j}}}}_{\partial\Omega}(t)\right)\,\mathrm{d}t \end{aligned} \tag{3.165}$$

Again using the interchangeability of the time integration and the dual discrete curl operator, we arrive at Maxwell's second topological grid equation discrete in space and time:

$$\begin{aligned} \Leftrightarrow \quad & \underset{\sim}{\mathbf{C}} \int_{\underset{\sim}{t}_n}^{\underset{\sim}{t}_{n+1}} \underset{\sim}{\widehat{\mathbf{h}}}(t)\,\mathrm{d}t = \underset{\sim}{\widehat{\widehat{\mathbf{d}}}}(\underset{\sim}{t}_{n+1}) - \underset{\sim}{\widehat{\widehat{\mathbf{d}}}}(\underset{\sim}{t}_n) + \int_{\underset{\sim}{t}_n}^{\underset{\sim}{t}_{n+1}} \underset{\sim}{\widehat{\widehat{\mathbf{j}}}}(t)\,\mathrm{d}t + \int_{\underset{\sim}{t}_n}^{\underset{\sim}{t}_{n+1}} \underset{\sim}{\widehat{\widehat{\mathbf{j}}}}_{\partial\Omega}(t)\,\mathrm{d}t \\ \Leftrightarrow \quad & \boxed{\underset{\sim}{\mathbf{C}}\, \underset{\sim}{\overline{\widehat{\mathbf{h}}}}^{n+1} = \underset{\sim}{\widehat{\widehat{\mathbf{d}}}}^{n+1} - \underset{\sim}{\widehat{\widehat{\mathbf{d}}}}^{n} + \underset{\sim}{\overline{\widehat{\widehat{\mathbf{j}}}}}^{n+1} + \underset{\sim}{\overline{\widehat{\widehat{\mathbf{j}}}}}_{\partial\Omega}^{n+1}} \qquad \forall\, n \in \mathbb{Z} \end{aligned} \tag{3.166}$$

where we have introduced the magnetic grid voltage pulses $\underset{\sim}{\overline{\widehat{\mathbf{h}}}}^n$ as the grid projection of the magnetic grid voltages $\underset{\sim}{\widehat{\mathbf{h}}}(t)$ onto the dual temporal edges $\underset{\sim}{\Delta t}_n$ by the grid projection operator $\underset{\sim}{L}^1_{\underset{\sim}{\mathrm{T}}_{\Delta t},n}$

$$\underset{\sim}{\overline{\widehat{\mathbf{h}}}}^n \equiv \underset{\sim}{L}^1_{\underset{\sim}{\mathrm{T}}_{\Delta t},n} \underset{\sim}{\widehat{\mathbf{h}}}(t) \equiv \int_{\underset{\sim}{\Delta t}_n} \underset{\sim}{\widehat{\mathbf{h}}}(t)\,\mathrm{d}t \tag{3.167}$$

the electric grid source current pulses $\underset{\sim}{\overline{\widehat{\widehat{\mathbf{j}}}}}^n$ as the grid projection of the source currents $\underset{\sim}{\widehat{\widehat{\mathbf{j}}}}(t)$ onto the dual temporal edges $\underset{\sim}{\Delta t}_n$

$$\underset{\sim}{\overline{\widehat{\widehat{\mathbf{j}}}}}^n \equiv \underset{\sim}{L}^1_{\underset{\sim}{\mathrm{T}}_{\Delta t},n} \underset{\sim}{\widehat{\widehat{\mathbf{j}}}}(t) = \int_{\underset{\sim}{\Delta t}_n} \underset{\sim}{\widehat{\widehat{\mathbf{j}}}}(t)\,\mathrm{d}t \tag{3.168}$$

the equivalent electric boundary grid current pulses $\underset{\sim}{\overline{\hat{\mathbf{j}}}}^{n}_{\partial\Omega}$ as the grid projection of the equivalent electric boundary grid currents $\underset{\sim}{\hat{\mathbf{j}}}_{\partial\Omega}(t)$ onto the dual temporal edges $\underset{\sim}{\Delta t}_n$

$$\underset{\sim}{\overline{\hat{\mathbf{j}}}}^{n}_{\partial\Omega} \equiv \underset{\sim}{L}^{1}_{\underset{\sim}{\mathrm{T}}_{\Delta t},n} \underset{\sim}{\hat{\mathbf{j}}}_{\partial\Omega}(t) = \int_{\underset{\sim}{\Delta t}_n} \underset{\sim}{\hat{\mathbf{j}}}_{\partial\Omega}(t)\,\mathrm{d}t \tag{3.169}$$

and the electric grid fluxes $\underset{\sim}{\hat{\mathbf{d}}}^{n}$ as the grid projection of the time-continuous electric grid fluxes $\underset{\sim}{\hat{\mathbf{d}}}(t)$ onto the dual temporal nodes $\underset{\sim}{t}_n$ by the grid projection operator $\underset{\sim}{L}^{0}_{\underset{\sim}{\mathrm{T}}_{\Delta t},n}$:

$$\underset{\sim}{\hat{\mathbf{d}}}^{n} \equiv \underset{\sim}{L}^{0}_{\underset{\sim}{\mathrm{T}}_{\Delta t},n} \underset{\sim}{\hat{\mathbf{d}}}(t) \equiv \underset{\sim}{\hat{\mathbf{d}}}(\underset{\sim}{t}_n) \tag{3.170}$$

Later, we will split the equivalent electric boundary grid current pulses $\underset{\sim}{\overline{\hat{\mathbf{j}}}}^{n}_{\partial\Omega}$ into the boundary parts $\underset{\sim}{\overline{\hat{\mathbf{j}}}}^{n}_{\Gamma_1}$ and $\underset{\sim}{\overline{\hat{\mathbf{j}}}}^{n}_{\Gamma_2}$ defined equivalently to equation (3.169).

Let us take a look back at what we have done: Fig. 3.16 shows the association of the time and space discretized quantities with the introduced primal and dual temporal grids $\mathrm{T}_{\Delta t}$ and $\underset{\sim}{\mathrm{T}}_{\Delta t}$. These quantities actually live on Cartesian product spaces of the spatial and the temporal grids, e.g. on $\Omega_h \times \mathrm{T}_{\Delta t}$ and $\underset{\sim}{\Omega}_h \times \underset{\sim}{\mathrm{T}}_{\Delta t}$. This greatly restricts our time-stepping schemes: Firstly, no local time-stepping is possible with this approach as the temporal discretization is assumed the same for each spatial grid element. Secondly, the topology of the spatial grid is the same for all time-steps which does not allow for a time-adjusted topology of the grid. The first drawback can be handled by simplectic time integrators with local time-stepping, e.g. as nicely presented in [72]. The second drawback calls for a rigorous discretization of Maxwell's equations on a 4-dimensional space-time grid.

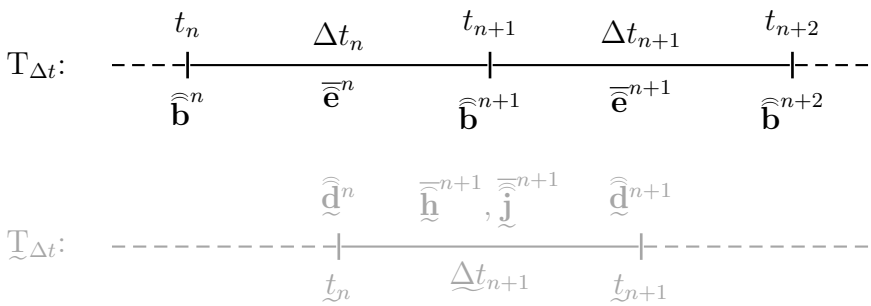

Fig. 3.16: Primal and dual temporal grids $\mathrm{T}_{\Delta t}$ and $\underset{\sim}{\mathrm{T}}_{\Delta t}$. Shown are the nodes and edges of the grids as well as the association of the quantities from the space- and time-discrete Maxwell's Grid Equations (3.164) and (3.166) with the temporal grid elements.

3.3.2 Maxwell's Discrete Material Laws

The space and time discrete material laws transfer the grid quantities from the primal space-time grid $\Omega_h \times \mathrm{T}_{\Delta t}$ to the dual space-time grid $\underset{\sim}{\Omega}_h \times \underset{\sim}{\mathrm{T}}_{\Delta t}$ and vice versa. Maxwell's first material law transfers the electric grid voltage pulses $\overline{\hat{\mathbf{e}}}^m$ to the electric grid fluxes

$\underset{\sim}{\widehat{\overline{\mathbf{d}}}}^n$ by the *space-time permittivity matrices* $\dot{\mathbf{M}}_\varepsilon(n,m)$:

$$\boxed{\underset{\sim}{\widehat{\overline{\mathbf{d}}}}^n = \sum_{m=-\infty}^{+\infty} \dot{\mathbf{M}}_\varepsilon(n,m)\overline{\widehat{\mathbf{e}}}^m} \qquad \forall\, n \in \mathbb{Z} \tag{3.171}$$

The discrete space-time permittivity matrices $\dot{\mathbf{M}}_\varepsilon(n,m)$ include temporal metric information to transfer between the temporal primal and dual grids as well as spatial metric information to transfer between the spatial primal and dual grids. Due to changes in the time-steps, the space-time material matrices $\dot{\mathbf{M}}_\varepsilon(n,m)$ can change over time and thus carry the arguments n and m.

Using the *space-time reluctivity matrices* $\overline{\mathbf{M}}_\nu(n,m)$, we write Maxwell's second material law transferring the magnetic grid fluxes $\widehat{\overline{\mathbf{b}}}^m$ to the magnetic grid voltage pulses $\underset{\sim}{\overline{\widehat{\mathbf{h}}}}^n$ as:

$$\boxed{\underset{\sim}{\overline{\widehat{\mathbf{h}}}}^n = \sum_{m=-\infty}^{+\infty} \overline{\mathbf{M}}_\nu(n,m)\widehat{\overline{\mathbf{b}}}^m} \qquad \forall\, n \in \mathbb{Z} \tag{3.172}$$

Again, the space-time reluctivity matrices $\overline{\mathbf{M}}_\nu(n,m)$ might differ at different time instants.

Although it would be interesting to propose general properties of the discrete space-time matrices and derive properties for Maxwell's Grid Equations just from these, this was not the aim of this thesis. As we will apply the Newmark-Θ time-stepping scheme in the applications, its specific space-time material relations are used in the next chapters to derive its metric properties in parallel to the continuous and semi-discrete cases.

Newmark-Θ Time-Stepping

The cell-based Newmark-Θ time-stepping scheme introduced in [76] can be recast in the FIT formalism using special material laws. In order to simplify the presentation, we will assume the same constant time-steps for both temporal grids

$$\Delta t_n = \underset{\sim}{\Delta} t_n = \Delta t \qquad \forall\, n \in \mathbb{Z} \tag{3.173}$$

and assume the dual temporal grid to be centered with respect to the primal temporal grid, i.e.:

$$\underset{\sim}{t}_n = \frac{1}{2}\left(t_n + t_{n+1}\right) \qquad \forall\, n \in \mathbb{Z} \tag{3.174}$$

The Newmark-Θ time-stepping scheme was developed in [76] to handle hybrid FD/FE schemes. The parameters Θ_m defined for each cell S_m^3 allow to construct a provably stable hybrid FD/FE scheme without further reduction of the time-step in the FEM part. In the formalism of the FIT, using the diagonal standard FIT spatial material matrices as defined in chapter 3.2.2 renders the FD scheme, while using the Whitney-FEM material matrices to be defined in chapter 4 renders the FE scheme. Now one part of the domain is discretized using cells with the local diagonal standard FIT spatial material matrices $\mathbf{M}_{\mathrm{sFIT},\varepsilon}^{1,m}$ and $\mathbf{M}_{\mathrm{sFIT},\nu}^{2,m}$ defined in equations (3.85) on page 59 and (3.91)

on page 61, respectively. The other part is discretized using cells with local Whitney-FEM spatial material matrices $\mathbf{M}^{1,m}_{\mathrm{FEM},\varepsilon}$ and $\mathbf{M}^{1,m}_{\mathrm{FEM},\nu}$ which will be defined in chapter 4. Let $\mathrm{I}^3_{\mathrm{sFIT}}$ denote the indices of the cells with diagonal sFIT material matrices and $\mathrm{I}^3_{\mathrm{FEM}}$ the indices of the cells with Whitney-FEM material matrices. Then the permittivity matrix $\mathbf{M}_\varepsilon$ used below in the Newmark-Θ space-time material relations is defined as:

$$\mathbf{M}_\varepsilon \equiv \sum_{m\in\mathrm{I}^3_{\mathrm{sFIT}}} \mathbf{M}^{1,m}_{\mathrm{sFIT},\varepsilon} + \sum_{m\in\mathrm{I}^3_{\mathrm{FEM}}} \mathbf{M}^{1,m}_{\mathrm{FEM},\varepsilon} \tag{3.175a}$$

For the reluctivity matrix, the weighing coefficient vector $\boldsymbol{\Theta} \in \mathbb{R}^{n^3}$ is introduced with one entry Θ_m for each primal grid cell. These weighing coefficients will be used to control the time-stepping scheme of each cell to render the explicit leapfrog time-stepping[13] for the standard FIT cells and an unconditionally stable time-stepping for the Whitney-FEM cells. The weighted reluctivity matrix $\mathbf{M}^{\boldsymbol{\Theta}}_\nu$ used below in the Newmark-Θ space-time material relations is defined as:

$$\mathbf{M}^{\boldsymbol{\Theta}}_\nu \equiv \sum_{m\in\mathrm{I}^3_{\mathrm{sFIT}}} \Theta_m\, \mathbf{M}^{2,m}_{\mathrm{sFIT},\nu} + \sum_{m\in\mathrm{I}^3_{\mathrm{FEM}}} \Theta_m\, \mathbf{M}^{2,m}_{\mathrm{FEM},\nu} \tag{3.175b}$$

For later use, we note the following relation for weighted material matrices:

$$\mathbf{M}^{a\boldsymbol{\alpha}+b\boldsymbol{\beta}}_\nu = a\,\mathbf{M}^{\boldsymbol{\alpha}}_\nu + b\,\mathbf{M}^{\boldsymbol{\beta}}_\nu \qquad \forall\, a,b\in\mathbb{R}, \quad \boldsymbol{\alpha},\boldsymbol{\beta}\in\mathbb{R}^{n_3} \tag{3.176}$$

Using $\mathbf{1}$ to denote the weighing vector with only ones as entries, we can write the standard global reluctivity matrix $\mathbf{M}_\nu$ as

$$\mathbf{M}_\nu = \sum_{m=1}^{n^3} \mathbf{M}^m_\nu = \mathbf{M}^{\mathbf{1}}_\nu \tag{3.177}$$

The above defined material matrices fulfill the properties outlined in chapter 3.1.4: The permittivity matrix $\mathbf{M}_\varepsilon$ and the reluctivity matrix $\mathbf{M}_\nu$ are symmetric positive definite. For non-negative parameters α_m, the weighted reluctivity matrix $\mathbf{M}^{\boldsymbol{\alpha}}_\nu$ is symmetric positive semi-definite.

We propose the following Maxwell's electric and magnetic material grid laws for the Newmark-Θ scheme:

$$\boxed{\widehat{\underset{\sim}{\mathbf{d}}}^n = \mathbf{M}_\varepsilon \frac{1}{\Delta t}\widehat{\overline{\mathbf{e}}}^n} \qquad \forall\, n\in\mathbb{Z} \tag{3.178a}$$

$$\boxed{\widehat{\overline{\underset{\sim}{\mathbf{h}}}}^n = \Delta t\left(\mathbf{M}^{\boldsymbol{\Theta}}_\nu\, \widehat{\mathbf{b}}^{n-1} + \mathbf{M}^{\mathbf{1}-2\boldsymbol{\Theta}}_\nu\, \widehat{\mathbf{b}}^{n} + \mathbf{M}^{\boldsymbol{\Theta}}_\nu\, \widehat{\mathbf{b}}^{n+1}\right)} \qquad \forall\, n\in\mathbb{Z} \tag{3.178b}$$

Setting the control parameters Θ_m to zero for all indices m renders the standard conditionally stable leapfrog time-stepping scheme. Setting the control parameters Θ_m to $\frac{1}{4}$ renders the unconditionally stable Newmark time-stepping scheme. For the Newmark-Θ scheme, the parameters Θ_m are set to zero for the sFIT cells, i.e. for $m \in \mathrm{I}^3_{\mathrm{sFIT}}$, and to $\frac{1}{4}$ for the Whitney-FEM cells, i.e. for $m \in \mathrm{I}^3_{\mathrm{FEM}}$. This renders a scheme with explicit time-stepping for the sFIT cells. As we will see in chapter 3.3.5, the Newmark-Θ scheme is conditionally stable with a time-step restriction only due to the sFIT cells.

[13] The leapfrog time-stepping scheme is widely used in time domain simulations, as it often renders an explicit time-stepping scheme [95, pp. 304]. For Maxwell's equations, together with spatial finite difference approximations, it is known as Yee algorithm [100].

3.3.3 Maxwell's Topological Properties

Maxwell's topological properties only make use of Maxwell's topological laws (3.164) on page 76 and (3.166) on page 77, as in the continuous and semi-discrete cases. No metric and thus no specific time-discretization scheme are needed to state Maxwell's topological properties.

Conservation of Charge

The conservation of charge is established in parallel to the time continuous and the semi-discrete Maxwell's equations. We define the magnetic and electric grid charges $\widehat{\widehat{\boldsymbol{\varrho}}}_m^n$ and $\underset{\sim}{\widehat{\widehat{\boldsymbol{\varrho}}}}_e^{*n}$ as

$$\widehat{\widehat{\boldsymbol{\varrho}}}_m^n \equiv \mathbf{S}\,\widehat{\widehat{\mathbf{b}}}^n \tag{3.179}$$

$$\underset{\sim}{\widehat{\widehat{\boldsymbol{\varrho}}}}_e^{*n} \equiv \underset{\sim}{\mathbf{S}}\,\underset{\sim}{\widehat{\widehat{\mathbf{d}}}}^n \tag{3.180}$$

where the superscript $*$ is used as a reminder that the electric grid charges $\underset{\sim}{\widehat{\widehat{\boldsymbol{\varrho}}}}_e^{*n}$ do contain equivalent boundary charges. We apply the discrete divergence grid operators $\mathbf{S}$ and $\underset{\sim}{\mathbf{S}}$ to Maxwell's topological grid laws (3.164) on page 76 and (3.166) on page 77 to arrive at the conservation of the magnetic and electric charges for the space- and time-discrete case:

$$\boxed{\widehat{\widehat{\boldsymbol{\varrho}}}_m^{n+1} - \widehat{\widehat{\boldsymbol{\varrho}}}_m^n = \mathbf{0}} \tag{3.181}$$

$$\boxed{\underset{\sim}{\widehat{\widehat{\boldsymbol{\varrho}}}}_e^{*n+1} - \underset{\sim}{\widehat{\widehat{\boldsymbol{\varrho}}}}_e^{*n} = -\underset{\sim}{\mathbf{S}}\,\underset{\sim}{\overline{\widehat{\dot{\mathbf{j}}}}}^{n+1} - \underset{\sim}{\mathbf{S}}\,\underset{\sim\partial\Omega}{\overline{\widehat{\dot{\mathbf{j}}}}}^{n+1}} \tag{3.182}$$

Potential Formulations

In parallel to the continuous and semi-discrete case, we will under the assumption of absence of magnetic charges introduce a magnetic vector potential $\widehat{\mathbf{a}}_m^n$ and rewrite the electric grid voltage pulses $\overline{\mathbf{e}}^n$ in terms of this vector potential and a scalar electric potential $\overline{\boldsymbol{\varphi}}_e^n$.

Assuming no magnetic charges to exist at an arbitrary time-step t_{n_0}, the conservation of charge in equation (3.181) renders zero magnetic charges at all time-steps:

$$\widehat{\widehat{\boldsymbol{\varrho}}}_m^n = \mathbf{S}\,\widehat{\widehat{\mathbf{b}}}^n = \mathbf{0} \qquad \forall\, n \in \mathbb{Z} \tag{3.183}$$

Then according to the Poincaré Lemma (3.47) on page 46, we can introduce for all time-steps a magnetic vector potential $\widehat{\mathbf{a}}_m^n$ such that

$$\widehat{\widehat{\mathbf{b}}}^n = \mathbf{C}\,\widehat{\mathbf{a}}_m^n \qquad \forall\, n \in \mathbb{Z} \tag{3.184}$$

Maxwell's first topological grid law (3.164) on page 76 then renders:

$$\begin{aligned} & \mathbf{C}\,\overline{\mathbf{e}}^n = \mathbf{C}\,\widehat{\mathbf{a}}_m^n - \mathbf{C}\,\widehat{\mathbf{a}}_m^{n+1} \\ \Leftrightarrow \qquad & \mathbf{C}\left(\overline{\mathbf{e}}^n - \widehat{\mathbf{a}}_m^n + \widehat{\mathbf{a}}_m^{n+1}\right) = \mathbf{0} \end{aligned} \tag{3.185}$$

By the Poincaré Lemma (3.46) on page 46, the existence of some electric scalar grid potential $\overline{\boldsymbol{\varphi}}_e^n$ fulfilling the following equation is assured:

$$\begin{aligned} & \overline{\mathbf{e}}^n - \widehat{\mathbf{a}}_m^n + \widehat{\mathbf{a}}_m^{n+1} = -\,\mathbf{G}\,\overline{\boldsymbol{\varphi}}_e^n \\ \Leftrightarrow \quad & \overline{\mathbf{e}}^n = \widehat{\mathbf{a}}_m^n - \widehat{\mathbf{a}}_m^{n+1} - \mathbf{G}\,\overline{\boldsymbol{\varphi}}_e^n \end{aligned} \tag{3.186}$$

Maxwell's equations can now be rewritten in the unknown vector and scalar potentials $\widehat{\mathbf{a}}_m^n$ and $\overline{\boldsymbol{\varphi}}_e^n$. Note that again, the choice of the magnetic vector and electric scalar potentials is not unique and special gauges can be used.

Discrete Poynting's Theorem

We assume Maxwell's topological grid laws (3.164) on page 76 and (3.166) on page 77 to hold and derive a version of a discrete Poynting's Theorem from these. The interpretation of the preserved quantities as energies is only possible together with the metric laws and will be done in the next chapter.

Actually, several different conserved energy-like quantities can be derived from Maxwell's spatially and temporally discrete topological grid laws. Following the ideas of [30], we choose to derive energy terms at the dual time instants $\underset{\sim}{t}_n$ and therefore look at their change over the dual time intervals $\underset{\sim}{\Delta t}_n$. This leads us to consider the exterior product of the Maxwell's second topological grid law (3.166) with averaged electric grid voltage pulses[14]:

$$\left(\underset{\sim}{\mathbf{C}}\,\underset{\sim}{\overline{\widehat{\mathbf{h}}}}^{n+1}\right)^{\mathrm{T}} \frac{1}{2}\left(\overline{\widehat{\mathbf{e}}}^{n+1} + \overline{\widehat{\mathbf{e}}}^{n}\right) = \left(\underset{\sim}{\widehat{\mathbf{d}}}^{n+1} - \underset{\sim}{\widehat{\mathbf{d}}}^{n} + \underset{\sim}{\overline{\widehat{\mathbf{j}}}}^{n+1} + \underset{\sim}{\overline{\widehat{\mathbf{j}}}}_{\partial\Omega}^{n+1}\right)^{\mathrm{T}} \frac{1}{2}\left(\overline{\widehat{\mathbf{e}}}^{n+1} + \overline{\widehat{\mathbf{e}}}^{n}\right)$$

Using the duality of the discrete curl operators in equation (3.52) on page 46, we can write the left hand side as

$$= \left(\underset{\sim}{\overline{\widehat{\mathbf{h}}}}^{n+1}\right)^{\mathrm{T}} \frac{1}{2}\left(\mathbf{C}\,\overline{\widehat{\mathbf{e}}}^{n+1} + \mathbf{C}\,\overline{\widehat{\mathbf{e}}}^{n}\right)$$

which plugging in Maxwell's first topological grid law (3.164) renders:

$$\begin{aligned} &= \left(\underset{\sim}{\overline{\widehat{\mathbf{h}}}}^{n+1}\right)^{\mathrm{T}} \frac{1}{2}\left(\widehat{\mathbf{b}}^{n+1} - \widehat{\mathbf{b}}^{n+2} + \widehat{\mathbf{b}}^{n} - \widehat{\mathbf{b}}^{n+1}\right) \\ &= \left(\underset{\sim}{\overline{\widehat{\mathbf{h}}}}^{n+1}\right)^{\mathrm{T}} \frac{1}{2}\left(\widehat{\mathbf{b}}^{n} - \widehat{\mathbf{b}}^{n+2}\right) \end{aligned}$$

Rearranging terms, we arrive at a space-time discrete Poynting's Theorem:

$$\begin{aligned} & \left(\underset{\sim}{\widehat{\mathbf{d}}}^{n+1} - \underset{\sim}{\widehat{\mathbf{d}}}^{n}\right)^{\mathrm{T}} \frac{1}{2}\left(\overline{\widehat{\mathbf{e}}}^{n+1} + \overline{\widehat{\mathbf{e}}}^{n}\right) + \left(\underset{\sim}{\overline{\widehat{\mathbf{h}}}}^{n+1}\right)^{\mathrm{T}} \frac{1}{2}\left(\widehat{\mathbf{b}}^{n+2} - \widehat{\mathbf{b}}^{n}\right) \\ & \quad + \left(\underset{\sim}{\overline{\widehat{\mathbf{j}}}}^{n+1}\right)^{\mathrm{T}} \frac{1}{2}\left(\overline{\widehat{\mathbf{e}}}^{n+1} + \overline{\widehat{\mathbf{e}}}^{n}\right) + \left(\underset{\sim}{\overline{\widehat{\mathbf{j}}}}_{\partial\Omega}^{n+1}\right)^{\mathrm{T}} \frac{1}{2}\left(\overline{\widehat{\mathbf{e}}}^{n+1} + \overline{\widehat{\mathbf{e}}}^{n}\right) = 0 \end{aligned} \tag{3.187}$$

The discrete Poynting's Theorem in this form is still a fairly abstract topological conservation law and its selection from the conservation laws that we can derive seems to some extent arbitrary. The reason for choosing this version will be revealed when we define the space-time discrete energies and insert the Newmark-Θ material laws in the next chapter.

[14] We can equivalently derive a discrete Poynting's Theorem for the primal time intervals Δt_n to arrive at conserved energy terms at the primal time instants t_n.

3.3.4 Maxwell's Metric Properties

Although, as hinted at above, a discussion of the metric properties for general space-time material relations seems desirable at this point, this is outside the scope of this thesis. We will analyze the properties stemming from the full set of Maxwell's Grid Equations only for the case of the Newmark-Θ material laws (3.178a) and (3.178b) on page 80.

Conservation of Energy

For the space-time material relations of the Newmark-Θ scheme, we define the space-time discrete electric energy W_e^n, magnetic energy W_m^n, and total energy W^n at the dual time instants $\underset{\sim}{t}_n$ by

$$W_e^n \equiv \frac{1}{2\Delta t^2} \left(\overline{\mathbf{e}}^n\right)^T \mathbf{M}_\varepsilon \, \overline{\mathbf{e}}^n \tag{3.188}$$

$$W_m^n \equiv \frac{1}{2} \left[\left(\widehat{\overline{\mathbf{b}}}^n\right)^T \mathbf{M}_\nu^{\mathbf{\Theta}} \, \widehat{\overline{\mathbf{b}}}^n + \left(\widehat{\overline{\mathbf{b}}}^n\right)^T \mathbf{M}_\nu^{\mathbf{1}-2\mathbf{\Theta}} \, \widehat{\overline{\mathbf{b}}}^{n+1} + \left(\widehat{\overline{\mathbf{b}}}^{n+1}\right)^T \mathbf{M}_\nu^{\mathbf{\Theta}} \, \widehat{\overline{\mathbf{b}}}^{n+1} \right] \tag{3.189}$$

$$W^n \equiv W_e^n + W_m^n \tag{3.190}$$

We first note that the magnetic energy W_m^n might become negative due to the mixed terms. This raises the question whether the total discrete energy W^n does even define a norm on the unknowns $\overline{\mathbf{e}}^n$ and $\widehat{\overline{\mathbf{b}}}^n$. The following theorem does assure this under a constraint on the time-step of the Newmark-Θ scheme:

Theorem 3.9. *For the Newmark-Θ scheme, the total electromagnetic energy W^n defined by equation (3.190) defines a norm on the unknown vector $\mathbf{x}^n$*

$$\mathbf{x}^n \equiv \begin{pmatrix} \overline{\mathbf{e}}^n \\ \widehat{\overline{\mathbf{b}}}^n \end{pmatrix} \tag{3.191}$$

if the time-step Δt obeys the following criteria:

$$\Delta t < \frac{2}{\max_{m \in \mathrm{I}^3_{\mathrm{sFIT}}} \sqrt{\lambda_{\mathbf{L}^m,\max}}} \tag{3.192}$$

where $\mathrm{I}^3_{\mathrm{sFIT}}$ denotes the indices of the cells with standard diagonal FIT material matrix contributions and $\lambda_{\mathbf{L}^m,\max}$ denotes the maximum eigenvalue of the matrix $\mathbf{L}^m$ defined as

$$\mathbf{L}^m \equiv \mathbf{C} \left(\mathbf{M}^{1,m}_{\mathrm{sFIT},\varepsilon}\right)^{-1} \underset{\sim}{\mathbf{C}} \, \mathbf{M}^{2,m}_{\mathrm{sFIT},\nu} \tag{3.193}$$

The proof of Theorem 3.9 can be found in appendix F.1.1 on page 215.

Let us define the space-time discrete *electric loss pulses* $\overline{P}_e^n$ and the *equivalent boundary electric grid loss pulses* $\overline{P}_P^n$ as

$$\overline{P}_e^n = \frac{1}{2\Delta t} \left(\overline{\widehat{\underset{\sim}{\mathbf{j}}}}^n\right)^T \left(\overline{\mathbf{e}}^n + \overline{\mathbf{e}}^{n-1}\right) \tag{3.194}$$

$$\overline{P}_P^n = \frac{1}{2\Delta t} \left(\overline{\widehat{\underset{\sim}{\mathbf{j}}}}^n_{\partial\Omega}\right)^T \left(\overline{\mathbf{e}}^n + \overline{\mathbf{e}}^{n-1}\right) \tag{3.195}$$

Then after some calculation, we can rewrite the discrete Poynting's Theorem (3.187) by using the Newmark-Θ material relations (3.178a) and (3.178b) on page 80 as:

$$\boxed{\left(W^{n+1} - W^n\right) + \overline{P}_e^{n+1} + \overline{P}_P^{n+1} = 0} \tag{3.196}$$

This conservation law for the total energy W^n for the cell-based Newmark-Θ scheme has, to the authors knowledge, not been reported before. Setting the control parameters Θ_m to zero, one arrives at the standard conservation law for the discrete energy of the FIT-leapfrog as stated e.g. in [30], extended for non-zero boundary terms.

3.3.5 Temporally and Spatially Discrete Maxwell's Initial Boundary Value Problem

As in the continuous and the semi-discrete cases, the temporally and spatially discrete Maxwell's equations have to be supplemented by suitable initial and boundary conditions to arrive at a fully discrete IBVP with a unique solution. In this chapter, we will state a fully discrete IBVP employing the Newmark-Θ time-stepping scheme, show existence and uniqueness of a solution, and prove its conditional stability.

A Discrete Initial Boundary Value Problem for Maxwell's Grid Equations

We assume the continuous Maxwell's IBVP in equations (2.57a) to (2.57h) on page 21 to be given along with the boundary data $\vec{E}_{\Gamma_1}(\vec{r},t)$ and $\vec{H}_{\Gamma_2}(\vec{r},t)$ and the source current $\vec{J}(\vec{r},t)$ with unbounded temporal domain T. Alternatively, the semi-discrete Maxwell's grid IBVP in equations (3.132a) to (3.132h) on page 68 along with the boundary data $\widehat{\mathbf{e}}_{\Gamma_1}(t)$ and $\underset{\sim}{\widehat{\mathbf{h}}}_{\Gamma_2}(t)$ and the source current $\underset{\sim}{\widehat{\widehat{\mathbf{j}}}}(t)$ can be assumed given with unbounded temporal domain T. Then we arrive at space- and time-discrete boundary and source data by the following grid projections:

$$\overline{\widehat{\mathbf{e}}}^n_{\Gamma_1} = L^1_{\mathrm{T}_{\Delta t},n}\,\widehat{\mathbf{e}}_{\Gamma_1}(t) = L^1_{\mathrm{T}_{\Delta t},n}\,\mathrm{L}^1_{\overline{\Gamma}_{1,h}}\,\vec{E}_{\Gamma_1}(\vec{r},t) \qquad \forall\, n \in \mathbb{Z} \tag{3.197}$$

$$\underset{\sim}{\overline{\widehat{\mathbf{h}}}}^n_{\Gamma_2} = \underset{\sim}{L}^1_{\underset{\sim}{\mathrm{T}}_{\Delta t},n}\,\underset{\sim}{\widehat{\mathbf{h}}}_{\Gamma_2}(t) = \underset{\sim}{L}^1_{\underset{\sim}{\mathrm{T}}_{\Delta t},n}\,\underset{\sim}{\mathrm{L}}^1_{\overline{\Gamma}_{2,h}}\,\vec{H}_{\Gamma_2}(\vec{r},t) \qquad \forall\, n \in \mathbb{Z} \tag{3.198}$$

$$\underset{\sim}{\overline{\widehat{\widehat{\mathbf{j}}}}}^n = \underset{\sim}{L}^1_{\underset{\sim}{\mathrm{T}}_{\Delta t},n}\,\underset{\sim}{\widehat{\widehat{\mathbf{j}}}}(t) = \underset{\sim}{L}^1_{\underset{\sim}{\mathrm{T}}_{\Delta t},n}\,\underset{\sim}{\mathrm{L}}^2\,\vec{J}(\vec{r},t) \qquad \forall\, n \in \mathbb{Z} \tag{3.199}$$

The temporal primal and dual grid projection operators $L^1_{\mathrm{T}_{\Delta t},n}$ and $\underset{\sim}{L}^1_{\underset{\sim}{\mathrm{T}}_{\Delta t},n}$ were defined in equation (3.162) on page 76 and equation (3.167) on page 77, respectively.

For the spatially and temporally discrete Maxwell's IBVP, we have assumed an unbounded temporal domain T. Thus we do not truly have any temporal boundary. Nevertheless, we need the field values at some time instants to arrive at uniqueness of the solution. From these initial values, we can calculate the fields forward or backward in time to arrive at the solution for all discrete temporal grid elements. We assume the continuous values of the electric field strength $\vec{E}(\vec{r},t)$ to be given over the primal temporal edge Δt_0 and the magnetic flux density $\vec{B}(\vec{r},t)$ at the primal temporal node t_0. Alternatively, the equivalent

data of the semi-discrete case can be given. Then we can use the following grid projected initial data:

$$\overline{\mathbf{e}}^0 = L^1_{\mathrm{T}_{\Delta t},0}\mathbf{e}(t) = L^1_{\mathrm{T}_{\Delta t},0}\mathrm{L}^1\vec{E}(\vec{r},t) \tag{3.200}$$

$$\widehat{\overline{\mathbf{b}}}^0 = L^0_{\mathrm{T}_{\Delta t},0}\widehat{\mathbf{b}}(t) = L^0_{\mathrm{T}_{\Delta t},0}\mathrm{L}^2\vec{B}(\vec{r},t) \tag{3.201}$$

The initial data is again required to be compatible with the boundary conditions, i.e.:

$$\mathbf{T}_{\Gamma_1}\,\overline{\mathbf{e}}^0 = \overline{\mathbf{e}}^0_{\Gamma_1} \tag{3.202}$$

Now we can collect Maxwell's topological grid laws in equations (3.164) on page 76 and (3.166) on page 77, Maxwell's material laws for the specific Newmark-Θ scheme in equations (3.178a) and (3.178b) on page 80 and impose the initial and boundary conditions to arrive at Maxwell's space- and time-discrete IBVP:

$$\mathbf{C}\,\overline{\mathbf{e}}^n = \widehat{\overline{\mathbf{b}}}^n - \widehat{\overline{\mathbf{b}}}^{n+1} \qquad \forall\, n \in \mathbb{Z} \tag{3.203a}$$

$$\underset{\sim}{\mathbf{C}}\,\underset{\sim}{\overline{\mathbf{h}}}^{n+1} = \underset{\sim}{\widehat{\overline{\mathbf{d}}}}^{n+1} - \underset{\sim}{\widehat{\overline{\mathbf{d}}}}^{n} + \underset{\sim}{\widehat{\overline{\mathbf{j}}}}^{n+1} + \underset{\sim}{\widehat{\overline{\mathbf{j}}}}^{n+1}_{\Gamma_1} + \underset{\sim}{\widehat{\overline{\mathbf{j}}}}^{n+1}_{\Gamma_2} \qquad \forall\, n \in \mathbb{Z} \tag{3.203b}$$

$$\underset{\sim}{\widehat{\overline{\mathbf{d}}}}^{n} = \mathbf{M}_\varepsilon\,\frac{1}{\Delta t}\overline{\mathbf{e}}^n \qquad \forall\, n \in \mathbb{Z} \tag{3.203c}$$

$$\underset{\sim}{\overline{\mathbf{h}}}^{n} = \Delta t\left(\mathbf{M}_\nu^{\boldsymbol{\Theta}}\,\widehat{\overline{\mathbf{b}}}^{n-1} + \mathbf{M}_\nu^{\mathbf{1}-2\boldsymbol{\Theta}}\,\widehat{\overline{\mathbf{b}}}^{n} + \mathbf{M}_\nu^{\boldsymbol{\Theta}}\,\widehat{\overline{\mathbf{b}}}^{n+1}\right) \qquad \forall\, n \in \mathbb{Z} \tag{3.203d}$$

$$\mathbf{T}_{\Gamma_1}\,\overline{\mathbf{e}}^n = \overline{\mathbf{e}}^n_{\Gamma_1} \qquad \forall\, n \in \mathbb{Z} \tag{3.203e}$$

$$\underset{\sim}{\widehat{\overline{\mathbf{j}}}}^{n}_{\Gamma_2} = -\left(\mathbf{T}_{\Gamma_2}\right)^{\mathrm{T}}\,\underset{\sim}{\overline{\mathbf{h}}}^{n}_{\Gamma_2} \qquad \forall\, n \in \mathbb{Z} \tag{3.203f}$$

$$\overline{\mathbf{e}}^0 \quad \text{given} \tag{3.203g}$$

$$\widehat{\overline{\mathbf{b}}}^0 \quad \text{given} \tag{3.203h}$$

The source current pulses $\underset{\sim}{\widehat{\overline{\mathbf{j}}}}^{n}$ and the boundary data $\overline{\mathbf{e}}^n_{\Gamma_1}$ and $\underset{\sim}{\overline{\mathbf{h}}}^{n}_{\Gamma_2}$ are assumed known for all $n \in \mathbb{Z}$. The initial data $\overline{\mathbf{e}}^0$ and $\widehat{\overline{\mathbf{b}}}^0$ is also assumed to be given. All other quantities are assumed unknown.

Existence and Uniqueness of the Solution to Maxwell's Spatially and Temporally Discrete Initial Boundary Value Problem

Theorem 3.10. *Maxwell's space- and time-discrete IBVP (3.203) with given initial data* $\overline{\mathbf{e}}^0$ *and* $\widehat{\overline{\mathbf{b}}}^0$*, compatible boundary data* $\overline{\mathbf{e}}^n_{\Gamma_1}$ *and* $\underset{\sim}{\overline{\mathbf{h}}}^{n}_{\Gamma_2}$*, and source data* $\underset{\sim}{\widehat{\overline{\mathbf{j}}}}^{n}$ *has a unique solution for* $n \in \mathbb{Z}$*.*

Proof. Again for ease of the presentation, we will assume only magnetic boundary conditions on all the boundary $\partial\Omega$, i.e. we assume Γ_1 to be empty. The treatment for electric boundary conditions can be included in parallel to the semi-discrete case in appendix B on page 181.

Existence and uniqueness will be proven by a direct construction of the unique solution. We can rewrite equations (3.203a) to (3.203d) on the preceding page in the unknown $\mathbf{x}^n$ defined by equation (3.191):

$$\begin{pmatrix} \frac{1}{\Delta t^2}\,\mathbf{M}_\varepsilon + \underset{\sim}{\mathbf{C}}\,\mathbf{M}_\nu^{\boldsymbol{\Theta}}\,\mathbf{C} & 0 \\ 0 & \mathbf{M}_\nu \end{pmatrix} \mathbf{x}^n = \begin{pmatrix} \frac{1}{\Delta t^2}\,\mathbf{M}_\varepsilon - \underset{\sim}{\mathbf{C}}\,\mathbf{M}_\nu^{\mathbf{1}-\boldsymbol{\Theta}}\,\mathbf{C} & \underset{\sim}{\mathbf{C}}\,\mathbf{M}_\nu \\ -\,\mathbf{M}_\nu\,\mathbf{C} & \mathbf{M}_\nu \end{pmatrix} \mathbf{x}^{n-1} - \begin{pmatrix} \frac{1}{\Delta t}\left(\underset{\sim}{\overline{\overline{\hat{\mathbf{j}}}}}^{n} + \underset{\sim}{\overline{\overline{\hat{\mathbf{j}}}}}^{n}_{\Gamma_2}\right) \\ \mathbf{0} \end{pmatrix} \tag{3.204}$$

The matrix on the left hand side is easily shown to be positive definite: The material matrices $\mathbf{M}_\varepsilon$ and $\mathbf{M}_\nu$ are positive definite. The weighted material matrix $\mathbf{M}_\nu^{\boldsymbol{\Theta}}$ is symmetric positive semi-definite, as the control parameters Θ_m are non-negative and each local material matrix $\mathbf{M}_{\nu,\mathrm{sFIT/FEM}}^{2,m}$ is symmetric positive semi-definite. Thus, according to Theorem F.7 on page 217, we can write the weighted material matrix $\mathbf{M}_\nu^{\boldsymbol{\Theta}}$ as

$$\mathbf{M}_\nu^{\boldsymbol{\Theta}} = \mathbf{X}_{\boldsymbol{\Theta}}\mathbf{E}_{\boldsymbol{\Theta}}\mathbf{X}_{\boldsymbol{\Theta}}^{\mathrm{T}} = \mathbf{X}_{\boldsymbol{\Theta}}\mathbf{E}_{\boldsymbol{\Theta}}^{\frac{1}{2}}\left(\mathbf{E}_{\boldsymbol{\Theta}}^{\frac{1}{2}}\right)^{\mathrm{T}}\mathbf{X}_{\boldsymbol{\Theta}}^{\mathrm{T}} \tag{3.205}$$

The term $\underset{\sim}{\mathbf{C}}\,\mathbf{M}_\nu^{\boldsymbol{\Theta}}\,\mathbf{C}$ can thus be written in the form:

$$\underset{\sim}{\mathbf{C}}\,\mathbf{M}_\nu^{\boldsymbol{\Theta}}\,\mathbf{C} = \underbrace{\underset{\sim}{\mathbf{C}}\,\mathbf{X}_{\boldsymbol{\Theta}}\mathbf{E}_{\boldsymbol{\Theta}}^{\frac{1}{2}}}_{\mathbf{F}}\underbrace{\left(\mathbf{E}_{\boldsymbol{\Theta}}^{\frac{1}{2}}\right)^{\mathrm{T}}\mathbf{X}_{\boldsymbol{\Theta}}^{\mathrm{T}}\,\mathbf{C}}_{\mathbf{F}^{\mathrm{T}}} = \mathbf{F}\mathbf{F}^{\mathrm{T}} \tag{3.206}$$

According to [77, p. 32] this term is symmetric positive semi-definite. Thus the matrix on the left hand side of equation (3.204) is symmetric positive definite and invertible.

In addition, we know the initial vector $\mathbf{x}^0$ and the source and boundary data $\underset{\sim}{\overline{\overline{\hat{\mathbf{j}}}}}^{n}$ and $\underset{\sim}{\overline{\overline{\hat{\mathbf{j}}}}}^{n}_{\Gamma_2}$ for all $n \in \mathbb{Z}$. So we can calculate the unique solutions inductively for each $n \in [1, \infty)$. For the time-steps $n \in (-\infty, -1]$, we can equivalently proof existence and uniqueness. □

Stability of the Spatially and Temporally Discrete Maxwell's Initial Boundary Value Problem

In parallel to the semi-discrete case on page 70, we will simplify the problem for proving stability: We assume magnetic boundary conditions on all of the boundary, i.e. the electric boundary part Γ_1 is empty. Also, we assume the source current $\underset{\sim}{\overline{\overline{\hat{\mathbf{j}}}}}^{n}$ to be zero for all $n \in \mathbb{Z}$ and the magnetic boundary condition to be homogeneous, i.e. the equivalent boundary current $\underset{\sim}{\overline{\overline{\hat{\mathbf{j}}}}}^{n}_{\Gamma_2}$ to be zero for all $n \in \mathbb{Z}$.

We now want to rewrite the IBVP for a sequence of spatial and temporal grids with indices $h, \Delta t$ in the form:

$$\mathrm{L}_{h,\Delta t}\left(\mathbf{x}_{h,\Delta t}\right) = b_{h,\Delta t} \tag{3.207}$$

Let us define the matrices $\mathbf{A}_{h,\Delta t}$ and $\mathbf{B}_{h,\Delta t}$ as

$$\mathbf{A}_{h,\Delta t} = \begin{pmatrix} \frac{1}{\Delta t^2}\,\mathbf{M}_\varepsilon + \underset{\sim}{\mathbf{C}}\,\mathbf{M}_\nu^{\boldsymbol{\Theta}}\,\mathbf{C} & 0 \\ 0 & \mathbf{M}_\nu \end{pmatrix}, \qquad \mathbf{B}_{h,\Delta t} = \begin{pmatrix} \underset{\sim}{\mathbf{C}}\,\mathbf{M}_\nu\,\mathbf{C} & -\,\underset{\sim}{\mathbf{C}}\,\mathbf{M}_\nu \\ \mathbf{M}_\nu\,\mathbf{C} & 0 \end{pmatrix} \tag{3.208}$$

where we have suppressed the indices $h, \Delta t$ for the matrices on the right hand sides for better readability. Define the unknown vectors $\mathbf{x}_{h,\Delta t}$ as

$$\mathbf{x}_{h,\Delta t} \equiv \left[\mathbf{x}^n_{h,\Delta t}\right]_{n\in\mathbb{Z}} = \left[\begin{pmatrix} \overline{\widehat{\mathbf{e}}}^n_{h,\Delta t} \\ \widehat{\mathbf{b}}^n_{h,\Delta t} \end{pmatrix}\right]_{n\in\mathbb{Z}} \tag{3.209}$$

the operators $\mathrm{L}_{h,\Delta t}$ as

$$\mathrm{L}_{h,\Delta t}\left(\mathbf{x}_{h,\Delta t}\right) = \begin{pmatrix} \left[\mathbf{A}_{h,\Delta t}\left(\mathbf{x}^n_{h,\Delta t} - \mathbf{x}^{n-1}_{h,\Delta t}\right) + \mathbf{B}_{h,\Delta t}\mathbf{x}^{n-1}_{h,\Delta t}\right]_{n\in\mathbb{Z}} \\ \mathbf{x}^0_{h,\Delta t} \end{pmatrix} \tag{3.210}$$

and the right hand sides $b_{h,\Delta t}$ as:

$$b_{h,\Delta t} = \begin{pmatrix} [0]_{n\in\mathbb{Z}} \\ \mathbf{x}^0_{h,\Delta t} \end{pmatrix} \tag{3.211}$$

Then the general form in equation (3.207) is equivalent to Maxwell's space- and time-discrete IBVP (3.203) on page 85.

Now we have to specify the discrete norms in which we want to discuss stability. For the norm in the domain $U_{h,\Delta t}$ of the operator $\mathrm{L}_{h,\Delta t}$, we will choose the discrete total energy norm defined in equation (3.190) on page 83 for the spatial variables and the maximum norm in the temporal index:

$$\|\mathbf{x}_{h,\Delta t}\|^2_{U_{h,\Delta t}} \equiv \max_{n\in\mathbb{Z}} 2W^n_{h,\Delta t} \tag{3.212}$$

As norm on the range $F_{h,\Delta t}$ of the operator $\mathrm{L}_{h,\Delta t}$, we will choose the discrete total energy norm of the initial field:

$$\|b_{h,\Delta t}\|^2_{F_{h,\Delta t}} \equiv 2W^0_{h,\Delta t} \tag{3.213}$$

The choice of the discrete energies only renders a norm in the unknown vector $\mathbf{x}_{h,\Delta t}$, if the time-step restriction (3.192) on page 83 is fulfilled for the grids at hand as stated in Theorem 3.9 on page 83. Thus we put this as a requirement on the grid sequence to prove stability:

Theorem 3.11 (Stability)**.** *Let a sequence of space- and time-discrete Maxwell's grid IBVP (3.203) with homogeneous magnetic boundary conditions on all of the boundary and no source currents be given in reduced form as in equation (3.207). Also assume each grid to fulfill the restriction on the time-step given by equation (3.192). Then the sequence of operators* $\mathrm{L}_{h,\Delta t}$ *is stable according to Definition E.3 in the discrete norms defined above.*

Proof. The conservation for the discrete total energy in equation (3.196) on page 84 renders:

$$W^{n+1}_{h,\Delta t} - W^n_{h,\Delta t} + \overline{P}^{n+1}_{e,h,\Delta t} + \overline{P}^{n+1}_{P,h,\Delta t} = W^{n+1}_{h,\Delta t} - W^n_{h,\Delta t} = 0 \tag{3.214}$$

where the electric loss pulses and equivalent boundary loss pulses are zero due to the zero source current and the homogeneous boundary conditions, respectively. Thus we know that the total energy is constant for all times:

$$W^n_{h,\Delta t} = W^0_{h,\Delta t} \qquad \forall\, n \in \mathbb{Z} \tag{3.215}$$

This renders stability of the scheme:

$$\|\mathbf{x}_{h,\Delta t}\|^2_{U_{h,\Delta t}} = \max_{n\in\mathbb{Z}} 2W^n_{h,\Delta t} = 2W^0_{h,\Delta t} = \|b_{h,\Delta t}\|^2_{F_{h,\Delta t}} \tag{3.216}$$

$$\Leftrightarrow \qquad \|\mathrm{L}^{-1}_{h,\Delta t} b_{h,\Delta t}\|_{U_{h,\Delta t}} = \|b_{h,\Delta t}\|_{F_{h,\Delta t}} \tag{3.217}$$

□

4. DISCRETE MATERIAL OPERATORS FOR POLYHEDRAL GRIDS

The Finite Integration Technique (FIT) described in chapter 3 is a numerical recipe for discretizing Maxwell's and similar IBVPs. It is based on the general class of consistent grids and their duals. Only very weak restrictions are put on the actual shape of the grid elements, thus these consistent grids facilitate arbitrary polyhedral cell shapes, even with curved boundaries. A selection of polyhedral elements is shown in Fig. 4.1, where actually only the hexahedron in Fig. 4.1b shows curved surfaces.

For consistent grids with such polyhedral cells, all discrete *topological* operators as the discrete gradient, curl, and divergence are fixed by the topology of the primal grid. The *metric* operators were only explicitly given for the standard FIT material laws, though, requiring dual orthogonal grids. Although they have been extended to non-orthogonal hexahedral grids in [79], this still restricts the cell shapes greatly. The Whitney-Finite Element Method (Whitney-FEM) provides a way to extend the FIT to tetrahedral, prism, and pyramidal cells. The name Whitney-FEM stems from the early work of H. Whitney, who introduced in [96, pp. 138] basis functions for simplicial and therefore tetrahedral grids which were later used in FEM formulations. The special cases of edge and face basis functions have independently been developed by Nédélec in [69]. It has been realized that the lowest order Whitney-FEM can be recast in the formalism of the FIT simply by deriving the material matrices from the Whitney-FEM basis functions [7]. Whitney-FEM basis functions have been generalized to hexahedral [69], prism [29], and pyramidal cells [40]. Thus all these cell shapes can be used in the framework of the FIT. Basis functions for general polyhedral grids had been missing so far, though.

Based on the ideas outlined in [19], we present lowest order Whitney-FEM-like basis functions for arbitrary straight-edged, planar-faced polyhedral cells in this chapter. The derived material matrices for such polyhedral cells greatly enhance the flexibility of grid types to use in the FIT. E.g. the grid cells shown in Fig. 4.1f to 4.1h can be employed in numerical simulations. The cells in Fig. 4.1e and Fig. 4.1f are useful for coupling grids consisting of hexahedra and tetrahedra consistently. The element in Fig. 4.1g can be employed for consistent subgridding.

The construction of the Whitney-FEM material operators from Whitney-FEM basis functions is presented in chapter 4.1. Certain properties of the Whitney-FEM basis functions which are used in the convergence analysis in [48] are stated. These properties guide the development of new polyhedral basis functions in the following chapters, from which polyhedral material operators can be derived in the same manner as the standard Whitney-FEM material operators. As the mentioned properties do not define the polyhedral basis functions uniquely, there are many possibilities to define construction schemes for them.

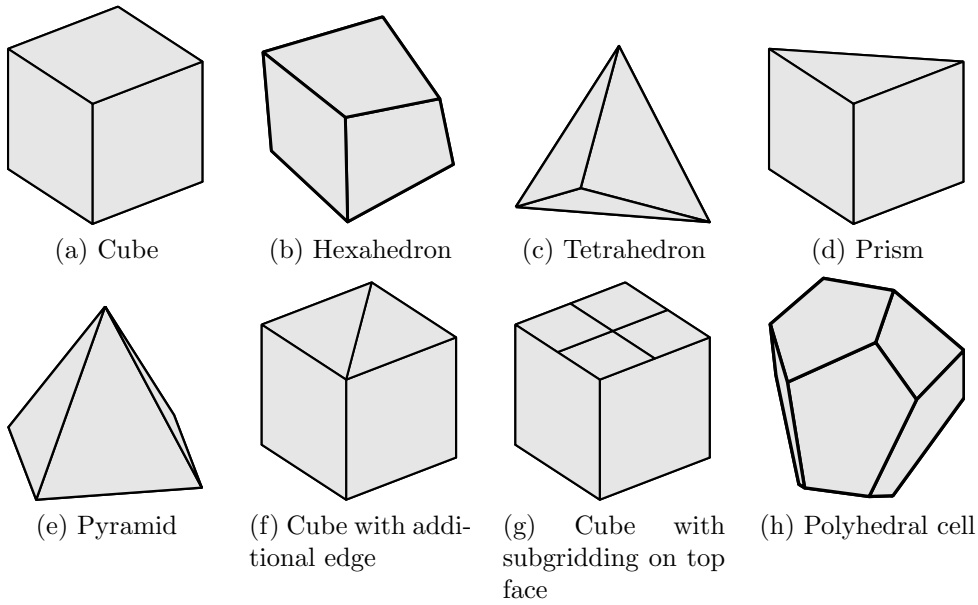

Fig. 4.1: Examples for polyhedral cell shapes allowed in a consistent grid.

We introduce three variants in this chapter which are closely related.

In a first variant in chapter 4.2, the polyhedral basis functions are defined as analytical solutions to general BVPs. The analytical solutions are readily available only for simplicial elements, i.e. tetrahedra, or Cartesian product space elements, i.e. cuboids, though. For tetrahedra and cuboids, the resulting basis functions coincide with the known lowest order Whitney-FEM basis functions and their tensor products, respectively.

In order to obtain numerically available basis functions for arbitrarily shaped cells, we discretize the BVP in chapters 4.3 and 4.4. Different discretization methods arrive at different polyhedral basis functions, but they all fulfill the basic properties of the Whitney-FEM basis functions stated in chapter 4.1.

In chapter 4.5, we shortly discuss some polygonal and polyhedral schemes available in the literature and how they fit into the framework discussed here.

4.1 Whitney-FEM Material Operators

For the lowest order Whitney-FEM, the degrees of freedom can be chosen such that they correspond exactly to the integral grid quantity coefficients (cochain coefficients) discussed on page 37 in the framework of the general FIT [7]. Then all the operators and methodology drop out as described in chapter 3.1, just with a special set of material matrices, called Whitney-FEM material matrices. In this chapter, we describe the derivation of the Whitney-FEM material matrices from Whitney-FEM basis functions.

We use the language of differential geometry introduced in chapter 2.1 and the general FIT notation introduced in chapter 3.1 in the following for a unified presentation of the Whitney-FEM material matrices of all degrees.

At this point, we finally need to introduce Sobolev-type k-form spaces. These have been found convenient for discussing problems with jumping material coefficients for which the analytical solutions are not smooth any more, but nevertheless exhibit certain regularity properties. The Sobolev-type space $\mathcal{F}_{\mathrm{d}}^k(\Omega)$ contains integral k-forms with bounded energy and bounded energy of their exterior derivatives. The spaces $\vec{\mathcal{F}}_{\mathrm{d}}^k(\Omega)$ of their vector proxies, i.e. vector field representations, are for $k = 0, 1, 2$ sometimes called gradient-, curl-, or divergence-conforming spaces and for $k = 3$ are simply the square integrable functions. As in [49, p. 49], they are often denoted as:

$$H_{\mathrm{grad}}(\Omega) \equiv \vec{\mathcal{F}}_{\mathrm{d}}^0(\Omega) \tag{4.1a}$$

$$\vec{H}_{\mathrm{curl}}(\Omega) \equiv \vec{\mathcal{F}}_{\mathrm{d}}^1(\Omega) \tag{4.1b}$$

$$\vec{H}_{\mathrm{div}}(\Omega) \equiv \vec{\mathcal{F}}_{\mathrm{d}}^2(\Omega) \tag{4.1c}$$

$$L^2(\Omega) \equiv \vec{\mathcal{F}}_{\mathrm{d}}^3(\Omega) \tag{4.1d}$$

Definition 4.1. The *Sobolev-type k-form spaces* $\mathcal{F}_{\mathrm{d}}^k(\Omega)$ for a domain $\Omega \subset \mathbb{R}^l$ with piecewise smooth boundary are defined as

$$\mathcal{F}_{\mathrm{d}}^k(\Omega) \equiv \left\{\omega^k \in \mathcal{F}_{\mathrm{I}}^k(\Omega) : \|\omega^k\| < \infty \quad \text{and} \quad \|\mathrm{d}^k\,\omega^k\| < \infty\right\} \tag{4.2}$$

where $\mathcal{F}_{\mathrm{I}}^k(\Omega)$ is to denote the general class of integral k-forms and $\|.\|$ denotes the norm induced by the Euclidean metric as defined in equation (2.36) on page 15. The spaces of their vector proxies are denoted by $\vec{\mathcal{F}}_{\mathrm{d}}^k(\Omega)$.

We now consider an IBVP with possibly jumping material coefficients that has solutions in the spaces $\mathcal{F}_{\mathrm{d}}^k(\Omega)$. We call this the continuous setting and $\mathcal{F}_{\mathrm{d}}^k(\Omega)$ the continuous Sobolev-type k-form spaces[1]. The FIT discretization of this IBVP renders discrete solutions in the spaces of primal and dual k-cochains $\mathcal{F}_h^k(\Omega_h)$ and $\underset{\sim}{\mathcal{F}}_h^k(\underset{\sim}{\Omega}_h)$ as introduced in Definition 3.5 on page 37. In the FIT framework presented in chapter 3, no recipe was given to reconstruct approximate solutions in the continuous spaces $\mathcal{F}_{\mathrm{d}}^k(\Omega)$ from these discrete solutions. In the Whitney-FEM, *Whitney reconstruction operators*, or Whitney maps, W^k are introduced which provide such continuous approximations for primal k-cochains $\boldsymbol{\omega}^k$:

$$\mathrm{W}^k : \qquad \boldsymbol{\omega}^k \in \mathcal{F}_h^k(\Omega_h) \longmapsto \mathrm{W}^k\boldsymbol{\omega}^k \in \mathcal{F}_{\mathrm{d}}^k(\Omega) \tag{4.3}$$

The Whitney reconstruction operators are defined in terms of the *Whitney basis forms*, or in short *Whitney forms*, B_i^k. There is exactly one Whitney form B_i^k associated with each primal grid element S_i^k and the Whitney reconstruction simply adds all these basis functions weighted with the corresponding cochain coefficient $\left(\boldsymbol{\omega}^k\right)_i$:

$$\mathrm{W}^k\boldsymbol{\omega}^k \equiv \sum_{i=1}^{n^k} \left(\boldsymbol{\omega}^k\right)_i B_i^k \tag{4.4}$$

The vector proxies $\vec{B}_i^k$ of the Whitney forms are called *Whitney basis functions*. The Whitney basis functions are commonly called nodal, edge, face, and volume basis functions

[1] The term *continuous* is used here in contrast to the *discrete* setting. There is thus no connection of the *continuous k-form spaces* with the mathematical notion of continuous functions.

for $k = 0, 1, 2, 3$, respectively. As in chapter 2, we will use the notation of differential geometry when considering k-forms of general degree and the notation of the vector proxies when considering k-forms of specific degree.

The spaces spanned by the Whitney basis forms are called *Whitney approximation spaces* $\mathcal{W}^k(\Omega_h)$:

$$\mathcal{W}^k(\Omega_h) \equiv \mathrm{span}_{i\in n^k}\left\{B_i^k\right\} = \mathrm{R}\big(\mathrm{W}^k\big) \tag{4.5}$$

These actually define the range of the Whitney reconstruction operators W^k, as easily seen from equation (4.4). Thus we can rewrite equation (4.3) as:

$$\mathrm{W}^k : \qquad \boldsymbol{\omega}^k \mathcal{F}_h^k(\Omega_h) \longmapsto \mathrm{W}^k \boldsymbol{\omega}^k \in \mathcal{W}^k(\Omega_h) \tag{4.6}$$

Example 4.1. To show an example of such a Whitney reconstruction operator, let us reconsider the grid discretization example from Fig. 3.7 on page 38 and include the nodal Whitney reconstruction operator W^0: In Fig. 4.2, the 0-form ω^0 is discretized by the nodal grid discretization operator L^0 into the 0-cochain $\boldsymbol{\omega}^0$. This 0-cochain contains simply the values of the 0-form ω^0 at the vertices S_i^0 of the one-dimensional grid Ω_h. The nodal Whitney reconstruction operator W^0 reconstructs an approximate 0-form ω_A^0 from the 0-cochain $\boldsymbol{\omega}^0$. It does so by adding the Whitney forms B_i^0 associated with each vertex S_i^0 weighted by the corresponding coefficient of the 0-cochain $\boldsymbol{\omega}^0$. The approximate 0-form ω_A^0 can again be discretized by the grid discretization operator rendering a 0-cochain.

Further comments can be found in the discussion of possible error definitions in discrete and continuous norms in appendix D. When Whitney reconstruction operators are available, we can compare the reconstructed approximate solution to the continuous solutions in continuous norms.

Before discussing the properties of the Whitney basis functions, we will describe how to derive the Whitney-FEM material matrices from the Whitney basis forms B_i^k:

Definition 4.2 (Whitney-FEM material matrices)**.** The *Whitney-FEM material matrices* $\mathbf{M}_{\mathrm{FEM},\alpha}^k$ for the metric α are defined for $k \in [0..3]$ as:

$$\left(\mathbf{M}_{\mathrm{FEM},\alpha}^k\right)_{ij} \equiv \left\langle\!\left\langle B_i^k \middle| B_j^k \right\rangle\!\right\rangle_\alpha = \int_\Omega B_i^k \wedge \star_\alpha B_j^k, \qquad i,j \in [1..n^k] \tag{4.7}$$

where the inner product $\langle\!\langle .|. \rangle\!\rangle_\alpha$ is defined in equation (2.35) on page 14. The *local Whitney-FEM material matrices* $\mathbf{M}_{\mathrm{FEM},\alpha}^{k,m}$ rendering a splitting according to Definition 3.12 on page 49 are constructed by integrating only over one primal cell S_m^3:

$$\left(\mathbf{M}_{\mathrm{FEM},\alpha}^{k,m}\right)_{ij} \equiv \int_{S_m^3} B_i^k \wedge \star_\alpha B_j^k \equiv \left\langle\!\left\langle B_i^k \middle| B_j^k \right\rangle\!\right\rangle_{\alpha,S_m^3}, \qquad i,j \in [1..n^k] \tag{4.8}$$

where we have introduced the new continuous local inner product $\langle\!\langle .|. \rangle\!\rangle_{\alpha,S_m^3}$. The *reduced local Whitney-FEM material matrices* $\widehat{\mathbf{M}}_{\mathrm{FEM},\alpha}^{k,m}$ are defined as

$$\widehat{\mathbf{M}}_{\mathrm{FEM},\alpha}^{k,m} \equiv \mathbf{T}_{S_m^3}^k \, \mathbf{M}_{\mathrm{FEM},\alpha}^{k,m} \left(\mathbf{T}_{S_m^3}^k\right)^{\mathrm{T}} \tag{4.9}$$

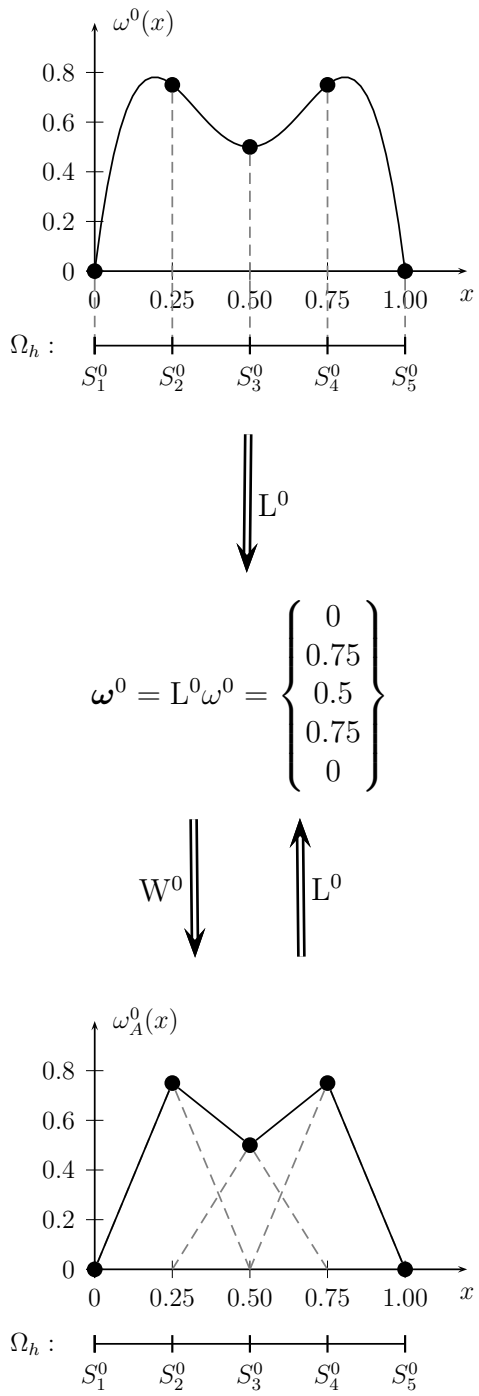

Fig. 4.2: Illustration of the grid discretization operator L^0 and the Whitney reconstruction operator W^0 for the one-dimensional grid Ω_h: The grid discretization operator L^0 discretizes the 0-form ω^0 into the 0-cochain $\boldsymbol{\omega}^0$. The Whitney reconstruction operator W^0 reconstructs the approximating 0-form $\omega_A^0 = \mathrm{W}^0\boldsymbol{\omega}^0 \in \mathcal{W}^0(\Omega_h) \subset \mathcal{F}_{\mathrm{d}}^0(\Omega)$ from the 0-cochain $\boldsymbol{\omega}^0$ by adding the Whitney basis 0-forms associated with the nodes S_i^0 of the grid weighted by the corresponding coefficients of the 0-cochain $\boldsymbol{\omega}^0$.

Specifically, we get the following Whitney-FEM permittivity and reluctivity material matrices in vector proxy notation:

$$(\mathbf{M}_{\mathrm{FEM},\varepsilon})_{ij} = \int_\Omega \varepsilon \vec{B}_i^1(\vec{r}) \cdot \vec{B}_j^1(\vec{r})\,\mathrm{d}V, \qquad i,j \in [1..n^1] \tag{4.10a}$$

$$(\mathbf{M}_{\mathrm{FEM},\nu})_{ij} = \int_\Omega \nu \vec{B}_i^2(\vec{r}) \cdot \vec{B}_j^2(\vec{r})\,\mathrm{d}V, \qquad i,j \in [1..n^2] \tag{4.10b}$$

Theorem 4.1. *For linearly independent basis forms B_i^k and positive definite metric α, the material matrices $\mathbf{M}_{\mathrm{FEM},\alpha}^k$ and the local reduced material matrices $\widehat{\mathbf{M}}_{\mathrm{FEM},\alpha}^{k,m}$ defined above for $k \in [0..3]$ are symmetric positive definite.*

Proof. For any k-cochain $\boldsymbol{\omega}^k$, we directly get from equation (4.7) of the definition of the material matrix $\mathbf{M}_{\mathrm{FEM},\alpha}^k$:

$$\begin{aligned}
\left(\boldsymbol{\omega}^k\right)^T \mathbf{M}_{\mathrm{FEM},\alpha}^k\, \boldsymbol{\omega}^k &= \sum_{i=1}^{n^k}\sum_{j=1}^{n^k} \left(\boldsymbol{\omega}^k\right)_i \left(\boldsymbol{\omega}^k\right)_j \left\langle\!\left\langle B_i^k \middle| B_j^k \right\rangle\!\right\rangle_\alpha \\
&= \left\langle\!\left\langle \sum_i \left(\boldsymbol{\omega}^k\right)_i B_i^k \middle| \sum_i \left(\boldsymbol{\omega}^k\right)_i B_i^k \right\rangle\!\right\rangle_\alpha \\
&= \|\sum_i \left(\boldsymbol{\omega}^k\right)_i B_i^k\|_\alpha \geq 0
\end{aligned} \tag{4.11}$$

The positive definite metric α renders $\|.\|_\alpha$ defined according to equation (2.36) on page 15 a norm. As the basis forms B_i^k are linearly independent, the equality to zero only holds for $\boldsymbol{\omega}^k = 0$. Thus the matrix $\mathbf{M}_{\mathrm{FEM},\alpha}^k$ is symmetric positive definite. A similar reasoning shows symmetric positive definiteness of the local reduced material matrices $\widehat{\mathbf{M}}_{\mathrm{FEM},\alpha}^{k,m}$. □

Equivalence of the FIT using these Whitney-FEM material matrices to a standard FEM formulation using Whitney-FEM basis forms is shown in appendix C. Note that we did not specify the dual grid for which the Whitney-FEM material operators were defined. Although for tetrahedral grids, the barycentric dual grid has been recognized as a sensible choice for a dual grid for the Whitney-FEM [9, pp. 99], for the arbitrary polyhedral primal grids introduced here, this question is still open. Thus to state the IBVP in the FIT, we rely on the duality relations in equations (3.51) on page 46 to define the dual grid exterior derivatives $\underset{\sim}{\mathbf{D}}^k$. To discretize the boundary and source data allocated on the dual grid, we introduce an alternative version of the dual grid discretization operators $\underset{\sim}{\mathrm{L}}^k$ based on the Whitney-FEM basis forms in appendix C.

In order to guide the search for basis forms B_i^k for polyhedral cells, we will propose certain properties as requirements. Property I is needed to be able to recast the FEM formulation using the basis forms in terms of the FIT. Property II ensures that the FEM formulation is conforming. Properties III and IV are basic tools in the convergence analysis. Property V is proposed to obtain convergence rates as for standard FIT or lowest order Whitney-FEM material matrices. And the last property VI will lead to a sparse numerical scheme.

As stated above, we require one basis form B_i^k to be associated with each primal grid element S_i^k:

I. For each element S_i^k of the grid, there exists exactly one basis form B_i^k defining the Whitney reconstruction operator for the i-th cochain coefficient according to equation (4.4) on page 91.

We also require the basis forms B_i^k to be conforming:

II. The Whitney basis forms should be conforming, i.e. the Whitney spaces should be subspaces of the Sobolev-type spaces $\mathcal{F}_{\mathrm{d}}^k(\Omega)$:

$$\operatorname{span}_{i\in n^k}\left\{B_i^k\right\} = \mathcal{W}^k(\Omega_h) \subset \mathcal{F}_{\mathrm{d}}^k(\Omega) \tag{4.12}$$

Now it seems sensible to require that the grid discretization of a reconstructed cochain should again render the same cochain, i.e. that the lower part in Fig. 4.2 does commute:

III. The grid discretization operator L^k should be the left inverse of the Whitney reconstruction operator W^k:

$$\mathrm{L}^k\mathrm{W}^k\boldsymbol{\omega}^k = \boldsymbol{\omega}^k \qquad \forall\, \boldsymbol{\omega}^k \in \mathcal{F}_h^k(\Omega_h) \tag{4.13}$$

From this requirement, it actually follows that the grid discretization operator L^k is also the right inverse of the Whitney reconstruction operator W^k:

Lemma 4.2. *Assuming property III to hold,* L^k *is the right inverse of the Whitney reconstruction operator* W^k*.*

Proof. The Whitney space $\mathcal{W}^k$ is the range of the Whitney reconstruction operator W^k, as seen in equation (4.5) on page 92. Thus for any $\omega^k \in \mathcal{W}^k$, there exists a k-cochain $\boldsymbol{\omega}^k$ such that:

$$\omega^k = \mathrm{W}^k\boldsymbol{\omega}^k \qquad \forall\, \omega^k \in \mathcal{W}^k \tag{4.14}$$

Then assuming property III to hold we can write this as

$$\omega^k = \mathrm{W}^k\mathrm{L}^k\mathrm{W}^k\boldsymbol{\omega}^k = \mathrm{W}^k\mathrm{L}^k\omega^k \qquad \forall\, \omega^k \in \mathcal{W}^k \tag{4.15}$$

which shows that the grid discretization operator L^k is the right inverse of the Whitney reconstruction operator W^k. □

Property III and Lemma 4.2 establish a one-to-one correspondence between elements in the space of cochains $\mathcal{F}_h^k(\Omega_h)$ and in the Whitney spaces $\mathcal{W}^k(\Omega_h)$. In order to complete this correspondence, we require the continuous exterior derivative d^k and the discrete exterior derivative $\mathbf{D}^k$ to commute under the Whitney reconstruction operators:

IV. The exterior derivative should commute with the Whitney map W^k:

$$\mathrm{d}^k\,\mathrm{W}^k = \mathrm{W}^{k+1}\,\mathbf{D}^k \tag{4.16}$$

Properties II, III, and IV can be nicely added to the commuting diagram (3.37) on page 44 (replacing the smooth k-form spaces $\mathcal{F}_s^k$ by the Sobolev-type k-form spaces $\mathcal{F}_\mathrm{d}^k$). Note that Fig. 4.2 illustrates the left-most column of this diagram:

$$\begin{tikzcd}
\mathcal{F}_\mathrm{d}^0(\Omega) \arrow[r, "\mathrm{d}^0\,(=\mathrm{grad})"] \arrow[d, "\mathrm{L}^0"'] & \mathcal{F}_\mathrm{d}^1(\Omega) \arrow[r, "\mathrm{d}^1\,(=\mathrm{curl})"] \arrow[d, "\mathrm{L}^1"'] & \mathcal{F}_\mathrm{d}^2(\Omega) \arrow[r, "\mathrm{d}^2\,(=\mathrm{div})"] \arrow[d, "\mathrm{L}^2"'] & \mathcal{F}_\mathrm{d}^3(\Omega) \arrow[d, "\mathrm{L}^3"'] \\
\mathcal{F}_h^0(\Omega_h) \arrow[r, "\mathbf{D}^0\,(=\mathbf{G})"] \arrow[d, shift right, "\mathrm{W}^0"'] & \mathcal{F}_h^1(\Omega_h) \arrow[r, "\mathbf{D}^1\,(=\mathbf{C})"] \arrow[d, shift right, "\mathrm{W}^1"'] & \mathcal{F}_h^2(\Omega_h) \arrow[r, "\mathbf{D}^2\,(=\mathbf{S})"] \arrow[d, shift right, "\mathrm{W}^2"'] & \mathcal{F}_h^3(\Omega_h) \arrow[d, shift right, "\mathrm{W}^3"'] \\
\mathcal{W}^0(\Omega_h) \arrow[r, "\mathrm{d}^0\,(=\mathrm{grad})"] \arrow[u, shift right, "\mathrm{L}^0"'] \arrow[d, phantom, "\cap"] & \mathcal{W}^1(\Omega_h) \arrow[r, "\mathrm{d}^1\,(=\mathrm{curl})"] \arrow[u, shift right, "\mathrm{L}^1"'] \arrow[d, phantom, "\cap"] & \mathcal{W}^2(\Omega_h) \arrow[r, "\mathrm{d}^2\,(=\mathrm{div})"] \arrow[u, shift right, "\mathrm{L}^2"'] \arrow[d, phantom, "\cap"] & \mathcal{W}^3(\Omega_h) \arrow[u, shift right, "\mathrm{L}^3"'] \arrow[d, phantom, "\cap"] \\
\mathcal{F}_\mathrm{d}^0(\Omega) & \mathcal{F}_\mathrm{d}^1(\Omega) & \mathcal{F}_\mathrm{d}^2(\Omega) & \mathcal{F}_\mathrm{d}^3(\Omega)
\end{tikzcd} \tag{4.17}$$

Using the grid discretization operator L^k and the Whitney reconstruction operator W^k, we can define the *Whitney projector* P^k from the spaces of continuous Sobolev-type k-forms into the Whitney approximation spaces:

$$\begin{aligned}
&\mathrm{P}^k: \quad \omega^k \in \mathcal{F}_\mathrm{d}^k(\Omega) \longmapsto \mathrm{P}^k\omega^k \in \mathcal{W}^k(\Omega_h) \\
&\mathrm{P}^k \equiv \mathrm{W}^k\mathrm{L}^k
\end{aligned} \tag{4.18}$$

For convergence, we require this Whitney projector P^k to be exact for constant k-forms[2]:

V. The Whitney projector P^k should exactly reproduce constant k-forms:

$$\mathrm{P}^k c^k = \mathrm{W}^k\mathrm{L}^k c^k = c^k \qquad \forall\,\text{constant } k\text{-forms } c^k \tag{4.19}$$

The next and last property required of the Whitney basis functions is due to computational reasons: We require the basis functions to be local. Then the above defined Whitney material matrices are sparse, which is advantageous for storage and calculation.

VI. The Whitney basis form B_i^k should be local, i.e. be non-zero only in the associated grid element S_i^k and adjacent grid elements of higher dimension. More precisely, adjacent grid elements are elements that have the associated grid element S_i^k in their boundary.

Requirements III and IV are essential in the convergence analysis for tetrahedral basis forms presented in [48]. Although we do not carry out the convergence analysis here, it is believed that the above requirements along with certain restrictions on the grid sequence (equivalent to the angle condition for tetrahedral grids) are sufficient to prove convergence of the scheme. We will observe the expected convergence rates for the polyhedral scheme in the applications in chapter 5.

Requirement III renders linear independence of the Whitney basis forms B_i^k:

[2] Constant k-forms in the domain Ω, which is a submanifold of $\mathbb{R}^3$, can be characterized as k-forms whose vector proxies are component-wise constant in the Cartesian coordinate system.

Lemma 4.3. *Whitney basis forms fulfilling property III are linearly independent.*

Proof. The dimension of the cochain space $\mathcal{F}_h^k(\Omega_h)$ is n^k. As noted above, property III establishes an isomorphism between each cochain space $\mathcal{F}_h^k(\Omega_h)$ and the Whitney space $\mathcal{W}^k(\Omega_h)$. Therefore the dimension of the Whitney space $\mathcal{W}^k(\Omega_h)$ is also n^k. As the Whitney spaces are defined by equation (4.5) as the span of the n^k Whitney basis forms B_i^k, the Whitney basis forms must be a basis of the Whitney spaces $\mathcal{W}^k(\Omega_h)$ and thus are linearly independent. □

The following lemma gives an equivalent formulation of the commuting property IV:

Lemma 4.4. *Assuming property III to hold, the commuting property IV can be restated as:*

$$\mathrm{d}^k\,\mathcal{W}^k \subset \mathcal{W}^{k+1} \tag{4.20}$$

Proof. It is easily seen that (4.20) follows from property IV:

$$\mathrm{d}^k\,\mathcal{W}^k = \mathrm{R}\big(\mathrm{d}^k\,\mathrm{W}^k\big) = \mathrm{R}\big(\mathrm{W}^{k+1}\,\mathbf{D}^k\big) \subset \mathrm{R}\big(\mathrm{W}^{k+1}\big) = \mathcal{W}^{k+1} \tag{4.21}$$

So we are left to prove that property IV holds assuming (4.20) to be true and property III to hold. Let us consider an arbitrary k-cochain $\boldsymbol{\omega}^k$. From equation (4.20), we know that the exterior derivative of its Whitney reconstruction is in the Whitney space $\mathcal{W}^{k+1}$:

$$\eta^{k+1} \equiv \mathrm{d}^k\,\mathrm{W}^k\boldsymbol{\omega}^k \quad \in \quad \mathcal{W}^{k+1}$$

Using equation (4.15), which follows from property III, we can represent η^{k+1} as

$$\eta^{k+1} = \mathrm{W}^{k+1}\mathrm{L}^{k+1}\eta^{k+1} = \mathrm{W}^{k+1}\mathrm{L}^{k+1}\,\mathrm{d}^k\,\mathrm{W}^k\boldsymbol{\omega}^k$$

Using the commuting property of the exterior derivative with the grid discretization operator stated in equation (3.38) on page 44

$$= \mathrm{W}^{k+1}\,\mathbf{D}^k\,\mathrm{L}^k\mathrm{W}^k\boldsymbol{\omega}^k \tag{4.22}$$

and equation (4.13) of property III we get our result:

$$= \mathrm{W}^{k+1}\,\mathbf{D}^k\,\boldsymbol{\omega}^k \qquad \forall\,\boldsymbol{\omega}^k \in \mathcal{F}_h^k(\Omega_h) \tag{4.23}$$

□

Having stated the properties required of polyhedral Whitney basis forms, we can now start to search for these. As the properties do not uniquely define the basis forms, there are many possibilities to construct conforming basis forms. In the next chapters, we will formulate three possible construction schemes which are closely related.

4.2 Continuous Construction Algorithm for Polyhedral Whitney Basis Functions

In this chapter, we introduce sets of basis forms which fulfill the properties I to VI proposed in chapter 4.1. They are defined as the solutions to continuous generalized Laplace-Beltrami BVPs. Each basis form B_i^k is built hierarchically by defining its traces $\mathrm{t}_{S_j^l}^k B_i^k$ on the grid elements S_j^l of higher and higher dimension l.

For nodal basis forms B_i^0, we start with their values on the grid vertices and then calculate step by step their values on the edges, faces, and cells of the grid. For the edge basis forms B_i^1, we start with their values on the edges, as their traces on the vertices of the grid is zero by Definition 2.2. Equivalently, for the face basis forms B_i^2, we will start with their values on the faces and for the volume basis forms B_i^3, we will directly define their values on the grid cells.

Although this scheme seems fairly complicated, it is stated very compactly in the language of differential geometry as one general BVP in chapter 4.2.1. In this form, we can conveniently prove that the solutions B_i^k of the BVPs fulfill the requirements I to VI proposed in chapter 4.1. In chapter 4.2.2, this general construction algorithm is written explicitly in vector proxy notation for all basis functions step by step. The solutions for simplicial elements, i.e. straight edges, planar triangles, and planar-faced tetrahedra, are stated, leading to the known Whitney basis functions on tetrahedra.

Example 4.2. As example, we consider the vector proxy of a basis 0-form B_i^0: The (scalar) nodal basis function $\vec{B}_i^0$. The construction steps for this nodal basis function are illustrated by Fig. 4.3. We first define the values of $\vec{B}_i^0$ on all vertices S_j^0 of the grid as shown in Fig. 4.3a. The solution of value 1 for the vertex S_i^0 and value 0 on all other vertices, written with the Kronecker delta δ_{ij} as

$$\vec{B}_i^0(S_j^0) = \delta_{ij} \tag{4.24}$$

should not come as a surprise: This basis function is associated with the vertex S_i^0. It reconstructs a continuous 0-form with value one at this vertex and, by looking at requirement III, with value zero at all other vertices.

Now the values of the nodal basis function $\vec{B}_i^0$ are calculated on the edges S_j^1 of the grid by a BVP using the values at the vertices as boundary conditions. The resulting values are shown in Fig. 4.3b. For straight edges, these are either the linear functions going from value 1 at the node S_i^0 to value 0 at the other node, or, for non-adjacent edges, simply the zero function.

Once the values of the nodal basis function $\vec{B}_i^0$ are known on all edges, these are taken as boundary conditions for a BVP on the faces S_j^2 of the grid to calculate the values of the basis function $\vec{B}_i^0$ on the faces as shown in Fig. 4.3c. For the planar-faced polyhedra considered here, these are the first non-trivial results.

Once the values of the nodal basis functions $\vec{B}_i^0$ are known on all faces, these are taken as boundary conditions for a BVP on the grid cells S_j^3 to finally arrive at the values of the basis forms on all of the domain Ω. In Fig. 4.3d its values for a single grid cell are shown.

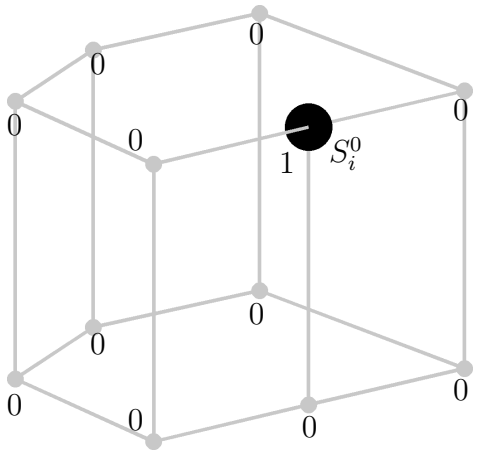

(a) Values of the nodal basis function $\vec{B}_i^0$ at the nodes of the example polyhedral element. The nodal value is 1 for the associated node S_i^0 and zero for all other nodes.

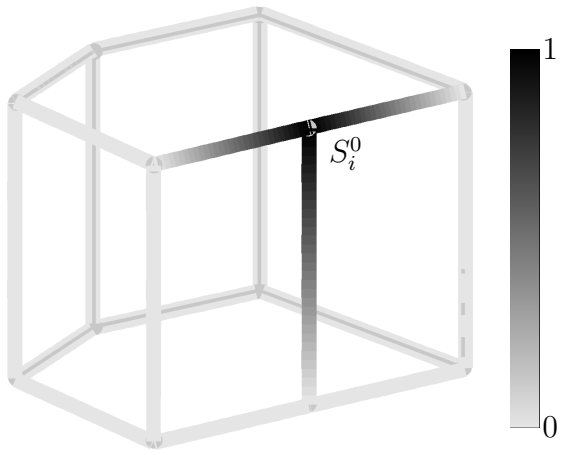

(b) Values of the nodal basis function $\vec{B}_i^0$ along the edges of the example polyhedral element. The nodal basis function $\vec{B}_i^0$ varies linearly from value 1 at its associated node S_i^0 to value zero along edges adjacent to the associated node. On all other edges, the nodal basis function $\vec{B}_i^0$ is zero.

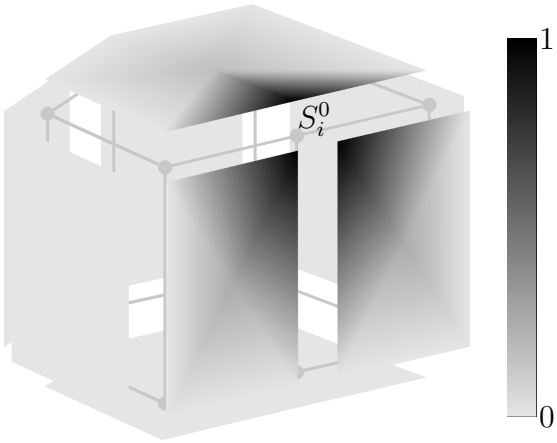

(c) Values of the nodal basis function $\vec{B}_i^0$ on the faces of the example polyhedral element. The nodal basis function $\vec{B}_i^0$ is only non-zero on the faces adjacent to the associated node S_i^0.

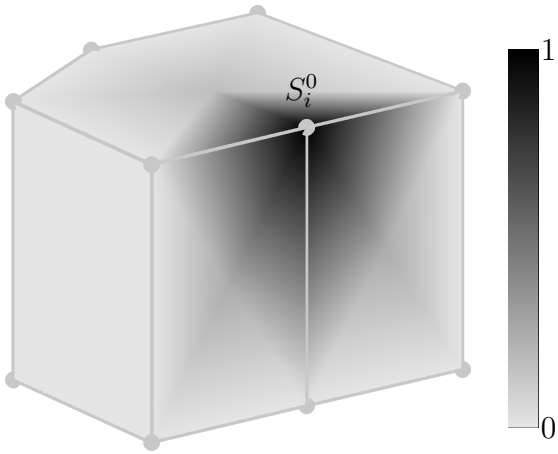

(d) Values of the nodal basis function $\vec{B}_i^0$ on the example polyhedral element.

Fig. 4.3: Illustration of the construction scheme for the nodal basis function $\vec{B}_i^0$ on a polyhedron: First, the values of the basis function are defined on the vertices of the grid. Then its values along the edges, faces, and on the complete polyhedral element are calculated step by step by solving BVPs. For these BVPs, the values on the lower-dimensional grid elements are needed as boundary conditions. The example shows the results of using the discrete construction algorithm described by equations (4.90) on page 117 employing discrete harmonic coordinates as intermediate basis functions as described in Example 4.13.

4.2.1 General Construction Algorithm

In this chapter, we describe the general construction algorithm for the continuous polyhedral Whitney basis forms in the language of differential geometry. We also state that they fulfill the requirements I to VI on pages 95–96 proposed in chapter 4.1.

In the BVP, we will make use of the local exterior derivative $\mathrm{d}^k_{S^l_j}$ on the grid elements S^l_j

$$\mathrm{d}^k_{S^l_j}: \quad \omega^k \in \mathcal{F}^k_s(S^l_j) \longmapsto \mathrm{d}^k_{S^l_j}\,\omega^k \in \mathcal{F}^{k+1}_s(S^l_j) \tag{4.25}$$

and the local hodge operator $\star^l_{S^l_j}$ on the grid elements S^l_j

$$\star^l_{S^l_j}: \quad \omega^k \in \mathcal{F}^k_s(S^l_j) \longmapsto \star^l_{S^l_j}\omega^k \in \mathcal{F}^{l-k}_s(S^l_j) \tag{4.26}$$

These are simply the local l-dimensional equivalents of the exterior derivative and hodge operators introduced in chapter 2. We additionally introduce the local *coderivative* $\delta^k_{S^l_j}$ which is defined as:

$$\delta^k_{S^l_j}: \omega^k \in \mathcal{F}^k_s(S^l_j) \longmapsto \delta^k_{S^l_j}\,\omega^k \in \mathcal{F}^{k-1}_s(S^l_j) \tag{4.27}$$

$$\delta^k_{S^l_j} \equiv (-1)^{l(k-1)+1}\,\star^l_{S^l_j}\,\mathrm{d}^{l-k}_{S^l_j}\,\star^l_{S^l_j} \tag{4.28}$$

Now we are ready to state the construction scheme for the continuous polyhedral Whitney basis forms:

Definition 4.3 (Continuous Polyhedral Whitney Basis Forms)**.** Let a consistent grid Ω_h with planar faces and straight edges be given. The *continuous polyhedral Whitney basis forms* B^k_i of degree k associated with the primal grid element S^k_i are defined for $i \in [1..n^k]$ by the following inductive scheme, letting l go from k to 3:

Assume the traces $\mathrm{t}^k_{S^{l-1}_p}\,B^k_i$ of the basis form B^k_i on all $(l-1)$-dimensional grid elements S^{l-1}_p to be known. For $l = k$ this renders the trivial traces $\mathrm{t}^k_{S^{k-1}_p}\,B^k_i = 0$. Then for each l-dimensional element of the grid S^l_j, the trace $\mathrm{t}^k_{S^l_j}\,B^k_i$ of the basis form B^k_i on the element S^l_j is defined as the unique solution to the following BVP: Find the trace

$$\mathrm{t}^k_{S^l_j}\,B^k_i \in \mathcal{F}^k_s(S^l_j) \tag{4.29}$$

such that

$$\delta^{k+1}_{S^l_j}\,\mathrm{d}^k_{S^l_j}\left(\mathrm{t}^k_{S^l_j}\,B^k_i\right) = 0 \qquad \text{in } S^l_j \tag{4.30a}$$

$$\delta^k_{S^l_j}\left(\mathrm{t}^k_{S^l_j}\,B^k_i\right) = 0 \qquad \text{in } S^l_j \tag{4.30b}$$

$$\mathrm{t}^k_{\partial S^l_j}\left(\mathrm{t}^k_{S^l_j}\,B^k_i\right) = \psi \qquad \text{known on } \partial S^l_j \tag{4.30c}$$

$$\int_{S^k_j}\left(\mathrm{t}^k_{S^k_j}\,B^k_i\right) = \delta_{ij} \qquad \text{if } l = k \tag{4.30d}$$

where ψ denotes the known traces on ∂S_j^l. For $l = k$, the additional constraint (4.30d) is needed to ensure uniqueness of the solution. For $l = 3$, we arrive at the final basis form B_i^k by

$$B_i^k \equiv \sum_{j=1}^{n^3} \mathrm{t}_{S_j^3}^k \, B_i^k \tag{4.31}$$

where we assume the local traces $\mathrm{t}_{S_j^3}^k \, B_i^k$ extended by zero to the complete domain Ω.

Note that, according to Definition 2.2 on page 10, the traces of the basis form B_i^k on all elements of the grid of dimension less than the degree of the basis form are trivial:

$$\mathrm{t}_{S_p^l}^k \, B_i^k = 0 \qquad \forall\, p \in [1..n^l], \quad \forall\, l < k \tag{4.32}$$

This allows us to start the above inductive scheme at $l = k$.

Now the first question is whether the BVP (4.30) does indeed have a unique solution. The following theorem assures this:

Theorem 4.5. *The BVP (4.30) has a unique solution* $\mathrm{t}_{S_j^l}^k \, B_i^k$ *in* $\mathcal{F}_s^k(S_j^l)$ *for* $k \leq l$.

The proof for Theorem 4.5 can be found in appendix F.2.1 on page 225. The next theorem assures that requirements I to VI on pages 95–96 are fulfilled by the above defined continuous polyhedral Whitney basis forms B_i^k. The proof can be found in appendix F.2.2 on page 227.

Theorem 4.6. *The continuous polyhedral Whitney basis forms defined in Definition 4.3 fulfill the requirements I to VI on pages 95–96.*

4.2.2 Specific Construction Algorithm

In this chapter, we will write down the equations of the BVP (4.30) specifying the polyhedral Whitney basis functions in vector proxy language. We will list them step by step for basis functions[3] $\vec{B}_i^k$ of each degree k.

For simplicial grid elements of the various dimensions, i.e. vertices, straight edges, triangles, and tetrahedra, explicit solutions are given as examples. These solutions coincide with the standard Whitney basis functions for simplicial grid elements.

To state the local BVP in vector proxy notation for the edges and faces of the grid, we introduce a local coordinate system for each edge and face. We also use the local coordinate systems to write down the vector proxy equivalents of the traces defined for k-forms in Definition 2.2 on page 10.

[3] The arrow in the symbol $\vec{B}_i^k$ for the basis function of degree k indicates that we are considering the vector proxy of the basis k-form B_i^k as defined in Definition 2.1. As described in remark 2.1, these are scalar functions for 0-forms and 3-forms and vector fields for 1-forms and 2-forms.

For each edge of the grid S^1_j we introduce a local coordinate $\hat{x}_1$ and describe the edge by the curve $\vec{s}(\hat{x}_1)$:

$$\vec{s}(\hat{x}_1) \in \Omega \subset \mathbb{R}^3, \qquad \hat{x}_1 \in (0..1) \tag{4.33}$$

with the metric coefficient h_1 defined as:

$$h_1 \equiv \left| \frac{\partial \vec{s}(\hat{x}_1)}{\partial \hat{x}_1} \right| \tag{4.34}$$

The unit tangential vector $\vec{t}_{S^1_j}$ along the edge is defined as:

$$\vec{t}_{S^1_j}(\hat{x}_1) \equiv \frac{1}{h_1} \frac{\partial \vec{s}(\hat{x}_1)}{\partial \hat{x}_1} \tag{4.35}$$

The trace of the scalar nodal basis function $\vec{B}^0_i$ along the edge S^1_j is simply its values along the edge. Using the equivalence symbol between forms and their vector proxies introduced in (2.8) on page 9, we write this as:

$$\mathrm{t}^k_{S^1_j} B^0_i \quad \multimap \quad \vec{B}^0_i \tag{4.36}$$

The trace of the edge basis function $\vec{B}^1_i$, which is a vector field in $\mathbb{R}^3$, is simply its tangential component along the edge. It is thus a scalar function and we will denote it by $(\vec{B}^1_i)_{t_{S^1_j}}$:

$$\mathrm{t}^k_{S^1_j} B^1_i \quad \multimap \quad \vec{B}^1_i \cdot \vec{t}_{S^1_j} \equiv (\vec{B}^1_i)_{t_{S^1_j}} \tag{4.37}$$

The traces of the face and volume basis functions on the edges are by definition zero.

Each of the faces S^2_j of the grid will be described parametrically by a surface $\vec{s}(\hat{x}_1, \hat{x}_2)$:

$$\vec{s}(\hat{x}_1, \hat{x}_2) \in \Omega \subset \mathbb{R}^3, \qquad (\hat{x}_1, \hat{x}_2) \in \Sigma \subset \mathbb{R}^2 \tag{4.38}$$

where the local coordinates $\hat{x}_1$ and $\hat{x}_2$ are taken in some set Σ. For simplicity, we assume the local coordinates to be orthogonal. The metric coefficients h_m for this surface are defined as:

$$h_m \equiv \left| \frac{\partial \vec{s}(\hat{x}_1, \hat{x}_2)}{\partial \hat{x}_m} \right| \qquad m \in [1, 2] \tag{4.39}$$

The unit tangential vectors on the surface $\vec{t}_{S^2_j, m}$ are defined as:

$$\vec{t}_{S^2_j, m}(\hat{x}_1, \hat{x}_2) \equiv \frac{1}{h_m} \frac{\partial \vec{s}(\hat{x}_1, \hat{x}_2)}{\partial \hat{x}_m} \qquad m \in [1, 2] \tag{4.40}$$

We assume the unit tangential vectors $\vec{t}_{S^2_j, 1}$ and $\vec{t}_{S^2_j, 2}$ to form in that order a positively oriented basis of the face S^2_j. The normal vector on the surface $\vec{n}_{S^2_j}$ is defined as the cross product of the tangential vectors:

$$\vec{n}_{S^2_j}(\hat{x}_1, \hat{x}_2) \equiv \vec{t}_{S^2_j, 1}(\hat{x}_1, \hat{x}_2) \times \vec{t}_{S^2_j, 2}(\hat{x}_1, \hat{x}_2) \tag{4.41}$$

Now we can describe the traces of the basis functions on the surfaces. The trace of a scalar nodal basis function $\vec{B}_i^0$ is again simply its values on the surface:

$$\mathrm{t}^k_{S_j^2}\, B_i^0 \quad \multimap \quad \vec{B}_i^0 \tag{4.42}$$

The trace of the edge basis function $\vec{B}_i^1$ is its tangential component on the face. It is thus a 2-component vector field. The components of the trace vector are denoted by $(\vec{B}_i^1)_{t_{S_j^2,m}}$ and the 2-component trace vector by $(\vec{B}_i^1)_{t_{S_j^2}}$:

$$\mathrm{t}^k_{S_j^2}\, B_i^1 \quad \multimap \quad \begin{pmatrix} \vec{B}_i^1 \cdot \vec{t}_{S_j^2,1} \\ \vec{B}_i^1 \cdot \vec{t}_{S_j^2,2} \end{pmatrix} \equiv \begin{pmatrix} (\vec{B}_i^1)_{t_{S_j^2,1}} \\ (\vec{B}_i^1)_{t_{S_j^2,2}} \end{pmatrix} \equiv (\vec{B}_i^1)_{t_{S_j^2}} \tag{4.43}$$

The trace of a face basis function $\vec{B}_i^2$ on a face translates to its normal vector component on the face. It is thus a scalar function on the face and we denote it by $(\vec{B}_i^2)_{n_{S_j^2}}$:

$$\mathrm{t}^k_{S_j^2}\, B_i^2 \quad \multimap \quad \vec{B}_i^2 \cdot \vec{n}_{S_j^2} \equiv (\vec{B}_i^2)_{n_{S_j^2}} \tag{4.44}$$

The trace of the volume basis functions on the faces are by definition zero.

To translate the general construction algorithm, i.e. the BVP (4.30) on page 100, for each type of basis function on each type of grid element into vector proxy notation, we still have to find the equivalents of the exterior derivative and coderivative for the vector proxies. For the 0-dimensional case, these are the trivial zero operators. For the 1-dimensional case, they are either the zero or the 1-dimensional gradient operator. The equivalences for the 2- and 3-dimensional case, i.e. faces and cells, can be found in [42, pp.246]. In the 3-dimensional case, they are described by the gradient, curl, and divergence operators already introduced in chapter 2. For the 2-dimensional case, we need to introduce the surface gradient denoted by $\overrightarrow{\mathrm{grad}}_{\mathrm{2D}}$, the tangential part of the surface curl denoted by $\overrightarrow{\mathrm{curl}}_{\mathrm{2D}}$, the normal part of the surface curl denoted by $\mathrm{curl}_{\mathrm{2D}}$, and the surface divergence denoted by $\mathrm{div}_{\mathrm{2D}}$. For the above introduced traces, these are defined as:

$$\overrightarrow{\mathrm{grad}}_{\mathrm{2D}}\, \vec{B}_i^0 \equiv \begin{pmatrix} \frac{\partial}{\partial x_1} \vec{B}_i^0 \\ \frac{\partial}{\partial x_2} \vec{B}_i^0 \end{pmatrix} \tag{4.45a}$$

$$\overrightarrow{\mathrm{curl}}_{\mathrm{2D}}\, \vec{B}_i^0 \equiv \begin{pmatrix} -\frac{\partial}{\partial x_2} \vec{B}_i^0 \\ \frac{\partial}{\partial x_1} \vec{B}_i^0 \end{pmatrix} \tag{4.45b}$$

$$\mathrm{curl}_{\mathrm{2D}}(\vec{B}_i^1)_{t_{S_j^2}} \equiv \frac{1}{h_1 h_2} \left(\frac{\partial}{\partial \hat{x}_1} \left(h_2 (\vec{B}_i^1)_{t_{S_j^2,2}} \right) - \frac{\partial}{\partial \hat{x}_2} \left(h_1 (\vec{B}_i^1)_{t_{S_j^2,1}} \right) \right) \tag{4.45c}$$

$$\mathrm{div}_{\mathrm{2D}}(\vec{B}_i^1)_{t_{S_j^2}} \equiv \frac{1}{h_1 h_2} \left(\frac{\partial}{\partial \hat{x}_1} \left(h_2 (\vec{B}_i^1)_{t_{S_j^2,1}} \right) + \frac{\partial}{\partial \hat{x}_2} \left(h_1 (\vec{B}_i^1)_{t_{S_j^2,2}} \right) \right) \tag{4.45d}$$

Now we are ready to state the construction algorithm for the basis functions for each degree in vector proxy language.

Polyhedral Nodal Basis Functions

The nodal basis functions $\vec{B}_i^0$ associated with the nodes of the grid $S_i^0 \in \boldsymbol{S}^0(\Omega_h)$ are first defined by their values on the nodes of the grid, then on the edges, then on the faces, and finally in the cells of the grid, as was depicted schematically in Fig. 4.3. Keep in mind that the nodal basis functions $\vec{B}_i^0$ are scalar functions on the domain Ω.

For each type of grid element, we will give the analytical solutions for simplicial grid elements as examples. Note that all grid vertices are simplicial as are the straight grid edges, thus the solutions for all vertices and edges are given. Simplicial faces are planar triangles and simplicial cells are tetrahedrons.

For the nodes of the grid, the first three equations of the BVP (4.30a)- (4.30c) on page 100 reduce to stating $0=0$. The only remaining condition is the constraint (4.30d) which directly gives the solution:

$$\int_{S_j^0} \vec{B}_i^0(S_j^0) = \vec{B}_i^0(S_j^0) = \delta_{ij} \qquad \forall\, S_j^0 \in \boldsymbol{S}^0(\Omega_h) \tag{4.46d}$$

Example 4.3. The BVP directly states the solution for the basis function $\vec{B}_i^0$ on the nodes of the grid: Its value is one at its associated node S_i^0 and zero at all other nodes of the grid. For a sample tetrahedron, the values for a basis function $\vec{B}_i^0$ are depicted in Fig. 4.4a.

Now we consider the BVP (4.30) for the nodal basis functions $\vec{B}_i^0$ on the edges of the grid S_j^1:

$$\frac{1}{h_1}\frac{\partial}{\partial \hat{x}_1}\left(\frac{1}{h_1}\frac{\partial}{\partial \hat{x}_1}\vec{B}_i^0(\vec{s}(\hat{x}_1))\right) = 0 \qquad \forall\, \vec{s}(\hat{x}_1) \in S_j^1 \tag{4.47a}$$

$$\vec{B}_i^0\left(\vec{s}(\hat{x}_1)\right) \qquad \text{known on } \partial S_j^1 \tag{4.47c}$$

The boundary conditions in equation (4.47c) are known from the solution on the grid nodes above.

Example 4.4. All grid edges are assumed to be simplicial, i.e. straight. Then the unique solution for the edge S_j^1 from point S_p^0 to S_q^0 reads:

$$\vec{B}_i^0(\vec{r}) = \delta_{ip}\frac{|S_q^0 - \vec{r}|}{|S_q^0 - S_p^0|} + \delta_{iq}\frac{|S_p^0 - \vec{r}|}{|S_p^0 - S_q^0|} \qquad \forall\, \vec{r} \in S_j^1 \subset \mathbb{R}^3 \tag{4.48}$$

For the edges adjacent to the node S_i^0, this renders the linear function going from 1 at the node S_i^0 to zero on the other node. For all other edges, this is the zero function. For the edges of a sample tetrahedron, a solution is shown in Fig. 4.4b.

On the faces of the grid S_j^2, the BVP (4.30) for the nodal basis functions reads:

$$\mathrm{div}_{2\mathrm{D}}\, \overrightarrow{\mathrm{grad}}_{2\mathrm{D}}\, \vec{B}_i^0(\vec{s}(\hat{x}_1, \hat{x}_2)) = 0 \qquad \forall\, \vec{s}(\hat{x}_1, \hat{x}_2) \in S_j^2 \tag{4.49a}$$

$$\vec{B}_i^0(\vec{s}(\hat{x}_1, \hat{x}_2)) \qquad \text{known on } \partial S_j^2 \tag{4.49b}$$

Again, the boundary conditions in equation (4.49b) are known from the solution on the grid edges above.

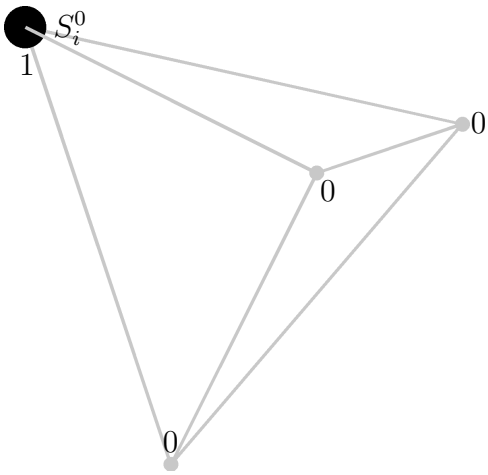

(a) Values of the nodal basis function $\vec{B}_i^0$ at the nodes of the example tetrahedral element. The nodal value is 1 for the associated node S_i^0 and zero for all other nodes.

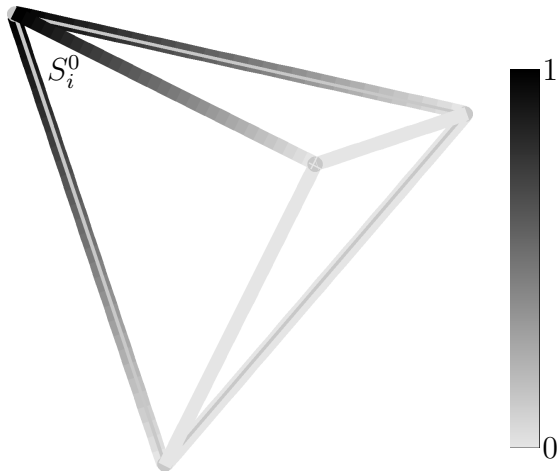

(b) Values of the nodal basis function $\vec{B}_i^0$ along the edges of the example tetrahedral element. The nodal basis function $\vec{B}_i^0$ varies linearly from value 1 at its associated node S_i^0 to value zero along edges adjacent to the associated node. On all other edges, the nodal basis function $\vec{B}_i^0$ is zero.

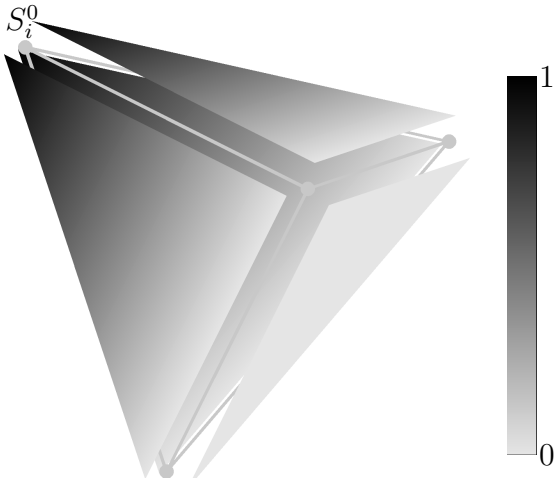

(c) Values of the nodal basis function $\vec{B}_i^0$ on the faces of the example tetrahedral element. The nodal basis function $\vec{B}_i^0$ is only non-zero on the faces adjacent to the associated node S_i^0.

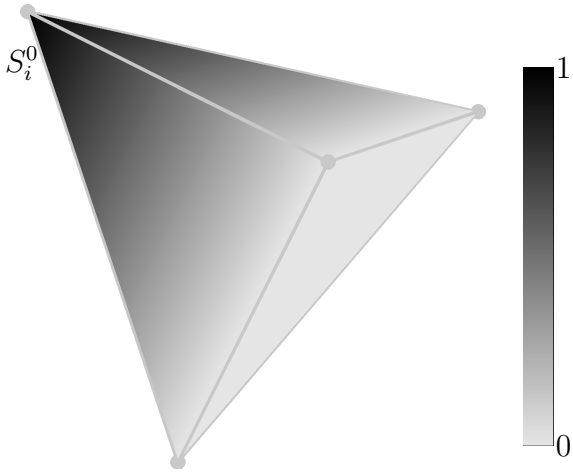

(d) The nodal basis function $\vec{B}_i^0$ on the example tetrahedral element varies linearly from value 1 on the associated vertex S_i^0 to value 0 on the opposite face.

Fig. 4.4: Continuous polyhedral nodal basis function $\vec{B}_i^0$ for an example tetrahedron. The resulting nodal basis function coincides with the standard Whitney-FEM nodal basis function of lowest order for the tetrahedron.

Example 4.5. For simplicial faces, i.e. planar triangles, we can write down the analytical solution to this BVP. Denoting the corner points of the triangle S_j^2 by S_p^0, S_q^0, and S_r^0, the basis function $\vec{B}_p^0$ reads:

$$\vec{B}_p^0(\vec{r}) = \frac{|(S_q^0 - \vec{r}) \times (S_r^0 - \vec{r})|}{|(S_q^0 - S_p^0) \times (S_r^0 - S_p^0)|} \qquad \forall\, \vec{r} \in S_j^2 \subset \mathbb{R}^3 \tag{4.50}$$

This is the standard Whitney nodal basis function for triangles. The basis functions associated with a node that is not contained in the face are zero on that face. For the faces of a tetrahedron, a solution is shown in Fig. 4.4c.

Now taking the solutions on the faces as boundary values, we arrive at the BVP for the nodal basis functions on the grid cells S_j^3:

$$\operatorname{div}\operatorname{grad}\vec{B}_i^0 = 0 \qquad \text{in } S_j^3 \tag{4.51a}$$

$$\vec{B}_i^0 \qquad \text{known on } \partial S_j^3 \tag{4.51c}$$

Example 4.6. For simplicial grid cells, i.e. tetrahedra with planar faces, the solution can again be written analytically. For a tetrahedron S_j^3 with the corner points S_p^0, S_q^0, S_r^0, and S_s^0, the solution for the nodal basis function $\vec{B}_p^0$ reads:

$$\vec{B}_p^0(\vec{r}) = \frac{|((S_q^0 - \vec{r}) \times (S_r^0 - \vec{r})) \cdot (S_s^0 - \vec{r})|}{|((S_q^0 - S_p^0) \times (S_r^0 - S_p^0)) \cdot (S_s^0 - S_p^0)|} \qquad \forall\, \vec{r} \in S_j^3 \subset \mathbb{R}^3 \tag{4.52}$$

This is the standard Whitney nodal basis function for tetrahedra shown in Fig. 4.4d.

Polyhedral Edge Basis Functions

The edge basis functions $\vec{B}_i^1$ are first defined by their tangential components on the edges, then by their tangential components on the faces, and finally on all cells of the grid. On the edge S_j^1, the trace $(\vec{B}_i^1)_{t_{S_j^1}}$ as defined in equation (4.37) on page 102 is a scalar function. The BVP (4.30) on page 100 for this trace reads:

$$\frac{\partial}{\partial \hat{x}_1}(\vec{B}_i^1(\vec{s}(\hat{x}_1)))_{t_{S_j^1}} = 0 \qquad \text{in } S_j^1 \tag{4.53b}$$

$$\int_{S_j^1} (\vec{B}_i^1(\vec{s}(\hat{x}_1)))_{t_{S_j^1}}\, \mathrm{d}s = 1 \tag{4.53d}$$

Example 4.7. For the case of straight edges, the unique solution for the edge S_j^1 reads:

$$(\vec{B}_i^1(\vec{r}))_{t_{S_j^1}} = \delta_{ij}\frac{1}{|S_j^1|} \qquad \forall\, \vec{r} \in S_i^1 \subset \mathbb{R}^3 \tag{4.54}$$

The trace is thus constant on all edges and only non-zero on the associated edge S_i^1. An example edge basis function is shown on the edges of a tetrahedron in Fig. 4.5a.

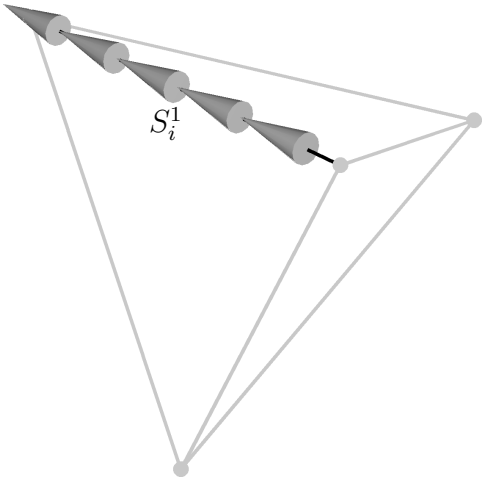

(a) Tangential component of the edge basis function $\vec{B}_i^1$ along the edges of the example tetrahedral element. The edge basis function $\vec{B}_i^1$ has constant tangential component along its associated edge S_i^1. On all other edges, the tangential component of the edge basis function $\vec{B}_i^1$ is zero.

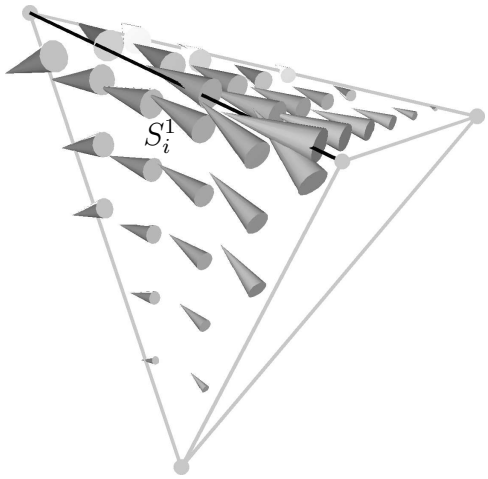

(b) Tangential components of the edge basis function $\vec{B}_i^1$ on the faces of the example tetrahedral element. The tangential components of the edge basis function $\vec{B}_i^1$ are only nonzero on the faces adjacent to the associated edge S_i^1.

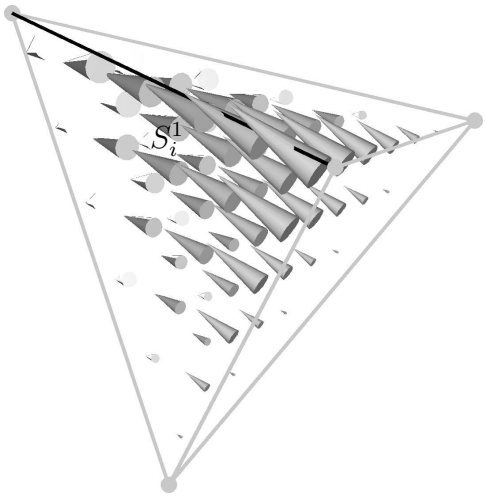

(c) The edge basis function $\vec{B}_i^1$ on the example tetrahedral element.

Fig. 4.5: Continuous polyhedral edge basis function $\vec{B}_i^1$ for an example tetrahedron. The resulting edge basis function coincides with the standard Whitney-FEM edge basis function of lowest order for the tetrahedron.

The tangential component vector $(\vec{B}_i^1)_{t_{S_j^2}}$ of edge basis functions on a face S_j^2 is a 2-component vector field on the face as defined in equation (4.37) on page 102. Assuming the tangential components $(\vec{B}_i^1)_{t_{S_m^1}}$ on the edges of the grid known from above, the BVP on the faces reads:

$$\overrightarrow{\mathrm{curl}}_{\mathrm{2D}}\,\mathrm{curl}_{\mathrm{2D}}(\vec{B}_i^1)_{t_{S_j^2}} = 0 \qquad \text{in } S_j^2 \tag{4.55a}$$

$$\mathrm{div}_{\mathrm{2D}}(\vec{B}_i^1)_{t_{S_j^2}} = 0 \qquad \text{in } S_j^2 \tag{4.55b}$$

$$(\vec{B}_i^1)_{t_{\partial S_j^2}} \qquad \text{known on } \partial S_j^2 \tag{4.55c}$$

Example 4.8. Let S_p^0, S_q^0, and S_r^0 denote the vertices of the triangle S_j^2 and S_{pq}^1 the edge from vertex S_p^0 to vertex S_q^0. Then the unique solution for the edge basis function $\vec{B}_{pq}^1$ associated with the edge S_{pq}^1 reads:

$$(\vec{B}_{pq}^1)_{t_{S_j^2}} = \vec{B}_p^0(\vec{r})\,\overrightarrow{\mathrm{grad}}_{\mathrm{2D}}\,\vec{B}_q^0(\vec{r}) - \vec{B}_q^0(\vec{r})\,\overrightarrow{\mathrm{grad}}_{\mathrm{2D}}\,\vec{B}_p^0(\vec{r}) \qquad \forall\,\vec{r} \in S_j^2 \subset \mathbb{R}^3 \tag{4.56}$$

where we have used the scalar nodal basis functions $\vec{B}_i^0$ defined on the face S_j^2 in equation (4.50). An example edge basis function is shown on the faces of a tetrahedron in Fig. 4.5b.

In a grid cell S_j^3, the BVP for the edge basis function $\vec{B}_i^1$ reads:

$$\mathrm{curl}\,\mathrm{curl}\,\vec{B}_i^1 = 0 \qquad \text{in } S_j^3 \tag{4.57a}$$

$$\mathrm{div}\,\vec{B}_i^1 = 0 \qquad \text{in } S_j^3 \tag{4.57b}$$

$$(\vec{B}_i^1)_{t_{\partial S_j^3}} \qquad \text{known on } \partial S_j^3 \tag{4.57c}$$

Example 4.9. For the tetrahedron S_j^3 with the corner points S_p^0, S_q^0, S_r^0, and S_s^0, let S_{pq}^1 denote the edge from node S_p^0 to node S_p^0 and $\vec{B}_{pq}^1$ the associated edge basis function. Then the solution for the edge basis function $\vec{B}_{pq}^1$ reads:

$$\vec{B}_{pq}^1(\vec{r}) = \vec{B}_p^0(\vec{r})\,\mathrm{grad}\,\vec{B}_q^0(\vec{r}) - \vec{B}_q^0(\vec{r})\,\mathrm{grad}\,\vec{B}_p^0(\vec{r}) \qquad \forall\,\vec{r} \in S_j^3 \subset \mathbb{R}^3 \tag{4.58}$$

where we have used the scalar nodal basis functions $\vec{B}_i^0$ defined on the cell S_j^3 in equation (4.52). These are the standard edge Whitney basis functions for a tetrahedron. An example edge basis function is shown for a tetrahedron in Fig. 4.5c.

Polyhedral Face Basis Functions

The face basis functions $\vec{B}_i^2$ are first defined by their normal vector components on the grid faces and then in all vector component on the grid cells.

For the normal vector component of the face basis functions $(\vec{B}_i^2)_{n_{S_j^2}}$ on the faces S_j^2 of the grid, we get the following BVP:

$$\overrightarrow{\mathrm{grad}}_{\mathrm{2D}}(\vec{B}_i^2)_{n_{S_j^2}} = 0 \qquad \text{in } S_j^2 \tag{4.59b}$$

$$\int_{S_j^2} (\vec{B}_i^2)_{n_{S_j^2}}\,\mathrm{d}A = 1 \tag{4.59d}$$

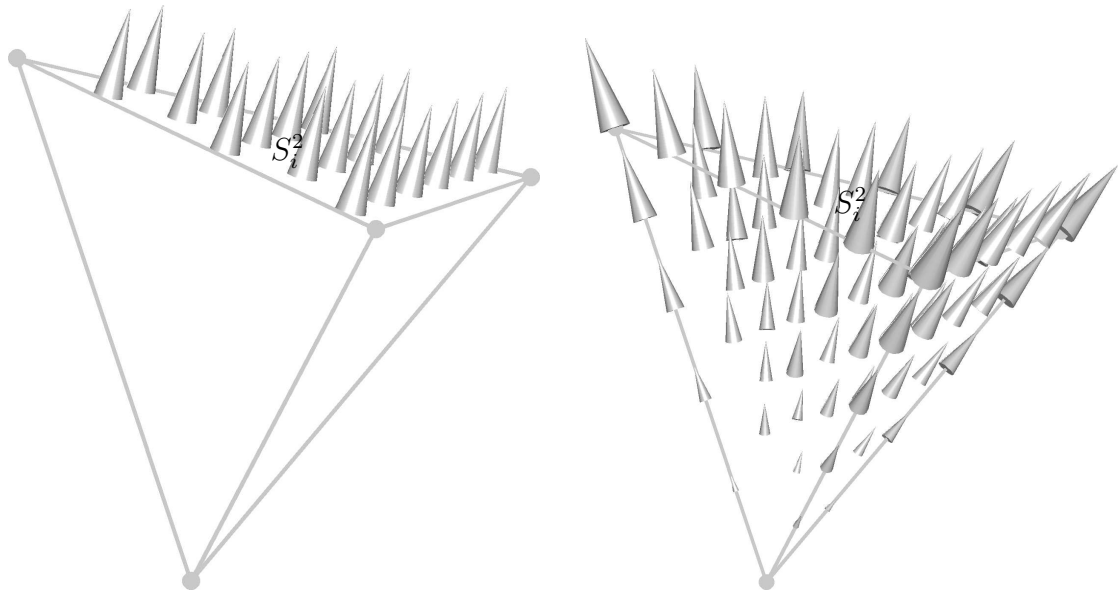

(a) Normal vector component of the face basis function $\vec{B}_i^2$ on the faces of the example tetrahedral element. The normal vector component is constant on the associated face S_i^2 and zero on all other faces.

(b) Values of the face basis function $\vec{B}_i^2$ on the example tetrahedral element.

Fig. 4.6: Continuous polyhedral face basis function $\vec{B}_i^2$ for an example tetrahedron. The resulting face basis function coincides with the standard Whitney-FEM face basis function of lowest order for the tetrahedron.

Example 4.10. We directly see that the constant function $\delta_{ij}\frac{1}{|S_j^2|}$ solves this BVP and therefore is its unique solution:

$$(\vec{B}_i^2(\vec{r}))_{n_{S_j^2}} = \delta_{ij}\frac{1}{|S_j^2|} \qquad \forall\, \vec{r} \in S_j^2 \subset \mathbb{R}^3 \tag{4.60}$$

The normal vector component of an example face basis function is shown on the faces of a tetrahedron in Fig. 4.6a.

In the grid cells S_j^3, the BVP defining the face basis functions $\vec{B}_i^2$ reads:

$$\operatorname{grad}\operatorname{div}\vec{B}_i^2 = 0 \qquad \text{in } S_j^3 \tag{4.61a}$$

$$\operatorname{curl}\vec{B}_i^2 = 0 \qquad \text{in } S_j^3 \tag{4.61b}$$

$$(\vec{B}_i^2)_{n_{\partial S_j^3}} \qquad \text{known on } \partial S_j^3 \tag{4.61c}$$

Example 4.11. For the tetrahedron S_j^3 with the corner points S_p^0, S_q^0, S_r^0, and S_s^0, let S_{pqr}^2 denote the face with the nodes S_p^0, S_p^0, and S_r^0 in its boundary in that order. Then the solution for the face basis function $\vec{B}_{pqr}^2$ associated with that face reads:

$$\begin{aligned}\vec{B}_{pqr}^2(\vec{r}) = {} & \vec{B}_p^0(\vec{r})\operatorname{curl}\vec{B}_{qr}^1(\vec{r}) + \vec{B}_q^0(\vec{r})\operatorname{curl}\vec{B}_{rp}^1(\vec{r}) \\ & + \vec{B}_r^0(\vec{r})\operatorname{curl}\vec{B}_{pq}^1(\vec{r}) \qquad \forall\, \vec{r} \in S_j^3 \subset \mathbb{R}^3\end{aligned} \tag{4.62}$$

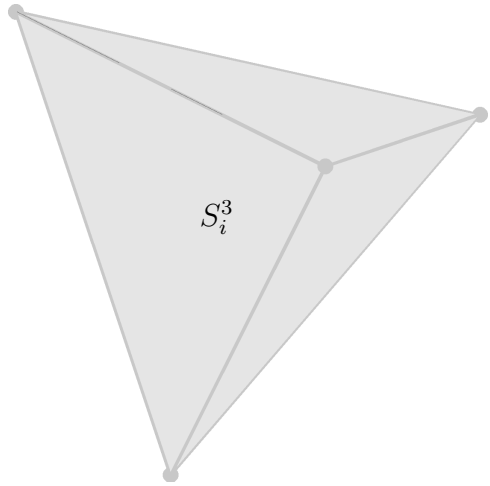

Fig. 4.7: Continuous polyhedral volume basis function $\vec{B}_i^3$ for an example tetrahedron S_i^3. The volume basis function $\vec{B}_i^3$ has constant value on the associated element and zero value on all other elements. This coincides with the standard Whitney volume basis function of lowest order for the tetrahedron.

using the nodal and edge basis functions defined in equations (4.52) and (4.58). These are the standard lowest order Whitney face basis functions on a tetrahedron. An example face basis function is shown for an example tetrahedron in Fig. 4.6b.

Polyhedral Volume Basis Functions

The volume basis functions $\vec{B}_i^3$ are directly defined by a BVP on the grid cells S_j^3:

$$\operatorname{grad} \vec{B}_i^3 = 0 \qquad \text{in } S_j^3 \tag{4.63b}$$

$$\int_{S_j^3} \vec{B}_i^3 \, \mathrm{d}V = 1 \tag{4.63d}$$

Example 4.12. Again, we notice that the scalar function $\delta_{ij} \frac{1}{|S_j^3|}$ solves the BVP (4.63) and therefore is its unique solution:

$$\vec{B}_i^3(\vec{r}) = \delta_{ij} \frac{1}{|S_j^3|} \qquad \forall \, \vec{r} \in S_j^3 \subset \mathbb{R}^3 \tag{4.64}$$

These are the standard Whitney volume basis functions of lowest order. An example volume basis function is shown in Fig. 4.7.

4.3 Discrete Construction Algorithm for Polyhedral Whitney Basis Functions by the FIT

Although the continuous BVP (4.30) on page 100 does describe basis functions for arbitrary polyhedrons, analytical solutions are only available for a few element shapes: Besides

the solutions for simplicial elements given in the examples above, they are also known for Cartesian product cells, i.e. cubes, or combinations of simplicial and Cartesian product cells like the prism. In this and the following chapter, we will discover that consistent discretizations of the continuous BVP do render discrete solutions which also fulfill the properties I to VI on pages 95–96 required of the Whitney-FEM-like basis functions. We call these discrete solutions *discrete polyhedral Whitney basis functions*. There are many possibilities to consistently discretize the BVP. In this chapter, we will shortly describe the discretization by the FIT introduced in chapter 3 using element shapes for which material matrices are known. Although the discretization by the FIT seems very promising, especially for subgridding or multigrid schemes, the numerical examples in chapter 5 use a more general consistent Galerkin formulation. The Galerkin formulation will be discussed in chapter 4.4.

At first, it might seem much effort to solve a discrete BVP for each grid element in order to construct each Whitney-like basis function. Due to the locality condition, the discrete BVP has only to be solved for grid elements adjacent to the associated grid element, though. More importantly, the solutions always fulfill the required properties I to VI and thus the same order of consistency is expected for any solution. As more expensive discrete solutions that approximate the continuous solutions of the BVP better do not necessarily render a better overall polyhedral scheme, the discretization can be chosen as coarse and as cheap as possible. Another argument is that most application examples in chapter 5 use polyhedral cells of a single type. Then it is sufficient to calculate the discrete Whitney basis functions only once and use them for all cells of the same type in the grid.

As stated before, the FIT formalism introduced in chapter 3 is a general method for discretizing a BVP. As such, we can employ it to discretize the BVP (4.30) rendering approximate discrete solutions for the Whitney basis functions. We will only discuss this scheme very briefly, as it is not used directly in the applications in chapter 5.

The continuous BVP (4.30) has to be discretized on each primal grid element S_j^l. For each primal grid element S_j^l, we thus introduce again a consistent grid and call this the *intermediate grid part* $\left(S_j^l\right)_h$. In order to be able to solve the discrete version of the BVP (4.30), only element shapes with known material matrices should be employed, e.g only simplicial or Cartesian product elements.

We require the intermediate grid parts to fit together consistently, that is the discretizations in intersecting boundary parts to be the same. We call this union the *intermediate grid* $(\Omega_h)_h$. Note that the intermediate grid $(\Omega_h)_h$ is a consistent grid of the domain Ω and the intermediate grid parts $\left(S_j^l\right)_h$ are consistent grid parts of the intermediate grid according to Definition 3.7. In this case, the resulting discrete Whitney basis functions fulfill equivalent discrete versions to the properties I to VI. Although these are not stated or proven here, this can be done in analogy to the continuous case and the Galerkin formulation in the next chapter.

The discrete Whitney basis functions $\boldsymbol{B}_i^k$ sought for are primal k-cochains of the intermediate grid $(\Omega_h)_h$:

$$\boldsymbol{B}_i^k \in \mathcal{F}_h^k((\Omega_h)_h) \tag{4.65}$$

The unknown for the discrete BVP on each grid element S_j^l is the trace of this k-cochain onto the grid element S_j^l (or more precisely: onto the grid part $\left(S_j^l\right)_h$):

$$\left(\mathbf{T}^k_{(\Omega_h)_h,\left(S_j^l\right)_h} \boldsymbol{B}_i^k\right) \quad \in \mathcal{F}_h^k(\left(S_j^l\right)_h) \tag{4.66}$$

using the intermediate grid trace operator $\mathbf{T}^k_{(\Omega_h)_h,\left(S_j^l\right)_h}$. In order to state the discretized version of the BVP (4.30) on the grid element S_j^l, we need local equivalents of the primal and dual discrete exterior derivatives, the material matrices, the primal discrete trace operator, and the discrete integral. They are simply the l-dimensional generalizations of the operators introduced for the 3-dimensional case in chapter 3. We will here only state their domains and ranges to get enough intuition about them to state the discrete BVP:

$$\mathbf{D}^k_{\left(S_j^l\right)_h} : \qquad \mathcal{F}_h^k(\left(S_j^l\right)_h) \longrightarrow \mathcal{F}_h^{k+1}(\left(S_j^l\right)_h) \tag{4.67}$$

$$\underset{\sim}{\mathbf{D}}^k_{\left(S_j^l\right)_h} : \qquad \underset{\sim}{\mathcal{F}}_h^k(\left(S_j^l\right)_h) \longrightarrow \underset{\sim}{\mathcal{F}}_h^{k+1}(\left(S_j^l\right)_h) \tag{4.68}$$

$$\mathbf{M}^k_{\left(S_j^l\right)_h} : \qquad \mathcal{F}_h^k(\left(S_j^l\right)_h) \longrightarrow \underset{\sim}{\mathcal{F}}_h^{l-k}(\left(S_j^l\right)_h) \tag{4.69}$$

$$\mathbf{T}^k_{\left(S_j^l\right)_h,\left(\Gamma_h^m\right)_h} : \qquad \mathcal{F}_h^k(\left(S_j^l\right)_h) \longrightarrow \mathcal{F}_h^k((\Gamma_h^m)_h) \tag{4.70}$$

$$\int_{S_j^l} . : \qquad \mathcal{F}_h^k(\left(S_j^l\right)_h) \longrightarrow \mathbb{R} \tag{4.71}$$

Now we can state the FIT discretized version of the BVP (4.30) on each grid element S_j^l:

$$\left(\mathbf{M}^k_{\left(S_j^l\right)_h}\right)^{-1} \underset{\sim}{\mathbf{D}}^{l-k-1}_{\left(S_j^l\right)_h} \mathbf{M}^{k+1}_{\left(S_j^l\right)_h} \mathbf{D}^k_{\left(S_j^l\right)_h} \left(\mathbf{T}^k_{(\Omega_h)_h,\left(S_j^l\right)_h} \boldsymbol{B}_i^k\right) = 0 \tag{4.72a}$$

$$\left(\mathbf{M}^{k-1}_{\left(S_j^l\right)_h}\right)^{-1} \underset{\sim}{\mathbf{D}}^{l-k}_{\left(S_j^l\right)_h} \mathbf{M}^k_{\left(S_j^l\right)_h} \left(\mathbf{T}^k_{(\Omega_h)_h,\left(S_j^l\right)_h} \boldsymbol{B}_i^k\right) = 0 \tag{4.72b}$$

$$\mathbf{T}^k_{\left(S_j^l\right)_h,\left(\partial S_j^l\right)_h} \left(\mathbf{T}^k_{(\Omega_h)_h,\left(S_j^l\right)_h} \boldsymbol{B}_i^k\right) \qquad \text{given} \tag{4.72c}$$

$$\int_{S_j^k} \left(\mathbf{T}^k_{(\Omega_h)_h,\left(S_j^l\right)_h} \boldsymbol{B}_i^k\right) = \delta_{ij} \qquad \text{if } l = k \tag{4.72d}$$

Solving the discrete BVP (4.72) for all grid elements S_j^l letting l go from k to 3 renders all entries of the discrete Whitney basis functions $\boldsymbol{B}_i^k$. As mentioned above, this discretization should only contain elements for which material matrices $\mathbf{M}^k_{\left(S_j^l\right)_h}$ can be derived, i.e. at this point simplicial or orthogonal product elements. In the setting of chapter 3, existence and uniqueness of the solutions as well as the fulfillment of discrete equivalents to the properties I to VI can be proven.

As denoted by equation (4.65), the solutions $\boldsymbol{B}_i^k$ of the above discrete BVP are primal k-cochains of the intermediate grid $(\Omega_h)_h$. As Whitney maps for these are not necessarily available, e.g. for the standard FIT formulation with dual orthogonal grids, we do not get continuous approximations for the basis functions. So if not by equation (4.7) on page 92, how do we derive the polyhedral material matrices? We can directly calculate

the polyhedral material matrices from the local FIT material matrices $\mathbf{M}^k_{(S^3_m)_h}$ according to:

$$\left(\mathbf{M}^k\right)_{ij} = \left(\boldsymbol{B}^k_i\right)^{\mathrm{T}} \sum_{m=1}^{n^3} \left(\left(\mathbf{T}^k_{(\Omega_h)_h,(S^3_m)_h}\right)^{\mathrm{T}} \mathbf{M}^k_{(S^3_m)_h} \mathbf{T}^k_{(\Omega_h)_h,(S^3_m)_h} \right) \boldsymbol{B}^k_j \tag{4.73}$$

As the global material matrix for the intermediate grid $(\Omega_h)_h$ is equivalent to

$$\mathbf{M}^k_{(\Omega_h)_h} = \sum_{m=1}^{n^3} \left(\mathbf{T}^k_{(\Omega_h)_h,(S^3_m)_h}\right)^{\mathrm{T}} \mathbf{M}^k_{(S^3_m)_h} \mathbf{T}^k_{(\Omega_h)_h,(S^3_m)_h} \tag{4.74}$$

we recognize equation (4.73) as the discrete inner product for k-cochains as defined by equation (3.63) on page 49 for the intermediate grid $(\Omega_h)_h$. Weighted material matrices for material coefficients α can be calculated by using the appropriate local weighted material matrices.

Remark 4.1. When using Whitney-FEM material matrices for the FIT discretization, equation (4.73) renders exactly the same material matrices as when plugging the Whitney reconstructed discrete solution into equation (4.7) on page 92.

4.4 Discrete Construction Algorithm for Polyhedral Whitney Basis Functions by a Galerkin Formulation

In this chapter, we discretize the continuous BVP (4.30) on page 100 by a conforming Galerkin formulation. As the first step, we state the continuous variational formulation of the BVP (4.30). The discretization is achieved by choosing finite-dimensional approximation spaces for this variational formulation. These approximation spaces are called *intermediate approximation spaces* and denoted by $\widetilde{\mathcal{W}}^k$. The basis functions spanning the search spaces are called *intermediate basis functions* and denoted by $\widetilde{B}^k_i$. Under certain restrictions on the intermediate approximation spaces, the resulting discrete BVPs do have unique solutions and the resulting approximate Whitney basis functions do fulfill properties I to VI on pages 95–96. This is actually the original setting of the construction algorithm as presented in [19].

A special class of global basis functions, the so-called barycentric coordinates and derived basis functions, is given in the examples as a possible choice for the intermediate basis functions of the variational formulation. Basis functions derived according to this scheme are used in the applications in chapter 5. These global basis functions seem interesting as they hint at geometrical construction schemes for discrete Whitney basis functions. For the 2-dimensional faces, an equivalent geometric construction scheme is proposed. The proof for its general validity is an open problem, though, as is its extension to 3-dimensional grid cells.

4.4.1 Continuous Variational Formulation of the Construction Boundary Value Problem

We here state the variational formulation of the BVP (4.30) on page 100. We again use the notation of differential geometry in order to unify the presentation.

We first need to define the search and test spaces for this formulation based on the Sobolev-type spaces defined in equation (4.2) on page 91. The search spaces $\mathcal{F}^k_{\mathrm{d}}(S^l_j, \mathrm{t}^k_{\partial S^l_j} B^k_i)$ directly impose the boundary conditions $\mathrm{t}^k_{\partial S^l_j} B^k_i$:

$$\mathcal{F}^k_{\mathrm{d}}(S^l_j, \mathrm{t}^k_{\partial S^l_j} B^k_i) \equiv \left\{ \omega \in \mathcal{F}^k_{\mathrm{d}}(S^l_j) : \mathrm{t}^k_{\partial S^l_j} \omega = \mathrm{t}^k_{\partial S^l_j} B^k_i \right\} \tag{4.75}$$

As test spaces, we will employ the spaces $\mathcal{F}^k_{\mathrm{d}}(S^l_j, 0)$, which have zero trace on the boundary.

The variational formulation uses the local inner product $\langle\!\langle .|. \rangle\!\rangle_{S^l_j}$ on the grid elements S^l_j defined as:

$$\langle\!\langle .|. \rangle\!\rangle_{S^l_j} : \quad \left(\omega^k, \eta^k\right) \in \mathcal{F}^k_{\mathrm{d}}(S^l_j) \times \mathcal{F}^k_{\mathrm{d}}(S^l_j) \longmapsto \langle\!\langle \omega^k | \eta^k \rangle\!\rangle_{S^l_j} \in \mathbb{R} \tag{4.76a}$$

$$\langle\!\langle \omega^k | \eta^k \rangle\!\rangle_{S^l_j} \equiv \int_{S^l_j} \omega^k \wedge \star^l_{S^l_j} \eta^k \tag{4.76b}$$

We finally state the BVP (4.30) in variational form: Find the k-form $\left(\mathrm{t}^k_{\partial S^l_j} B^k_i\right)$ in the search space $\mathcal{F}^k_{\mathrm{d}}(S^l_j, \mathrm{t}^k_{S^l_j} B^k_i)$ that fulfills the equations:

$$\langle\!\langle \mathrm{d}^k_{S^l_j} \left(\mathrm{t}^k_{S^l_j} B^k_i\right) \,|\, \mathrm{d}^k_{S^l_j} \eta^k \rangle\!\rangle_{S^l_j} = 0 \qquad \forall\, \eta^k \in \mathcal{F}^k_{\mathrm{d}}(S^l_j, 0) \tag{4.77a}$$

$$\langle\!\langle \left(\mathrm{t}^k_{S^l_j} B^k_i\right) \,|\, \mathrm{d}^{k-1} \eta^{k-1} \rangle\!\rangle_{S^l_j} = 0 \qquad \forall\, \eta^{k-1} \in \mathcal{F}^{k-1}_{\mathrm{d}}(S^l_j, 0) \tag{4.77b}$$

$$\int_{S^k_j} \left(\mathrm{t}^k_{S^l_j} B^k_i\right) = \delta_{ij} \qquad \text{if } l = k \tag{4.77d}$$

This variational formulation is called the weak formulation of the BVP (4.30). Existence of a solution is easily seen, as the solution to the BVP (4.30) also fulfills the variational formulation. Uniqueness is not proven here but also holds.

To arrive at the approximate Galerkin discretization of the BVP (4.30) on page 100, we now simply use finite-dimensional search and test spaces.

4.4.2 Discrete Galerkin Formulation of the Construction Boundary Value Problem

For a Galerkin discretization of the variational BVP (4.77), we simply replace the infinite-dimensional search and test spaces by finite-dimensional search and test spaces based on finite-dimensional *intermediate approximation spaces* $\widetilde{\mathcal{W}}^k(S^l_j)$. These spaces will be characterized later on and a specific choice is presented in the examples.

The intermediate approximation spaces are assumed to be conforming, i.e.:

$$\widetilde{\mathcal{W}}^k(S_j^l) \subset \mathcal{F}_{\mathrm{d}}^k(S_j^l) \tag{4.78}$$

The boundary condition is directly imposed on the search space for the discrete formulation which is defined as:

$$\widetilde{\mathcal{W}}^k(S_j^l, \mathrm{t}^k_{\partial S_j^l} B_i^k) \equiv \widetilde{\mathcal{W}}^k(S_j^l) \cap \mathcal{F}_{\mathrm{d}}^k(S_j^l, \mathrm{t}^k_{\partial S_j^l} B_i^k) \tag{4.79}$$

As test space, we will use the space $\widetilde{\mathcal{W}}^k(S_j^l, 0)$ with zero boundary condition. Then the Galerkin discretization of the variational BVP (4.77) reads: Find the k-form $\left(\mathrm{t}^k_{S_j^l} B_i^k\right) \in \widetilde{\mathcal{W}}^k(S_j^l, \mathrm{t}^k_{\partial S_j^l} B_i^k)$ such that

$$\left\langle\!\left\langle \mathrm{d}^k_{S_j^l} \left(\mathrm{t}^k_{S_j^l} B_i^k\right) \,\middle|\, \mathrm{d}^k_{S_j^l} \eta^k \right\rangle\!\right\rangle_{S_j^l} = 0 \qquad \forall\, \eta^k \in \widetilde{\mathcal{W}}^k(S_j^l, 0) \tag{4.80a}$$

$$\left\langle\!\left\langle \left(\mathrm{t}^k_{S_j^l} B_i^k\right) \,\middle|\, \mathrm{d}^{k-1}_{S_j^l} \eta^{k-1} \right\rangle\!\right\rangle_{S_j^l} = 0 \qquad \forall\, \eta^{k-1} \in \widetilde{\mathcal{W}}^{k-1}(S_j^l, 0) \tag{4.80b}$$

$$\int_{S_j^k} \left(\mathrm{t}^k_{S_j^l} B_i^k\right) = \delta_{ij} \qquad \text{if } l = k \tag{4.80d}$$

Remark 4.2. When Whitney spaces are chosen again as intermediate approximation spaces $\widetilde{\mathcal{W}}^k$, the resulting discrete BVP (4.80) is equivalent to the FIT discretized BVP (4.72) on page 112 with Whitney-FEM material matrices defined by the basis functions spanning the intermediate approximation spaces. This equivalence was shown in the case of Maxwell's BVP in appendix C on page 183.

Theorem 4.7. *If the intermediate approximation spaces form a complex under the operator* d^k*, i.e. the following holds*

$$\mathrm{d}^k : \widetilde{\mathcal{W}}^k \to \widetilde{\mathcal{W}}^{k+1} \tag{4.81a}$$

$$\mathrm{d}^{k+1}\,\mathrm{d}^k = 0 \tag{4.81b}$$

and the full and relative discrete cohomology spaces $\mathcal{H}^k$ *and* $\mathcal{H}_c^k$ *for the discrete approximation spaces defined as*

$$\mathcal{H}^k \equiv \frac{\mathrm{K}\big(\mathrm{d}^k : \widetilde{\mathcal{W}}^k \to \widetilde{\mathcal{W}}^{k+1}\big)}{\mathrm{R}\big(\mathrm{d}^{k-1} : \widetilde{\mathcal{W}}^{k-1} \to \widetilde{\mathcal{W}}^k\big)} \tag{4.82}$$

$$\mathcal{H}_c^k \equiv \frac{\mathrm{K}\big(\mathrm{d}^k : \widetilde{\mathcal{W}}_c^k \to \widetilde{\mathcal{W}}_c^{k+1}\big)}{\mathrm{R}\big(\mathrm{d}^{k-1} : \widetilde{\mathcal{W}}_c^{k-1} \to \widetilde{\mathcal{W}}_c^k\big)} \tag{4.83}$$

have the same dimensions as the continuous cohomology spaces, i.e.:

$$\dim\left(\mathcal{H}^k\right) = \begin{cases} 1 & \text{for } k = 0, \\ 0 & \text{otherwise} \end{cases} \tag{4.84}$$

$$\dim\left(\mathcal{H}_c^k\right) = \begin{cases} 1 & \text{for } k = n = 3, \\ 0 & \text{otherwise} \end{cases} \tag{4.85}$$

then the discrete system of equations (4.80) has a unique solution for each grid element $S_j^l, j \in [1..n^l]$.

The sequence property $\mathrm{d}^{k+1}\,\mathrm{d}^k = 0$ is actually always fulfilled, so the requirement of the complex property is that the range of d^k is part of the domain of d^{k+1}. The proof of existence and uniqueness has striking similarities to the continuous case and can be found in [19].

4.4.3 General Construction Algorithm

Definition 4.4 (Discrete Galerkin Polyhedral Whitney Basis Functions)**.** Let a consistent grid Ω_h with planar faces and straight edges be given. Introduce on each grid element S_j^l an intermediate approximation space $\widetilde{\mathcal{W}}^k(S_j^l)$ which fulfills the requirements in Theorem 4.7 and further on is conforming, i.e.

$$\widetilde{\mathcal{W}}^k(S_j^l) \subset \mathcal{F}_{\mathrm{d}}^k(S_j^l) \tag{4.86}$$

constant exact, i.e.

$$c^k \in \widetilde{\mathcal{W}}^k(S_j^l) \qquad \forall\, \text{constant } k\text{-forms } c^k \tag{4.87}$$

and fulfills the following compatibility condition for the traces:

$$\mathrm{t}^k_{S_p^{l-1}}\, \widetilde{\mathcal{W}}^k(S_j^l) = \widetilde{\mathcal{W}}^k(S_p^{l-1}) \tag{4.88}$$

Then the *discrete Galerkin polyhedral Whitney basis forms* B_i^k of degree k associated with the primal grid element S_i^k are defined for $i \in [1..n^k]$ by the following inductive scheme, letting l go from k to 3:

Assume the traces $\left(\mathrm{t}^k_{S_p^{l-1}}\, B_i^k\right) \in \widetilde{\mathcal{W}}^k(S_p^{l-1})$ of the basis function B_i^k on all (l–1)-dimensional grid elements S_p^{l-1} to be known. For $l = k$ this renders the trivial traces $\mathrm{t}^k_{S_p^{k-1}}\, B_i^k = 0$. Then for each l-dimensional element of the grid S_j^l, the trace $\mathrm{t}^k_{S_j^l}\, B_i^k$ of the basis function B_i^k on the element S_j^l is defined as the unique solution to the discrete Galerkin BVP (4.80) in the intermediate approximation space $\widetilde{\mathcal{W}}^k(S_j^l, \mathrm{t}^k_{\partial S_j^l}\, B_i^k)$.

We arrive at the final discrete Galerkin polyhedral Whitney basis form B_i^k as

$$B_i^k \equiv \sum_{j=1}^{n^3} \mathrm{t}^k_{S_j^3}\, B_i^k \tag{4.89}$$

where we assume the local traces $\mathrm{t}^k_{S_j^3}\, B_i^k$ extended by zero to the complete domain Ω.

Theorem 4.8. *The discrete Galerkin polyhedral Whitney basis forms B_i^k given by Definition 4.4 fulfill the properties I to VI on pages 95–96.*

The proof for this theorem is given in appendix F.2.3 on page 233. It is in parallel to the one for the continuous construction scheme given in appendix F.2.2 on page 227.

Remark 4.3. Note that the inner products $\langle\!\langle .|. \rangle\!\rangle_{S_j^l}$ defined in equation (4.76b) and used in the BVP (4.77) for the construction algorithm contain continuous integrations. If no analytical formula for the integrals is available, numerical integration schemes have to be employed. If these numerical integrations are not exact, the resulting solutions do not fulfill the discrete BVP exactly, but again are only approximations. As a result, Theorem 4.8 does not hold. This renders the construction scheme useless for cases where no exact integration for the chosen intermediate approximation spaces are available.

4.4.4 Specific Construction Algorithm

In this chapter, we state the Galerkin discretized BVP (4.80) on page 115 for each type of basis function on each type of grid element.

In the examples, a special choice for the intermediate approximation spaces $\widetilde{\mathcal{W}}^k$ is given: The intermediate approximation spaces $\widetilde{\mathcal{W}}^k$ are taken as the span of global basis functions. These special choices hint at geometrical construction formulas, which could not be fully realized for the 3-dimensional case, though. On the other hand, the global basis functions chosen in the examples lead to full matrices for the discrete problems. For polyhedra with many nodes, the number of global basis functions increases drastically leading to large full system matrices. In these cases, one should resort to sparse discretization methods e.g. by employing local basis functions or the FIT construction scheme presented in chapter 4.3. Nonetheless, the specific scheme presented in the examples is used to calculate the basis functions for the material matrices employed in the numerical simulations in chapter 5.

We now switch again to vector proxy notation and use the 2-dimensional derivative operators introduced in equations (4.45) on page 103.

Polyhedral Nodal Basis Functions

We collect all equations of the discrete Galerkin BVP (4.80) needed to construct the nodal basis functions $\vec{B}_i^0$. Many of the equations are trivial; the final construction algorithm reads: For each grid node S_i^0, search the unique basis function $\vec{B}_i^0$ in the search spaces that fulfills the following equations:

$$\vec{B}_i^0(S_j^0) = \delta_{ij} \qquad \forall\, j \in [1..n^0] \tag{4.90a}$$

$$\langle\!\langle \frac{\partial}{\partial \hat{x}_1}\vec{B}_i^0 \,|\, \frac{\partial}{\partial \hat{x}_1}\vec{\tilde{B}}_p^0 \rangle\!\rangle_{S_j^1} = 0 \qquad \forall\, \vec{\tilde{B}}_p^0 \in \vec{\widetilde{\mathcal{W}}}^0(S_j^1, 0) \qquad \forall\, j \in [1..n^1] \tag{4.90b}$$

$$\langle\!\langle \overrightarrow{\operatorname{grad}}_{2\mathrm{D}}\, \vec{B}_i^0 \,|\, \overrightarrow{\operatorname{grad}}_{2\mathrm{D}}\, \vec{\tilde{B}}_p^0 \rangle\!\rangle_{S_j^2} = 0 \qquad \forall\, \vec{\tilde{B}}_p^0 \in \vec{\widetilde{\mathcal{W}}}^0(S_j^2, 0) \qquad \forall\, j \in [1..n^2] \tag{4.90c}$$

$$\langle\!\langle \operatorname{grad} \vec{B}_i^0 \,|\, \operatorname{grad} \vec{\tilde{B}}_p^0 \rangle\!\rangle_{S_j^3} = 0 \qquad \forall\, \vec{\tilde{B}}_p^0 \in \vec{\widetilde{\mathcal{W}}}^0(S_j^3, 0) \qquad \forall\, j \in [1..n^3] \tag{4.90d}$$

This completely fixes each nodal basis function $\vec{B}_i^0$.

Example 4.13. For the nodal intermediate approximation spaces $\widetilde{\mathcal{W}}(S_j^3)$ on each grid cell S_j^3, we can choose the space of so-called generalized barycentric coordinate functions

$\vec{\widetilde{B}}_i^0$. On the lower dimensional grid elements S_j^l, we will simply take the traces of this space as intermediate approximation spaces $\widetilde{\mathcal{W}}(S_j^l)$. Generalized barycentric coordinate functions are functions fulfilling the following properties[4]:

$$\sum_{i=1}^{n^0} \vec{\widetilde{B}}_i^0(\vec{r}) = 1 \qquad \forall\, \vec{r} \in S_j^3 \tag{4.91a}$$

$$\sum_{i=1}^{n^0} \vec{\widetilde{B}}_i^0(\vec{r}) S_i^0 = \vec{r} \qquad \forall\, \vec{r} \in S_j^3 \tag{4.91b}$$

$$\vec{\widetilde{B}}_i^0(\vec{r}) = 0 \qquad \forall\, \vec{r} \in S_j^l,\ \forall\, \overline{S_j^l} \cap S_i^0 = \emptyset \quad \forall\, l \in [0..3] \tag{4.91c}$$

In equation (4.91b), as before, we use the symbol S_i^0 to also denote the point in $\mathbb{R}^3$ that the node S_i^0 is located at. Property (4.91a) ensures constant exactness, property (4.91b) linear exactness, and property (4.91c) locality of the basis functions. For tetrahedra, these requirements uniquely define the well-known nodal Whitney basis functions of lowest order. For more complex polyhedra, there are infinitely many possibilities to construct basis functions fulfilling these requirements. Geometric construction algorithms for barycentric coordinates for convex polyhedra are given in [55] or [91]. For arbitrary 3-dimensional polyhedra, the mean-value coordinates [37], [54] or the harmonic coordinates [25] fulfill these properties. Note that the harmonic coordinates are themselves exactly the solutions to the continuous construction algorithm in equations (4.46), (4.47), (4.49), and (4.51). As these are not directly available for arbitrary polyhedra, the solutions were calculated numerically in [25]. For the applications in chapter 5, we have chosen the solutions to equations (4.90) of the equivalent discrete construction algorithm. We will call these basis functions the *discrete harmonic barycentric coordinates*.

Choosing some barycentric coordinates as intermediate basis functions, we have exactly one intermediate basis function associated with each node of the grid. We now show that the barycentric coordinates fulfill equations (4.90) and thus are themselves the solutions for the construction algorithm: From equations (4.91a) and (4.91c), we conclude that each intermediate basis function $\vec{\widetilde{B}}_i^0$ has value 1 at the grid node S_i^0 and value 0 on the other nodes. Thus the intermediate basis functions fulfill equation (4.90a). Equations (4.90b) to (4.90d) are trivially fulfilled as the test spaces contain only the zero element: The intermediate basis functions $\vec{\widetilde{B}}_i^0$ all have non-zero trace on grid elements adjacent to the associated grid element S_i^0. On non-adjacent grid elements, they are zero due to the locality condition in equation (4.91c). Thus we conclude that the resulting test spaces, which only contain functions with zero trace, are trivial for any grid element S_j^l:

$$\vec{\widetilde{\mathcal{W}}}^0(S_j^l, 0) = \{0\} \qquad \forall\, l \in [1..3] \tag{4.92}$$

[4] Note that the definition of a generalized barycentric coordinate function given here deviates slightly from the standard one: We do not require positivity of the function, but instead enforce the locality condition (4.91c). Often, positivity is desired to get a quasi-maximum principle for the values inside the elements, but neither from the computational nor the convergence point of view, positivity is required. For convex elements, the positivity ensures locality, as derived for the 2-dimensional case in [36].

So the intermediate nodal basis functions already fulfill all requirements on the final nodal basis functions and thus are the solutions:

$$\vec{B}_i^0 = \vec{\tilde{B}}_i^0 \qquad \forall\, i \in [1..n^0] \tag{4.93}$$

Now the motivation for using the generalized barycentric coordinates becomes clear: We do not have to solve a BVP but directly obtain the final basis functions. As stated above, there exist infinitely many choices for generalized barycentric coordinate functions on general polyhedra and several explicit construction formulas are available. Two criteria guide our choice of a barycentric coordinate formula: On one hand, the calculation of the material matrices according to equation (4.7) on page 92 should be computationally cheap. On the other hand, the approximation properties of the basis functions, i.e. the absolute approximation error against the searched solutions, should be small. The discrete harmonic coordinates are themselves built from the BVP (4.90) using lowest order Whitney-FEM tetrahedral basis functions. For a very coarse discretization they are cheap to evaluate and the integration in the calculation of the material matrices can be done exactly. Thus these were employed in the applications in chapter 5 with the edge, face, and volume basis functions resulting from the schemes given in the examples. The calculations needed for their construction are computationally more expensive than using local edge, face, and volume Whitney-FEM basis functions for the intermediate approximation spaces, though. For future implementations, local basis functions seem thus more promising.

For an example of a polyhedral nodal basis functions $\vec{B}_i^0$ constructed with this scheme using discrete harmonic barycentric coordinates, see Fig. 4.3 on page 99.

Polyhedral Edge Basis Functions

Collecting all equations of the discrete Galerkin BVP (4.80) needed to construct the edge basis functions $\vec{B}_i^1$, the final construction algorithm reads: For each grid edge S_i^1, search the unique basis function $\vec{B}_i^1$ in the search spaces that fulfills the following equations:

$$\left\langle\!\left\langle (\vec{B}_i^1)_{t_{S_j^1}} \middle| \frac{\partial}{\partial \hat{x}_1} \vec{\tilde{B}}_p^0 \right\rangle\!\right\rangle_{S_j^1} = 0 \qquad \forall\, \vec{\tilde{B}}_p^0 \in \vec{\widetilde{\mathcal{W}}}^0(S_j^1, 0) \qquad \forall\, j \in [1..n^1] \tag{4.94a}$$

$$\int_{S_j^1} (\vec{B}_i^1)_{t_{S_j^1}} \,\mathrm{d}s = \delta_{ij} \qquad \forall\, j \in [1..n^1] \tag{4.94b}$$

$$\left\langle\!\left\langle \operatorname{curl}_{2\mathrm{D}}(\vec{B}_i^1)_{t_{S_j^2}} \middle| \operatorname{curl}_{2\mathrm{D}}(\vec{\tilde{B}}_p^1)_{t_{S_j^2}} \right\rangle\!\right\rangle_{S_j^2} = 0 \qquad \forall\, (\vec{\tilde{B}}_p^1)_{t_{S_j^2}} \in \vec{\widetilde{\mathcal{W}}}^1(S_j^2, 0) \qquad \forall\, j \in [1..n^2] \tag{4.94c}$$

$$\left\langle\!\left\langle (\vec{B}_i^1)_{t_{S_j^2}} \middle| \overrightarrow{\operatorname{grad}}_{2\mathrm{D}}\, \vec{\tilde{B}}_p^0 \right\rangle\!\right\rangle_{S_j^2} = 0 \qquad \forall\, \vec{\tilde{B}}_p^0 \in \vec{\widetilde{\mathcal{W}}}^0(S_j^2, 0) \qquad \forall\, j \in [1..n^2] \tag{4.94d}$$

$$\left\langle\!\left\langle \operatorname{curl} \vec{B}_i^1 \middle| \operatorname{curl} \vec{\tilde{B}}_p^1 \right\rangle\!\right\rangle_{S_j^3} = 0 \qquad \forall\, \vec{\tilde{B}}_p^1 \in \vec{\widetilde{\mathcal{W}}}^1(S_j^3, 0) \qquad \forall\, j \in [1..n^3] \tag{4.94e}$$

$$\left\langle\!\left\langle \vec{B}_i^1 \middle| \operatorname{grad} \vec{\tilde{B}}_p^0 \right\rangle\!\right\rangle_{S_j^3} = 0 \qquad \forall\, \vec{\tilde{B}}_p^0 \in \vec{\widetilde{\mathcal{W}}}^0(S_j^3, 0) \qquad \forall\, j \in [1..n^3] \tag{4.94f}$$

Example 4.14. As a specific choice for the intermediate approximation spaces $\vec{\widetilde{\mathcal{W}}}^1(S_j^3)$, we take the span of the following intermediate basis functions:

$$\vec{\tilde{B}}_{kl}^1 = \vec{\tilde{B}}_k^0 \operatorname{grad} \vec{\tilde{B}}_l^0 - \vec{\tilde{B}}_l^0 \operatorname{grad} \vec{\tilde{B}}_k^0 \qquad \forall\, k, l \in [1..n^0] \tag{4.95}$$

where $\vec{\tilde{B}}_i^0$ denotes the choice of barycentric coordinates from Example 4.13. Note that the intermediate basis functions $\vec{\tilde{B}}_{kl}^1$ might be linearly dependent. The intermediate approximation spaces $\vec{\widetilde{\mathcal{W}}}^1(S_j^l)$ are again taken as the traces of these spaces on the grid elements S_j^l. Notice that for the case of simplicial cells, i.e. tetrahedra, the intermediate basis functions are exactly the Whitney edge basis functions.

Requirements (4.94a), (4.94d), and (4.94f) are automatically fulfilled, as by equation (4.92), the test spaces are trivial. Let $\vec{B}_{pq}^1$ denote the final basis function associated with the edge S_{pq}^1 from node S_p^0 to node S_q^0. We can write the final basis function $\vec{B}_{pq}^1$ as a linear combination of the intermediate basis functions from equation (4.95). We will choose for this the following form:

$$\vec{B}_{pq}^1 = \sum_{k=1}^{n^0} \sum_{l=1}^{n^0} \left(\frac{1}{2} \alpha_{kl}^{pq} \right) \vec{\tilde{B}}_{kl}^1 \tag{4.96}$$

with the unknown coefficients α_{kl}^{pq}.

In [32], we have stated the following conjecture for a solution for the coefficients α_{kl}^{pq} solving equations (4.94b) and (4.94c):

Conjecture 4.9. *Let the coefficients α_{kl}^{pq} for all nodes S_k^0, S_l^0 that lie in the boundary of a common face S_j^2 be defined as follows:*

$$\alpha_{kl}^{pq} = \begin{cases} +\frac{A_{kl}^{pq}}{|S_j^2|}, & \textit{if the lines } \overline{S_q^0 S_k^0},\ \overline{S_p^0 S_l^0} \textit{ intersect,} \\ -\frac{A_{kl}^{pq}}{|S_j^2|}, & \textit{otherwise} \end{cases} \tag{4.97}$$

where A_{kl}^{pq} is the area included by the line $\overline{S_k^0 S_l^0}$ and the side of the element opposite *of the grid edge S_{pq}^1, as shown in Fig. 4.8. Then the basis functions $\vec{B}_{pq}^1$ defined by equation (4.96) fulfill equations (4.94b) and (4.94c).*

Remark 4.4. This conjecture has been proven using geometric formulas for polygons with up to 5 vertices. As the proof is very lengthy and does not seem to give any insight into a generalization for polygons with more vertices, it is not reproduced here.

Conjecture 4.9 only defines the coefficients α_{kl}^{pq} for nodes S_k^0, S_l^0 that lie in the boundary of a common face. Thus for the construction of fully 3-dimensional basis functions, the coefficients α_{kl}^{pq} for nodes S_k^0 and S_l^0 that do not lie in the boundary of a common face are still missing. These are fixed by equations (4.94e), though, which can be solved directly. We hope to also find a geometric formula for calculating these coefficients in future work, removing the need to solve equations (4.94e) explicitly.

For an example of a polyhedral edge basis functions $\vec{B}_i^1$ constructed with this scheme using discrete harmonic barycentric coordinates, see Fig. 4.9 on page 122.

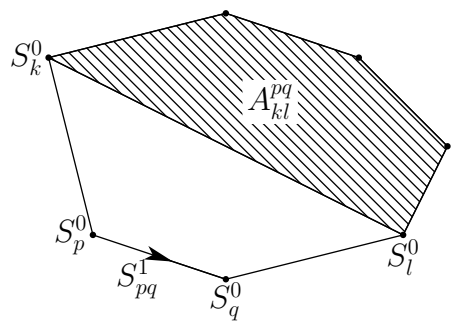

Fig. 4.8: Definition of the terms A_{kl}^{pq} used in equation (4.97) for a polygon S_j^2. The area enclosed by the line $\overline{S_k^0 S_l^0}$ and the polygon side opposite of the grid edge S_{pq}^1 is denoted by A_{kl}^{pq}. We define $A_{kl}^{pq} = \left|S_j^2\right|$ if $k = p$ and $l = q$ and $A_{kl}^{pq} = 0$ if $\overline{S_k^0 S_l^0}$ coincides with any other grid edge in the boundary of S_j^2. For concave polygons, parts of the area outside the polygon are counted negative.

Polyhedral Face Basis Functions

Collecting all equations in the discrete Galerkin BVP (4.80) needed to construct the face basis functions $\vec{B}_i^2$, the final construction algorithm reads: For each grid face S_i^2, search the unique basis function $\vec{B}_i^2$ in the search spaces that fulfills the following equations:

$$\left\langle\!\left\langle (\vec{B}_i^2)_{n_{S_j^2}} \middle| \operatorname{curl}(\vec{\tilde{B}}_p^1)_{t_{S_j^2}} \right\rangle\!\right\rangle_{S_j^2} = 0 \qquad \forall\, (\vec{\tilde{B}}_p^1)_{t_{S_j^2}} \in \vec{\widetilde{\mathcal{W}}}^1(S_j^2, 0) \qquad \forall\, j \in [1..n^2] \tag{4.98a}$$

$$\int_{S_j^2} (\vec{B}_i^2)_{n_{S_j^2}} \,\mathrm{d}A = \delta_{ij} \qquad \forall\, j \in [1..n^2] \tag{4.98b}$$

$$\left\langle\!\left\langle \operatorname{div} \vec{B}_i^2 \middle| \operatorname{div} \vec{\tilde{B}}_p^2 \right\rangle\!\right\rangle_{S_j^3} = 0 \qquad \forall\, \vec{\tilde{B}}_p^2 \in \vec{\widetilde{\mathcal{W}}}^2(S_j^3, 0) \qquad \forall\, j \in [1..n^3] \tag{4.98c}$$

$$\left\langle\!\left\langle \vec{B}_i^2 \middle| \operatorname{curl} \vec{\tilde{B}}_p^1 \right\rangle\!\right\rangle_{S_j^3} = 0 \qquad \forall\, \vec{\tilde{B}}_p^1 \in \vec{\widetilde{\mathcal{W}}}^1(S_j^3, 0) \qquad \forall\, j \in [1..n^3] \tag{4.98d}$$

Example 4.15. As a specific choice for the intermediate approximation space $\vec{\widetilde{\mathcal{W}}}^2$, we will take the span of the following intermediate basis functions:

$$\begin{aligned}
\vec{\tilde{B}}_{klm}^2 &= \vec{\tilde{B}}_k^0 \operatorname{curl} \vec{\tilde{B}}_{lm}^1 + \vec{\tilde{B}}_l^0 \operatorname{curl} \vec{\tilde{B}}_{mk}^1 + \vec{\tilde{B}}_m^0 \operatorname{curl} \vec{\tilde{B}}_{kl}^1 \\
&= 2 \Bigg(\vec{\tilde{B}}_k^0 \operatorname{grad} \vec{\tilde{B}}_l^0 \times \operatorname{grad} \vec{\tilde{B}}_m^0 + \vec{\tilde{B}}_l^0 \operatorname{grad} \vec{\tilde{B}}_m^0 \times \operatorname{grad} \vec{\tilde{B}}_k^0 \\
&\quad + \vec{\tilde{B}}_m^0 \operatorname{grad} \vec{\tilde{B}}_k^0 \times \operatorname{grad} \vec{\tilde{B}}_l^0 \Bigg) \qquad \forall\, k, l, m \in [1..n^0]
\end{aligned} \tag{4.99}$$

where $\vec{\tilde{B}}_i^0$ and $\vec{\tilde{B}}_{pq}^1$ denote the basis functions chosen in Examples 4.13 and 4.14, respectively.

The hope is again, that in future works, a geometric formula can be derived for the coefficients in the following general representation formula for the solutions $\vec{B}_i^2$:

$$\vec{B}_i^2 = \sum_k \sum_l \sum_m \left(\frac{1}{6} \beta_{klm}^i \right) \vec{\tilde{B}}_{klm}^2 \tag{4.100}$$

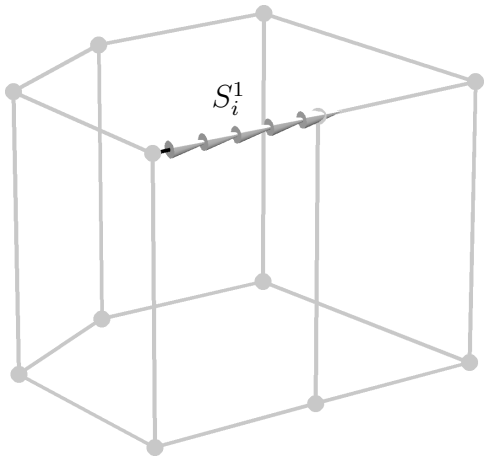

(a) Tangential component of the edge basis function $\vec{B}_i^1$ along the edges of the example polyhedral element. The edge basis function $\vec{B}_i^1$ has constant tangential component along its associated edge S_i^1. On all other edges, the edge basis function $\vec{B}_i^1$ is zero.

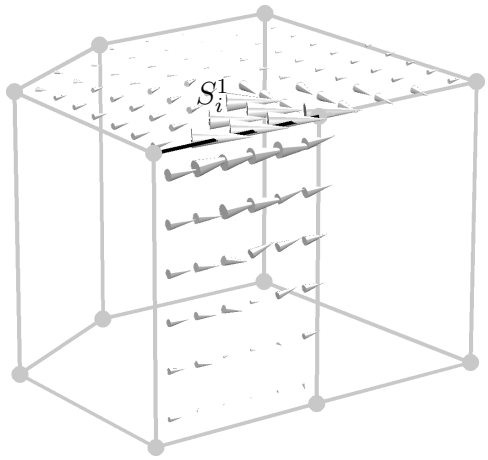

(b) Tangential components of the edge basis function $\vec{B}_i^1$ on the faces of the example polyhedral element. The edge basis function $\vec{B}_i^1$ is only non-zero on the faces adjacent to the associated edge S_i^1.

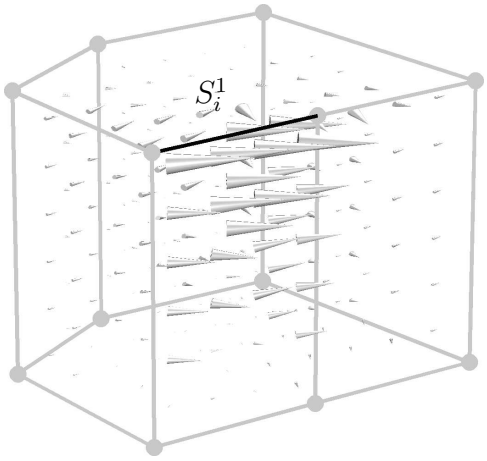

(c) Values of the edge basis function $\vec{B}_i^1$ on the example polyhedral element.

Fig. 4.9: Discrete polyhedral edge basis function $\vec{B}_i^1$ for an example polyhedron. The basis function $\vec{B}_i^1$ was derived using the construction algorithm in equations (4.94) employing the discrete harmonic intermediate basis functions as described in Example 4.14.

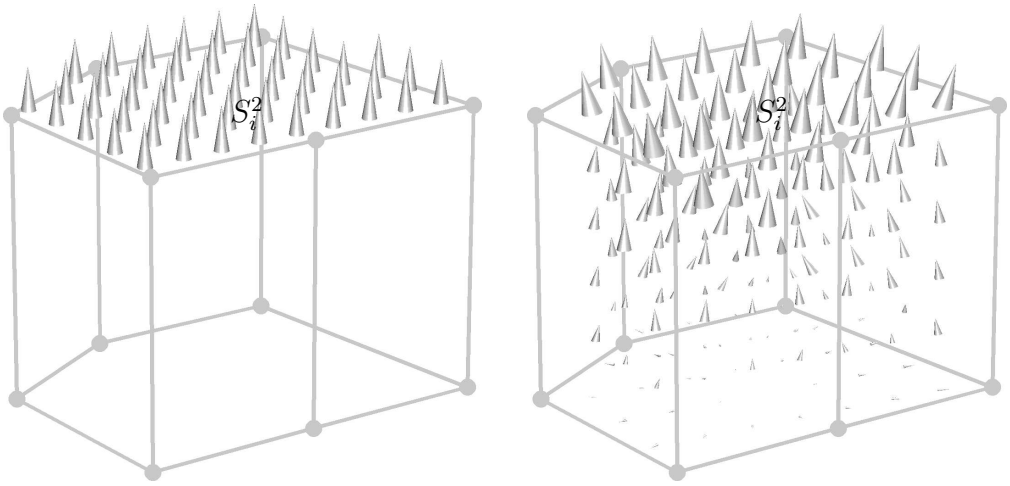

(a) Normal vector component of the face basis function $\vec{B}_i^2$ on the faces of the example polyhedral element. The normal vector component is constant on the associated face S_i^2 and zero on all other faces.

(b) Values of the face basis function $\vec{B}_i^2$ on the example polyhedral element.

Fig. 4.10: Discrete polyhedral face basis function $\vec{B}_i^2$ for an example polyhedron. The basis function $\vec{B}_i^2$ was derived using the construction algorithm in equations (4.98) employing the discrete harmonic intermediate basis functions as described in Example 4.15.

So far, the discrete equations (4.98a) to (4.98d) are solved explicitly.

For an example of a polyhedral face basis function $\vec{B}_i^2$ constructed with this scheme using discrete harmonic barycentric coordinates, see Fig. 4.10.

Polyhedral Volume Basis Functions

The final construction algorithm for the volume basis functions $\vec{B}_i^3$ reads: For each grid cell S_i^3, search the unique basis function $\vec{B}_i^3$ in the search spaces that fulfills the following equations:

$$\left\langle\!\left\langle \vec{B}_i^3 \middle| \operatorname{div} \vec{\tilde{B}}_p^2 \right\rangle\!\right\rangle_{S_j^3} = 0 \qquad \forall\, \vec{\tilde{B}}_p^2 \in \vec{\widetilde{\mathcal{W}}}^2(S_j^3, 0) \qquad \forall\, j \in [1..n^3] \tag{4.101a}$$

$$\int_{S_j^3} \vec{B}_i^3 \,\mathrm{d}V = \delta_{ij} \qquad \forall\, j \in [1..n^3] \tag{4.101b}$$

Example 4.16. We will choose the constant basis functions as defined in equation (4.64) on page 110 which was a solution of the continuous problem as the only intermediate basis functions. They also solve equations (4.101): While equation (4.101b) is easily verified, it might be surprising at first sight that equation (4.101a) is fulfilled. Using the definition of the local inner product in equation (4.76b) on page 114, we can rewrite equation (4.101a) for the constant basis functions as:

$$\int_{S_j^3} \operatorname{div} \vec{\tilde{B}}_p^2 \,\mathrm{d}V = 0 \qquad \forall\, \vec{\tilde{B}}_p^2 \in \vec{\widetilde{\mathcal{W}}}^2(S_j^3, 0) \qquad \forall\, j \in [1..n^3] \tag{4.102}$$

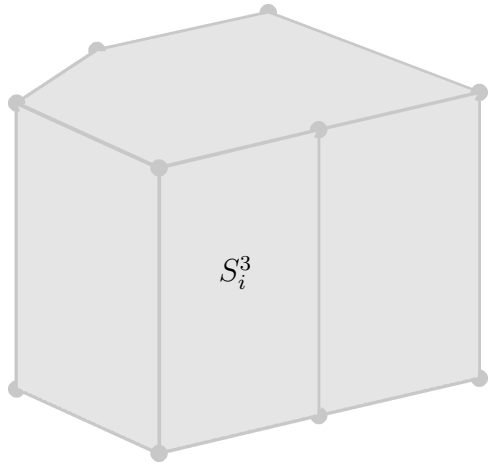

Fig. 4.11: Discrete polyhedral volume basis function $\vec{B}_i^3$ for an example associated polyhedron S_i^3. The volume basis function $\vec{B}_i^3$ was derived using the construction algorithm in equations (4.101) as described in Example 4.16. The volume basis function $\vec{B}_i^3$ has constant value on the associated element and zero value on all other elements, exactly as the solutions to the continuous construction algorithm.

Using Gauss' law (2.16) on page 11 renders:

$$\Leftrightarrow \qquad \int_{\partial S_j^3} \vec{\widetilde{B}}_p^2 \cdot \vec{n}_{\partial S_j^3} \, \mathrm{d}A = 0 \qquad \forall \, \vec{\widetilde{B}}_p^2 \in \vec{\widetilde{\mathcal{W}}}^2(S_j^3, 0) \qquad \forall \, j \in [1..n^3] \tag{4.103}$$

As all test functions in $\vec{\widetilde{\mathcal{W}}}^2(S_j^3, 0)$ do have zero trace on the grid cell boundary ∂S_j^3, this does indeed hold and the constant basis functions as defined in equation (4.64) on page 110 are directly valid as discrete volume basis functions.

For an example of a constant polyhedral volume basis functions $\vec{B}_i^3$, see Fig. 4.11.

Remarks on the Example Intermediate Approximation Spaces

Remark 4.5. In Examples 4.13 to 4.16 on pages 117–123, we have chosen intermediate approximation spaces $\widetilde{\mathcal{W}}^k$ based on generalized barycentric coordinates. For Theorem 4.8 on page 116 to hold, certain properties were required of the intermediate approximation spaces: The complex property in equations (4.81), the cohomology requirements (4.82), conformity in equation (4.86), constant exactness in equation (4.87), and the trace compatibility condition in equation (4.88). These properties have so far not been checked for the chosen intermediate approximation spaces. Constant exactness is inherent for the nodal intermediate approximation spaces $\widetilde{\mathcal{W}}^0$ by equation (4.91a). From the linear exactness of the nodal barycentric coordinates in equation (4.91b), one can also prove constant exactness of the edge and face intermediate approximation spaces $\widetilde{\mathcal{W}}^1$ and $\widetilde{\mathcal{W}}^2$. The volume intermediate approximation $\widetilde{\mathcal{W}}^3$ spaces were directly chosen as the piecewise constant functions and thus are constant exact. The conformity of the spaces is easily shown, as is the complex property. Trace compatibility according to equation (4.88) holds, as the compatibility equations have actually been used to define the intermediate

approximation spaces on the lower-dimensional grid elements based on the intermediate approximation spaces $\widetilde{\mathcal{W}}^k(S_j^3)$. What has not been established by the author are the cohomology requirements for all intermediate approximation spaces. For the applications in chapter 5, these were checked numerically and observed to hold for all tested cases, though.

Remark 4.6. The intermediate approximation spaces in the examples based on generalized barycentric coordinates could also be used directly in a Finite Element formulation instead of deriving basis functions according to the above scheme. We would not recover the association of the degrees of freedom with the grid elements, though. Also, the additional degrees of freedom do not help to improve the convergence rate in any way, but their number and therefore the computational cost grows very fast with the number of edges and faces of the polyhedra.

4.5 Discussion of Existing Polygonal and Polyhedral Schemes

As stated in the introduction, several methods incorporating polytope, that is polygonal and polyhedral, grids or similar ideas already exist. Most of these can actually be interpreted as realizations of parts of the construction schemes presented in chapters 4.2 to 4.4.

In Example 4.13 on page 117, we have seen that any choice of generalized barycentric coordinates already fulfill the requirements on the nodal basis functions and can be used directly to calculate material matrices of degree 0. Numerical simulations requiring only nodal basis functions or material matrices of degree 0 can thus easily be extended to polytope grids as done in [82]. The Examples 4.13 to 4.16 on pages 117–123 can be viewed as realizations of the basic idea put forward in [26] that the generalized barycentric coordinates can be used to derive Whitney forms on general polytopes.

In [16], polygonal basis functions are derived on the barycentric dual grid of a triangular grid to derive a preconditioner for boundary integral formulations. This work actually led to the generalization in [19], which is the basis for the polytope scheme described by this thesis. For the preconditioner, the approximation properties are not as stringent, though, such that the basis functions are in general not constant exact. Lifting the restriction of straight edges and employing a special non-Euclidean metric in the construction process outlined in chapter 4.4 leads to the scheme in [16].

In [57], the specific continuous construction formulas (4.55) on page 108 were used to derive 2-dimensional polygonal edge basis functions. For the solution of the continuous construction scheme, a boundary integral formulation was derived which apparently was solved numerically. For such a numerical solution, one would have to prove that the requirements I to VI on pages 95–96 are still fulfilled to assure convergence and solutions free of spurious modes, though.

In [45], centered so-called hanging nodes have been incorporated consistently for nodal and edge basis functions for triangles and tetrahedra. The method employed can be interpreted as a special case of the discrete construction algorithms in chapter 4.4. The

construction algorithms presented in chapter 4.4 thus generalize the method to more complex elements and non-centered node allocations.

In [40], special basis functions have been derived for pyramidal cells. For special choices of the intermediate approximation spaces in the discrete construction algorithm in chapter 4, we arrive at the same basis functions.

In [24], a special scheme removes an additional edge degree of freedom for two tetrahedrons glued together. The calculated removal coefficients nicely fit the theory in chapter 4 and thus the scheme can be reinterpreted as a construction of material coefficients for a consistent polyhedral grid element. For the formulation of the discrete problem, Nitsche's method [43] [71] was employed in [24]. The perspective of Nitsche's method has some interesting consequences for the polyhedral basis functions: In Nitsche's method, there exists a whole equivalence class of traces whose integrated surface jumps evaluates to zero. In chapter 4, we required the basis functions of all elements sharing part of the boundary to have the same trace on these parts. Using Nitsche's method, one can relax this requirement and just state the traces to be in the same equivalence class. Thereby, one gains more flexibility for the local construction of the Whitney forms.

For the Mimetic Finite Difference Method, polyhedral elements with certain shape restrictions are introduced for diffusion type problems in [14]. The presentation can be reinterpreted as providing material matrices of degree 2, that is for face degrees of freedom. The connections to the scheme presented here are not yet fully understood, but further investigation of these seems promising for future developments for both schemes.

5. APPLICATION OF POLYTOPE ELEMENTS IN ELECTROMAGNETIC SIMULATIONS

The material relations for polyhedral cells developed in chapter 4 can be employed for numerical simulations in the framework of the general FIT described in chapter 3. They have been successfully applied in high-frequency and quasistatic problems both in frequency and time domain as well as in electro- and magnetostatic problems. In the following numerical examples, a variation from these fields was chosen to show the general validity of the approach. The specific examples highlight different application scenarios of polyhedral cells: The new gridding flexibility in general, enhanced boundary approximation in structured grids, consistent subgridding for hexagonal grids, and hybrid hexagonal/tetrahedral grids. The examples cover 3-dimensional as well as 2-dimensional cases.

The polyhedral material matrices employed in this chapter are derived by the Galerkin construction scheme based on discrete harmonic barycentric coordinates described in the Examples 4.13 to 4.16. The resulting basis functions are not affine invariant, but only invariant under similarity transformations, i.e. scaling, translation, and rotation. The integrals for the calculation of the material matrices according to equation (4.7) on page 92 have to be calculated for each invariant type of polyhedral cells. In the worst case, they have to be calculated on each element of the grid. As most examples only contain a single type of polyhedral cell, the construction and integral evaluation has to be performed only once, though.

For future implementations, using the sparse construction algorithm outlined in chapter 4.3 for constructing polyhedral material matrices seems promising. It can handle complex polyhedra more efficiently.

All calculations were performed using the double precision floating point format [51].

5.1 New Gridding Flexibility

Using the material relations from chapter 4, consistent grids with arbitrary polytope element shapes can be used in numerical simulations. In order to demonstrate this flexibility, the following 2-dimensional waveguide eigenproblem features a wide variety of grids. The convergence properties are shown to be qualitatively the same as for standard rectangular or triangular grids.

5.1.1 2-Dimensional Eigenproblem Example: Rectangular Waveguide with Polygonal Grids

We calculate the eigenmodes of the waveguide depicted in Fig. 5.1 for the time-harmonic case in the frequency domain. The inner of the waveguide Ω is filled homogeneously with vacuum. On its boundary $\Gamma_1 = \partial\Omega$, homogeneous electric (PEC) boundary conditions are applied. The problem is translationally invariant in the z-direction and we therefore can reduce it to a 2-dimensional problem in the transverse xy-plane. Here, we employ the formulation described in the standard FIT setting in [93] but include the boundary conditions rigorously in the notation. The equivalent formulation in the FEM setting along with a nice discussion of the continuous problem can be found in [89]. For a discussion of alternate formulations for this problem, see [34].

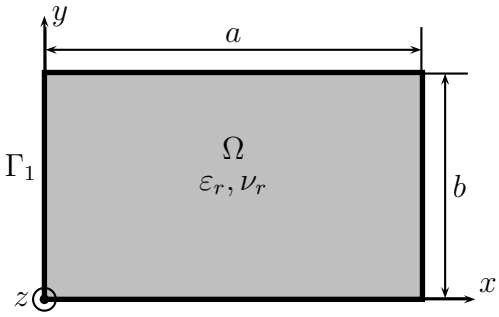

Fig. 5.1: Homogeneously filled rectangular waveguide. The inner domain Ω is filled with a homogeneous material with relative permittivity $\varepsilon_r = 1$ and the relative reluctivity $\nu_r = 1$. On the boundary $\Gamma_1 = \partial\Omega$, homogeneous electric (PEC) boundary conditions are applied. The relation of the dimensions of the waveguide is $b = 0.6a$ and a is arbitrarily chosen at $a = 1$mm. The longitudinal wavenumber k_z was calculated at the frequency $f = \frac{c_0}{1.875a} \approx 160$ GHz, i.e. $k_0 \approx 1.067\frac{\pi}{a}$.

Let k_0 denote the free space wavenumber and $k_{z,c}$ the wavenumber in the longitudinal direction for the continuous problem. Then the continuous problem in the complex amplitude of the transverse electric field strength $\underline{\vec{E}}_t(\vec{r}) \in \mathbb{C}^2$ and the longitudinal electric field strength $\underline{E}_z(\vec{r}) \in \mathbb{C}$ as unknowns reads for $k_{z,c} \neq 0$:

$$\overrightarrow{\mathrm{curl}}_{2\mathrm{D}}\left(\nu_r \,\mathrm{curl}_{2\mathrm{D}}\, \underline{\vec{E}}_t\right) - k_0^2\varepsilon_r\underline{\vec{E}}_t + k_{z,c}^2\nu_r\underline{\vec{E}}_t - ik_{z,c}\nu_r\,\overrightarrow{\mathrm{grad}}_{2\mathrm{D}}\,\underline{E}_z = 0 \qquad \text{in } \Omega \tag{5.1a}$$

$$\mathrm{div}_{2\mathrm{D}}\left(\varepsilon_r\underline{\vec{E}}_t\right) - ik_{z,c}\varepsilon_r\underline{E}_z = 0 \tag{5.1b}$$

$$\underline{\vec{E}}_t \times \vec{n}_{\Gamma_1} = 0 \qquad \text{on } \Gamma_1 \tag{5.1c}$$

$$\underline{E}_z = 0 \qquad \text{on } \Gamma_1 \tag{5.1d}$$

where $\vec{n}_{\Gamma_1}$ denotes the outward unit normal vector on the boundary Γ_1 and the 2-dimensional exterior derivatives are defined according to equations (4.45) on page 103.

For translating the eigenproblem (5.1) into its discrete form in the language of the FIT, we introduce a 2-dimensional grid Ω_h of the problem domain Ω including the discretization $\overline{\Gamma}_{1,h}$ of its boundary $\Gamma_1 = \partial\Omega$. Some example grids are shown in Fig. 5.2. In chapter 3, we have only introduced the 3-dimensional definitions and notation of the discrete primal

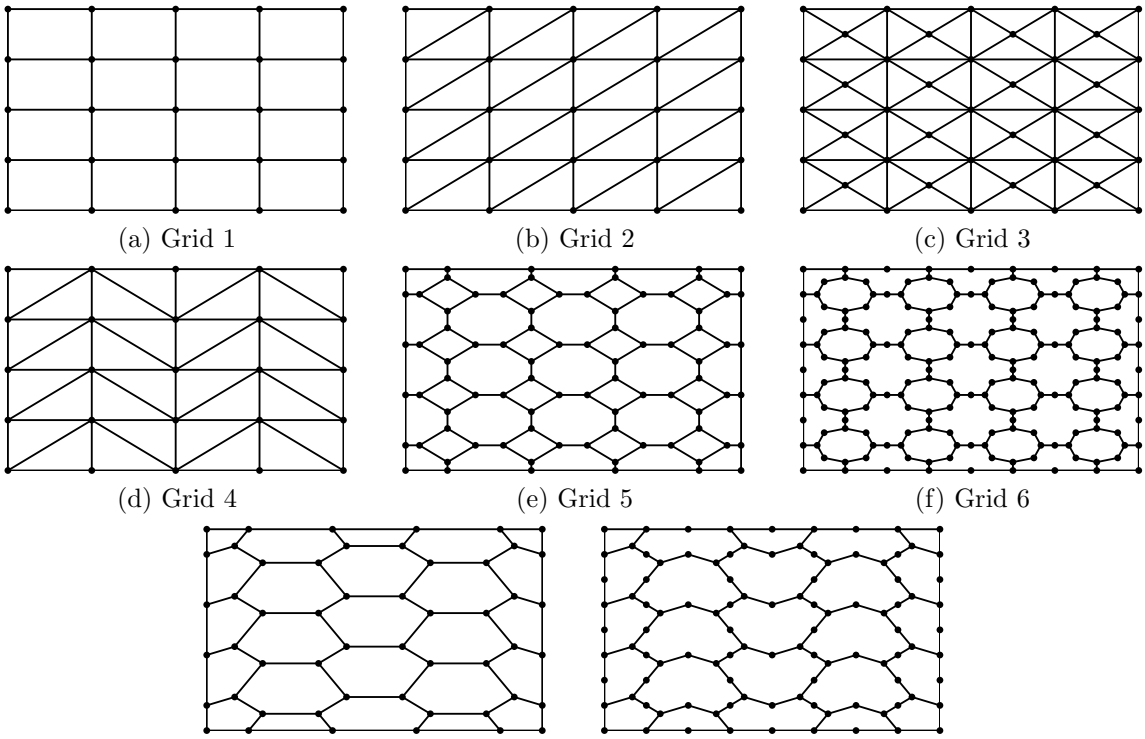

(a) Grid 1 (b) Grid 2 (c) Grid 3

(d) Grid 4 (e) Grid 5 (f) Grid 6

(g) Grid 7 (h) Grid 8

Fig. 5.2: Different grid types for discretizing the domain shown in Fig. 5.1. Grid 1 is a standard rectangular grid. Grids 2 to 4 are standard triangular grids. Grids 5 to 8 are examples for new polygonal grids.

and dual exterior derivatives, discrete material matrices, and discrete trace operators. In parallel to the continuous (local) l-dimensional equivalents introduced in equations (4.67) to (4.70) on page 112, we introduce discrete 2-dimensional operators: Let $\mathbf{D}^k_{\mathrm{2D}}$ and $\underset{\sim}{\mathbf{D}}^k_{\mathrm{2D}}$ denote the 2-dimensional primal and dual exterior derivatives, $\mathbf{M}^k_{\mathrm{2D},\alpha}$ the 2-dimensional primal material matrices for the material metric α, and $\mathbf{T}^k_{\mathrm{2D},\overline{\Gamma}_{1,h}}$ the 2-dimensional trace operators onto the electric boundary grid part $\overline{\Gamma}_{1,h}$. For a consistent discretization of the exterior derivative for the dual quantities, we have to include boundary terms in equivalence to the discrete dual curl in Maxwell's second topological grid law (3.73) on page 56. This renders the following terms for a consistent discretization of $\overrightarrow{\mathrm{curl}}_{\mathrm{2D}}$ and $\mathrm{div}_{\mathrm{2D}}$ used in equations (5.1a) and (5.1b):

$$\overrightarrow{\mathrm{curl}}_{\mathrm{2D}}\,\underline{H}_z \quad \rightsquigarrow \quad \underset{\sim}{\mathbf{D}}^0_{\mathrm{2D}}\underset{\simeq}{\widehat{\mathbf{h}}}_{\mathrm{2D},z} + (\mathbf{T}^1_{\mathrm{2D},\overline{\Gamma}_{1,h}})^{\mathrm{T}}\underset{\simeq}{\widehat{\mathbf{h}}}_{\mathrm{2D},z,\overline{\Gamma}_{1,h}} \tag{5.2a}$$

$$\mathrm{div}_{\mathrm{2D}}\,\underline{\vec{D}}_t \quad \rightsquigarrow \quad \underset{\sim}{\mathbf{D}}^1_{\mathrm{2D}}\underset{\simeq}{\widehat{\mathbf{d}}}_{\mathrm{2D},t} + (\mathbf{T}^0_{\mathrm{2D},\overline{\Gamma}_{1,h}})^{\mathrm{T}}\underset{\simeq}{\widehat{\mathbf{d}}}_{\mathrm{2D},t,\overline{\Gamma}_{1,h}} \tag{5.2b}$$

where the rightmost term represents the boundary contributions. Now we can consistently discretize equations (5.1) into the following discrete problem in the complex amplitudes of the transverse electric grid voltages $\underline{\widehat{\mathbf{e}}}_{\mathrm{2D},t}$, the longitudinal electric grid voltages $\underline{\mathbf{e}}_{\mathrm{2D},z}$,

and the discrete longitudinal wavenumber k_z as unknowns:

$$\underset{\sim}{\mathbf{D}}^0_{2\mathrm{D}}\mathbf{M}^2_{2\mathrm{D},\nu_r}\mathbf{D}^1_{2\mathrm{D}}\underline{\widehat{\mathbf{e}}}_{2\mathrm{D},t} + (\mathbf{T}^1_{2\mathrm{D},\overline{\Gamma}_{1,h}})^{\mathrm{T}}\underline{\widehat{\mathbf{h}}}_{2\mathrm{D},z,\overline{\Gamma}_{1,h}} - k_0^2\mathbf{M}^1_{2\mathrm{D},\varepsilon_r}\underline{\widehat{\mathbf{e}}}_{2\mathrm{D},t}$$
$$+ k_z^2\mathbf{M}^1_{2\mathrm{D},\nu_r}\underline{\widehat{\mathbf{e}}}_{2\mathrm{D},t} - ik_z\mathbf{M}^1_{2\mathrm{D},\nu_r}\mathbf{D}^0_{2\mathrm{D}}\underline{\mathbf{e}}_{2\mathrm{D},z} = 0 \tag{5.3a}$$

$$\underset{\sim}{\mathbf{D}}^1_{2\mathrm{D}}\mathbf{M}^1_{2\mathrm{D},\varepsilon_r}\underline{\widehat{\mathbf{e}}}_{2\mathrm{D},t} + (\mathbf{T}^0_{2\mathrm{D},\overline{\Gamma}_{1,h}})^{\mathrm{T}}\underline{\widehat{\mathbf{d}}}_{2\mathrm{D},t,\overline{\Gamma}_{1,h}} - ik_z\mathbf{M}^0_{2\mathrm{D},\varepsilon_r}\underline{\mathbf{e}}_{2\mathrm{D},z} = 0 \tag{5.3b}$$

$$\mathbf{T}^1_{2\mathrm{D},\overline{\Gamma}_{1,h}}\underline{\widehat{\mathbf{e}}}_{2\mathrm{D},t} = 0 \tag{5.3c}$$

$$\mathbf{T}^0_{2\mathrm{D},\overline{\Gamma}_{1,h}}\underline{\mathbf{e}}_{2\mathrm{D},z} = 0 \tag{5.3d}$$

We will now transform this problem into an eigenproblem for the inner degrees of freedom of the complex amplitudes of the transverse electric grid voltages $\underline{\widehat{\mathbf{e}}}_{2\mathrm{D},t}$. The resulting eigenproblem can be solved by standard eigenproblem solvers while it reduces the degrees of freedom to a necessary minimum. Let $\mathbf{T}^k_{2\mathrm{D},\Omega_h\setminus\overline{\Gamma}_{1,h}}$ denote the trace operator onto the interior of the grid excluding the boundary $\overline{\Gamma}_{1,h}$. This trace operator simply singles out the interior degrees of freedom. Then we define the following reduced electric field strengths:

$$\underline{\widehat{\mathbf{e}}}_{2\mathrm{D},t,\mathrm{red}} \equiv \mathbf{T}^1_{2\mathrm{D},\Omega_h\setminus\overline{\Gamma}_{1,h}}\underline{\widehat{\mathbf{e}}}_{2\mathrm{D},t} \tag{5.4a}$$

$$\underline{\mathbf{e}}_{2\mathrm{D},z,\mathrm{red}} \equiv \mathbf{T}^0_{2\mathrm{D},\Omega_h\setminus\overline{\Gamma}_{1,h}}\underline{\mathbf{e}}_{2\mathrm{D},z} \tag{5.4b}$$

Due to the zero boundary conditions from equations (5.3c) and (5.3d), we can recover the full electric field strengths simply by:

$$\underline{\widehat{\mathbf{e}}}_{2\mathrm{D},t} = (\mathbf{T}^1_{2\mathrm{D},\Omega_h\setminus\overline{\Gamma}_{1,h}})^{\mathrm{T}}\underline{\widehat{\mathbf{e}}}_{2\mathrm{D},t,\mathrm{red}} \tag{5.5a}$$

$$\underline{\mathbf{e}}_{2\mathrm{D},z} = (\mathbf{T}^0_{2\mathrm{D},\Omega_h\setminus\overline{\Gamma}_{1,h}})^{\mathrm{T}}\underline{\mathbf{e}}_{2\mathrm{D},z,\mathrm{red}} \tag{5.5b}$$

The trace operators onto the boundary and the interior of the primal grid select disjunct sets of indices, thus we note the relation:

$$\mathbf{T}^k_{2\mathrm{D},\Omega_h\setminus\overline{\Gamma}_{1,h}}(\mathbf{T}^k_{2\mathrm{D},\overline{\Gamma}_{1,h}})^{\mathrm{T}} = 0 \tag{5.6}$$

This relation allows us to drop the boundary terms in equations (5.3a) and (5.3b) by multiplying the equations with $\mathbf{T}^1_{2\mathrm{D},\Omega_h\setminus\overline{\Gamma}_{1,h}}$ and $\mathbf{T}^0_{2\mathrm{D},\Omega_h\setminus\overline{\Gamma}_{1,h}}$, respectively, from the left. We thereby only state the equations for the interior of the grid, where the boundary terms do not matter:

$$\mathbf{T}^1_{2\mathrm{D},\Omega_h\setminus\overline{\Gamma}_{1,h}}\underset{\sim}{\mathbf{D}}^0_{2\mathrm{D}}\mathbf{M}^2_{2\mathrm{D},\nu_r}\mathbf{D}^1_{2\mathrm{D}}\underline{\widehat{\mathbf{e}}}_{2\mathrm{D},t} - k_0^2\mathbf{T}^1_{2\mathrm{D},\Omega_h\setminus\overline{\Gamma}_{1,h}}\mathbf{M}^1_{2\mathrm{D},\varepsilon_r}\underline{\widehat{\mathbf{e}}}_{2\mathrm{D},t}$$
$$+ k_z^2\mathbf{T}^1_{2\mathrm{D},\Omega_h\setminus\overline{\Gamma}_{1,h}}\mathbf{M}^1_{2\mathrm{D},\nu_r}\underline{\widehat{\mathbf{e}}}_{2\mathrm{D},t} - ik_z\mathbf{T}^1_{2\mathrm{D},\Omega_h\setminus\overline{\Gamma}_{1,h}}\mathbf{M}^1_{2\mathrm{D},\nu_r}\mathbf{D}^0_{2\mathrm{D}}\underline{\mathbf{e}}_{2\mathrm{D},z} = 0 \tag{5.7a}$$

$$\mathbf{T}^0_{2\mathrm{D},\Omega_h\setminus\overline{\Gamma}_{1,h}}\underset{\sim}{\mathbf{D}}^1_{2\mathrm{D}}\mathbf{M}^1_{2\mathrm{D},\varepsilon_r}\underline{\widehat{\mathbf{e}}}_{2\mathrm{D},t} - ik_z\mathbf{T}^0_{2\mathrm{D},\Omega_h\setminus\overline{\Gamma}_{1,h}}\mathbf{M}^0_{2\mathrm{D},\varepsilon_r}\underline{\mathbf{e}}_{2\mathrm{D},z} = 0 \tag{5.7b}$$

Now using equation (5.5b), we can solve equation (5.7b) for the reduced longitudinal electric field strength:

$$\mathbf{T}^0_{2\mathrm{D},\Omega_h\setminus\overline{\Gamma}_{1,h}}\underset{\sim}{\mathbf{D}}^1_{2\mathrm{D}}\mathbf{M}^1_{2\mathrm{D},\varepsilon_r}\underline{\widehat{\mathbf{e}}}_{2\mathrm{D},t} - ik_z\mathbf{T}^0_{2\mathrm{D},\Omega_h\setminus\overline{\Gamma}_{1,h}}\mathbf{M}^0_{2\mathrm{D},\varepsilon_r}(\mathbf{T}^0_{2\mathrm{D},\Omega_h\setminus\overline{\Gamma}_{1,h}})^{\mathrm{T}}\underline{\mathbf{e}}_{2\mathrm{D},z,\mathrm{red}} = 0 \tag{5.8}$$

$$\Leftrightarrow \quad \underline{\mathbf{e}}_{2\mathrm{D},z,\mathrm{red}} = \frac{1}{ik_z}\left(\mathbf{M}^0_{2\mathrm{D},\Omega_h\setminus\overline{\Gamma}_{1,h},\varepsilon_r}\right)^{-1}\mathbf{T}^0_{2\mathrm{D},\Omega_h\setminus\overline{\Gamma}_{1,h}}\underset{\sim}{\mathbf{D}}^1_{2\mathrm{D}}\mathbf{M}^1_{2\mathrm{D},\varepsilon_r}\underline{\widehat{\mathbf{e}}}_{2\mathrm{D},t} \tag{5.9}$$

where we have introduced the reduced nodal permittivity matrix $\mathbf{M}^0_{2\mathrm{D},\Omega_h\setminus\overline{\Gamma}_{1,h},\varepsilon_r}$ to shorten the notation:

$$\mathbf{M}^0_{2\mathrm{D},\Omega_h\setminus\overline{\Gamma}_{1,h},\varepsilon_r} \equiv \mathbf{T}^0_{2\mathrm{D},\Omega_h\setminus\overline{\Gamma}_{1,h}}\mathbf{M}^0_{2\mathrm{D},\varepsilon_r}\left(\mathbf{T}^0_{2\mathrm{D},\Omega_h\setminus\overline{\Gamma}_{1,h}}\right)^{\mathrm{T}} \tag{5.10}$$

We can plug equation (5.9) into equation (5.7a) by using equation (5.5b):

$$\begin{aligned}
&\mathbf{T}^1_{2\mathrm{D},\Omega_h\setminus\overline{\Gamma}_{1,h}}\underset{\sim}{\mathbf{D}}^0_{2\mathrm{D}}\mathbf{M}^2_{2\mathrm{D},\nu_r}\mathbf{D}^1_{2\mathrm{D}}\underline{\widehat{\mathbf{e}}}_{2\mathrm{D},t} - k_0^2\mathbf{T}^1_{2\mathrm{D},\Omega_h\setminus\overline{\Gamma}_{1,h}}\mathbf{M}^1_{2\mathrm{D},\varepsilon_r}\underline{\widehat{\mathbf{e}}}_{2\mathrm{D},t} + k_z^2\mathbf{T}^1_{2\mathrm{D},\Omega_h\setminus\overline{\Gamma}_{1,h}}\mathbf{M}^1_{2\mathrm{D},\nu_r}\underline{\widehat{\mathbf{e}}}_{2\mathrm{D},t}\\
&\quad - \mathbf{T}^1_{2\mathrm{D},\Omega_h\setminus\overline{\Gamma}_{1,h}}\mathbf{M}^1_{2\mathrm{D},\nu_r}\mathbf{D}^0_{2\mathrm{D}}(\mathbf{T}^0_{2\mathrm{D},\Omega_h\setminus\overline{\Gamma}_{1,h}})^{\mathrm{T}}\left(\mathbf{M}^0_{2\mathrm{D},\Omega_h\setminus\overline{\Gamma}_{1,h},\varepsilon_r}\right)^{-1}\mathbf{T}^0_{2\mathrm{D},\Omega_h\setminus\overline{\Gamma}_{1,h}}\underset{\sim}{\mathbf{D}}^1_{2\mathrm{D}}\mathbf{M}^1_{2\mathrm{D},\varepsilon_r}\underline{\widehat{\mathbf{e}}}_{2\mathrm{D},t}\\
&\quad = 0
\end{aligned} \tag{5.11}$$

Now using equation (5.5a) to introduce the reduced transverse electric field strength, we arrive at the final eigenproblem:

$$\begin{aligned}
&\mathbf{T}^1_{2\mathrm{D},\Omega_h\setminus\overline{\Gamma}_{1,h}}\underset{\sim}{\mathbf{D}}^0_{2\mathrm{D}}\mathbf{M}^2_{2\mathrm{D},\nu_r}\mathbf{D}^1_{2\mathrm{D}}(\mathbf{T}^1_{2\mathrm{D},\Omega_h\setminus\overline{\Gamma}_{1,h}})^{\mathrm{T}}\underline{\widehat{\mathbf{e}}}_{2\mathrm{D},t,\mathrm{red}}\\
&\quad - k_0^2\mathbf{T}^1_{2\mathrm{D},\Omega_h\setminus\overline{\Gamma}_{1,h}}\mathbf{M}^1_{2\mathrm{D},\varepsilon_r}(\mathbf{T}^1_{2\mathrm{D},\Omega_h\setminus\overline{\Gamma}_{1,h}})^{\mathrm{T}}\underline{\widehat{\mathbf{e}}}_{2\mathrm{D},t,\mathrm{red}}\\
&\quad - \mathbf{T}^1_{2\mathrm{D},\Omega_h\setminus\overline{\Gamma}_{1,h}}\mathbf{M}^1_{2\mathrm{D},\nu_r}\mathbf{D}^0_{2\mathrm{D}}(\mathbf{T}^0_{2\mathrm{D},\Omega_h\setminus\overline{\Gamma}_{1,h}})^{\mathrm{T}}\left(\mathbf{M}^0_{2\mathrm{D},\Omega_h\setminus\overline{\Gamma}_{1,h},\varepsilon_r}\right)^{-1}\\
&\qquad \cdot \mathbf{T}^0_{2\mathrm{D},\Omega_h\setminus\overline{\Gamma}_{1,h}}\underset{\sim}{\mathbf{D}}^1_{2\mathrm{D}}\mathbf{M}^1_{2\mathrm{D},\varepsilon_r}(\mathbf{T}^1_{2\mathrm{D},\Omega_h\setminus\overline{\Gamma}_{1,h}})^{\mathrm{T}}\underline{\widehat{\mathbf{e}}}_{2\mathrm{D},t,\mathrm{red}}\\
&= -k_z^2\mathbf{T}^1_{2\mathrm{D},\Omega_h\setminus\overline{\Gamma}_{1,h}}\mathbf{M}^1_{2\mathrm{D},\nu_r}(\mathbf{T}^1_{2\mathrm{D},\Omega_h\setminus\overline{\Gamma}_{1,h}})^{\mathrm{T}}\underline{\widehat{\mathbf{e}}}_{2\mathrm{D},t,\mathrm{red}}
\end{aligned} \tag{5.12}$$

This formulation now does include all boundary conditions explicitly and can be directly coded into a computer program.

In the standard FIT with diagonal material matrices, the formulation (5.12) has the advantage of reducing the unknowns to the necessary minimum while the reduced nodal permittivity matrix $\mathbf{M}^0_{2\mathrm{D},\Omega_h\setminus\overline{\Gamma}_{1,h},\varepsilon_r}$ can be inverted explicitly. In the general polygonal case, the reduced nodal permittivity matrix is non-diagonal and thus not easily inverted. Nonetheless, we will use formulation (5.12) for the problem at hand, keeping in mind that for different setups, other formulations might be better suited.

In the eigenproblem (5.12), we nicely see the involvement of material matrices of all possible degrees $k = 0, 1, 2$, that is for nodal, edge, and face grid quantities, and discrete differential operators of all possible degrees $k = 0, 1$. Therefore, it is almost guaranteed that errors in the scheme will destroy the convergence properties rendering a nice test case for the scheme.

We will employ a wide variety of grids as shown in Fig. 5.2 and compare the convergence properties of the new polygonal scheme with those of standard quadrilateral and triangular schemes. Grid 1 in Fig. 5.2a will be used with standard FIT diagonal material relations. Grids 2 through 4 (Fig. 5.2b to 5.2d) are examples for triangular grids employing standard triangular Whitney-FEM material relations. Grids 5 through 8 (Fig. 5.2e to 5.2h) are examples for new polygonal grids and employ the new material relations derived in chapter 4 adjusted to the 2-dimensional case. All grids shown in Fig. 5.2 are the coarsest ones used in the simulations and are refined regularly for the convergence study.

Convergence rates are usually stated in regard to some grid parameter h based on the lengths of the grid edges, as this often proves to be independent of the dimension of the

problem. Here we do state convergence rates in the number of unknowns, i.e. edges, though. This allows for a better comparison of the computational effort for the different grids. For regular grid refinements in the 2-dimensional case, the number of unknowns is roughly proportional to the square of a grid parameter h. Therefore, the convergence rates in the number of unknowns is only $\frac{1}{2}$ that of the usually stated convergence rates in some grid parameter h.

For all types of grids employed, the condition number of the left hand side system matrix of equation (5.12) is observed in Fig. 5.3 to be roughly proportional to the number of unknowns.

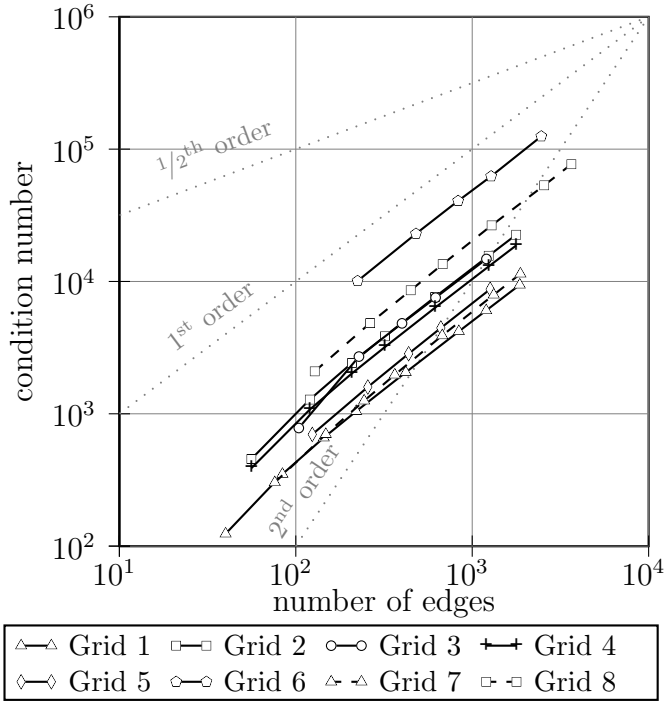

Fig. 5.3: Condition number of the system matrix on the left hand side of equation (5.12) for a regular refinement of the grids shown in Fig. 5.2.

The relative error in the longitudinal wavenumber k_z compared to the continuous value $k_{z,c}$ is defined as:

$$\frac{|k_{z,c} - k_z|}{k_{z,c}} \tag{5.13}$$

For the first 6 modes, we observe in Fig. 5.4 first order convergence in the number of unknowns, i.e. second order convergence in the grid size parameter h, for all grids. This order of convergence is well-known for the standard FIT with rectangular grids, as shown by a dispersion analysis for homogeneous regions [85, pp. 60]. For the FEM, a convergence analysis was carried out in [89] for triangular and quadrilateral grids. Although certain grids show a better performance for certain modes, the overall quantitative error seems similar for all chosen grids. Interesting in this context is also the discussion of the quantitative error in the dispersion relation for different grids for 2-dimensional TE- and TM-waves in [99].

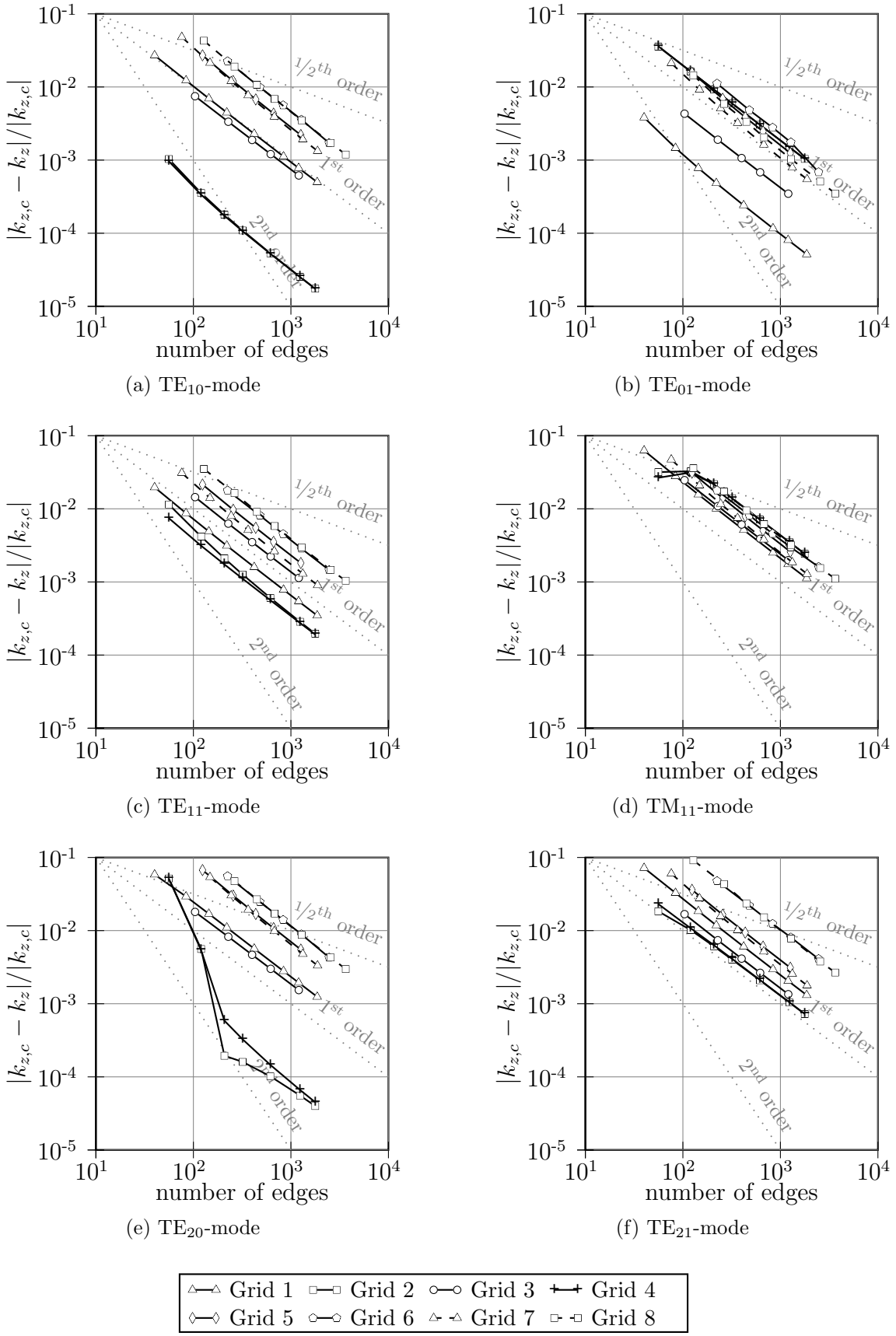

(a) TE_{10}-mode (b) TE_{01}-mode

(c) TE_{11}-mode (d) TM_{11}-mode

(e) TE_{20}-mode (f) TE_{21}-mode

Fig. 5.4: Relative errors in the longitudinal wavenumber k_z for the first 6 modes of the discrete eigenproblem stated in equation (5.12). The results are shown for a regular refinement of the different grids depicted in Fig. 5.2.

In appendix D.2, different error definitions for the error in the transverse and longitudinal electric grid voltages $\underline{\widehat{\mathbf{e}}}_{2\mathrm{D},t}$ and $\underline{\mathbf{e}}_{2\mathrm{D},z}$ are discussed. Also for these errors, the polygonal scheme is observed to behave comparably to the standard quadrilateral and triangular schemes.

5.2 Enhanced Boundary Approximation in Structured Grids

For grid-based numerical simulations, there is always the choice of either using structured or unstructured grids. Structured grids allow for an efficient implementation of large grids as no connectivity matrices have to be stored or accessed. Their disadvantage is the inflexibility regarding the resolution of small structures and the approximation of material boundaries not conforming to the grid faces if a fixed node distribution is used. Although these disadvantages are tackled by subgridding [73] and boundary approximation techniques like edge-, face-, and volume-averaging [35] or the conformal FD [101], there are situations where better local approximation properties are needed. The use of unstructured grids solves these disadvantages of structured grids, as they can be locally refined to conform to small features and quite arbitrary boundaries. Unstructured grids imply additional memory and computational cost due to the need for saving and accessing connectivity information, though. Also, the material relations for unstructured grids do in general not allow for an explicit time discretization.

Usually, diagonal material matrices as the standard FIT material relations described on pages 58-61 are used for structured grids and non-diagonal material matrices like the Whitney-FEM material relations described in chapter 4.1 for unstructured grids. The numerical discretization described in chapter 3 provides an efficient framework incorporating these different methods just by cell-wise using the appropriate discrete material relations. Thereby great flexibility is gained and hybrid schemes using different material relations are directly available.

For computational reasons, we propose to use structured grids with a regular node distribution in regions where no problems due to small features or boundaries exist. In the problematic regions, we propose to use unstructured grids either to resolve these problems directly or to provide a transition to structured grids with higher resolution (subgridding).

5.2.1 2-Dimensional Electrostatic Example: Dielectric Cylinder in Homogeneous Field

We first treat an example from electrostatics with curved dielectric boundary. Problems in convergence are observed when the curved dielectric boundaries are discretized with staircase grids and standard FIT material relations or even with edge- or face-averaged material relations [35]. The example consists of a vacuum cylinder enclosed by a dielectric medium as depicted in Fig. 5.5. As excitation, an external electric field $\vec{E}_0$ is applied in the y-direction. As the external electric field is oriented perpendicular to the axis of the cylinder, we obtain the following 2-dimensional boundary value problem in the unknown electric scalar potential φ_e and the unknown transverse electric (TE) field strength $\vec{E}_t$:

$$\vec{E}_t = -\overrightarrow{\mathrm{grad}}_{2\mathrm{D}}\,\varphi_e \qquad \text{in } \mathbb{R}^2 \tag{5.14a}$$

$$\mathrm{div}_{2\mathrm{D}}\,\varepsilon\vec{E}_t = -\,\mathrm{div}_{2\mathrm{D}}\,\varepsilon\,\overrightarrow{\mathrm{grad}}_{2\mathrm{D}}\,\varphi_e = 0 \qquad \text{in } \mathbb{R}^2 \tag{5.14b}$$

$$\lim_{r\to\infty}\vec{E}_t = \vec{E}_0 = E_0\vec{e}_y \tag{5.14c}$$

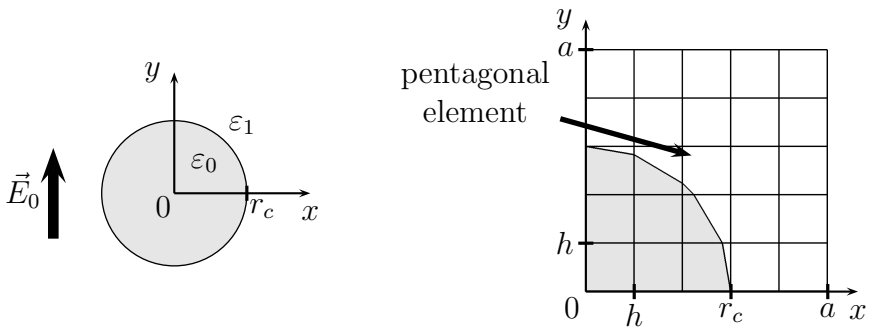

(a) Problem setup. (b) Gridded problem domain.

Fig. 5.5: Problem domain and example polygonal grid: (a) A vacuum cylinder of radius $r_c = 0.3\,\mathrm{mm}$ and permittivity ε_0 is enclosed by a surrounding dielectric medium with permittivity $\varepsilon_1 = 1000\,\varepsilon_0$. An external electrostatic field $\vec{E}_0$ is applied in the y-direction. (b) For the discretization, only one fourth of the problem domain reduced to $x \in [0, a]$ and $y \in [0, a]$ with $a = 0.5\,\mathrm{mm}$ is discretized. A structured grid employing a locally unstructured section of the grid along the boundary of the cylinder is used. The curved cylinder boundary is approximated piecewise linearly. Shown is the coarsest grid used with grid parameter $h = 0.1\mathrm{mm}$.

with the arbitrary gauge

$$\varphi_e(\vec{r}=0) = 0 \tag{5.15}$$

The 2-dimensional gradient and divergence operators are defined in equations (4.45) on page 103.

In order to discretize this problem by the FIT, we truncate the domain as shown in Fig. 5.5b. We again use the 2-dimensional discrete FIT exterior derivative, material and trace operators introduced on page 128. For discretizing the boundary data, we use the 2-dimensional grid discretization operators $\mathrm{L}^k_{2\mathrm{D}}$. The resulting discretized system of equations with the electric scalar grid potentials $\boldsymbol{\varphi}_{e,2\mathrm{D}}$, the transverse electric grid voltages $\widehat{\mathbf{e}}_{2\mathrm{D},t}$, and the dual electric boundary fluxes $\widehat{\underset{\sim}{\mathbf{d}}}_{2\mathrm{D},t,\overline{\Gamma}_{1,h}}$ as unknowns reads:

$$\widehat{\mathbf{e}}_{2\mathrm{D},t} = -\mathbf{D}^0_{2\mathrm{D}}\boldsymbol{\varphi}_{e,2\mathrm{D}} \tag{5.16a}$$

$$\underset{\sim}{\mathbf{D}}^1_{2\mathrm{D}}\mathbf{M}^1_{2\mathrm{D},\varepsilon}\widehat{\mathbf{e}}_{2\mathrm{D},t} + (\mathbf{T}^0_{2\mathrm{D},\overline{\Gamma}_{1,h}})^{\mathrm{T}}\widehat{\underset{\sim}{\mathbf{d}}}_{2\mathrm{D},t,\overline{\Gamma}_{1,h}} = 0 \tag{5.16b}$$

$$\mathbf{T}^0_{2\mathrm{D},\overline{\Gamma}_{1,h}}\boldsymbol{\varphi}_{e,2\mathrm{D}} = \mathbf{T}^0_{2\mathrm{D},\overline{\Gamma}_{1,h}}\mathrm{L}^0_{2\mathrm{D}}\varphi_e \tag{5.16c}$$

Equation (5.16c) imposes the values of the continuous solution as boundary potentials at the boundary of the truncated domain. The boundary terms $\widehat{\underset{\sim}{\mathbf{d}}}_{2\mathrm{D},t,\overline{\Gamma}_{1,h}}$ need to be included to arrive at a consistent discretization of the continuous equations up to the boundary as introduced in equation (5.2b) on page 129.

Defining the reduced electric scalar grid potentials $\boldsymbol{\varphi}_{e,2\mathrm{D,red}}$ as the values associated with the interior nodes

$$\boldsymbol{\varphi}_{e,2\mathrm{D,red}} \equiv \mathbf{T}^0_{2\mathrm{D},\Omega_h\setminus\overline{\Gamma}_{1,h}}\boldsymbol{\varphi}_{e,2\mathrm{D}} \tag{5.17}$$

we can deduce from equations (5.16) the following reduced formulation:

$$\begin{aligned} &- \mathbf{T}^0_{2\mathrm{D},\Omega_h\setminus\overline{\Gamma}_{1,h}} \underset{\sim}{\mathbf{D}}^1_{2\mathrm{D}} \mathbf{M}^1_{2\mathrm{D},\varepsilon} \mathbf{D}^0_{2\mathrm{D}} \left(\mathbf{T}^0_{2\mathrm{D},\Omega_h\setminus\overline{\Gamma}_{1,h}}\right)^{\mathrm{T}} \boldsymbol{\varphi}_{e,2\mathrm{D},\mathrm{red}} \\ &\quad = \mathbf{T}^0_{2\mathrm{D},\Omega_h\setminus\overline{\Gamma}_{1,h}} \underset{\sim}{\mathbf{D}}^1_{2\mathrm{D}} \mathbf{M}^1_{2\mathrm{D},\varepsilon} \mathbf{D}^0_{2\mathrm{D}} \left(\mathbf{T}^0_{2\mathrm{D},\overline{\Gamma}_{1,h}}\right)^{\mathrm{T}} \mathbf{T}^0_{2\mathrm{D},\overline{\Gamma}_{1,h}} \mathrm{L}^0_{2\mathrm{D}} \varphi_e \end{aligned} \tag{5.18}$$

This is a formulation in the unknown reduced electric scalar grid potentials $\boldsymbol{\varphi}_{e,2\mathrm{D},\mathrm{red}}$ with symmetric system matrix which includes all boundary conditions that can be directly coded in a program.

We will discuss the errors in the grid quantities, i.e. in discrete error norms comparing the numerical solutions $\boldsymbol{\varphi}_{e,2\mathrm{D}}$ and $\widehat{\mathbf{e}}_{2\mathrm{D},t}$ with the projections $\boldsymbol{\varphi}_{e,2\mathrm{D},c}$ and $\widehat{\mathbf{e}}_{2\mathrm{D},t,c}$ of the continuous solutions φ_e and $\vec{E}_t$ onto the grid:

$$\boldsymbol{\varphi}_{e,2\mathrm{D},c} \equiv \mathrm{L}^0_{2\mathrm{D}} \varphi_e \tag{5.19}$$

$$\widehat{\mathbf{e}}_{2\mathrm{D},t,c} \equiv \mathrm{L}^1_{2\mathrm{D}} \vec{E}_t \tag{5.20}$$

The discrete relative 2-norm and ∞-norm errors are defined by the standard vector norms $\|.\|_2$ and $\|.\|_\infty$ as:

$$\frac{\|\boldsymbol{\varphi}_{e,2\mathrm{D}} - \boldsymbol{\varphi}_{e,2\mathrm{D},c}\|_2}{\|\boldsymbol{\varphi}_{e,2\mathrm{D},c}\|_2}, \qquad \frac{\|\boldsymbol{\varphi}_{e,2\mathrm{D}} - \boldsymbol{\varphi}_{e,2\mathrm{D},c}\|_\infty}{\|\boldsymbol{\varphi}_{e,2\mathrm{D},c}\|_\infty} \tag{5.21}$$

$$\frac{\|\widehat{\mathbf{e}}_{2\mathrm{D},t} - \widehat{\mathbf{e}}_{2\mathrm{D},t,c}\|_2}{\|\widehat{\mathbf{e}}_{2\mathrm{D},t,c}\|_2}, \qquad \frac{\|\widehat{\mathbf{e}}_{2\mathrm{D},t} - \widehat{\mathbf{e}}_{2\mathrm{D},t,c}\|_\infty}{\|\widehat{\mathbf{e}}_{2\mathrm{D},t,c}\|_\infty} \tag{5.22}$$

Note that the scaling of the discrete relative norm in the grid potentials is quite arbitrary due to the integration constant in the scalar potential, which was fixed by equation (5.15).

For homogeneous problems with sufficient regularity of the solutions, where the boundary can be reproduced perfectly, and regular grids, [67] has observed second order convergence of the scalar potential as well as the electric field strength in both norms. For slightly irregular grids, the convergence rate for the maximum error in the electric field strength can drop down to first order as described in [68]. These are the best convergence rates to expect for the non-homogeneous case if the grid can approximate the material boundaries at least piecewise linearly.

For a standard staircase approximation, we note a decrease in the convergence rates in Fig. 5.6: The errors in the scalar potential converge only roughly first order; in the electric field strength, the 2-norm error converges with order less then $\frac{1}{2}$ and the ∞-norm error does not converge at all.

These problems in convergence of the staircase approximation are well-known. In [35], it was shown that even for face- or edge-averaged material relations taking the partial dielectric fillings into account, the ∞-norm error does not converge. There, an adopted scheme resulting in non-symmetric material matrices was derived recovering first order convergence of the electric field strength in the ∞-norm. Another possibility for improving convergence for structured quadrilateral meshes is to move nodes close to the boundary onto the boundary. This results in a piecewise linear approximation of the boundary. This would retain the topology of the grid and only change the material relations. A

drawback might be the need for a finer grid resolution to capture the dielectric boundary, which results for structured quadrilateral meshes in a finer grid in the complete calculation domain.

Here we propose the local use of polygonal elements piecewise linearly conforming to the dielectric boundary, as shown in Fig. 5.5b, to improve convergence rates. This results in symmetric material relations and provably stable schemes. The striking feature is the use of a structured grid in the homogeneous regions with a locally unstructured polygonal grid at the curved cylinder boundary only. A simple cutting algorithm not only renders standard triangular and quadrilateral but also pentagonal elements. Although in the 2-dimensional case, these could be split into standard triangular elements, in the 3-dimensional case, the resulting tetrahedra could not be consistently coupled to a hexahedral grid. With the availability of polyhedral cells, a polyhedral splitting can be directly employed in the 3-dimensional case.

In Fig. 5.6, we see that convergence rates considerably improve for the polygonal grid: For the scalar potential, convergence rates of approximately order 2 are recovered. By linear regression, we get orders 2.13 and 1.93 for the 2-norm and the ∞-norm, respectively. For the electric field strength, the convergence rates have improved but are less than expected in the homogeneous case: By linear regression, we get orders 1.53 and 0.85 for the 2-norm and ∞-norm, respectively.

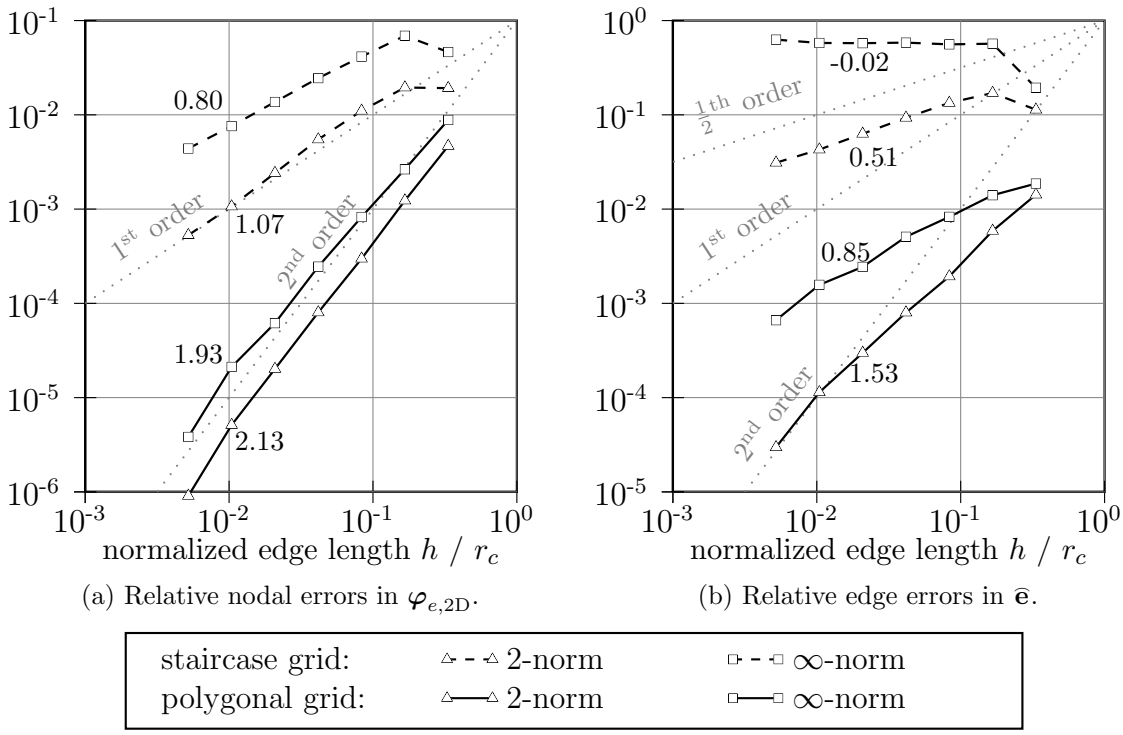

(a) Relative nodal errors in $\boldsymbol{\varphi}_{e,2\mathrm{D}}$.

(b) Relative edge errors in $\widehat{\mathbf{e}}$.

Fig. 5.6: Relative errors in the electric grid potentials $\boldsymbol{\varphi}_{e,2\mathrm{D}}$ and the electric grid voltages $\widehat{\mathbf{e}}_{2\mathrm{D},t}$ as defined in equations (5.21) and (5.22) for a staircase grid and the conforming polygonal grid shown in Fig. 5.5b. Inset are the convergence orders calculated by linear regression.

5.3 Subgridding for Structured Grids

In the previous example, better approximation of dielectric boundaries is achieved by polygonal elements. In the following examples, we study grids with better local approximation achieved by using locally refined grids, as e.g. required by locally higher dielectric constants.

5.3.1 2-Dimensional Eigenproblem Example: Partially Filled Waveguide with Subgridding

We reconsider the waveguide eigenproblem described in the discrete setting by equation (5.12) on page 131, but now for a partially filled waveguide as depicted in Fig. 5.7. This waveguide features longitudinal-section electric (LSE) and longitudinal-section magnetic (LSM) modes [4, pp. 398] [22, pp. 411].

The grid is chosen to be a regular rectangular grid within each material, but with smaller elements in the high-dielectric region. The elements on the material border of the low-dielectric region are polygonal elements (here octagons). For the material relations, standard diagonal FIT relations are used in the homogeneous rectangular grid regions while the polygonal material relations from chapter 4 are used for the 1-dimensional layer of octagonal elements.

The coarse grid shown in Fig. 5.7b is refined regularly. In Fig. 5.8, we observe convergence of the numerical longitudinal wavenumber k_z in the grid parameter $h_{x,c}$ with order slightly less than 2. The convergence rates calculated by linear regression based on the values for the 3 finest grids for the first 10 modes are 1.74, 1.84, 1.84, 1.86, 1.88, 1.93, 1.86, 1.97, 1.79, and 1.95, respectively. The condition number of the system matrix is roughly proportional to $(h_{x,c})^{-2}$.

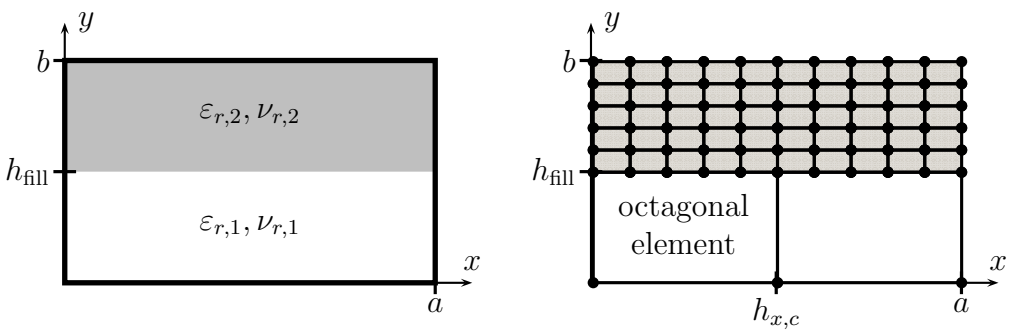

(a) Problem setup. (b) Consistent subgridding grid.

Fig. 5.7: Partially filled rectangular waveguide. (a) The dimensions of the waveguide are chosen at $b = 0.6a$ with $a = 1$ mm. The filling height is $h_{\text{fill}} = \frac{b}{2}$. The relative permittivities are $\varepsilon_{r,1} = 1$ and $\varepsilon_{r,2} = 25$, the relative reluctivities are $\nu_{r,1} = 1$ and $\nu_{r,2} = 1$. The wavenumber k_z was calculated at the frequency $f = \frac{c_0}{1.875a} \approx 160\,\text{GHz}$, i.e. $k_0 \approx 1.067\frac{\pi}{a}$. (b) Coarsest grid used. The grid parameter $h_{x,c}$ for this coarse grid is $h_{x,c} = \frac{a}{2}$.

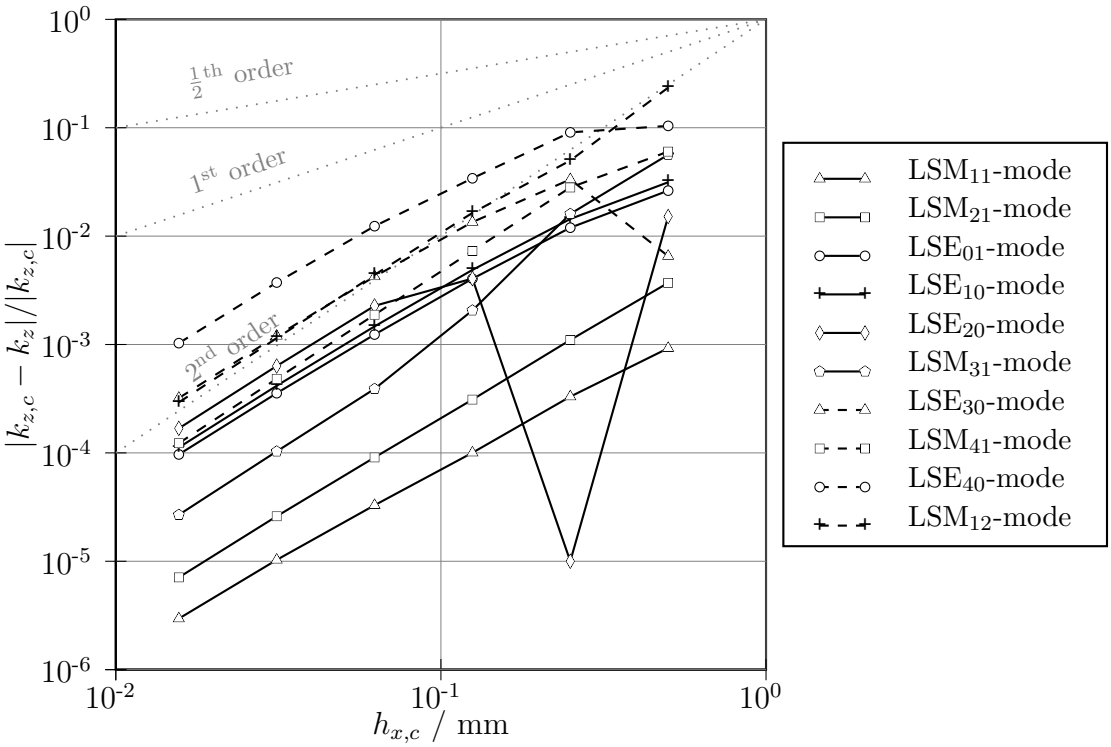

Fig. 5.8: Convergence study of the wavenumber k_z of the first 10 eigenmodes of the filled rectangular waveguide depicted in Fig. 5.7. The grid shown in Fig. 5.7b was refined regularly in the mesh parameter $h_{x,c}$.

5.3.2 3-Dimensional Eigenproblem Example: Homogeneously Filled Resonator with Subgridding

In this example, we study the convergence of the eigenvalues of the rectangular resonator depicted in Fig. 5.9. The boundary conditions are chosen such that zero eigenvalues are to be expected even for space-charge free solutions: Homogeneous electric (PEC) boundaries are chosen in the z-direction and homogeneous magnetic (PMC) boundaries in the x- and y-directions. The domain is homogeneously filled with vacuum (permittivity ε_0 and reluctivity ν_0). The eigenmodes are labeled as TE-, TM-, or TEM-modes, according to whether the z-component of the electric, the magnetic, or the electric and magnetic fields are zero.

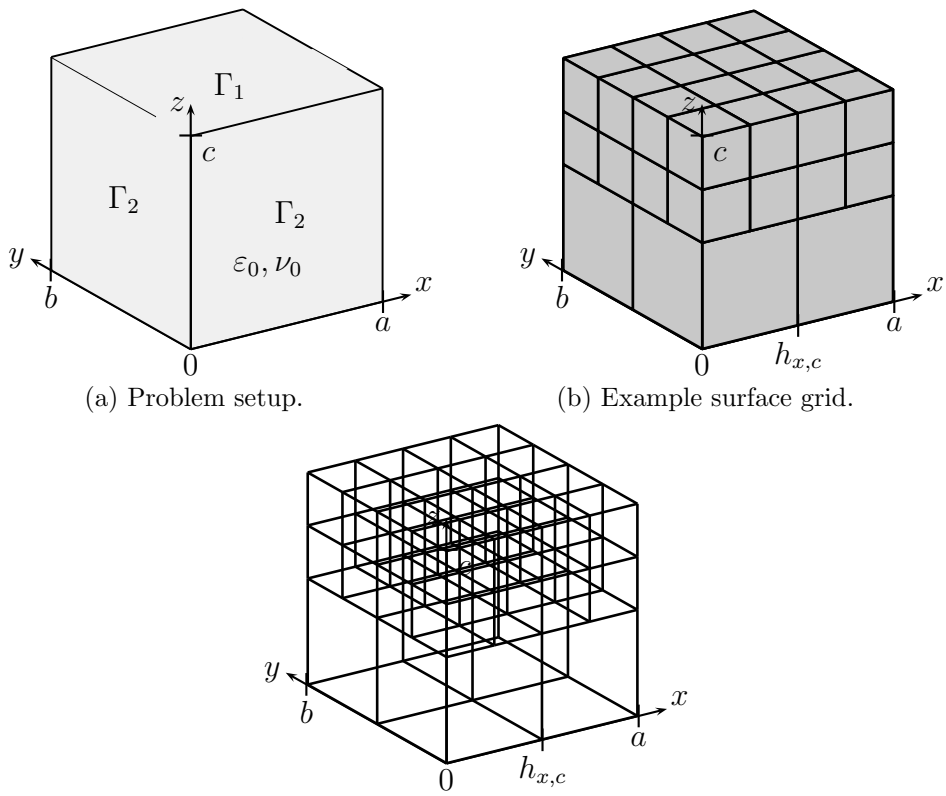

(a) Problem setup.

(b) Example surface grid.

(c) Example volume grid.

Fig. 5.9: (a) Rectangular resonator with $a = 1\,\text{mm}$, $b = 1.1\,\text{mm}$, $c = 1\,\text{mm}$. The inner domain Ω of the resonator is homogeneously filled with vacuum (ε_0, ν_0). Homogeneous electric (PEC) boundary conditions are applied at the boundary Γ_1 located at $z = 0$ and $z = c$. Homogeneous magnetic (PMC) boundary conditions are applied at the boundary Γ_2 located at $x = 0$, $x = a$, $y = 0$, and $y = b$. (b) and (c) The coarsest grid used in the convergence study. The special polyhedral grid cell depicted in Fig. 5.10 is used to connect the coarse to the fine grid.

The continuous boundary value problem for the resonator with the complex amplitude of the electric field strength $\underline{\vec{E}}$ and the continuous resonance frequency ω_c as unknowns

reads:

$$\operatorname{curl} \nu \operatorname{curl} \underline{\vec{E}} = \omega_c^2 \, \varepsilon \underline{\vec{E}} \qquad \text{in } \Omega \tag{5.23a}$$

$$\left(\nu \operatorname{curl} \underline{\vec{E}} \right) \times \vec{n}_{\Gamma_2} = 0 \qquad \text{on } \Gamma_2 \tag{5.23b}$$

$$\underline{\vec{E}} \times \vec{n}_{\Gamma_1} = 0 \qquad \text{on } \Gamma_1 \tag{5.23c}$$

Discretizing this boundary value problem by the FIT, we obtain the following discrete boundary value problem in the complex amplitude of the electric grid voltages $\underline{\widehat{\mathbf{e}}}$, the equivalent boundary currents $\underset{\simeq}{\widehat{\dot{\mathbf{j}}}}_{\Gamma_1}$, and the discrete resonance frequency ω as unknowns:

$$\underset{\sim}{\mathbf{C}} \, \mathbf{M}_\nu \, \mathbf{C} \, \underline{\widehat{\mathbf{e}}} = \omega^2 \, \mathbf{M}_\varepsilon \, \underline{\widehat{\mathbf{e}}} - i\omega \left(\underset{\simeq}{\widehat{\dot{\mathbf{j}}}}_{\Gamma_1} + \underset{\simeq}{\widehat{\dot{\mathbf{j}}}}_{\Gamma_2} \right) \tag{5.24a}$$

$$\underset{\simeq}{\widehat{\dot{\mathbf{j}}}}_{\Gamma_2} = - \left(\mathbf{T}^1_{\overline{\Gamma}_{2,h}} \right)^{\mathrm{T}} \underset{\simeq}{\widehat{\mathbf{h}}}_{\Gamma_2} = 0 \tag{5.24b}$$

$$\mathbf{T}^1_{\overline{\Gamma}_{1,h}} \, \underline{\widehat{\mathbf{e}}} = 0 \tag{5.24c}$$

To arrive at a reduced eigenproblem, we introduce the reduced unknown vector of the electric grid voltages $\underline{\widehat{\mathbf{e}}}_{\Omega \setminus \overline{\Gamma}_1}$:

$$\underline{\widehat{\mathbf{e}}}_{\Omega \setminus \overline{\Gamma}_1} \equiv \mathbf{T}^1_{\Omega_h \setminus \overline{\Gamma}_{1,h}} \, \underline{\widehat{\mathbf{e}}} \tag{5.25}$$

Due to the homogeneous boundary condition in equation (5.24c), we can recover the full vector of electric grid voltages by:

$$\underline{\widehat{\mathbf{e}}} = \left(\mathbf{T}^1_{\Omega_h \setminus \overline{\Gamma}_{1,h}} \right)^{\mathrm{T}} \underline{\widehat{\mathbf{e}}}_{\Omega \setminus \overline{\Gamma}_1} \tag{5.26}$$

Now we can reduce equations (5.24) to the following eigenproblem:

$$\mathbf{T}^1_{\Omega_h \setminus \overline{\Gamma}_{1,h}} \, \underset{\sim}{\mathbf{C}} \, \mathbf{M}_\nu \, \mathbf{C} \left(\mathbf{T}^1_{\Omega_h \setminus \overline{\Gamma}_{1,h}} \right)^{\mathrm{T}} \underline{\widehat{\mathbf{e}}}_{\Omega \setminus \overline{\Gamma}_1} = \omega^2 \, \mathbf{T}^1_{\Omega_h \setminus \overline{\Gamma}_{1,h}} \, \mathbf{M}_\varepsilon \left(\mathbf{T}^1_{\Omega_h \setminus \overline{\Gamma}_{1,h}} \right)^{\mathrm{T}} \underline{\widehat{\mathbf{e}}}_{\Omega \setminus \overline{\Gamma}_1} \tag{5.27}$$

The solutions to this problem contain many zero eigenvalues associated with solutions containing space-charges inside the calculation domain, so-called static solutions. In order to obtain only space-charge free solutions, we have to require the electric charges on the dual volumes inside the calculation domain and on the boundary part Γ_2 (that is not on the boundary part Γ_1) to be zero:

$$\mathbf{T}^0_{\Omega_h \setminus \overline{\Gamma}_{1,h}} \, \underset{\sim}{\mathbf{S}} \, \mathbf{M}_\varepsilon \, \underline{\widehat{\mathbf{e}}} = 0 \tag{5.28}$$

$$\Rightarrow \quad \mathbf{T}^0_{\Omega_h \setminus \overline{\Gamma}_{1,h}} \, \underset{\sim}{\mathbf{S}} \, \mathbf{M}_\varepsilon \left(\mathbf{T}^1_{\Omega_h \setminus \overline{\Gamma}_{1,h}} \right)^{\mathrm{T}} \underline{\widehat{\mathbf{e}}}_{\Omega \setminus \overline{\Gamma}_1} = 0 \tag{5.29}$$

For solving the discrete eigenvalue problem (5.27) under the constraint (5.29), the projected Jacobi-Davidson algorithm described along with other methods in [38] and implemented in the Python package PyFemax [39] is used. It is specifically adapted to handling the divergence-free constraint (5.29) while preserving possible zero eigenvalues of the space-charge free solutions.

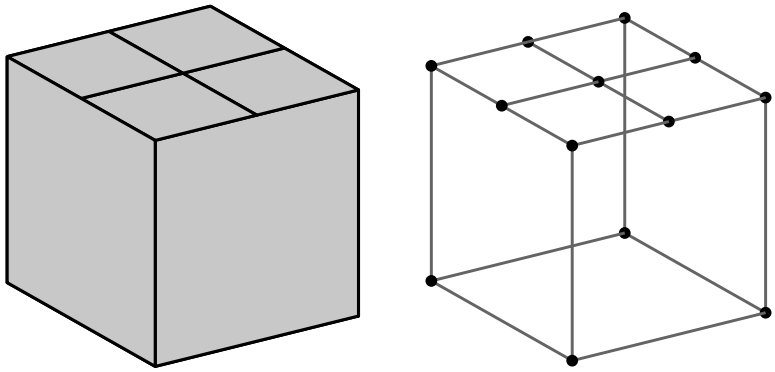

(a) Surface grid. (b) Volume grid.

Fig. 5.10: This special polyhedral grid cell is used to consistently connect the fine and coarse grids in Fig. 5.9.

The grid is split into a coarse and a fine part, as seen in Fig. 5.9b and 5.9c. The special subgridding element depicted in Fig. 5.10 connects the coarse and the fine grid parts consistently. Within the regular grid regions, the standard diagonal FIT material relations are used. For the subgridding element, the non-diagonal polyhedral material relations are employed. The convergence study for uniformly refined grids in Fig. 5.11 shows approximately second order convergence of the eigenvalues ω in the grid size parameter $h_{x,c}$. The zero eigenvalue of the TEM_{000}-mode is captured down to machine precision and therefore not plotted in Fig. 5.11. Note that for the finest calculated grid resolution of $\frac{h_{x,c}}{a} = 2^{-5}$, there are more than 430,000 edge degrees of freedom.

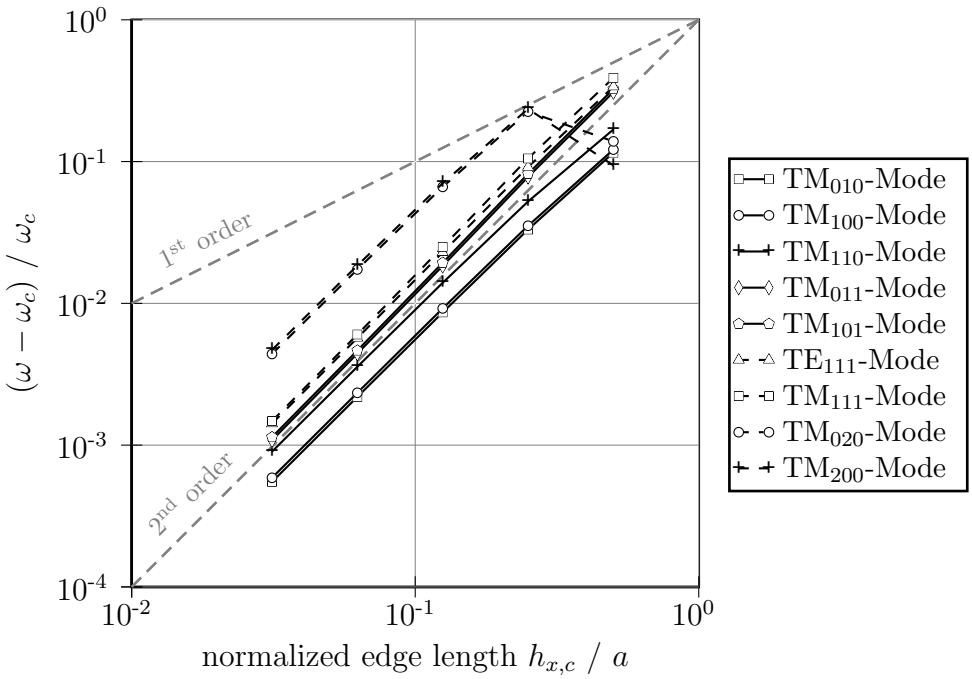

Fig. 5.11: Convergence of the eigenvalues of the first modes for the homogeneous rectangular resonator problem depicted in Fig. 5.9. The error for the constant TEM_{000}-mode is not plotted as its zero eigenvalue is solved for to machine precision. Linear regression analysis gives orders 1.93, 1.93, 1.90, 2.05, 2.05, 1.98, 2.02, 1.37, and 1.23 for the modes plotted in the listed order.

5.3.3 3-Dimensional Eigenproblem Example: Partially Filled Resonator with Subgridding

In order to show that material fillings can be used in the primary grid cells as usual, the partially filled rectangular resonator depicted in Fig. 5.12 is studied next. The resonator is filled with medium 1 for $0 < y < h_{\text{fill}}$ and with medium 2 for $h_{\text{fill}} < y < b$. The material filling is chosen to cut through the polyhedral layer to show that this does not pose any problem for convergence. The permittivity and reluctivity of the medium 1 and 2 are $\varepsilon_1 = \varepsilon_0$, $\nu_1 = \nu_0$ and $\varepsilon_2 = 10\,\varepsilon_0$, $\nu_2 = \nu_0$, respectively. Note that homogeneous electric (PEC) boundary conditions are chosen everywhere on the boundary. The eigenmodes of this resonator are denoted as LSE- or LSM-modes, depending on whether the normal y-component of the electric or the magnetic field strength is zero at the material interface. The discrete eigenvalue problem (5.27) and the divergence-free constraint (5.29) read the same as before and the same subgridding element depicted in Fig. 5.10 is used. In Fig. 5.13, we again observe roughly second order convergence of the eigenvalues ω in the grid size parameter $h_{x,c}$, as expected.

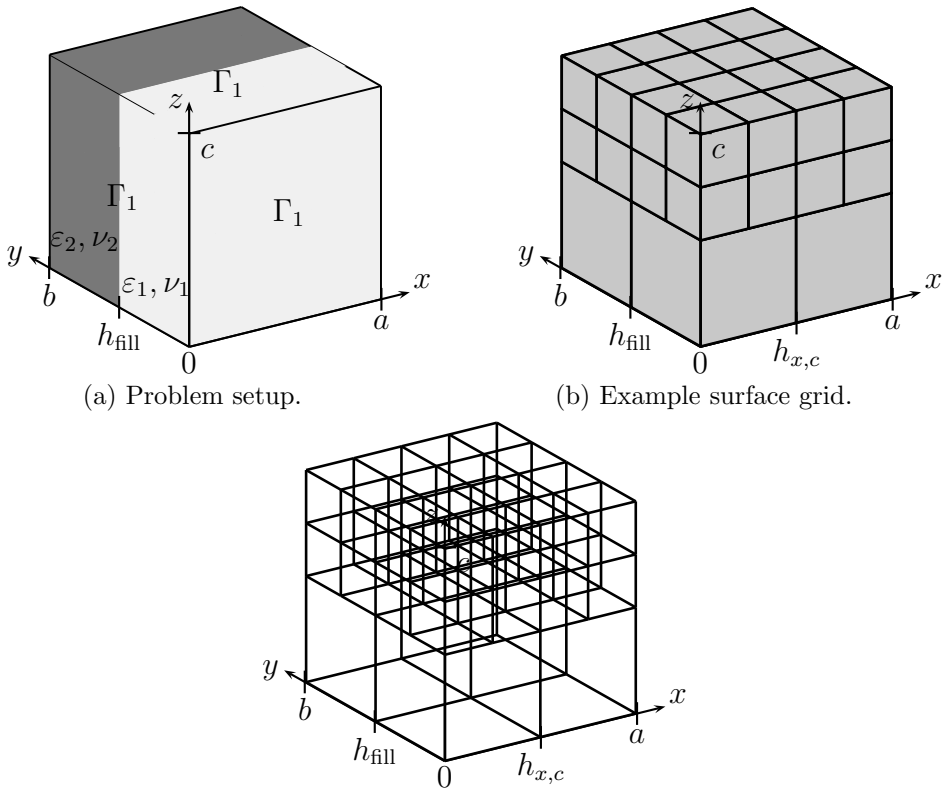

(a) Problem setup.

(b) Example surface grid.

(c) Example volume grid.

Fig. 5.12: (a) Rectangular resonator with $a = 1\,\text{mm}$, $b = 1.1\,\text{mm}$, $c = 1\,\text{mm}$. The inner domain Ω of the resonator is filled with material 1 (ε_1, ν_1) for $0 < y < h_{\text{fill}}$ and with material 2 (ε_2, ν_2) for $h_{\text{fill}} < y < b$. Homogeneous electric (PEC) boundary conditions are applied at the boundary $\Gamma_1 = \partial\Omega$ at $x = 0$, $x = a$, $y = 0$, $y = b$, $z = 0$, and $z = c$. (b) and (c) The coarsest grid used in the convergence study. The special polyhedral grid cell depicted in Fig. 5.10 is used to connect the coarse to the fine grid.

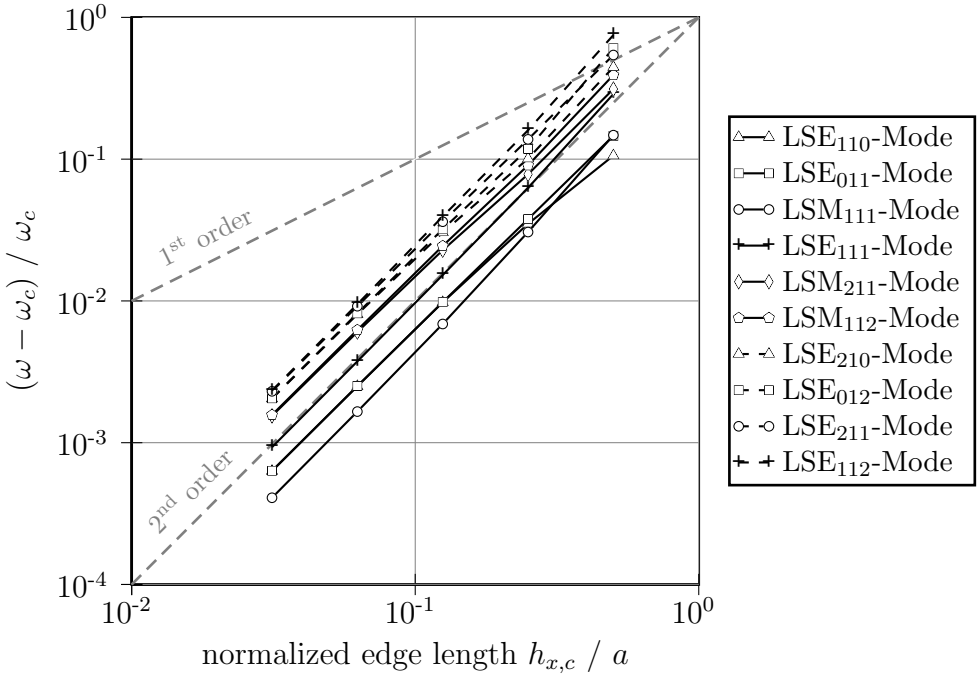

Fig. 5.13: Convergence of the eigenvalues of the first modes for the partially filled rectangular resonator problem depicted in Fig. 5.12. Linear regression analysis gives orders 1.86, 1.96, 2.12, 2.06, 1.90, 1.98, 1.92, 2.02, 1.97, and 2.07 for the modes plotted in the listed order.

5.3.4 3-Dimensional Time Domain Example: Reflection Analysis from Subgridding Interface

In this example, reflections from a subgridding interface realized by polyhedral cells are examined. The first setup is a parallel plate waveguide with a subgridding step in the longitudinal z-direction. Examining the reflections of the TEM-mode of this waveguide is equivalent to normal incidence of a plane wave on the subgridding interface. The second setup is a rectangular waveguide. Looking at the reflections of the TE_{10}-mode for different frequencies is similar to examining the reflection of plane waves incident at varying angles to the subgridding interface, as the TE_{10}-mode is equivalent to a superposition of two plane waves incident at a frequency dependent angle to the transverse xy-plane.

TEM-Mode of a Parallel Plate Waveguide

As shown in Fig. 5.14, a parallel plate waveguide is discretized using a coarse grid with grid step size h_c and a fine grid with grid step size $h_f = \frac{1}{2}h_c$ connected by a polyhedral cell. The medium inside the waveguide is assumed to have permittivity $\varepsilon = 1\frac{\mathrm{F}}{\mathrm{m}}$ and reluctivity $\nu = 1\frac{\mathrm{m}}{\mathrm{H}}$. The TEM-mode is input either at port 1 on the coarse grid side or at port 2 on the fine grid side and the reflection coefficients S_{11} or S_{22}, respectively, are investigated. The Newmark-Θ time discretization scheme described on page 79 is employed for the time-domain simulation. The modulated Gaussian pulse shown in Fig. 5.15 is used as input signal. The reflection coefficients gathered from the time-domain simulations are transformed into the frequency domain by a discrete-time Fourier transform.

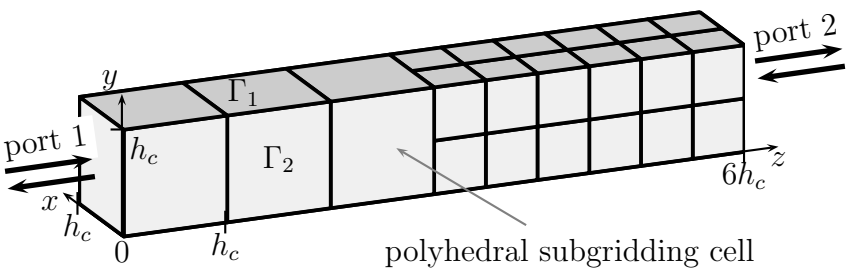

Fig. 5.14: Parallel plate waveguide employing the polyhedral subgridding cell from Fig. 5.10 on page 143. At $z=0$ and $z=6h_c$, waveguide ports are implemented. At the boundary Γ_1 at $y=0$ and $y=h_c$, homogeneous electric (PEC) boundary conditions are applied. At the boundary Γ_2 at $x=0$ and $x=h_c$, homogeneous magnetic (PMC) boundary conditions are applied. Due to the symmetry of the system, only this portion of the parallel plate waveguide shrinking in size with reduction of the mesh step h_c has to be calculated.

In the standard hexagonal coarse and fine grid regions, the standard diagonal FIT material relations described in chapter 3.2.2 are used and the parameters Θ_i of the Newmark-Θ scheme are set to zero. This renders the standard explicit FIT time domain leapfrog algorithm. Only for the polyhedral cells in the 2-dimensional transition region, polyhedral material relations from chapter 4 are employed[1] with the control parameters Θ_i set to $\frac{1}{4}$. This renders an implicit but unconditionally stable time-stepping scheme for these

[1] Special attention was paid to derive material relations exhibiting the same symmetries as the subgrid-

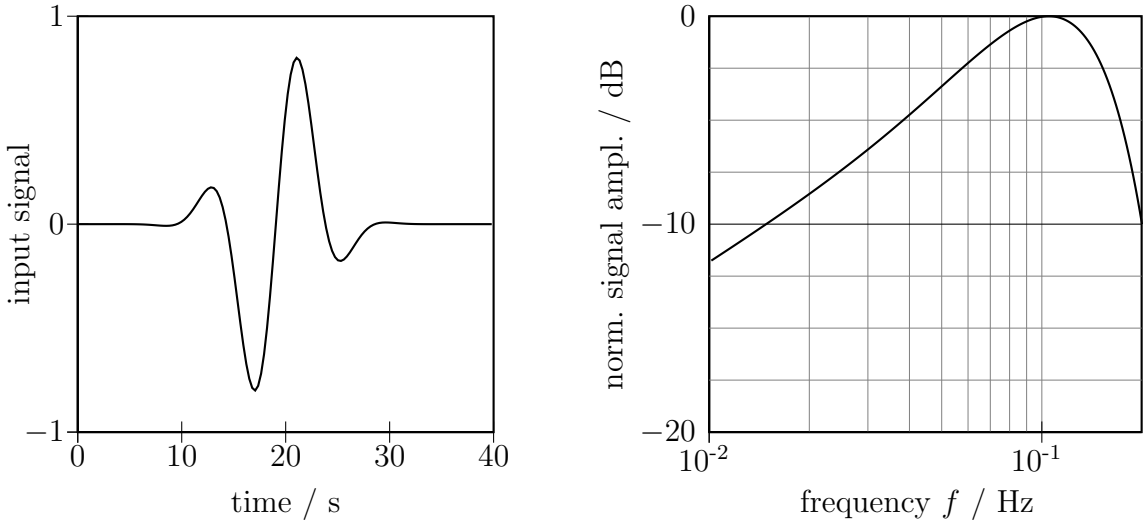

(a) time domain (b) frequency spectrum

Fig. 5.15: Input signal for the time domain simulation.

elements. As the subgridding interface employing polyhedral cells is only 2-dimensional, the complexity of the numerical solution of this implicit part is lower than the complexity of the 3-dimensional problem and therefore does not pose a problem in practical implementations.

The ports (with homogeneous grid step in the longitudinal direction) are implemented as described in [85, pp. 109][2]. These port implementations work extremely well for homogeneous materials and allow for an almost perfect removal of the energy from the calculation domain (see Fig. 5.16a), as the dispersion relation of the waveguide modes is captured down to machine precision. We do not observe a constant energy in time, as the simulation domain is shorter than the input signal wave. The error in the energy balance in the frequency domain, i.e. after a discrete-time Fourier transform of the discrete time domain signal, is also extremely low, as seen in Fig. 5.16b.

The reflection coefficients S_{11} and S_{22} for TEM-waves entering at the coarse and the fine grid ports, respectively, are depicted for different grid size parameters h_c in Fig. 5.17. Fixing a single frequency and refining the grid results in Fig. 5.18. We observe second order convergence of the reflection coefficients. For high resolutions of $h_c < 2^{-6}$, some artifacts are observed which can be removed by using more exact representations of the time signal and longer simulation times.

ding element to keep the symmetry of the system and to avoid mode-conversion. Although material relations not conforming to the element symmetry do not pose any problem in terms of convergence of the scheme, it does effect the high precision reflection analysis performed here.

[2] An additional correction for the frequency dependent wave impedance accounting for its dependence on the grid step size Δz at the port was taken into account to arrive at correct energy balances.

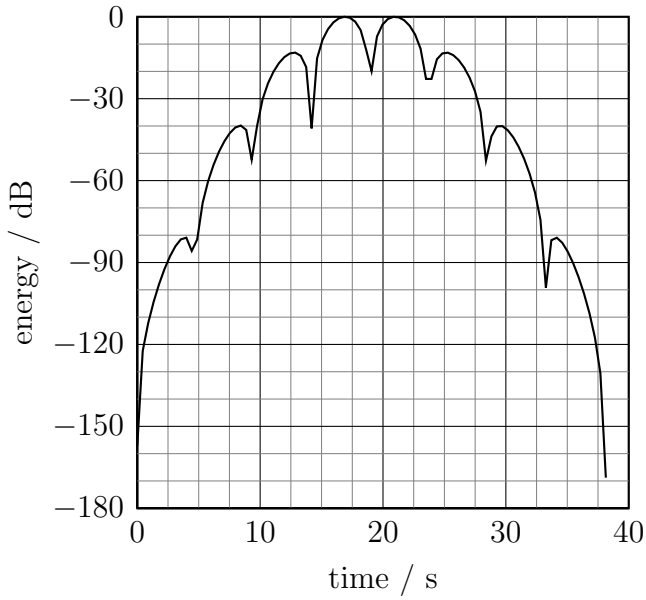

(a)

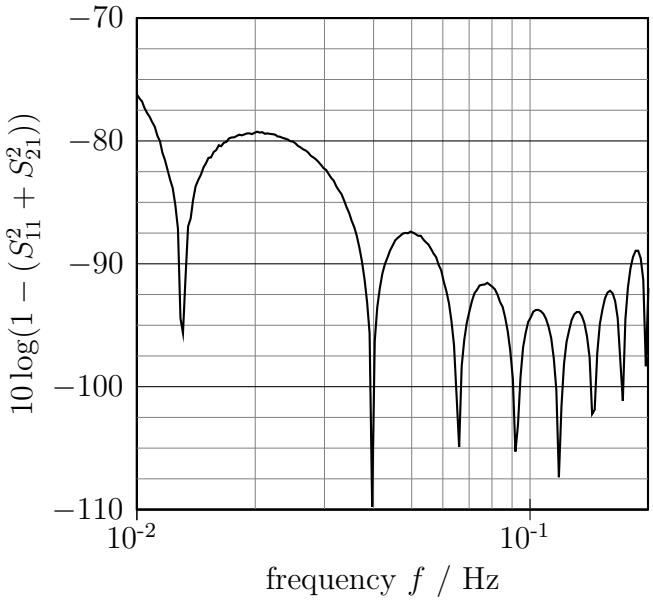

(b)

Fig. 5.16: (a): Total electromagnetic energy in the calculation domain as defined by equation (3.190) on page 83 for $h_c = 2^{-6}$ and signal input at the coarse grid port 1. (b): Energy balance error for $h_c = 2^{-6}$ m and signal input at the coarse grid port 1.

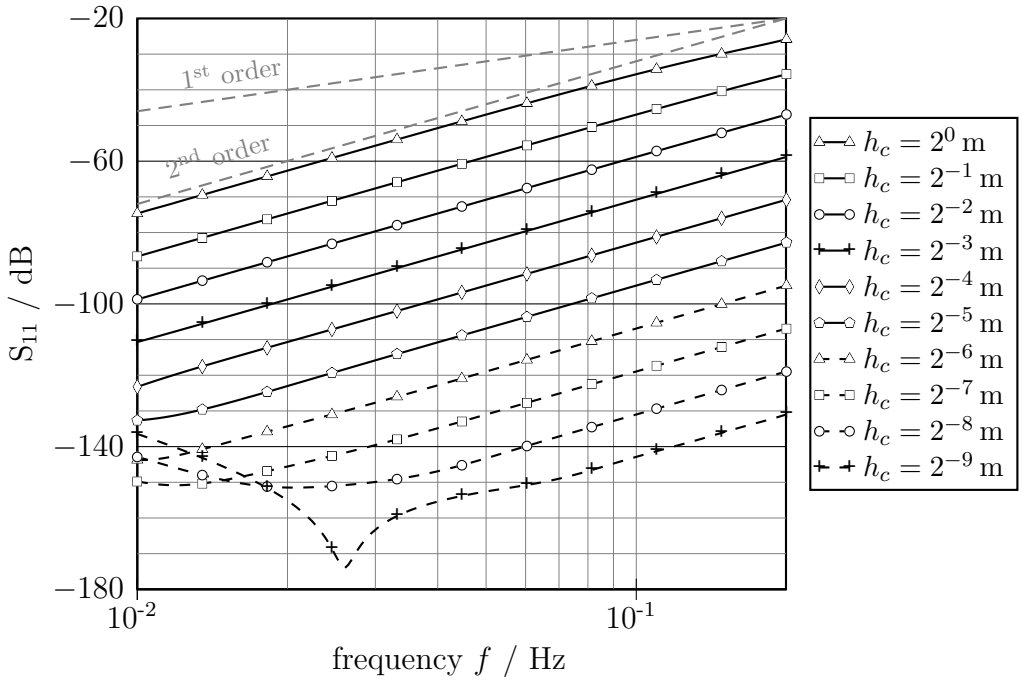

(a) S_{11}

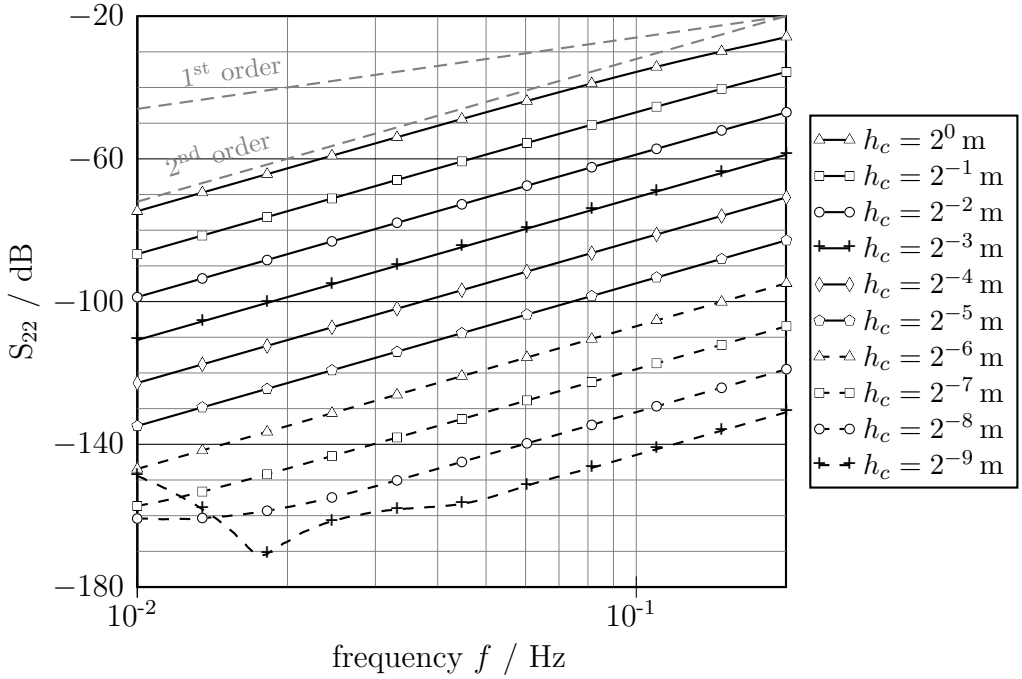

(b) S_{22}

Fig. 5.17: S-parameters over frequency for different grid discretizations for the parallel plate waveguide depicted in Fig. 5.14.

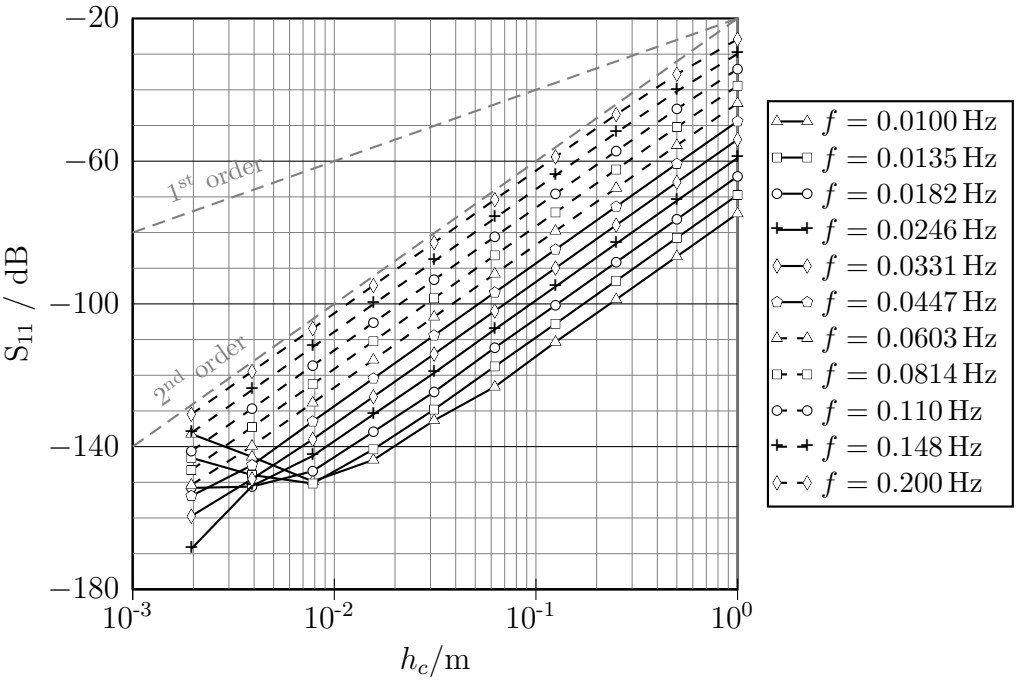

(a) S_{11}

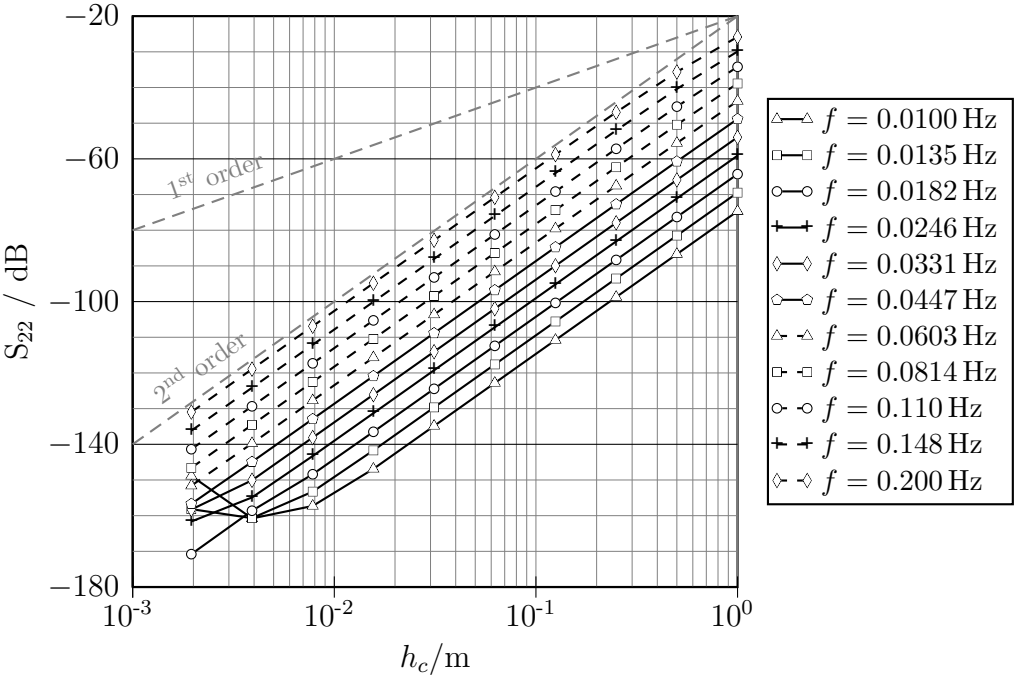

(b) S_{22}

Fig. 5.18: S-parameters over grid size parameter h_c for different frequencies for the parallel plate waveguide depicted in Fig. 5.14.

TE_{10}-Mode of a Rectangular Waveguide

The second example for the subgridding reflection analysis is a rectangular waveguide discretized with a grid similar to the one above (see Fig. 5.19). Again, we have chosen $\varepsilon = 1\,\frac{\mathrm{F}}{\mathrm{m}}$ and $\nu = 1\,\frac{\mathrm{m}}{\mathrm{H}}$. Although there is only a slight variation in the boundary conditions to the example above, now the eigenmodes of the waveguide are superpositions of plane waves propagating at an angle to the longitudinal z-direction. Therefore, this example predicts the reflection coefficients of plane waves incident at an angle to the subgridding interface. We only consider the TE_{10}-mode here and again input it at either the coarse grid side or at the fine grid side. Using the Newmark-Θ time discretization scheme described in chapter 3.3.2 with the modulated Gaussian pulse shown in Fig. 5.20 as input signal, the frequency response is recovered by a discrete-time Fourier transform of the discrete time domain port signals.

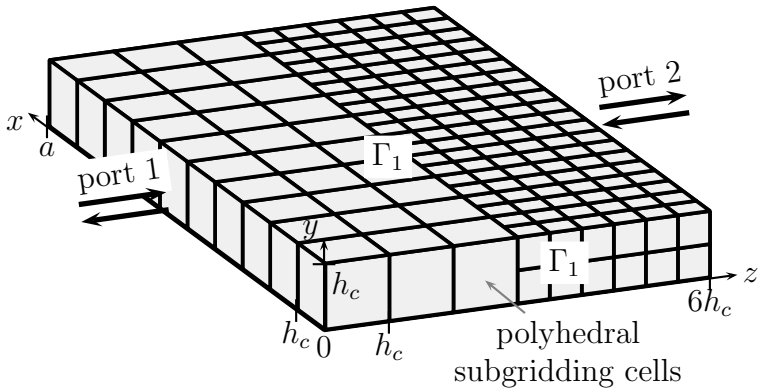

Fig. 5.19: Rectangular waveguide employing the polyhedral subgridding cell from Fig. 5.10 on page 143. At $z=0$ and $z=6h_c$, waveguide ports are implemented. At the boundary Γ_1 at $x=0$, $x=a$, $y=0$, and $y=h_c$ homogeneous electric (PEC) boundary conditions are applied. Due to the symmetry of the system, only this portion of the parallel plate waveguide shrinking in size in the y- and z-directions with reduction of the mesh step h_c has to be calculated.

The cutoff frequency f_c for the TE_{10}-mode

$$f_c = \frac{c_0}{2a} \tag{5.30}$$

is used to normalize the curves. The time signal in Fig. 5.20 is chosen such that the energy density at the cutoff frequency is low to avoid long simulation times. The good performance of the ports is again observed in Fig. 5.21a and 5.21b. The error in the energy balance in Fig. 5.21b is not as good as in the previous example for the TEM-mode, though. This is due to the excitation of the mode around the cut-off frequency: Without further techniques like signal prediction, any excitation around the cut-off frequency causes long simulation times. For this reason, the input signal was chosen with a small bandwidth and a power level of -50dB at the spectrum edges. The simulation was stopped when the energy in the domain reached a level of less than -160dB, as seen in Fig. 5.21a. This causes an error in the port signal calculation which is roughly constant in frequency. As the power level of the input signal at the spectrum edges is 50dB less than at the main frequency, the resulting error in the energy balance at the spectrum edges is 50dB higher than at the main frequency as observed in Fig. 5.21b.

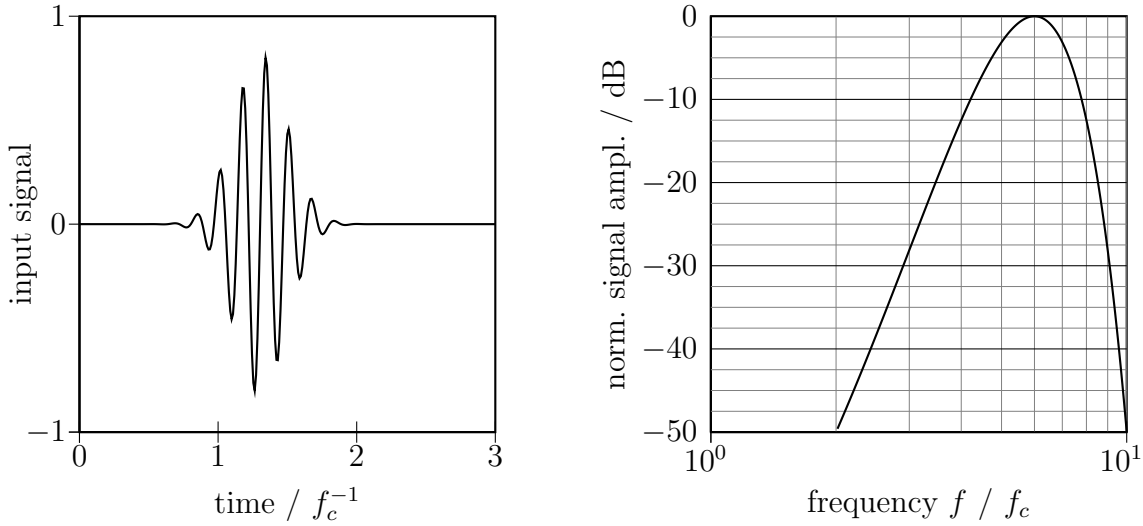

(a) time domain (b) frequency spectrum

Fig. 5.20: Signal for time domain simulation.

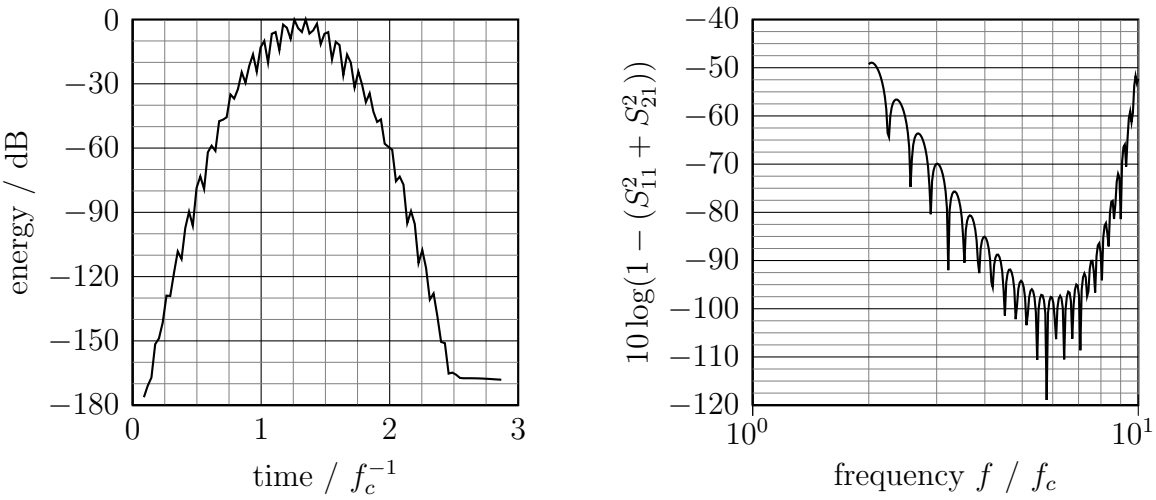

(a) (b)

Fig. 5.21: (a): Total electromagnetic energy in the calculation domain as defined by (3.190) on page 83 for $h_c = 2^{-5}\frac{a}{10}$ with signal input at the coarse grid port 1. (b): Energy balance error, for $h_c = 2^{-5}\frac{a}{10}$ with signal input at the coarse grid port 1.

The reflection coefficients S_{11} and S_{22} for TE_{10}-waves entering at the coarse and the fine grid ports for different discretizations are depicted in Fig. 5.22. Again, artifacts show for higher resolutions, which can be removed by using more exact representations of the time signal and longer simulation times. Fixing a single frequency and refining the grid results in Fig. 5.23. We note convergence of approximately second order in the grid parameter h_c.

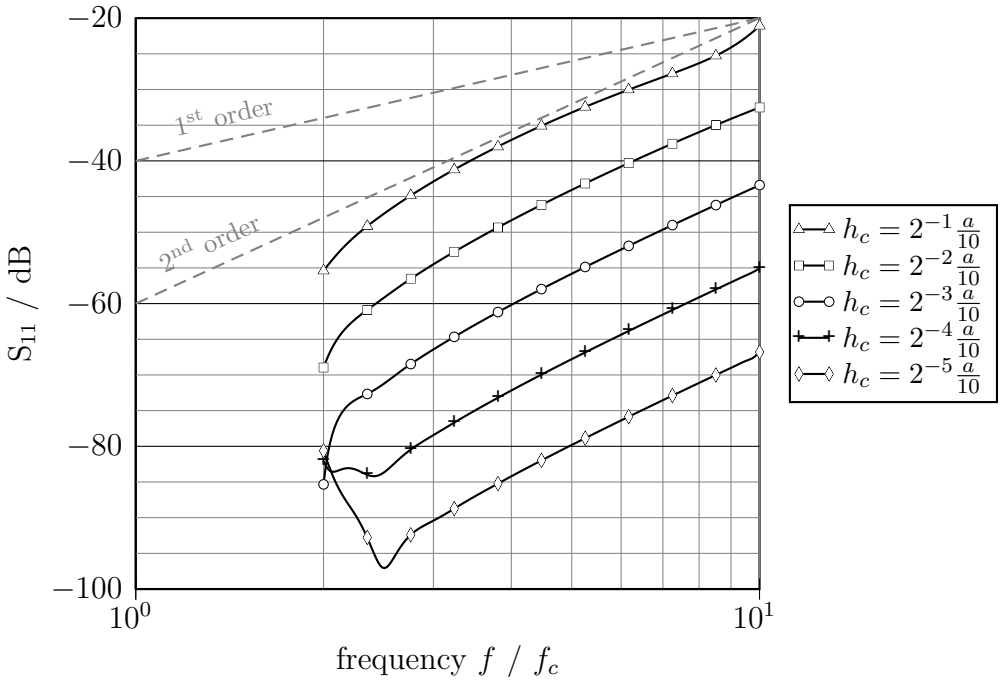

(a) S_{11}

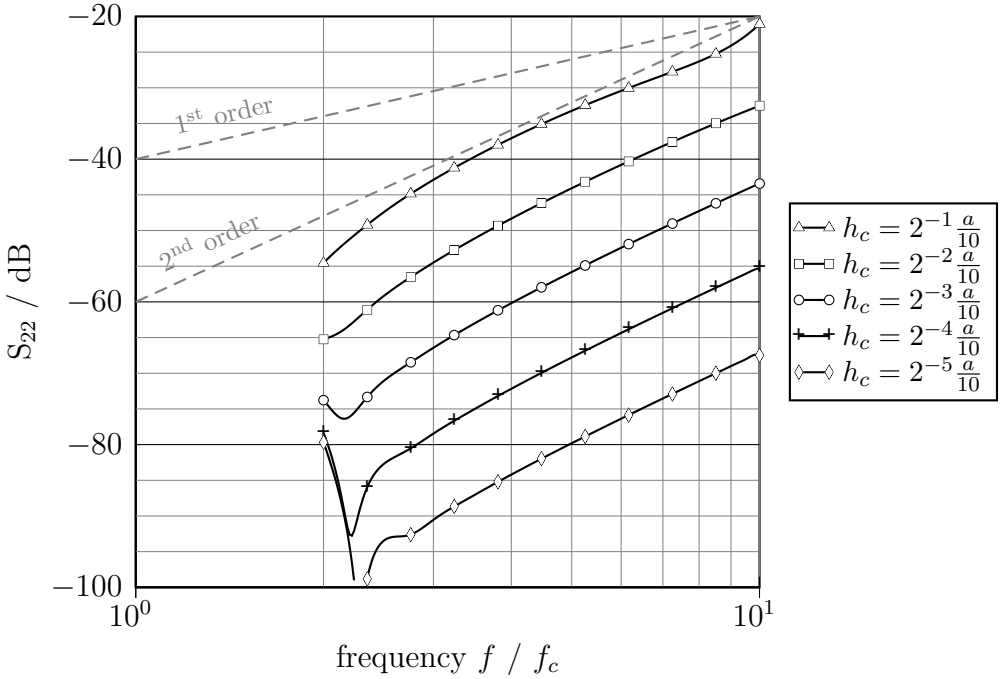

(b) S_{22}

Fig. 5.22: S-parameters over frequency for different grid discretizations for the rectangular waveguide depicted in Fig. 5.19.

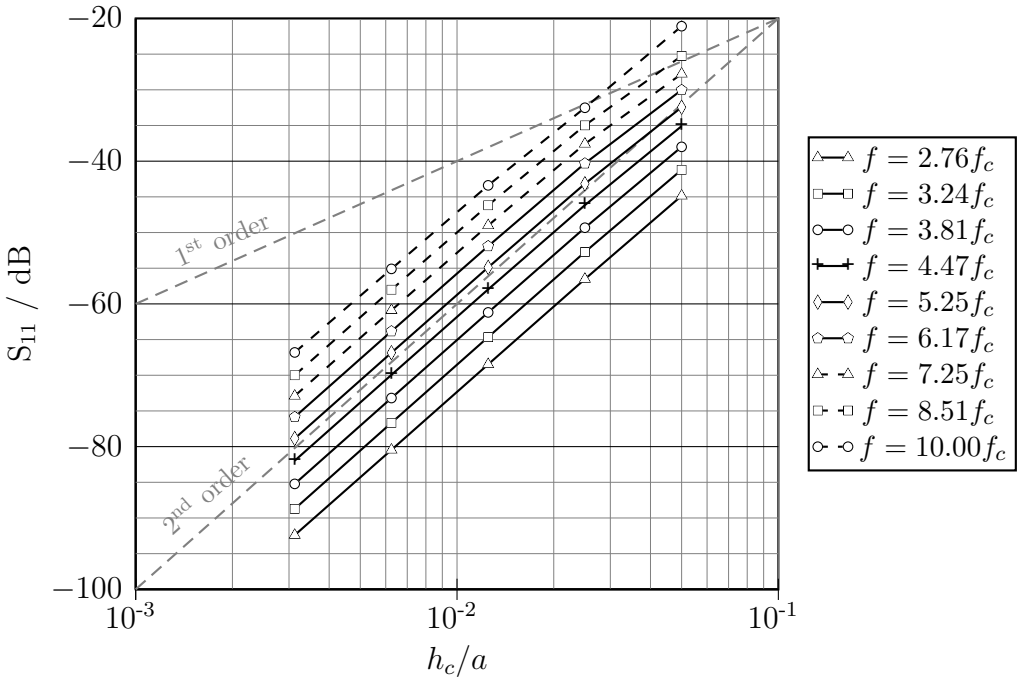

(a) S_{11}

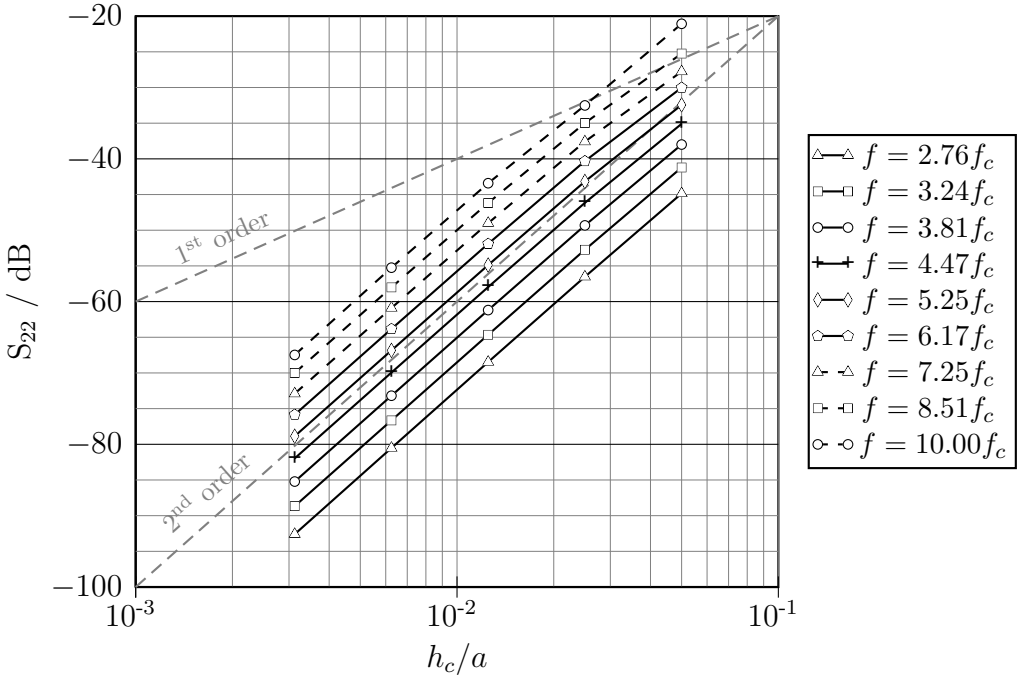

(b) S_{22}

Fig. 5.23: S-parameters over grid size parameter h_c for different frequencies for the rectangular waveguide depicted in Fig. 5.19.

5.4 Hybrid Hexahedral/Tetrahedral Grids

Another application area for polyhedral cells is the use of hybrid hexahedral and tetrahedral grids. Polyhedral grid cells are suited to consistently connect the hexahedral and tetrahedral grid regions. As shortly discussed in chapter 4.5, a pyramidal cell shape was introduced in [40] specifically for this application and is used for hybrid time domain simulations e.g. in [31] and [76]. The consistent removal of additional degrees of freedoms on the tetrahedral side of the coupling region described in [24] can also be reinterpreted as using polyhedral material relations.

5.4.1 3-Dimensional Eigenproblem Example: Partially Filled Resonator with Hybrid Hexahedral/Tetrahedral Grid

We revisit the discrete eigenproblem presented in chapter 5.3.3 but now employ the hybrid hexahedral / tetrahedral grid depicted in Fig. 5.24. The discrete eigenvalue problem and the divergence-free constraint were stated in equations (5.27) and (5.29) on page 142. In

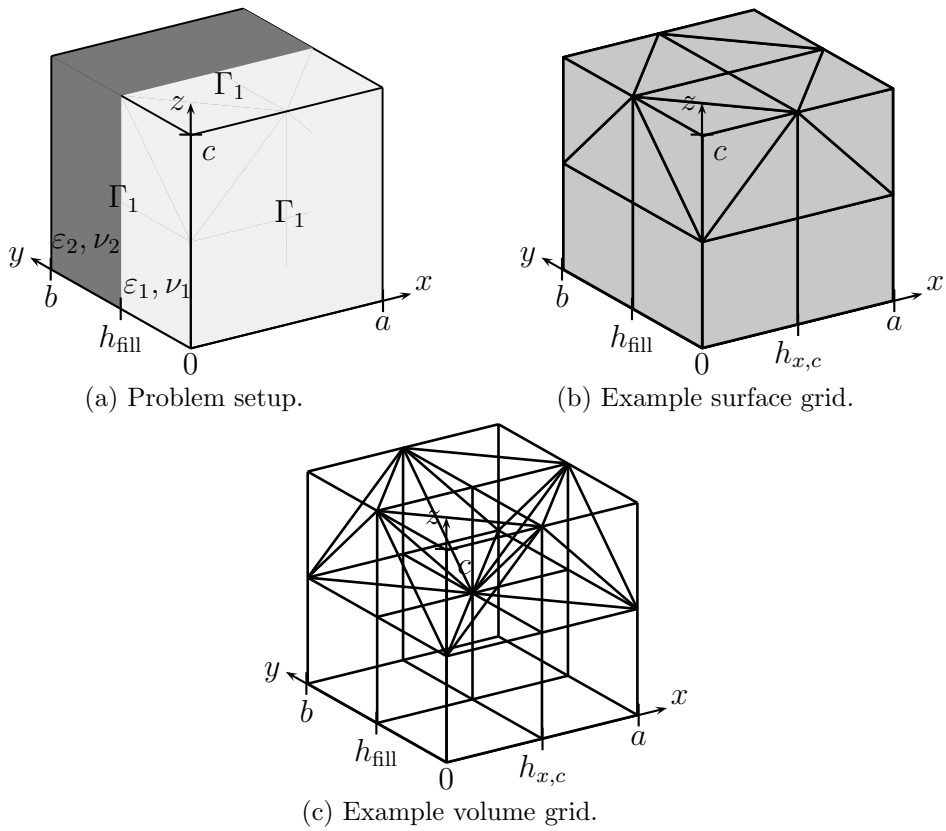

(a) Problem setup.

(b) Example surface grid.

(c) Example volume grid.

Fig. 5.24: (a) Rectangular resonator with $a=1\,\text{mm}$, $b=1.1\,\text{mm}$, $c=1\,\text{mm}$. The resonator is filled with material 1 (ε_1, ν_1) for $0<y<h_{\text{fill}}$ and with material 2 (ε_2, ν_2) for $h_{\text{fill}}<y<b$. Homogeneous electric (PEC) boundary conditions are applied at the boundary $\Gamma_1 = \partial\Omega$ at $x=0$, $x=a$, $y=0$, $y=b$, $z=0$, and $z=c$. (b) and (c) The coarsest grid used in the convergence study. The special polyhedral grid cell depicted in Fig. 5.25 is used to connect the hexahedral to the tetrahedral grid.

the purely hexahedral grid part, standard diagonal FIT material relations are used while in the tetrahedral part standard tetrahedral Whitney-FEM material relations are employed. In order to consistently connect the two grid types, the polyhedral cell depicted in Fig. 5.25 is used with polyhedral material relations as developed in chapter 4. In Fig. 5.26, we again observe second order convergence of the eigenvalues ω in the grid size parameter $h_{x,c}$, as expected.

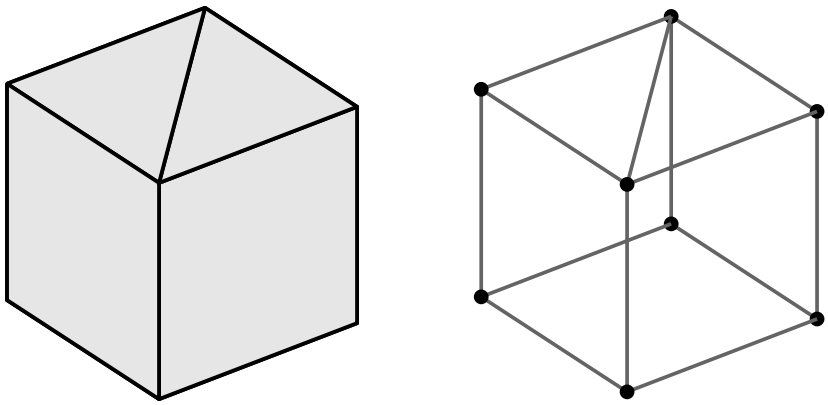

(a) Surface grid. (b) Volume grid.

Fig. 5.25: This special polyhedral grid cell is used to consistently connect the hexahedral and the tetrahedral grids in Fig. 5.24.

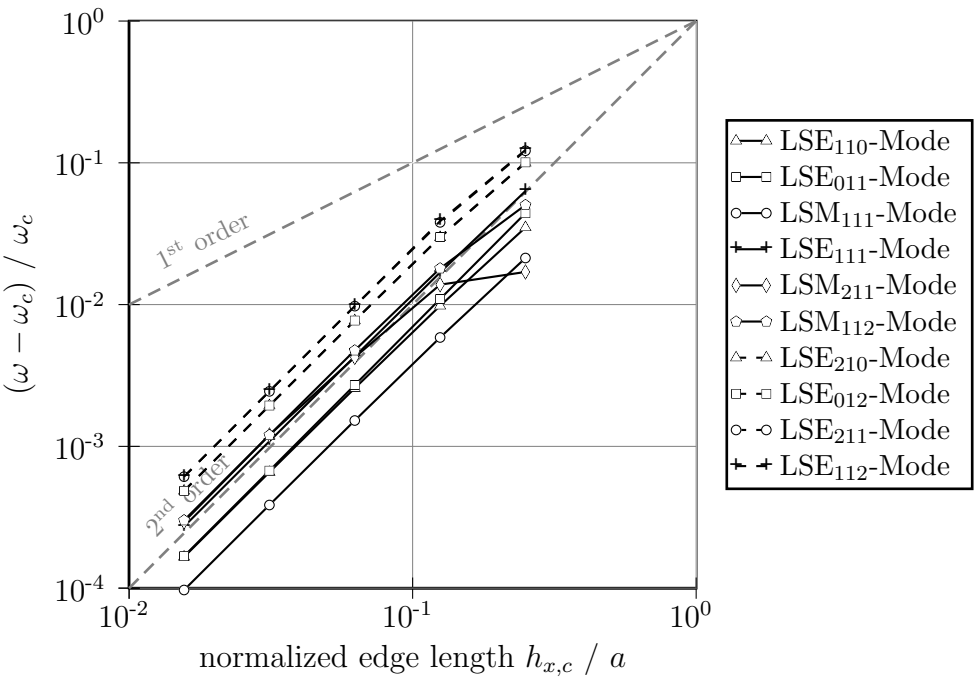

Fig. 5.26: Convergence of the eigenvalues of the first modes for the partially filled rectangular resonator problem depicted in Fig. 5.24 and described by equations (5.27) and (5.29).

5.4.2 3-Dimensional Frequency Domain Example: Dielectric Filter

In this example, the frequency response of a dielectric filter using a hybrid hexahedral / tetrahedral grid is calculated in the frequency domain. The dielectric filter is depicted in Fig. 5.27: It is a 4-pole bandpass filter working around 4GHz with rectangular waveguide feeds. Dielectric disc resonators couple through the waveguide section below cut-off to create the filter characteristic.

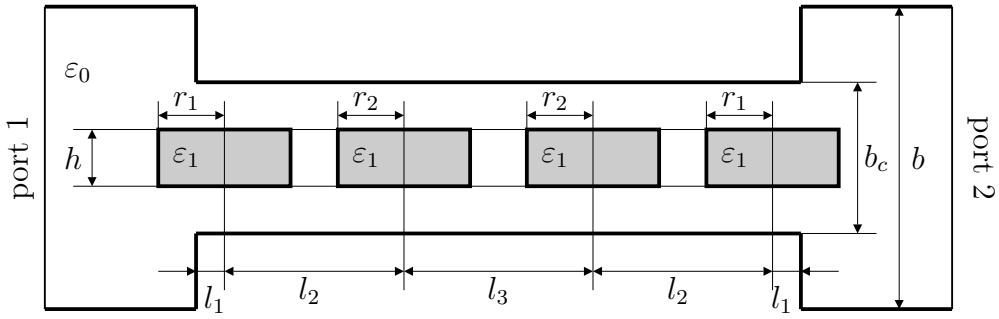

(a) Side view

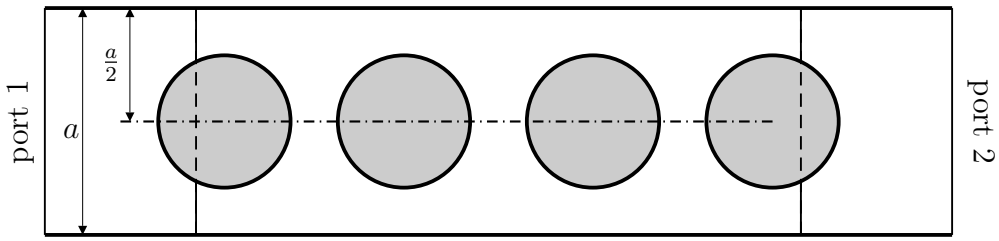

(b) Top view

Fig. 5.27: Rectangular waveguide filter. The design is based on [56, pp. 436]. The rectangular waveguide with perfect electrically conducting side walls is filled with vacuum with permittivity ε_0 and reluctivity ν_0. The dielectric resonators have permittivity $\varepsilon_1 = 36\varepsilon_0$ and reluctivity ν_0. The width of the waveguide is $a = 22.5$mm, the height $b = 47.5$mm and the height of the coupling section is $b_c = 13.1$mm. The radii of the resonators are $r_1 = 6.8775$mm and $r_2 = 7$mm and their height is $h = 7$mm. The placement measures are $l_1 = 5.21$mm, $l_2 = 22.873$mm, and $l_3 = 23.761$mm.

The method described in [79, pp. 124] is used to calculate the S-parameters: First, the port modes are calculated by a 2-dimensional simulation. Then two curl-curl equations in the complex amplitudes of the electric grid voltages $\underline{\widehat{\mathrm{e}}}$ are solved for each frequency using simple electric and magnetic boundary conditions. The S-parameters are extracted by post-processing.

Due to the symmetry of the problem, only one-fourth of the domain was discretized and simulated with the grid shown in Fig. 5.28. Tetrahedral grid cells were used in the region of the dielectric resonators to accurately resolve the curved dielectric boundaries and assure a sufficient resolution for the fields in the coupling section. There are several reasons for using hexahedral grid cells in other parts of the simulation domain, though: E.g. for other connected waveguide components, hexahedral grids might be advantageous in terms of

degrees of freedom or accuracy; for hexahedral grids, port implementations with very low reflections exist; or in time-domain simulations, the coupling to explicit FIT with leapfrog time-discretization might be desired. Thus a hexahedral grid was used in the standard waveguide sections. The consistent transition between the two grid regions is achieved by the special polyhedral cell shown in Fig. 5.25. The transition region between both grid types is shown in Fig. 5.28b.

(a) Complete grid.

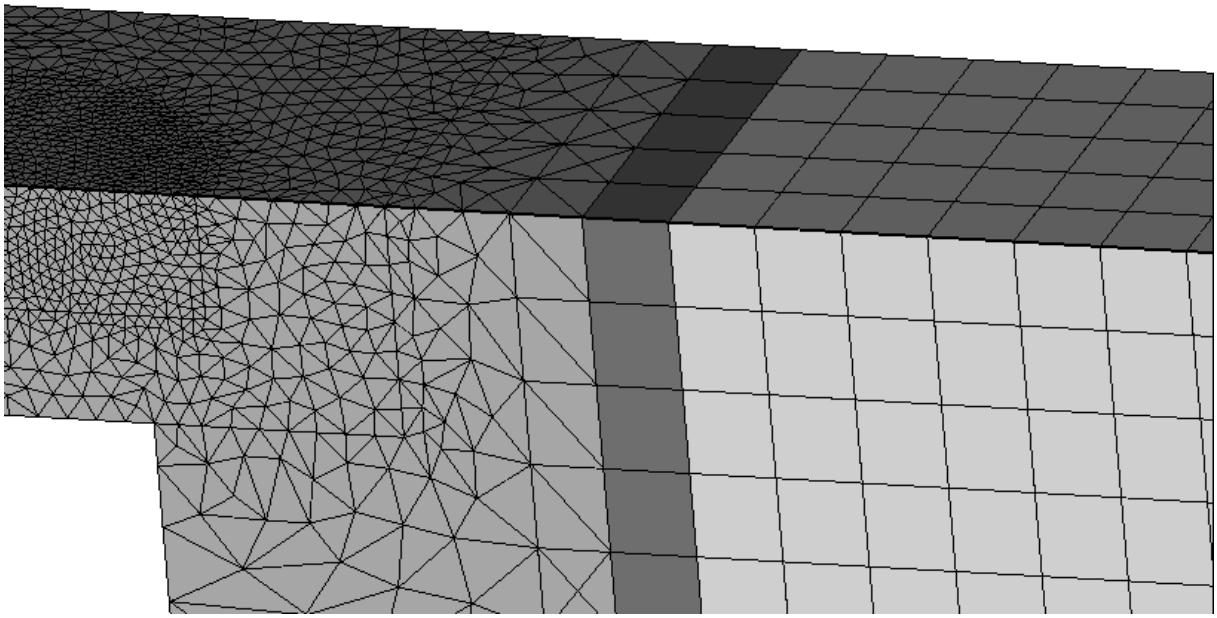

(b) Zoom into transition layer. Shown in dark gray is the transition layer of polyhedral cells.

Fig. 5.28: Grid for the simulation of the waveguide filter depicted in Fig. 5.27. Using the symmetry of the problem, only one-fourth of the problem is discretized and simulated.

The S-parameters calculated in frequency domain are compared with a calculation by CST Microwave Studio® [23] employing a tetrahedral grid in Fig. 5.29. Very good agreement of the results is observed. The maximum difference in S_{21} is 0.3 dB.

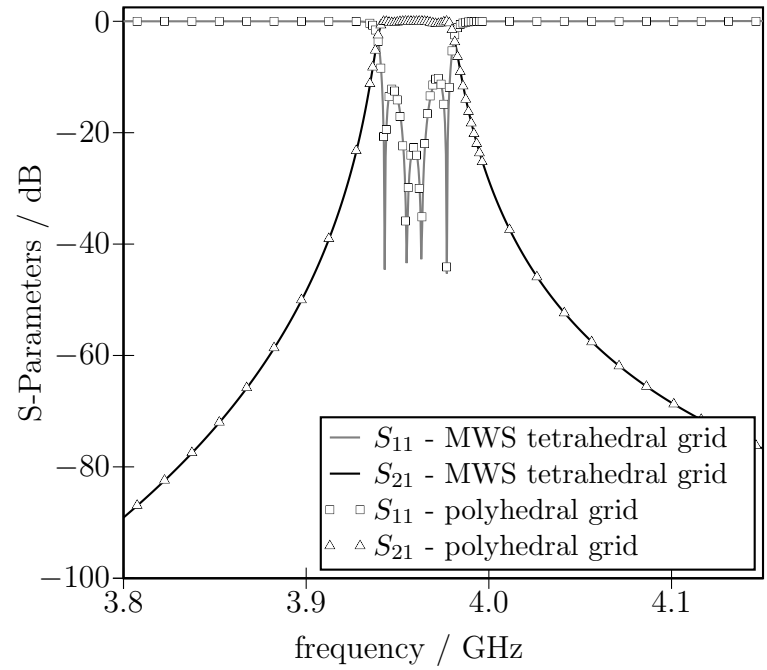

(a)

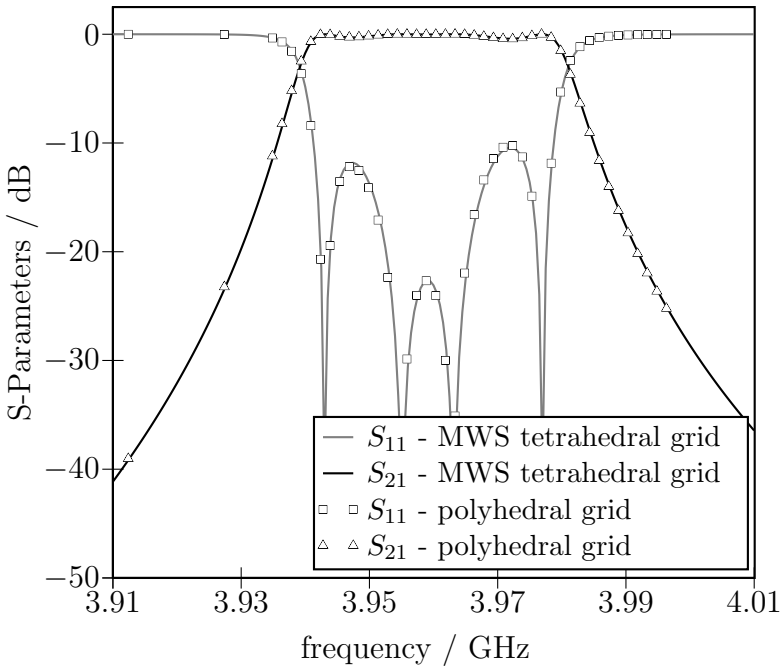

(b)

Fig. 5.29: S-parameters for the dielectric bandpass filter depicted in Fig. 5.27 calculated by CST Microwave Studio® (MWS) [23] employing a tetrahedral grid and by the proposed polyhedral scheme. In (b), an enlargement of the bandpass characteristic of (a) is shown.

6. SUMMARY AND OUTLOOK

The main aim of this thesis was to introduce polyhedral cell shapes into the formalism of the FIT and show their practicability in electromagnetic simulations.

Maxwell's equations in the continuous setting were introduced in chapter 2. In chapter 2.1, the basic mathematical terms and tools needed to state Maxwell's equations were introduced in the language of differential geometry. The separation into topological and metric tools became evident. In chapter 2.2, Maxwell's topological and metric laws were stated separately. Useful topological and metric properties were derived. Complementing Maxwell's equations with suitable initial and boundary values led to Maxwell's initial boundary value problem (IBVP) for which existence and uniqueness of the solution was claimed.

Chapter 3 introduced the discrete Maxwell's Grid Equations of the FIT for general consistent grids. Chapter 3.1 presented the basic mathematical terms and tools needed for the discretization of the spatial variable in analogy to the continuous presentation in chapter 2.1. Maxwell's semi-discrete and fully discrete grid equations were developed in chapters 3.2 and 3.3. For both cases, Maxwell's topological and metric laws were stated, useful topological and metric properties were derived, and existence and uniqueness of the solution for Maxwell's discrete IBVP was shown. Although the question of the discrete material relations for polyhedral cells was postponed until chapter 4, all other needed topological and metric tools were provided for general consistent grids.

The mathematical rigorous treatment of the discrete setting in parallel to the continuous setting clarified many concepts. E.g. the conservation of charge is recognized as direct consequence of the sequence property, the existence of potentials to hinge on the Poincaré Lemma and deRham Theorem, and Poynting's Theorem to result from a specific partial integration formula. The interpretation of Poynting's Theorem as a conservation law for energy required the continuous or discrete metrics to be positive definite. The positive definite metric also led to existence and uniqueness of the solutions as well as stability of the discrete scheme.

The setting of the FIT as presented in chapter 3 is already general enough to define all discrete operators except for the material matrices for general consistent grids. General requirements on the discrete material relations had been stated in chapter 3, though. Therefore, chapter 4 concentrated on constructing material relations for planar-faced polyhedral grid cells fulfilling these requirements. As basis for the construction scheme, Whitney-FEM material operators were introduced in the FIT in chapter 4.1. The Whitney-FEM material operators were generalized to polyhedral grid elements in the following chapters based on the scheme outlined in [19]: Chapter 4.2 used analytical BVPs to derive the discrete material operators, while in chapters 4.3 and 4.4, discretized versions of the BVPs

were discussed. Although the presentation concentrated on the 3-dimensional case, it can be directly generalized to n-dimensional polytope grid cells.

The availability of polyhedral grid cells allows for a completely new gridding flexibility. Cases like subgridding, hybrid hexahedral / tetrahedral grids, or domain coupling along arbitrary interfaces can now be treated consistently in the FIT. As the construction algorithms of material relations seem too expensive for complicated arbitrary polyhedral grids and anyway no grid generators are known for such complicated grids, it is believed that polyhedral elements will first be used for such special application scenarios. The 2- and 3-dimensional applications in chapter 5 showed hybrid hexahedral / tetrahedral grids and subgridding scenarios from the fields of electrostatics and electrodynamics both in frequency- and time-domain. The expected convergence rates were verified by the numerical experiments.

Besides the main goal of distilling the known concepts of the FIT for arbitrary consistent grids and filling the gap of material relations for polyhedral cells, several minor achievements have been accomplished in this thesis:

- Maxwell's IBVP for the semi-discrete and fully discrete case have been stated rigorously and existence and uniqueness of their solutions were shown. Although several simplifications were made to shorten the presentation, extensions to conductive materials, more complex material relations, and more complex boundary conditions are possible.

- The boundary of the dual grid was rigorously included in the development of Maxwell's Grid Equations. This rendered a consistent discretization of the exterior derivative on the dual grid up to the boundary. All boundary terms needed e.g. for developing open boundary conditions, coupling to other domains, and the statement of the global Poynting's Theorem have been retained in this development. For simplicial grids, this rigorous boundary treatment has been found to be similar to the treatment in [3].

- The enhanced dual grid introduced in appendix A generalizes the concept of consistent discretizations on the dual grid. It allows for the calculation of local exterior products of primal and dual quantities for all degrees. Thus a local Poynting's Theorem has been derived.

- The use of the term stability and its application to the FIT was clarified in the stability discussions in chapters 3.2 and 3.3. To set the stage for a convergence analysis, the inclusion of source terms is missing, but the basic concepts were presented in a stream-lined manner.

- As a specific time-discretization allowing for hybrid explicit / implicit schemes, the Newmark-Θ method was incorporated in chapter 3.3 into the FIT formalism. A preserved energy quantity was derived, which has, to the author's knowledge, not been reported before.

There are several topics for further research of the polyhedral material relations:

- Although the notion of *stability* was considered in this thesis, *consistency* and *convergence* have not been proven for the derived polyhedral numerical schemes. The development of the polyhedral material relations was guided by the properties used in [48] for convergence analysis of the tetrahedral Whitney-FEM. It is believed that convergence for the polyhedral scheme can thus be proven in analogue to [48]. Interesting ideas for the framework of the FIT can also be found in [47], where the convergence analysis of the scheme is reduced to the consistency analysis of the material relations.

- The framework of the FIT can be extended to higher order schemes in the sense of the Whitney-FEM as described in [48]. The question of finding higher order material relations, that is higher order basis functions, for general polyhedral cells is still open. An interesting start might be the development of higher order basis functions for pyramidal cells in [41].

- The polyhedral scheme was presented and tested for straight-edged flat-faced polyhedra. The construction algorithm for the basis functions can directly be generalized to arbitrarily curved polyhedra, though. The convergence properties of such elements is not clear at this point. Especially the realization of *bent* edges with corners would open new possibilities: One could directly construct material relations on the barycentric dual grid of an arbitrary tetrahedral grid and thereby arrive at explicit time domain schemes. In multigrid schemes for unstructured grids, bent edges and surfaces allow for arbitrary coarsening while retaining the original material boundaries.

- Possible multigrid schemes hinted at above lead to the question on whether and how one can include material distributions in the construction of the polyhedral material relations. The convergence properties are again unclear at this point.

- The construction scheme for the polyhedral material relations required the solution of either analytical or discrete BVPs. First steps were taken to reduce the construction scheme to geometric computations. Although for the 2-dimensional case, a geometric construction formula was found for practical applications, the proof for this formula to hold in general and its extension to the 3-dimensional setting are open problems. Also, one can search for simpler construction methods of consistent polyhedral material relations, e.g. by algebraically stating the requirements for consistency on some intermediate approximation spaces. This idea seems similar to the approach taken by the polyhedral mimetic scheme presented in [14] for certain approximation spaces. To this end, the basic requirements for consistency and convergence have to be better understood.

- The polyhedral basis functions derived in chapter 4 all have pointwise continuous trace across inter-element boundaries. As discussed shortly in chapter 4.5, Nitsche's method opens a possibility to use basis functions for which only the integral values of the jump terms evaluate to zero. This possibility can be explored further.

- When introducing the polyhedral material relations, no explicit definition of a dual grid was needed, as for standard Whitney-FEM schemes. For the Whitney-FEM with tetrahedral cells, the barycentric dual grid has been realized as a suitable choice

[9, pp. 99]. Are there suitable choices for a dual grid for the polyhedral material relations stated in this thesis?

- The polyhedral scheme needs to be tested in practical problems and compared to existing schemes in order to assess the computational advantages and disadvantages in different application scenarios. For this, an efficient implementation of the polyhedral scheme is required.

Further research topics in regards to the FIT for consistent grids are:

- The conductivity law, more complex material relations, as well as more general boundary conditions need to be included in the treatment of chapter 3.
- There are still open questions regarding quantities stemming from products of primal with dual quantities. The energies as exterior products of a primal with a dual quantity are widely used, but interpretations in the discrete setting do not seem satisfactory. The enhanced dual grid introduced in appendix A localizes all products on (clusters of) primal grid elements. Other interpretations are possible, see e.g. the localization on dual grid elements for the energy and Poynting vector in [13].
- Some questions regarding the enhanced dual grid introduced in appendix A are still open. The point of view of more general dual, or better secondary, grids can be further explored upon.
- The calculation of forces and momenta, inclusion of moving media, and the incorporation of time-adaptive grids for arbitrary consistent grids in the framework of the FIT is unclear. To this end, the concepts of contraction and Lie derivative from differential geometry need to be translated consistently into the discrete setting. For tetrahedral grids, ideas on this can be found in [12] and [13].

APPENDIX

A. ENHANCED DUAL GRID

As mentioned in [47], one has more leeway in the choice of the dual grid as may seem at first sight. In this appendix, we will basically work out the ideas given in [47] for a general consistent splitting of our grid into several parts. In the extreme case, one can take an element by element splitting. The resulting enhanced dual grid provides a consistent boundary treatment, allows for the calculation of local outer products, and provides a local partial integration formula. For the setting of Maxwell's equations, the local partial integration formula leads to a local discrete Poynting's Theorem.

The formulation is derived for a general n-dimensional domain denoted by Ω^n. The definitions of primal and dual grid, cochains, etc. given in chapter 3 are assumed generalized to the n-dimensional setting.

A.1 Definitions and Topological Tools and Properties

In order to calculate local quantities like energies in some part of the grid or the energy flux through some collection of faces in the grid, we have to identify these grid parts of interest. In this chapter, the primal grid is divided into the grid parts of interest and a local dual grid is introduced on each of the resulting primal grid parts. The union of all local dual grids then results in the enhanced dual grid allowing for the local calculation of the wanted quantities. The enhanced dual grid is already useful in the case of a single domain of interest with boundaries: It enhances the standard dual grid of the domain by a boundary discretization and thus provides a consistent discretization of the exterior derivative up to the boundary. It also allows e.g. for the calculation of the Poynting vector on the domain boundary.

The scheme is illustrated by Fig. A.1: Fig. A.1a shows an example consistent primal grid Ω_h^2 of a 2-dimensional domain Ω^2. Fig. A.1b depicts a standard dual grid $\underset{\sim}{\Omega}_h^2$ of this primal grid. In Fig. A.1c, different parts of interest Γ_i^l of the primal grid are shown in an explosive view. Note that the parts of interest are each open, that they can be built from the union of elements of the primal grid and that they themselves are a consistent grid of the domain Ω^2. Such a division of the domain Ω^2 for the grid Ω_h^2 will be called a *consistent subdivision* for the grid Ω_h^2. The parts of the primal grid Ω_h^2 in each subdivision element Γ_i^l define a consistent grid for Γ_i^l, which is called the grid part $\overline{\Gamma}_{i,h}^l$ in accordance with Definition 3.7 on page 40. The grid parts $\overline{\Gamma}_{i,h}^l$ are depicted in Fig. A.1d. On each grid part $\overline{\Gamma}_{i,h}^l$, we can introduce a *local dual grid* $\underset{\sim}{\Gamma}_{i,h}^l$ as illustrated in Fig. A.1e. The union of

all local dual grids $\underset{\sim}{\Gamma}^l_{i,h}$ forms the enhanced dual grid $\overline{\underset{\sim}{\Omega}}^2_h$ as shown in Fig. A.1f. Note that the enhanced dual grid $\overline{\underset{\sim}{\Omega}}^2_h$ is now a consistent grid of the complete domain Ω^2 including its boundary. Thus it is suited not only to solve the problem of calculating local exterior products, but also to introduce a rigorous boundary treatment for the dual quantities. It generalizes the boundary treatment of the dual grid established in chapter 3.2.1 for the specific case of Maxwell's equations.

In the following, we formalize the definition of the enhanced dual grid for a consistent primal grid Ω^n_h of an n-dimensional domain Ω^n. We first define the *subdivision* of the primal grid into the parts of interest:

Definition A.1 (Consistent subdivision for a consistent grid)**.** A subdivision of a consistent grid Ω^n_h into disjunct l-dimensional elements Γ^l_i, $i = [1..n_{\Gamma^l}]$, $l = [0..n]$ with the following properties

I. All elements Γ^l_i are contractible open unions of elements $S^k_j \in \boldsymbol{S}^k(\Omega^n_h)$, $k \leq l$ of the grid Ω^n_h.

II. The boundary of each element Γ^l_i is the union of the closure of elements Γ^{l-1}_j.

III. For $l < n$, each element Γ^l_i is contained in the boundary of an element Γ^{l+1}_j.

IV. For each element Γ^l_i, an arbitrary inner orientation is chosen.

is called a *consistent subdivision* for the consistent grid Ω^n_h and denoted by $\mathrm{Sub}(\Omega^n_h)$. By $\overline{\Gamma}^l_i$, we want to denote the closure of Γ^l_i and by $\overline{\Gamma}^l_{i,h}$ the primal grid part of Ω^n_h defined by the elements in $\overline{\Gamma}^l_i$ according to Definition 3.7 on page 40. The set of grid elements in the grid part $\overline{\Gamma}^l_{i,h}$ are denoted by $\boldsymbol{S}^k(\overline{\Gamma}^l_{i,h})$. The set of indices of the elements $\boldsymbol{S}^k(\overline{\Gamma}^l_{i,h})$ in the global numbering is denoted by $\mathrm{I}^k_{\overline{\Gamma}^l_{i,h}}$ and the number of entries in $\mathrm{I}^k_{\overline{\Gamma}^l_{i,h}}$ by $n^k_{\overline{\Gamma}^l_{i,h}}$.

This definition is very close to the one of the consistent grid Ω^n_h itself; in particular, the set of elements of the consistent grid Ω^n_h forms a consistent subdivision of Ω^n_h.

Also a splitting of Ω^n_h into the interior $\mathring{\Omega}^n$ and the disjunct boundary parts Γ^{n-1}_j is a consistent subdivision of Ω^n_h.

For the subdivision $\mathrm{Sub}(\Omega^n_h)$, the boundary operator $\boldsymbol{\partial}^l_{\mathrm{Sub}}$ is defined in matrix notation as follows:

$$\boldsymbol{\partial}^l_{\mathrm{Sub}} \in \mathbb{R}^{n_{\Gamma^{l-1}} \times n_{\Gamma^l}} \tag{A.1a}$$

$$\left(\boldsymbol{\partial}^l_{\mathrm{Sub}}\right)_{ij} = \begin{cases} \pm 1 & \text{if } \Gamma^{l-1}_i \text{ lies in } \partial\Gamma^l_j \text{ in positive/negative direction} \\ 0 & \text{otherwise} \end{cases} \tag{A.1b}$$

We can restrict primal cochains $\boldsymbol{\omega}^k \in \mathcal{F}^k_h(\Omega^n_h)$ onto the grid parts $\overline{\Gamma}^l_{i,h}$ by the primal trace operators $\mathbf{T}^k_{\overline{\Gamma}^l_{i,h}}$ defined according to Definition 3.8 on page 41. The resulting *local primal cochains* will be denoted by the subscript $\overline{\Gamma}^l_{i,h}$:

$$\boldsymbol{\omega}^k_{\overline{\Gamma}^l_{i,h}} \equiv \mathbf{T}^k_{\overline{\Gamma}^l_{i,h}} \boldsymbol{\omega}^k \tag{A.2}$$

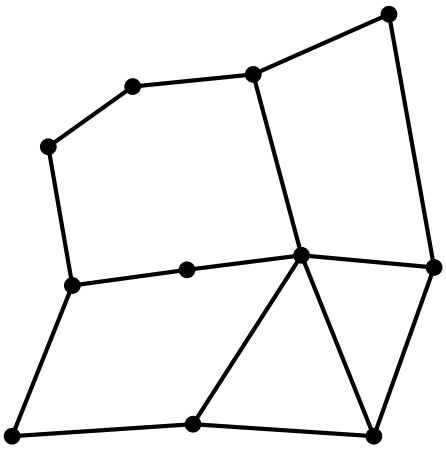

(a) Primal grid Ω_h^2 of the domain Ω^2.

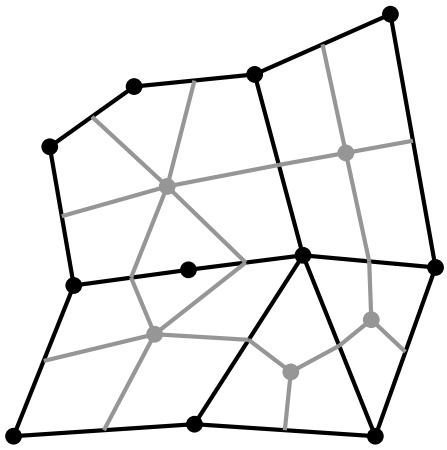

(b) Primal grid Ω_h^2 (in black) with a standard dual grid $\underset{\sim}{\Omega}_h^2$ (in gray).

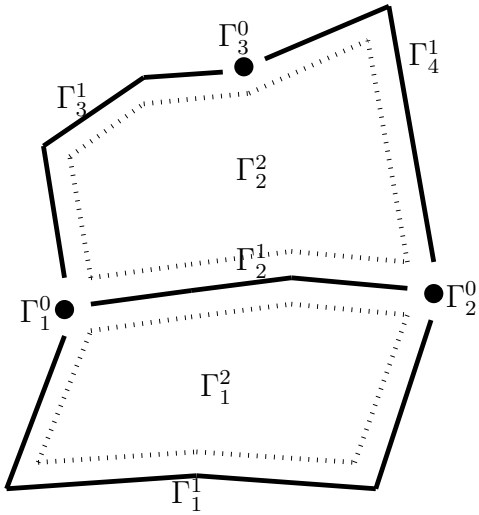

(c) Consistent subdivision for the primal grid Ω_h^2 into open subdivision elements Γ_i^l (explosive view).

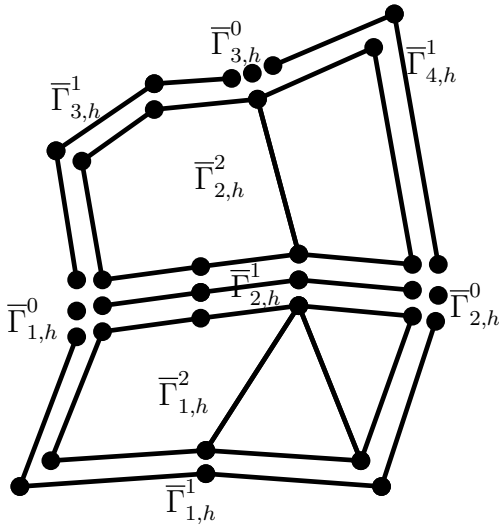

(d) Primal grid parts $\overline{\Gamma}_{i,h}^l$ for the consistent subdivision shown in Fig. A.1c (explosive view).

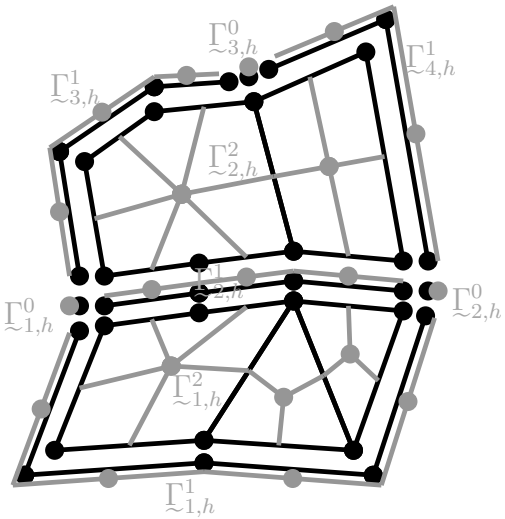

(e) Local dual grids $\underset{\sim}{\Gamma}_{i,h}^l$ (in gray) for the primal grid parts $\overline{\Gamma}_{i,h}^l$ (in black; explosive view).

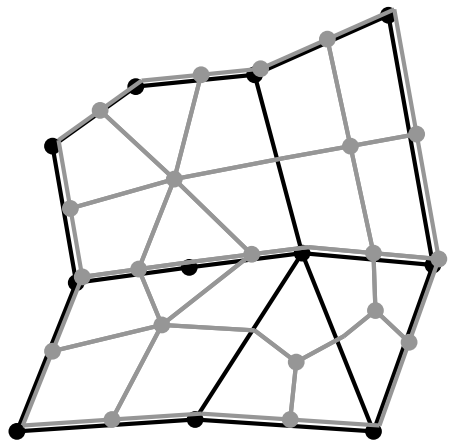

(f) Primal grid Ω_h^2 (in black) with an enhanced dual grid $\overline{\underset{\sim}{\Omega}}_h^2$ (slightly offset, in gray) for the subdivision shown in Fig. A.1c.

Fig. A.1: Illustration of the construction steps for an enhanced dual grid. The orientations of the grid and subdivision elements have been omitted for better view.

We introduce the *local primal exterior derivatives* $\mathbf{D}^k_{\overline{\Gamma}^l_{i,h}}$:

$$\mathbf{D}^k_{\overline{\Gamma}^l_{i,h}} \equiv \mathbf{T}^{k+1}_{\overline{\Gamma}^l_{i,h}} \mathbf{D}^k \left(\mathbf{T}^k_{\overline{\Gamma}^l_{i,h}}\right)^{\mathrm{T}} \tag{A.3}$$

Because the exterior derivative acts only locally, we note the following relation:

$$\mathbf{D}^k_{\overline{\Gamma}^l_{i,h}} \boldsymbol{\omega}^k_{\overline{\Gamma}^l_{i,h}} = \mathbf{D}^k_{\overline{\Gamma}^l_{i,h}} \mathbf{T}^k_{\overline{\Gamma}^l_{i,h}} \boldsymbol{\omega}^k = \mathbf{T}^{k+1}_{\overline{\Gamma}^l_{i,h}} \mathbf{D}^k \left(\mathbf{T}^k_{\overline{\Gamma}^l_{i,h}}\right)^{\mathrm{T}} \mathbf{T}^k_{\overline{\Gamma}^l_{i,h}} \boldsymbol{\omega}^k = \mathbf{T}^{k+1}_{\overline{\Gamma}^l_{i,h}} \mathbf{D}^k \boldsymbol{\omega}^k \tag{A.4}$$

which states the commutativity of the primal exterior derivatives with the primal trace operators.

Now we define the *enhanced dual grid* for a consistent subdivision $\mathrm{Sub}(\Omega^n_h)$:

Definition A.2 (Enhanced dual grid)**.** Denote by $\underset{\sim}{\Gamma}^l_{i,h}$ the (open) dual grid of the primal grid part $\overline{\Gamma}^l_{i,h}$, i.e. the collection $\underset{\sim}{\boldsymbol{S}}^k(\underset{\sim}{\Gamma}^l_{i,h})$ of elements $\underset{\sim}{S}^m_{\underset{\sim}{\Gamma}^l_{i,h},j}$ dual to each element $S^m_{\overline{\Gamma}^l_{i,h},j} \in \boldsymbol{S}^m(\overline{\Gamma}^l_{i,h})$ for $m \leq l$. The outer orientations of the dual elements are chosen as induced by the inner orientations of the defining primal elements. Then the collection of all outer-oriented dual grid elements $\underset{\sim}{\boldsymbol{S}}^m(\underset{\sim}{\Gamma}^l_{i,h})$ for $l = [0..n]$ and $m \leq l$ defines the *enhanced dual grid* and is denoted by $\overline{\underset{\sim}{\Omega}}^n_h$. Let $\underset{\sim}{\mathrm{I}}^k_{\underset{\sim}{\Gamma}^l_{i,h}}$ denote the indices of the elements dual to the primal ones with indices $\mathrm{I}^k_{\overline{\Gamma}^l_{i,h}}$ in the same order, i.e. $\underset{\sim}{\mathrm{I}}^k_{\underset{\sim}{\Gamma}^l_{i,h}} = \mathrm{I}^k_{\overline{\Gamma}^l_{i,h}}$. There are $\underset{\sim}{n}^k_{\underset{\sim}{\Gamma}^l_{i,h}} = n^k_{\overline{\Gamma}^l_{i,h}}$ entries in $\underset{\sim}{\mathrm{I}}^k_{\underset{\sim}{\Gamma}^l_{i,h}}$. The k-dimensional elements of $\overline{\underset{\sim}{\Omega}}^n_h$ are denoted by $\overline{\underset{\sim}{S}}^k_i \in \overline{\underset{\sim}{\boldsymbol{S}}}^k(\overline{\underset{\sim}{\Omega}}^n_h)$. The number of k-dimensional grid elements in $\overline{\underset{\sim}{\Omega}}^n_h$ denoted by $\overline{\underset{\sim}{n}}^k$ is

$$\overline{\underset{\sim}{n}}^k = \sum_{l=k}^{n} \sum_{i=1}^{n_{\Gamma^l}} \underset{\sim}{n}^k_{\underset{\sim}{\Gamma}^l_{i,h}} = \sum_{l=k}^{n} \sum_{i=1}^{n_{\Gamma^l}} n^k_{\overline{\Gamma}^l_{i,h}} \tag{A.5}$$

Note that we do have more elements in the enhanced dual grid than in the primal grid. Also note that the enhanced dual grid is a consistent grid for the complete problem domain $\overline{\Omega}^n$. So all quantities and operators defined in chapter 3 for a (primal) consistent grid are available for the enhanced dual grid. The grid discretization operators according to Definition 3.6 on page 37 will be denoted by $\overline{\underset{\sim}{\mathrm{L}}}^k$ and called the *enhanced dual grid discretization operators*. The discrete exterior derivatives of this consistent grid $\overline{\underset{\sim}{\Omega}}^n_h$ according to Definition 3.10 on page 43 will be denoted by $\overline{\underset{\sim}{\mathbf{D}}}^k$ and called the *enhanced dual exterior derivatives*. Note that the discrete exterior derivative $\overline{\underset{\sim}{\mathbf{D}}}^k$ and the continuous exterior derivative d^k do commute under the enhanced dual grid discretization operator $\overline{\underset{\sim}{\mathrm{L}}}^k$, as the enhanced dual grid describes a consistent grid of the complete domain including the boundary:

$$\overline{\underset{\sim}{\mathrm{L}}}^{k+1} \mathrm{d}^k \omega^k = \overline{\underset{\sim}{\mathbf{D}}}^k \overline{\underset{\sim}{\mathrm{L}}}^k \omega^k \tag{A.6}$$

Thus the enhanced dual grid is suitable for a consistent discretization of differential equations on a domain with boundary. The boundary treatments introduced in chapter 3.2 and used for the application examples in chapter 5 are special examples for the use of enhanced dual grids.

The space of k-cochains on the enhanced dual grid according to Definition 3.5 is denoted by $\mathcal{F}_h^k(\underset{\sim}{\overline{\Omega}}_h^n)$ and will be called the *space of enhanced dual k-cochains*. The elements of these spaces will be called *enhanced dual k-cochains* and denoted by $\underset{\sim}{\overline{\boldsymbol{\omega}}}^k$. We define the *enhanced dual trace operators* $\underset{\sim}{\overline{\mathbf{T}}}^k_{\underset{\sim}{\Gamma}^l_{i,h}}$ as:

$$\underset{\sim}{\overline{\mathbf{T}}}^k_{\underset{\sim}{\Gamma}^l_{i,h}} : \qquad \underset{\sim}{\overline{\boldsymbol{\omega}}}^k \in \mathcal{F}_h^k(\underset{\sim}{\overline{\Omega}}_h^n) \longmapsto \underset{\sim}{\overline{\mathbf{T}}}^k_{\underset{\sim}{\Gamma}^l_{i,h}} \underset{\sim}{\overline{\boldsymbol{\omega}}}^k \in \underset{\sim}{\mathcal{F}}_h^k(\underset{\sim}{\Gamma}^l_{i,h}) \tag{A.7}$$

$$\left(\underset{\sim}{\overline{\mathbf{T}}}^k_{\underset{\sim}{\Gamma}^l_{i,h}}\right)_{mn} = \begin{cases} +1 & \text{if } \underset{\sim}{\Gamma}^k_{\underset{\sim}{\Gamma}^l_{i,h}}(m) = n \\ 0 & \text{otherwise} \end{cases} \tag{A.8}$$

Note that the ranges of these trace operators are the spaces of cochains on the local dual grids, while the domains are the spaces of cochains on the (consistent) enhanced dual grid. The ranges of different enhanced dual trace operators are always disjunct, so we get:

$$\underset{\sim}{\overline{\mathbf{T}}}^k_{\underset{\sim}{\Gamma}^l_{i,h}} \left(\underset{\sim}{\overline{\mathbf{T}}}^m_{\underset{\sim}{\Gamma}^p_{j,h}}\right)^{\mathrm{T}} = \begin{cases} \mathbf{I} & \text{if } k = m \text{ and } l = p \text{ and } i = j \\ \mathbf{0} & \text{otherwise} \end{cases} \tag{A.9}$$

where $\mathbf{I}$ denotes the identity matrix of appropriate dimension. The *local dual k-cochains* will be denoted by the subscript $\underset{\sim}{\Gamma}^l_{i,h}$:

$$\underset{\sim}{\boldsymbol{\omega}}^k_{\underset{\sim}{\Gamma}^l_{i,h}} \equiv \underset{\sim}{\overline{\mathbf{T}}}^k_{\underset{\sim}{\Gamma}^l_{i,h}} \underset{\sim}{\overline{\boldsymbol{\omega}}}^k \tag{A.10}$$

and the *local dual exterior derivative* by $\underset{\sim}{\mathbf{D}}^{l-k}_{\underset{\sim}{\Gamma}^l_{i,h}}$:

$$\underset{\sim}{\mathbf{D}}^k_{\underset{\sim}{\Gamma}^l_{i,h}} \equiv \underset{\sim}{\overline{\mathbf{T}}}^{k+1}_{\underset{\sim}{\Gamma}^l_{i,h}} \underset{\sim}{\overline{\mathbf{D}}}^k \left(\underset{\sim}{\overline{\mathbf{T}}}^k_{\underset{\sim}{\Gamma}^l_{i,h}}\right)^{\mathrm{T}} \tag{A.11}$$

Note that in contrast to the local primal cochains $\boldsymbol{\omega}^k_{\overline{\Gamma}^l_{i,h}}$, the local dual cochains $\underset{\sim}{\boldsymbol{\omega}}^k_{\underset{\sim}{\Gamma}^l_{i,h}}$ describe only the quantities truly inside the subdivision elements Γ^l_i and not the quantities on their boundaries. Similarly, the local dual exterior derivatives only describe the contributions from within the subdivision elements Γ^l_i to the exterior derivative and do not include any contributions from the boundaries. For each subdivision element Γ^l_i, the local dual exterior derivative is equivalent to the standard dual exterior derivative defined in chapter 3.2. So according to equations (3.51) on page 46, the following local duality relation of the local primal and dual exterior derivatives holds:

$$\underset{\sim}{\mathbf{D}}^{l-k}_{\underset{\sim}{\Gamma}^l_{i,h}} = (-1)^k \left(\mathbf{D}^{k-1}_{\overline{\Gamma}^l_{i,h}}\right)^{\mathrm{T}} \tag{A.12}$$

Using the definitions in equations (A.3) and (A.11), this renders:

$$\Leftrightarrow \qquad \underset{\sim}{\overline{\mathbf{T}}}^{l-k+1}_{\underset{\sim}{\Gamma}^l_{i,h}} \underset{\sim}{\overline{\mathbf{D}}}^{l-k} \left(\underset{\sim}{\overline{\mathbf{T}}}^{l-k}_{\underset{\sim}{\Gamma}^l_{i,h}}\right)^{\mathrm{T}} = (-1)^k \left(\mathbf{T}^k_{\overline{\Gamma}^l_{i,h}} \mathbf{D}^{k-1} \left(\mathbf{T}^{k-1}_{\overline{\Gamma}^l_{i,h}}\right)^{\mathrm{T}}\right)^{\mathrm{T}} \tag{A.13}$$

Further on, we note the following local splitting of the (local trace of the) enhanced dual exterior derivative into the contributions from the inner part of Γ_i^l and the boundary parts of Γ_i^l:

$$\overline{\underset{\sim}{\mathbf{T}}}^{k+1}_{\underset{\sim}{\Gamma}^l_{i,h}} \overline{\underset{\sim}{\mathbf{D}}}^k = \underset{\sim}{\mathbf{D}}^k_{\underset{\sim}{\Gamma}^l_{i,h}} \overline{\underset{\sim}{\mathbf{T}}}^k_{\underset{\sim}{\Gamma}^l_{i,h}} + \sum_{j=1}^{n_{\Gamma^{l-1}}} \left(\boldsymbol{\partial}^l_{\mathrm{Sub}}\right)_{ji} \mathbf{T}^{l-k-1}_{\overline{\Gamma}^l_{i,h}} \left(\mathbf{T}^{l-k-1}_{\overline{\Gamma}^{l-1}_{j,h}}\right)^{\mathrm{T}} \overline{\underset{\sim}{\mathbf{T}}}^k_{\underset{\sim}{\Gamma}^{l-1}_{j,h}} \tag{A.14}$$

So the enhanced dual exterior derivative and the local dual exterior derivative do not directly commute under the enhanced dual trace operators. Equation (A.14) leads us to define the boundary to inner part contributions for the enhanced dual grid exterior derivative as:

$$\overline{\underset{\sim}{\mathbf{D}}}^k_{\underset{\sim}{\Gamma}^{l-1}_{j,h} \mapsto \underset{\sim}{\Gamma}^l_{i,h}} \equiv \mathbf{T}^{l-k-1}_{\overline{\Gamma}^l_{i,h}} \left(\mathbf{T}^{l-k-1}_{\overline{\Gamma}^{l-1}_{j,h}}\right)^{\mathrm{T}} \tag{A.15}$$

So we can rewrite equation (A.14) as:

$$\overline{\underset{\sim}{\mathbf{T}}}^{k+1}_{\underset{\sim}{\Gamma}^l_{i,h}} \overline{\underset{\sim}{\mathbf{D}}}^k = \underset{\sim}{\mathbf{D}}^k_{\underset{\sim}{\Gamma}^l_{i,h}} \overline{\underset{\sim}{\mathbf{T}}}^k_{\underset{\sim}{\Gamma}^l_{i,h}} + \sum_{j=1}^{n_{\Gamma^{l-1}}} \left(\boldsymbol{\partial}^l_{\mathrm{Sub}}\right)_{ji} \overline{\underset{\sim}{\mathbf{D}}}^k_{\underset{\sim}{\Gamma}^{l-1}_{j,h} \mapsto \underset{\sim}{\Gamma}^l_{i,h}} \overline{\underset{\sim}{\mathbf{T}}}^k_{\underset{\sim}{\Gamma}^{l-1}_{j,h}} \tag{A.16}$$

Collecting all contributions for the enhanced dual exterior derivative, we arrive at the splitting[1]:

$$\overline{\underset{\sim}{\mathbf{D}}}^k = \sum_{l=k+1}^{n} \sum_{i=1}^{n_{\Gamma^l}} \left(\overline{\underset{\sim}{\mathbf{T}}}^{k+1}_{\underset{\sim}{\Gamma}^l_{i,h}}\right)^{\mathrm{T}} \left(\underset{\sim}{\mathbf{D}}^k_{\underset{\sim}{\Gamma}^l_{i,h}} \overline{\underset{\sim}{\mathbf{T}}}^k_{\underset{\sim}{\Gamma}^l_{i,h}} + \sum_{j=1}^{n_{\Gamma^{l-1}}} \left(\boldsymbol{\partial}^l_{\mathrm{Sub}}\right)_{ji} \overline{\underset{\sim}{\mathbf{D}}}^k_{\underset{\sim}{\Gamma}^{l-1}_{j,h} \mapsto \underset{\sim}{\Gamma}^l_{i,h}} \overline{\underset{\sim}{\mathbf{T}}}^k_{\underset{\sim}{\Gamma}^{l-1}_{j,h}}\right) \tag{A.17}$$

Let us now define the *discrete local exterior product*[2] of a primal k-cochain with an enhanced dual $(l-k)$-cochain on the grid part $\overline{\Gamma}^l_{i,h}$:

$$\int_{\Gamma^l_i} \boldsymbol{\omega}^k \wedge \overline{\underset{\sim}{\boldsymbol{\eta}}}^{l-k} \equiv \left(\mathbf{T}^k_{\overline{\Gamma}^l_{i,h}} \boldsymbol{\omega}^k\right)^{\mathrm{T}} \overline{\underset{\sim}{\mathbf{T}}}^{l-k}_{\underset{\sim}{\Gamma}^l_{i,h}} \overline{\underset{\sim}{\boldsymbol{\eta}}}^{l-k} = \left(\boldsymbol{\omega}^k_{\overline{\Gamma}^l_{i,h}}\right)^{\mathrm{T}} \underset{\sim}{\boldsymbol{\eta}}^{l-k}_{\underset{\sim}{\Gamma}^l_{i,h}} \tag{A.18}$$

We can now derive a local partial integration formula by starting with the expression

$$\int_{\Gamma^l_i} \left(\mathbf{D}^{k-1} \boldsymbol{\omega}^{k-1}\right) \wedge \overline{\underset{\sim}{\boldsymbol{\eta}}}^{l-k} = \left(\mathbf{T}^k_{\overline{\Gamma}^l_{i,h}} \mathbf{D}^{k-1} \boldsymbol{\omega}^{k-1}\right)^{\mathrm{T}} \overline{\underset{\sim}{\mathbf{T}}}^{l-k}_{\underset{\sim}{\Gamma}^l_{i,h}} \overline{\underset{\sim}{\boldsymbol{\eta}}}^{l-k}$$

using equation (A.4) to get

$$= \left(\mathbf{D}^{k-1}_{\overline{\Gamma}^l_{i,h}} \mathbf{T}^{k-1}_{\overline{\Gamma}^l_{i,h}} \boldsymbol{\omega}^{k-1}\right)^{\mathrm{T}} \overline{\underset{\sim}{\mathbf{T}}}^{l-k}_{\underset{\sim}{\Gamma}^l_{i,h}} \overline{\underset{\sim}{\boldsymbol{\eta}}}^{l-k}$$

[1] This formula for the splitting of the enhanced dual exterior derivative into standard dual exterior derivatives plus boundary contributions is the generalization of the consistent boundary treatment in Maxwell's second topological grid equation (3.73) on page 56 and equations (5.2) on page 129.

[2] As for the global exterior product in Definition 3.10 on page 43, this is not an exterior product in the mathematical sense, but a bilinear pairing used to approximate the continuous exterior product.

equation (A.12) to get

$$= (-1)^k \left(\mathbf{T}^{k-1}_{\overline{\Gamma}^l_{i,h}} \boldsymbol{\omega}^{k-1} \right)^{\mathrm{T}} \left(\underset{\sim}{\mathbf{D}}^{l-k}_{\underset{\sim}{\Gamma}^l_{i,h}} \underset{\sim}{\overline{\mathbf{T}}}^{l-k}_{\underset{\sim}{\Gamma}^l_{i,h}} \right) \underset{\sim}{\overline{\boldsymbol{\eta}}}^{l-k}$$

and equation (A.16) to arrive at:

$$\begin{aligned}
&= (-1)^k \left(\mathbf{T}^{k-1}_{\overline{\Gamma}^l_{i,h}} \boldsymbol{\omega}^{k-1} \right)^{\mathrm{T}} \left(\underset{\sim}{\overline{\mathbf{T}}}^{l-k+1}_{\underset{\sim}{\Gamma}^l_{i,h}} \underset{\sim}{\overline{\mathbf{D}}}^{l-k} - \sum_{j=1}^{n_{\Gamma^{l-1}}} \left(\boldsymbol{\partial}^l_{\mathrm{Sub}} \right)_{ji} \underset{\sim}{\overline{\mathbf{D}}}^{l-k}_{\underset{\sim}{\Gamma}^{l-1}_{j,h} \mapsto \underset{\sim}{\Gamma}^l_{i,h}} \underset{\sim}{\overline{\mathbf{T}}}^{l-k}_{\underset{\sim}{\Gamma}^{l-1}_{j,h}} \right) \underset{\sim}{\overline{\boldsymbol{\eta}}}^{l-k} \\
&= (-1)^k \left(\mathbf{T}^{k-1}_{\overline{\Gamma}^l_{i,h}} \boldsymbol{\omega}^{k-1} \right)^{\mathrm{T}} \underset{\sim}{\overline{\mathbf{T}}}^{l-k+1}_{\underset{\sim}{\Gamma}^l_{i,h}} \underset{\sim}{\overline{\mathbf{D}}}^{l-k} \underset{\sim}{\overline{\boldsymbol{\eta}}}^{l-k} \\
&\quad - (-1)^k \sum_{j=1}^{n_{\Gamma^{l-1}}} \left(\boldsymbol{\partial}^l_{\mathrm{Sub}} \right)_{ji} \left(\mathbf{T}^{k-1}_{\overline{\Gamma}^l_{i,h}} \boldsymbol{\omega}^{k-1} \right)^{\mathrm{T}} \underset{\sim}{\overline{\mathbf{T}}}^{l-k+1}_{\underset{\sim}{\Gamma}^{l-1}_{j,h}} \left(\underset{\sim}{\overline{\mathbf{T}}}^{l-k+1}_{\underset{\sim}{\Gamma}^{l-1}_{j,h}} \right)^{\mathrm{T}} \underset{\sim}{\overline{\mathbf{D}}}^{l-k}_{\underset{\sim}{\Gamma}^{l-1}_{j,h} \mapsto \underset{\sim}{\Gamma}^l_{i,h}} \underset{\sim}{\overline{\mathbf{T}}}^{l-k}_{\underset{\sim}{\Gamma}^{l-1}_{j,h}} \underset{\sim}{\overline{\boldsymbol{\eta}}}^{l-k} \\
&= (-1)^k \int_{\Gamma^l_i} \boldsymbol{\omega}^{k-1} \wedge \left(\underset{\sim}{\overline{\mathbf{D}}}^{l-k} \underset{\sim}{\overline{\boldsymbol{\eta}}}^{l-k} \right) \\
&\quad - (-1)^k \sum_{j=1}^{n_{\Gamma^{l-1}}} \left(\boldsymbol{\partial}^l_{\mathrm{Sub}} \right)_{ji} \int_{\Gamma^{l-1}_j} \boldsymbol{\omega}^{k-1} \wedge \left[\left(\underset{\sim}{\overline{\mathbf{T}}}^{l-k+1}_{\underset{\sim}{\Gamma}^{l-1}_{j,h}} \right)^{\mathrm{T}} \underset{\sim}{\overline{\mathbf{D}}}^{l-k}_{\underset{\sim}{\Gamma}^{l-1}_{j,h} \mapsto \underset{\sim}{\Gamma}^l_{i,h}} \underset{\sim}{\overline{\mathbf{T}}}^{l-k}_{\underset{\sim}{\Gamma}^{l-1}_{j,h}} \underset{\sim}{\overline{\boldsymbol{\eta}}}^{l-k} \right]
\end{aligned} \tag{A.19}$$

We know that the sequence property holds for the enhanced dual grid exterior derivative:

$$\underset{\sim}{\overline{\mathbf{D}}}^{k+1} \underset{\sim}{\overline{\mathbf{D}}}^{k} = 0 \tag{A.20}$$

Now we can derive properties of the local exterior derivatives by plugging the splitting of the exterior derivatives according to equation (A.17) into equation (A.20):

$$\begin{aligned}
\underset{\sim}{\overline{\mathbf{D}}}^{k+1} \underset{\sim}{\overline{\mathbf{D}}}^{k} &= \sum_{l_a=k+2}^{n} \sum_{i_a=1}^{n_{\Gamma^{l_a}}} \left(\underset{\sim}{\overline{\mathbf{T}}}^{k+2}_{\underset{\sim}{\Gamma}^{l_a}_{i_a,h}} \right)^{\mathrm{T}} \left(\underset{\sim}{\mathbf{D}}^{k+1}_{\underset{\sim}{\Gamma}^{l_a}_{i_a,h}} \underset{\sim}{\overline{\mathbf{T}}}^{k+1}_{\underset{\sim}{\Gamma}^{l_a}_{i_a,h}} + \sum_{j_a=1}^{n_{\Gamma^{l_a-1}}} \left(\boldsymbol{\partial}^{l_a}_{\mathrm{Sub}} \right)_{j_a i_a} \underset{\sim}{\overline{\mathbf{D}}}^{k+1}_{\underset{\sim}{\Gamma}^{l_a-1}_{j_a,h} \mapsto \underset{\sim}{\Gamma}^{l_a}_{i_a,h}} \underset{\sim}{\overline{\mathbf{T}}}^{k+1}_{\underset{\sim}{\Gamma}^{l_a-1}_{j_a,h}} \right) \\
&\quad \cdot \sum_{l_b=k+1}^{n} \sum_{i_b=1}^{n_{\Gamma^{l_b}}} \left(\underset{\sim}{\overline{\mathbf{T}}}^{k+1}_{\underset{\sim}{\Gamma}^{l_b}_{i_b,h}} \right)^{\mathrm{T}} \left(\underset{\sim}{\mathbf{D}}^{k}_{\underset{\sim}{\Gamma}^{l_b}_{i_b,h}} \underset{\sim}{\overline{\mathbf{T}}}^{k}_{\underset{\sim}{\Gamma}^{l_b}_{i_b,h}} + \sum_{j_b=1}^{n_{\Gamma^{l_b-1}}} \left(\boldsymbol{\partial}^{l_b}_{\mathrm{Sub}} \right)_{j_b i_b} \underset{\sim}{\overline{\mathbf{D}}}^{k}_{\underset{\sim}{\Gamma}^{l_b-1}_{j_b,h} \mapsto \underset{\sim}{\Gamma}^{l_b}_{i_b,h}} \underset{\sim}{\overline{\mathbf{T}}}^{k}_{\underset{\sim}{\Gamma}^{l_b-1}_{j_b,h}} \right)
\end{aligned}$$

We can simplify this expression by using equation (A.9):

$$\begin{aligned}
&= \sum_{l=k+2}^{n} \sum_{i=1}^{n_{\Gamma^l}} \left(\underset{\sim}{\overline{\mathbf{T}}}^{k+2}_{\underset{\sim}{\Gamma}^l_{i,h}} \right)^{\mathrm{T}} \left[\underset{\sim}{\mathbf{D}}^{k+1}_{\underset{\sim}{\Gamma}^l_{i,h}} \left(\underset{\sim}{\mathbf{D}}^{k}_{\underset{\sim}{\Gamma}^l_{i,h}} \underset{\sim}{\overline{\mathbf{T}}}^{k}_{\underset{\sim}{\Gamma}^l_{i,h}} + \sum_{j=1}^{n_{\Gamma^{l-1}}} \left(\boldsymbol{\partial}^l_{\mathrm{Sub}} \right)_{ji} \underset{\sim}{\overline{\mathbf{D}}}^{k}_{\underset{\sim}{\Gamma}^{l-1}_{j,h} \mapsto \underset{\sim}{\Gamma}^l_{i,h}} \underset{\sim}{\overline{\mathbf{T}}}^{k}_{\underset{\sim}{\Gamma}^{l-1}_{j,h}} \right) \right. \\
&\quad \left. + \sum_{j=1}^{n_{\Gamma^{l-1}}} \left(\boldsymbol{\partial}^l_{\mathrm{Sub}} \right)_{ji} \underset{\sim}{\overline{\mathbf{D}}}^{k+1}_{\underset{\sim}{\Gamma}^{l-1}_{j,h} \mapsto \underset{\sim}{\Gamma}^l_{i,h}} \left(\underset{\sim}{\mathbf{D}}^{k}_{\underset{\sim}{\Gamma}^{l-1}_{j,h}} \underset{\sim}{\overline{\mathbf{T}}}^{k}_{\underset{\sim}{\Gamma}^{l-1}_{j,h}} + \sum_{p=1}^{n_{\Gamma^{l-2}}} \left(\boldsymbol{\partial}^{l-1}_{\mathrm{Sub}} \right)_{pj} \underset{\sim}{\overline{\mathbf{D}}}^{k}_{\underset{\sim}{\Gamma}^{l-2}_{p,h} \mapsto \underset{\sim}{\Gamma}^{l-1}_{j,h}} \underset{\sim}{\overline{\mathbf{T}}}^{k}_{\underset{\sim}{\Gamma}^{l-2}_{p,h}} \right) \right] \\
&= 0
\end{aligned} \tag{A.21}$$

Now we can again use equation (A.9) to extract the following formulas:

$$\underset{\sim}{\overline{\mathbf{T}}}^{k+2}_{\underset{\sim}{\Gamma}^s_{q,h}} \underset{\sim}{\overline{\mathbf{D}}}^{k+1} \underset{\sim}{\overline{\mathbf{D}}}^{k} \left(\underset{\sim}{\overline{\mathbf{T}}}^{k}_{\underset{\sim}{\Gamma}^s_{q,h}} \right)^{\mathrm{T}} = \underset{\sim}{\mathbf{D}}^{k+1}_{\underset{\sim}{\Gamma}^s_{q,h}} \underset{\sim}{\mathbf{D}}^{k}_{\underset{\sim}{\Gamma}^s_{q,h}} = 0 \tag{A.22a}$$

$$\left(\boldsymbol{\partial}^s_{\mathrm{Sub}} \right)_{rq} \underset{\sim}{\overline{\mathbf{T}}}^{k+2}_{\underset{\sim}{\Gamma}^s_{q,h}} \underset{\sim}{\overline{\mathbf{D}}}^{k+1} \underset{\sim}{\overline{\mathbf{D}}}^{k} \left(\underset{\sim}{\overline{\mathbf{T}}}^{k}_{\underset{\sim}{\Gamma}^{s-1}_{r,h}} \right)^{\mathrm{T}} = \underset{\sim}{\mathbf{D}}^{k+1}_{\underset{\sim}{\Gamma}^s_{q,h}} \underset{\sim}{\overline{\mathbf{D}}}^{k}_{\underset{\sim}{\Gamma}^{s-1}_{r,h} \mapsto \underset{\sim}{\Gamma}^s_{q,h}} + \underset{\sim}{\overline{\mathbf{D}}}^{k+1}_{\underset{\sim}{\Gamma}^{s-1}_{r,h} \mapsto \underset{\sim}{\Gamma}^s_{q,h}} \underset{\sim}{\mathbf{D}}^{k}_{\underset{\sim}{\Gamma}^{s-1}_{r,h}} = 0 \tag{A.22b}$$

$$\underset{\sim}{\overline{\mathbf{T}}}^{k+2}_{\underset{\sim}{\Gamma}^s_{q,h}} \underset{\sim}{\overline{\mathbf{D}}}^{k+1} \underset{\sim}{\overline{\mathbf{D}}}^{k} \left(\underset{\sim}{\overline{\mathbf{T}}}^{k}_{\underset{\sim}{\Gamma}^{s-2}_{r,h}} \right)^{\mathrm{T}} = \sum_{j=1}^{n_{\Gamma^{s-1}}} \left(\boldsymbol{\partial}^s_{\mathrm{Sub}} \right)_{jq} \left(\boldsymbol{\partial}^{s-1}_{\mathrm{Sub}} \right)_{rj} \underset{\sim}{\overline{\mathbf{D}}}^{k+1}_{\underset{\sim}{\Gamma}^{s-1}_{j,h} \mapsto \underset{\sim}{\Gamma}^s_{q,h}} \underset{\sim}{\overline{\mathbf{D}}}^{k}_{\underset{\sim}{\Gamma}^{s-2}_{r,h} \mapsto \underset{\sim}{\Gamma}^{s-1}_{j,h}} = 0 \tag{A.22c}$$

where we assume $s \geq k+2$. Statement (A.22a) is already known as the sequence property of the local dual exterior derivatives. Statement (A.22b) connects the inner and the boundary parts of the enhanced dual exterior derivatives. Statement (A.22c) boils down to the sequence property of the local boundary exterior derivatives.

A.2 Example Application for Grid Equations of Maxwell's Type

We show for the example of grid equations of Maxwell's type what we can do with the enhanced dual grid: We calculate local energies, local energy fluxes, and a local Poynting's Theorem. Assume the n-dimensional primal grid Ω_h^n with outward-oriented boundary parts Γ_i^{n-1}, $i \in [1..n_{\Gamma^{n-1}}^{\text{outer}}]$ to be given along with a standard dual grid $\underset{\sim}{\Omega}_h$. Following the reasoning in chapter 3.2, there exists a unique solution to the following discrete boundary value problem:

$$\mathbf{D}^{k-1}\,\boldsymbol{\omega}^{k-1} = (-1)^{k+1}\,\partial_t \boldsymbol{\eta}^k \tag{A.23a}$$

$$\underset{\sim}{\mathbf{D}}^{n-k}\,\underset{\sim}{\boldsymbol{\eta}}^{n-k} + \sum_{i=1}^{n_{\Gamma^{n-1}}^{\text{outer}}} \left(\mathbf{T}^{k-1}_{\overline{\Gamma}_{i,h}^{n-1}}\right)^{\mathrm{T}} \underset{\sim}{\boldsymbol{\eta}}^{n-k}_{\underset{\sim}{\Gamma}_{i,h}^{n-1}} = \partial_t \underset{\sim}{\boldsymbol{\omega}}^{n-k+1} \tag{A.23b}$$

$$\underset{\sim}{\boldsymbol{\omega}}^{n-k+1} = \mathbf{M}^{k-1}\,\boldsymbol{\omega}^{k-1} \tag{A.23c}$$

$$\underset{\sim}{\boldsymbol{\eta}}^{n-k} = \mathbf{M}^{k}\,\boldsymbol{\eta}^{k} \tag{A.23d}$$

$$\mathbf{T}^{k-1}_{\overline{\Gamma}_{i,h}^{n-1}}\,\boldsymbol{\omega}^{k-1} = \boldsymbol{\omega}^{k-1}_{\overline{\Gamma}_{i,h}^{n-1}} \qquad \text{known for } i \in [1..n_{\Gamma^{n-1}}^{\text{EBC}}] \tag{A.23e}$$

$$\underset{\sim}{\boldsymbol{\eta}}^{n-k}_{\underset{\sim}{\Gamma}_{i,h}^{n-1}} \qquad \text{known for } i \in [n_{\Gamma^{n-1}}^{\text{EBC}}+1..n_{\Gamma^{n-1}}^{\text{outer}}] \tag{A.23f}$$

$$\boldsymbol{\omega}^{k-1}(t_0) \qquad \text{known} \tag{A.23g}$$

$$\boldsymbol{\eta}^{k}(t_0) \qquad \text{known} \tag{A.23h}$$

with $0 \leq n_{\Gamma^{n-1}}^{\text{EBC}} \leq n_{\Gamma^{n-1}}^{\text{outer}}$. We then know the following Poynting's Theorem to hold in analogy to the conservation law for the energy stated in equation (3.118) on page 66:

$$\frac{1}{2}\partial_t \left(\left(\boldsymbol{\omega}^{k-1}\right)^{\mathrm{T}} \mathbf{M}^{k-1}\,\boldsymbol{\omega}^{k-1} + \left(\boldsymbol{\eta}^{k}\right)^{\mathrm{T}} \mathbf{M}^{k}\,\boldsymbol{\eta}^{k} \right) = \sum_{i=1}^{n_{\Gamma^{n-1}}^{\text{outer}}} \left(\boldsymbol{\omega}^{k-1}_{\overline{\Gamma}_{i,h}^{n-1}}\right)^{\mathrm{T}} \underset{\sim}{\boldsymbol{\eta}}^{k}_{\underset{\sim}{\Gamma}_{i,h}^{n-1}} \tag{A.24}$$

Now assume we are interested in the local energies in several n-dimensional regions and the energy fluxes through several $(n-1)$-dimensional hyper-surfaces. Also assume that these regions and hyper-surfaces are consistently discretized by primal grid elements. Then the enhanced dual grid provides the tools for local energy and flux calculations as shown in the following. Choose a consistent subdivision $\mathrm{Sub}(\Omega_h)$ of the primal grid which contains these regions, hypersurfaces, and the boundary patches Γ_i^{n-1}, $i \in [1..n_{\Gamma^{n-1}}^{\text{outer}}]$ consistently. We restrict the subdivision to contain no additional inner subdivision parts of dimension less than $(n-1)$.[3] Using the local splitting of the material matrices onto the primal grid elements S_i^n according to formula (3.58) on page 48, we create the local material matrices $\mathbf{M}^k_{\overline{\Gamma}_{i,h}^n}$ for the n-dimensional grid parts $\overline{\Gamma}_{i,h}^n$:

$$\mathbf{M}^k_{\overline{\Gamma}_{i,h}^n} \equiv \sum_{j \in \mathrm{I}^n_{\overline{\Gamma}_{i,h}^n}} \mathbf{T}^k_{\overline{\Gamma}_{i,h}^n}\,\mathbf{M}^{k,j}_{\alpha}\left(\mathbf{T}^k_{\overline{\Gamma}_{i,h}^n}\right)^{\mathrm{T}} \qquad \forall\, k \in [0..n] \tag{A.25}$$

[3] The restriction to take $l \geq n-1$ was posed in order to ensure uniqueness of the additional quantities. Possibilities on lifting this restriction will be discussed below.

Now we plug these local material matrices into equation (A.24) in order to arrive at a local Poynting's Theorem for the grid part $\overline{\Gamma}^n_{j,h}$:

$$\frac{1}{2}\partial_t \left[\left(\boldsymbol{\omega}^{k-1}\right)^{\mathrm{T}} \sum_{i=1}^{n_{\Gamma^n}} \left(\mathbf{T}^{k-1}_{\overline{\Gamma}^n_{i,h}}\right)^{\mathrm{T}} \mathbf{M}^{k-1}_{\overline{\Gamma}^n_{i,h}} \mathbf{T}^{k-1}_{\overline{\Gamma}^n_{i,h}} \boldsymbol{\omega}^{k-1} + \left(\boldsymbol{\eta}^{k}\right)^{\mathrm{T}} \sum_{i=1}^{n_{\Gamma^n}} \left(\mathbf{T}^{k}_{\overline{\Gamma}^n_{i,h}}\right)^{\mathrm{T}} \mathbf{M}^{k}_{\overline{\Gamma}^n_{i,h}} \mathbf{T}^{k}_{\overline{\Gamma}^n_{i,h}} \boldsymbol{\eta}^{k} \right]$$
$$= \sum_{i=1}^{n^{\mathrm{outer}}_{\Gamma^{n-1}}} \left(\boldsymbol{\omega}^{k-1}_{\overline{\Gamma}^{n-1}_{i,h}}\right)^{\mathrm{T}} \underset{\sim}{\boldsymbol{\eta}}^{n-k}_{\underset{\sim}{\Gamma}^{n-1}_{i,h}} \tag{A.26}$$

which we can rewrite as:

$$\frac{1}{2}\partial_t \left[\left(\boldsymbol{\omega}^{k-1}_{\overline{\Gamma}^n_{j,h}}\right)^{\mathrm{T}} \mathbf{M}^{k-1}_{\overline{\Gamma}^n_{j,h}} \boldsymbol{\omega}^{k-1}_{\overline{\Gamma}^n_{j,h}} + \left(\boldsymbol{\eta}^{k}_{\overline{\Gamma}^n_{j,h}}\right)^{\mathrm{T}} \mathbf{M}^{k}_{\overline{\Gamma}^n_{j,h}} \boldsymbol{\eta}^{k}_{\overline{\Gamma}^n_{j,h}} \right]$$
$$= \sum_{i=1}^{n^{\mathrm{outer}}_{\Gamma^{n-1}}} \left(\boldsymbol{\omega}^{k-1}_{\overline{\Gamma}^{n-1}_{i,h}}\right)^{\mathrm{T}} \underset{\sim}{\boldsymbol{\eta}}^{n-k}_{\underset{\sim}{\Gamma}^{n-1}_{i,h}}$$
$$- \frac{1}{2}\partial_t \sum_{i=1, i\neq j}^{n_{\Gamma^n}} \left[\left(\boldsymbol{\omega}^{k-1}_{\overline{\Gamma}^n_{i,h}}\right)^{\mathrm{T}} \mathbf{M}^{k-1}_{\overline{\Gamma}^n_{i,h}} \boldsymbol{\omega}^{k-1}_{\overline{\Gamma}^n_{i,h}} + \left(\boldsymbol{\eta}^{k}_{\overline{\Gamma}^n_{i,h}}\right)^{\mathrm{T}} \mathbf{M}^{k}_{\overline{\Gamma}^n_{i,h}} \boldsymbol{\eta}^{k}_{\overline{\Gamma}^n_{i,h}} \right] \tag{A.27}$$

Assuming the terms on the left hand side of equation (A.27) to approximate the analytical energies in the region Γ^n_j, the term on the right hand side of equation (A.27) will approximate the integrated Poynting vector through the boundary of Γ^n_j.

Although we have formulated a local Poynting's Theorem by equation (A.27), we do not want to stop at this point. We will now use the enhanced dual grid to derive local Poynting vector quantities. In that spirit, we try to recast the discrete problem (A.23) in a local form using the enhanced dual grid. We first define the enhanced dual quantities in the grid parts $\overline{\Gamma}^n_{i,h}$ as:

$$\underset{\sim}{\boldsymbol{\omega}}^{n-k+1}_{\underset{\sim}{\Gamma}^n_{i,h}} \equiv \mathbf{M}^{k-1}_{\overline{\Gamma}^n_{i,h}} \boldsymbol{\omega}^{k-1}_{\overline{\Gamma}^n_{i,h}} \tag{A.28a}$$

$$\underset{\sim}{\boldsymbol{\eta}}^{n-k}_{\underset{\sim}{\Gamma}^n_{i,h}} \equiv \mathbf{M}^{k}_{\overline{\Gamma}^n_{i,h}} \boldsymbol{\eta}^{k}_{\overline{\Gamma}^n_{i,h}} \tag{A.28b}$$

We will interpret these already as local versions of (A.23c) and (A.23d). Equation (A.23a) is easily put into local form:

$$\mathbf{D}^{k-1}_{\overline{\Gamma}^n_{i,h}} \boldsymbol{\omega}^{k-1}_{\overline{\Gamma}^n_{i,h}} = (-1)^{k+1} \partial_t \boldsymbol{\eta}^{k}_{\overline{\Gamma}^n_{i,h}} \tag{A.29}$$

The difficult part is the local version of equation (A.23b). We note that we can recast the standard dual quantities in terms of the enhanced dual quantities as:

$$\underset{\sim}{\boldsymbol{\omega}}^{n-k+1} = \sum_{i=1}^{n_{\Gamma^n}} \left(\mathbf{T}^{k-1}_{\overline{\Gamma}^n_{i,h}}\right)^{\mathrm{T}} \underset{\sim}{\boldsymbol{\omega}}^{n-k+1}_{\underset{\sim}{\Gamma}^n_{i,h}} \tag{A.30a}$$

$$\underset{\sim}{\boldsymbol{\eta}}^{n-k} = \sum_{i=1}^{n_{\Gamma^n}} \left(\mathbf{T}^{k}_{\overline{\Gamma}^n_{i,h}}\right)^{\mathrm{T}} \underset{\sim}{\boldsymbol{\eta}}^{n-k}_{\underset{\sim}{\Gamma}^n_{i,h}} \tag{A.30b}$$

Further on, we can recast the standard dual exterior derivative in terms of the local dual exterior derivative as:

$$\underset{\sim}{\mathbf{D}}^{n-k} \left(\mathbf{T}^{k}_{\overline{\Gamma}^n_{i,h}}\right)^{\mathrm{T}} = \left(\mathbf{T}^{k-1}_{\overline{\Gamma}^n_{i,h}}\right)^{\mathrm{T}} \underset{\sim}{\mathbf{D}}^{n-k}_{\underset{\sim}{\Gamma}^n_{i,h}} \tag{A.31}$$

We will also need the following relation:

$$\mathbf{T}^{k-1}_{\overline{\Gamma}^n_{m,h}} \left(\mathbf{T}^{k-1}_{\overline{\Gamma}^n_{i,h}}\right)^{\mathrm{T}} = \begin{cases} \mathbf{I} & \text{for } i = m \\ \mathbf{T}^{k-1}_{\overline{\Gamma}^n_{m,h}} \sum\limits_{j=n^{\text{outer}}_{\Gamma^{n-1}}+1}^{n_{\Gamma^{n-1}}} \left(\mathbf{T}^{k-1}_{\overline{\Gamma}^{n-1}_{j,h}}\right)^{\mathrm{T}} \mathbf{T}^{k-1}_{\overline{\Gamma}^{n-1}_{j,h}} \left(\mathbf{T}^{k-1}_{\overline{\Gamma}^n_{i,h}}\right)^{\mathrm{T}} & \text{for } i \neq m \end{cases} \tag{A.32}$$

This relation is only true under the restriction put forward above, that no inner grid part $\overline{\Gamma}^l_{i,h}$ exists with dimension $l < (n-1)$. Otherwise, we have multiple additions of the terms along the lower dimensional grid parts. This restriction could be lifted by using the following relation:

$$\begin{aligned} \mathbf{T}^{k-1}_{\overline{\Gamma}^n_{m,h}} \left(\mathbf{T}^{k-1}_{\overline{\Gamma}^n_{i,h}}\right)^{\mathrm{T}} = \mathbf{T}^{k-1}_{\overline{\Gamma}^n_{m,h}} \sum_{l=k-1}^{n-1} \Bigg[& \sum_{j=n^{\text{outer}}_{\Gamma^l}+1}^{n_{\Gamma^l}} \left(\mathbf{T}^{k-1}_{\overline{\Gamma}^l_{j,h}}\right)^{\mathrm{T}} \mathbf{T}^{k-1}_{\overline{\Gamma}^l_{j,h}} \\ & - \sum_{p=n^{\text{outer}}_{\Gamma^{l-1}}+1}^{n_{\Gamma^{l-1}}} (\boldsymbol{\partial}^n_{\text{Sub}})_{pj} \left(\mathbf{T}^{k-1}_{\overline{\Gamma}^{l-1}_{p,h}}\right)^{\mathrm{T}} \mathbf{T}^{k-1}_{\overline{\Gamma}^{l-1}_{p,h}} \Bigg] \left(\mathbf{T}^{k-1}_{\overline{\Gamma}^n_{i,h}}\right)^{\mathrm{T}} \end{aligned} \tag{A.33}$$

We will run into problems for uniquely splitting the quantities at lower dimensional boundaries, anyway, so we keep the restriction at this point and use the simplified formula (A.32). Now we can localize each term in equation (A.23b) onto the dual grid parts $\underset{\sim}{\Gamma}^n_{m,h}$ by applying the primal trace operator $\mathbf{T}^{k-1}_{\overline{\Gamma}^n_{m,h}}$. For the first term, we use equations (A.30b) and (A.31) to deduce:

$$\mathbf{T}^{k-1}_{\overline{\Gamma}^n_{m,h}} \underset{\sim}{\mathbf{D}}^{n-k} \underset{\sim}{\boldsymbol{\eta}}^{n-k} = \mathbf{T}^{k-1}_{\overline{\Gamma}^n_{m,h}} \sum_{i=1}^{n_{\Gamma^n}} \left(\mathbf{T}^{k-1}_{\overline{\Gamma}^n_{i,h}}\right)^{\mathrm{T}} \underset{\sim}{\mathbf{D}}^{n-k}_{\underset{\sim}{\Gamma}^n_{i,h}} \underset{\sim}{\boldsymbol{\eta}}^{n-k}_{\underset{\sim}{\Gamma}^n_{i,h}}$$

Now we employ equation (A.32) to get

$$= \underset{\sim}{\mathbf{D}}^{n-k}_{\underset{\sim}{\Gamma}^n_{m,h}} \underset{\sim}{\boldsymbol{\eta}}^{n-k}_{\underset{\sim}{\Gamma}^n_{m,h}} + \mathbf{T}^{k-1}_{\overline{\Gamma}^n_{m,h}} \sum_{j=n^{\text{outer}}_{\Gamma^{n-1}}+1}^{n_{\Gamma^{n-1}}} \sum_{i=1, i\neq m}^{n_{\Gamma^n}} \left(\mathbf{T}^{k-1}_{\overline{\Gamma}^{n-1}_{j,h}}\right)^{\mathrm{T}} \mathbf{T}^{k-1}_{\overline{\Gamma}^{n-1}_{j,h}} \left(\mathbf{T}^{k-1}_{\overline{\Gamma}^n_{i,h}}\right)^{\mathrm{T}} \underset{\sim}{\mathbf{D}}^{n-k}_{\underset{\sim}{\Gamma}^n_{i,h}} \underset{\sim}{\boldsymbol{\eta}}^{n-k}_{\underset{\sim}{\Gamma}^n_{i,h}}$$

and equation (A.15) to write the first term as:

$$\begin{aligned} &= \underset{\sim}{\mathbf{D}}^{n-k}_{\underset{\sim}{\Gamma}^n_{m,h}} \underset{\sim}{\boldsymbol{\eta}}^{n-k}_{\underset{\sim}{\Gamma}^n_{m,h}} \\ &\quad + \sum_{j=n^{\text{outer}}_{\Gamma^{n-1}}+1}^{n_{\Gamma^{n-1}}} (\boldsymbol{\partial}^n_{\text{Sub}})_{jm} \underset{\sim}{\overline{\mathbf{D}}}^{n-k}_{\underset{\sim}{\Gamma}^{n-1}_{j,h} \mapsto \underset{\sim}{\Gamma}^n_{m,h}} \sum_{i=1, i\neq m}^{n_{\Gamma^n}} (\boldsymbol{\partial}^n_{\text{Sub}})_{jm} \left(\underset{\sim}{\overline{\mathbf{D}}}^{n-k}_{\underset{\sim}{\Gamma}^{n-1}_{j,h} \mapsto \underset{\sim}{\Gamma}^n_{i,h}}\right)^{\mathrm{T}} \underset{\sim}{\mathbf{D}}^{n-k}_{\underset{\sim}{\Gamma}^n_{i,h}} \underset{\sim}{\boldsymbol{\eta}}^{n-k}_{\underset{\sim}{\Gamma}^n_{i,h}} \end{aligned} \tag{A.34a}$$

For the second term, we employ equation (A.30a)

$$\mathbf{T}^{k-1}_{\overline{\Gamma}^n_{m,h}} \partial_t \underset{\sim}{\boldsymbol{\omega}}^{n-k+1} = \mathbf{T}^{k-1}_{\overline{\Gamma}^n_{m,h}} \partial_t \sum_{i=1}^{n_{\Gamma^n}} \left(\mathbf{T}^{k-1}_{\overline{\Gamma}^n_{i,h}}\right)^{\mathrm{T}} \underset{\sim}{\boldsymbol{\omega}}^{n-k+1}_{\underset{\sim}{\Gamma}^n_{i,h}}$$

equation (A.32)

$$= \partial_t \underset{\sim}{\boldsymbol{\omega}}^{n-k+1}_{\underset{\sim}{\Gamma}^n_{m,h}} + \mathbf{T}^{k-1}_{\overline{\Gamma}^n_{m,h}} \sum_{j=n^{\text{outer}}_{\Gamma^{n-1}}+1}^{n_{\Gamma^{n-1}}} \sum_{i=1, i\neq m}^{n_{\Gamma^n}} \left(\mathbf{T}^{k-1}_{\overline{\Gamma}^{n-1}_{j,h}}\right)^{\mathrm{T}} \mathbf{T}^{k-1}_{\overline{\Gamma}^{n-1}_{j,h}} \left(\mathbf{T}^{k-1}_{\overline{\Gamma}^n_{i,h}}\right)^{\mathrm{T}} \partial_t \underset{\sim}{\boldsymbol{\omega}}^{n-k+1}_{\underset{\sim}{\Gamma}^n_{i,h}}$$

and equation (A.15) to arrive at:

$$
\begin{aligned}
&= \partial_t \underset{\sim}{\boldsymbol{\omega}}^{n-k+1}_{\underset{\sim}{\Gamma}^n_{m,h}} \\
&\quad + \sum_{j=n^{\text{outer}}_{\Gamma^{n-1}}+1}^{n_{\Gamma^{n-1}}} (\boldsymbol{\partial}^n_{\text{Sub}})_{jm} \, \overline{\underset{\sim}{\mathbf{D}}}^{n-k}_{\underset{\sim}{\Gamma}^{n-1}_{j,h} \mapsto \underset{\sim}{\Gamma}^n_{m,h}} \sum_{i=1, i\neq m}^{n_{\Gamma^n}} (\boldsymbol{\partial}^n_{\text{Sub}})_{jm} \left(\overline{\underset{\sim}{\mathbf{D}}}^{n-k}_{\underset{\sim}{\Gamma}^{n-1}_{j,h} \mapsto \underset{\sim}{\Gamma}^n_{i,h}} \right)^{\mathrm{T}} \partial_t \underset{\sim}{\boldsymbol{\omega}}^{n-k+1}_{\underset{\sim}{\Gamma}^n_{i,h}}
\end{aligned}
\tag{A.34b}
$$

For the third term, we use equation (A.15) and the fact that $(\boldsymbol{\partial}^n_{\text{Sub}})_{jm} = +1$ for the indices j belonging to an outer boundary part to arrive at:

$$
\mathbf{T}^{k-1}_{\overline{\Gamma}^n_{m,h}} \sum_{j=1}^{n^{\text{outer}}_{\Gamma^{n-1}}} \left(\mathbf{T}^{k-1}_{\overline{\Gamma}^{n-1}_{j,h}} \right)^{\mathrm{T}} \underset{\sim}{\boldsymbol{\eta}}^{n-k}_{\underset{\sim}{\Gamma}^{n-1}_{j,h}} = \sum_{j=1}^{n^{\text{outer}}_{\Gamma^{n-1}}} (\boldsymbol{\partial}^n_{\text{Sub}})_{jm} \, \overline{\underset{\sim}{\mathbf{D}}}^{n-k}_{\underset{\sim}{\Gamma}^{n-1}_{j,h} \mapsto \underset{\sim}{\Gamma}^n_{m,h}} \underset{\sim}{\boldsymbol{\eta}}^{n-k}_{\underset{\sim}{\Gamma}^{n-1}_{i,h}}
\tag{A.34c}
$$

Multiplying equation (A.23b) with the trace operator $\mathbf{T}^{k-1}_{\overline{\Gamma}^n_{m,h}}$ from the left and using the relations (A.34), we get a local version of equation (A.23b) for each dual grid part $\underset{\sim}{\Gamma}^n_{m,h}$:

$$
\begin{aligned}
&\underset{\sim}{\mathbf{D}}^{n-k}_{\underset{\sim}{\Gamma}^n_{m,h}} \underset{\sim}{\boldsymbol{\eta}}^{n-k}_{\underset{\sim}{\Gamma}^n_{m,h}} + \sum_{j=1}^{n^{\text{outer}}_{\Gamma^{n-1}}} (\boldsymbol{\partial}^n_{\text{Sub}})_{jm} \, \overline{\underset{\sim}{\mathbf{D}}}^{n-k}_{\underset{\sim}{\Gamma}^{n-1}_{j,h} \mapsto \underset{\sim}{\Gamma}^n_{m,h}} \underset{\sim}{\boldsymbol{\eta}}^{n-k}_{\underset{\sim}{\Gamma}^{n-1}_{j,h}} \\
&+ \sum_{j=n^{\text{outer}}_{\Gamma^{n-1}}+1}^{n_{\Gamma^{n-1}}} (\boldsymbol{\partial}^n_{\text{Sub}})_{jm} \, \overline{\underset{\sim}{\mathbf{D}}}^{n-k}_{\underset{\sim}{\Gamma}^{n-1}_{j,h} \mapsto \underset{\sim}{\Gamma}^n_{m,h}} \sum_{i=1, i\neq m}^{n_{\Gamma^n}} (\boldsymbol{\partial}^n_{\text{Sub}})_{jm} \left(\overline{\underset{\sim}{\mathbf{D}}}^{n-k}_{\underset{\sim}{\Gamma}^{n-1}_{j,h} \mapsto \underset{\sim}{\Gamma}^n_{i,h}} \right)^{\mathrm{T}} \left(\underset{\sim}{\mathbf{D}}^{n-k}_{\underset{\sim}{\Gamma}^n_{i,h}} \underset{\sim}{\boldsymbol{\eta}}^{n-k}_{\underset{\sim}{\Gamma}^n_{i,h}} - \partial_t \underset{\sim}{\boldsymbol{\omega}}^{n-k+1}_{\underset{\sim}{\Gamma}^n_{i,h}} \right) \\
&= \partial_t \underset{\sim}{\boldsymbol{\omega}}^{n-k+1}_{\underset{\sim}{\Gamma}^n_{m,h}}
\end{aligned}
\tag{A.35}
$$

Now it seems natural to define the following terms $\underset{\sim}{\boldsymbol{\eta}}^{n-k}_{\underset{\sim}{\Gamma}^{n-1}_{j,h}}(m)$ for $j > n^{\text{outer}}_{\Gamma^{n-1}}$:

$$
\underset{\sim}{\boldsymbol{\eta}}^{n-k}_{\underset{\sim}{\Gamma}^{n-1}_{j,h}}(m) \equiv \sum_{i=1, i\neq m}^{n_{\Gamma^n}} (\boldsymbol{\partial}^n_{\text{Sub}})_{jm} \left(\overline{\underset{\sim}{\mathbf{D}}}^{n-k}_{\underset{\sim}{\Gamma}^{n-1}_{j,h} \mapsto \underset{\sim}{\Gamma}^n_{i,h}} \right)^{\mathrm{T}} \left(\underset{\sim}{\mathbf{D}}^{n-k}_{\underset{\sim}{\Gamma}^n_{i,h}} \underset{\sim}{\boldsymbol{\eta}}^{n-k}_{\underset{\sim}{\Gamma}^n_{i,h}} - \partial_t \underset{\sim}{\boldsymbol{\omega}}^{n-k+1}_{\underset{\sim}{\Gamma}^n_{i,h}} \right)
\tag{A.36}
$$

Due to our restriction that no lower dimensional boundaries exist, each internal hyper-surface $\underset{\sim}{\Gamma}^{n-1}_{j,h}$ has exactly two neighboring n-dimensional regions. Let the indices of these neighboring regions be m_1 and m_2. Then we know:

$$
\begin{aligned}
\underset{\sim}{\boldsymbol{\eta}}^{n-k}_{\underset{\sim}{\Gamma}^{n-1}_{j,h}}(m_1) &= (\boldsymbol{\partial}^n_{\text{Sub}})_{jm_2} \left(\overline{\underset{\sim}{\mathbf{D}}}^{n-k}_{\underset{\sim}{\Gamma}^{n-1}_{j,h} \mapsto \underset{\sim}{\Gamma}^n_{m_2,h}} \right)^{\mathrm{T}} \left(\underset{\sim}{\mathbf{D}}^{n-k}_{\underset{\sim}{\Gamma}^n_{m_2,h}} \underset{\sim}{\boldsymbol{\eta}}^{n-k}_{\underset{\sim}{\Gamma}^n_{m_2,h}} - \partial_t \underset{\sim}{\boldsymbol{\omega}}^{n-k+1}_{\underset{\sim}{\Gamma}^n_{m_2,h}} \right) \\
&= (\boldsymbol{\partial}^n_{\text{Sub}})_{jm_1} \left(\overline{\underset{\sim}{\mathbf{D}}}^{n-k}_{\underset{\sim}{\Gamma}^{n-1}_{j,h} \mapsto \underset{\sim}{\Gamma}^n_{m_1,h}} \right)^{\mathrm{T}} \left(\underset{\sim}{\mathbf{D}}^{n-k}_{\underset{\sim}{\Gamma}^n_{m_1,h}} \underset{\sim}{\boldsymbol{\eta}}^{n-k}_{\underset{\sim}{\Gamma}^n_{m_1,h}} - \partial_t \underset{\sim}{\boldsymbol{\omega}}^{n-k+1}_{\underset{\sim}{\Gamma}^n_{m_1,h}} \right) = \underset{\sim}{\boldsymbol{\eta}}^{n-k}_{\underset{\sim}{\Gamma}^{n-1}_{j,h}}(m_2)
\end{aligned}
\tag{A.37}
$$

and we can define the $\underset{\sim}{\boldsymbol{\eta}}^{n-k}_{\underset{\sim}{\Gamma}^{n-1}_{j,h}}$ on the internal hyper-surfaces independent of the m. This allows us to combine the sums in equation (A.35):

$$
\underset{\sim}{\mathbf{D}}^{n-k}_{\underset{\sim}{\Gamma}^n_{m,h}} \underset{\sim}{\boldsymbol{\eta}}^{n-k}_{\underset{\sim}{\Gamma}^n_{m,h}} + \sum_{j=1}^{n_{\Gamma^{n-1}}} (\boldsymbol{\partial}^n_{\text{Sub}})_{jm} \, \overline{\underset{\sim}{\mathbf{D}}}^{n-k}_{\underset{\sim}{\Gamma}^{n-1}_{j,h} \mapsto \underset{\sim}{\Gamma}^n_{m,h}} \underset{\sim}{\boldsymbol{\eta}}^{n-k}_{\underset{\sim}{\Gamma}^{n-1}_{j,h}} = \partial_t \underset{\sim}{\boldsymbol{\omega}}^{n-k+1}_{\underset{\sim}{\Gamma}^n_{m,h}}
\tag{A.38}
$$

Collecting the local equations derived above, we finally arrive at the local version of equations (A.23) for each grid part $\overline{\Gamma}^n_{m,h}$:

$$\mathbf{D}^{k-1}_{\overline{\Gamma}^n_{m,h}}\,\boldsymbol{\omega}^{k-1}_{\overline{\Gamma}^n_{i,h}} = (-1)^{k+1}\,\partial_t \boldsymbol{\eta}^k_{\overline{\Gamma}^n_{m,h}} \tag{A.39a}$$

$$\underset{\sim}{\mathbf{D}}^{n-k}_{\underset{\sim}{\Gamma}^n_{m,h}}\,\underset{\sim}{\boldsymbol{\eta}}^{n-k}_{\underset{\sim}{\Gamma}^n_{m,h}} + \sum_{j=1}^{n_{\Gamma^{n-1}}} \left(\boldsymbol{\partial}^n_{\mathrm{Sub}}\right)_{jm} \underset{\sim}{\overline{\mathbf{D}}}^{n-k}_{\underset{\sim}{\Gamma}^{n-1}_{j,h}\mapsto\underset{\sim}{\Gamma}^n_{m,h}}\,\underset{\sim}{\boldsymbol{\eta}}^{n-k}_{\underset{\sim}{\Gamma}^{n-1}_{j,h}} = \partial_t \underset{\sim}{\boldsymbol{\omega}}^{n-k+1}_{\underset{\sim}{\Gamma}^n_{m,h}} \tag{A.39b}$$

$$\underset{\sim}{\boldsymbol{\omega}}^{n-k+1}_{\underset{\sim}{\Gamma}^n_{m,h}} = \mathbf{M}^{k-1}_{\overline{\Gamma}^n_{m,h}}\,\boldsymbol{\omega}^{k-1}_{\overline{\Gamma}^n_{m,h}} \tag{A.39c}$$

$$\underset{\sim}{\boldsymbol{\eta}}^{n-k}_{\underset{\sim}{\Gamma}^n_{m,h}} = \mathbf{M}^{k}_{\overline{\Gamma}^n_{m,h}}\,\boldsymbol{\eta}^{k}_{\overline{\Gamma}^n_{m,h}} \tag{A.39d}$$

$$\boldsymbol{\omega}^{k-1}_{\overline{\Gamma}^{n-1}_{i,h}} \qquad \text{known } \forall\, i \in [1..n^{\mathrm{EBC}}_{\Gamma^{n-1}}] \tag{A.39e}$$

$$\underset{\sim}{\boldsymbol{\eta}}^{n-k}_{\underset{\sim}{\Gamma}^{n-1}_{i,h}} \qquad \text{known for } \forall\, i \in [n^{\mathrm{EBC}+1}_{\Gamma^{n-1}}..n^{\mathrm{outer}}_{\Gamma^{n-1}}] \tag{A.39f}$$

$$\boldsymbol{\omega}^{k-1}_{\overline{\Gamma}^n_{m,h}}(t_0) \qquad \text{known} \tag{A.39g}$$

$$\boldsymbol{\eta}^{k}_{\overline{\Gamma}^n_{m,h}}(t_0) \qquad \text{known} \tag{A.39h}$$

The system of equations (A.39) has a unique solution and could have been stated to start with. Its derivation from the standard form was only chosen to illuminate their connections. The additional unknowns $\underset{\sim}{\boldsymbol{\eta}}^{n-k}_{\underset{\sim}{\Gamma}^{n-1}_{j,h}}$ on the inner boundaries between the grid parts $\overline{\Gamma}^n_{m,h}$ are uniquely defined by equation (A.39b) under the restriction of no inner grid parts with dimension lower than $(n-1)$. These additional unknowns allow for conveniently stating the following local Poynting's Theorem, which can be derived from equations (A.39) by the help of equations (A.15), (A.19), and (A.37):

$$\begin{aligned}\frac{1}{2}\partial_t \left[\left(\boldsymbol{\omega}^{k-1}_{\overline{\Gamma}^n_{m,h}}\right)^{\mathrm{T}} \mathbf{M}^{k-1}_{\overline{\Gamma}^n_{m,h}}\,\boldsymbol{\omega}^{k-1}_{\overline{\Gamma}^n_{m,h}} + \left(\boldsymbol{\eta}^{k}_{\overline{\Gamma}^n_{m,h}}\right)^{\mathrm{T}} \mathbf{M}^{k}_{\overline{\Gamma}^n_{m,h}}\,\boldsymbol{\eta}^{k}_{\overline{\Gamma}^n_{m,h}}\right] \\ = \sum_{i=1}^{n_{\Gamma^{n-1}}} \left(\boldsymbol{\partial}^n_{\mathrm{Sub}}\right)_{im} \left(\boldsymbol{\omega}^{k-1}_{\overline{\Gamma}^{n-1}_{i,h}}\right)^{\mathrm{T}} \underset{\sim}{\boldsymbol{\eta}}^{n-k}_{\underset{\sim}{\Gamma}^{n-1}_{i,h}}\end{aligned} \tag{A.40}$$

If we allow for a subdivision with inner grid parts of dimension lower than $(n-1)$ to be present, we run into problems: Besides rendering slightly more complicated formulas, there does not exist a unique solution any more. Our definition of the local quantities $\underset{\sim}{\boldsymbol{\eta}}^{n-k}_{\underset{\sim}{\Gamma}^{n-1}_{i,h}}$ was based on the locally unique transfer of energies between two domains. But in the presence of lower dimensional grid parts, there can arise situations with several unknowns in the $\underset{\sim}{\boldsymbol{\eta}}^{n-k}_{\underset{\sim}{\Gamma}^{n-1}_{i,h}}$ with only a single equation dictated by the energy conservation. E.g. when a primal edge on the boundary between two domains has several dual surface edges or when three grid domains exchanging energy meet, the splitting is not unique any more. The right hand side of the local Poynting's Theorem (A.40) is unique, though, as the sums of the energy exchange for each domain is fixed.

A physically sound splitting if the local quantities $\underset{\sim}{\boldsymbol{\eta}}^{n-k}_{\underset{\sim}{\Gamma}^{n-1}_{j,h}}$ are of interest for these cases has not been found by the author. Uniqueness of the solution could be recovered again by several methods: One could require the square sum of the enhanced dual surface edges to

be minimal:

$$\sum_{i=1}^{n_{\Gamma^{n-1}}} ||\underset{\sim}{\boldsymbol{\eta}}^{n-k}_{\underset{\sim}{\Gamma}^{n-1}_{i,h}}||_2^2 \longrightarrow \min \tag{A.41}$$

This is actually equivalent to minimizing the square sum of the Poynting vector entries. Another possibility would be to require the circulation of energy flow around the primal surface edges in $(n-2)$ dimensional grid parts to be zero, i.e.:

$$\sum_{i=1}^{n_{\Gamma^{n-1}}} (\boldsymbol{\partial}^n_{\mathrm{Sub}})_{ji}\, \underset{\sim}{\boldsymbol{\eta}}^{n-k}_{\underset{\sim}{\Gamma}^{n-1}_{i,h}} = 0 \qquad \forall j \in [1..n_{\Gamma^{n-2}}] \tag{A.42}$$

These splittings do not take any metric into account, though. If one keeps the subdivision fixed, this does not seem a problem. If one refines the subdivision with the grid refinement, the convergence of the local quantities certainly requires the involvement of some metric in the splitting scheme, though. As mentioned above, these splittings do not have a physical interpretation and remain an open problem if the local quantities $\underset{\sim}{\boldsymbol{\eta}}^{n-k}_{\underset{\sim}{\Gamma}^{n-1}_{j,h}}$ are needed.

B. ELECTRIC BOUNDARY CONDITIONS IN THE FIT

In order to include electric boundary conditions in the proof of Theorem 3.7 on page 68, we will rewrite Maxwell's semi-discrete IBVP (3.132) in the standard form of equation (3.137) keeping the unknowns in the variable $\mathbf{x}$ and the knowns in the right hand sides $\mathbf{b}$ and $\mathbf{x}_0$.

We will need the discrete trace operators $\mathbf{T}^1_{\overline{\Gamma}_{1,h}}$ defined according to Definition 3.8 on page 41 onto the boundary discretization $\overline{\Gamma}_{1,h}$ of the electric boundary part Γ_1. The discrete trace operator $\mathbf{T}^1_{\overline{\Gamma}_{1,h}}$ simply picks out the edge cochain coefficients on the boundary grid part $\overline{\Gamma}_{1,h}$. Also needed will be the discrete trace operator $\mathbf{T}^1_{\Omega_h\setminus\overline{\Gamma}_{1,h}}$, which picks out the left over cochain coefficients for the primal grid Ω_h which are not in the boundary discretization $\overline{\Gamma}_{1,h}$.

Equation (3.127) on page 67 defines $\widehat{\mathbf{e}}_{\Gamma_1}$ as the electric grid voltages in the boundary part Γ_1. Equivalently, we define $\widehat{\mathbf{e}}_{\Omega\setminus\overline{\Gamma}_1}$ as the electric grid voltages on all other edges as:

$$\widehat{\mathbf{e}}_{\Omega\setminus\overline{\Gamma}_1} \equiv \mathbf{T}^1_{\Omega_h\setminus\overline{\Gamma}_{1,h}}\,\widehat{\mathbf{e}} \tag{B.1}$$

Now we are in the position to split the electric grid voltage vector $\widehat{\mathbf{e}}$ into its known boundary part $\widehat{\mathbf{e}}_{\Gamma_1}$ and its unknown part $\widehat{\mathbf{e}}_{\Omega\setminus\overline{\Gamma}_1}$. The magnetic boundary grid voltage $\widehat{\underset{\sim}{\mathbf{h}}}_{\Gamma_1}$ on the boundary discretization $\overline{\Gamma}_{1,h}$ is also an unknown quantity. Thus we define the vector $\mathbf{x}$ of unknowns as:

$$\begin{aligned}
\mathbf{x}(t) &\equiv \begin{pmatrix}\mathbf{x}_1(t)\\ \mathbf{x}_2(t)\end{pmatrix},\\
\mathbf{x}_1(t) &\equiv \begin{pmatrix}\widehat{\mathbf{e}}_{\Omega\setminus\overline{\Gamma}_1}(t)\\ \widehat{\overline{\mathbf{b}}}(t)\end{pmatrix},\\
\mathbf{x}_2(t) &\equiv \widehat{\underset{\sim}{\mathbf{h}}}_{\Gamma_1}(t)
\end{aligned} \tag{B.2}$$

The electric grid fluxes $\widehat{\overline{\underset{\sim}{\mathbf{d}}}}$ and magnetic grid voltages $\widehat{\underset{\sim}{\mathbf{h}}}$ can easily be computed by equations (3.132c) and (3.132d) on page 68 and are thus eliminated in the reduced system.

Defining the following matrices

$$
\begin{aligned}
\mathbf{A} &\equiv \begin{pmatrix} \mathbf{A}_{11} & 0 \\ \mathbf{A}_{21} & 0 \end{pmatrix}, \\
\mathbf{A}_{11} &\equiv \begin{pmatrix} \mathbf{T}^1_{\Omega_h \setminus \overline{\Gamma}_{1,h}} \mathbf{M}_\varepsilon \left(\mathbf{T}^1_{\Omega_h \setminus \overline{\Gamma}_{1,h}}\right)^{\mathrm{T}} & 0 \\ 0 & \mathbf{M}_\nu \end{pmatrix}, \\
\mathbf{A}_{21} &\equiv \begin{pmatrix} \mathbf{T}^1_{\overline{\Gamma}_{1,h}} \mathbf{M}_\varepsilon \left(\mathbf{T}^1_{\Omega_h \setminus \overline{\Gamma}_{1,h}}\right)^{\mathrm{T}} & 0 \end{pmatrix} \qquad \text{(B.3)} \\
\mathbf{B} &\equiv \begin{pmatrix} \mathbf{B}_{11} & 0 \\ \mathbf{B}_{21} & -\mathbf{I} \end{pmatrix}, \\
\mathbf{B}_{11} &\equiv \begin{pmatrix} 0 & -\mathbf{T}^1_{\Omega_h \setminus \overline{\Gamma}_{1,h}} \underset{\sim}{\mathbf{C}} \mathbf{M}_\nu \\ \mathbf{M}_\nu \mathbf{C} \left(\mathbf{T}^1_{\Omega_h \setminus \overline{\Gamma}_{1,h}}\right) & 0 \end{pmatrix}, \\
\mathbf{B}_{21} &\equiv \begin{pmatrix} 0 & -\mathbf{T}^1_{\overline{\Gamma}_{1,h}} \underset{\sim}{\mathbf{C}} \mathbf{M}_\nu \end{pmatrix} \qquad \text{(B.4)}
\end{aligned}
$$

and the right hand side vector $\mathbf{b}$ as:

$$
\begin{aligned}
\mathbf{b}(t) &\equiv \begin{pmatrix} \mathbf{b}_1(t) \\ \mathbf{b}_2(t) \end{pmatrix}, \\
\mathbf{b}_1(t) &\equiv \begin{pmatrix} \mathbf{T}^1_{\Omega_h \setminus \overline{\Gamma}_{1,h}} \left[-\underset{\sim}{\widehat{\dot{\mathbf{j}}}}(t) + \left(\mathbf{T}^1_{\overline{\Gamma}_{2,h}}\right)^{\mathrm{T}} \underset{\sim}{\widehat{\mathbf{h}}}_{\Gamma_2}(t) - \partial_t \mathbf{M}_\varepsilon \left(\mathbf{T}^1_{\overline{\Gamma}_{1,h}}\right)^{\mathrm{T}} \widehat{\mathbf{e}}_{\Gamma_1}(t) \right] \\ -\mathbf{C} \left(\mathbf{T}^1_{\overline{\Gamma}_{1,h}}\right)^{\mathrm{T}} \widehat{\mathbf{e}}_{\Gamma_1}(t) \end{pmatrix}, \\
\mathbf{b}_2(t) &\equiv \mathbf{T}^1_{\overline{\Gamma}_{1,h}} \left(-\underset{\sim}{\widehat{\dot{\mathbf{j}}}}(t) + \left(\mathbf{T}^1_{\overline{\Gamma}_{2,h}}\right)^{\mathrm{T}} \underset{\sim}{\widehat{\mathbf{h}}}_{\Gamma_2}(t) - \partial_t \mathbf{M}_\varepsilon \left(\mathbf{T}^1_{\overline{\Gamma}_{1,h}}\right)^{\mathrm{T}} \widehat{\mathbf{e}}_{\Gamma_1}(t) \right) \qquad \text{(B.5)}
\end{aligned}
$$

we can recast Maxwell's semi-discrete IBVP (3.132) on page 68 in the standard form of equation (3.137):

$$
\partial_t \begin{pmatrix} \mathbf{A}_{11} & 0 \\ \mathbf{A}_{21} & 0 \end{pmatrix} \mathbf{x}(t) + \begin{pmatrix} \mathbf{B}_{11} & 0 \\ \mathbf{B}_{21} & -\mathbf{I} \end{pmatrix} \mathbf{x}(t) = \begin{pmatrix} \mathbf{b}_1(t) \\ \mathbf{b}_2(t) \end{pmatrix} \qquad \text{(B.6a)}
$$

$$
\mathbf{x}_1(t_0) = \begin{pmatrix} \mathbf{T}^1_{\Omega_h \setminus \overline{\Gamma}_{1,h}} \widehat{\mathbf{e}}_0 \\ \widehat{\overline{\mathbf{b}}}_0 \end{pmatrix} \qquad \text{(B.6b)}
$$

We now note that we can solve the first line of equation (B.6a) independently:

$$
\partial_t \mathbf{A}_{11} \mathbf{x}_1(t) + \mathbf{B}_{11} \mathbf{x}_1(t) = \mathbf{b}_1(t) \qquad \text{(B.7)}
$$

Existence and uniqueness for equation (B.7) with initial condition (B.6b) can be shown in analogy to the case of purely magnetic boundary conditions: The matrix $\mathbf{A}_{11}$ is shown to be invertible and then uniqueness and existence follow from the standard theory in [15, pp. 493].

From the solution to equation (B.7), we can calculate the solution to the second line of equation (B.6a) by the Schur complement:

$$
\mathbf{x}_2(t) = \partial_t \mathbf{A}_{21} \mathbf{x}_1(t) + \mathbf{B}_{21} \mathbf{x}_1(t) - \mathbf{b}_2(t) \qquad \text{(B.8)}
$$

C. EQUIVALENCE OF THE WHITNEY-FEM TO THE FIT

For Maxwell's IBVP, we will show the equivalence of the standard Whitney-FEM method to the FIT discretization described in chapter 3 employing the Whitney-FEM material matrices defined in equations (4.10a) and (4.10b) on page 94. To simplify the derivation, we only consider the case of homogeneous magnetic boundary conditions on all of the boundary, i.e. $\Gamma_1 = \emptyset$ and the tangential magnetic field strength on $\Gamma_2 = \partial\Omega$ to be zero. Further on, we assume the source current $\vec{J}$ to be zero.

A standard time-domain Whitney-FEM formulation of the reduction of Maxwell's IBVP to the electric grid voltages $\widehat{\mathbf{e}}(t)$ as unknowns as derived e.g. in [58] reads:

$$\int_\Omega \nu \operatorname{curl} \underbrace{\left(\sum_{k=1}^{n^1} \widehat{\mathrm{e}}_k \vec{B}_k^1\right)}_{\mathrm{W}^1\widehat{\mathbf{e}}} \cdot \operatorname{curl} \underbrace{\left(\sum_{k=1}^{n^1} \widehat{\mathrm{e}}_{0,k} \vec{B}_k^1\right)}_{\mathrm{W}^1\widehat{\mathbf{e}}_0} \mathrm{d}V$$
$$+ \int_\Omega \partial_t^2 \varepsilon \left(\sum_{k=1}^{n^1} \widehat{\mathrm{e}}_k \vec{B}_k^1\right) \cdot \left(\sum_{k=1}^{n^1} \widehat{\mathrm{e}}_{0,k} \vec{B}_k^1\right) \mathrm{d}V = 0 \qquad \forall\, \widehat{\mathbf{e}}_0 \in \mathbb{R}^{n^1} \tag{C.1}$$

plus appropriate initial conditions. Here $\widehat{\mathrm{e}}_k$ and $\widehat{\mathrm{e}}_{0,k}$ denote the k-th component of the vectors $\widehat{\mathbf{e}}$ and $\widehat{\mathbf{e}}_0$, respectively.

Using the definition of the Whitney reconstruction operator (4.4) on page 91 we can write equation (C.1) as:

$$0 = \int_\Omega \nu \operatorname{curl} \mathrm{W}^1\widehat{\mathbf{e}} \cdot \operatorname{curl} \mathrm{W}^1\widehat{\mathbf{e}}_0 \,\mathrm{d}V + \int_\Omega \partial_t^2 \varepsilon \mathrm{W}^1\widehat{\mathbf{e}} \cdot \mathrm{W}^1\widehat{\mathbf{e}}_0 \,\mathrm{d}V$$

Using the commuting property IV in equation (4.16) on page 95 of the Whitney reconstruction operator with the exterior derivatives

$$= \int_\Omega \nu \mathrm{W}^2\, \mathbf{C}\, \widehat{\mathbf{e}} \cdot \mathrm{W}^2\, \mathbf{C}\, \widehat{\mathbf{e}}_0 \,\mathrm{d}V + \int_\Omega \partial_t^2 \varepsilon \mathrm{W}^1\widehat{\mathbf{e}} \cdot \mathrm{W}^1\widehat{\mathbf{e}}_0 \,\mathrm{d}V$$

again the definition of the Whitney reconstruction operator in equation (4.4) on page 91 and further transformations

$$= \int_\Omega \nu \sum_{i=1}^{n^2} \vec{B}_i^2 \sum_{l=1}^{n^1} (\mathbf{C}_{il}\, \widehat{\mathrm{e}}_l) \cdot \sum_{j=1}^{n^2} \vec{B}_j^2 \sum_{m=1}^{n^1} (\mathbf{C}_{jm}\, \widehat{\mathrm{e}}_{0,m}) \,\mathrm{d}x + \int_\Omega \partial_t^2 \varepsilon \sum_{i=1}^{n^1} \vec{B}_i^1 \widehat{\mathrm{e}}_i \cdot \sum_{j=1}^{n^1} \vec{B}_j^1 \widehat{\mathrm{e}}_{0,j} \,\mathrm{d}V$$
$$= \sum_{i=1}^{n^2} \sum_{j=1}^{n^2} \left(\sum_{l=1}^{n^1} \mathbf{C}_{il}\, \widehat{\mathrm{e}}_l\right) \left(\sum_{m=1}^{n^1} \mathbf{C}_{jm}\, \widehat{\mathrm{e}}_{0,m}\right) \int_\Omega \nu \vec{B}_i^2 \cdot \vec{B}_j^2 \,\mathrm{d}x + \sum_{i=1}^{n^1} \sum_{j=1}^{n^1} \partial_t^2 \widehat{\mathrm{e}}_i \widehat{\mathrm{e}}_{0,j} \int_\Omega \varepsilon \vec{B}_i^1 \cdot \vec{B}_j^1 \,\mathrm{d}x$$

the definition of the material matrices in equations (4.10a) and (4.10b) on page 94

$$
\begin{aligned}
&= \sum_{j=1}^{n^2} \left(\sum_{m=1}^{n^1} \mathbf{C}_{jm}\, \widehat{\mathrm{e}}_{0,m} \right) \left(\sum_{l=1}^{n^1} \sum_{i=1}^{n^2} (\mathbf{M}_\nu)_{ji}\, \mathbf{C}_{il}\, \widehat{\mathrm{e}}_l \right) + \sum_{j=1}^{n^1} \widehat{\mathrm{e}}_{0,j} \partial_t^2 \sum_{i=1}^{n^1} (\mathbf{M}_\varepsilon)_{ji}\, \widehat{\mathrm{e}}_i \\
&= \sum_{j=1}^{n^2} (\mathbf{C}\, \widehat{\mathrm{e}}_0)_j\, (\mathbf{M}_\nu\, \mathbf{C}\, \widehat{\mathrm{e}})_j + \sum_{j=1}^{n^1} \widehat{\mathrm{e}}_{0,j} \partial_t^2\, (\mathbf{M}_\varepsilon\, \widehat{\mathbf{e}})_j \\
&= (\mathbf{C}\, \widehat{\mathbf{e}}_0)^T\, (\mathbf{M}_\nu\, \mathbf{C}\, \widehat{\mathbf{e}}) + \widehat{\mathbf{e}}_0^T \left(\partial_t^2\, \mathbf{M}_\varepsilon\, \widehat{\mathbf{e}} \right)
\end{aligned}
$$

and finally the duality relation (3.52) on page 46 for the primal and dual grid curl operators $\mathbf{C}$ and $\underset{\sim}{\mathbf{C}}$, we arrive at:

$$
= \widehat{\mathbf{e}}_0^T \left(\underset{\sim}{\mathbf{C}}\, \mathbf{M}_\nu\, \mathbf{C}\, \widehat{\mathbf{e}} + \partial_t^2\, \mathbf{M}_\varepsilon\, \widehat{\mathbf{e}} \right) \qquad \forall\, \widehat{\mathbf{e}}_0 \in \mathbb{R}^{n^1} \tag{C.2}
$$

We can restate this as

$$
\underset{\sim}{\mathbf{C}}\, \mathbf{M}_\nu\, \mathbf{C}\, \widehat{\mathbf{e}} + \partial_t^2\, \mathbf{M}_\varepsilon\, \widehat{\mathbf{e}} = 0 \tag{C.3}
$$

Equation (C.3) together with discrete initial conditions is easily shown to be a reduced form of Maxwell's IBVP (3.132) on page 68 for homogeneous magnetic boundary conditions.

The inclusion of non-homogeneous boundary data as well as electric boundary conditions and source currents is straight forward. Possible differences between the FIT and the Whitney-FEM arise in the grid discretization of the given initial, boundary, and source data: While the FIT uses the grid discretization operators operators L^k and $\underset{\sim}{\mathrm{L}}^k$ introduced in chapter 3, the Whitney-FEM usually employs Galerkin discretizations.

For the polyhedral FIT developed in chapter 4, no explicit dual grid and thus no dual grid discretization operators $\underset{\sim}{\mathrm{L}}^k$ are available. To arrive at discrete source data on the dual grid, the following *dual FEM grid discretization operators* $\underset{\sim}{\mathrm{L}}^{FEM,k}$ are suitable Galerkin discretizations[1]:

$$
\left(\underset{\sim}{\mathrm{L}}^{\mathrm{FEM},k} \omega^k \right)_i \equiv \left\langle\!\left\langle \omega^k \middle| B_i^{3-k} \right\rangle\!\right\rangle = \int_\Omega \omega^k \wedge B_i^{3-k} \qquad \forall\, i \in [1..\underset{\sim}{n}^k] \tag{C.4}
$$

For discretizing non-homogeneous magnetic boundary data on the dual boundary grid part $\underset{\sim}{\Gamma}_{2,h}$, the following *dual FEM boundary grid discretization operators* $\underset{\sim}{\mathrm{L}}^{FEM,k}_{\underset{\sim}{\Gamma}_{2,h}}$ are a suitable choice:

$$
\left(\underset{\sim}{\mathrm{L}}^{\mathrm{FEM},k}_{\underset{\sim}{\Gamma}_{2,h}} \omega^k \right)_i \equiv \int_{\Gamma_2} \omega^k \wedge B_p^{2-k}, \qquad p = \underset{\sim}{\mathrm{I}}^k_{\Gamma_2}(i), \quad \forall\, i \in [1..\underset{\sim}{n}^k_{\underset{\sim}{\Gamma}_{2,h}}] \tag{C.5}
$$

[1] The dual FEM grid discretization operators again commute with the exterior derivative in the inner part of the grid and show the same problems at the grid boundary as the dual grid discretization operators $\underset{\sim}{\mathrm{L}}^k$ for an explicit dual grid.

D. ERROR DEFINITIONS

D.1 General Discussion

In chapter 3.2.5, we have discussed existence and uniqueness of solutions to the semi-discrete Maxwell's IBVP. Assuming we have found a discrete solution, how does this discrete solution relate to the continuous solution of Maxwell's equations? Using the grid discretization operators L^k and $\underset{\sim}{\mathrm{L}}^k$ from Definition 3.6 on page 37, we can *grid discretize* the continuous solution as shown in the top row of Fig. D.1. Now we can compare this *grid discretized continuous solution* to the discrete solution in discrete norms as shown in the center column of Fig. D.1. As discussed in chapter 3.2, the discrete solution contains equivalent boundary terms in the electric grid current $\underset{\sim}{\hat{\hat{\mathbf{j}}}}{}^*_d$ and the magnetic grid charge $\underset{\sim}{\hat{\hat{\boldsymbol{\varrho}}}}{}^*_{e,d}$ due to the defect of the dual grid at the boundary. To be able to compare the grid discretized continuous solution to the discrete solution, the dual grid discretization operators $\underset{\sim}{\mathrm{L}}^{k,*}$ in Fig. D.1 are assumed to take into account needed equivalent boundary terms. Maxwell's discrete topological equations do hold for the primal and, due to the included equivalent boundary terms, dual quantities of the grid discretized continuous solution. Maxwell's discrete material relations do not hold for the dual quantities of the discretized solution, though, as the discrete material relations in general only approximate the continuous ones.

In order to compare the discrete and the continuous solution in continuous error norms, we need to reconstruct an approximate continuous solution from the discrete quantities. The Whitney reconstruction operators W^k introduced in chapter 4 provide such a reconstruction. The Whitney reconstruction operators only reconstruct continuous quantities for the primal grid quantities, though. Thus we can compare the primal quantities of the continuous solution to the primal quantities of the Whitney reconstructed discrete solution as shown by the left column of Fig. D.1. Alternatively, we can compare the primal quantities of the Whitney reconstruction of the grid discretized continuous solution to the primal quantities of the Whitney reconstructed discrete solution as shown by the right column of Fig. D.1. The later error comparisons are equivalent to the error comparisons in the discrete norms, as the primal grid discretization operators and the Whitney reconstruction operators describe isomorphisms from the primal cochain spaces $\mathcal{F}_h^k(\Omega_h)$ to the approximating Whitney spaces $\mathcal{W}^k(\Omega_h)$.

So how about dual Whitney reconstruction operators and error comparisons for the dual quantities in continuous norms? One could calculate continuous dual quantities from the reconstructed discrete solutions by using the continuous material relations, e.g. defining

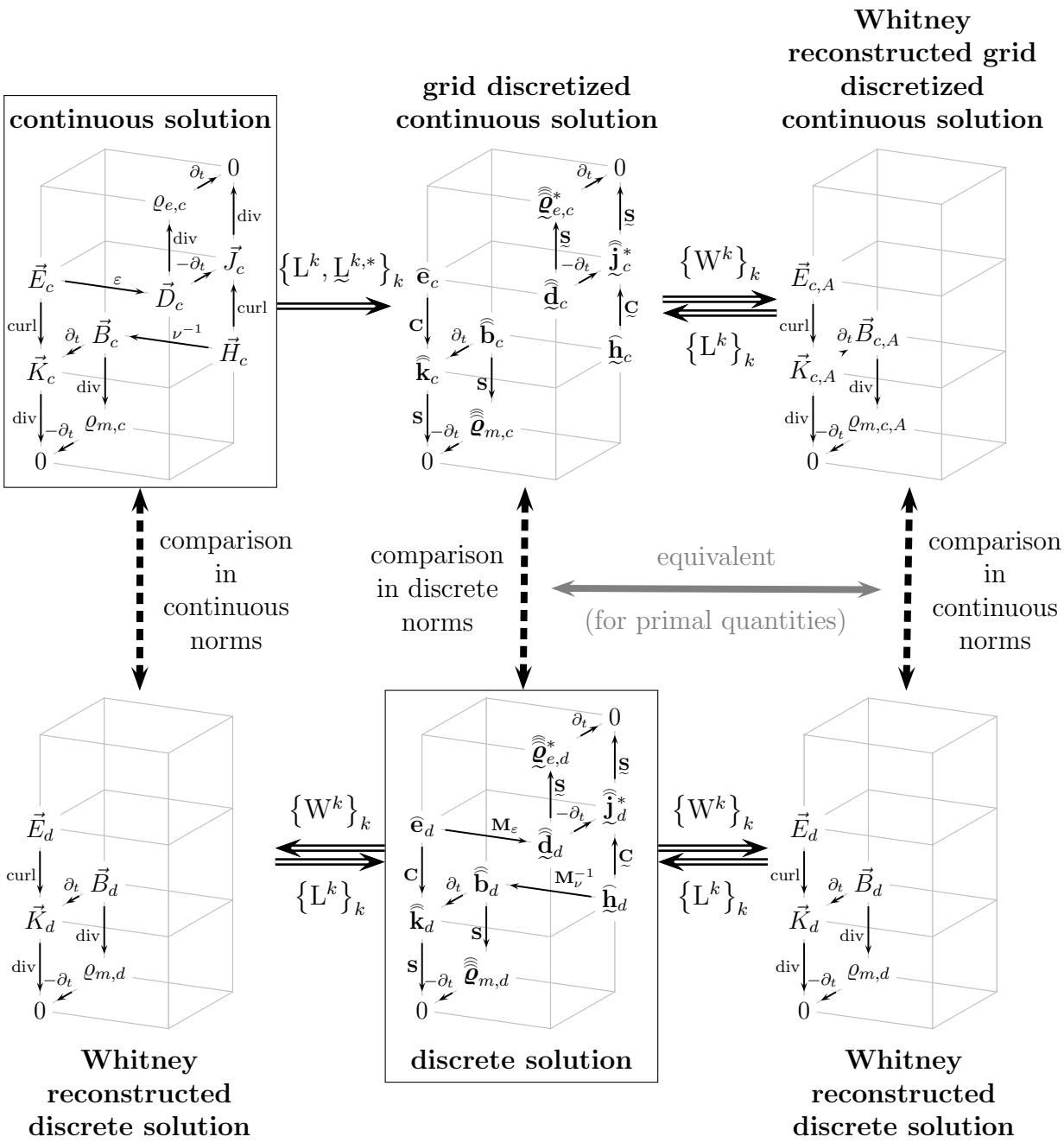

Fig. D.1: Possible error comparisons of the field quantities: Using the primal and dual grid discretization operators L^k and $\underset{\sim}{\mathrm{L}}^{k,*}$, the continuous solution denoted by the subscript c can be discretized and compared in discrete norms to the discrete solution denoted by the subscript d (center column). The $*$ in the dual grid discretization operator denotes that boundary terms are taken into account such that one can compare the resulting quantities to the FIT quantities containing equivalent boundary terms. Using the primal Whitney reconstruction operators W^k, one can reconstruct continuous quantities from the primal discrete quantities. Thus, for the primal quantities, one can compare the Whitney reconstructed discrete solution to the continuous solution (left column) or to the Whitney reconstruction of the grid discretized continuous solution (right column) in continuous norms.

the dual Whitney reconstruction operators $\underset{\sim}{\mathrm{W}}^k$ as:

$$\underset{\sim}{\mathrm{W}}^k \underset{\sim}{\boldsymbol{\omega}}^k \equiv \star \mathrm{W}^{3-k} \left(\mathbf{M}^{\mathrm{FEM},3-k}\right)^{-1} \underset{\sim}{\boldsymbol{\omega}}^k \qquad \notin \mathcal{F}_{\mathrm{d}}^k(\Omega) \tag{D.1}$$

The resulting functions are in general not in the subspace of the continuous problem spaces, though. Another possibility would be to define an explicit dual grid and then define dual Whitney reconstruction operators for the resulting polyhedral cells. The construction of a dual grid for a primal grid containing arbitrary polyhedral cells itself seems an open question and does depend on the choice for the discrete material operators, though. Thus we leave the question of how to compare dual quantities in continuous error norms open.

Often, not the errors in the field quantities themselves are of interest but errors of functionals of the field quantities. E.g. one needs to know the error in calculated forces, electromagnetic energy, or eigenfrequencies. If these functionals return scalar quantities in the continuous and in the discrete setting, as e.g. the continuous and discrete total electromagnetic energies W and W^d, one can directly compare these quantities in scalar norms.

The decision of which error norms to consider has to be guided by the application at hand. If one is interested in the field quantities in general, energy norms of the error are usually a good choice. Sometimes the maximum field error might be of interest, though, e.g. when the electric field strength has to stay below a certain electric strength. In the numerical example in chapter 5.2.1, the error was calculated in the discrete maximum error norm[1]. Of physical interest is the continuous maximum error norm, though. For the considered case of curved boundaries which are approximated piecewise linearly, their definition is non-trivial. These are only short comments trying to raise the awareness of the need for careful consideration of meaningful error definitions to use in each specific application.

[1] The error in the discrete maximum norm is often called the *local* error, as it describes the maximum local error. Errors in energy norms are in contrast often called *global* errors.

D.2 Example Error Discussion for the Eigenproblem Example from Chapter 5.1.1

In this chapter, we discuss the convergence of different error norms of the different quantities for the eigenproblem example of the rectangular waveguide with polygonal grids introduced in chapter 5.1.1. We do restrict ourselves to errors in the transverse and longitudinal electric field strength, although if other quantities are of interest, their error quantities should be considered. Due to the absence of reentrant corners or material jumps in the problem, the continuous solution is infinitely often continuously differentiable in the whole domain and exhibits no singularities. Therefore, the highest possible convergence rates for the specific grid type are to be expected.

Leaving the numerical solution at the side for the moment, we can consider the relative error in the projection of the continuous solution onto the Whitney approximation spaces by the Whitney projectors $P^k \equiv W^k \mathrm{L}^k$ defined on page 96. E.g. for the continuous solution of the transverse electric field strength $\underline{\vec{E}}_{t,c}$, we can consider the relative projection error

$$\|\underline{\vec{E}}_{t,c} - W^1 \mathrm{L}^1 \underline{\vec{E}}_{t,c}\|_2 \,/\, \|\underline{\vec{E}}_{t,c}\|_2 \tag{D.2}$$

where $\|.\|_p$ denotes the continuous p-norm defined as:

$$\|\underline{\mathrm{a}}\|_2 = \langle\!\langle \underline{\mathrm{a}} | \underline{\mathrm{a}} \rangle\!\rangle = \int_\Omega \underline{\mathrm{a}}^{\mathrm{H}} \cdot \underline{\mathrm{a}} \,\mathrm{d}A \tag{D.3}$$

and is calculated by high-order quadrature rules.

In Fig. D.2 and D.3, we notice convergence of the relative projection error with order $\frac{1}{2}$ in the number of unknowns, i.e. order 1 in h, for all grids. This is as expected for constant-exact basis functions / schemes. For the continuous solution of the longitudinal electric field strength $\underline{\mathrm{E}}_{z,c}$, we define the relative projection error as:

$$\|\underline{\mathrm{E}}_{z,c} - W^0 \mathrm{L}^0 \underline{\mathrm{E}}_{z,c}\|_2 \,/\, \|\underline{\mathrm{E}}_{z,c}\|_2 \tag{D.4}$$

The longitudinal electric field strength is only non-zero for the TM-modes, for which it converges with order 1 in the number of unknowns for all grids (see Fig. D.4). This is as expected for the linear-exact scheme. For the TE-modes, the zero longitudinal electric field strength is captured down to machine precision, so no error plots are given.

Let us now turn to errors between the numerically calculated solutions $\underline{\widehat{\mathbf{e}}}_{2\mathrm{D},t}$ and $\underline{\mathbf{e}}_{2\mathrm{D},z}$ and the continuous solutions $\underline{\vec{E}}_{t,c}$ and $\underline{\mathrm{E}}_{z,c}$. First, we discuss errors in discrete norms between the grid discretized continuous solution and the numerical solution as sketched in the center column of Fig. D.1. We define three different types of relative discrete errors for the edge-based quantity:

$$\|\mathrm{L}^1 \underline{\vec{E}}_{t,c} - \underline{\widehat{\mathbf{e}}}_{2\mathrm{D},t}\|_2 \,/\, \|\mathrm{L}^1 \underline{\vec{E}}_{t,c}\|_2 \tag{D.5}$$

$$\|\mathrm{L}^1 \underline{\vec{E}}_{t,c} - \underline{\widehat{\mathbf{e}}}_{2\mathrm{D},t}\|_E \,/\, \|\mathrm{L}^1 \underline{\vec{E}}_{t,c}\|_E \tag{D.6}$$

$$\|\mathrm{L}^1 \underline{\vec{E}}_{t,c} - \underline{\widehat{\mathbf{e}}}_{2\mathrm{D},t}\|_\infty \,/\, \|\mathrm{L}^1 \underline{\vec{E}}_{t,c}\|_\infty \tag{D.7}$$

and equivalently for the node-based quantity:

$$\|\mathrm{L}^0\underline{\mathrm{E}}_{z,c} - \underline{\mathbf{e}}_{2\mathrm{D},z}\|_2 \,/\, \|\mathrm{L}^0\underline{\mathrm{E}}_{z,c}\|_2 \tag{D.8}$$

$$\|\mathrm{L}^0\underline{\mathrm{E}}_{z,c} - \underline{\mathbf{e}}_{2\mathrm{D},z}\|_E \,/\, \|\mathrm{L}^0\underline{\mathrm{E}}_{z,c}\|_E \tag{D.9}$$

$$\|\mathrm{L}^0\underline{\mathrm{E}}_{z,c} - \underline{\mathbf{e}}_{2\mathrm{D},z}\|_\infty \,/\, \|\mathrm{L}^0\underline{\mathrm{E}}_{z,c}\|_\infty \tag{D.10}$$

where we define the discrete 2-, energy- and maximum-norms as:

$$\|\underline{\widehat{\mathbf{e}}}_{2\mathrm{D},t}\|_2 = \sqrt{\underline{\widehat{\mathbf{e}}}_{2\mathrm{D},t}{}^{\mathrm{H}} \cdot \underline{\widehat{\mathbf{e}}}_{2\mathrm{D},t}} \tag{D.11}$$

$$\|\underline{\widehat{\mathbf{e}}}_{2\mathrm{D},t}\|_E = \sqrt{\underline{\widehat{\mathbf{e}}}_{2\mathrm{D},t}{}^{\mathrm{H}}\mathbf{M}^1_{2\mathrm{D},\varepsilon_r}\underline{\widehat{\mathbf{e}}}_{2\mathrm{D},t}} \tag{D.12}$$

$$\|\underline{\widehat{\mathbf{e}}}_{2\mathrm{D},t}\|_\infty = \max\left|\underline{\widehat{\mathbf{e}}}_{2\mathrm{D},t}\right| \tag{D.13}$$

$$\|\underline{\mathbf{e}}_{2\mathrm{D},z}\|_2 = \sqrt{\underline{\mathbf{e}}_{2\mathrm{D},z}{}^{\mathrm{H}} \cdot \underline{\mathbf{e}}_{2\mathrm{D},z}} \tag{D.14}$$

$$\|\underline{\mathbf{e}}_{2\mathrm{D},z}\|_E = \sqrt{\underline{\mathbf{e}}_{2\mathrm{D},z}{}^{\mathrm{H}}\mathbf{M}^0_{2\mathrm{D},\varepsilon_r}\underline{\mathbf{e}}_{2\mathrm{D},z}} \tag{D.15}$$

$$\|\underline{\mathbf{e}}_{2\mathrm{D},z}\|_\infty = \max\left|\underline{\mathbf{e}}_{2\mathrm{D},z}\right| \tag{D.16}$$

The general constant in the eigenvector solutions is set to minimize the error (D.5), which can be done analytically.

The 2-norm and the energy norm errors should show equivalent convergence rates as the only difference is a scaling by the material matrix. Apparently due to the high regularity of the solutions, the ∞-norm errors also shows equivalent convergence rates.

The relative errors for the transverse electric voltages are shown in Fig. D.5 to D.10 for the first 10 modes. The minimal expected convergence rate in the number of edges is $\frac{1}{2}$. Certainly for all grids and all modes this is fulfilled. For certain grids and certain modes, the convergence rates are higher, though. For the standard diagonal FIT with grid 1, all quasi-1-dimensional modes, i.e. TE_{x0}- and TE_{0x}-modes, are captured down to machine precision, and therefore are not even shown on the convergence plots. This property is well-known, as for this quasi-1-dimensional case, the discrete scheme has exactly the grid discretizations of the continuous solution as eigensolutions[2]. Even for the other grids, so-called superconvergence results are observed for the quasi-1-dimensional modes: Grid 3 shows second order convergence for the TE_{10}-, TE_{01}-, TE_{20}-, TE_{30}-, and TE_{02}-modes, while grid 4 shows second order convergence for the TE_{01}- and the TE_{02}-mode. Also interesting to note is the superconvergence of at least first order (for the TM-modes seemingly in the limit case) for the grids 1, 2, and 4 and the constant low order of $\frac{1}{2}$ for grids 6 and 8. Grids 1, 2, and 4 all have the same tensor-product-like distribution of the grid nodes, while grids 6 and 8 have 2 common edges joined by most adjacent grid faces, which might hint at these being somehow good and bad grid properties.

For the nodal-based errors in the longitudinal electric voltages $\underline{\mathbf{e}}_{2\mathrm{D},z}$ of the TM-modes, we observe first order convergence in the number of edges for all grids in Fig. D.11 to

[2] More precisely, plane waves of the same form as in the continuous case are solutions to the discrete scheme without boundaries. The quasi-1-dimensional modes can be viewed as superpositions of these plane wave solutions with the same discrete wavenumber k_z which together fulfill the boundary conditions. For the fully 2-dimensional modes, the discrete wavenumber k_z of the modes needed for the superposition are in general not equivalent, so the exact eigenvectors are not captured any more.

D.13. This is the minimum order expected for solutions with such a high regularity. For the TE-modes, the zero longitudinal electric field strength is captured down to machine precision, so no error plots are given.

We can now use the Whitney reconstruction operator to compare the discrete and the continuous solutions in continuous norms by the following error definitions:

$$\|\underline{\vec{E}}_{t,c} - W^1 \underline{\widehat{\mathbf{e}}}_{2\mathrm{D},t}\|_2 \,/\, \|\underline{\vec{E}}_{t,c}\|_2 \tag{D.17}$$

$$\|W^1 \mathrm{L}^1 \underline{\vec{E}}_{t,c} - W^1 \underline{\widehat{\mathbf{e}}}_{2\mathrm{D},t}\|_2 \,/\, \|W^1 \mathrm{L}^1 \underline{\vec{E}}_{t,c}\|_2 \tag{D.18}$$

$$\|\underline{\mathrm{E}}_{z,c} - W^0 \underline{\mathbf{e}}_{2\mathrm{D},z}\|_2 \,/\, \|\underline{\mathrm{E}}_{z,c}\|_2 \tag{D.19}$$

$$\|W^0 \mathrm{L}^0 \underline{\mathrm{E}}_{z,c} - W^0 \underline{\mathbf{e}}_{2\mathrm{D},z}\|_2 \,/\, \|W^0 \mathrm{L}^0 \underline{\mathrm{E}}_{z,c}\|_2 \tag{D.20}$$

For grid 1 with the standard FIT with diagonal material matrices, reconstruction operators from an FEM formulation were used, as none are available in the standard FIT setting. The continuous relative error (D.17) converges as seen in Fig. D.14 and D.15 with order $\frac{1}{2}$, as expected. The relative error (D.18) shown in Fig. D.16 and D.17 behaves the same as the discrete 2-norm error (D.5), which is also to be expected, as these norms are equivalent on the discrete isomorphic spaces. The errors (D.19) and (D.20) are observed to converge with order 1 in Fig. D.18 and D.19, as expected.

In some error discussions, the values of the reconstructed solution and the continuous solution for the edge-based quantities are compared at the midpoints of the edges only:

$$\|[\underline{\vec{E}}_{t,c}(m_i) - W^1 \underline{\widehat{\mathbf{e}}}_{2\mathrm{D},t}(m_i)] \cdot \vec{t}_i\|_2 \,/\, \|\underline{\vec{E}}_{t,c}(m_i) \cdot \vec{t}_i\|_2 \tag{D.21}$$

$$\|[\underline{\vec{E}}_{t,c}(m_i) - W^1 \underline{\widehat{\mathbf{e}}}_{2\mathrm{D},t}(m_i)] \cdot \vec{t}_i\|_\infty \,/\, \|\underline{\vec{E}}_{t,c}(m_i) \cdot \vec{t}_i\|_\infty \tag{D.22}$$

The convergence plots for these errors in Fig. D.20 to D.23 are observed to be almost equivalent to the discrete error norms (D.5) and (D.7), with the exception of the missing super-convergence properties.

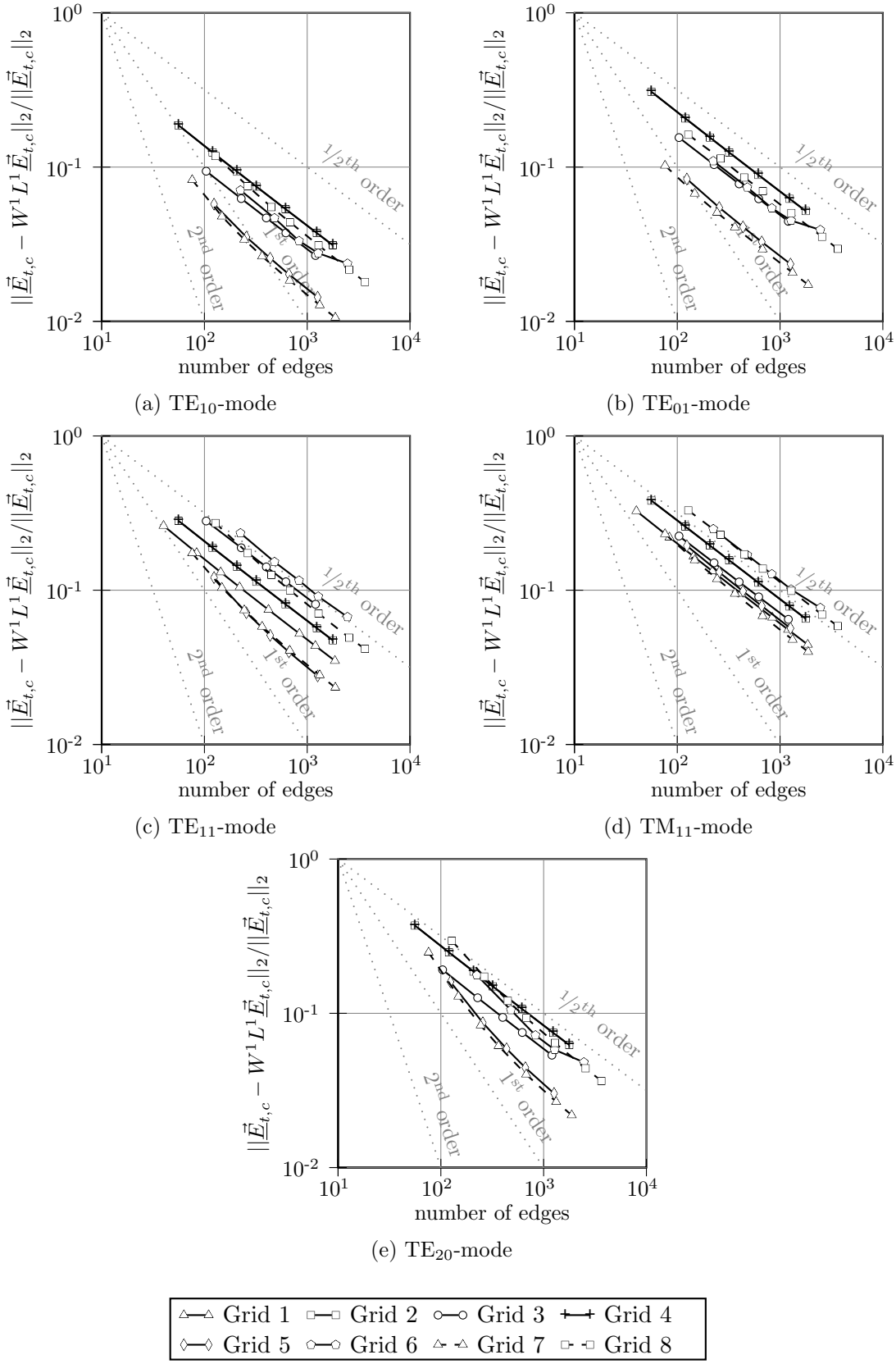

(a) TE_{10}-mode

(b) TE_{01}-mode

(c) TE_{11}-mode

(d) TM_{11}-mode

(e) TE_{20}-mode

Fig. D.2: Relative projection errors for the continuous solution of the transverse electric field strength $\vec{\underline{E}}_{t,c}$ in the continuous 2-norm for the first 5 modes.

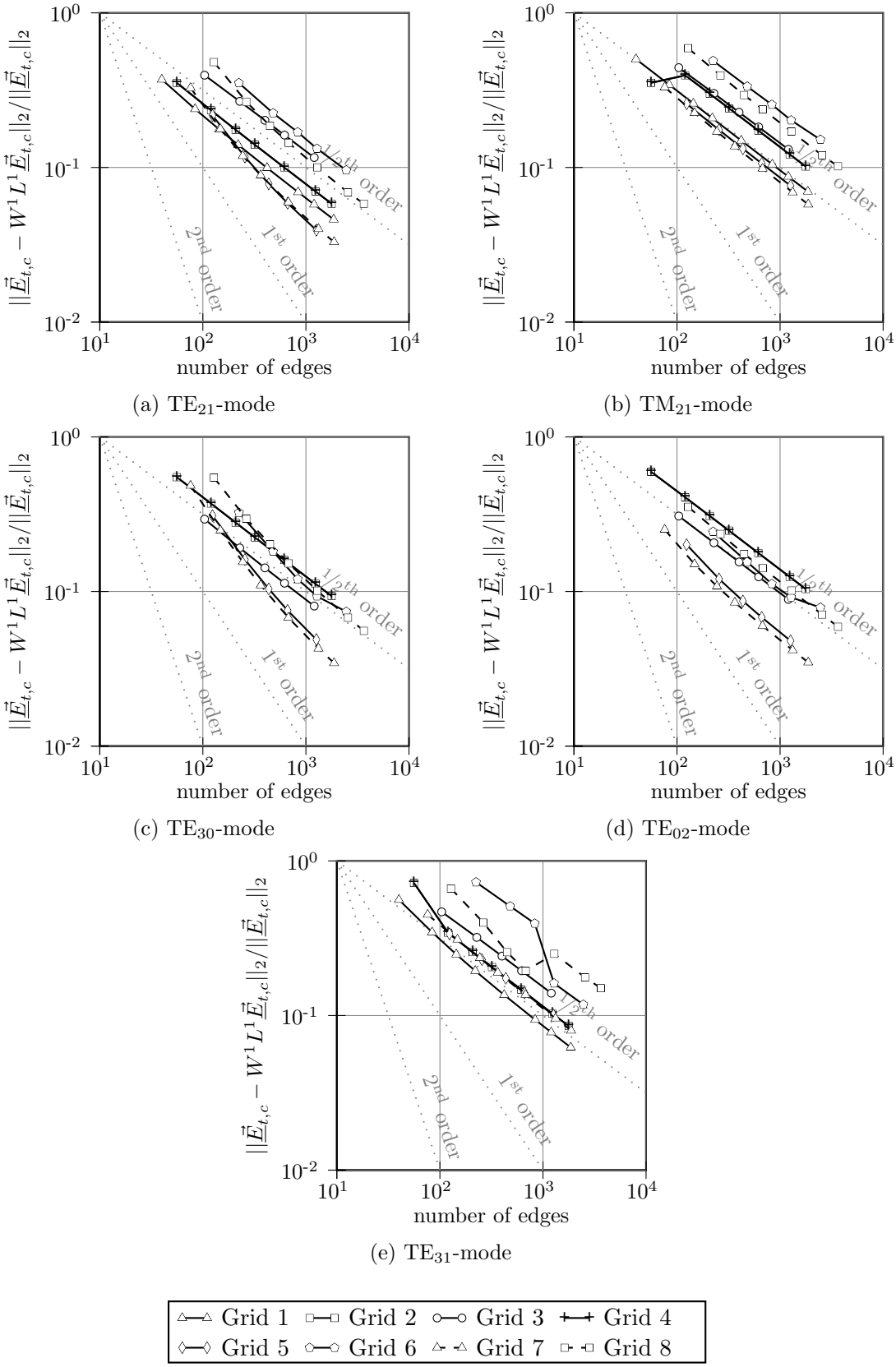

Fig. D.3: Relative projection errors for the continuous solution of the transverse electric field strength $\vec{\underline{E}}_{t,c}$ in the continuous 2-norm for the second 5 modes.

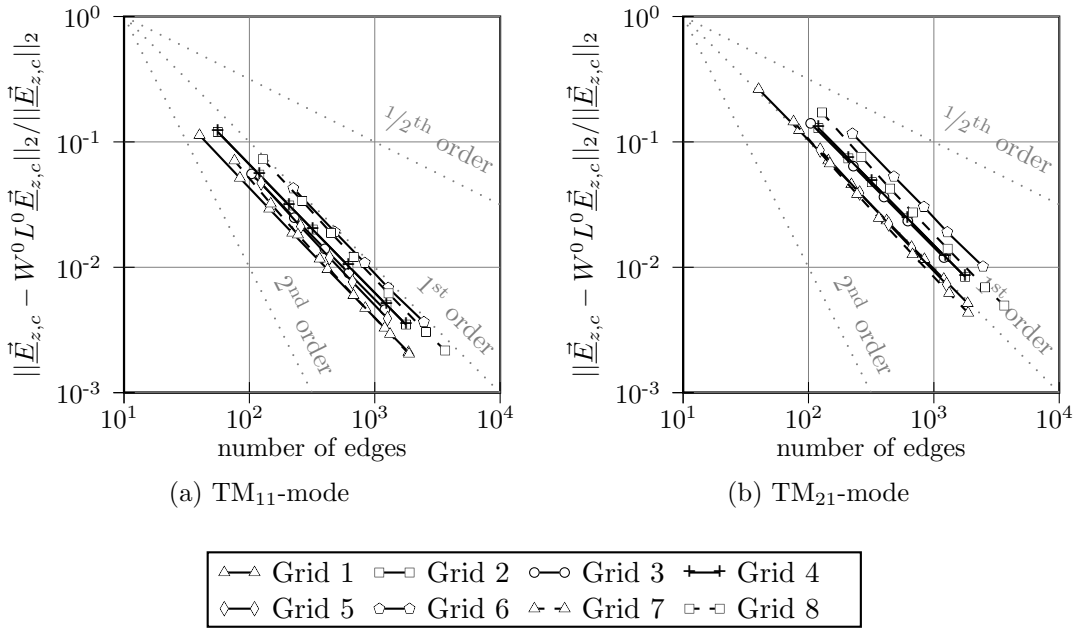

(a) TM_{11}-mode (b) TM_{21}-mode

Fig. D.4: Relative projection errors for the continuous solution of the longitudinal electric field strength $\underline{E}_{z,c}$ in the continuous 2-norm for the TM-modes.

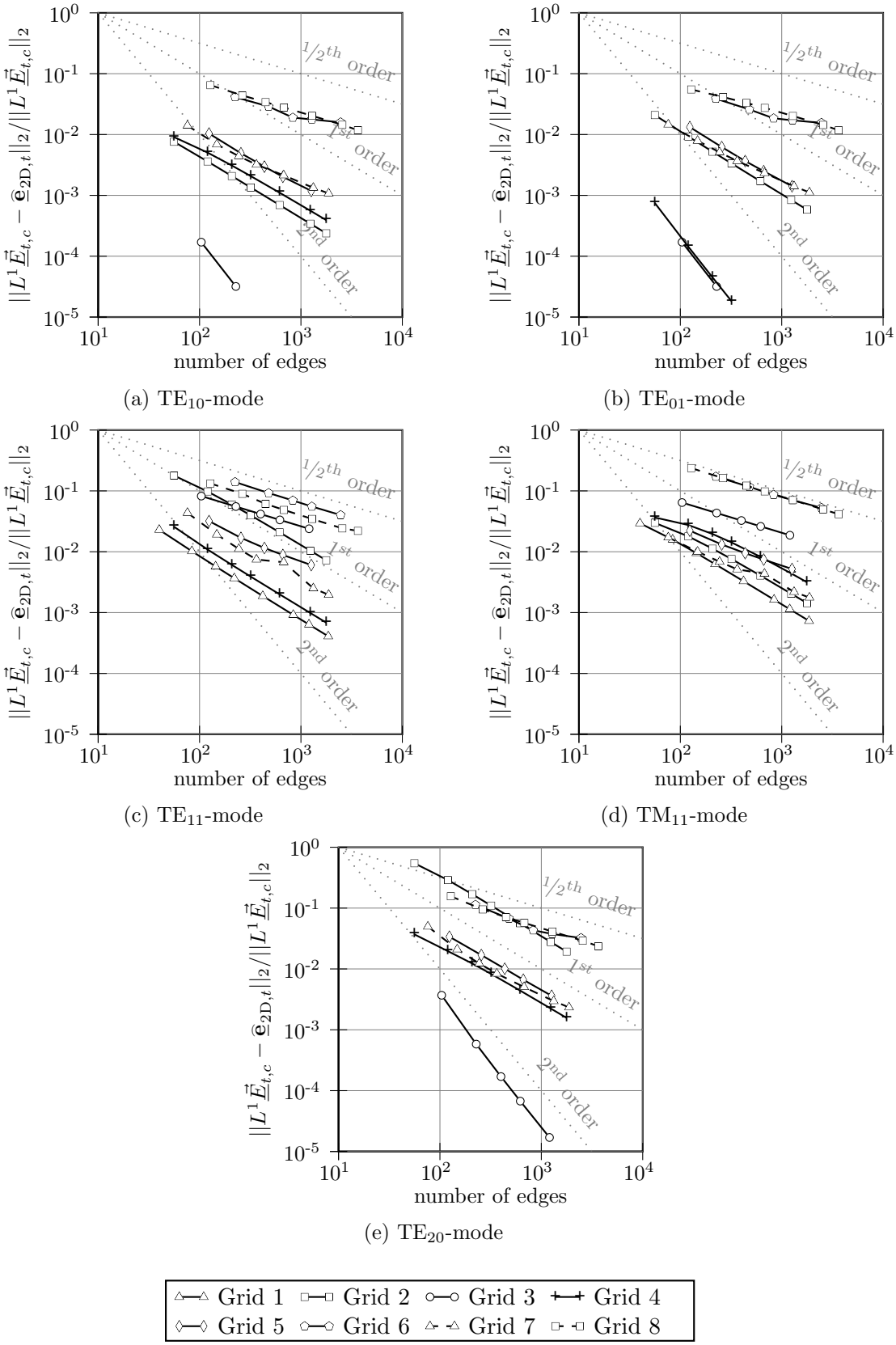

(a) TE_{10}-mode

(b) TE_{01}-mode

(c) TE_{11}-mode

(d) TM_{11}-mode

(e) TE_{20}-mode

Fig. D.5: Relative errors in the discrete 2-norm for the transverse electric field strength of the first 5 modes.

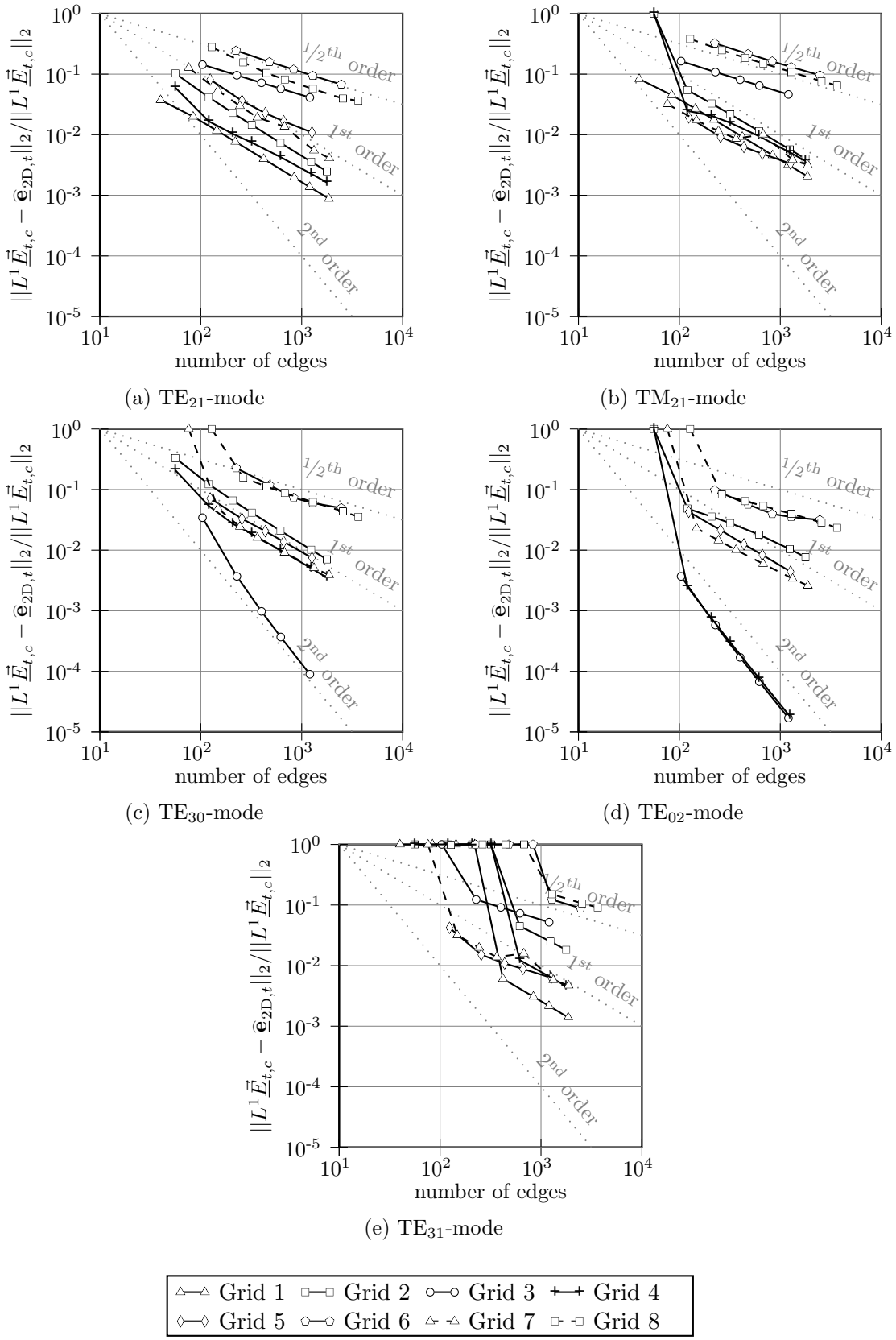

(a) TE_{21}-mode

(b) TM_{21}-mode

(c) TE_{30}-mode

(d) TE_{02}-mode

(e) TE_{31}-mode

Fig. D.6: Relative errors in the discrete 2-norm for the transverse electric field strength of the second 5 modes.

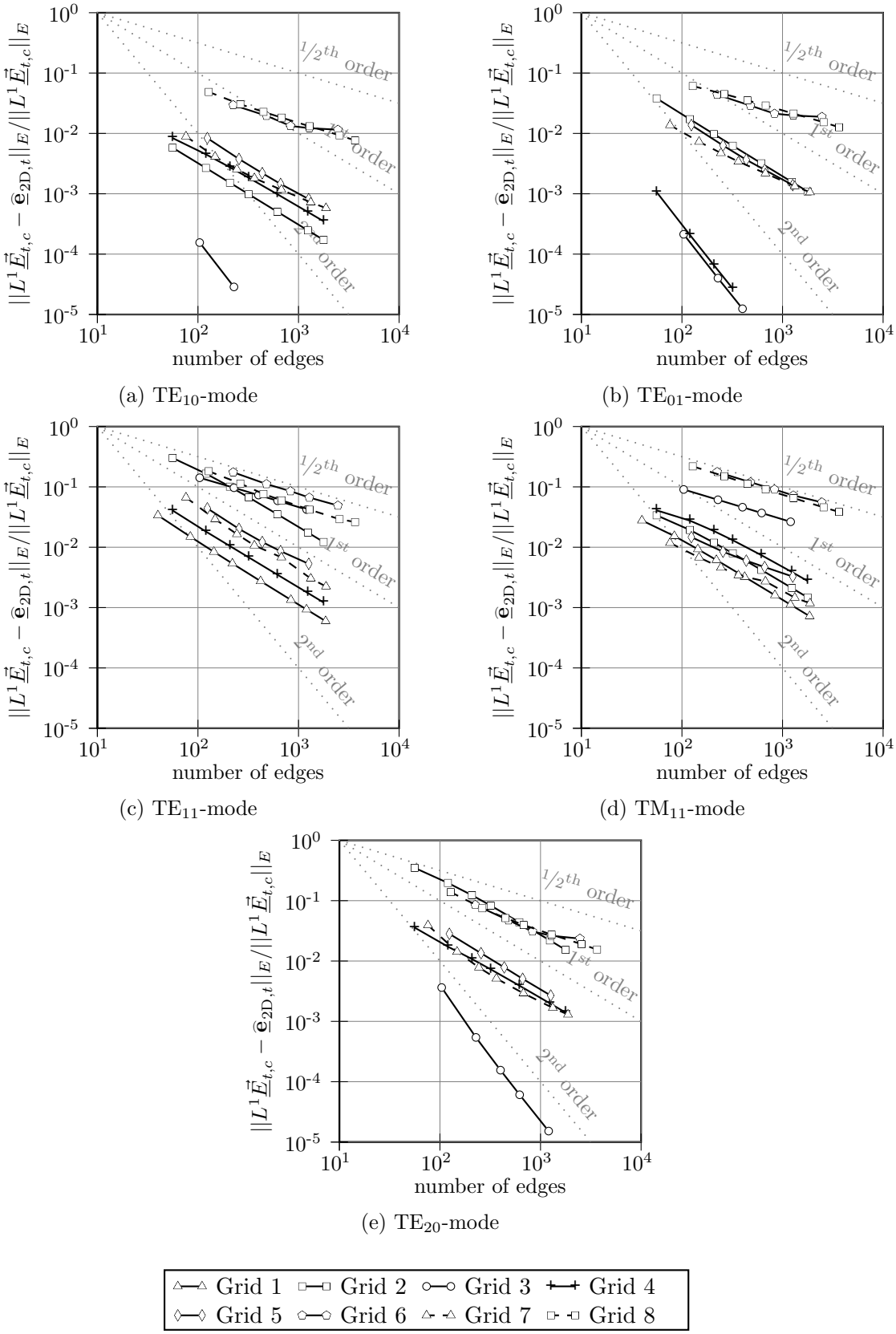

Fig. D.7: Relative errors in the discrete energy-norm for the transverse electric field strength of first 5 modes.

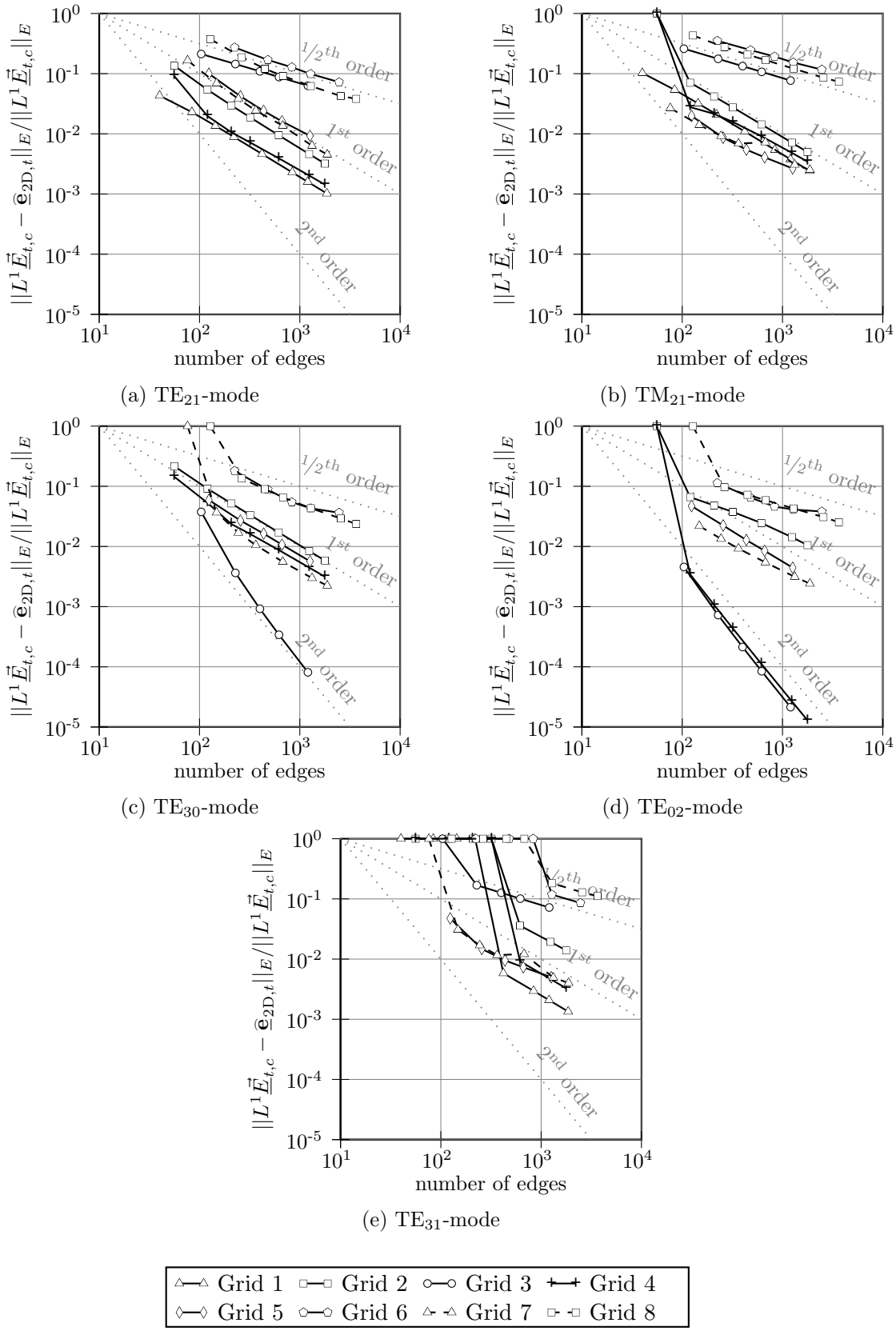

Fig. D.8: Relative errors in the discrete energy-norm for the transverse electric field strength of the second 5 modes.

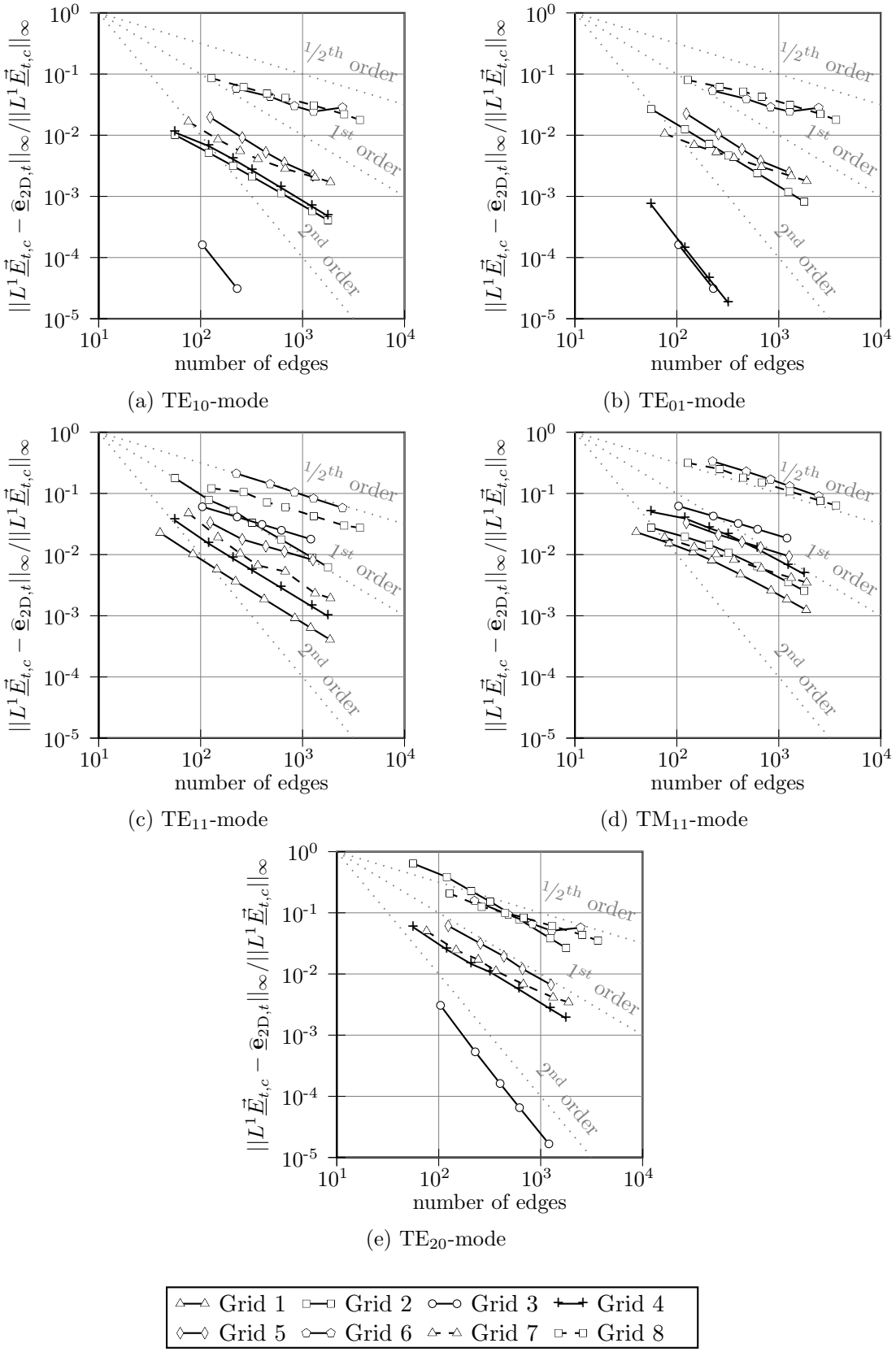

Fig. D.9: Relative errors in the discrete maximum-norm for the transverse electric field strength of the first 5 modes.

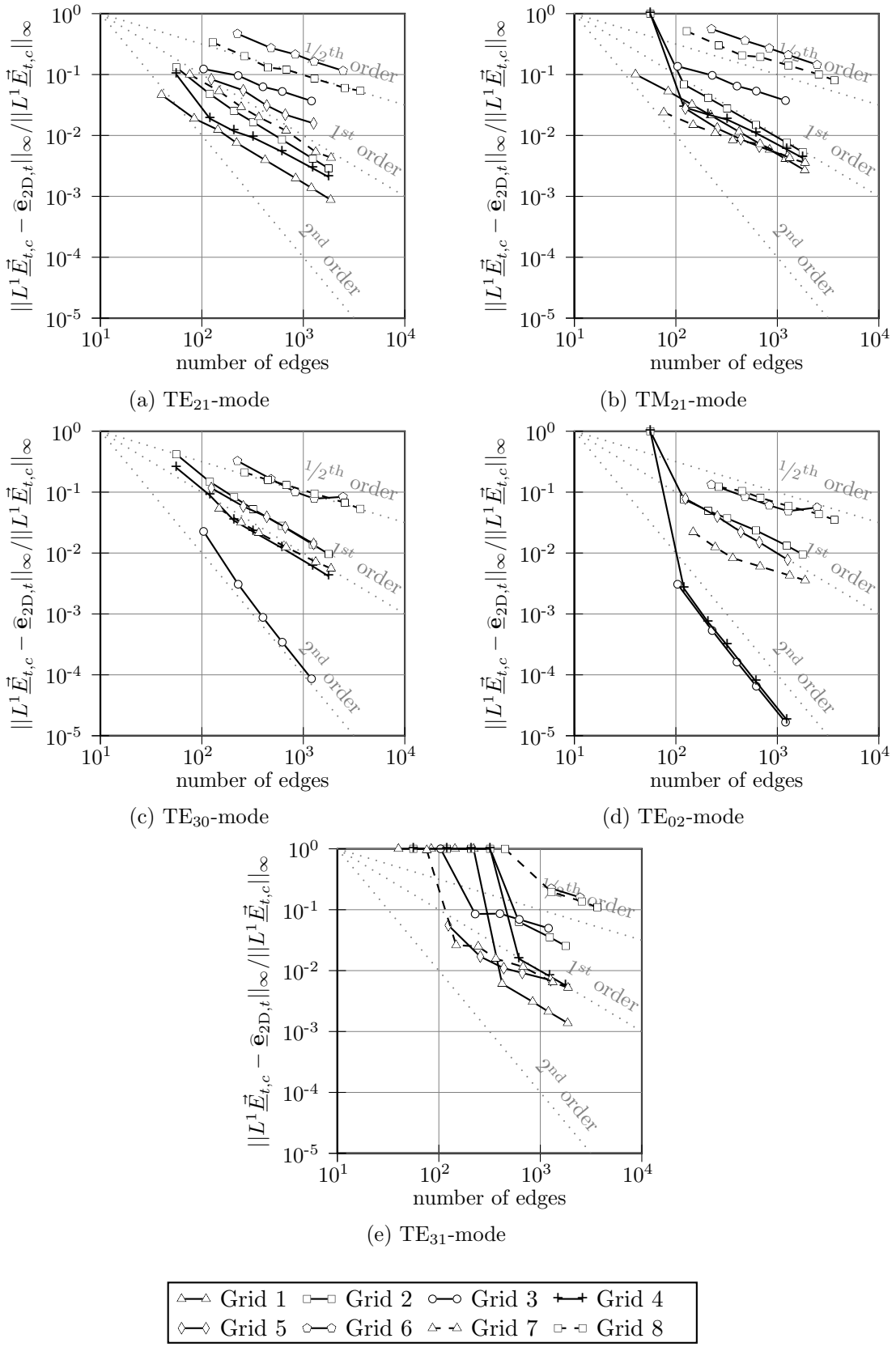

Fig. D.10: Relative errors in the discrete maximum-norm for the transverse electric field strength of the second 5 modes.

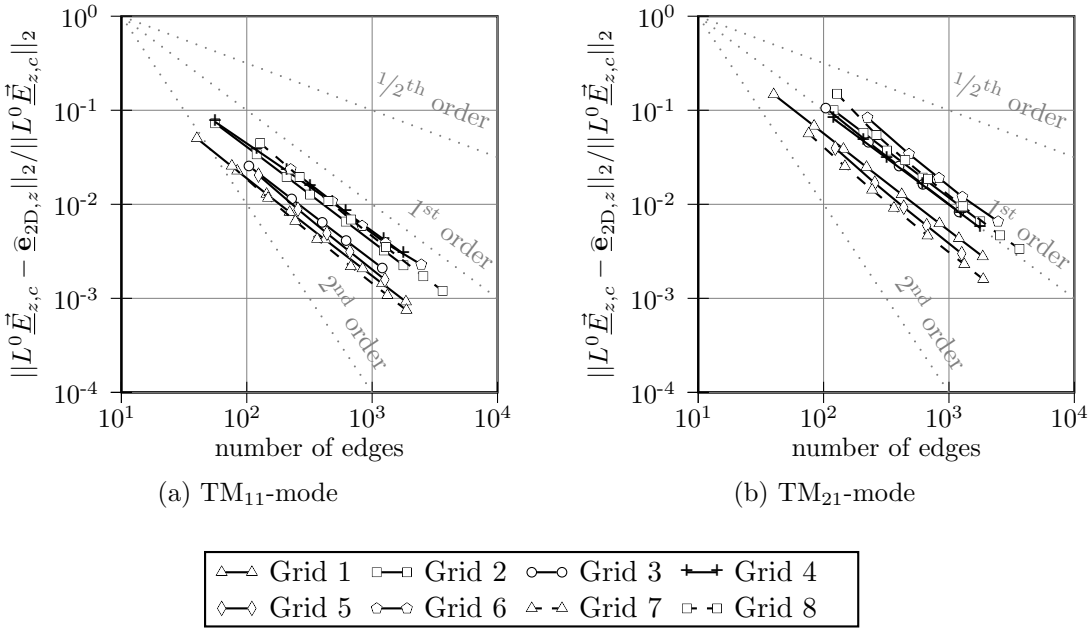

(a) TM_{11}-mode (b) TM_{21}-mode

Fig. D.11: Relative errors in the discrete 2-norm for the longitudinal electric field strength of the TM-modes.

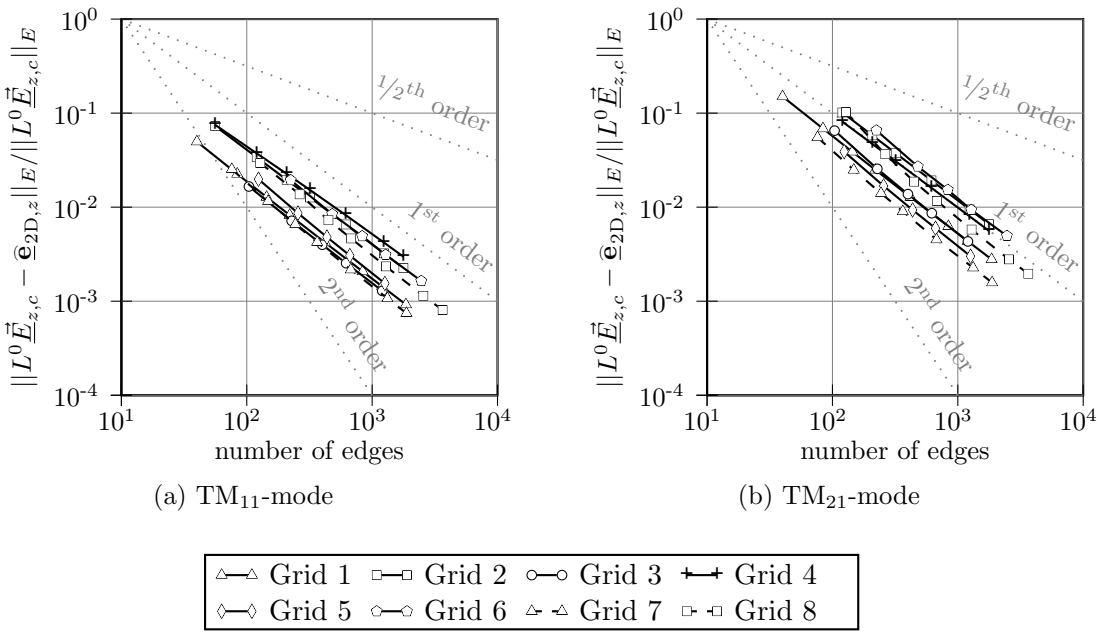

(a) TM_{11}-mode (b) TM_{21}-mode

Fig. D.12: Relative errors in the discrete energy-norm for the longitudinal electric field strength of the TM-modes.

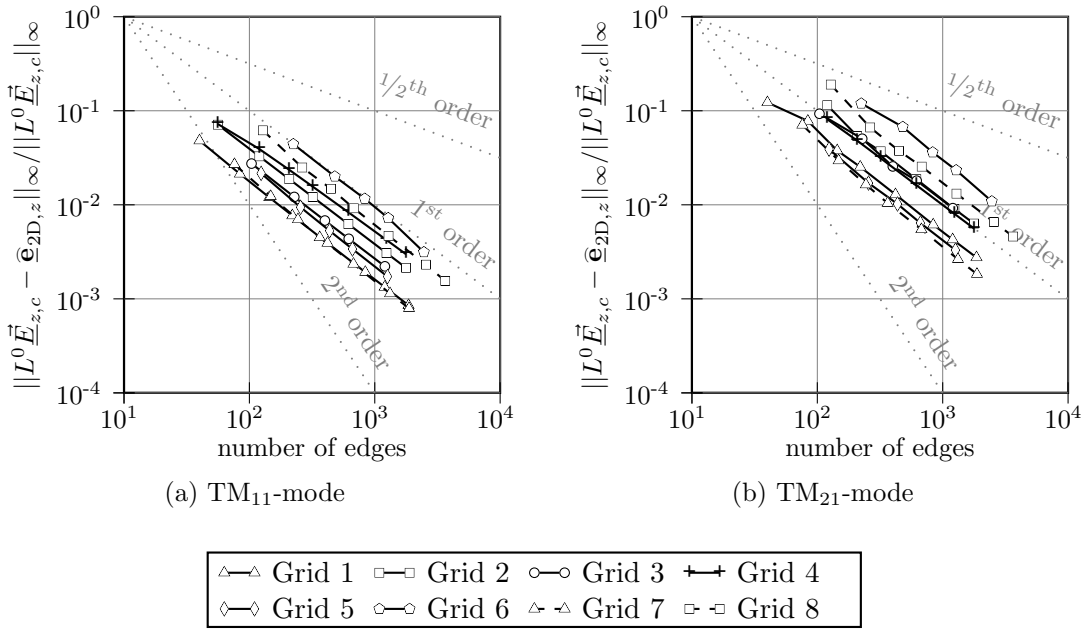

(a) TM_{11}-mode (b) TM_{21}-mode

Fig. D.13: Relative errors in the discrete maximum-norm for the longitudinal electric field strength of the TM-modes.

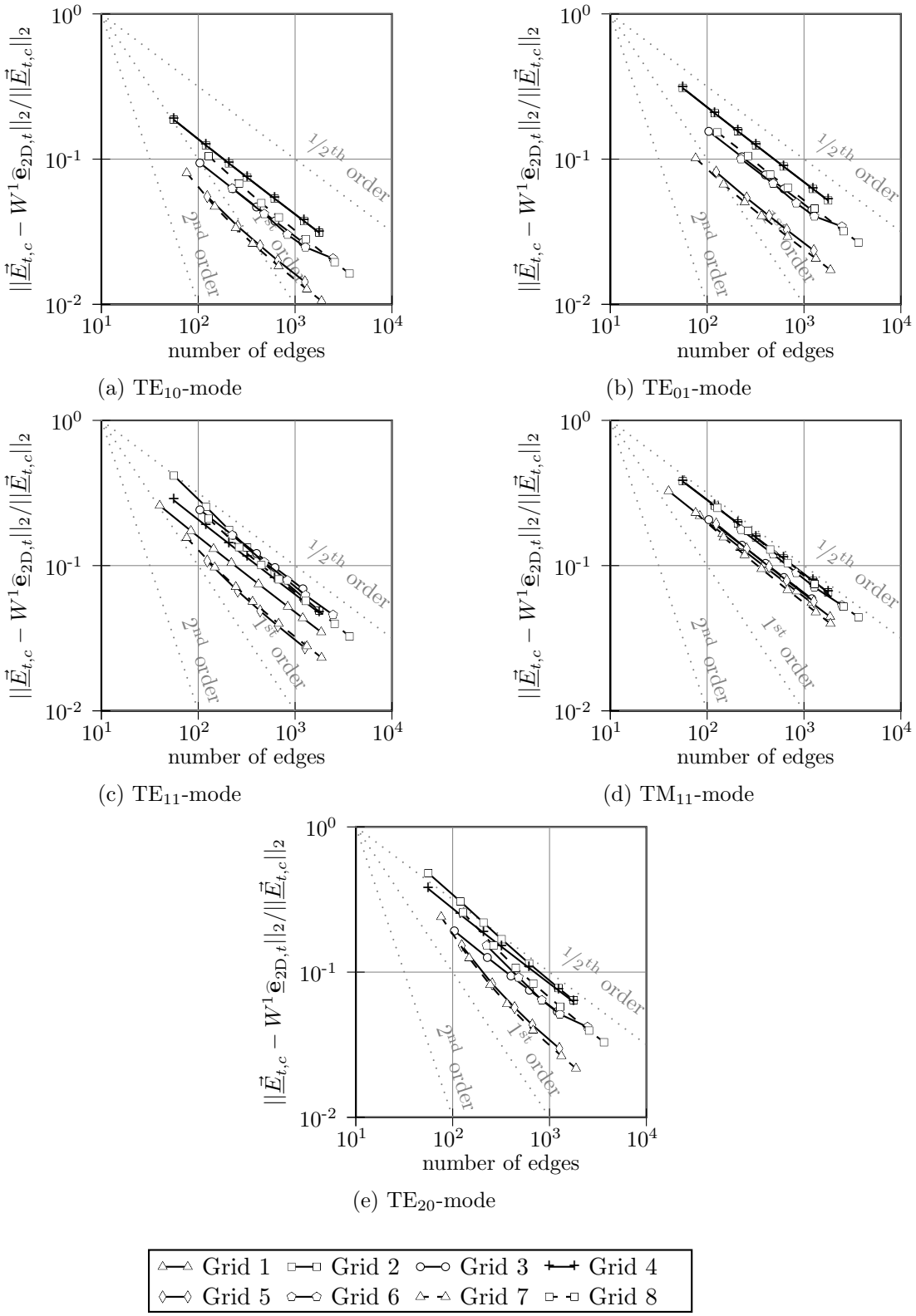

Fig. D.14: Relative errors in the continuous 2-norm for the transverse electric field strength of the first 5 modes.

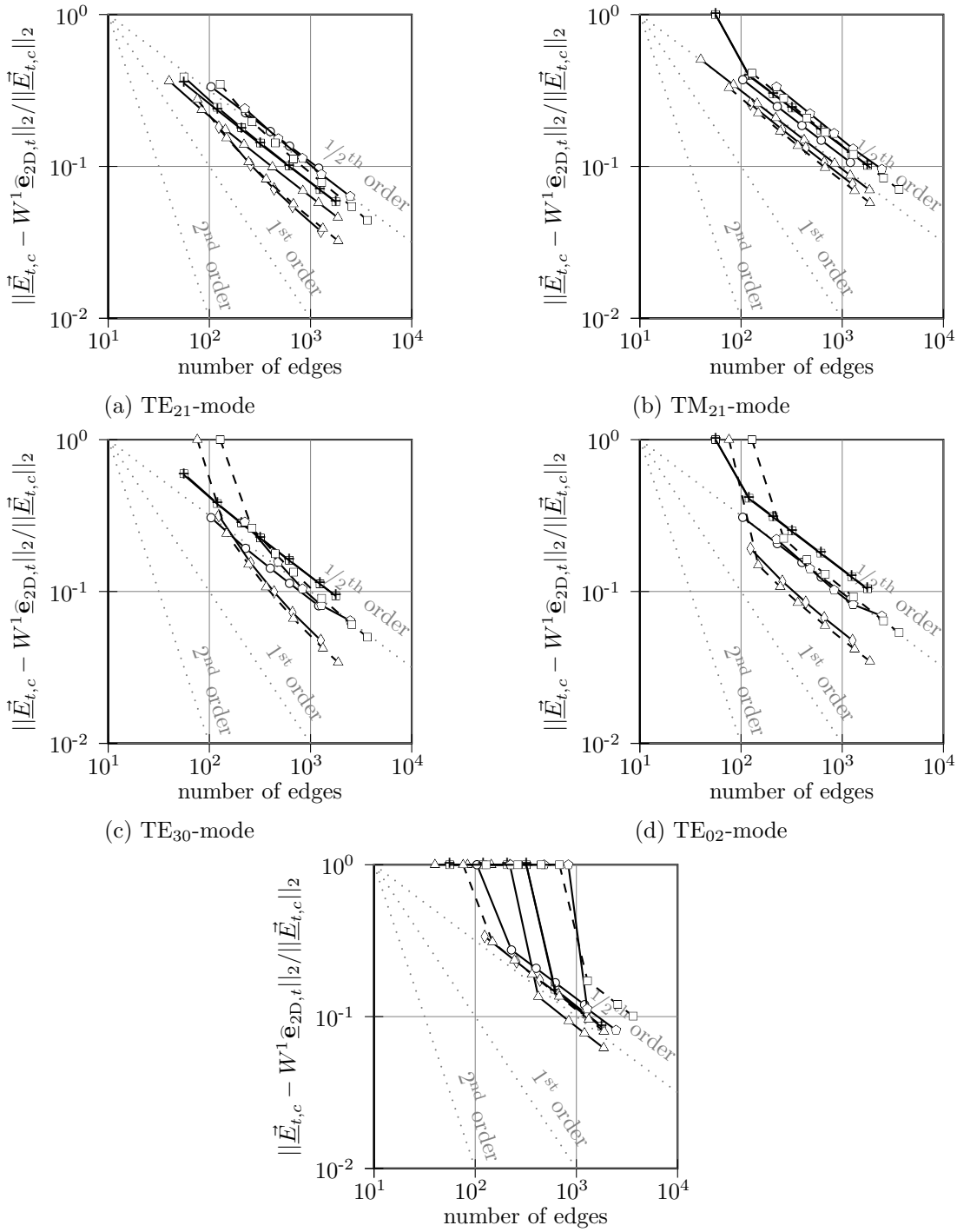

(a) TE_{21}-mode

(b) TM_{21}-mode

(c) TE_{30}-mode

(d) TE_{02}-mode

(e) TE_{31}-mode

Grid 1 Grid 2 Grid 3 Grid 4
Grid 5 Grid 6 Grid 7 Grid 8

Fig. D.15: Relative errors in the continuous 2-norm for the transverse electric field strength of the second 5 modes.

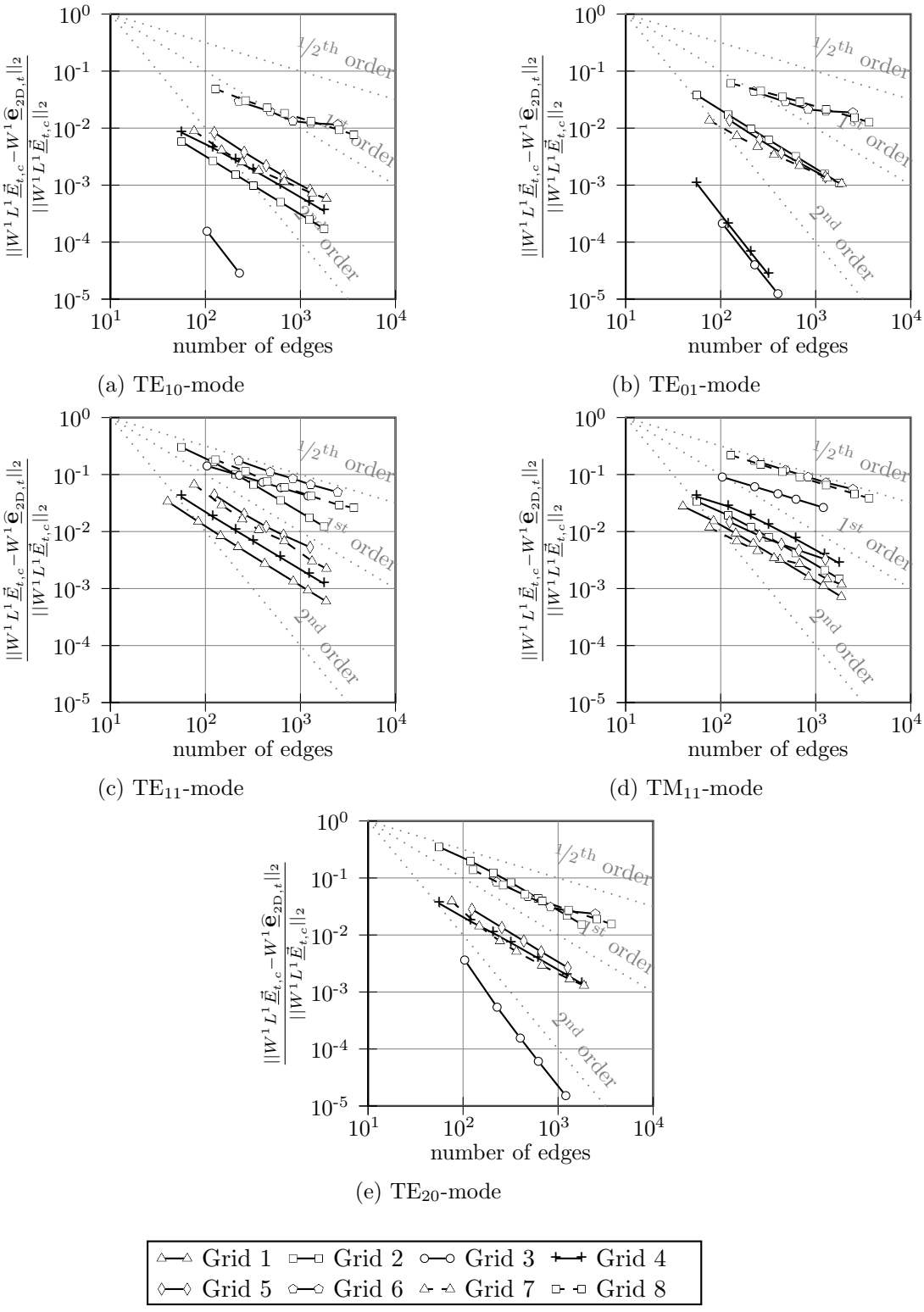

Fig. D.16: Relative errors in the continuous 2-norm for the transverse electric field strength of the first 5 modes.

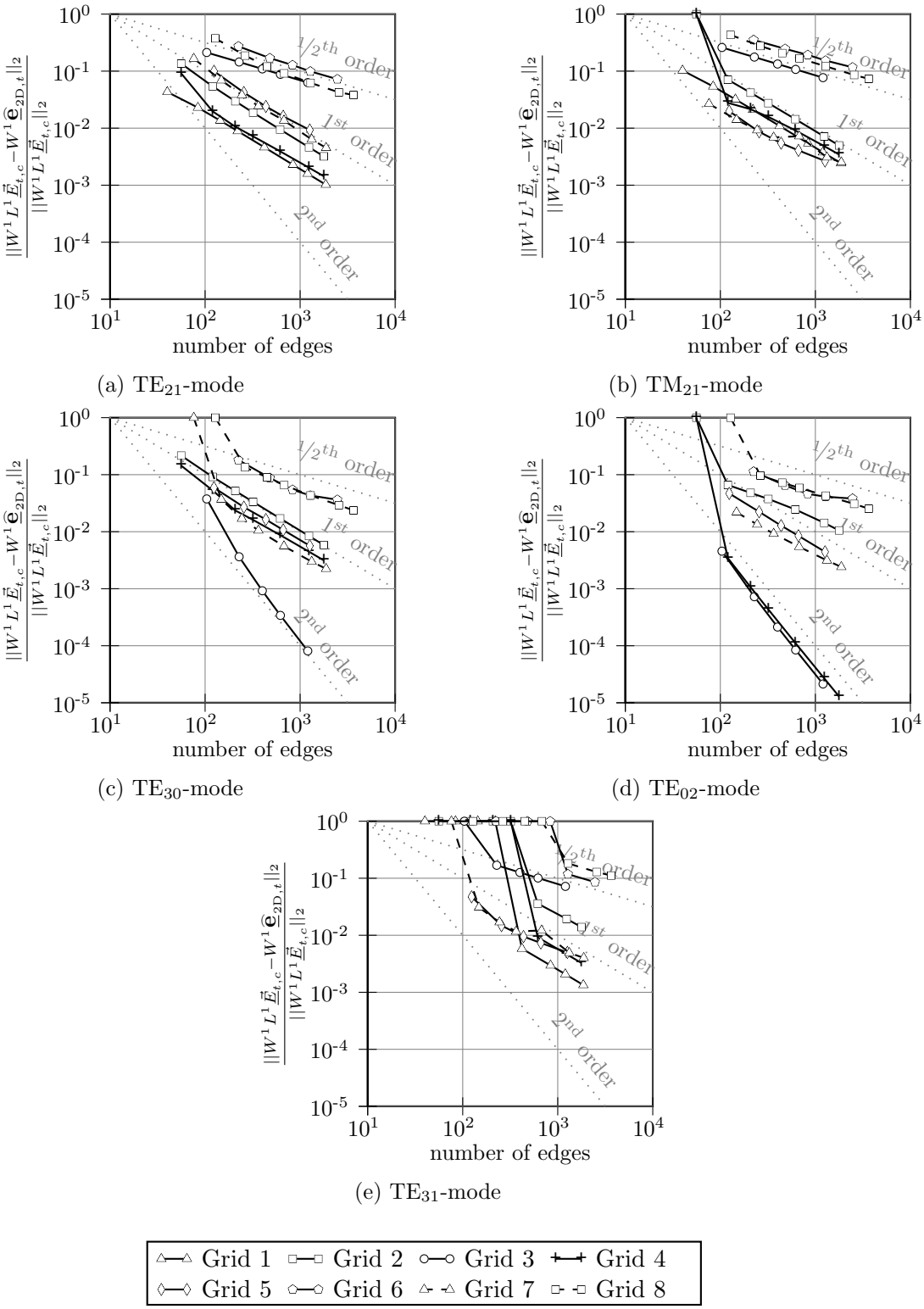

Fig. D.17: Relative errors in the continuous 2-norm for the transverse electric field strength of the second 5 modes.

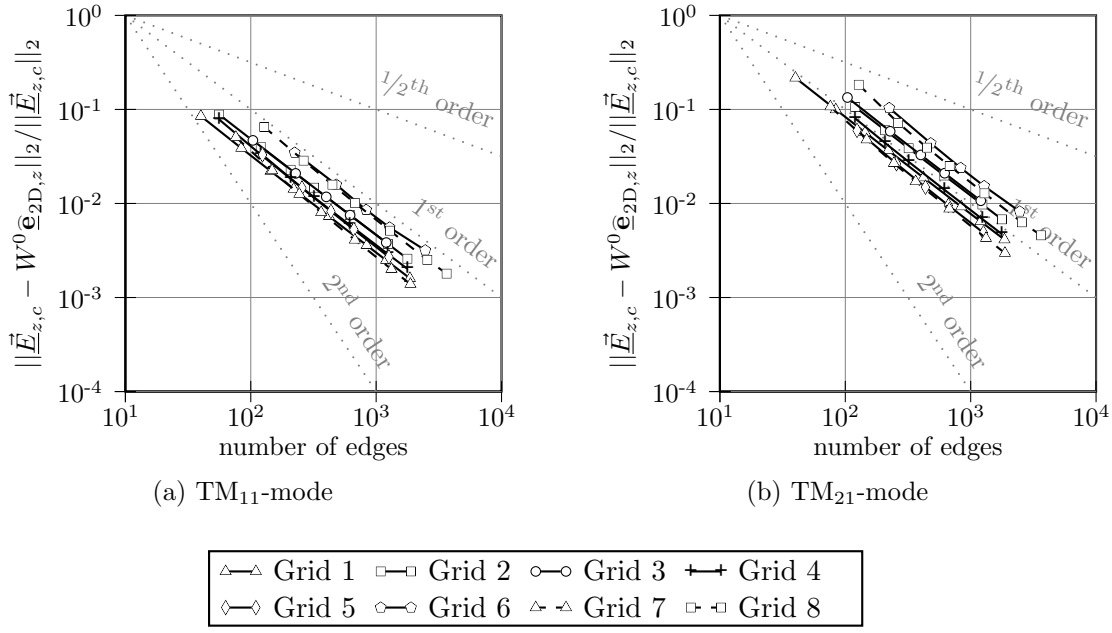

(a) TM_{11}-mode (b) TM_{21}-mode

Fig. D.18: Relative errors in the continuous 2-norm for the longitudinal electric field strength of the TM-modes.

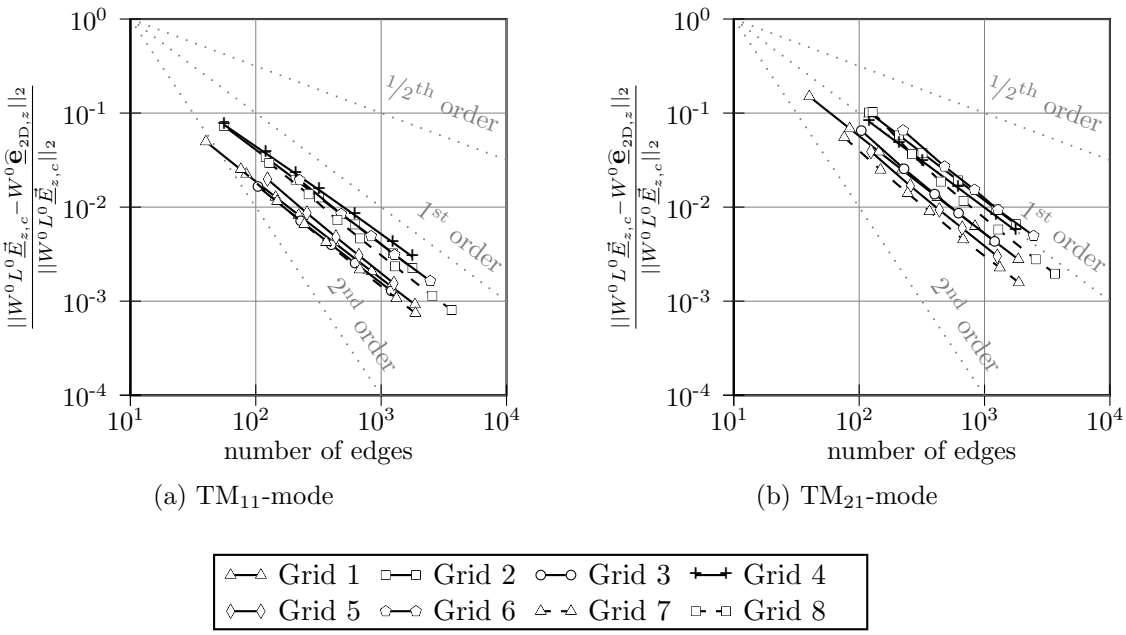

(a) TM_{11}-mode (b) TM_{21}-mode

Fig. D.19: Relative errors in the continuous 2-norm for the longitudinal electric field strength of the TM-modes.

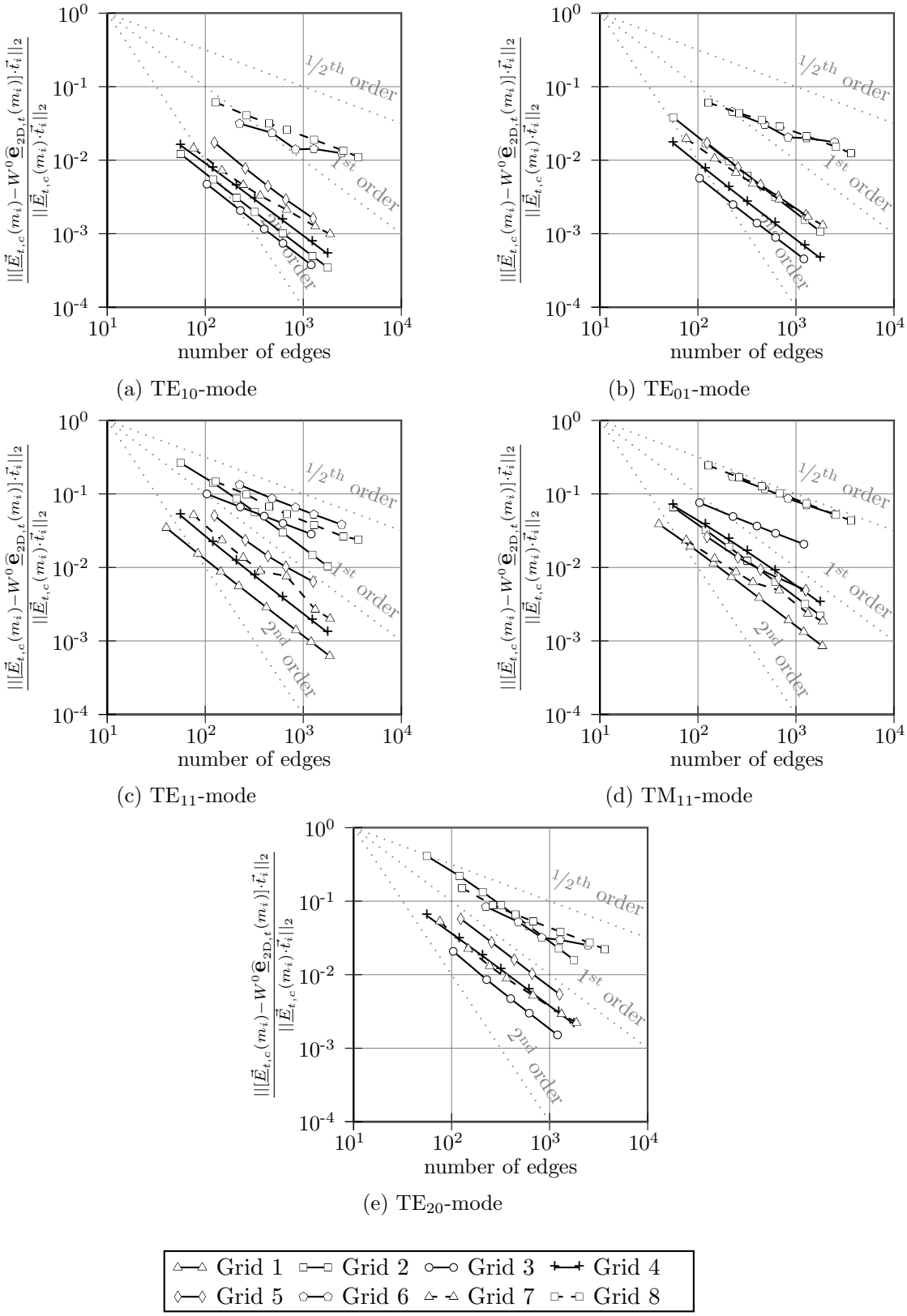

(a) TE_{10}-mode

(b) TE_{01}-mode

(c) TE_{11}-mode

(d) TM_{11}-mode

(e) TE_{20}-mode

Fig. D.20: Relative errors of the tangential component of the transverse electric field strength at the edge midpoints in the discrete 2-norm of the first 5 modes.

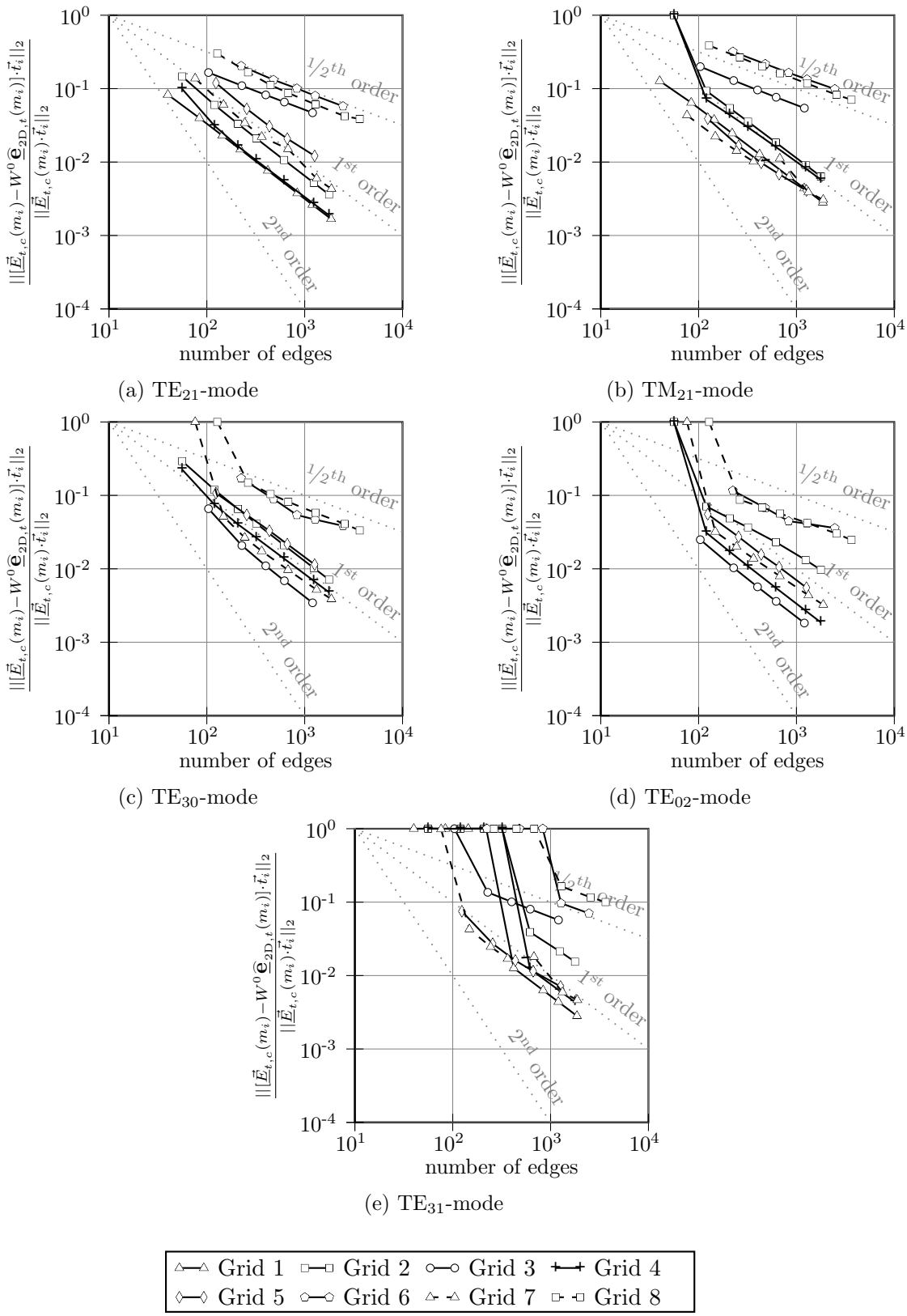

(a) TE_{21}-mode

(b) TM_{21}-mode

(c) TE_{30}-mode

(d) TE_{02}-mode

(e) TE_{31}-mode

Fig. D.21: Relative errors of the tangential component of the transverse electric field strength at the edge midpoints in the discrete 2-norm of the second 5 modes.

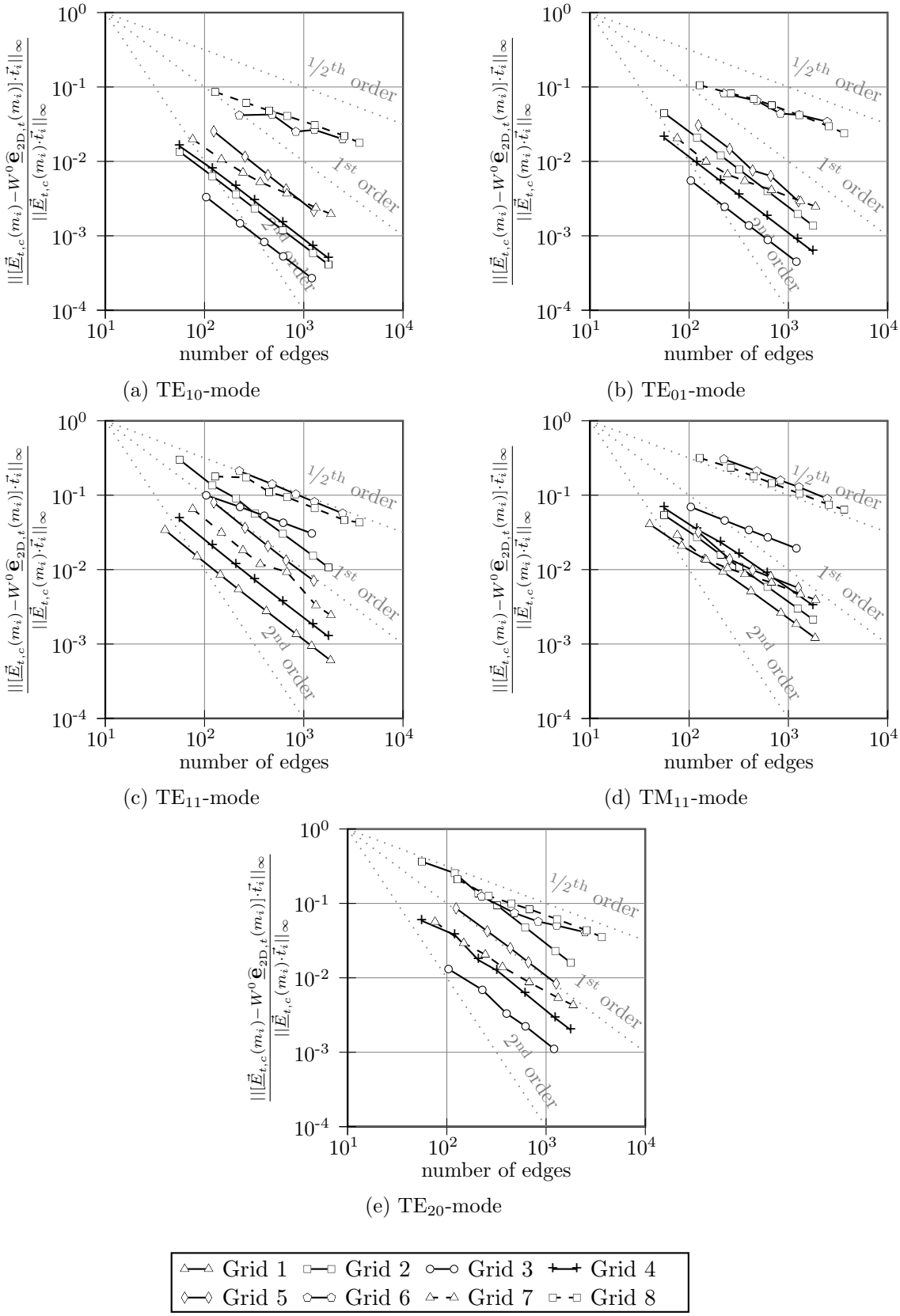

(a) TE_{10}-mode

(b) TE_{01}-mode

(c) TE_{11}-mode

(d) TM_{11}-mode

(e) TE_{20}-mode

Fig. D.22: Relative errors of the tangential component of the transverse electric field strength at the edge midpoints in the discrete maximum-norm of the first 5 modes.

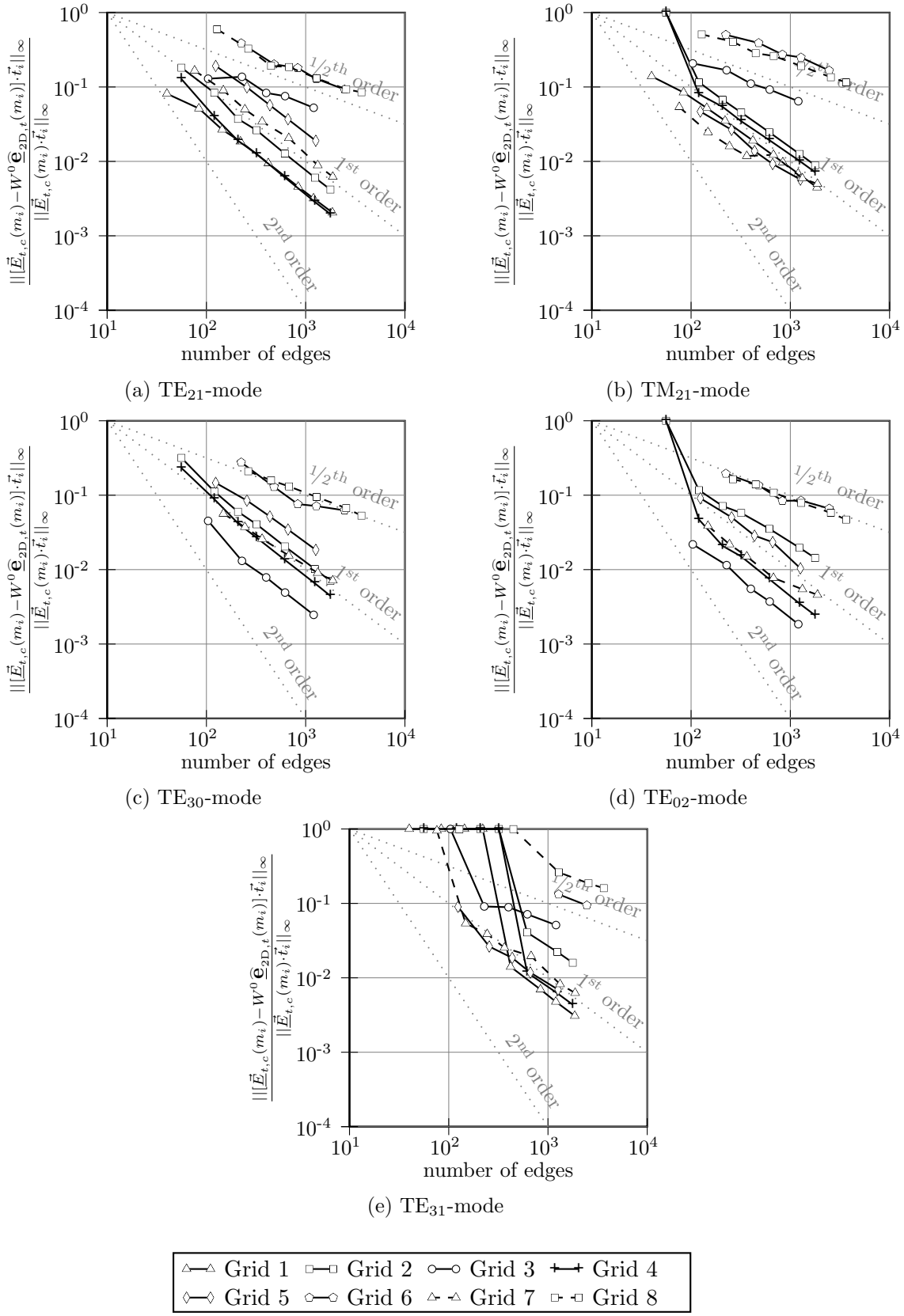

(a) TE_{21}-mode

(b) TM_{21}-mode

(c) TE_{30}-mode

(d) TE_{02}-mode

(e) TE_{31}-mode

Fig. D.23: Relative errors of the tangential component of the transverse electric field strength at the edge midpoints in the discrete maximum-norm of the second 5 modes.

E. STABILITY, CONSISTENCY, AND CONVERGENCE OF DISCRETE APPROXIMATION SCHEMES

The term *stability* is used in the computational engineering community to denote various different concepts. We resort to basic mathematical definitions [75, p. 312] and [75, pp. 320] to clarify these concepts.

We first state a continuous linear problem and then describe a sequence of discrete schemes to approximate this linear problem. This is the correct setup to discuss *stability*, *consistency*, and *convergence* of discrete approximation schemes. The analysis will be very abstract, but allows for the concepts to stay clear.

The continuous linear problem to be approximated reads:

$$\mathrm{L}\mathbf{x} = b \tag{E.1}$$

with the unknown $\mathbf{x}$, the given data b, and the invertible linear operator L:

$$\mathrm{L}: \qquad U \longrightarrow F \tag{E.2}$$

The inverse L^{-1} of the operator L is assumed to be *bounded*:

Definition E.1 (Bounded operator)**.** A linear operator $\mathrm{A} : F \longrightarrow U$ with F and U normed spaces with norms $\|.\|_F$ and $\|.\|_U$, respectively, is called *bounded*, if there exists a constant $C \in \mathbb{R}$ such that for all $b \in F$

$$\|\mathrm{A}b\|_U \leq C\|b\|_F \tag{E.3}$$

Considering an IBVP, the data b actually contains initial and boundary conditions as well as source terms.

We assume a sequence of discrete operators $\{\mathrm{L}_h\}_h$

$$\mathrm{L}_h: \qquad U_h \longrightarrow F_h \tag{E.4}$$

along with discretization operators P_{U_h} and P_{F_h}

$$\mathrm{P}_{U_h}: \qquad U \longrightarrow U_h \tag{E.5}$$

$$\mathrm{P}_{F_h}: \qquad F \longrightarrow F_h \tag{E.6}$$

given for some sequence parameter h with $h \to 0$. Then the sequence of discrete approximation problems reads

$$\mathrm{L}_h \mathbf{x}_h = \mathrm{P}_{F_h} b \qquad \forall\, h \tag{E.7}$$

rendering the sequence $\{\mathbf{x}_h\}_h$ of discrete approximate solutions. Usually, not a specific sequence of discrete problems is examined but a class of sequences fulfilling restrictions on certain discretization parameters as the time-step or grid size.

We also need the concept of *uniform boundedness* for a sequence of operators:

Definition E.2 (Uniform boundedness)**.** A sequence of linear operators $\mathrm{A}_h : F_h \longrightarrow U_h$ with the sequences F_h and U_h of normed spaces with norms $\|.\|_{F_h}$ and $\|.\|_{U_h}$, respectively, is called *uniformly bounded*, if there exists a constant $C \in \mathbb{R}$ independent of h such that for all h and for all $b_h \in F_h$ the following holds:

$$\|\mathrm{A}_h b_h\|_{U_h} \leq C \|b_h\|_{F_h} \tag{E.8}$$

We are now in the position to define *stability*, *consistency*, and *convergence* of the approximation scheme:

Definition E.3 (Stability)**.** A sequence of linear operators $\mathrm{L}_h : U_h \longrightarrow F_h$ with U_h and F_h normed spaces with norms $\|.\|_{U_h}$ and $\|.\|_{F_h}$, respectively, is called *stable*, if there exists an h_0 such that for all $h \leq h_0$ the operators L_h are invertible and their inverses L_h^{-1} are uniformly bounded.

Definition E.4 (Consistency)**.** A sequence of discrete approximation problems given in equation (E.7) is said to be *consistent* with the original problem (E.1), if the following approximation property holds for any $\mathbf{x} \in U$:

$$\lim_{h \to 0} \|\mathrm{L}_h \mathrm{P}_{U_h} \mathbf{x} - \mathrm{P}_{F_h} \mathrm{L} \mathbf{x}\|_{F_h} = 0 \tag{E.9}$$

Definition E.5 (Convergence)**.** A sequence of discrete approximation problems given in the form of equation (E.7) *converges* to the original problem (E.1), if for any given source term $b \in U$ the sequence of discrete solutions $\{\mathbf{x}_h\}_h$ converges to the discretization of the true solution $\mathbf{x}$:

$$\lim_{h \to 0} \|\mathbf{x}_h - \mathrm{P}_{U_h} \mathbf{x}\|_{U_h} = 0 \tag{E.10}$$

Theorem E.1. *A sequence of discrete approximation problems given in the form of equation (E.7) which is stable and consistent in the same norms is convergent in that norm.*

Proof. We can plug the inverted original problem in equation (E.1) and the approximating problem in equation (E.7) into the error estimate:

$$\begin{aligned} \|\mathbf{x}_h - \mathrm{P}_{U_h} \mathbf{x}\|_{U_h} &= \|\mathrm{L}_h^{-1} \mathrm{P}_{F_h} b - \mathrm{P}_{U_h} \mathbf{x}\|_{U_h} \\ &= \|\mathrm{L}_h^{-1} \mathrm{P}_{F_h} b - \mathrm{L}_h^{-1} \mathrm{L}_h \mathrm{P}_{U_h} \mathbf{x}\|_{U_h} \end{aligned}$$

Denoting by $\|\mathrm{L}_h^{-1}\|$ the operator norm of the inverse discrete operator L_h^{-1}, we can estimate:

$$\begin{aligned} &\leq \|\mathrm{L}_h^{-1}\| \|\mathrm{P}_{F_h} b - \mathrm{L}_h \mathrm{P}_{U_h} \mathbf{x}\|_{F_h} \\ &= \|\mathrm{L}_h^{-1}\| \|\mathrm{P}_{F_h} \mathrm{L}\mathbf{x} - \mathrm{L}_h \mathrm{P}_{U_h} \mathbf{x}\|_{F_h} \end{aligned}$$

As we have assumed stability of the discretization scheme, the operator norm of L_h^{-1} is bounded uniformly by a constant C; so we arrive at

$$\leq C \|\mathrm{P}_{F_h} \mathrm{L}\mathbf{x} - \mathrm{L}_h \mathrm{P}_{U_h} \mathbf{x}\|_{F_h} \tag{E.11}$$

Consistency ensures the convergence of the last term, so we have proven convergence of the discrete solution. □

Remark E.1. We have stated stability, consistency, and convergence in discrete norms. Using discrete norms, convergence does not necessarily have a useful physical meaning, though. If the discrete spaces U_h and F_h converge to the continuous spaces U and F in the sense that the chosen norms are compatible

$$\lim_{h\to 0} \|\mathrm{P}_{U_h} \mathbf{x}\|_{U_h} = \|\mathbf{x}\|_U \qquad \forall\, \mathbf{x} \in U \tag{E.12a}$$

$$\lim_{h\to 0} \|\mathrm{P}_{F_h} b\|_{F_h} = \|b\|_F \qquad \forall\, b \in F \tag{E.12b}$$

then from Theorem E.1, one also obtains convergence in the continuous norms.

Remark E.2. Defining the sequence of operators to render approximate solutions in the continuous function spaces, i.e. such that $U_h \subset U$ and $F_h \subset F$, we can directly replace the discrete norms by continuous norms $\|.\|_U$ and $\|.\|_F$. We then arrive at the setting for proving convergence in these continuous norms. The consistency definition then has to be changed to the following requirements:

$$\lim_{h\to 0} \|\mathrm{P}_{U_h} \mathbf{x} - \mathbf{x}\|_U = 0 \qquad \forall\, \mathbf{x} \in U \tag{E.13a}$$

$$\lim_{h\to 0} \|\mathrm{P}_{F_h} b - b\|_F = 0 \qquad \forall\, b \in F \tag{E.13b}$$

$$\lim_{h\to 0} \|\mathrm{L}_h \mathrm{P}_{U_h} \mathbf{x} - \mathrm{L}\mathbf{x}\|_F = 0 \qquad \forall\, \mathbf{x} \in U \tag{E.13c}$$

and the convergence requirement to:

$$\lim_{h\to 0} \|\mathbf{x}_h - \mathbf{x}\|_U = 0 \tag{E.13d}$$

The proof of Theorem E.1 can then be adjusted to the continuous error estimates provided that P_{U_h} and P_{F_h} define projections onto U_h and F_h, respectively.

Remark E.3. For the estimate (E.11), only the specific solution $\mathbf{x}$ for the problem at hand is actually needed. This can be used to relax the consistency requirement (E.9) to hold only for the specific solution $\mathbf{x}$.

F. PROOFS OF THEOREMS

F.1 Proofs of Theorems for Chapter 3

F.1.1 Proof of Theorem 3.9

We will first state some theorems and lemmas used later on in the proof of Theorem 3.9.

Theorem F.1 (Woodbury Formula)**.** *Let a square invertible matrix* $\mathbf{A} \in \mathbb{R}^{n\times n}$*, the matrices* $\mathbf{U}$ *and* $\mathbf{V}$ *both in* $\mathbb{R}^{n\times k}$ *with* $k \leq n$*, and* $\beta \in \mathbb{R}$ *be given. If the matrix* $\mathbf{\Sigma}$ *defined by*

$$\mathbf{\Sigma} \equiv \mathbf{I} + \beta \mathbf{V}^{\mathrm{T}} \mathbf{A}^{-1} \mathbf{U} \tag{F.1}$$

is invertible, then the following holds:

$$\left(\mathbf{A} + \beta \mathbf{U}\mathbf{V}^{\mathrm{T}}\right)^{-1} = \mathbf{A}^{-1} - \beta \mathbf{A}^{-1}\mathbf{U}\mathbf{\Sigma}^{-1}\mathbf{V}^{\mathrm{T}}\mathbf{A}^{-1} \tag{F.2}$$

The proof of this theorem can be found in [98].

Lemma F.2. *For any square matrices* $\mathbf{A}$ *and* $\mathbf{B}$ *of the same size,* $\mathbf{AB}$ *and* $\mathbf{BA}$ *have the same eigenvalues.*

A proof of this lemma can be found in [61].

Theorem F.3. *Let a real square matrix* $\mathbf{B}$ *be given in the form*

$$\mathbf{B} = \begin{pmatrix} 0 & \mathbf{F} \\ \mathbf{F}^{\mathrm{T}} & 0 \end{pmatrix} \tag{F.3}$$

with $\mathbf{F} \in \mathbb{R}^{m\times n}$*. Then for the eigenvalues* $\lambda_{\mathbf{B}}$ *of the matrix* $\mathbf{B}$ *and the eigenvalues* $\lambda_{\mathbf{F}\mathbf{F}^{\mathrm{T}}}$ *and* $\lambda_{\mathbf{F}^{\mathrm{T}}\mathbf{F}}$ *of the matrices* $\mathbf{F}\mathbf{F}^{\mathrm{T}}$ *and* $\mathbf{F}^{\mathrm{T}}\mathbf{F}$*, respectively, the following holds:*

$$\max|\lambda_{\mathbf{B}}| = \sqrt{\max|\lambda_{\mathbf{F}\mathbf{F}^{\mathrm{T}}}|} = \sqrt{\max|\lambda_{\mathbf{F}^{\mathrm{T}}\mathbf{F}}|} \tag{F.4}$$

Proof. As the matrix $\mathbf{B}$ is hermitian, its eigenvectors $x_{\mathbf{B}}$ can be chosen as an orthogonal basis of $\mathbb{C}^{m+n}$. Then the splitting of the eigenvectors $x_{\mathbf{B}}$ according to

$$x_{\mathbf{B}} = \begin{pmatrix} x_1 \\ x_2 \end{pmatrix} \tag{F.5}$$

with $x_1 \in \mathbb{C}^n$ and $x_2 \in \mathbb{C}^m$ renders the x_1 and x_2 an orthogonal basis of $\mathbb{C}^n$ and $\mathbb{C}^m$, respectively. As $x_{\mathbf{B}}$ is an eigenvector of $\mathbf{B}$, we know:

$$\mathbf{B}x = \begin{pmatrix} \mathbf{F}x_2 \\ \mathbf{F}^{\mathrm{T}}x_1 \end{pmatrix} = \begin{pmatrix} \lambda_{\mathbf{B}}x_1 \\ \lambda_{\mathbf{B}}x_2 \end{pmatrix} \tag{F.6}$$

We can deduce that for any non-zero $\lambda_{\mathbf{B}}$, the corresponding eigenvectors x have non-zero parts x_1 and x_2. (Assume there exists a non-zero eigenvector x where $x_1 = 0$ ($x_2 = 0$). Then from the equation above, we get that either $x_2 = 0$ ($x_1 = 0$) or that $\lambda_{\mathbf{B}} = 0$, both contradicting our assumptions.) Then using

$$\mathbf{B}\mathbf{B}x = \begin{pmatrix} \mathbf{F}\mathbf{F}^{\mathrm{T}}x_1 \\ \mathbf{F}^{\mathrm{T}}\mathbf{F}x_2 \end{pmatrix} = \begin{pmatrix} \lambda_{\mathbf{B}}^2x_1 \\ \lambda_{\mathbf{B}}^2x_2 \end{pmatrix} \tag{F.7}$$

we get that the square of any non-zero eigenvalue $\lambda_{\mathbf{B}}$ is also an eigenvalue of $\mathbf{F}\mathbf{F}^{\mathrm{T}}$ and $\mathbf{F}^{\mathrm{T}}\mathbf{F}$. We also note that the non-zero x_1 and x_2 of eigenvectors with zero eigenvalues $\lambda_{\mathbf{B}}$ are also eigenvectors of $\mathbf{F}\mathbf{F}^{\mathrm{T}}$ and $\mathbf{F}^{\mathrm{T}}\mathbf{F}$ with zero eigenvalues $\lambda_{\mathbf{F}\mathbf{F}^{\mathrm{T}}}$ and $\lambda_{\mathbf{F}^{\mathrm{T}}\mathbf{F}}$, respectively. As the set of x_1 and x_2 for all eigenvalues of $\mathbf{B}$ form a basis of $\mathbb{C}^n$ and $\mathbb{C}^m$ as noted above, we have thus characterized all eigenvalues of $\mathbf{F}\mathbf{F}^{\mathrm{T}}$ and $\mathbf{F}^{\mathrm{T}}\mathbf{F}$.

So the eigenvalues of $\mathbf{F}\mathbf{F}^{\mathrm{T}}$ and $\mathbf{F}^{\mathrm{T}}\mathbf{F}$ are the square of the non-zero eigenvalues of $\mathbf{B}$ plus possibly further zero eigenvalues. This leads to the statement in the theorem. □

Theorem F.4. *For a symmetric positive definite matrix* $\mathbf{A}$ *with a splitting*

$$\mathbf{A} = \sum_i \mathbf{A}^i \tag{F.8}$$

the intersection of the kernels of the contributions $\mathbf{A}^i$ *is the zero element:*

$$\cap_i \mathrm{K}\big(\mathbf{A}^i\big) = \{0\} \tag{F.9}$$

Proof. As the matrix $\mathbf{A}$ is symmetric positive definite, we know that for any $x \neq 0$

$$x^{\mathrm{T}}\mathbf{A}x > 0 \tag{F.10}$$

The zero element is in the kernels of all $\mathbf{A}^i$. Now assume there exists a $x \neq 0$ in the intersection of the kernels of the $\mathbf{A}^i$. Then we get

$$x^{\mathrm{T}}\mathbf{A}^i x = 0 \qquad \forall\, i \tag{F.11}$$

and therefore

$$\sum_i x^{\mathrm{T}}\mathbf{A}^i x = x^{\mathrm{T}}\mathbf{A}x = 0 \tag{F.12}$$

Because of the positive definiteness of $\mathbf{A}$, we have $x = 0$ in contradiction to the assumption above. So only the zero element is in the intersection of the kernels of the $\mathbf{A}^i$. □

Theorem F.5. *Any* $\mathbf{M} \in \mathbb{R}^{n\times n}$ *given in the form*

$$\mathbf{M} = \sum_i \big(\mathbf{H}^i\big)^{\mathrm{T}}\, \widehat{\mathbf{M}}^i \mathbf{H}^i \tag{F.13}$$

with symmetric positive definite $\widehat{\mathbf{M}}^i$ *and* $\mathbf{H}^i$ *such that* $\cap_i \mathrm{K}\big(\mathbf{H}^i\big) = \{0\}$ *is symmetric positive definite.*

Proof. As $\widehat{\mathbf{M}}^i$ is symmetric positive definite, we easily get that $\mathbf{M}$ is symmetric positive semi-definite:

$$x^{\mathrm{T}}\,\mathbf{M}\,x = \sum_i \left(\mathbf{H}^i x\right)^{\mathrm{T}} \widehat{\mathbf{M}}^i \left(\mathbf{H}^i x\right) \geq 0 \qquad \forall\, x \in \mathbb{R}^{sn} \tag{F.14}$$

Now assume there exists an $x \neq 0$ such that

$$x^{\mathrm{T}}\,\mathbf{M}\,x = \sum_i \left(\mathbf{H}^i x\right)^{\mathrm{T}} \widehat{\mathbf{M}}^i \left(\mathbf{H}^i x\right) = 0 \tag{F.15}$$

Then using the positive definiteness of $\widehat{\mathbf{M}}^i$, we get

$$\mathbf{H}^i x = 0 \qquad \forall\, i \tag{F.16}$$

and thus that x is in the kernel of all $\mathbf{H}^i$. As the intersection of the kernel of all $\mathbf{H}^i$ is the zero element, we get

$$x = 0 \tag{F.17}$$

which contradicts our assumption. So no $x \neq 0$ exists such that equation (F.15) holds. Thus $\mathbf{M}$ is symmetric positive definite. □

Theorem F.6. *For any matrix* $\mathbf{H} \in \mathbb{R}^{m\times n}$ *of the form*

$$\mathbf{H} = \begin{pmatrix} \mathbf{H}_1 & 0 \\ 0 & \mathbf{H}_2 \end{pmatrix}, \qquad \mathbf{H}_1 \in \mathbb{R}^{m_1\times n_1}, \mathbf{H}_2 \in \mathbb{R}^{m_2\times n_2} \tag{F.18}$$

the following holds:

$$\mathrm{K}\big(\mathbf{H}\big) = \mathrm{K}\big(\mathbf{H}_1\big) \times \mathrm{K}\big(\mathbf{H}_2\big) \tag{F.19}$$

where $\times$ *denotes the Cartesian product.*

Proof. We can write any $x \in \mathrm{K}\big(\mathbf{H}\big)$ as

$$x = \begin{pmatrix} x_1 \\ x_2 \end{pmatrix} \tag{F.20}$$

and get from

$$\mathbf{H}x = \begin{pmatrix} \mathbf{H}_1 x_1 \\ \mathbf{H}_2 x_2 \end{pmatrix} = 0 \tag{F.21}$$

that $x_1 \in \mathrm{K}\big(\mathbf{H}_1\big)$ and $x_2 \in \mathrm{K}\big(\mathbf{H}_2\big)$. Thus $x \in \mathrm{K}\big(\mathbf{H}_1\big) \times \mathrm{K}\big(\mathbf{H}_2\big)$. □

Theorem F.7. *For any symmetric positive semi-definite matrix* $\mathbf{A}$ *we can find a unitary matrix* $\mathbf{X_A}$ *and a diagonal matrix* $\mathbf{E_A}$ *such that* $\mathbf{A}$ *can be written as*

$$\mathbf{A} = \mathbf{X_A}\mathbf{E_A}\mathbf{X_A}^T \tag{F.22}$$

The proof of Theorem F.7 can be found in [77, Thm. 1.8]. The diagonal entries of $\mathbf{E_A}$ are the eigenvalues of $\mathbf{A}$ and the columns of $\mathbf{X_A}$ are the corresponding eigenvectors.

Definition F.1 (Matrix Powers)**.** For any symmetric positive semi-definite matrix $\mathbf{A}$ chose a unitary matrix $\mathbf{X_A}$ and a diagonal matrix $\mathbf{E_A}$ such that the splitting according to Theorem F.7 holds. Then the matrix power of $\mathbf{A}$ to the number $\alpha \in \mathbb{R}$, denoted by $\mathbf{A}^\alpha$, is defined as:

$$\mathbf{A}^\alpha \equiv \mathbf{X_A}\mathbf{E_A^\alpha}\mathbf{X_A^T} \tag{F.23}$$

where the matrix powers of the diagonal matrix $\mathbf{E_A}$ are defined as:

$$(\mathbf{E_A^\alpha})_{ij} \equiv \begin{cases} (\mathbf{E_A})_{ij}^\alpha & \text{, if } (\mathbf{E_A})_{ij} \neq 0 \\ 0 & \text{, otherwise} \end{cases} \tag{F.24}$$

Remark F.1. Using this definition of the matrix power, $\mathbf{A}^{-1}$ renders the Penrose pseudo inverse for symmetric positive semi-definite matrices.

Theorem F.8. *For any symmetric positive semi-definite matrix* $\mathbf{A}$*, the kernel of any matrix power is the same:*

$$\mathrm{K}\big(\mathbf{A}\big) = \mathrm{K}\big(\mathbf{A}^\alpha\big) \qquad \forall\, \alpha \in \mathbb{R} \tag{F.25}$$

Proof.

$$\begin{aligned} x \in \mathrm{K}\big(\mathbf{A}\big) \quad &\Leftrightarrow \quad \mathbf{A}x = 0 \quad \Leftrightarrow \quad \mathbf{X_A}\mathbf{E_A}\mathbf{X_A^T}x = 0 \quad \Leftrightarrow \quad \mathbf{E_A}\mathbf{X_A^T}x = 0 \\ \Leftrightarrow \quad \mathbf{E_A^\alpha}\mathbf{X_A^T}x = 0 \quad &\Leftrightarrow \quad \mathbf{X_A}\mathbf{E_A^\alpha}\mathbf{X_A^T}x = 0 \quad \Leftrightarrow \quad \mathbf{A}^\alpha x = 0 \quad \Leftrightarrow \quad x \in \mathrm{K}\big(\mathbf{A}^\alpha\big) \end{aligned}$$

□

Theorem F.9. *For symmetric positive semi-definite* $\mathbf{A}$*, the following two statements are equal:*

$$x^{\mathrm{T}}\mathbf{A}x = 0 \qquad \Leftrightarrow \qquad x \in \mathrm{K}\big(\mathbf{A}\big) \tag{F.26}$$

Proof. The way from right to left is easily proven: For $x \in \mathrm{K}\big(\mathbf{A}\big)$ we directly get:

$$x^{\mathrm{T}}\mathbf{A}x = 0 \tag{F.27}$$

Now assume the statement on the left holds. Then we can rewrite:

$$\begin{aligned} & \left(\mathbf{A}^{\frac{1}{2}}x\right)^{\mathrm{T}}\left(\mathbf{A}^{\frac{1}{2}}x\right) = 0 \\ \Leftrightarrow \qquad & \mathbf{A}^{\frac{1}{2}}x = 0 \qquad\qquad \Leftrightarrow \qquad x \in \mathrm{K}\big(\mathbf{A}^{\frac{1}{2}}\big) \end{aligned} \tag{F.28}$$

By Theorem F.8, we know $\mathrm{K}\big(\mathbf{A}^{\frac{1}{2}}\big) = \mathrm{K}\big(\mathbf{A}\big)$ and therefore the statement on the right to hold. □

Theorem F.10. *For any symmetric positive semi-definite matrix* $\mathbf{A}$*, its zero power matrix* $\mathbf{A}^0$ *defines an orthogonal projector and the following holds:*

$$\mathrm{R}\big(\mathbf{I} - \mathbf{A}^0\big) = \mathrm{K}\big(\mathbf{A}^0\big) \tag{F.29}$$

Proof. We have

$$\begin{aligned}\mathbf{A}^0\mathbf{A}^0 &= \mathbf{X}_\mathbf{A}\mathbf{E}^0_\mathbf{A}\mathbf{X}^T_\mathbf{A}\mathbf{X}_\mathbf{A}\mathbf{E}^0_\mathbf{A}\mathbf{X}^T_\mathbf{A} \\ &= \mathbf{X}_\mathbf{A}\mathbf{E}^0_\mathbf{A}\mathbf{X}^T_\mathbf{A} = \mathbf{A}^0 \end{aligned} \tag{F.30}$$

and $\mathbf{A}^0$ is symmetric. So $\mathbf{A}^0$ is an orthogonal projector onto $\mathrm{R}\big(\mathbf{A}^0\big)$ and $\mathbf{I}-\mathbf{A}^0$ is an orthogonal projector onto $\mathrm{R}\big(\mathbf{I}-\mathbf{A}^0\big) = \mathrm{R}\big(\mathbf{A}^0\big)^\perp = \mathrm{K}\big(\mathbf{A}^0\big)$. □

We will now consider the Newmark-Θ scheme as presented on page 79. Assume the local standard FIT material matrices $\mathbf{M}^{k,i}_{\mathrm{sFIT},\alpha}$ derived similar to equations (3.85) on page 59 and (3.91) on page 61 and the local Whitney-FEM material matrices $\mathbf{M}^{k,i}_{\mathrm{FEM},\alpha}$ derived according to equation (4.8) on page 92. We will from now on simply denote the local material matrices by $\mathbf{M}^{k,i}_\alpha$ implying that these matrices are standard FIT material matrices for $i \in \mathrm{I}^3_{\mathrm{sFIT}}$ and Whitney-FEM material matrices for $i \in \mathrm{I}^3_{\mathrm{FEM}}$. Recall that the Θ_i denote the cell-wise control parameters of the Newmark-Θ scheme. Then we define the following matrices to be used as short hands in the following theorems:

$$\mathbf{A}^i = \frac{1}{\Delta t^2}\,\mathbf{M}^{1,i}_\varepsilon + \Theta_i\,\underset{\sim}{\mathbf{C}}\,\mathbf{M}^{2,i}_\nu\,\mathbf{C} \tag{F.31}$$

$$\mathbf{B}^i = -\frac{1}{2}\,\underset{\sim}{\mathbf{C}}\,\mathbf{M}^{2,i}_\nu \tag{F.32}$$

$$\mathbf{H}^i = \begin{pmatrix} \big(\mathbf{A}^i\big)^{\frac{1}{2}} & 0 \\ 0 & \big(\mathbf{M}^{2,i}_\nu\big)^{\frac{1}{2}} \end{pmatrix} \tag{F.33}$$

$$\mathbf{F}^i = \big(\mathbf{A}^i\big)^{-1/2}\,\mathbf{B}^i\,\big(\mathbf{M}^{2,i}_\nu\big)^{-1/2} \tag{F.34}$$

$$\mathbf{P}^i = \begin{pmatrix} 0 & \mathbf{F}^i \\ \big(\mathbf{F}^i\big)^{\mathrm{T}} & 0 \end{pmatrix} \tag{F.35}$$

$$\widehat{\mathbf{M}}^i = \mathbf{I} + \mathbf{P}^i \tag{F.36}$$

$$\mathbf{M}^i = \begin{pmatrix} \mathbf{A}^i & \mathbf{B}^i \\ \big(\mathbf{B}^i\big)^{\mathrm{T}} & \mathbf{M}^{2,i}_\nu \end{pmatrix} \tag{F.37}$$

Theorem F.11. *For the local standard FIT and the local FEM material relations* $\mathbf{M}^{k,i}_{\mathrm{sFIT},\alpha}$ *and* $\mathbf{M}^{k,i}_{\mathrm{FEM},\alpha}$ *defined similar to equation (3.85) and according to equation (4.8), respectively, and the discrete exterior derivative* $\mathbf{D}^k$ *defined in (3.33b), the following holds:*

$$\mathbf{D}^k\,\mathrm{K}\big(\mathbf{M}^{k,i}_\alpha\big) \subset \mathrm{K}\big(\mathbf{M}^{k+1,i}_\alpha\big) \tag{F.38}$$

Proof. Using equation (3.60) on page 48, we can write the local material relations $\mathbf{M}^{k,i}_\alpha$ in terms of the symmetric positive matrices $\widehat{\mathbf{M}}^{k,i}_\alpha$ (see theorems 3.6 on page 61 and 4.1 on page 94):

$$\mathbf{M}^{k,i}_\alpha = \Big(\mathbf{T}^k_{S^3_i}\Big)^{\mathrm{T}}\,\widehat{\mathbf{M}}^{k,i}_\alpha\,\mathbf{T}^k_{S^3_i} \tag{F.39}$$

For any $\boldsymbol{\omega}^k$ in the kernel of $\mathbf{M}^{k,i}_\alpha$, we know by Theorem F.9 that

$$\big(\boldsymbol{\omega}^k\big)^{\mathrm{T}}\,\mathbf{M}^{k,i}_\alpha\,\boldsymbol{\omega}^k = \Big(\mathbf{T}^k_{S^3_i}\,\boldsymbol{\omega}^k\Big)^{\mathrm{T}}\,\widehat{\mathbf{M}}^{k,i}_\alpha\,\Big(\mathbf{T}^k_{S^3_i}\,\boldsymbol{\omega}^k\Big) = 0 \tag{F.40}$$

As $\widehat{\mathbf{M}}_{\alpha}^{k,i}$ is symmetric positive definite, it follows that

$$\mathbf{T}_{S_i^3}^{k}\,\boldsymbol{\omega}^k = 0 \tag{F.41}$$

Now let us consider the term $\mathbf{T}_{S_i^3}^{k+1}\,\mathbf{D}^k\,\boldsymbol{\omega}^k$:

$$\begin{aligned}\mathbf{T}_{S_i^3}^{k+1}\,\mathbf{D}^k\,\boldsymbol{\omega}^k &= \mathbf{T}_{S_i^3}^{k+1}\,\mathbf{D}^k\left(\left(\mathbf{T}_{S_i^3}^{k}\right)^{\mathrm{T}}\mathbf{T}_{S_i^3}^{k} + \left(\mathbf{I} - \left(\mathbf{T}_{S_i^3}^{k}\right)^{\mathrm{T}}\mathbf{T}_{S_i^3}^{k}\right)\right)\boldsymbol{\omega}^k \\ &= \mathbf{T}_{S_i^3}^{k+1}\,\mathbf{D}^k\left(\mathbf{T}_{S_i^3}^{k}\right)^{\mathrm{T}}\mathbf{T}_{S_i^3}^{k}\,\boldsymbol{\omega}^k = 0 \end{aligned} \tag{F.42}$$

We have used the fact that $\mathbf{D}^k$ only acts locally in the second equal sign. So we know for any $\boldsymbol{\omega}^k$ in the kernel of $\mathbf{M}_{\alpha}^{k,i}$ that also the following quantity is zero:

$$\begin{aligned} & \left(\mathbf{T}_{S_i^3}^{k+1}\,\mathbf{D}^k\,\boldsymbol{\omega}^k\right)^{\mathrm{T}}\widehat{\mathbf{M}}_{\alpha}^{k+1,i}\left(\mathbf{T}_{S_i^3}^{k+1}\,\mathbf{D}^k\,\boldsymbol{\omega}^k\right) = 0 \\ \Leftrightarrow \quad & \left(\mathbf{D}^k\,\boldsymbol{\omega}^k\right)^{\mathrm{T}}\mathbf{M}_{\alpha}^{k+1,i}\left(\mathbf{D}^k\,\boldsymbol{\omega}^k\right) = 0 \end{aligned} \tag{F.43}$$

From Theorem F.9 we get that:

$$\mathbf{D}^k\,\boldsymbol{\omega}^k \in \mathrm{K}\big(\mathbf{M}_{\alpha}^{k+1,i}\big) \tag{F.44}$$

As this holds for any $\boldsymbol{\omega}^k$ in the kernel of $\mathbf{M}_{\alpha}^{k,i}$, we have concluded the proof. □

Theorem F.12. *For $\mathbf{A}^i$ defined in equation (F.31) and the symmetric positive semi-definite $\mathbf{M}_{\varepsilon}^{1,i}$, the following holds:*

$$\mathrm{K}\big(\mathbf{A}^i\big) = \mathrm{K}\big(\mathbf{M}_{\varepsilon}^{1,i}\big) \tag{F.45}$$

Proof. Using Theorem F.11, we easily get that any $\widehat{\mathbf{e}}_{\varepsilon}^{0}$ in the kernel of $\mathbf{M}_{\varepsilon}^{1,i}$ is in the kernel of $\mathbf{A}^i$:

$$\mathbf{A}^i\widehat{\mathbf{e}}_{\varepsilon}^{0} = \left(\frac{1}{\Delta t^2}\,\mathbf{M}_{\varepsilon}^{1,i} + \Theta_i\,\underset{\sim}{\mathbf{C}}\,\mathbf{M}_{\nu}^{2,i}\,\mathbf{C}\right)\widehat{\mathbf{e}}_{\varepsilon}^{0} = 0 \tag{F.46}$$

So we know

$$\mathrm{K}\big(\mathbf{M}_{\varepsilon}^{1,i}\big) \subset \mathrm{K}\big(\mathbf{A}^i\big) \tag{F.47}$$

Now take any $\widehat{\mathbf{e}} \in \mathrm{K}\big(\mathbf{A}^i\big)$. Then we know that

$$\begin{aligned} & \widehat{\mathbf{e}}^{\mathrm{T}}\mathbf{A}^i\widehat{\mathbf{e}} = 0 \\ \Leftrightarrow \quad & \underbrace{\frac{1}{\Delta t^2}\widehat{\mathbf{e}}^{\mathrm{T}}\,\mathbf{M}_{\varepsilon}^{1,i}\,\widehat{\mathbf{e}}}_{\geq 0} + \underbrace{\Theta_i\widehat{\mathbf{e}}^{\mathrm{T}}\,\underset{\sim}{\mathbf{C}}\,\mathbf{M}_{\nu}^{2,i}\,\mathbf{C}\,\widehat{\mathbf{e}}}_{\geq 0} = 0 \end{aligned} \tag{F.48}$$

where the second term is seen to be positive semi-definite due to a possible splitting of the term $\underset{\sim}{\mathbf{C}}\,\mathbf{M}_{\nu}^{2,i}\,\mathbf{C}$ into the form $\left(\underset{\sim}{\mathbf{C}}\left(\mathbf{M}_{\nu}^{2,i}\right)^{\frac{1}{2}}\right)^{\mathrm{T}}\left(\underset{\sim}{\mathbf{C}}\left(\mathbf{M}_{\nu}^{2,i}\right)^{\frac{1}{2}}\right)$ which is always symmetric

positive semi-definite. As the contributions are all non-negative, they have to be zero and we get

$$\widehat{\mathbf{e}}^{\mathrm{T}}\,\mathbf{M}_{\varepsilon}^{1,i}\,\widehat{\mathbf{e}} = 0 \tag{F.49}$$

By Theorem F.9 we then know $\widehat{\mathbf{e}}$ to be in the kernel of $\mathbf{M}_{\varepsilon}^{1,i}$ and we have

$$\mathrm{K}\big(\mathbf{A}^i\big) \subset \mathrm{K}\big(\mathbf{M}_{\varepsilon}^{1,i}\big) \tag{F.50}$$

Together with equation (F.47), we get the result. □

Theorem F.13. *For any $\widehat{\mathbf{e}} \in \mathbb{R}^{n^1}$, there exists an $\widehat{\mathbf{e}}_{\varepsilon}^{0} \in \mathrm{K}\big(\mathbf{M}_{\varepsilon}^{1,i}\big)$ such that*

$$\Big(\mathbf{I} - \big(\mathbf{A}^i\big)^0\Big)\,\widehat{\mathbf{e}} = \widehat{\mathbf{e}}_{\varepsilon}^{0} \tag{F.51}$$

Proof. By Theorem F.10, we know that

$$\mathrm{R}\big(\mathbf{I} - \big(\mathbf{A}^i\big)^0\big) = \mathrm{K}\big(\big(\mathbf{A}^i\big)^0\big) \tag{F.52}$$

by Theorem F.8, that

$$\mathrm{K}\big(\big(\mathbf{A}^i\big)^0\big) = \mathrm{K}\big(\mathbf{A}^i\big) \tag{F.53}$$

and by Theorem F.12 that

$$\mathrm{K}\big(\mathbf{A}^i\big) = \mathrm{K}\big(\mathbf{M}_{\varepsilon}^{1,i}\big) \tag{F.54}$$

□

Theorem F.14. *The local Newmark metric term $\mathbf{M}^i$ defined in equation (F.37) can be split according to*

$$\mathbf{M}^i = \big(\mathbf{H}^i\big)^{\mathrm{T}}\,\widehat{\mathbf{M}}^i\,\mathbf{H}^i \tag{F.55}$$

Proof. The right hand term evaluates as:

$$\big(\mathbf{H}^i\big)^{\mathrm{T}}\,\widehat{\mathbf{M}}^i\,\mathbf{H}^i = \begin{pmatrix} \mathbf{A}^i & \big(\mathbf{A}^i\big)^0\,\mathbf{B}^i\,\big(\mathbf{M}_{\nu}^{2,i}\big)^0 \\ \big(\mathbf{M}_{\nu}^{2,i}\big)^0\,\big(\mathbf{B}^i\big)^{\mathrm{T}}\,\big(\mathbf{A}^i\big)^0 & \mathbf{M}_{\nu}^{2,i} \end{pmatrix} \tag{F.56}$$

So what is left to prove is the equivalence of $\mathbf{B}^i$ and $\big(\mathbf{A}^i\big)^0\,\mathbf{B}^i\,\big(\mathbf{M}_{\nu}^{2,i}\big)^0$. For the term $\mathbf{B}^i\,\big(\mathbf{M}_{\nu}^{2,i}\big)^0$ we easily get:

$$\mathbf{B}^i\,\big(\mathbf{M}_{\nu}^{2,i}\big)^0 = -\frac{1}{2}\,\underset{\sim}{\mathbf{C}}\,\mathbf{M}_{\nu}\,\big(\mathbf{M}_{\nu}^{2,i}\big)^0 = -\frac{1}{2}\,\underset{\sim}{\mathbf{C}}\,\mathbf{M}_{\nu} = \mathbf{B}^i \tag{F.57}$$

According to Theorem F.13, we can find for any $\widehat{\mathbf{e}} \in \mathbb{R}^{n^1}$ some $\widehat{\mathbf{e}}_{\varepsilon}^{0} \in \mathrm{K}\big(\mathbf{M}_{\varepsilon}^{1,i}\big)$ such that

$$\begin{aligned} \big(\mathbf{B}^i\big)^{\mathrm{T}}\,\widehat{\mathbf{e}} &= \big(\mathbf{B}^i\big)^{\mathrm{T}}\,\big(\mathbf{A}^i\big)^0\,\widehat{\mathbf{e}} + \big(\mathbf{B}^i\big)^{\mathrm{T}}\,\Big(\mathbf{I} - \big(\mathbf{A}^i\big)^0\Big)\,\widehat{\mathbf{e}} \\ &= \big(\mathbf{B}^i\big)^{\mathrm{T}}\,\big(\mathbf{A}^i\big)^0\,\widehat{\mathbf{e}} + \big(\mathbf{B}^i\big)^{\mathrm{T}}\,\widehat{\mathbf{e}}_{\varepsilon}^{0} \end{aligned} \tag{F.58}$$

and, using Theorem F.11, this is equal to:

$$= \left(\mathbf{B}^i\right)^{\mathrm{T}} \left(\mathbf{A}^i\right)^0 \widehat{\mathbf{e}} \tag{F.59}$$

So we know that

$$\mathbf{B}^i = \left(\mathbf{A}^i\right)^0 \mathbf{B}^i \left(\mathbf{M}_\nu^{2,i}\right)^0 \tag{F.60}$$

and thus that the splitting in (F.55) does hold. □

Theorem F.15. *For the* $\mathbf{H}^i$ *defined in equation (F.33), the following holds:*

$$\cap_i \mathrm{K}\big(\mathbf{H}^i\big) = \{0\} \tag{F.61}$$

Proof. Using Theorem F.6, we know

$$\cap_i \mathrm{K}\big(\mathbf{H}^i\big) = \cap_i \left(\mathrm{K}\big(\big(\mathbf{A}^i\big)^{\frac{1}{2}}\big) \times \mathrm{K}\big(\big(\mathbf{M}_\nu^{2,i}\big)^{\frac{1}{2}}\big)\right) \tag{F.62}$$

using Theorem F.8, this is equal to

$$= \cap_i \left(\mathrm{K}\big(\mathbf{A}^i\big) \times \mathrm{K}\big(\mathbf{M}_\nu^{2,i}\big)\right) = \cap_i \left(\mathrm{K}\big(\mathbf{A}^i\big)\right) \times \cap_i \left(\mathrm{K}\big(\mathbf{M}_\nu^{2,i}\big)\right) \tag{F.63}$$

which, using Theorem F.4, is equal to

$$= \{0\} \times \{0\} = \{0\} \tag{F.64}$$

□

Theorem F.16. *The matrices* $\widehat{\mathbf{M}}^i$ *defined in equation (F.36) are symmetric positive definite if the following requirement holds:*

$$\frac{\Delta t}{2} \sqrt{\frac{\lambda_{\mathbf{L}^i,\max}}{1 + \Delta t^2 \Theta_i \lambda_{\mathbf{L}^i,\max}}} < 1 \tag{F.65}$$

where $\lambda_{\mathbf{L}^i,\max}$ *denotes the maximum eigenvalue of the matrix* $\mathbf{L}^i$ *defined as*

$$\mathbf{L}^i \equiv \mathbf{C} \left(\mathbf{M}_\varepsilon^{1,i}\right)^{-1} \underset{\sim}{\mathbf{C}} \, \mathbf{M}_\nu^{2,i} \tag{F.66}$$

Proof. From the definition of $\widehat{\mathbf{M}}^i$ in equation (F.36), we note that the eigenvalues $\lambda_{\widehat{\mathbf{M}}^i}$ of the matrix $\widehat{\mathbf{M}}^i$ can be calculated from the eigenvalues $\lambda_{\mathbf{P}^i}$ of the matrix $\mathbf{P}^i$ defined in (F.35) by

$$\lambda_{\widehat{\mathbf{M}}^i} = 1 + \lambda_{\mathbf{P}^i} \tag{F.67}$$

We can estimate the minimal eigenvalue $\lambda_{\widehat{\mathbf{M}}^i,\min}$ of $\widehat{\mathbf{M}}^i$ by

$$\lambda_{\widehat{\mathbf{M}}^i,\min} \geq 1 - \max |\lambda_{\mathbf{P}^i}| \tag{F.68}$$

and using Theorem F.3 we get

$$\lambda_{\widehat{\mathbf{M}}^i,\min} \geq 1 - \max|\lambda_{\mathbf{P}^i}| = 1 - \sqrt{\lambda_{\mathbf{F}^i\mathbf{F}^{i\mathrm{T}},\max}} = 1 - \sqrt{\lambda_{\mathbf{F}^{i\mathrm{T}}\mathbf{F}^i,\max}} \tag{F.69}$$

where $\lambda_{\mathbf{F}^i\mathbf{F}^{i\mathrm{T}},\max}$ and $\lambda_{\mathbf{F}^{i\mathrm{T}}\mathbf{F}^i,\max}$ denote the maximum of the (non-negative) eigenvalues of the symmetric positive semi-definite matrices $\mathbf{F}^i\mathbf{F}^{i\mathrm{T}}$ and $\mathbf{F}^{i\mathrm{T}}\mathbf{F}^i$, respectively. The matrix $\mathbf{F}^i$ was defined in equation (F.35). We will now calculate the eigenvalues of $\lambda_{\mathbf{F}^{i\mathrm{T}}\mathbf{F}^i}$ in order to establish the theorem. Defining the matrix $\mathbf{G}$ as

$$\mathbf{G} \equiv \mathbf{M}_\varepsilon^{i\,-1/2}\,\underset{\sim}{\mathbf{C}}\,\mathbf{M}_\nu^{i\,1/2} \tag{F.70}$$

we can rewrite $\mathbf{F}^{i\mathrm{T}}\mathbf{F}^i$:

$$\mathbf{F}^{i\mathrm{T}}\mathbf{F}^i = \frac{\Delta t^2}{4}\mathbf{G}^{\mathrm{T}}\left(\mathbf{I} + \Delta t^2\Theta_i\mathbf{G}\mathbf{G}^{\mathrm{T}}\right)^{-1}\mathbf{G} \tag{F.71}$$

Using the Woodbury Formula (Theorem F.1), we know that

$$\left(\mathbf{I} + \Delta t^2\Theta_i\mathbf{G}\mathbf{G}^{\mathrm{T}}\right)^{-1} = \mathbf{I} - \Delta t^2\Theta_i\mathbf{G}\left(\mathbf{I} + \Delta t^2\Theta_i\mathbf{G}^{\mathrm{T}}\mathbf{G}\right)^{-1}\mathbf{G}^{\mathrm{T}} \tag{F.72}$$

and we get

$$\mathbf{F}^{i\mathrm{T}}\mathbf{F}^i = \frac{\Delta t^2}{4}\left(\mathbf{G}^{\mathrm{T}}\mathbf{G} - \Delta t^2\Theta_i\mathbf{G}^{\mathrm{T}}\mathbf{G}\left(\mathbf{I} + \Delta t^2\Theta_i\mathbf{G}^{\mathrm{T}}\mathbf{G}\right)^{-1}\mathbf{G}^{\mathrm{T}}\mathbf{G}\right) \tag{F.73}$$

For any eigenvector/eigenvalue pair $(\lambda_{\mathbf{G}^{\mathrm{T}}\mathbf{G}}, x)$ of the matrix $\mathbf{G}^{\mathrm{T}}\mathbf{G}$, we get:

$$\begin{aligned}
\mathbf{F}^{i\mathrm{T}}\mathbf{F}^i x &= \frac{\Delta t^2}{4}\left(\mathbf{G}^{\mathrm{T}}\mathbf{G} - \Delta t^2\Theta_i\mathbf{G}^{\mathrm{T}}\mathbf{G}\left(\mathbf{I} + \Delta t^2\Theta_i\mathbf{G}^{\mathrm{T}}\mathbf{G}\right)^{-1}\mathbf{G}^{\mathrm{T}}\mathbf{G}\right)x \\
&= \frac{\Delta t^2}{4}\left(\lambda_{\mathbf{G}^{\mathrm{T}}\mathbf{G}} - \Delta t^2\Theta_i\frac{\lambda^2_{\mathbf{G}^{\mathrm{T}}\mathbf{G}}}{1 + \Delta t^2\Theta_i\lambda_{\mathbf{G}^{\mathrm{T}}\mathbf{G}}}\right)x \\
&= \frac{\Delta t^2}{4}\frac{\lambda_{\mathbf{G}^{\mathrm{T}}\mathbf{G}}}{1 + \Delta t^2\Theta_i\lambda_{\mathbf{G}^{\mathrm{T}}\mathbf{G}}}x
\end{aligned} \tag{F.74}$$

As the eigenvectors of $\mathbf{G}^{\mathrm{T}}\mathbf{G}$ span $\mathbb{C}^n$, all eigenvalues of $\mathbf{F}^{i\mathrm{T}}\mathbf{F}^i$ can be calculated by

$$\lambda_{\mathbf{F}^{i\mathrm{T}}\mathbf{F}^i} = \frac{\Delta t^2}{4}\frac{\lambda_{\mathbf{G}^{\mathrm{T}}\mathbf{G}}}{1 + \Delta t^2\Theta_i\lambda_{\mathbf{G}^{\mathrm{T}}\mathbf{G}}} \tag{F.75}$$

As the function $\lambda_{\mathbf{F}^{i\mathrm{T}}\mathbf{F}^i}(\lambda_{\mathbf{G}^{\mathrm{T}}\mathbf{G}})$ is concave (for positive $\lambda_{\mathbf{G}^{\mathrm{T}}\mathbf{G}}$), we also know for the maximum eigenvalue $\lambda_{\mathbf{F}^{i\mathrm{T}}\mathbf{F}^i,\max}$:

$$\lambda_{\mathbf{F}^{i\mathrm{T}}\mathbf{F}^i,\max} = \frac{\Delta t^2}{4}\frac{\lambda_{\mathbf{G}^{\mathrm{T}}\mathbf{G},\max}}{1 + \Delta t^2\Theta_i\lambda_{\mathbf{G}^{\mathrm{T}}\mathbf{G},\max}} \tag{F.76}$$

Defining the matrix $\mathbf{L}^i$ as in equation (F.66), we know due to Lemma F.2, that the eigenvalues of $\mathbf{L}^i$ and those of $\mathbf{G}^{\mathrm{T}}\mathbf{G}$ are the same and thus get:

$$\lambda_{\mathbf{F}^{i\mathrm{T}}\mathbf{F}^i,\max} = \frac{\Delta t^2}{4}\frac{\lambda_{\mathbf{L}^i,\max}}{1 + \Delta t^2\Theta_i\lambda_{\mathbf{L}^i,\max}} \tag{F.77}$$

where $\lambda_{\mathbf{L}^i,\max}$ denotes the maximum eigenvalue of $\mathbf{L}^i$. Using equations (F.67), (F.69), and (F.77), we can estimate $\lambda_{\widehat{\mathbf{M}}^i}$ by

$$\begin{aligned}\lambda_{\widehat{\mathbf{M}}^i} &= 1 + \lambda_{\mathbf{P}^i} \geq 1 - \max|\lambda_{\mathbf{P}^i}| = 1 - \sqrt{\lambda_{\mathbf{F}^{i\mathrm{T}}\mathbf{F}^i,\max}} \\ &= 1 - \frac{\Delta t}{2}\sqrt{\frac{\lambda_{\mathbf{L}^i,\max}}{1 + \Delta t^2 \Theta_i \lambda_{\mathbf{L}^i,\max}}} \end{aligned} \tag{F.78}$$

A necessary and sufficient condition for the symmetric $\widehat{\mathbf{M}}^i$ to be positive definite is the positiveness of all its eigenvalues $\lambda_{\widehat{\mathbf{M}}^i}$. So equation (F.65) is a sufficient condition. □

Now we can prove Theorem 3.9 on page 83:

Proof of Theorem 3.9. Defining the Newmark-Θ energy matrix $\mathbf{M}$ as

$$\mathbf{M} \equiv \begin{pmatrix} \frac{1}{\Delta t^2}\,\mathbf{M}_\varepsilon + \underset{\sim}{\mathbf{C}}\,\mathbf{M}_\nu^{\boldsymbol{\Theta}}\,\mathbf{C} & -\frac{1}{2}\,\underset{\sim}{\mathbf{C}}\,\mathbf{M}_\nu \\ -\frac{1}{2}\,\mathbf{M}_\nu\,\mathbf{C} & \mathbf{M}_\nu \end{pmatrix} \tag{F.79}$$

we can, after some calculations using equation (3.164) on page 76, rewrite the total energy defined by equation (3.190) on page 83 as follows:

$$W^n = \frac{1}{2}\left(\mathbf{x}^n\right)^{\mathrm{T}} \mathbf{M}\,\mathbf{x}^n \tag{F.80}$$

In the remaining part, we prove that the energy matrix $\mathbf{M}$ is symmetric positive definite for the time-step restriction given by equation (3.192) and thus the total energy defines a norm on the unknown vector $\mathbf{x}^n$.

According to Theorem F.14, the following splitting holds:

$$\mathbf{M} = \sum_{i=1}^{n^3} \mathbf{M}^i = \sum_{i=1}^{n^3} \left(\mathbf{H}^i\right)^{\mathrm{T}} \widehat{\mathbf{M}}^i \mathbf{H}^i \tag{F.81}$$

By Theorem F.16, we know that the matrices $\widehat{\mathbf{M}}^i$ are symmetric positive definite under the requirement (F.65). For the standard FIT material cells, the control parameters Θ_i are set to zero and thus requirement (F.65) reads:

$$\Delta t < \frac{2}{\sqrt{\lambda_{\mathbf{L}^i,\max}}}, \qquad \forall\, i \in \mathrm{I}^3_{\mathrm{sFIT}} \tag{F.82}$$

where $\mathrm{I}^3_{\mathrm{sFIT}}$ denotes the indices of the cells with standard FIT material matrix contributions. For the FEM material cells with indices in $\mathrm{I}^3_{\mathrm{FEM}}$, the control parameters Θ_i are set to $\frac{1}{4}$ and thus requirement (F.65) reads:

$$\begin{aligned} & \frac{\lambda_{\mathbf{L}^i,\max}}{1 + \Delta t^2 \Theta_i \lambda_{\mathbf{L}^i,\max}} < \frac{4}{\Delta t^2}, && \forall\, i \in \mathrm{I}^3_{\mathrm{FEM}} \\ \Leftrightarrow \quad & \frac{1}{1 + \frac{4}{\Delta t^2 \lambda_{\mathbf{L}^i,\max}}} < 1, && \forall\, i \in \mathrm{I}^3_{\mathrm{FEM}} \end{aligned} \tag{F.83}$$

which is always fulfilled. The time-step condition (3.192) is sufficient to guarantee equation (F.82) and thus the matrices $\widehat{\mathbf{M}}^i$ are positive definite for all $i \in [1..n^3]$.

By Theorem F.15, we get equation (F.61). Thus all requirements for Theorem F.5 are fulfilled and we conclude that the matrix $\mathbf{M}$ is symmetric positive definite under the condition (3.192) on the time-step. □

F.2 Proof of Theorems from Chapter 4

F.2.1 Proof of Theorem 4.5

The proof of Theorem 4.5 is based on the existence and uniqueness properties for the following generalized Laplace-Beltrami BVP for the unknown $\left(\mathrm{t}^k_{S^l_j} B^k_i\right)$ as given in [80, Lemma 3.4.7]:

$$\Delta^k_{S^l_j}\left(\mathrm{t}^k_{S^l_j} B^k_i\right) = 0 \qquad \text{in } S^l_j \tag{F.84a}$$

$$\mathrm{t}^k_{\partial S^l_j}\left(\mathrm{t}^k_{S^l_j} B^k_i\right) = \psi \qquad \text{known on } \partial S^l_j \tag{F.84b}$$

$$\mathrm{t}^{k-1}_{\partial S^l_j}\,\delta^k_{S^l_j}\left(\mathrm{t}^k_{S^l_j} B^k_i\right) = 0 \qquad \text{on } \partial S^l_j \tag{F.84c}$$

with the additional uniqueness constraint for $l = k$:

$$\int_{S^k_j}\left(\mathrm{t}^k_{S^l_j} B^k_i\right) = \delta_{ij} \qquad \text{if } l = k \tag{F.84d}$$

where the general Laplace-Beltrami operator $\Delta^k_{S^l_j}$ is defined as:

$$\Delta^k_{S^l_j} = \left(\mathrm{d}^{k-1}_{S^l_j}\,\delta^k_{S^l_j} + \delta^{k+1}_{S^l_j}\,\mathrm{d}^k_{S^l_j}\right) \tag{F.85}$$

As the proof in [80] is based on smooth domains, strictly speaking, the following derivation is only valid for smooth grid elements without corners or edges. We assume the theorem to be valid also for the piecewise smooth polyhedral elements under consideration, though. For some work in this direction see [65] [66].

According to [80, Lemma 3.4.7], we know a solution to exist for the BVP (F.84a)-(F.84c) under certain regularity assumptions on $\mathrm{t}^k_{\partial S^l_j} B^k_i$ and for smooth domains S^l_j. This solution is unique up to a set of solutions called Dirichlet fields. For simply connected domains, the set of Dirichlet fields is only non-empty if B^k_i is a form of the same degree as the dimension of S^l_j, i.e. $l = k$, and then the constraint (F.84d) ensures uniqueness.

Lemma F.17. *The BVP (F.84) is equivalent to the BVP (4.30) on page 100.*

Proof. We first derive a partial integration formula that we need later in the proof: Formally, using the two relations

$$\star^l_{S^l_j}\star^l_{S^l_j}\omega^k = (-1)^{k(l-k)}\omega^k \tag{F.86}$$

$$\omega^k \wedge \star^l_{S^l_j}\eta^m = \eta^m \wedge \star^l_{S^l_j}\omega^k \tag{F.87}$$

we can derive the following partial integration formula from equation (2.25) on page 13:

$$\begin{aligned}\int_{S_j^l} \omega^k \wedge \star_{S_j^l}^l \, \mathrm{d}_{S_j^l}^{k-1} \, \eta^{k-1} \\ = \int_{S_j^l} \delta_{S_j^l}^k \, \omega^k \wedge \star_{S_j^l}^l \eta^{k-1} + \int_{\partial S_j^l} \mathrm{t}_{\partial S_j^l}^{l-k} \, \eta^{k-1} \wedge \mathrm{t}_{\partial S_j^l}^k \star_{S_j^l}^l \omega^k\end{aligned} \tag{F.88}$$

where we have included the trace operators in the boundary term. Using the element-wise local inner product defined in equation (4.76b) on page 114, we rewrite equation (F.88) as:

$$\left\langle\!\!\left\langle \omega^k \middle| \, \mathrm{d}_{S_j^l}^{k-1} \, \eta^{k-1} \right\rangle\!\!\right\rangle_{S_j^l} = \left\langle\!\!\left\langle \, \delta_{S_j^l}^k \, \omega^k \middle| \eta^{k-1} \right\rangle\!\!\right\rangle_{S_j^l} + \int_{\partial S_j^l} \mathrm{t}_{\partial S_j^l}^{l-k+1} \, \eta^{k-1} \wedge \mathrm{t}_{\partial S_j^l}^k \star_{S_j^l}^l \omega^k \tag{F.89}$$

This partial integration formula will be used later in the proof. Let us first prove that equation (F.84) follows from (4.30). We will use the following short hand notation to ease readability:

$$\xi \equiv \left(\mathrm{t}_{S_j^l}^k \, B_i^k \right) \tag{F.90}$$

Note that the trace conditions (4.30d) on page 100 and (F.84d) are directly equivalent as well as the uniqueness requirements (4.30d) on page 100 and (F.84d). Thus we only have to show equivalence of the other two equations. Assuming (4.30) on page 100 to hold, we get easily:

$$\Delta_{S_j^l}^k \xi = \mathrm{d}_{S_j^l}^{k-1} \, \delta_{S_j^l}^k \, \xi + \delta_{S_j^l}^{k+1} \, \mathrm{d}_{S_j^l}^k \, \xi = 0 \tag{F.91a}$$

$$\mathrm{t}_{\partial S_j^l}^{k-1} \, \delta_{S_j^l}^k \, \xi = \mathrm{t}_{\partial S_j^l}^{k-1} \, 0 = 0 \tag{F.91b}$$

Let us now prove that (4.30) on page 100 follows from equations (F.84). From equation (F.84a)

$$\Delta_{S_j^l}^k \xi = 0 \tag{F.92}$$

we get (leaving out the indices for the differential operators for better readability):

$$\begin{aligned} 0 = \left\langle\!\!\left\langle \Delta\xi \middle| \Delta\xi \right\rangle\!\!\right\rangle_{S_j^l} = \left\langle\!\!\left\langle \, (\delta \, \mathrm{d} + \mathrm{d} \, \delta) \, \xi \middle| \, (\delta \, \mathrm{d} + \mathrm{d} \, \delta) \, \xi \right\rangle\!\!\right\rangle_{S_j^l} \\ = \|\delta \, \mathrm{d} \, \xi\|_{S_j^l}^2 + \|\mathrm{d} \, \delta \, \xi\|_{S_j^l}^2 + 2 \left\langle\!\!\left\langle \, \delta \, \mathrm{d} \, \xi \middle| \, \mathrm{d} \, \delta \, \xi \right\rangle\!\!\right\rangle_{S_j^l} \end{aligned} \tag{F.93}$$

where $\|.\|_{S_j^l}$ denotes the local norm induced by the local inner product $\langle\!\langle .|. \rangle\!\rangle_{S_j^l}$. Using the partial integration formula developed in equation (F.89), the sequence property, the commuting property of the trace and the exterior derivative, and equation (F.84c), we get:

$$\begin{aligned} &= \|\delta \, \mathrm{d} \, \xi\|_{S_j^l}^2 + \|\mathrm{d} \, \delta \, \xi\|_{S_j^l}^2 + 2 \Bigg(\left\langle\!\!\left\langle \underbrace{\delta \, \delta}_{=0} \, \mathrm{d} \, \xi \middle| \, \delta \, \xi \right\rangle\!\!\right\rangle_{S_j^l} \\ &\quad + \int_{\partial S_j^l} \underbrace{\mathrm{t}_{\partial S_j^l} \, \delta \, \xi}_{=0} \wedge \mathrm{t}_{\partial S_j^l} \star \delta \, \mathrm{d} \, \xi \Bigg) \\ &= \|\delta \, \mathrm{d} \, \xi\|_{S_j^l}^2 + \|\mathrm{d} \, \delta \, \xi\|_{S_j^l}^2 \end{aligned} \tag{F.94}$$

This renders the following two terms zero:

$$\delta \, \mathrm{d} \, \xi = 0 \tag{F.95}$$
$$\mathrm{d} \, \delta \, \xi = 0 \tag{F.96}$$

We recognize equation (F.95) as proof for equation (4.30a) on page 100 to hold. Using the second equation (F.96) to prove equation (4.30b) on page 100 to hold requires more work: Defining a as

$$a \equiv \delta \, \xi \tag{F.97}$$

we recognize that a fulfills the following BVP (using equation (F.96), the sequence property, and equation (F.84c)):

$$\mathrm{d} \, a = 0 \tag{F.98a}$$
$$\delta \, a = \delta \, \delta \, \xi = 0 \tag{F.98b}$$
$$\mathrm{t}_{\partial S_j^l} \, a = \mathrm{t}_{\partial S_j^l} \, \delta \, \xi = 0 \tag{F.98c}$$

According to [80, Theorem 3.2.5], we know a unique solution up to the set of Dirichlet fields to exist. As $a = 0$ solves this BVP, it is the unique solution up to the set of Dirichlet fields. This renders the prove for equation (4.30b) on page 100:

$$\delta \, \xi = 0 \tag{F.99}$$

Therefore, we have proved equivalence of the two BVP (4.30) on page 100 and (F.84) on page 225. □

Proof of Theorem 4.5. With Lemma F.17 and the existence and uniqueness of a solution to the BVP (F.84) on page 225 from [80, Lemma 3.4.7], we have existence and uniqueness of a solution to the BVP (4.30) on page 100. □

F.2.2 Proof of Theorem 4.6

We will need the following lemma characterizing constant k-forms:

Lemma F.18. *The following two statements for a k-form c^k are equal for a manifold $S_j^l \subset \mathbb{R}^l$ with piecewise planar boundaries:*

1. *c^k is constant in $\overline{S_j^l}$*
2. *c^k has the following properties:*

$$\delta^k_{S_j^l} \, \mathrm{d}^k_{S_j^l} \, c^k = 0 \qquad \text{in } S_j^l \tag{F.100a}$$
$$\delta^k_{S_j^l} \, c^k = 0 \qquad \text{in } S_j^l \tag{F.100b}$$
$$\mathrm{t}^k_{\partial S_j^l} \, c^k = \mathrm{t}^k_{\partial S_j^l} \, \hat{c}^k \qquad \text{for some constant } k\text{-form } \hat{c}^k \text{ on } \partial S_j^l \tag{F.100c}$$
$$\int_{S_j^k} c^k = c_j^k \qquad \text{for } k = l, \text{ for some } c_j^k \in \mathbb{R} \tag{F.100d}$$

Proof. Considering 1 to hold, the statements in 2 can be verified by using the definitions of the exterior derivative, coderivative, and the trace. Intuitively considering the vector proxy of the constant k-form c^k, which has constant components in a Cartesian coordinate system, its exterior derivative and coderivative are zero as they contain first derivatives of the constant components. The trace of the constant k-form c^k is certainly that of a constant k-form, e.g. for itself. And the integral over the manifold S_j^k does definitely render some scalar.

To prove that statement 1 follows from statement 2, we notice that the equations (F.100) are equivalent to the BVP described by equations (4.30) on page 100. Theorem 4.5 on page 101 ensures uniqueness of the solution to this BVP. As the constant k-form $\hat{c}^k$ fulfills equations (F.100), it is the unique solution to equations (F.100). □

Proof of Theorem 4.6. Given existence and uniqueness of solutions to the BVP (4.30) on page 100, the requirements I to V on pages 95–96 are surprisingly easy to verify. We will prove the requirements one by one:

I. The construction algorithm given in Definition 4.3 on page 100 directly defines a basis form B_i^k for each grid element S_i^k.

II. From equation (4.29) on page 100 in the construction algorithm, we know that the traces $\mathrm{t}^k_{S_j^3} B_i^k$ on the local grid cells S_j^3 are smooth:

$$\mathrm{t}^k_{S_j^3} B_i^k \in \mathcal{F}_s^k(S_j^3) \tag{F.101}$$

Continuity of the traces $\mathrm{t}^k_{S_j^l} B_i^k$ for $l < 3$ across the inter-cell boundaries is sufficient to ensure that the patched global basis form B_i^k defined by equation (4.89) on page 116 is in the global Sobolev-type space $\mathcal{F}_\mathrm{d}^k(\Omega)$[1]. This continuity is fulfilled, because the traces $\mathrm{t}^k_{S_j^l} B_i^k$ are taken as boundary condition in equation (4.30c) on page 100 and thus are the same for all cells sharing the grid element S_j^l. The Whitney spaces $\mathcal{W}^k(\Omega_h)$ are spanned by the basis forms B_i^k; therefore we know:

$$\mathcal{W}^k(\Omega_h) \subset \mathcal{F}_\mathrm{d}^k(\Omega) \tag{F.102}$$

III. Using the definition of the grid discretization operators in equation (3.19) on page 37 and of the Whitney reconstruction operator in equation (4.4) on page 91, we can write:

$$\mathrm{L}_j^k \mathrm{W}^k \boldsymbol{\omega}^k = \int_{S_j^l} \sum_{i=1}^{n_k} \left(\boldsymbol{\omega}^k\right)_i B_i^k = \sum_{i=1}^{n_k} \left(\boldsymbol{\omega}^k\right)_i \int_{S_j^l} B_j^k \tag{F.103}$$

With the definition of the trace operator in equation (2.11) on page 10 and the relation (4.30d) on page 100 from the construction algorithm, we deduce:

$$= \sum_{i=1}^{n_k} \left(\boldsymbol{\omega}^k\right)_i \int_{S_j^l} \mathrm{t}^k_{S_j^l} B_j^k = \left(\boldsymbol{\omega}^k\right)_j \qquad \forall\, j \in [1..n^k] \tag{F.104}$$

which proofs equation (4.13) on page 95.

[1] Compare [49, Lemma 2.30] extended by the argument in [49, Remark 2.40] and the resulting presentation in [49, p. 77].

IV. We will show the property

$$\mathrm{d}^k\, \mathcal{W}^k(\Omega_h) \subseteq \mathcal{W}^{k+1}(\Omega_h) \tag{F.105}$$

and then conclude, using property III on page 95, by Lemma 4.4 on page 97 that property IV holds.

The statement in equation (F.105) will be verified by proving that the $(k+1)$-forms v_i^{k+1} defined as

$$v_i^{k+1} \equiv \mathrm{d}^k\, B_i^k \tag{F.106}$$

which form a basis of the space $\mathrm{d}^k\, \mathcal{W}^k(\Omega_h)$, are all in the Whitney space $\mathcal{W}^{k+1}(\Omega_h)$. Note that the trace commutes with the exterior derivative, so for the trace of v_i^{k+1} on the grid elements S_j^l we can write:

$$\mathrm{t}_{S_j^l}^{k+1}\, v_i^{k+1} = \mathrm{d}_{S_j^l}^k\, \mathrm{t}_{S_j^l}^k\, B_i^k \tag{F.107}$$

Also, for any l-dimensional grid element S_j^l, we know due to the sequence property (2.20) on page 12:

$$\delta_{S_j^l}^{k+2}\, \mathrm{d}_{S_j^l}^{k+1}\, \mathrm{t}_{S_j^l}^{k+1}\, v_i^{k+1} = \delta_{S_j^l}^{k+2}\, \mathrm{d}_{S_j^l}^{k+1}\, \mathrm{d}_{S_j^l}^k\, \mathrm{t}_{S_j^l}^k\, B_i^k = 0 \qquad \text{in } S_j^l \quad \forall\, S_j^l \tag{F.108}$$

From equation (4.30a) on page 100, we get:

$$\delta_{S_j^l}^{k+1}\, \mathrm{t}_{S_j^l}^{k+1}\, v_i^{k+1} = \delta_{S_j^l}^{k+1}\, \mathrm{d}_{S_j^l}^k\, \mathrm{t}_{S_j^l}^k\, B_i^k = 0 \qquad \text{in } S_j^l \quad \forall\, S_j^l \tag{F.109}$$

According to Definition 2.2 on page 10, the trace of v_i^{k+1} is trivial for all grid elements S_j^l with dimension l less than $k+1$:

$$\mathrm{t}_{S_j^l}^{k+1}\, v_i^{k+1} = 0 \qquad \forall\, l < k+1 \tag{F.110}$$

For any grid element of dimension $k+1$, we conclude from equation (4.30d) on page 100:

$$\int_{S_j^{k+1}} \mathrm{t}_{S_j^{k+1}}^{k+1}\, v_i^{k+1} = \int_{S_j^{k+1}} \mathrm{d}_{S_j^l}^k\, \mathrm{t}_{S_j^{k+1}}^k\, B_i^k \tag{F.111}$$

using Gauss' law (2.16) on page 11, this renders

$$\int_{S_j^{k+1}} \mathrm{t}_{S_j^{k+1}}^{k+1}\, v_i^{k+1} = \int_{\partial S_j^{k+1}} B_i^k \equiv a_j \quad \in \mathbb{R} \tag{F.112}$$

where we have defined the scalars a_j for later use. According to Lemma F.18 on page 227, the BVP in the unknown $\mathrm{t}_{S_j^{k+1}}^{k+1}\, v_i^{k+1}$ described by equations (F.108), (F.109), and (F.112) for $l = k+1$ has a constant k-form as unique solution:

$$\mathrm{t}_{S_j^{k+1}}^{k+1}\, v_i^{k+1} \quad \text{is a constant } k\text{-form} \tag{F.113}$$

Assuming property V on page 96 to hold, $\mathcal{W}^{k+1}(\Omega_h)$ contains all constant $(k+1)$-forms. Then $\mathrm{t}^{k+1}_{S^l_j}\,\mathcal{W}^{k+1}(\Omega_h)$ contains all constant $(k+1)$-forms on S^l_j and we get:

$$\mathrm{t}^{k+1}_{S^{k+1}_j}\,v^{k+1}_i \in \mathrm{t}^{k+1}_{S^{k+1}_j}\,\mathcal{W}^{k+1} \qquad \forall\, j \in [1..n^{k+1}] \tag{F.114}$$

For any $(l-1)$-dimensional grid element S^{l-1}_j with $k+2 < l < 4$ we will prove the following equivalent statement inductively:

$$\mathrm{t}^{k+1}_{S^{l-1}_j}\,v^{k+1}_i \in \mathrm{t}^{k+1}_{S^{l-1}_j}\,\mathcal{W}^{k+1} \qquad \forall\, j \in [1..n^{l-1}] \tag{F.115}$$

Assume equation (F.115) to hold for some $l > k+1$. Then for any l-dimensional grid element S^l_j we deduce that the traces on its boundary are in the Whitney spaces:

$$\mathrm{t}^{k+1}_{\partial S^l_j}\left(\mathrm{t}^{k+1}_{S^l_j}\,v^{k+1}_i\right) \in \mathrm{t}^{k+1}_{\partial S^l_j}\,\mathcal{W}^{k+1} \qquad \forall\, j \in [1..n^l] \tag{F.116}$$

The BVP defined by equations (F.108), (F.109), and (F.116) has according to Theorem 4.5 on page 101 a unique solution for the trace $\mathrm{t}^{k+1}_{S^l_j}\,v^{k+1}_i$. Consider the $(k+1)$-form $\hat{v}^{k+1}_i$ defined with the a_m from equation (F.112) as:

$$\hat{v}^{k+1}_i \equiv \sum_{m=1}^{n^{k+1}} a_m B^{k+1}_m \quad \in \mathcal{W}^{k+1}(\Omega_h) \tag{F.117}$$

We easily see, that its trace $\mathrm{t}^{k+1}_{S^l_j}\,\hat{v}^{k+1}_i$ also fulfills equations (F.108), (F.109), and (F.116) and thus these two solutions must be equal:

$$\mathrm{t}^{k+1}_{S^l_j}\,v^{k+1}_i = \mathrm{t}^{k+1}_{S^l_j}\,\hat{v}^{k+1}_i \quad \in \mathrm{t}^{k+1}_{S^l_j}\,\mathcal{W}^{k+1}(\Omega_h) \qquad \forall\, j \in [1..n^l] \tag{F.118}$$

Together with the induction start by equation (F.114), this proves:

$$\mathrm{t}^{k+1}_{S^3_j}\,v^{k+1}_i \quad \in \mathrm{t}^{k+1}_{S^3_j}\,\mathcal{W}^{k+1}(\Omega_h) \qquad \forall\, j \in [1..n^3] \tag{F.119}$$

$$\Leftrightarrow \qquad v^{k+1}_i \quad \in \mathcal{W}^{k+1}(\Omega_h) \tag{F.120}$$

Thus statement (F.105) is verified.

Assuming property III on page 95 to hold, this implies by Lemma 4.4 on page 97

$$\mathrm{d}^k\,\mathcal{W}^k = \mathcal{W}^{k+1}\,\mathbf{D}^k \qquad \forall\, k \in [0..2] \tag{F.121}$$

and thus concludes the proof.

V. Take any constant k-form c^k. We define $\hat{c}^k$ as

$$\hat{c}^k \equiv \sum_{i=1}^{n^k} \underbrace{\left(\int_{S^k_i} c^k\right)}_{c^k_i} B^k_i \quad \in \mathcal{W}^k(\Omega_h) \tag{F.122}$$

In the following, we will show that $\hat{c}^k$ and c^k are equal by showing that their traces on all grid elements are equal. Then it follows that all constant k-forms are in the Whitney space $\mathcal{W}^k(\Omega_h)$. First note that by Definition 2.2 on page 10 all grid elements S_j^l with lower dimension than the degree k of the constant k-form are zero:

$$\mathrm{t}^k_{S_j^l}\, c^k = \mathrm{t}^k_{S_j^l}\, \hat{c}^k = 0 \qquad \forall\, S_j^l, \quad \forall\, l < k \tag{F.123}$$

For any grid element S_j^l, we arrive using equations (4.30a) and (4.30b) on page 100 at:

$$\delta^k_{S_j^l}\, \mathrm{d}^k_{S_j^l}\, \mathrm{t}^k_{S_j^l}\, \hat{c}^k = \sum_{i=1}^{n^k} \left(c_i^k\right) \delta^k_{S_j^l}\, \mathrm{d}^k_{S_j^l}\, \mathrm{t}^k_{S_j^l}\, B_i^k = 0 \qquad \forall\, S_j^l \tag{F.124a}$$

$$\delta^k_{S_j^l}\, \mathrm{t}^k_{S_j^l}\, \hat{c}^k = \sum_{i=1}^{n^k} \left(c_i^k\right) \delta^k_{S_j^l}\, \mathrm{t}^k_{S_j^l}\, B_i^k = 0 \qquad \forall\, S_j^l \tag{F.124b}$$

Now consider the grid elements S_j^k, i.e. the grid elements having the same dimension as the degree of the k-form $\hat{c}^k$. From equation (F.123), we can conclude that the trace on the boundaries of these grid elements is zero:

$$\mathrm{t}^k_{\partial S_j^k}\, \hat{c}^k = 0 \tag{F.125}$$

Using equation (4.30d) on page 100, we can also calculate its integral over the grid element S_j^k:

$$\int_{S_j^k} \mathrm{t}^k_{S_j^k}\, \hat{c}^k = \sum_{i=1}^{n^k} c_i^k \int_{S_j^k} \mathrm{t}^k_{S_j^k}\, B_i^k \tag{F.126}$$

Now the BVP described by equations (F.124a) and (F.124b) with $l = k$ and equations (F.125) and (F.126) has, according to Theorem 4.5 on page 101, a unique solution. The trace of the constant k-form c^k does also fulfill these equations (see Lemma F.18 on page 227), so these two solutions must be equal:

$$\mathrm{t}^k_{S_j^k}\, c^k = \mathrm{t}^k_{S_j^k}\, \hat{c}^k \qquad \forall\, S_j^k \tag{F.127}$$

For $l > k$, we will prove the equivalent statement inductively: Assume the traces of $\hat{c}^k$ and c^k to be equal on all grid elements S_j^{l-1}:

$$\mathrm{t}^k_{S_j^{l-1}}\, c^k = \mathrm{t}^k_{S_j^{l-1}}\, \hat{c}^k \qquad \forall\, S_j^{l-1} \tag{F.128}$$

Then together with equations (F.124a) and (F.124b) this defines a BVP for the trace $\mathrm{t}^k_{S_j^l}\, \hat{c}^k$ and together with equations (F.100a) and (F.100b) on page 227 for the trace $\mathrm{t}^k_{S_j^l}\, c^k$. According to Theorem 4.5 on page 101, this BVP has a unique solution. Thus these traces are equal on S_j^l:

$$\mathrm{t}^k_{S_j^l}\, c^k = \mathrm{t}^k_{S_j^l}\, \hat{c}^k \qquad \forall\, S_j^l \tag{F.129}$$

Letting the induction start at $l = k$ by equation (F.127), this renders equality of c^k and $\hat{c}^k$:

$$c^k = \hat{c}^k \tag{F.130}$$

Thus any constant k-form c^k is in the Whitney space $\mathcal{W}^k(\Omega_h)$. Then there exists a $\boldsymbol{c}^k \in \mathcal{F}_h^k(\Omega_h)$ such that $c^k = \mathrm{W}^k \boldsymbol{c}^k$. Using property III on page 95 we can conclude the proof:

$$c^k = \mathrm{W}^k \boldsymbol{c}^k = \mathrm{W}^k \mathrm{L}^k \mathrm{W}^k \boldsymbol{c}^k = \mathrm{W}^k \mathrm{L}^k c^k \tag{F.131}$$

VI. Let us consider a basis form B_i^k associated with the element S_i^k. Immediately, we know that on all lower dimensional elements S_j^l with $l < k$, the trace of the basis function is zero:

$$\mathrm{t}^k_{S_j^l} B_i^k = 0 \qquad \forall\, S_j^l \quad \forall\, l < k \tag{F.132}$$

For $l = k$, we know by Theorem 4.5 on page 101 that the solution to the BVP (4.30) on page 100 is unique and by Lemma F.18 on page 227 that it is a constant function with integral value δ_{ij}. So on the grid elements S_j^k not associated with the basis function, its trace is zero:

$$\mathrm{t}^k_{S_j^k} B_i^k = 0 \qquad \forall\, j \in \big([1..n^k] \setminus i\big) \tag{F.133}$$

Now for $l > k$, we can prove inductively that the traces on all grid elements S_j^l which do not have S_j^l in its boundary, the trace of B_i^k on that element is zero:

Assume that for all grid elements S_m^{l-1} that do not have S_i^k in its boundary, the trace of B_i^k on these grid elements is zero:

$$\mathrm{t}^k_{S_m^l} B_i^k = 0 \qquad \forall\, S_m^l \text{ without } S_i^k \text{ in their boundaries} \tag{F.134}$$

Any element S_j^l that does not contain S_i^k in its boundary, only has such elements S_m^l in its boundary. Thus we know:

$$\mathrm{t}^k_{\partial S_j^l} B_i^k = 0 \qquad \forall\, j \in [1..n^l] \tag{F.135}$$

Together with equations (4.30a) and (4.30b) on page 100 we get by Theorem 4.5 on page 101 and by Lemma F.18 on page 227 the unique solution:

$$\mathrm{t}^k_{S_j^l} B_i^k = 0 \qquad \forall\, j \in [1..n^l] \tag{F.136}$$

Thus we know that the trace for all grid elements S_j^l that do not have S_i^k in its boundary, the trace of B_i^k on these grid elements is zero.

Together with the induction start at $l = k$ from equation (F.133) we thus know the function B_i^k to have zero trace on all grid elements that do not contain its associated grid element S_i^k in their boundaries.

□

F.2.3 Proof of Theorem 4.8

We will need the following lemma characterizing constant k-forms:

Lemma F.19. *Assume the spaces $\widetilde{\mathcal{W}}^k(S_j^l)$ fulfill the requirements put forward in Definition 4.4 and the spaces $\widetilde{\mathcal{W}}^k(S_j^l, \mathrm{t}^k_{\partial S_j^l} B_i^k)$ defined according to equation (4.79). Then the following two statements for a k-form c^k are equal for a manifold $S_j^l \subset \mathbb{R}^l$ with piecewise planar boundaries:*

1. *c^k is constant in $\overline{S_j^l}$*
2. *There exists a constant k-form $\hat{c}^k$ such that $c^k \in \widetilde{\mathcal{W}}^k(S_j^l, \mathrm{t}^k_{\partial S_j^l} \hat{c}^k)$ has the following properties:*

$$\left\langle\!\!\left\langle \mathrm{d}^k_{S_j^l} c^k \middle| \mathrm{d}^k_{S_j^l} \eta^k \right\rangle\!\!\right\rangle_{S_j^l} = 0 \qquad \forall\, \eta^k \in \widetilde{\mathcal{W}}^k(S_j^l, 0) \tag{F.137a}$$

$$\left\langle\!\!\left\langle c^k \middle| \mathrm{d}^{k-1}_{S_j^l} \eta^{k-1} \right\rangle\!\!\right\rangle = 0 \qquad \forall\, \eta^{k-1} \in \widetilde{\mathcal{W}}^{k-1}(S_j^l, 0) \tag{F.137b}$$

$$\int_{S_j^k} c^k = c_j^k \qquad \text{for } k = l, \text{ for some } c_j^k \in \mathbb{R} \tag{F.137c}$$

Proof. Considering 1 to hold, the statements in 2 can be verified by using the definitions of the exterior derivative, coderivative, and the trace and the partial integration formula (F.89) on page 226.

To prove that statement 1 follows from statement 2, we notice that the equations (F.137) are equivalent to the BVP described by equations (4.80) on page 115. Theorem 4.7 on page 115 ensures uniqueness of the solution to this BVP. As the constant k-form $\hat{c}^k \in \widetilde{\mathcal{W}}^k(S_j^l)$ fulfills equations (F.137), it is the unique solution to equations (F.137). □

Proof of Theorem 4.8. We prove the requirements I to V on pages 95–96 one by one in parallel to the proof for the continuous construction scheme given in chapter F.2.2:

I. The construction algorithm given in Definition 4.4 on page 116 directly defines a basis form B_i^k for each grid element S_i^k.

II. The traces $\mathrm{t}^k_{S_j^l} B_i^k$ on the local grid elements S_j^l are in the local intermediate approximation spaces $\widetilde{\mathcal{W}}^k(S_j^l)$:

$$\mathrm{t}^k_{S_j^l} B_i^k \in \widetilde{\mathcal{W}}^k(S_j^l) \tag{F.138}$$

Continuity of the traces $\mathrm{t}^k_{S_j^l} B_i^k$ for $l < 3$ across the inter-cell boundaries is sufficient to ensure that the patched global basis form B_i^k defined by equation (4.89) on page 116 is in the global Sobolev-type space $\mathcal{F}^k_{\mathrm{d}}(\Omega)$. This continuity is fulfilled, because the traces $\mathrm{t}^k_{S_j^l} B_i^k$ are taken as boundary condition by the discrete construction process and thus are the same for all cells sharing the grid element S_j^l. The Whitney spaces $\mathcal{W}^k(\Omega_h)$ are spanned by the basis forms B_i^k; therefore we know:

$$\mathcal{W}^k(\Omega_h) \subset \mathcal{F}^k_{\mathrm{d}}(\Omega) \tag{F.139}$$

III. This proof is completely analogous to the proof for the continuous BVP.

IV. We will show that equation (F.105) on page 229 holds and then conclude, using property III on page 95, by Lemma 4.4 on page 97 that property IV holds.

The statement in equation (F.105) will be verified by proving that the $(k+1)$-forms v_i^{k+1} defined by equation (F.106), which form a basis of the space $\mathrm{d}^k\,\mathcal{W}^k(\Omega_h)$, are all in the Whitney space $\mathcal{W}^{k+1}(\Omega_h)$.

Note that the trace commutes with the exterior derivative, so for the trace of v_i^{k+1} on the grid elements S_j^l we can use equation (F.107). Also, for any l-dimensional grid element S_j^l, we know due to the sequence property (2.20) on page 12:

$$\left\langle\!\!\left\langle \mathrm{d}^{k+1}_{S_j^l}\,\mathrm{t}^{k+1}_{S_j^l}\,v_i^{k+1}\middle|\,\mathrm{d}^{k+1}_{S_j^l}\,\eta^{k+1}\right\rangle\!\!\right\rangle_{S_j^l} = \left\langle\!\!\left\langle \mathrm{d}^{k+1}_{S_j^l}\,\mathrm{d}^{k}_{S_j^l}\,\mathrm{t}^{k}_{S_j^l}\,B_i^k\middle|\,\mathrm{d}^{k+1}_{S_j^l}\,\eta^{k+1}\right\rangle\!\!\right\rangle_{S_j^l} = 0$$
$$\forall\,\eta^{k+1} \in \widetilde{\mathcal{W}}^{k+1}(S_j^l, 0) \quad \forall\, S_j^l \tag{F.140}$$

From equation (4.80a) on page 115, we get:

$$\left\langle\!\!\left\langle \mathrm{t}^{k+1}_{S_j^l}\,v_i^{k+1}\middle|\,\mathrm{d}^{k}_{S_j^l}\,\eta^{k}\right\rangle\!\!\right\rangle_{S_j^l} = \left\langle\!\!\left\langle \mathrm{d}^{k}_{S_j^l}\,\mathrm{t}^{k}_{S_j^l}\,B_i^k\middle|\,\mathrm{d}^{k}_{S_j^l}\,\eta^{k}\right\rangle\!\!\right\rangle_{S_j^l} = 0$$
$$\forall\,\eta^{k} \in \widetilde{\mathcal{W}}^{k}(S_j^l, 0) \quad \forall\, S_j^l \tag{F.141}$$

According to Definition 2.2 on page 10, the trace of v_i^{k+1} is trivial for all grid elements S_j^l with dimension l less than $k+1$. For any grid element of dimension $k+1$, we conclude from equation (4.80d) on page 115 that equation (F.111) on page 229 holds. Using Gauss' law (2.16) on page 11, this renders equation (F.112). According to Lemma F.19, the BVP in the unknown $\mathrm{t}^{k+1}_{S_j^{k+1}}\,v_i^{k+1}$ described by equations (F.140), (F.141), and (F.112) for $l = k+1$ has a constant k-form as unique solution in the intermediate search space $\widetilde{\mathcal{W}}^k(S_j^l, \mathrm{t}^{k+1}_{\partial S_j^{k+1}}\,v_i^{k+1} = 0)$. Assuming property V on page 96 to hold, $\mathcal{W}^{k+1}(\Omega_h)$ contains all constant $(k+1)$-forms. Then $\mathrm{t}^{k+1}_{S_j^l}\,\mathcal{W}^{k+1}(\Omega_h)$ contains all constant $(k+1)$-forms on S_j^l and we get equation (F.114) on page 230. For any $(l-1)$-dimensional grid element S_j^{l-1} with $k+2 < l < 4$ we will prove equation (F.115) inductively: Assume equation (F.115) to hold for some $l > k+1$. Then for any l-dimensional grid element S_j^l we deduce that the traces on its boundary are in the Whitney spaces as stated in equation (F.116). The BVP defined by equations (F.140) and (F.141) has, according to Theorem 4.7 on page 115, a unique solution for the trace $\mathrm{t}^{k+1}_{S_j^l}\,v_i^{k+1}$ in the search space $\widetilde{\mathcal{W}}^{k+1}(S_j^l, \mathrm{t}^{k+1}_{\partial S_j^l}\,\mathrm{t}^{k+1}_{S_j^l}\,v_i^{k+1})$. The trace of the $(k+1)$-form $\hat{v}_i^{k+1}$ defined by equation (F.117) fulfills equations (F.140) and (F.141) and thus these two solutions must be equal. Together with the induction start by equation (F.114), this verifies statement (F.105) also for the approximation spaces resulting from the discrete construction algorithm. Assuming property III on page 95 to hold, this implies by Lemma 4.4 on page 97 that equation (F.121) on page 230 holds and thus concludes the proof.

V. Take any constant k-form c^k and define $\hat{c}^k$ by equation (F.122) on page 230. In the following, we will show that $\hat{c}^k$ and c^k are equal by showing that their traces on all grid elements are equal. Then it follows that all constant k-forms are in the Whitney

space $\mathcal{W}^k(\Omega_h)$. First note that by Definition 2.2 on page 10 all grid elements S_j^l with lower dimension than the degree k of the constant k-form are zero as stated by equation (F.123). For any grid element S_j^l, we arrive using equations (4.80a) and (4.80b) on page 115 at:

$$\langle\!\langle \mathrm{d}^k_{S_j^l}\, \mathrm{t}^k_{S_j^l}\, \hat{c}^k \,|\, \mathrm{d}^k_{S_j^l}\, \eta^k \rangle\!\rangle_{S_j^l} = \sum_{i=1}^{n^k} \left(c_i^k\right) \langle\!\langle \mathrm{d}^k_{S_j^l}\, \mathrm{t}^k_{S_j^l}\, B_i^k \,|\, \mathrm{d}^k_{S_j^l}\, \eta^k \rangle\!\rangle_{S_j^l} = 0 \qquad \forall\, \eta^k \in \widetilde{\mathcal{W}}^k(S_j^l, 0) \quad \forall\, S_j^l \tag{F.142a}$$

$$\langle\!\langle \mathrm{t}^k_{S_j^l}\, \hat{c}^k \,|\, \mathrm{d}^k_{S_j^l}\, \eta^k \rangle\!\rangle_{S_j^l} = \sum_{i=1}^{n^k} \left(c_i^k\right) \langle\!\langle \mathrm{t}^k_{S_j^l}\, B_i^k \,|\, \mathrm{d}^{k-1}_{S_j^l}\, \eta^{k-1} \rangle\!\rangle_{S_j^l} = 0 \qquad \forall\, \eta^{k-1} \in \widetilde{\mathcal{W}}^{k-1}(S_j^l, 0) \quad \forall\, S_j^l \tag{F.142b}$$

Now consider the grid elements S_j^k, i.e. the grid elements having the same dimension as the degree of the k-form $\hat{c}^k$. From equation (F.123), we can conclude that the trace on the boundaries of these grid elements is zero. Using equation (4.80d) on page 115, we can also calculate its integral over the grid element S_j^k according to equation (F.126) on page 231. The BVP described by equations (F.142a) and (F.142b) with $l = k$ and equation (F.126) has, according to Theorem 4.7 on page 115, a unique solution in the intermediate search space $\widetilde{\mathcal{W}}^k(S_j^l, 0)$. The trace of the constant k-form c^k does also fulfill these equations (see Lemma F.19), so these two solutions must be equal, as stated by equation (F.127). For $l > k$, we will prove the equivalent statement inductively: Assume the traces of $\hat{c}^k$ and c^k to be equal on all grid elements S_j^{l-1} as stated by equation (F.128) on page 231. Then together with equations (F.142a) and (F.142b), this defines a BVP for the trace $\mathrm{t}^k_{S_j^l}\, \hat{c}^k$ and together with equations (F.137a) and (F.137b) on page 233 for the trace $\mathrm{t}^k_{S_j^l}\, c^k$. According to Theorem 4.7 on page 115, this BVP has a unique solution. Thus these traces are equal on S_j^l. Letting the induction start at $l = k$ by equation (F.127), this renders equality of c^k and $\hat{c}^k$. Thus any constant k-form c^k is in the Whitney space $\mathcal{W}^k(\Omega_h)$. Then there exists a $\boldsymbol{c}^k \in \mathcal{F}_h^k(\Omega_h)$ such that $c^k = \mathrm{W}^k \boldsymbol{c}^k$. Using property III on page 95 we can conclude the proof:

$$c^k = \mathrm{W}^k \boldsymbol{c}^k = \mathrm{W}^k \mathrm{L}^k \mathrm{W}^k \boldsymbol{c}^k = \mathrm{W}^k \mathrm{L}^k c^k \tag{F.143}$$

VI. This proof is completely analogous to the proof for the continuous case.

□

ABBREVIATIONS AND SYMBOLS

List of Abbreviations

BEM	boundary element method
BVP	boundary value problem
FD	Finite Differences
FE	Finite Element
FEM	Finite Element Method
FIT	Finite Integration Technique
FV	Finite Volume
IBVP	initial boundary value problem
PEC	perfect electrically conducting (boundary condition)
PMC	perfect magnetically conducting (boundary condition)
TE	transverse electric
TEM	transverse electric-magnetic
TM	transverse magnetic

List of Symbols

General

$\mathbb{R}$	real numbers
$\mathbb{C}$	complex numbers
$\mathbb{Z}$	integers
δ_{ij}	Kronecker delta
$\mathrm{K}\big(L\big)$	kernel of operator L
$\mathrm{R}\big(L\big)$	range of operator L
$\vec{a} \cdot \vec{b}$	scalar product of vectors $\vec{a}$ and $\vec{b}$
$\vec{a} \times \vec{b}$	vector product of vectors $\vec{a}$ and $\vec{b}$
$[a_i]_{i \in \mathrm{I}}$	vector defined by components a_i for i in the index set I
$(\vec{a})_i$	i-th component of vector $\vec{a}$
$\{S_i\}_{i \in \mathrm{I}}$	set of elements S_i over the index set I
$(\mathbf{A})_{ij}$	entry in row i and column j of matrix $\mathbf{A}$
A_{ij}	entry in row i and column j of matrix $\mathbf{A}$
$\mathbf{A}^{\mathrm{T}}$	transpose of matrix $\mathbf{A}$
$\mathbf{A}^{\mathrm{H}}$	hermitian of matrix $\mathbf{A}$
$\mathbf{I}$	identity matrix

Continuous Setting

Ω	(3-dimensional) spatial domain, (Riemannian) manifold
$\vec{r}$	spatial variable
T	(1-dimensional) temporal domain
t	temporal variable
Γ^l	l-dimensional (Riemannian) submanifold
$\partial\Omega$	boundary of Ω
$\mathring{\Omega}$	interior of Ω
$\overline{\Omega}$	closure of Ω
$\Omega \times \mathrm{T}$	Cartesian product space of Ω with T
S^k	k-dimensional submanifold
$\boldsymbol{S}_s^k(\Omega)$	space of smooth oriented k-dimensional submanifolds of Ω
$\boldsymbol{S}^k(\Omega)$	space of non-pathological piecewise smooth oriented k-dimensional submanifolds of Ω
$\mathcal{F}_s^k(\Omega)$	space of smooth k-forms on the manifold Ω
$\vec{\mathcal{F}}_s^k(\Omega)$	space of vector proxies of smooth k-forms on the manifold Ω
ω^k, η^k	k-forms
$\vec{\omega}^k$, $\vec{\eta}^k$	vector proxies of k-forms
$\multimap$	association symbol for k-forms with their vector proxies
∂_t	temporal derivative
$\mathrm{t}_{\Gamma^l}^k$	trace operator onto Γ^l acting on k-forms
d^k	exterior derivative acting on k-forms
$\star_\alpha^n$	hodge operator for n-dimensional manifold based on Riemannian metric α
$\star_\alpha$	hodge operator for 3-dimensional manifold based on Riemannian metric α
$\star^n$	hodge operator for n-dimensional manifold based on Euclidean metric
$\star$	hodge operator for 3-dimensional manifold based on Euclidean metric
$\wedge$	exterior product
$\langle\!\langle .\vert . \rangle\!\rangle_\alpha$	global inner product based on metric α
$\langle\!\langle .\vert . \rangle\!\rangle$	global inner product based on Euclidean metric
$\Vert . \Vert_\alpha$	global norm induced by the inner product $\langle\!\langle .\vert . \rangle\!\rangle_\alpha$
$\Vert . \Vert$	global norm induced by the Euclidean inner product $\langle\!\langle .\vert . \rangle\!\rangle$
grad	3-dimensional gradient operator
curl	3-dimensional curl operator
div	3-dimensional divergence operator
$\int_{S^k} \omega^k$	integral of a k-form ω^k over a k-dimensional submanifold S^k
$\mathrm{d}s$	infinitesimal path length element
$\mathrm{d}A$	infinitesimal surface area element
$\mathrm{d}V$	infinitesimal volume element
$\vec{t}_{S^1}$	unit tangential vector along oriented path S^1
$\vec{n}_{S^2}$	unit normal vector perpendicular to oriented surface S^2
φ_e^0	electric scalar potential as 0-form

e^1	electric field strength as 1-form
h^1	magnetic field strength as 1-form
d^2	electric flux density as 2-form
b^2	magnetic flux density as 2-form
j^2	electric current density as 2-form
ϱ_e^3	electric charge density as 3-form
ϱ_m^3	magnetic charge density as 3-form
φ_e	electric scalar potential
$\vec{E}$	electric field strength
$\vec{E}_{\Gamma_1}$	tangential electric field strength on boundary part Γ_1
$\vec{H}$	magnetic field strength
$\vec{H}_{\Gamma_2}$	tangential magnetic field strength on boundary part Γ_2
$\vec{A}_m$	magnetic vector potential
$\vec{D}$	electric flux density
$\vec{B}$	magnetic flux density
$\vec{K}$	magnetic current density
$\vec{J}$	electric current density
ϱ_e	electric charge density
ϱ_m	magnetic charge density
ε	permittivity
ν	reluctivity
W_e	electric energy
W_m	magnetic energy
W	(total) electromagnetic energy
P_e	electric losses
P_P	radiation losses
Γ_1	electric boundary part (boundary part with electric boundary condition)
Γ_2	magnetic boundary part (boundary part with magnetic boundary condition)

Semi-Discrete FIT Setting

Ω_h	consistent primal grid
$\underset{\sim}{\Omega}_h$	dual grid of primal grid Ω_h
$\boldsymbol{S}^k(\Omega_h)$	space of k-dimensional primal grid elements
$\underset{\sim}{\boldsymbol{S}}^k(\underset{\sim}{\Omega}_h)$	space of k-dimensional dual grid elements
S_i^k	i-th k-dimensional primal grid element
$\underset{\sim}{S}_i^k$	i-th k-dimensional dual grid element
$\lvert S_i^k \rvert$	measure of grid element S_i^k
n^k	number of k-dimensional primal grid elements
$\underset{\sim}{n}^k$	number of k-dimensional dual grid elements
$\boldsymbol{C}^k(\Omega_h)$	space of primal k-chains on primal grid Ω_h
$\underset{\sim}{\boldsymbol{C}}^k(\underset{\sim}{\Omega}_h)$	space of dual k-chain on dual grid $\underset{\sim}{\Omega}_h$
$\boldsymbol{c}^k$	primal k-chains

$\underset{\sim}{\boldsymbol{c}}^k$	dual k-chains
$\mathcal{F}_h^k(\Omega_h)$	space of primal k-cochains on primal grid Ω_h
$\underset{\sim}{\mathcal{F}}_h^k(\underset{\sim}{\Omega}_h)$	space of dual k-cochain on dual grid $\underset{\sim}{\Omega}_h$
$\boldsymbol{\omega}^k, \boldsymbol{\eta}^k$	primal k-cochains
$\underset{\sim}{\boldsymbol{\omega}}^k, \underset{\sim}{\boldsymbol{\eta}}^k$	dual k-cochains
$\boldsymbol{\partial}^k$	discrete boundary operator acting on primal k-chains
$\underset{\sim}{\boldsymbol{\partial}}^k$	discrete boundary operator acting on dual k-chains
L^k	primal grid discretization operator / deRham map of degree k
L_i^k	primal grid discretization operator / deRham map of degree k for primal grid element S_i^k
$\underset{\sim}{\mathrm{L}}^k$	dual grid discretization operator / deRham map of degree k
$\underset{\sim}{L}_i^k$	dual grid discretization operator / deRham map of degree k for dual grid element $\underset{\sim}{S}_i^k$
$\overline{\Gamma}_h^l$	l-dimensional (primal) grid part; consistent (primal) grid of manifold Γ^l
$\underset{\sim}{\Gamma}_h^l$	dual grid of grid part $\overline{\Gamma}_h^l$; dual grid of primal grid $\overline{\Gamma}_h^l$
$\mathrm{I}^k_{\overline{\Gamma}_h^l}$	index list of k-dimensional primal grid elements in grid part $\overline{\Gamma}_h^l$
$\underset{\sim}{\mathrm{I}}^k_{\underset{\sim}{\Gamma}_h^l}$	index list of k-dimensional dual grid elements in dual grid $\underset{\sim}{\Gamma}_h^l$
$n^k_{\overline{\Gamma}_h^l}$	number of k-dimensional primal grid elements in grid part $\overline{\Gamma}_h^l$
$\underset{\sim}{n}^k_{\underset{\sim}{\Gamma}_h^l}$	number of k-dimensional dual grid elements in dual grid $\underset{\sim}{\Gamma}_h^l$
$\mathbf{T}^k_{\overline{\Gamma}_h^l}$	discrete (grid) trace operator onto grid part $\overline{\Gamma}_h^l$ acting on primal k-cochains
$\wedge$	discrete (grid) exterior product
$\int_{S_i^k} \boldsymbol{\omega}^k$	primal discrete (grid) integral of the k-cochain $\boldsymbol{\omega}^k$ over the grid element S_i^k
$\int_{\underset{\sim}{S}_i^k} \underset{\sim}{\boldsymbol{\omega}}^k$	dual discrete (grid) integral of the k-cochain $\underset{\sim}{\boldsymbol{\omega}}^k$ over the grid element $\underset{\sim}{S}_i^k$
$\mathbf{D}^k$	primal exterior grid derivative on k-cochains
$\underset{\sim}{\mathbf{D}}^k$	dual exterior grid derivative on k-cochains
$\mathrm{L}^k_{\overline{\Gamma}_h^l}$	primal boundary grid discretization operator of degree k on grid part $\overline{\Gamma}_h^l$
$\underset{\sim}{\mathrm{L}}^k_{\underset{\sim}{\Gamma}_h^l}$	dual boundary grid discretization operator of degree k on dual grid $\underset{\sim}{\Gamma}_h^l$
$\mathbf{M}^k_\alpha$	primal discrete hodge operator for Riemannian metric α
$\underset{\sim}{\mathbf{M}}^k_\alpha$	dual discrete hodge operator for Riemannian metric α
$\mathbf{M}^k$	primal discrete hodge operator for Euclidean metric
$\underset{\sim}{\mathbf{M}}^k$	dual discrete hodge operator for Euclidean metric
$\mathbf{M}^{k,m}_\alpha$	local discrete hodge operator for grid cell S_m^3 for metric α
$\widetilde{\mathbf{M}}^{k,m}_\alpha$	reduced local discrete hodge operator for grid cell S_m^3 for metric α
$\langle\!\langle \cdot \vert \cdot \rangle\!\rangle_\alpha$	primal grid inner product based on metric α
$\Vert \cdot \Vert_\alpha$	primal grid energy norm induced by the primal grid inner product $\langle\!\langle \cdot \vert \cdot \rangle\!\rangle_\alpha$
$\boldsymbol{\varphi}_e$	(primal) electric scalar grid potentials
$\underset{\sim}{\boldsymbol{\varphi}}_m$	(dual) magnetic scalar grid potentials

$\widehat{\mathbf{e}}$	(primal) electric grid voltages
$\widehat{\mathbf{e}}_{\Gamma_j}$	(primal) electric boundary grid voltages on boundary part Γ_j
$\widehat{\mathbf{h}}$	(dual) magnetic grid voltages
$\widehat{\mathbf{h}}_{\Gamma_j}$	(dual) magnetic boundary grid voltages on boundary part Γ_j
$\widehat{\widetilde{\mathbf{b}}}$	(primal) magnetic grid fluxes
$\widehat{\widetilde{\mathbf{k}}}$	(primal) magnetic grid currents
$\widehat{\widetilde{\mathbf{d}}}$	(dual) electric grid fluxes
$\widehat{\widetilde{\mathbf{j}}}$	(dual) electric grid currents
$\widehat{\widetilde{\mathbf{j}}}_{\Gamma_j}$	(dual) equivalent electric boundary grid current parts on boundary part Γ_j
$\widehat{\widetilde{\mathbf{j}}}_{\partial\Omega}$	(dual) equivalent electric boundary grid currents
$\widehat{\widetilde{\mathbf{j}}}^*$	(dual) total electric grid currents containing equivalent boundary currents
$\widehat{\widetilde{\boldsymbol{\varrho}}}_m$	(primal) magnetic grid charges
$\widehat{\widetilde{\boldsymbol{\varrho}}}_e$	(dual) electric grid charges
$\widehat{\widetilde{\boldsymbol{\varrho}}}_e^*$	(dual) electric grid charges containing equivalent boundary charges
$\widehat{\mathbf{a}}_m$	(primal) magnetic grid vector potential
W_e^d	electric grid energy
W_m^d	magnetic grid energy
W^d	(total) electromagnetic grid energy
P_e^d	electric grid losses
P_P^d	equivalent boundary electric grid losses
$\mathbf{M}_\varepsilon$	(primal) permittivity matrix
$\mathbf{M}_\nu$	(primal) reluctivity matrix
$\mathbf{M}_\varepsilon^{1,m}$	(primal) local permittivity matrix for grid cell S_m^3
$\mathbf{M}_\nu^{2,m}$	(primal) local reluctivity matrix for grid cell S_m^3
$\widetilde{\mathbf{M}}_\varepsilon^{1,m}$	(primal) reduced local permittivity matrix for grid cell S_m^3
$\widetilde{\mathbf{M}}_\nu^{2,m}$	(primal) reduced local reluctivity matrix for grid cell S_m^3
$\mathbf{M}_{\mathrm{sFIT},\varepsilon}$	standard FIT material matrix
$\mathbf{M}_{\mathrm{FEM},\varepsilon}$	Whitney-FEM material matrix
ε_m	permittivity of primal cell S_m^3
$\overline{\varepsilon}_i$	face-averaged permittivity for primal edge S_i^1
ν_m	reluctivity of primal cell S_m^3
$\overline{\nu}_i$	edge-averaged reluctivity for primal face S_i^2
$\mathbf{G}$	primal grid gradient
$\widetilde{\mathbf{G}}$	dual grid gradient
$\mathbf{C}$	primal grid curl
$\widetilde{\mathbf{C}}$	dual grid curl
$\mathbf{S}$	primal grid divergence
$\widetilde{\mathbf{S}}$	dual grid divergence

Fully-Discrete FIT Setting

$\mathrm{T}_{\Delta t}$	primal temporal grid

$\underset{\sim}{\mathrm{T}}_{\Delta t}$	dual temporal grid
t_n	primal temporal grid vertices
$\underset{\sim}{t}_n$	dual temporal grid vertices
Δt_n	primal temporal grid edges
$\underset{\sim}{\Delta t}_n$	dual temporal grid edges
$L^k_{\mathrm{T}_{\Delta t},n}$	local primal temporal grid discretization operator of degree k
$\underset{\sim}{L}^k_{\underset{\sim}{\mathrm{T}}_{\Delta t},n}$	local dual temporal grid discretization operator of degree k
$\overline{\widehat{\mathbf{e}}}^n$	electric grid voltage pulses
$\overline{\boldsymbol{\varphi}}^n_e$	electric grid potential pulses
$\widehat{\mathbf{a}}^n_m$	magnetic vector potential
$\overline{\widehat{\mathbf{h}}}^n$	magnetic grid voltage pulses
$\underset{\sim}{\overline{\widehat{\mathbf{d}}}}^n$	electric grid fluxes
$\overline{\widehat{\mathbf{b}}}^n$	magnetic grid fluxes
$\overline{\dot{\widehat{\mathbf{j}}}}^n$	electric grid current pulses
$\underset{\sim}{\overline{\dot{\widehat{\mathbf{j}}}}}^n_{\Gamma_j}$	equivalent boundary electric grid current pulse parts
$\underset{\sim}{\overline{\dot{\widehat{\mathbf{j}}}}}^n_{\partial\Omega}$	equivalent boundary electric grid current pulses
$\underset{\sim}{\overline{\widehat{\boldsymbol{\varrho}}}}^{*,n}_e$	electric grid charges containing equivalent boundary charges
$\overline{\widehat{\boldsymbol{\varrho}}}^n_m$	magnetic grid charges
$\dot{\mathbf{M}}_\varepsilon(n,m)$	space-time permittivity matrices
$\overline{\mathbf{M}}_\nu(n,m)$	space-time reluctivity matrices
$\mathbf{M}^{\boldsymbol{\alpha}}_\nu$	weighted reluctivity matrices
$\mathrm{I}^3_{\mathrm{sFIT}}$	index set of cells with standard FIT material relations
$\mathrm{I}^3_{\mathrm{FEM}}$	index set of cells with Whitney-FEM material relations
W^n	space-time discrete (total) electromagnetic grid energy
W^n_e	space-time discrete electric grid energy
W^n_m	space-time discrete magnetic grid energy
$\overline{P}^n_e$	space-time discrete electric grid losses
$\overline{P}^n_P$	space-time discrete equivalent boundary electric grid losses

Polyhedral Material Relations

$\mathcal{F}^k_{\mathrm{d}}(\Omega)$	space of Sobolev-type k-forms on the manifold Ω
$\vec{\mathcal{F}}^k_{\mathrm{d}}(\Omega)$	space of vector proxies of Sobolev-type k-forms on the manifold Ω
$\mathcal{F}^k_{\mathrm{I}}(\Omega)$	space of integral k-forms on the manifold Ω
B^k_i	Whitney-FEM basis form
$\vec{B}^k_i$	Whitney-FEM basis function
$\mathcal{W}^k(\Omega_h)$	Whitney approximation space of degree k for the consistent grid Ω_h
W^k	Whitney reconstruction operator / Whitney map
P^k	Whitney projector
$\langle\!\langle .\vert . \rangle\!\rangle_{\alpha,S^l_j}$	continuous local inner product over grid cell S^l_j based on metric α
$\langle\!\langle .\vert . \rangle\!\rangle_{S^l_j}$	continuous local inner product over grid cell S^l_j based on Euclidean metric

$\mathrm{d}^k_{S^l_j}$	local exterior derivative on the grid cell S^l_j
$\star^k_{S^l_j}$	local hodge operator on the grid cell S^l_j based on Euclidean metric
$\delta^k_{S^l_j}$	local exterior coderivative on the grid cell S^l_j
$\widetilde{\mathcal{W}}^k(S^l_j)$	intermediate approximation space of degree k on the grid element S^l_j
$\widetilde{\mathcal{W}}^k(S^l_j, \mathrm{t}^k_{\partial S^{l_j}} B^k_i)$	intermediate search space on the grid element S^l_j
$\widetilde{\mathcal{W}}^k(S^l_j, 0)$	intermediate test space on the grid element S^l_j
$\overrightarrow{\mathrm{grad}}_{2\mathrm{D}}$	2-dimensional gradient operator
$\mathrm{curl}_{2\mathrm{D}}$	2-dimensional longitudinal part curl operator
$\overrightarrow{\mathrm{curl}}_{2\mathrm{D}}$	2-dimensional transverse part curl operator
$\mathrm{div}_{2\mathrm{D}}$	2-dimensional divergence operator
$\mathcal{H}^k$	full discrete cohomology space of degree k
$\mathcal{H}^k_c$	relative discrete cohomology space of degree k

Numerical Examples

ε_0	free-space permittivity
ε_r	relative permittivity
ν_0	free-space reluctivity
ν_r	relative reluctivity
ω	resonance frequency
ω_c	resonance frequency of the continuous problem
f	frequency
f_c	cut-off frequency
k_0	free-space wavenumber
$k_{z,c}$	continuous longitudinal wavenumber
k_z	discrete longitudinal wavenumber
$\underline{\vec{E}}$	complex amplitude of the electric field strength
$\vec{E}_t$	2-dimensional transverse electric field strength
$\underline{\vec{E}}_t$	2-dimensional complex amplitude of the transverse electric field strength
$\underline{\mathrm{E}}_z$	2-dimensional complex amplitude of the longitudinal electric field strength
$\underline{\vec{D}}_t$	2-dimensional complex amplitude of the transverse electric flux density
$\underline{H}_z$	2-dimensional complex amplitude of the longitudinal magnetic field strength
$\mathrm{L}^k_{2\mathrm{D}}$	2-dimensional grid discretization operator
$\mathbf{D}^k_{2\mathrm{D}}$	2-dimensional primal exterior grid derivative
$\underset{\sim}{\mathbf{D}}^k_{2\mathrm{D}}$	2-dimensional dual exterior grid derivative
$\mathbf{M}^k_{2\mathrm{D},\alpha}$	2-dimensional primal material matrices for the material coefficient α
$\mathbf{M}^0_{2\mathrm{D},\Omega_h\setminus\overline{\Gamma}_{1,h},\varepsilon_r}$	2-dimensional primal reduced nodal permittivity matrix

$\mathbf{T}^k_{2\mathrm{D},\overline{\Gamma}_{1,h}}$	2-dimensional trace operators onto the electric boundary grid part $\overline{\Gamma}_{1,h}$
$\mathbf{T}^k_{2\mathrm{D},\Omega_h\setminus\overline{\Gamma}_{1,h}}$	2-dimensional trace operator onto the grid Ω_h without the electric boundary grid part $\overline{\Gamma}_{1,h}$
$\mathbf{T}^k_{\overline{\Gamma}_{1,h}}$	trace operator onto the boundary grid part $\overline{\Gamma}_{1,h}$
$\mathbf{T}^k_{\Omega_h\setminus\overline{\Gamma}_{j,h}}$	trace operator onto the grid Ω_h without the boundary grid part $\overline{\Gamma}_{j,h}$
$\boldsymbol{\varphi}_{e,2\mathrm{D}}$	2-dimensional electric scalar grid potentials
$\underline{\widehat{\mathbf{e}}}_{2\mathrm{D},t}$	2-dimensional complex amplitudes of the transverse electric grid voltages
$\underline{\mathbf{e}}_{2\mathrm{D},z}$	2-dimensional complex amplitudes of the longitudinal electric grid voltages
$\underline{\widehat{\mathbf{e}}}_{2\mathrm{D},t,\mathrm{red}}$	2-dimensional complex amplitudes of the reduced transverse electric grid voltages
$\underline{\mathbf{e}}_{2\mathrm{D},z,\mathrm{red}}$	2-dimensional complex amplitudes of the reduced longitudinal electric grid voltages
$\widehat{\mathbf{e}}_{2\mathrm{D},t}$	2-dimensional transverse electric grid voltages
$\underline{\widehat{\mathbf{h}}}_{2\mathrm{D},z,\overline{\Gamma}_{1,h}}$	2-dimensional complex amplitudes of the longitudinal magnetic grid voltages on the closure of the dual grid at the grid part $\overline{\Gamma}_{1,h}$
$\underline{\widehat{\mathbf{d}}}_{2\mathrm{D},t,\overline{\Gamma}_{1,h}}$	2-dimensional complex amplitudes of the transverse electric grid flux on the closure of the dual grid at the grid part $\overline{\Gamma}_{1,h}$
$\underline{\widehat{\mathbf{e}}}$	complex amplitudes of the electric grid voltages
$\underline{\widehat{\mathbf{e}}}_{\Omega\setminus\overline{\Gamma}_1}$	complex amplitudes of the reduced electric grid voltages
$\underline{\widehat{\mathbf{h}}}_{\Gamma_j}$	complex amplitudes of the (dual) magnetic boundary grid voltages on the closure of the dual grid at the boundary part Γ_j
$\underline{\widehat{\widehat{\mathbf{j}}}}_{\Gamma_j}$	complex amplitudes of the equivalent boundary electric grid current parts

CURRICULUM VITAE

since 2003	Promotionsstudium Technische Universität Darmstadt, Germany
2001 - 2002	Master of Science (major in Electrical and Computer Engineering) Georgia Institute of Technology, Atlanta, GA, USA
1998 - 2003	Diplom in Elektrotechnik und Informationstechnik Studienrichtung Theoretische Elektrotechnik Technische Universität Darmstadt, Germany
1995 - 1997	Allgemeine Hochschulreife Ulrich-von-Hutten-Gymnasium, Schlüchtern, Germany
1994 - 1995	Stockbridge High School, Stockbridge, GA, USA
1988 - 1994	Ulrich-von-Hutten-Gymnasium, Schlüchtern, Germany
1984 - 1988	Bergwinkel-Grundschule, Schlüchtern, Germany

BIBLIOGRAPHY

[1] I. Agricola and T. Friedrich, *Globale Analysis: Differentialformen in Analysis, Geometrie und Physik*. Braunschweig: Vieweg, 2001. 6

[2] D. N. Arnold, R. S. Falk, and R. Winther, "Finite element exterior calculus, homological techniques, and applications," *Acta Numerica*, vol. 15, pp. 1–155, May 2006. 27

[3] B. Auchmann, "The coupling of discrete electromagnetism and the boundary element method for the simulation of accelerator magnets," Ph.D. dissertation, CERN, AT/MEL-EM, Vienna University of Technology, Vienna, Dec. 2004. 162

[4] C. A. Balanis, *Advanced Engineering Electromagnetics*. New York: John Wiley & Sons, 1989. 139

[5] D. Baldomir and P. Hammond, *Geometry of Electromagnetic Systems*. New York: Oxford Univ. Press, 1996. 6

[6] P. B. Bochev and J. M. Hyman, "Principles of mimetic discretizations of differential operators," in *Compatible Spatial Discretizations*, D. Arnold, P. Bochev, R. Lehoucq, R. Nicolaides, and M. Shashkov, Eds. New York: Springer, 2006, pp. 89–119. 58

[7] A. Bossavit and L. Kettunen, "Yee-like schemes on staggered cellular grids: A synthesis between FIT and FEM approaches," *IEEE Transactions on Magnetics*, vol. 36, no. 4, pp. 861–867, July 2000. 1, 89, 90

[8] A. Bossavit, "Differential geometry for the student of numerical methods in electromagnetism," Aug. 1991. [Online]. Available: http://www.lgep.supelec.fr/mocosem/perso/ab/DGSNME.pdf 5

[9] ——, *Computational electromagnetism: Variational formulations, complementarity, edge elements*. San Diego, CA: Academic, 1998. 12, 25, 27, 94, 164

[10] ——, "'Generalized finite differences' in computational electromagnetics," *Progress In Electromagnetics Research (PIER)*, vol. 32, pp. 45–64, 2001. 27

[11] ——, "Applied differential geometry – A compendium," Sept. 2002. [Online]. Available: http://www.icm.edu.pl/edukacja/mat/compendium.pdf 31

[12] ——, "Extrusion, contraction: Their discretization via Whitney forms," *The International Journal for Computation and Mathematics in Electrical and Electronic Engineering (COMPEL)*, vol. 22, no. 3, pp. 470–480, 2003. 164

[13] ——, "Force-related nuts and bolts in the discretization toolkit for electromagnetics," in *Proc. 16th Conf. Computation of Electromagnetic Fields (COMPUMAG)*, Aachen, 2007, pp. 885–886. 164

[14] F. Brezzi, K. Lipnikov, and V. Simoncini, "A family of mimetic finite difference methods on polygonal and polyhedral meshes," *Mathematical Models and Methods in Applied Sciences*, vol. 15, no. 10, pp. 1533–1551, Oct. 2005. 2, 126, 163

[15] I. N. Bronstein, K. A. Semendjajew, G. Musiol, and H. Mühlig, *Taschenbuch der Mathematik*, 4th ed. Frankfurt a. M.: Harri Deutsch, 1999. 69, 182

[16] A. Buffa and S. H. Christiansen, "A dual finite element complex on the barycentric refinement," *Mathematics of Computation*, vol. 76, no. 260, pp. 1743–1769, Oct. 2007. 125

[17] W. L. Burke, *Applied Differential Geometry.* Cambridge: Cambridge Univ. Press, 1985. 31

[18] M. Cessenat, *Mathematical Methods in Electromagnetism: Linear Theory and Applications.* Singapore: World Scientific, 1996. 5, 6, 10, 14, 22

[19] S. H. Christiansen, "A construction of spaces of compatible differential forms on cellular complexes," Institut Mittag-Leffler, The Royal Swedish Academy of Sciences, Djursholm, Rep. 17, Dec. 2005. 3, 89, 113, 116, 125, 161

[20] M. Cinalli, F. Edelvik, R. Schuhmann, and T. Weiland, "Consistent material operators for tetrahedral grids based on geometrical principles," *International Journal of Numerical Modelling: Electronic Networks, Devices and Fields*, vol. 17, no. 5, pp. 487–507, Sept./Oct. 2004. 58

[21] M. Clemens and T. Weiland, "Discrete electromagnetism with the Finite Integration Technique," *Progress in Electromagnetics Research (PIER)*, vol. 32, pp. 65–87, 2001. 27

[22] R. E. Collin, *Field Theory of Guided Waves*, 2nd ed. Piscataway, NJ: IEEE Press, 1991. 139

[23] *CST Microwave Studio® 2006 – Getting Started*, Computer Simulation Technology GmbH, Darmstadt, 2006. 158, 159

[24] D. Degerfeldt and T. Rylander, "A brick-tetrahedron finite-element interface with stable hybrid explicit-implicit time-stepping for Maxwell's equations," *Journal of Computational Physics*, vol. 220, no. 1, pp. 383–393, Dec. 2006. 126, 155

[25] T. DeRose and M. Meyer, "Harmonic coordinates," Pixar Animation Studios, Emeryville, CA, Pixar Technical Memo #06-02, Jan. 2006. 118

[26] M. Desbrun, "From barycentric coordinates to Whitney forms: Turn your mesh into a computational structure," presented at the ACM SIGGRAPH 2005, Los Angeles, CA, July. [Online]. Available: www.geometry.caltech.edu/pubs/Courses/DDG/BC&Whitney.pdf 125

[27] M. Desbrun, A. N. Hirani, M. Leok, and J. E. Marsden, "Discrete exterior calculus," Aug. 2005, arXiv:math/0508341v2. [Online]. Available: http://arxiv.org/abs/math/0508341v2 27, 42

[28] G. A. Deschamps, "Electromagnetics and differential forms," *Proceedings of the IEEE*, vol. 69, no. 6, pp. 676–696, June 1981. 5, 6, 25

[29] P. Dular, J.-Y. Hody, A. Nicolet, A. Genon, and W. Legros, "Mixed finite elements associated with a collection of tetrahedra, hexahedra and prisms," *IEEE Transactions on Magnetics*, vol. 30, no. 5, pp. 2980–2983, Sept. 1994. 1, 89

[30] F. Edelvik, R. Schuhmann, and T. Weiland, "A general stability analysis of FIT/FDTD applied to lossy dielectrics and lumped elements," *International Journal of Numerical Modelling: Electronic Networks, Devices and Fields*, vol. 17, no. 4, pp. 407–419, July/Aug. 2004. 82, 84

[31] F. Edelvik, "Hybrid solvers for the Maxwell equations in time-domain," Uppsala Dissertations 40, Faculty of Science and Technology, Uppsala University, Uppsala, May 2002. [Online]. Available: http://urn.kb.se/resolve?urn=urn:nbn:se:uu:diva-2156 155

[32] T. Euler, R. Schuhmann, and T. Weiland, "Polygonal finite elements," *IEEE Transactions on Magnetics*, vol. 42, no. 4, pp. 675–678, Apr. 2006. 120

[33] L. C. Evans, *Partial Differential Equations*. Providence, RI: American Mathematical Society, 1998. 22

[34] O. Farle, V. Hill, and R. Dyczij-Edlinger, "Finite-element waveguide solvers revisited," *IEEE Transactions on Magnetics*, vol. 40, no. 2, pp. 1468–1471, Mar. 2004. 128

[35] S. Feigh, "Ein geometrisches Diskretisierungs- und Lösungsverfahren auf der Basis der Finiten-Integrations-Methode," D 17 Darmstädter Dissertation, Technische Universität Darmstadt, Germany, 2006. 58, 135, 137

[36] M. S. Floater, K. Hormann, and G. Kós, "A general construction of barycentric coordinates over convex polygons," *Advances in Computational Mathematics*, vol. 24, no. 1-4, pp. 311–331, Jan. 2006. 118

[37] M. S. Floater, G. Kós, and M. Reimers, "Mean value coordinates in 3D," *Computer Aided Geometric Design*, vol. 22, no. 7, pp. 623–631, Oct. 2005. 2, 118

[38] R. Geus, "The Jacobi-Davidson algorithm for solving large sparse symmetric eigenvalue problems with application to the design of accelerator cavities," Diss. ETH No. 14734, Swiss Federal Institute of Technology, Zurich, 2002. 142

[39] ——, "Pyfemax," Aug. 2003. [Online]. Available: http://people.web.psi.ch/geus/pyfemax/pyfemax.html 142

[40] V. Gradinaru and R. Hiptmair, "Whitney elements on pyramids," *Electronic Transactions on Numerical Analysis*, vol. 8, pp. 154–168, 1999. 1, 89, 126, 155

[41] R. Graglia and I.-L. Gheorma, "Higher order interpolatory vector bases on pyramidal elements," *IEEE Transactions on Antennas and Propagation*, vol. 47, no. 5, pp. 775–782, May 1999. 163

[42] P. W. Gross and P. R. Kotiuga, *Electromagnetic Theory and Computation.* Cambridge: Cambridge Univ. Press, 2004. 6, 10, 18, 103

[43] P. Hansbo, "Nitsche's method for interface problems in computational mechanics," *GAMM-Mitteilungen*, vol. 28, pp. 184–207, 2005. 126

[44] J. Harrison, "Lectures on chainlet geometry – new topological methods in geometric measure theory," Department of Mathematics, University of California, Berkeley, Tech. Rep., May 2005. [Online]. Available: http://arxiv.org/abs/math-ph/0505063 28

[45] V. Hill, O. Farle, and R. Dyczij-Edlinger, "Finite element basis functions for nested meshes of nonuniform refinement level," *IEEE Transactions on Magnetics*, vol. 40, no. 2, pp. 981–984, Mar. 2004. 2, 125

[46] R. Hiptmair, "Discrete hodge operators," SFB 382, Universität Tübingen, Tech. Rep. 126, Oct. 1999. 73

[47] ——, "Discrete hodge-operators: An algebraic perspective," *Progress in Electromagnetics Research (PIER)*, vol. 32, pp. 247–269, 2001. 32, 42, 59, 163, 167

[48] ——, "Finite elements in computational electromagnetism," *Acta Numerica*, vol. 11, pp. 237–339, Jan. 2002. 11, 12, 13, 27, 29, 46, 89, 96, 163

[49] R. Hiptmair and C. Schwab, "Numerical treatment of partial differential equations," lecture notes, Mar. 2004, Dep. Mathematics, ETH Zurich. 28, 91, 228

[50] J. M. Hyman and M. Shashkov, "Mimetic discretizations for Maxwell's equations," *Journal of Computational Physics*, vol. 151, no. 2, pp. 881–909, 1999. 58

[51] *IEEE Standard for Binary Floating-Point Arithmetic*, IEEE Std. 754, 1985. 127

[52] J. D. Jackson, *Classical electrodynamics*, 3rd ed. New York: John Wiley & Sons, 1998. 16

[53] K. Jänich, *Vektoranalysis*, 4th ed. Berlin: Springer, 2003. 6, 7, 8, 10, 11, 14

[54] T. Ju, S. Schaefer, and J. Warren, "Mean value coordinates for closed triangular meshes," in *ACM SIGGRAPH 2005*, Los Angeles, CA, July, pp. 561–566. 2, 118

[55] T. Ju, S. Schaefer, J. Warren, and M. Desbrun, "Geometric construction of coordinates for convex polyhedra using polar duals," in *Eurographics Symp. on Geometry Processing*, Vienna, July 2005, pp. 181–186. 118

[56] D. Kajfez and P. Guillon, Eds., *Dielectric resonators.* Dedham: Artech, 1986. 157

[57] L. Knockaert, J. Sercu, and D. De Zutter, "Generalized polygonal basis functions for the electromagnetic simulation of complex geometrical planar structures," in *2001 IEEE MTT-S Int. Microwave Symp. Dig.*, vol. 2, Phoenix, AZ, May 2001, pp. 1249–1252. 2, 125

[58] J.-F. Lee, R. Lee, and A. Cangellaris, "Time-domain finite-element methods," *IEEE Transactions on Antennas and Propagation*, vol. 45, no. 3, pp. 430–442, Mar. 1997. 183

[59] R. Leis, *Initial Boundary Value Problems in Mathematical Physics.* Stuttgart: Teubner, 1986. 5, 6, 22, 28

[60] I. V. Lindell, *Differential Forms in Electromagnetics.* New York: Wiley Interscience, 2004. 6

[61] L.-Z. Lu and C. E. M. Pearce, "Some new bounds for singular values and eigenvalues of matrix products," *Annals of Operations Research*, vol. 98, no. 1-4, pp. 141–148, Dec. 2000. 215

[62] M. Marrone, "The equivalence between cell method, FDTD and FEM," in *The Fourth Int. Conf. on Computation in Electromagnetics (CEM)*, Bournemouth, Apr. 2002, p. n.p. 58

[63] C. Mattiussi, "The finite volume, finite difference, and finite elements methods as numerical methods for physical field problems," *Advances in Imaging and Electron Physics*, vol. 113, pp. 1–146, 2000. 58

[64] J. C. Maxwell, *A Treatise on Electricity and Magnetism.* Oxford: Clarendon, 1873. 1, 5

[65] D. Mitrea and M. Mitrea, "Finite energy solutions of Maxwell's equations and constructive hodge decompositions on nonsmooth Riemannian manifolds," *Journal of Functional Analysis*, vol. 190, no. 2, pp. 339–417, Apr. 2002. 225

[66] M. Mitrea, "Sharp Hodge decompositions, Maxwell's equations, and vector Poisson problems on nonsmooth, three-dimensional Riemannian manifolds," *Duke Mathematical Journal*, vol. 125, no. 3, pp. 467–547, Dec. 2004. 225

[67] P. Monk, "A finite element method for approximating the time-harmonic Maxwell equations," *Numerische Mathematik*, vol. 63, pp. 243–261, 1992. 137

[68] P. Monk and K. Parrott, "Phase-accuracy comparisons and improved far-field estimates for 3-D edge elements on tetrahedral meshes," *Journal of Computational Physics*, vol. 170, no. 2, pp. 614–641, July 2001. 137

[69] J. C. Nédélec, "Mixed finite elements in $\mathbb{R}^3$," *Numerische Mathematik*, vol. 35, no. 3, pp. 315–341, Sept. 1980. 1, 89

[70] N. M. Newmark, "A method of computation for structural dynamics," *Journal of the Engineering Mechanics Division*, vol. 85, pp. 67–94, 1959. 75

[71] J. Nitsche, "Über ein Variationsprinzip zur Lösung von Dirichlet-Problemen bei Verwendung von Teilräumen, die keinen Randbedingungen unterworfen sind," *Abhandlungen aus dem Mathematischen Seminar der Universität Hamburg*, vol. 36, pp. 9–15, 1971. 126

[72] S. Piperno, "Symplectic local time-stepping in non-dissipative DGTD methods applied to wave propagation problems," Unité de recherche INRIA Sophia Antipolis, Tech. Rep. 5643, July 2005. [Online]. Available: http://cermics.enpc.fr/reports/CERMICS-2005/CERMICS-2005-282.pdf 78

[73] O. Podebrad, M. Clemens, and T. Weiland, "New flexible subgridding scheme for the Finite Integration Technique," *IEEE Transactions on Magnetics*, vol. 39, no. 3, pp. 1662–1665, May 2003. 3, 135

[74] P. Russer, *Electromagnetics, Microwave Circuit and Antenna Design for Communications Engineering.* Boston, MA: Artech, 2003. 6

[75] V. S. Ryaben'kii and S. V. Tsynkov, *A Theoretical Introduction to Numerical Analysis.* Boca Raton: Chapman & Hall, 2007. 211

[76] T. Rylander and A. Bondeson, "Stability of explicit-implicit hybrid time-stepping schemes for Maxwell's equations," *Journal of Computational Physics*, vol. 179, no. 2, pp. 426–438, Aug. 2002. 28, 75, 79, 155

[77] Y. Saad, *Numerical Methods for Large Eigenvalue Problems*, revised online ed. Manchester: Manchester Univ. Press, 1992. [Online]. Available: http://www-users.cs.umn.edu/~saad/EIGBOOK.tar.gz 86, 218

[78] R. Schuhmann and T. Weiland, "Conservation of discrete energy and related laws in the Finite Integration Technique," *Progress in Electromagnetic Research (PIER)*, vol. 32, pp. 301–316, 2001. 42

[79] R. Schuhmann, "Die Nichtorthogonale Finite-Integrations-Methode zur Simulation elektromagnetischer Felder," D 17 Darmstädter Dissertation, Technische Universität Darmstadt, Darmstadt, 1999. 1, 58, 89, 157

[80] G. Schwarz and J. Sniatycki, "Yang-Mills and Dirac fields in a bag, existence and uniqueness theorems," *Communications in Mathematical Physics*, vol. 168, no. 2, pp. 441–453, Mar. 1995. 225, 227

[81] G. S. Smith, *An Introduction to Classical Electromagnetic Radiation.* Cambridge: Cambridge Univ. Press, 1997. 22

[82] N. Sukumar and E. A. Malsch, "Recent advances in the construction of polygonal finite element interpolants," *Archives of Computational Methods in Engineering*, vol. 13, pp. 129–163, 2006. 2, 125

[83] T. Tarhasaari, L. Kettunen, and A. Bossavit, "Some realizations of a discrete Hodge operator: A reinterpretation of finite element techniques [for EM field analysis]," *IEEE Transactions on Magnetics*, vol. 35, no. 3, pp. 1494–1497, May 1999. 27

[84] F. L. Teixeira and W. C. Chew, "Lattice electromagnetic theory from a topological viewpoint," *Journal of Mathematical Physics*, vol. 40, pp. 169–187, Jan. 1999. 27

[85] P. Thoma, "Zur numerischen Lösung der Maxwellschen Gleichungen im Zeitbereich," D 17 Darmstädter Dissertation, Technische Universität Darmstadt, Darmstadt, 1997. 58, 59, 60, 64, 132, 147

[86] E. Tonti, "On the formal structure of physical theories," Istituto di Matematica del Politecnico di Milano, Tech. Rep., 1975. 25, 27

[87] ——, "A direct discrete formulation of field laws: The cell method," *Computer Modeling in Engineering & Sciences*, vol. 2, pp. 237–258, 2001. 1, 27

[88] ——, "Finite formulation of the electromagnetic field," *Progress in Electromagnetics Research (PIER)*, vol. 32, pp. 1–44, 2001. 32, 76

[89] L. Vardapetyan and L. Demkowicz, "Full-wave analysis of dielectric waveguides at a given frequency," *Mathematics of Computation*, vol. 72, no. 241, pp. 105–129, 2003. 128, 132

[90] E. L. Wachspress, *A Rational Finite Element Basis.* New York: Academic, 1975. 2

[91] J. Warren, "Barycentric coordinates for convex polytopes," *Advances in Computational Mathematics*, vol. 6, pp. 97–108, 1996. 118

[92] T. Weiland, "Eine Methode zur Lösung der Maxwellschen Gleichungen für sechskomponentige Felder auf diskreter Basis," *Electronics and Communication (AEÜ)*, vol. 31, pp. 116–120, 1977. 1, 27, 58

[93] ——, "Eine numerische Methode zur Lösung des Eigenwellenproblems längshomogener Wellenleiter," *Electronics and Communication (AEÜ)*, vol. 31, pp. 308–314, 1977. 128

[94] ——, "On the unique numerical solution of Maxwellian eigenvalueproblems in three dimensions," *Particle Accelerators*, vol. 17, pp. 227–242, 1985. 1, 27

[95] ——, "Time domain electromagnetic field computation with finite difference methods," *International Journal of Numerical Modelling: Electronic Networks, Devices and Fields*, vol. 9, pp. 295–319, 1996. 1, 3, 27, 45, 46, 50, 76, 80

[96] H. Whitney, *Geometric Integration Theory.* Princeton, NJ: Princeton Univ. Press, 1957. 89

[97] H. Windcliff, P. A. Forsyth, and K. R. Vetzal, "Analysis of the stability of the linear boundary condition for the black-scholes equation," *Journal of Computational Finance*, vol. 8, pp. 65–92, 2004. 73

[98] M. A. Woodbury, "Inverting modified matrices," Department of Statistics, Princeton Univ., Princeton, NJ, Tech. Rep., 1950. 215

[99] J.-Y. Wu and R. Lee, "The advantages of triangular and tetrahedral edge elements for electromagnetic modeling with the finite-element method," *IEEE Transactions on Antennas and Propagation*, vol. 45, no. 9, pp. 1431–1437, Sept. 1997. 132

[100] K. Yee, "Numerical solution of inital boundary value problems involving Maxwell's equations in isotropic media," *IEEE Transactions on Antennas and Propagation*, vol. 14, no. 3, pp. 302–307, May 1966. 80

[101] I. Zagorodnov, R. Schuhmann, and T. Weiland, "Conformal FDTD-methods to avoid time step reduction with and without cell enlargement," *Journal of Computational Physics*, vol. 225, no. 2, pp. 1493–1507, 2007. 58, 135